Volcanology and Geochemistry of the Kaingaroa Ignimbrite, Taupo Volcanic Zone, New Zealand.

A thesis
submitted in fulfilment
for the requirements for the degree
of
Doctor of Philosophy in Geological Sciences
at the
University of Canterbury
by

Stephen Willis Beresford

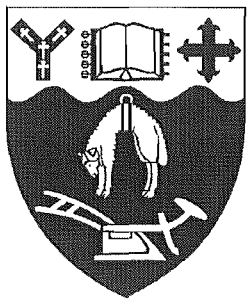

University of Canterbury
1997

Frontispiece: "Valley of death": A near complete section through the Kaingaroa Ignimbrite, Maungahekeke Valley. Geologists Steve Beresford and Dr Rod Burt for scale (Photograph courtesy of Al Ritchie).

Erratum

- Spelling of Rerewhakaaitu inconsistent throughout thesis.
- All Rare earth element plots are missing Pm (which was not analysed but is traditionally included between Sm and Nd).

Pg 8. (Line 24) R.J.Martin should read R.C. Martin.
Pg 33 (Line 7) west should read east
Pg 36, Figure 2.2, should read Figure 3.2.
Pg 44 (Line 8) coincendent should read coincident.
Pg 54, Fig 3.8. M_L in mm.
Pg 58, Table 3.2. correction
non-welded - Density < 1.3
Densely welded - Density >1.8
Pg 78 (Line 9). varies should read variation
Pg 84 (Line 1). median diameter -5.98 to -2.9.
Pg 98. (Fig 5.1 caption) Fig 5.6 should read Fig 5.5.
Pg 104 (Line 30). Fig 5.6 should read Fig 5.5.
Pg 110, Fig 5.5a + b. GBN should read GB.
Pg 180, Fig 7.4. Partial hydration? should read incipient alteration?
Pg 183, Fig 7.6. Rb missing off x axis.
Pg 312. Table of glass analyses.

Abstract

The 0.23 Ma Kaingaroa Ignimbrite is a composite multiple flow-unit ignimbrite erupted from Reporoa Caldera, Taupo Volcanic Zone (TVZ), New Zealand.

The Kaingaroa Ignimbrite has a complex internal stratigraphy with a complex basal tephra sequence of intercalated fall, surge and flow deposits, and three ignimbrite units, with strikingly proximal to medial facies variation. Proximal facies deposits are dominated by coarse lithic breccias up to 45 m thick which are interpreted as co-ignimbrite lag breccias. These lag breccias are some of the thickest so far documented. Welding and thickness variations in the extensive Old Waiotapu Rd (OWR; kg_1) and Webb ignimbrite unit (WIU; kg_2) suggests gradual thickening away from source, interpreted to represent ponding in a shallow alluvial lowland or basin.

A detailed lithic componentry study indicates changes in lithic diversity and abundance between stratigraphic units which mark changes in vent conditions, increasing depth of lithic provenance and hence inferred fragmentation level. Lithic fragments reveal aspects of the sub-caldera geology, which is dominated by an andesitic volcano with leuco-gabbroic subvolcanic roots, intercalated welded ignimbrites, rare low-grade metasedimentary basement and meta-rhyolites. Gabbros and meta-rhyolites suggest complex metasomatic and fumarolic processes adjacent to the Kaingaroa magma system. The presence of tourmaline-bearing meta-rhyolites and meta-ignimbrites and tourmalinite is the first documented occurrence of tourmaline and tourmalinite in TVZ.

Four pumice types are defined on pumice chemistry and mineralogy. These pumices are interpreted to represent samples of a weakly continuously zoned magma chamber (70-75% SiO_2), which was progressively tapped during the eruption. Trace element and rare earth element systematics are consistent with an origin of type A magma from a type D parent by minor fractionation of plagioclase, zircon, and trace contents of Fe/Ti oxides and orthopyroxene. An additional hornblende-, 2-pyroxene-phyric dacite pumice/bleb (69% SiO_2) was sampled from the Tokiaminga sub-unit, but is mineralogically and compositionally different from Kaingaroa $pumices_{s.s.}$. Post-caldera rhyolites are mineralogically and chemically variable, with broad similarities to Kaingaroa pumices. The Kaingaroa magma components show reverse isotopic zonation i.e. decreasing $^{87}Sr/^{86}Sr$ and increasing $^{143}Nd/^{144}Nd$ with differentiation, suggesting syn-eruptive mingling and evisceration of the multiple magma batches occurred during the climactic caldera collapse phase.

The Kaingaroa Ignimbrite has been mis-correlated by previous workers with the Matahina, Mamaku, and Rangatira Point ignimbrites, and three new units described in this thesis; Kawerau ignimbrite, Wheao sheet, and the welded ignimbrite of Wairakei drill holes. It is clear that ignimbrite correlation is difficult in TVZ because of the poor exposure and the limited stratigraphic sections that document multiple units. The Kawerau ignimbrite remains an enigma, largely because of the anomalously high Zr, Hf and Zn contents, suggestive of a relationship to 'alkaline' rhyolites, and the presence of unusual magnesium-poor manganoan fayalite of vapour-phase origin. Identification of these units and other intermediate size ignimbrite in the stratigraphic interval between Whakamaru-group, and Mamaku ignimbrites requires further careful documentation, but suggests a temporal clustering of ignimbrites sourced from throughout TVZ.

Table of Contents

CHAPTER ONE
Introduction

1.1 Introduction

The Kaingaroa Ignimbrite (formally Kaingaroa Ignimbrites), Taupo Volcanic Zone (TVZ), New Zealand, was erupted from Reporoa Caldera (Nairn et al. 1994), 230,000 years ago (Houghton et al. 1995). Until this study it was one of the few prominent ignimbrites in the central TVZ not to have been studied in detail (see Wilson et al. 1995a). This thesis reports the first results of major, trace elements, (including rare earth elements; REE), isotopes, a revised stratigraphy, detailed lithic componentry, and detailed analysis of the associated lag breccia, with the aim of producing an integrated eruptive and magma system model.

"The name Kaingaroa comes from a myth called Kaingaroa a Haungaroa - the long meal taking of Haungaroa. Haungaroa was a woman who took a long time over a meal when travelling across the Kaingaroa plateau. The males with her abused her for delaying them, so she responded by turning them into cabbage trees. These trees became landmarks for travellers for centuries after".

1.2 Location and physiography

The Kaingaroa Ignimbrite crops out around Reporoa Caldera, within the central Taupo Volcanic Zone, North Island, New Zealand (Fig 1.1). Kaingaroa Ignimbrite outcrop is principally in three prominent terrains, the Kaingaroa Plateau, Taupo-Reporoa basin and the rolling hills and abundant fault scarps of the Te Weta and Paeroa blocks.

Kaingaroa Plateau is a vast plateau, dominantly covered by the Kaingaroa forest which is the largest manmade forest in New Zealand, and during the 1960's and 1970's the largest manmade forest in the world. The surface of the plateau is controlled by ignimbrites gently dipping away from central TVZ towards the ranges; the northern part, near Lake Rerewhakaaitu, is unforested and forms farmland.

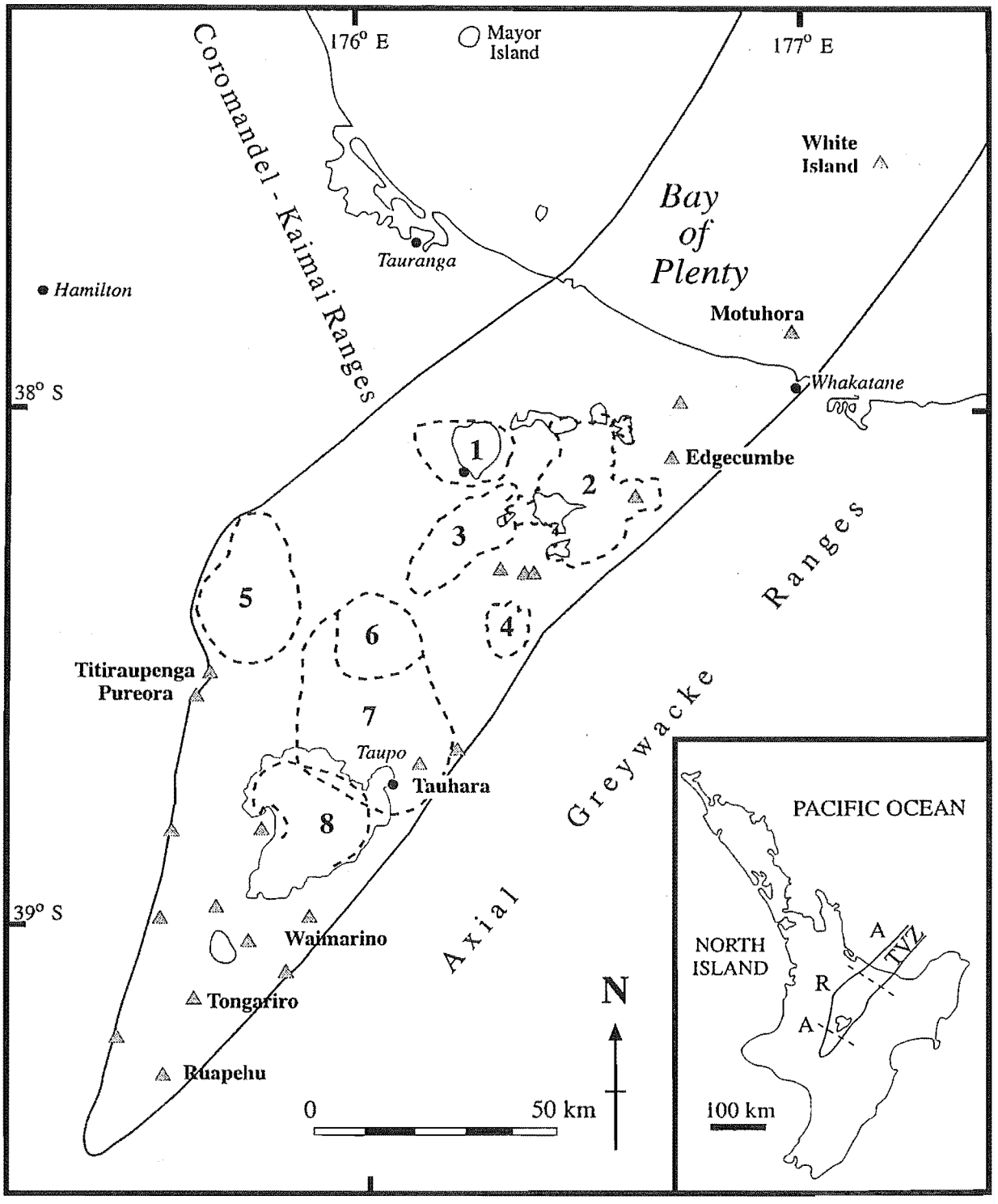

Figure 1.1 Location of Reporoa Caldera and Taupo Volcanic Zone, New Zealand. Caldera and caldera complex boundaries after Wilson et al. 1995; Cole et al. submitted. 1= Rotorua; 2=Okataina; 3=Kapenga; 4=Reporoa; 5=Mangakino; 6=Maroa; 7=Wairakei; 8=Taupo. Inset denotes andesitic (A) and rhyolitic (R) dominated domains of Taupo Volcanic Zone.

The Taupo-Reporoa basin is a depression that extends from Lake Taupo to Waiotapu. The northern part of this basin is marked by Maungaongaonga and Maungakakaramea (or "Rainbow Mountain"), two extensively hydrothermally dacite domes that occur within the 17 km^2 Waiotapu geothermal field. In the northern part of the depression is the 15 km long 10 km wide Reporoa Caldera, with well expressed topographic rims defined by large slump scallops cutting the pre-caldera Waiotapu and Whakamaru-group ignimbrites and the Trig 8566 rhyolite dome (Chapter 2). The central part of the Taupo-Reporoa basin is dominated by low-lying farmland, and intermittent geothermal areas e.g. Broadlands-Ohaaki. It is largely infilled with sediments, reflecting a prolonged and intermittent lacustrine history. The eastern edge of the basin is defined by the eastern edge of Reporoa Caldera, and the Kaingaroa fault, which defines the eastern boundary of the TVZ.

To the west of Taupo-Reporoa basin, is the Taupo fault belt, on the eastern side of which is the impressive 600 m high Paeroa Fault scarp. The area to the west of the fault was termed the Te Weta block by Lloyd (1972), and consists of highly faulted, rolling farmland.

1.3 Exposure

Outcrop within the Taupo Volcanic Zone is generally poor, due to abundant vegetation and the unconsolidated nature of most rock types. Despite the excellent preservation of the Kaingaroa Ignimbrite *surface* on the Kaingaroa Plateau, the unit is very poorly exposed. Exposures are limited to rare roadcuts, quarries, farm tracks and rivers that incise into the plateau, generally along its margins and discontinuously exposed welded ignimbrite on rolling farmland hills in the Te Weta block and near Lake Rerewhakaitu (Fig 1.2). The poorly welded nature of most units means outcrop is largely limited to proximal areas. Exposure within the forest is ephemeral, with best exposure occurring for a few years after clear felling. Exposures following clear felling can be patchy in areas of rolling topography (e.g. Northern Boundary Rd) or excellent adjacent to deeply incised gorges (e.g. Maungahekeke Valley, Main Gully Rd; Fig 1.3). Rare quarries provide excellent exposures e.g. Butchers Boundary Road, No 6 Road and Webb Quarry.

Figure 1.2 The Kaingaroa Ignimbrite surface in the Rerewhakaaitu area. Note the discontinuous exposure of the upper Kaingaroa Ignimbrite unit.

Figure 1.3. Semi-continuous exposure of welded portions of the middle and upper Kaingaroa Ignimbrite units along Main Gully Rd.

1.4 Taupo Volcanic Zone

The Taupo Volcanic Zone is a NNE trending arc-related rift zone c. 300 km (220 km on land) that is filled by voluminous Quaternary volcanism (Fig 1.1), a result of oblique westward subduction of the Pacific lithosphere beneath the Australian plate.

The Taupo Volcanic Zone has produced over 15-20000 km^3 DRE (dense rock equivalent) of volcanics (Wilson et al. 1995a) made up of 80% rhyolite, 20% andesite and dacite, and < 1% high alumina basalt (Hochstein et al. 1993). Rhyolitic volcanism in the TVZ is restricted to the central TVZ with the northern and southern ends dominated by andesitic/dacitic volcanism (Cole 1990; Wilson et. al. 1995a). Central TVZ is an extraordinarily productive area of rhyolitic volcanism and huge geothermal heat fluxes, and is the most productive and active rhyolitic volcanic system on Earth (Wilson 1996). There have been at least 34 major rhyolitic ignimbrite eruptions from an overlapping succession of *at least* eight 'calderas' (Houghton et al. 1995; Wilson et al. 1995a; Fig 1.1). In addition there have been a number of phases of lava effusion.

TVZ is currently defined by an envelope drawn around all known vent locations since 1.9 Ma (Wilson et al. 1995a). The 1.9 m.y age limit is defined as the onset of observable calc-alkaline volcanism in central North Island, and with an alignment reflecting the present-day stress regime (Houghton et al. 1995). The history of TVZ is divided into 'old TVZ' from c.2.0 Ma to 0.36 Ma, and 'young TVZ' from 0.36 Ma onwards, the division being the Whakamaru-group ignimbrites, which obscure much of the evidence for older activity. 'Modern TVZ' is defined by activity during and since the 0.065 Ma Rotoiti eruption (Wilson et al. 1995a), and is considered to represent the currently active part of the zone. Based on regional mapping, reconnaissance geochemistry and $^{40}Ar/^{39}Ar$ ages Houghton et al (1995) define six periods of caldera-forming ignimbrite activity (Fig 1.4):

Period I (1.6-1.45 Ma): The onset of ignimbritic and rhyolitic volcanism in the TVZ, evidence of which is preserved in western TVZ from the Mangakino 'caldera'.

Period IIA (1.25-0.9 Ma): An intense episode of large ignimbritic eruptions, preserved in western TVZ

Period IIB (0.8-0.7 Ma) Early eruptions from the Kapenga 'caldera', including the distinctive and widespread Waiotapu Ignimbrite.

Period IIIA (0.35-0.3 Ma) Whakamaru-group ignimbrites.

Period IIIB (0.28-0.10 Ma) Intensive period of smaller scale ignimbrite eruptions from six calderas. The Kaingaroa Ignimbrite erupted at 0.23 Ma (Houghton et al. 1995).

Period IIIC (0.10 Ma-present day) Eruptions of the Rotoiti Breccia, Oruanui and Taupo ignimbrites from Okataina and Taupo 'calderas'.

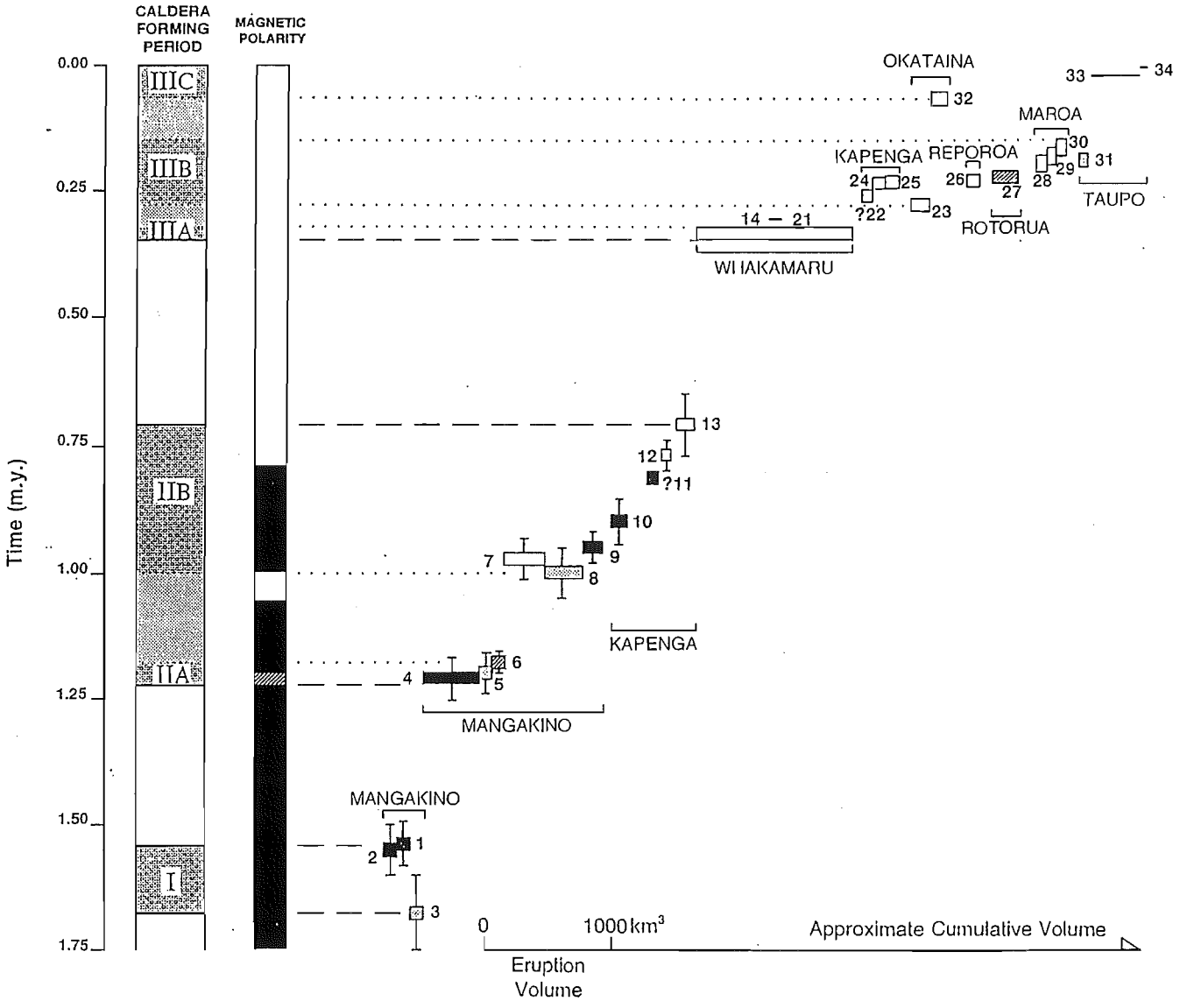

Figure 1.4. Periods of silicic volcanism after Houghton et al (1995).

The subvolcanic basement of TVZ is thought to conceal a terrane boundary between two largely Mesozoic quartzofeldspathic 'greywacke' terranes. The Torlesse terrane lies to the east of the TVZ (Fig 1.1); the Waipapa terrane to the west. Locally within TVZ, rare outcrops (e.g. Pekepeke and Matata) and geothermal drill holes (e.g. Rotokawa and Kawerau) reveal the complex boundary between the terranes. Greywacke and its metamorphic equivalent are considered assimilants in geochemical models for the origin of andesites and rhyolites (e.g. Graham and Hackett 1987, Graham et al. 1995). Along the flanks of the TVZ Tertiary sediments are unconformable over greywacke basement.

Aspects of regional geology within the study areas are outlined in Chapter 2.

1.5 Previous work

Grange (1937) mapped all the ignimbrites in the Reporoa-Paeroa area as Patetere Ignimbrite, but noted a dark grey ignimbrite "with small black glass shreds, outcropping on the Waiotapu-Murupara Road with widely spaced vertical joints". Grange describes the unit as a good cliff maker and contains " andesite lumps, mostly less than 1 inch in diameter". He traced the owharoite for seven miles (12 km) to the south from Waiotapu-Murupara Rd, and also describes andesitic gravels up to 30 ft, interbedded with owharoite, which are underlain by water sorted pumice silts containing pisolites, at two localities " one mile and half north of Wharekaunga Trig", and " about two miles south of Wharekaunga Trig". He also mentions a light grey ignimbrite which forms the surface of the Kaingaroa Plateau in this area. Grange's descriptions are notable as they are the first recognisable descriptions of a unit termed Kaingaroa Ignimbrite by Beck and Robertson (1955), but also because they accurately describe outcrops of inferred lag breccia and basal tephras (outcrops now covered in forest).

J.Healy and R.J.Martin (unpublished letters on IGNS files) first report stratigraphy on the Kaingaroa Ignimbrite, based on early unpublished mapping by L.Allen. They noted two units termed the Reporoa ignimbrite and Kaingaroa lenticulite. J. Healy (letter to A.Steiner 30/9/1958, unpublished letter on IGNS files) also noted the presence of conglomerate underlying the Kaingaroa 1 (formerly Reporoa ignimbrite) sheet.

"I was out yesterday afternoon with Mr Overington of the State Forest Service to look at a deposit they are working for road metal near Kaingaroa. It turns out to be from a andesite conglomerate interbedded with sandstones and pumiceous tuffs underlying the Kaingaroa Plateau east of Waiotapu.

What I think is Kaingaroa 1 sheet east of Waiotapu has over 300ft of sandstones, conglomerates and breccias under it, whereas near Kaingaroa it is underlain directly by another ignimbrite sheet."

Healy's descriptions closely match those of the lag breccia and underlying non-welded ignimbrite and basal tephras, outlined in Chapter 3 and 4.

Martin's (1961) seminal paper on TVZ ignimbrites outlines two ignimbrite members; a lower sandy-black ignimbrite, and an upper densely-welded lenticulite. Martin renamed the Reporoa ignimbrite as the lower member of the Kaingaroa Ignimbrites (Formation), and noted that the ignimbrites overlay the Matahina Ignimbrite. He described the upper member as " consisting of fine-textured, pinkish, welded tuff containing sparse pumice lenticules", and the lower member "consists of lightly welded, dark grey to black, pumice tuff containing light-grey pumice fragments". "Both are characterised by relatively abundant andesite fragments up to 1.5 in long". Martin defined type localities for the lower member as "three miles south-east of Lake Rotowhero on the Rotorua-Murupara Road", and for the upper member "at Webb Road quarry, one mile north-west of Kaingaroa Forest headquarters".

Healy et al (1964) placed the source of the entire Kaingaroa Ignimbrites in the southern part of Okataina Caldera. Later workers adopted this source (e.g. Nairn 1981, 1989: Wilson et al. 1984), but Martin (1961) gave a source for the upper member as "south of Haroharo Caldera (Okataina), near Kaingaroa Forest headquarters", on the basis of variations in grain size and thickness and degree of welding. Healy et al (1964) mapped the Kaingaroa Ignimbrites at 1: 250 000 and their distribution closely matches the distribution mapped during this project. Healy et al (1964) begun the 'kg' notation, and mapped the lower member as kg_1 and upper member as kg_2. Nairn (1973) recognised a third member of the Kaingaroa Ignimbrites, which he termed kg_0.

Nairn (1981, 1989) mapped the Kaingaroa Ignimbrite in the Rerewhakaitu and Puhipuhi Basin-Kawerau region. B.P.Kohn (in Nairn 1989) dated the unit in the Puhipuhi Basin at 0.24 Ma using the fission track method. Details concerning the correlation of this unit is addressed in Chapter 8.

New mapping along the eastern margin of the Reporoa Basin by Nairn et al (1994) identified a lithic lag breccia facies within the Kaingaroa Ignimbrites and interpreted the northern part of the depression as a caldera, which was the source of the Kaingaroa Ignimbrites. Nairn et al (1994) reported reconnaissance field studies and granulometry for the lag breccia, and petrography of the lithic components.

Houghton et al (1995) redefined the age of the Kaingaroa Ignimbrites to 0.23 Ma (Ar/Ar) and Grindley et al (1994) quoted a stratigraphically consistent 0.22 Ma fission track age which is within error of the Ar/Ar age. Black et al (1996) used the isothermal plateau fission track method on glass shards to obtain an eruption age for the Kaingaroa Ignimbrite of 0.31 ± 0.01 Ma.

1.6 Aims

The aims of this project has been to study the Kaingaroa Ignimbrite using a combination of field and geochemical techniques to develop a model of magmatic and eruptive evolution during (and prior) to the caldera-forming Kaingaroa Ignimbrite eruption.

The main objectives are to:

1. Establish an internal stratigraphy and define the distribution of the Kaingaroa Ignimbrite.
2. Describe the geology of the lag breccia and lateral equivalents to deduce features of proximal ignimbrite emplacement and deposition
3. Undertake a detailed study of lithic fragments to deduce features of lithic provenance, vent evolution and sub-caldera geology.
4. Investigate mineral and pumice compositional variation in order to establish a petrogenetic model for the Kaingaroa magma system.

CHAPTER TWO

Reporoa Caldera:

Morphology, structure, and circumcaldera geology

Figure 2.1 Reporoa Caldera viewed from the southeastern caldera rim (Butchers Boundary Rd quarry).

2.1 Introduction

There are two parts to this chapter. The first section introduces calderas and caldera structures in TVZ, and describes both the structure and interpretation of Reporoa Caldera (Fig 2.1), and the source of the Kaingaroa Ignimbrite. The second deals with reconnaissance mapping and previous work on the circumcaldera geology of the Reporoa Caldera. The purpose is to introduce the general geology of the region and the structure of the caldera to provide background information for discussion on lithic fragment correlation (see Chapter 5), and interpretation of the processes of caldera collapse and vent evolution (Chapter 9).

2.2 Calderas and caldera complexes

Eight calderas have been identified by previous workers in TVZ, all of which are restricted to the central TVZ (Fig 1.1), although Wilson et al (1995a) outline two possible additional structures in the Broadlands and northern Mamaku plateau region. Detailed reviews of TVZ calderas are outlined in Wilson et al (1984, 1995a) and Wood (1995).

There has been considerable debate on the location and nature of caldera structures in the TVZ. It is becoming increasingly apparent that many previously identified 'caldera' structures are complex features resulting from multiple episodes of caldera collapse. Many have been also strongly influenced by regional tectonics. Monogenetic caldera structures are rare in TVZ and previous workers have outlined both calderas and centres (both terms are often used for the same feature). The term centre has been used for both spatial and temporal association of caldera-forming events, and this has led to further confusion.

While much of the debate is semantic, its relevance to hazard assessment means that a general understanding of terminology is important. Terminology of calderas and caldera structures in this thesis follows Cole et al (1996):

Caldera: A volcanic depression, generally large, which is principally the result of collapse into the top of a magma reservoir during or immediately following eruptive activity.

Caldera complex: Spatially and structurally associated nested or overlapping calderas. Structures are poorly and incompletely preserved, therefore ignimbrites should be assigned to a caldera complex on the basis of volcanologic criteria (e.g. M_L, AMS, clast preferred orientation, and lithic componentry).

Centre: Spatially associated eruptives e.g. Tongariro volcanic centre.

Six caldera complexes are identified in the TVZ including Okataina, Kapenga, Mangakino, Whakamaru, Maroa, and Taupo. Two monogenetic calderas identified include Rotorua, and Reporoa.

Calderas and caldera complexes in TVZ exhibit variable structure due to differing roles of downsag, and regional tectonic influence and overprint. TVZ 'calderas' are strongly controlled by regional structure, with Okataina, Kapenga, Rotorua, and Taupo exhibiting caldera scarps, embayments, and basins parallel to the regional fault trend; presumed to be synchronous with caldera collapse.

2.3 Reporoa Caldera

Reporoa Caldera is situated in the northern part of the Taupo-Reporoa Basin (Fig1.1) and along the eastern margin of central TVZ. Modriniak and Studt (1959) interpreted this basin as a fault-angle depression between the Taupo fault belt and Kaingaroa Fault, and Nairn (1973) mapped scalloped margins around the northern side of the depression. Later, Nairn et al (1994) reinterpreted the northern part of the basin as a caldera and the source of the Kaingaroa Ignimbrite, based on the presence of proximal lag breccias, drillhole data, structural and geophysical evidence.

The Reporoa Caldera is 10 km wide and its boundary is well expressed along its northern and eastern margins (Fig 2.2). The southern margin of the caldera was inferred by Nairn et al (1994) to lie near the Deer Hill rhyolite dome. Nairn et al (1994) also interpret two rhyolite domes (Kairuru and Pukekahu) as intracaldera rhyolites possibly extruded on an inner caldera ring fault. Details of gravity, geothermal activity and seismic interpretation are given in Nairn et al (1994).

The surficial morphology of Reporoa Caldera (Fig 2.2, 2.3) is dominated by a scalloped margin along the northern end of the structure which resembles classic collapse scarps formed by surficial rotational slumping of an inferred ring fracture scarp (e.g. Lipman 1984; submitted). The western margin of the caldera is poorly defined due to the proximity of the Taupo fault belt, but broadly constrains an elliptical caldera which is open at the southern end, with its maximum diameter trending N-S.

Figure 2.2a Eastern margin of Reporoa Caldera illustrating scalloped margins.

Figure 2.2b Scalloped northern Reporoa Caldera margin, on the southern side of Trig 8566 rhyolite dome.

The northern and eastern margins are well defined and flanked by NE-trending normal faults, which may play a role in defining the geometry of the caldera.

The internal structure of Reporoa Caldera is obscured by caldera-fill, dominated by a prolonged history of lacustrine sedimentation, and at least two periods of post-collapse intrusion (Wood 1994a). Reporoa basin has been the site of temporary lakes on several occasions in the late Pleistocene and Holocene, including one period following the Oruanui and Taupo ignimbrite eruptions (Healy 1992). Evidence for a pre-0.23 Ma lake in the Reporoa Basin region is outlined in Chapter 3.

Soengkono and Hochstein (1996) identified the presence of reversely magnetised andesite along the northern and eastern edges of the caldera (Fig 2.4), which delineates a northern and eastern structural caldera boundary, a few kilometres in board of the current topographic boundary. Soengkono and Hochstein (1996) suggest the 'Kairuru rhyolite dome massif', a complex of rhyolite domes inferred from magnetic and gravity measurements, whose surface expression is expressed by Kairuru rhyolite dome (Fig 2.3, 2.4), lie within the structural caldera boundary, and extend to the southeast. The rhyolite massif inferred by Soengkono and Hochstein (1996) contrasts with the lineament of surficial and inferred rhyolite domes inferred by Nairn et al (1994), which they interpreted as reflecting extrusion along an intracaldera fault. The 'Kairuru rhyolite massif' is interpreted by Soengkono and Hochstein (1996) to extend to the southeast, beyond the topographic limits of the caldera outlined by Nairn et al (1994), within an area mapped as Waiora Formation, an assemblage of primary ignimbrites and breccias, sandstones and mudstones of lacustrine origin (Lloyd 1972).

The lacustrine nature of the Waiora Formation in this area is consistent with a complex pre- (and possibly syn-) Kaingaroa Ignimbrite paleotopography. Further work is required on the Waiora Formation to delineate primary units, and constrain geological events at ca.220-230ka. The 'Kairuru rhyolite massif' is interpeted as post-caldera rhyolites infilling complex pre-Kaingaroa topography.

Reporoa Caldera is flanked on its western side by the Taupo fault belt (Paeroa Fault) and on its eastern margin by the Kaingaroa Fault, the eastern boundary of the TVZ. The relationship between caldera collapse and faults whose orientations parallel the regional

trend is considered important, and it seems likely that regional structures control caldera collapse, and deposition of resultant ignimbrites.

Recent arcuate fault traces indicate post-caldera formation faulting.

Seismic evidence presented by Stagpoole (1994) suggest the Kaingaroa Plateau consists of 650 m of ignimbrites sitting on 'greywacke' basement (Fig 2.5), whereas over 1200 m of ignimbrites have been drilled to the west in the Waiotapu drill holes. Numerous units present in TVZ are inferred not to be represented underneath the Kaingaroa Plateau, including the Paeroa Range ignimbrites and Waiotapu Ignimbrite. This suggests the Kaingaroa Fault has been a fundamental structure in controlling ignimbrite distribution.

The Kaingaroa Plateau represents a portion of the sub-volcanic basement that has subsided relative to the main 1000-1700 m high axial ranges to the east (or the ranges have been uplifted relative to the plateau), but which has not been involved in the active rifting and extension in the TVZ itself (Healy 1992). The Kaingaroa Fault forms the western boundary of the plateau and is inferred on the basis of seismic, gravity and resistivity surveys to be a complex stepped structure (Risk et al. 1994; Stagpoole 1994). The complex nature of the structure may be (partly?) attributed to complex structural collapse on regional faults outside the topographic caldera boundary. Interpretation is difficult, because of the mantling effect of post-collapse sedimentation. South of Reporoa Caldera the Kaingaroa Fault offsets the 0.7 Ma Rolles Peak andesite and 0.32 Ma Rangitaiki Ignimbrite which suggest the structure has been fundamental in TVZ evolution for at least 0.7 Ma. Further work on southern Reporoa basin is in progress on the nature of the fault, and delineation of other (inferred) calderas (Bibby pers comm 1996).

In the Reporoa Caldera area a complex pre-Kaingaroa topography can be inferred from ignimbrite distribution. The early Kaingaroa flows were restricted to proximal areas, coincidental with a "hole" in the pre-caldera stratigraphy where Rangitaki Ignimbrite is missing, and the unusual presence of arroyos and "dry valleys" with deep and narrow gorges (Fig 2.3). This structure is inferred to represent a pre-Kaingaroa basin. Nairn et al (1994) suggested this structure may represent evidence of an early caldera boundary.

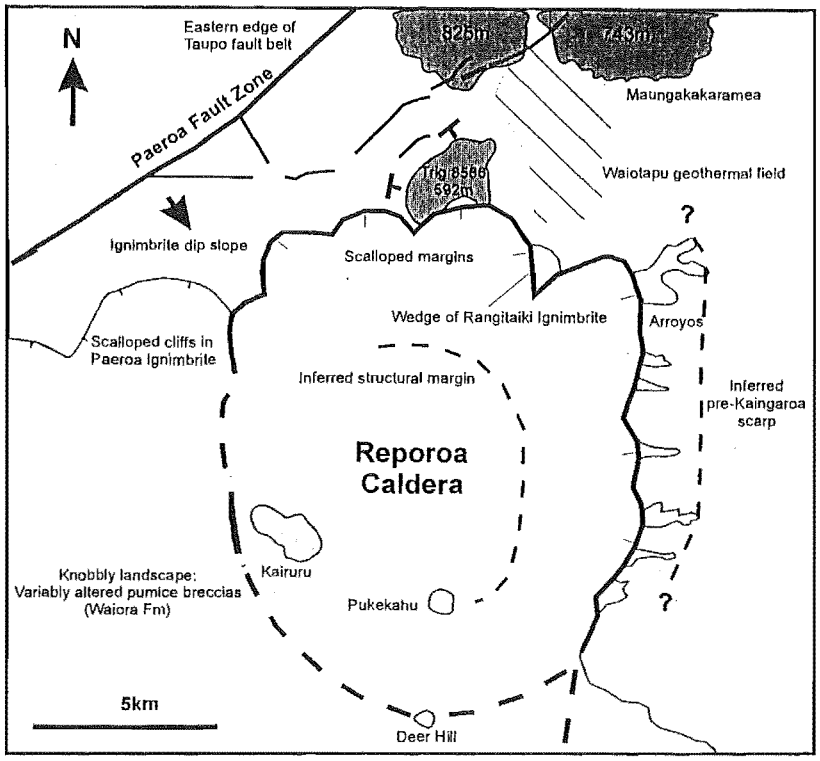

Figure 2.3 Geomorphology and structure of Reporoa Caldera, illustrating regional and caldera collapse-related structures including the Paeroa Fault, topographic caldera margins, post-caldera rhyolites. Geomorphology and structure from Pain and Pullar (1975), Hedenquist (1983), Nairn et al (1994), and this study.

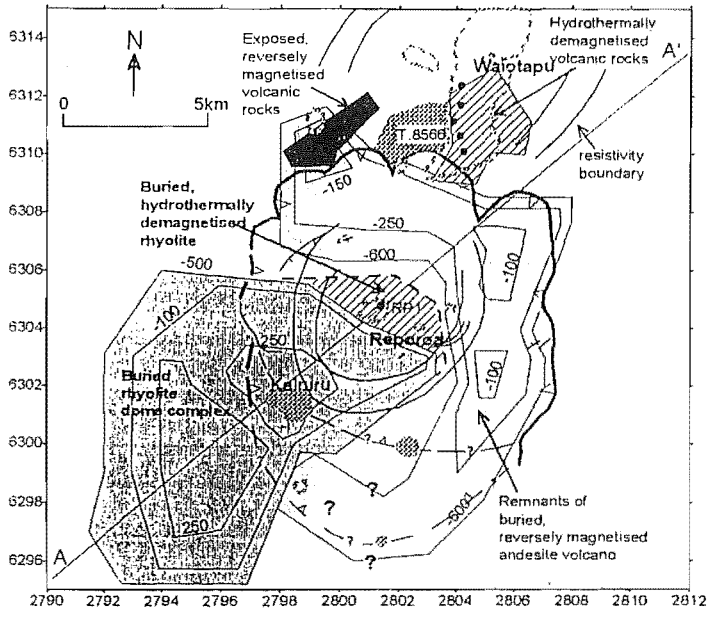

Figure 2.4 Inferences of caldera morphology, and distribution of pre-caldera andesite and post-caldera rhyolite domes based on magnetic and gravity data (from Soengkono and Hochstein 1996).

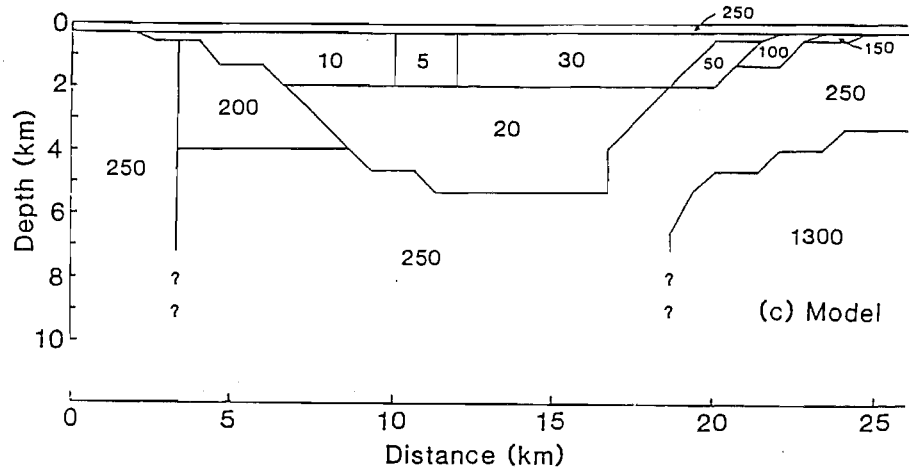

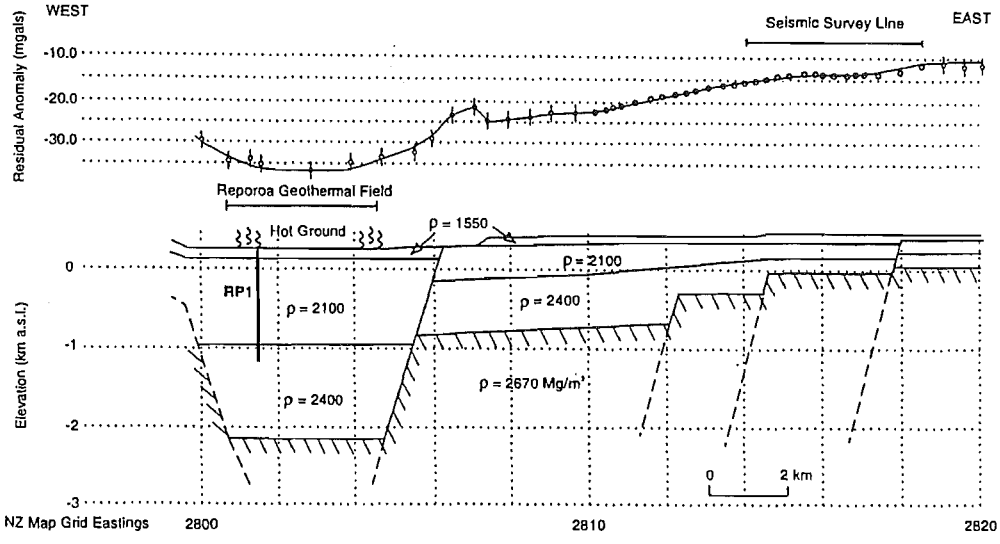

Depth (m)	Velocity	Stratigraphy
	200m/s	Pumice
3.5		
	1350m/s	Kaingaroa Ignimbrite
30		
	1100m/s	Tuff
70		
	1700m/s	Matahina Ignimbrite
110		
	1100m/s	Tuff
130		
	2200m/s	Rangitaiki Ignimbrite
190		
	1300m/s	Tuff
280		
	3250m/s	Older Ignimbrites
650		
	>4800m/s	Greywacke basement

Figure 2.5 Gravity and seismic interpretations of Reporoa Caldera area, and adjacent eastern margin of TVZ, illustrating complex stepped margin in Torlesse basement (Stagpoole 1994).

To the west the Paeroa Fault marks the eastern boundary of the Taupo fault belt (Tfb). Martin (1961) showed that Kaingaroa Ignimbrite occurs on both sides of the Paeroa Fault, which indicates that faulting has occurred since its emplacement about 0.23 Ma. In places the Paeroa Fault scarp is stepped and forms a composite topographic feature, suggesting multiple sites of displacement. Nairn and Hull (1986) also found increasing vertical separation of Taupo Pumice (186 AD), Rotoma Ash (9000 BP) and Earthquake Flat Breccia (60 ka) across the Paeroa Fault. This indicates that faulting was still active 1800 years ago.

Geothermal systems often occur in or adjacent to calderas in central TVZ. Wood (1994a, 1995) attributes this to a genetic relationship between caldera formation and geothermal plumes, although Wood notes that the genetic link between caldera-forming magmatism and geothermal systems cannot be directly proven. Bibby et al (1995) attribute the presence of geothermal systems adjacent to calderas as random coincidence.

The Reporoa region contains numerous geothermal fields, some of which are suspected of being related and connected at depth. Waiotapu and Reporoa are the two most prominent fields within or adjacent to Reporoa Caldera. Waiotapu and Reporoa geothermal fields occur at the south end of a 25 km long belt of low resistivity that includes Waimangu geothermal field. Debate continues about the location of plumes, and relationship at depth (Hunt and Glover 1994).

A wide range of thermal discharges occur in the 18km^2 Waiotapu field (New Zealand's largest geothermal field) including large hydrothermal eruption craters (Champagne pool), sinter terraces, mud volcanoes, geysers (Lady Knox Geyser), and fumaroles. Thermal features at Reporoa are less well known but include hot pools, mud pools and steaming ground (Hunt et al. 1994).

2.4 Basement

Mesozoic low grade metasediments, and interbedded volcanics are presumed to form the basement beneath TVZ, comprising two quartzofeldspathic terranes, the Waipapa and Torlesse terranes. Along the western margins of TVZ gravity models suggest the

'greywacke' should occur between 500-1000 m (Rogan 1982) or 1300 m RL (Modriniak and Studt 1959; Reduced Level = metres relative to sea level). At Ohaaki, to the south of Reporoa Caldera 'Torlesse-like greywacke' basement was drilled to -1977 m (Browne 1971). Torlesse 'greywacke' forms the ranges to the east of TVZ, and isolated inliers on the Kaingaroa Plateau, while Waipapa 'greywacke' outcrops extensively to the west of TVZ. The terrane boundary is inferred to lie within TVZ. Torlesse "greywacke', and its higher-grade equivalent is inferred to form the basement of the Kaingaroa Plateau-Reporoa region; a detailed discussion is given in Wood (1994a) and Mortimer (1995). To the west of TVZ are outcrops of Tertiary sediments, unconformably overlying 'greywacke' basement.

Ewart and Cole (1967) and Brown et al (submitted) report numerous granitoid lithics from large-scale ignimbrites in the TVZ. They infer that the blocks represent samples of the subvolcanic equivalents of TVZ rhyolites. South of Reporoa Caldera an altered quartz-diorite was drilled in the Ngatamariki drill hole, thought to represent the subvolcanic equivalents of coeval andesitic volcanics.

The evolution of volcanism in the Reporoa region can be divided into three stages: (1) pre-caldera stage; (2) 0.23 Ma caldera-forming Kaingaroa Ignimbrite eruption; (3) post-caldera stage. Pre- and post-caldera stages include a varied history of volcanism within the region and a history of ignimbrite eruptions from other source vents that have influenced the geology and geomorphology.

Stratigraphy of units in the Reporoa region is defined from three composite sections; Paeroa Scarp, Waiotapu drill hole and Kaingaroa Plateau. In addition aspects of circumcaldera geology are outlined below (Fig 2.6, Table 2.1):

2.5 Pre caldera stage

2.5.1 Pre-Waiotapu units

Akatarewa/ Rahopaka

Beneath Waiotapu Ignimbrite and Unit X along the Ngapouri Ridge is an ignimbrite termed Akatarewa A (Grindley et al. 1994) or Rahopaka (Wood 1994a), which has been

correlated with Akatarewa ignimbrites within the Waiotapu and Te Kopia drill holes. The unit is partially-welded, crystal-rich with plagioclase, orthopyroxene, quartz, augite, orthopyroxene and inferred pseudomorphed hornblende phenocrysts (Wood 1994a; pers comm 1994).

To the north of Reporoa Caldera is a unit mapped as Akatarewa A by Grindley et al (1994) (Waikite Valley Rd; U16/012151). Here this unit is a lithic-rich 'sandy-black' partially-welded ignimbrite with a 'salt and pepper' appearance, which locally resembles the Kaingaroa Ignimbrite and units within the Waiora Formation. The outcrop is hydrothermally altered from the adjacent Waikite geothermal field but consists of interbedded ignimbrites and lithic breccia. The presence of lithic breccias, interbedded ignimbrites and abundant gas segregation structures suggest the exposure is a proximal lag facies, indicating a nearby source. Insufficient outcrop precludes more detailed assessment. The units mapped as Akatarewa by Grindley seem to represent a group of different ignimbrites. Further work is required on these ignimbrites which is beyond the scope of this thesis.

Unit X

Unit X is a collection of poorly-exposed reversely magnetised pumiceous sediments that outcrop at the base of the Ngapouri Ridge and in the Waiotapu drill hole beneath Waiotapu Ignimbrite (Grindley et al. 1994). A common clast type in the sediments is the ignimbrite described above as Akatarewa A ignimbrite.

2.5.2 Ngakoro Andesite

Sheet C in the Waiotapu drill holes is overlain by Ngakoro Andesite (Hedenquist 1983). The andesite thickens to the south (Wood 1994a, Grindley et al. 1994). It consists of vesicular andesite lavas, with 30% plagioclase (An_{60-36}) orthopyroxene and augite phenocrysts (Hedenquist 1983). Nairn et al (1994) and Wood (1994a) correlate the Ngakoro Andesite with andesite lithics in the Kaingaroa Ignimbrite, and suggest the southward thinning of the unit is consistent with the distal flows of a buried andesite volcano in the Reporoa region.

Paeroa Range/ Ngapouri area (Grindley et al 1994; Wood 1994a; Keall 1988; Healy et al 1964; Martin 1961; this study)	**Waiotapu Geothermal area** (Grindley et al. 1994; Hedenquist 1983; Steiner 1963)	**Kaingaroa Plateau** (Nairn et al 1994; Wood 1994a, Brown 1994, Nairn 1989; Healy et al 1964; this study)
Kaingaroa Ignimbrite		Kaingaroa Ignimbrite
Onuku	Onuku	Onuku
Matahina Ignimbrite		Matahina/Wheao ignimbrites Bonisch
Paeroa Ignimbrite Te Weta Ignimbrite Te Kopia Ignimbrite	Rangitaiki Ignimbrite Unit W (?)	Rangitaiki Ignimbrite Quartz-biotite Ignimbrite Te Whaiti Ignimbrite
Waiotapu Ignimbrite	Waiotapu Ignimbrite	Unknown purple lenticulite
Unit X Akatarewa A/ Unit A/ Rahopaka	Unit X Ignimbrite A (Akatarewa) Unit Y_2 Unit Y_1 Ignimbrite B (Akatarewa) Unit Z Ngakoro Andesite Ignimbrite C	Unidentified ignimbrites?
Unidentified ignimbrites?		
Torlesse basement?		Gravels Torlesse basement

Table 2.1. Stratigraphy of the Reporoa region.

Soengkono and Hochstein (1996) inferred the distribution of reversely magnetised andesite within the Reporoa region using gravity and magnetics, thereby delineating the precaldera distribution of the andesites.

2.5.3 Waiotapu Ignimbrite

Waiotapu Ignimbrite is a distinctive densely-welded crystal-poor (9-17 vol%) grey-purple lenticulite thought to have erupted from the Kapenga area (Ritchie 1996). The ignimbrite contains abundant plagioclase phenocrysts with subordinate orthopyroxene, Fe/Ti oxides and hornblende. The ignimbrite outcrops along the Ngapouri Ridge northwest of Reporoa Caldera, and is up to 360m thick in the Waiotapu drill holes (Wood 1994a).

2.5.4 Northern boundary purple lenticulite

A purple-grey lenticulite was drilled to >84 m thickness in the Northern Boundary drill hole to the north end of the Reporoa area (Nairn 1984). The ignimbrite contains devitrified crystal-rich pumice lenticules, large amphibole phenocrysts and a moderate quartz and plagioclase content, with subordinate orthopyroxene and Fe/Ti oxides (Wood pers comm 1996). The unit underlies the Whakamaru-group ignimbrites and does not correlate with known outcropping ignimbrites.

2.5.5 Whakamaru-group ignimbrites

The term "Whakamaru-group" ignimbrites was coined by Wilson et al (1986) and continued by Brown (1994) to describe a series of geochemically, petrographically and age related caldera-forming ignimbrites. The ignimbrites are characterised by their crystal-rich quartz- and locally sanidine-bearing nature. The group consists of nine ignimbrites; Whakamaru, Manunui, Rangitaiki, Te Whaiti, Paeroa, Te Weta, Te Kopia, Quartz-biotite, and Wairakei (considered intracaldera), which range in age from 0.31 Ma to 0.36 Ma (Houghton et al.1995). Wilson et al (1986) and Brown (1994) propose a single caldera (Fig 2.2) in the Maroa-Taupo area as their source, though Nairn (1989) has suggested that the quartz-biotite ignimbrite has a grain-size consistent with a

Okataina source, and Keall (1988) suggests the source for the Te Weta and Te Kopia ignimbrites is to the north of the proposed caldera.

In the Reporoa region, Rangitaiki Ignimbrite is present along much of the Kaingaroa Plateau, underlying the Matahina and Kaingaroa Ignimbrites, and outcrops in the northeastern corner of Reporoa Caldera (Fig 2.6). A Whakamaru-group ignimbrite has also been identified in the Waiotapu drill hole, but the drill core is hydrothermally altered and petrographic correlation inconclusive (Wood 1994a). The Te Weta, Te Kopia and Paeroa ignimbrites, collectively termed Paeroa Range ignimbrites (Keall 1988), are present insitu only in the Paeroa Fault scarp and Paeroa Block west of Reporoa Caldera.

Paeroa Range ignimbrites

Paeroa Ignimbrite

The Paeroa Ignimbrite consists of at least three cooling units (up to 140 m thick) of crystal-rich quartz-bearing moderately-welded ignimbrite, which form the highest part of the Paeroa Scarp. The unit varies in colour from grey to pink, is rich in two-pyroxene andesite lithics, and has been locally mapped as two units (e.g. Grindley et al.1994). Keall (1988) describes the Paeroa Ignimbrite as containing 30-35% phenocrysts of plagioclase, quartz, sanidine, biotite, orthopyroxene, hornblende and Fe/Ti oxides.

Te Weta Ignimbrite

Te Weta Ignimbrite is a 110 m-240 m thick partially-welded ignimbrite that forms the middle unit along the Paeroa Fault scarp. The Te Weta Ignimbrite is a variable unit that consists of interbedded accretionary-lapilli bearing tephras, surges, lithic breccias and buff-light grey vapour-phase altered crystal- (25-35 vol%) and lithic-rich ignimbrite. Plagioclase is the dominant phenocryst phase with subordinate quartz, sanidine, biotite, orthopyroxene, hornblende, augite and Fe/Ti oxides (Keall 1988).

Te Kopia Ignimbrite

The Te Kopia Ignimbrite outcrops along the base of the Paeroa Fault scarp, is present to 360 m in the OK6 drill hole, and has also been identified in the Broadlands and Ngatamariki drill holes (Bignall et al. 1996). The Te Kopia Ignimbrite consists of three members; a lower member is a dark-grey densely-welded lithic-poor crystal-rich (35-

40%) ignimbrite with a plagioclase, quartz, orthopyroxene, hornblende, biotite, augite and Fe/Ti oxide assemblage (Keall 1988). The middle member is a lag breccia with andesite lithics up to 3 m, whereas the upper member is grey to buff densely-welded crystal-rich ignimbrite (Keall 1988).

2.5.6 Waiora Formation

The Waiora Formation consists of over 700 m thickness of pumiceous sandstones, mudstones, non-welded ignimbrites and tephras of poorly constrained age (330-230 ka). Recent Ar/Ar dating on the intercalated Kakuki Basalt constrains part of the sequence to ca. 220 ka (Tanaka et al. 1995; Houghton pers comm 1996). Keall (1988) describes a few examples as crystal-poor composed of plagioclase, orthopyroxene and rare quartz, hornblende and Fe/Ti oxides. Many of the exposures of the Waiora Formation are hydrothermally altered.

2.5.7 Matahina Ignimbrite

The 0.28 Ma (Houghton et al. 1995) Matahina Ignimbrite is the youngest pre-Kaingaroa ignimbrite in the Reporoa region. Matahina Ignimbrite is poorly exposed on both sides of Reporoa Caldera (Fig 2.6), overlying Rangitaiki Ignimbrite. The Matahina Ignimbrite is crystal-moderate with a plagioclase, orthopyroxene, hornblende, quartz and Fe/Ti oxide assemblage (Bailey and Carr 1994), and diagnostic vesiculated bladed obsidian lithics.

2.5.8 Onuku Pyroclastics

Miscellaneous non-welded fall, flow and reworked pyroclastics outcrop between Matahina and Kaingaroa ignimbrites and were termed Onuku Pyroclastics by Nairn (1989). Nairn (1989) inferred an Okataina source for the eruptives and Wood (1994a) suggests pumice breccias in the Waiotapu drill holes may be a correlative. Manning (1995) correlated one of the tephra units with the Kapenga-sourced Chimp Ignimbrite.

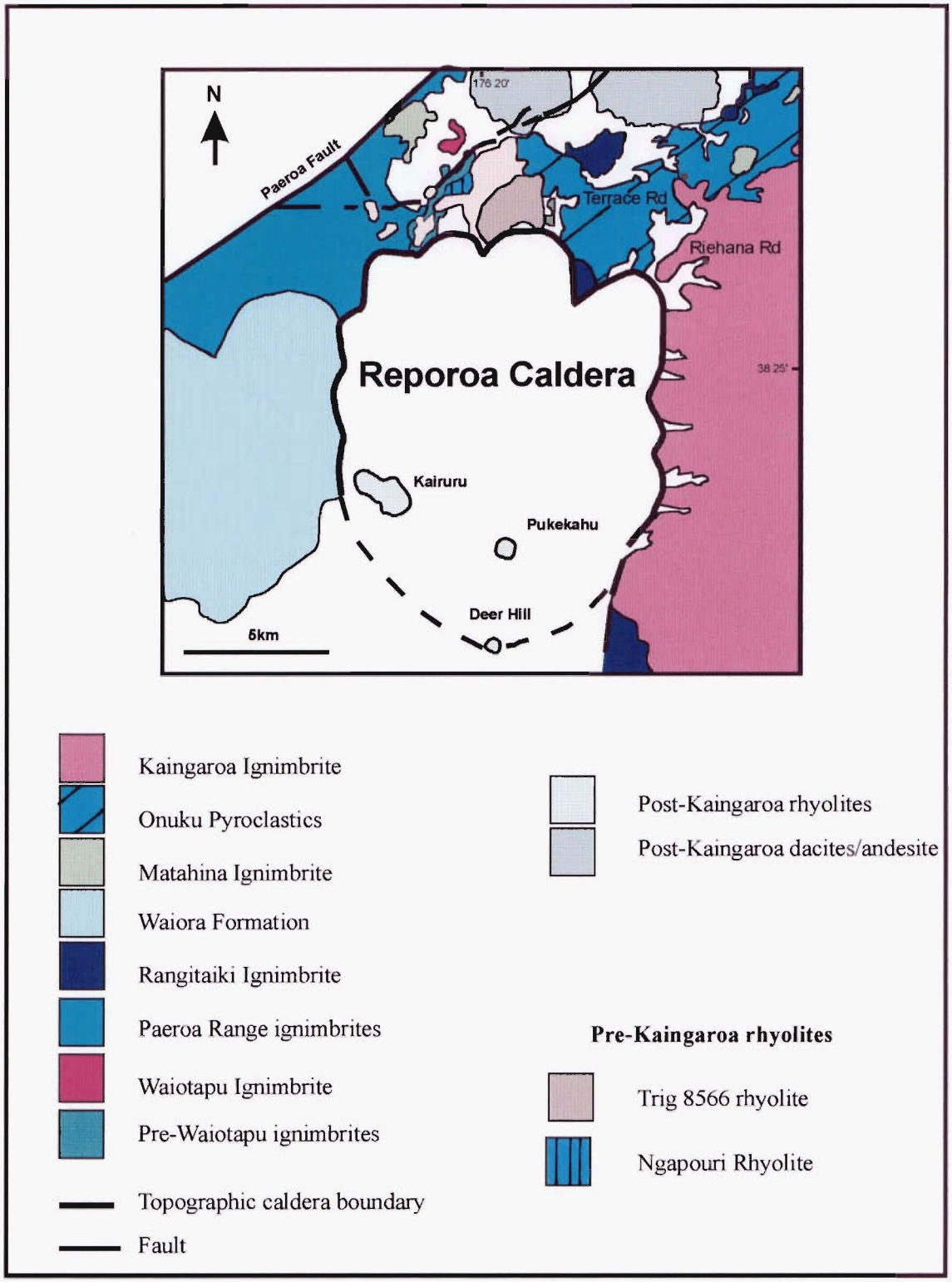

Figure 2.6 Map of pre-caldera geology. Terrace Rd locality is the location of Terrace Rd Basalt, and Riehana Rd locality refers to locality of Onuku Pyroclastics and Chimp Ignimbrite quoted in text. Geology from Nairn (1973, 1989); Nairn et al (1994); Wood (1994a); this study.

2.5.9 Terrace Rd Basalt

Interbedded within the Onuku Pyroclastics at U16/087115 is a thin well-stratified lithic-rich phreatomagmatic and reworked basaltic ash (Nairn 1981).Vesicular black scoria have a basaltic-andesite composition (53% SiO_2; Nairn 1981). A single scoria was sampled (KA439) which contains plagioclase (An_{75-70}) and skeletal augite phenocrysts and rare olivine microphenocrysts, rimmed by augite. Nairn (1981) also noted xenocrystic quartz. The groundmass consists of acicular plagioclase (An_{55}), rare augite laths and magnetite euhedra, and brown glass. Groundmass texture varies from pilotaxitic to intersertal.

2.5.10 Pre-caldera rhyolites

Pre-caldera rhyolites in the Reporoa region are limited to Trig 8566 and Ngapouri Rhyolite. Trig 8566 rhyolite dome (592 m) is cut by the Reporoa Caldera boundary, with a prominent arcuate and steep collapse scarp. The southern margin of Trig 8566 rhyolite domes was interpreted by Nairn et al (1994) as the northern topographic boundary of Reporoa Caldera, formed during caldera collapse and eruption of the Kaingaroa Ignimbrite. Ewart (1968) reports the Trig 8566 rhyolite as a crystal-moderate rhyolite with 27% phenocrysts of plagioclase, quartz, orthopyroxene, hornblende, biotite and Fe/Ti oxides.

Ngapouri Rhyolite is exposed along the Ngapouri Ridge (e.g. U16/005114), surrounded by normally magnetised 0.7 Ma Waiotapu Ignimbrite. Ngapouri Rhyolite is a purple-grey, flow-banded, reversely magnetised crystal-poor high-silica rhyolite (74.8-75.2% SiO_2) with up to 10% phenocrysts of plagioclase (An_{35}), orthopyroxene, quartz, and Fe/Ti oxide (Ritchie 1996).

Precursor rhyolite have been identified as lithics within the Kaingaroa Ignimbrite, but do not outcrop in the Reporoa region (see Chapter 5), indicating all pre-caldera domes were destroyed by caldera-collapse.

2.6 Kaingaroa Ignimbrite eruption

The Kaingaroa Ignimbrite include early airfall, surge, flows and the main caldera-forming ignimbrites. The onset of the Kaingaroa Ignimbrite eruption is defined as all the deposits lying above the paleosol on the Onuku Pyroclastics. Details of this event are described in Chapters 3,4,5,6,7, and 9. The eruption can be divided into two phases: single vent and ring vent phases which can be identified through stratigraphic relations (Chapter 3,4), lithic componentry (Chapter 5), and whole pumice chemistry (Chapter 7).

2.7 Post-caldera stage

2.7.1 Post-caldera rhyolites

Three rhyolite domes outcrop in the northern part of the Reporoa basin. Kairuru and Pukekahu form low-lying flat-topped domes while Deer Hill rhyolite dome lies to the south of Pukekahu, and consists of numerous blocks on a slightly elevated topography. Exposure is poor consisting of isolated outcrops on rolling farmland, and was thus considered insufficient for detailed structural analysis. A study of the domes was undertaken to ascertain field characteristics and petrology, and any relationship to Reporoa Caldera and the Kaingaroa magma system. Mineralogy and geochemistry are outlined in Chapter 7.

Kairuru

Kairuru rhyolite (Fig 2.7) is a pinkish-grey flow-banded devitrified crystal-poor rhyolite with localised irregular flow-layering, presence of obsidian-rich layers, lithophysae, vesicle-rich layers and flow banding on a range of scales.

Ewart (1968) noted the unusual mineralogy of Kairuru rhyolite in his regional synthesis of rhyolite petrography. Ewart pointed out that Kairuru is distinct from other rhyolites in TVZ, exhibiting low crystal-content and a low plagioclase/quartz ratio. Two samples from the dome (KA42, 43) were sampled for thin sectioning and geochemistry. Both samples are crystal-poor (10-11%) with subequal phenocryst proportions of plagioclase (An_{21-20}) and locally embayed quartz, rare orthopyroxene and Fe/Ti oxides, in a

spherulitic to felsitic groundmass. The mineralogy and geochemistry is discussed in Chapter 7, with reference to the Kaingaroa magma system.

A rhyolite dome was penetrated by Reporoa drill hole RP1. Aeromagnetic data (Bromley pers comm; in Wood 1994a) suggests that this rhyolite is part of a large buried dome complex which extends south and west towards the caldera boundary. Soengkono and Hochstein (1996) infer the Kairuru dome to represent the exposure of this dome complex.

Pukekahu

Pukekahu is a weakly flow-layered blue-green coloured rhyolite, which is well exposed along its southwestern margin. A single sample (KA387) was taken for petrographic and geochemical analysis. KA387 contains 2.5% phenocrysts of plagioclase, orthopyroxene, Fe/Ti oxides and hornblende.

Deer Hill

Deer Hill rhyolite dome is weakly flow-layered crystal-poor (6%) quartz-phenocryst free high silica rhyolite (74.5% SiO_2; Brown 1994). A K/Ar age of 216 $\pm$ 19 ka was obtained from Deer Hill (U17/015965; Houghton pers comm 1996), which is consistent with its stratigraphic position post-dating the 0.23 Ma Kaingaroa Ignimbrite.

Oscillatory-zoned plagioclase (andesine) is the dominant phenocryst with subordinate orthopyroxne, augite, and Fe/Ti oxides, in a spherulitic matrix. Euhedral to subhedral plagioclase commonly forms glomeroporphyritic clusters up to 3.5 mm, which contain numerous glass inclusions. The matrix consists of numerous feldspar microlites and microphenocrysts, which locally exhibit swallow tail morphology.

2.7.2 Andesites and dacites

North of Reporoa Caldera are the twin dacite domes of Maungaongaonga and Maungakakaramea (Rainbow Mountain) and eroded andesite cone (?) of Waikokomuka.

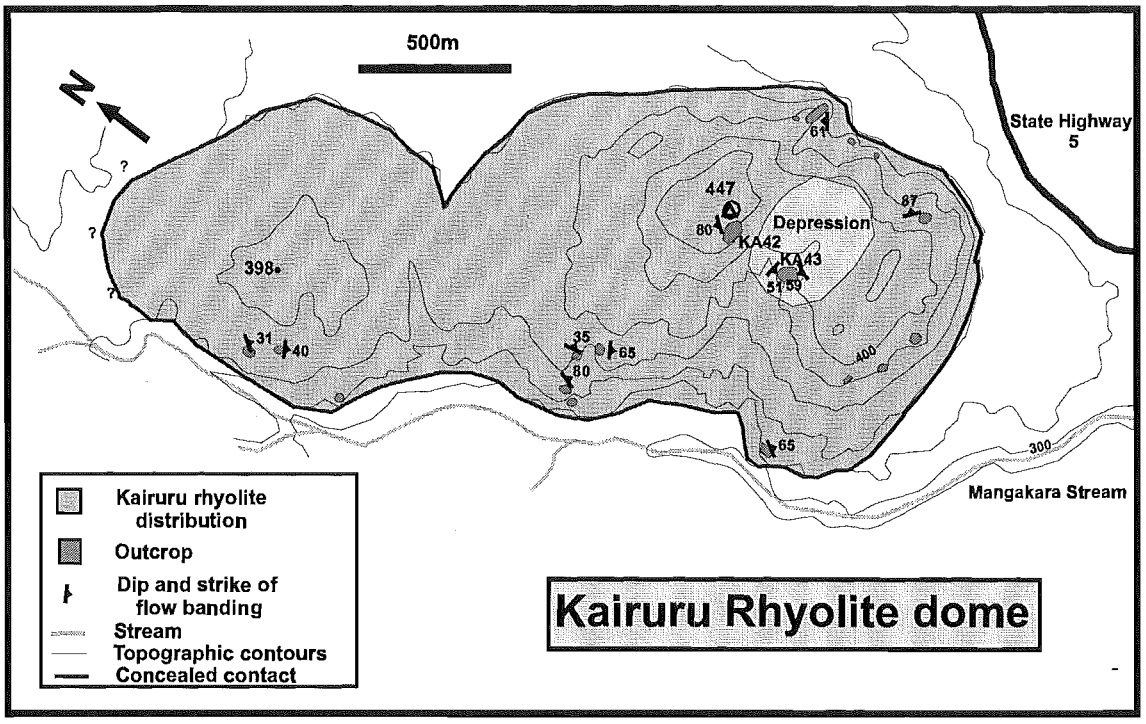

Figure 2.7 Geological map of Kairuru rhyolite dome, illustrating outcrop data, dip and strike of flow banding and sample localities.

Maungaongaonga and Maungakakaramea ('Rainbow Mountain')

Maungongaonga dacite (67.2-67.4% SiO_2; Reid and Cole 1983) which has been dated at 183 $\pm$ 9 ka (K/Ar age; Houghton pers comm 1996) contains plagioclase (oligoclase-andesine; Hedenquist 1983), orthopyoxene, rare augite and magnetite phenocrysts. Maungakakaramea is hydrothermally altered and considered to have a similar composition.

Waikokomuka

The eastern part of the Maungakakaramea dome complex (U16/005051) was noted by Nairn (1981) to be more mafic, and termed Waikokomuka Andesite. The unit is covered in forest and very poorly exposed, but seems to consist of a uniform composition (high Si andesite/dacite; 62% SiO_2, anhydrous; Nairn 1981); Waikokomuka Andesite was inferred to be older than Maungakakaramea, based on greater degree of dissection (Nairn 1981). A single sample (KA440) is a vesicular andesite with phenocrysts of plagioclase, orthopyroxene and augite, in a pilotaxitic to hyalopilitic matrix.

2.7.3 Recent pyroclastics

The Reporoa basin and surrounding region is largely covered by more recent primary and reworked ignimbrites (Earthquake Flat Breccia, Oruanui, and Taupo), and mantled by Okataina and Taupo tephras (Nairn 1973; Pain and Pullar 1975).

CHAPTER THREE

Kaingaroa Ignimbrite:

Eruptive stratigraphy and lithologic variation

3.1 Introduction

This chapter presents field characteristics of the Kaingaroa Ignimbrite. The principal aim of the field work was to examine the variation within the ignimbrite, and establish an internal stratigraphy. A single ignimbrite, named Kaingaroa Ignimbrite, is defined, combining all units previously mapped as Kaingaroa Ignimbrites (kg_0, kg_1, and kg_2) by Nairn et al (1994), and incorporating all units with similar pumice and lithic types, pumice mineralogy and chemistry. It overlies a paleosol developed in basal sections on the Onuku Pyroclastics and consists of a poorly exposed basal tephra unit and three non-welded to welded ignimbrite units. Aspects of depositional facies variation from proximal to medial facies is outlined in Chapter 4.

3.2 Distribution

The Kaingaroa Ignimbrite extends radially 20-30 km from its inferred source at Reporoa Caldera and underlies a 800 km^2 area mainly to the east, southeast and west (Fig 3.1; Map in pocket at back of thesis). The Kaingaroa Ignimbrite is exposed in two main areas: 1) east and southeast of Reporoa Caldera where it forms the capping unit of the Kaingaroa Plateau, extending from Rerewhakaitu to south of Wairapukao, and 2) west of the Paeroa Range, within the Te Weta Block, where it extends from Lake Ohakuri northwards to Waikite Valley (Fig 3.1). Isolated outcrops are also present northwest of Reporoa Caldera as outliers in the Ngapouri area. Kaingaroa Ignimbrite has also been identified in the Reporoa (RP1), Northern Boundary, Broadlands, and Murupara drill holes. North of the caldera no outcrops of Kaingaroa Ignimbrite are known, and the unit does not appear as a lithic type in post-Kaingaroa ignimbrites. Wilson et al (1995b) noted the marked asymmetry in distribution of the Kaingaroa Ignimbrite, in contrast to the symmetrical distribution of the energetically emplaced Taupo Ignimbrite. Wilson et al (1995b) interpreted the asymmetry of ignimbrite distribution as due to eruption from a ring vent (c.f. point source). The Taupo fault belt (Tfb), marked along its eastern

margin by the Paeroa Fault truncates the western margin of Reporoa Caldera (see Chapter 2), and the ignimbrite along this western margin has been strongly downfaulted. The presence of faulted ignimbrite remnants to the west of Reporoa Caldera (this study), and correlation of Kaingaroa Ignimbrite in the Broadlands drill hole (Bignall et al. 1996) highlights a need for caution with inferences based solely on ignimbrite asymmetry and its relationship to caldera dynamics, especially in older poorly-exposed units.

On the Kaingaroa Plateau to the west of Reporoa Caldera the upper unit of the Kaingaroa Ignimbrite terminates in an arcuate erosional scarp (Fig 3.1).

The mapped distribution closely follows that identified from earlier regional mapping (e.g. Healy et al. 1964; Nairn 1981,1989). Exceptions include a sandy-black ignimbrite mapped as Kaingaroa Ignimbrite in the Kawerau-Puhipuhi Basin region by Nairn (1981, 1989). This was found in the present study to contain distinctive lithic types, pumice chemistry and mineralogy which suggest it is a distinct unit. M_L and lithic componentry suggest an Okataina source. The unit has been termed the Kawerau ignimbrite and is discussed further in Chapter 8. A pink-coloured partially-welded lenticulite mapped by Nairn et al (1994) and noted by Wilson et al (1984) in the Flaxy and Wheao dam areas also contains different lithic fragments, crystal contents and pumice chemistry to Kaingaroa Ignimbrite, and is correlated with 0.28 Ma Matahina Ignimbrite. The unit has been termed the Wheao sheet (see Appendix A). Outliers of Kaingaroa Ignimbrite mapped by Healy et al (1964) in the Rangitaiki and Wheao river region were not identified during the course of this study.

There are no known outcrops of distal Kaingaroa Ignimbrite. It is likely flows dominantly travelled east. Remnant exposures and depositional facies suggest that the ignimbrite was strongly topographically controlled and never surmounted the ranges to the east in contrast to the Rangitaiki and Matahina ignimbrites.

3.3 Thickness and volume

The poor exposure of the Kaingaroa Ignimbrite makes any inferences on thickness and volume strongly interpretative. The Kaingaroa Ignimbrite ranges in thickness from

ca.80m in proximal regions to ca.30 m in distal areas (e.g. Murupara drill hole), but thickness determinations are minima, because of erosion and incomplete exposure. The base of the Kaingaroa Ignimbrite is exposed in only two localities at Riehana Rd and Maungahekeke Valley.

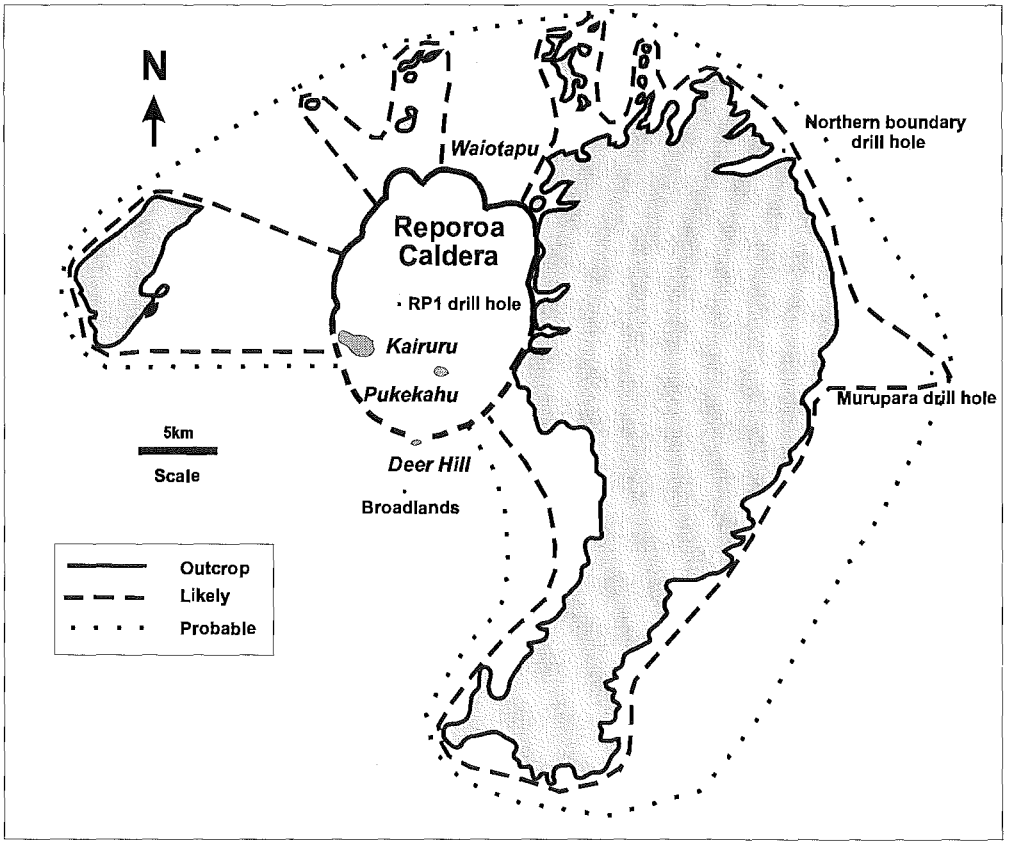

Figure 3.1 Distribution of the Kaingaroa Ignimbrite. Dashed and dotted lines denote likely and probable outcrop based on distribution of depositional facies, welding and thickness variation and presence of Kaingaroa Ignimbrite in drill holes.

The lower ignimbrite unit is present only in proximal regions, perhaps reflecting topographic control on emplacement. The upper and middle ignimbrite units maintain near uniform thickness across most of Kaingaroa Plateau (average thickness= 65 m) reflecting eruption onto flat or slightly undulose paleotopography. Localised thickness variations reflect the infilling of small alluvial valleys, and scouring of the underlying deposits by the pyroclastic flows (this point is discussed further in Chapter 4). A more

rugged topography would have generated more extreme facies variations, and more patchy distribution (e.g. Campanian Ignimbrite; Fisher et al. 1993). Distribution and rare sections of the lower and upper ignimbrite units in the Te Weta block, indicate the Kaingaroa Ignimbrite infilled valleys in the underlying Paeroa Ignimbrite (Lloyd 1972).

Three broad facies of ignimbrite are defined by Wilson (1993a):1) Landscape-mantling or ignimbrite veneer deposits; 2) Landscape-modifying or valley ponded ignimbrite; and 3) Landscape-burying deposits. The relationship between the ignimbrite facies is illustrated in Figure 3.2. The Kaingaroa Ignimbrite comprises predominantly landscape-burying ignimbrite facies. The surface is flat lying and forms the upper surface of the Kaingaroa Plateau, concealing the irregularities in the underlying paleotopography.

A common way of quantifying variation in thickness and area covered by an ignimbrite is by using aspect ratio - the ratio of the average thickness to the diameter of circle enclosing all outcrops. Aspect ratio in ignimbrite varies from high-aspect ratio (HARI; e.g. Valley of Ten Thousand Smokes; 1:135) to low-aspect ratio (LARI; e.g. Taupo Ignimbrite; 1:107000; Wilson 1986). High aspect ratio ignimbrites are thought to be erupted at relatively slow rates, and low-aspect ratio ignimbrites at high rates. Reconstruction of original distribution is critical for estimates of aspect ratio and volume (Streck and Grunder 1995). Figure 3.1 illustrates the distribution and inferred distribution of the Kaingaroa Ignimbrite. Methodology largely follows Streck and Grunder (1995), with divisions of reconstructed distribution divided into three categories, 'outcrop', 'likely', and 'probable'. 'Outcrop' refers to current outcrop of the Kaingaroa Ignimbrite mapped during this study. 'Likely' distribution included lobes needed to connect outliers of the ignimbrite, and 'probable' distribution includes a more reasonable interpretation of lobe emplacement directed towards outliers.

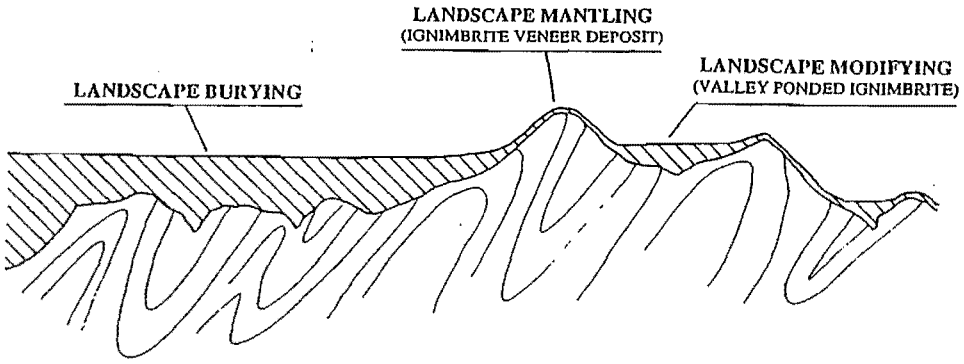

Figure 2.2 Broad ignimbrite facies after Wilson (1993a).

The inferred outflow area estimated from thickness and distribution data ranges from 800 km^2 to 1870 km^2, depending on the extent of inferred distribution. A moderate to high aspect ratio of 1:920 and estimated 'probable' volume of 120 km^3 is estimated from outflow area, and average thicknesses. The volume of associated fall and intracaldera ignimbrite is difficult to estimate. The fall deposits, where exposed, are thick (even at 5 km from the inferred vent area) and complex similar to phreatomagmatic (phreatoplinian) eruptions (C.J.N.Wilson pers comm 1996) such as the 22 ka Oruanui eruption, which is inferred to have erupted >500 km^3 (DRE) of airfall material (Wilson 1994). Nairn (1981) calculated a magmatic volume of 100 km^3 (DRE) for the entire Kaingaroa Ignimbrite based on sparse thickness data, which is consistent with inferred caldera volume (Nairn et al.1994). The average thickness and distribution described in this study suggests a larger volume is likely, especially when fall and intracaldera deposits are taken into account. Due to the large uncertainties in calculating volume, especially in poorly exposed ignimbrites, and the large lateral and vertical variation in density, a magmatic volume of not less than 100 km^3 (DRE) and (depending on the inferred volumes of intracaldera and fall deposits) possibly as high as 200 km^3 (DRE) is inferred, which is thought to be representative of distribution, and thickness data of similar ignimbrites in TVZ.

Individual ignimbrite units display a wide range of aspect ratio and thickness that suggest composite thickness and aspect ratios are meaningless. Paleotopography has

largely controlled thickness variations of individual units, so the lower ignimbrite unit is localised, varies in thickness from 50 m+ in exposures adjacent to Reporoa Caldera to >2 m in more distal exposures, and forms a classical high aspect ratio ignimbrite deposit (ca. 1:670). The middle and upper ignimbrite units vary in thickness from 10 m and ca.8 m to 30 m and 12 m, and are relatively uniform in thickness (notably the upper unit; see below) across the Kaingaroa Plateau. Both middle and upper ignimbrite units, therefore have moderate aspect ratios, related to the low-lying paleotopography they were emplaced onto. Their passive response to the limited topography (and limited facies variation in medial facies; Chapter 4), suggests relatively low velocity of emplacement. Similar moderate to low-aspect ratio ignimbrites have been described by Streck and Grunder (1995; Rattlesnake Tuff) and Schumacher and Mues-Schumacher (1996; Kizilkaya Ignimbrite), and are ascribed to emplacement onto shallow topography rather than high emplacement rate.

3.4 Age and stratigraphic relations

The middle ignimbrite unit of the Kaingaroa Ignimbrite is a regionally distinctive unit due to its 'sandy-black' appearance, and abundance of andesite lithics. Zircon from pumice in the lower sandy black ignimbrite in Puhipuhi Basin was dated by fission track method (Kohn in Nairn 1989) at 240 ka. This unit has now been correlated with the newly recognised Kawerau ignimbrite (Chapter 8). Grindley et al (1994) dated the 'sandy black' unit at Coates Rd at 0.22 $\pm$ 0.04 Ma age (zircon fission track), and Houghton et al (1995) using Ar/Ar dated the 'sandy black' ignimbrite unit at the Old Waiotapu Rd type locality at 0.23 $\pm$ 0.03 Ma. Black et al (1996) dated the Kaingaroa Ignimbrite at 0.31 $\pm$ 0.01 Ma by the isothermal plateau fission track method. The ages determined by Houghton et al (1995) and Grindley et al (1994) are consistent with stratigraphic position and other dated TVZ ignimbrites, and are adopted in this thesis.

On the eastern Kaingaroa Plateau the Kaingaroa Ignimbrite overlies the quartz-poor 0.28 Ma Matahina Ignimbrite, and crystal-rich quartzose Rangitaiki and Te Whaiti ignimbrites (Whakamaru-group ignimbrites). Locally between the Matahina and Kaingaroa Ignimbrite are variable thicknesses of Onuku Pyroclastics, a well bedded sequence of unconsolidated obsidian-lithic-bearing rhyolitic pyroclastics (Nairn 1989) containing several paleosols including one particularly well developed directly beneath the Kaingaroa Ignimbrite basal tephras.

To the west of Reporoa Caldera the Kaingaroa Ignimbrite overlies the Matahina Ignimbrite and 0.33 ± 10 Ma (Ar/Ar age; Houghton et al. 1995) Paeroa Ignimbrite. The Kaingaroa Ignimbrite is locally overlain by Earthquake Flat Breccia and numerous recent tephras.

3.5 Lithology

The Kaingaroa Ignimbrite is characterised by its crystal-poor nature, containing 0.1-3.5 % crystals of plagioclase + orthopyroxene + Fe/Ti oxides ± hornblende, with very rare augite and xenocrystic biotite and quartz in whole rock specimens (see Chapter 7). Petrographic evidence indicates that there is little change in crystal content or mineralogy throughout the entire thickness. The abundance of plagioclase-pyroxene-phyric andesite lithics is unique in ignimbrites of similar stratigraphic position. It is mineralogically distinct from underlying ignimbrites. The underlying Matahina Ignimbrite contains 4-16% phenocrysts of plagioclase, quartz, hornblende, orthopyroxene, Fe/Ti oxides, and rare augite (Bailey and Carr 1994), and Whakamaru-group ignimbrites are coarse-grained quartz-rich ignimbrites, with quartz, plagioclase, sanidine, biotite, hornblende, and Fe/Ti oxides (Brown 1994).

3.6 Internal stratigraphy

The internal stratigraphy of the Kaingaroa Ignimbrite is based on field appearance, lithic abundances and proportions, and pumice chemistry. Details of lithic componentry, and chemistry are presented in Chapters 5 and 7 respectively.

3.6.1 Basal tephras (BT)

Intercalated surge, fall and flow tephras are present at the base of the Kaingaroa Ignimbrite at four localities adjacent to the eastern margin of Reporoa Caldera. The type locality is defined at a roadside outcrop on Riehana Rd. The limited and sporadic exposure makes correlation from locality to locality difficult and means there is insufficient thickness and M_L data to create isopachs and isopleths. Tephras have not been observed intercalated with the middle and upper ignimbrite units, and are interpreted as preceeding the ignimbrite-forming eruption phase.

At Riehana Rd (Fig 3.3) the basal tephras consist of numerous intercalated fine-grained accretionary lapilli-bearing and pumiceous lapilli-bearing tephras which sit on a carbonaceous paleosol developed on Onuku Pyroclastics, thought to represent the initial phreatoplinian tephras, surges and flows of the Kaingaroa Ignimbrite eruption (Nairn et al. 1994). A similar sequence is observed in the adjacent Maungahekeke Valley.

The basal tephras consist of eight recognisable units: unit A, B, C, D, E, F, G, and H (Fig 3.3), many of which have localised distribution and can not be correlated from locality to locality.

The base of the tephra sequence consists of a variable thickness basal pale-grey to white cross-bedded accretionary lapilli-bearing deposit (unit A), which thickens to 70 cm in shallow valleys in the underlying Onuku Pyroclastics. Bedding is marked by pumice concentration zones which are locally distinct and planar but commonly cross bedded, and pinch and swell independent of topography. Erosional scours to low angle truncations of bedding are common. The juvenile fragments range from rounded commonly 'woody' white crystal-poor pumice (up to 28 mm) to dense black obsidian (up to 38mm). Rare rhyolitic lithics are generally less than 25 mm in diameter. The stratified nature, thickening into valleys and locally scoured basal contact suggest the unit was laterally emplaced by a low particle concentration volcanic density current or surge. The presence of 'woody' pumice with variable vesicularities, and accretionary lapilli indicate a degree of water:magma interaction.

Overlying the basal surge is >5 m of topography-mantling intercalated, variably white, grey, red or yellow fine-grained ash and coarser relatively well sorted pumiceous lapilli-bearing ash (unit B). Juvenile fragments are predominantly white to yellow variably vesicular pumice and dense black to colourless conchoidally fractured angular obsidian or vitrophyric ignimbrite. Pumice fragments range in size from sub mm to 8 cm in a coarse obsidian and pumice-rich bed. Lithic fragments are predominantly rhyolite and a distinctive welded pink 'Matahina-like' ignimbrite. Accretionary lapilli up to 20 mm are locally abundant. Individual beds are commonly finely stratified, contain abundant accretionary lapilli, and localised iron-stained horizons.

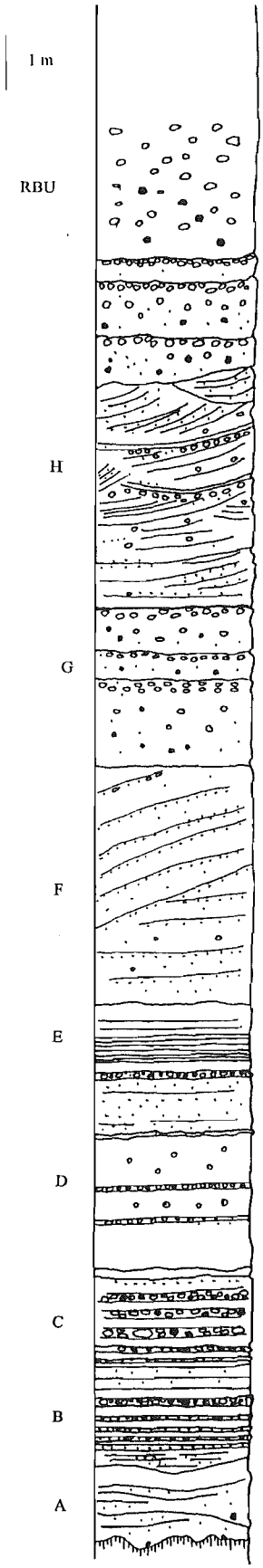

Figure 3.3. Stratigraphic log of basal tephras and Reporoa Boundary Unit at Riehana Rd.

The high content of accretionary lapilli, grainsize, fine-grained nature and topography mantling occurrence suggest the tephra deposits are phreatomagmatic fall deposits. Variable thicknesses and inferred dispersal suggest many of the units may have been phreatoplinian in size. The coarser interbedded tephras contain abundant lithics and large angular pumices, and are relatively well sorted and broadly 'plinian' in style. A phreatomagmatic origin is inferred to represent bulk-interaction between magma and a shallow lake within the Reporoa region. The eruption began with a phreatomagmatic style and continued until water supply was exhausted, when eruptions became magmatic. Similar alternations in style were reported by Self (1983) for Oruanui eruptive products, and were attributed to differing mixing ratios of water and magma. The intercalation of deposits of plinian style and finer grained phreatoplinian style is attributed to variable magma-water interaction. The lack of exposure prevents detailed assessment of changing vent patterns, as has been documented during other large scale phreatoplinian eruptions (e.g. Smith and Houghton 1996).

Charcoal fragments (up to 4 cm) are sparse, and limited to the basal surge. This may be because of limited vegetation or the phreatoplinian nature of the eruption meant that vegetation may not always have been carbonised and hence would have rotted away, as advocated by Wilson et al (1988) for the Oruanui eruption.
Overlying the phreatoplinian tephras is unit C, a planar stratified 75 cm thick coarse pumiceous lapilli and obsidian block bed. Pumice up to 80 mm and obsidian fragments up to 38 mm are angular and similar to underlying units A and B.

Unit D is marked at the base by a thin (9 cm) yellow weakly stratified fine-grained ash, similar to unit B, which passes up into a 1 m thick weakly stratified accretionary lapilli-rich fine grained ash with diffuse pumiceous lapilli up to 20 mm and obsidian lithic layers, of probable fall origin. Unit E superficially resembles unit B, but is marked by an iron-stained horizon at the base passing up into variably pink, grey or yellow interbedded fine-grained ashes and pumiceous lapilli and obsidian-rich layers. As with unit B, accretionary lapilli are common, and a similar fall origin is inferred.

Unit F consists of >2 m thick cross stratified pumiceous lapilli and fine-grained ash with rare accretionary lapilli. There is a localised basal erosive scoured contact into unit E. Unit F resembles unit A and is presumed to have a similar surge origin.

Unit G typically contains at least three reverse graded yellow pumiceous lapilli poorly sorted ashes, which resemble the overlying Reporoa Boundary Unit (RBU). Pumiceous lapilli (up to 50 mm) are concentrated in upper concentration zones, and moderate number of lithics up to 30 mm are disseminated throughout the unit. Individual packets vary in thickness from 30 cm to 60 cm, but the presence of reverse grading, fine grained basal layers and poor sorting indicate deposition from high particle concentration flows, in contrast with the flanking surge deposits. Individual reverse graded packets are interpreted as distinct flow units.

Unit H resembles unit F surge deposits, with up to 4 m thickness of cross stratified pumiceous lapilli and fine grained ash. Individual flow units (up to 60 cm thick) are recognised by reverse grading of pumice, basal and upper fine-grained ash layers, and localised weakly developed basal lithic concentration zones. Unit H marks the incoming of variable ignimbrite and andesite lithics up to 25 mm in diameter. Pumice is generally rounded in contrast to underlying fall deposits and locally is up to 41 mm in diameter. Pumice type is similar to underlying tephras.

The overlying RBU consists of numerous well defined flow units marked by reverse grading of pumice and upper pumice concentration zones. The basal contact is erosive and scours into unit H surges. Evidence of flow units is poorly defined further up sequence.

At Plateau Rd the base of the tephra sequence is not exposed, but over 10 m of interbedded variably coloured pink, yellow, and grey accretionary-lapilli-bearing fine-grained ash and pumiceous lapilli and obsidian lithic beds similar to unit B are present, overlain by a 70 cm thick cross stratified pumiceous lapilli and obsidian lithic similar to surges observed at Riehana Rd and Maungahekeke Valley. The sequence is overlain by a 2 m thick yellow-grey pyroclastic flow unit, with obsidian and no andesite lithics suggesting the flow is a correlative of flow deposits in the upper parts of the Basal Tephra sequence (c.f. RBU). Overlying this pyroclastic flow deposit is Old Waiotapu Rd unit (OWR; see below). No RBU is present at this locality. A notable feature of all the basal tephra units at Plateau Rd is the fine grain size, with M_P and M_L rarely exceed 10 mm, thus indicating the distal nature of this outcrop.

Dense components in the basal tephras are dominated by black/red obsidian or vitrophyric ignimbrite-like rhyolite, which are interpreted as dense juvenile components of the Kaingaroa magma system. The obsidian pyroclasts are commonly subrounded, and exhibit breadcrusted surfaces, with rare vesicular interiors. The mineralogy and chemistry of the pyroclasts is similar to that of the Kaingaroa pumices (Chapter 7).

The basal tephras are divided into two packages of units defined by the incoming of yellow pumice-poor lithic-rich(er) surge and flow deposits which become more numerous towards the top of the succession. The absence of interbedded paleosols suggest all units represent part of a single eruption with no significant hiatus. Juvenile products consisted of a single grey/white pumice and obsidian, while lithics are generally rhyolite and ignimbrite. Unit G marks the incoming of a variety of lithic types including ignimbrites, rhyolites and andesite, generally fumarolically altered. The change in lithic content from juvenile obsidian, rhyolites and rare ignimbrites to a diversity of ignimbrites and andesites marks a fundamental change in eruption dynamics (Chapters 5 and 9).

3.6.2 Reporoa Boundary unit (RBU)

Nairn (1973, 1981) identified a lower non-welded ignimbrite member at Old Waiotapu Rd, at least 50 m thickness and gradational into the overlying 'sandy-black' unit. Nairn termed this unit kg_0. The unit is renamed here 'Reporoa Boundary unit' (RBU) because of its localised distribution adjacent to Reporoa Caldera (Fig 3.4a), near Reporoa Boundary Rd. The type section is defined as a roadside exposure on Old Waiotapu Rd (U16/ 085108).

RBU is gradational upwards into the similar-looking transition zone and lag breccia, and at its base the presence of interbedded surges and falls, mark the transition from the underlying basal tephras. The base of RBU is defined as the last appearance of surges and fall deposits.

RBU is a rhyolitic pumice-poor pyroclastic flow deposit, which consists of several flow units, defined by localised pumice concentration zones, and is everywhere non-welded, although densely-welded RBU-like ignimbrite lithics (Chapter 5 and 7) present in the

overlying lag breccia suggest a densely welded proximal facies was destroyed during caldera-collapse. Similar disruption and incorporation of fragments of early flow deposits in later flows of the same eruption has been documented by numerous workers e.g. Rosi et al (1996).

The unit is very poorly exposed, confined to valleys eroded headward into the eastern rim of Reporoa Caldera, and rare tentatively identified deposits in the Northern Boundary drill hole (Nairn 1984). This localised distribution adjacent to the scarp suggests the pyroclastic flows were strongly topographically controlled, coincendent with the undulating Rangitaiki and Onuku surface in this area, and the possible basinal structure inferred from the presence of dry valleys (Chapter 2). Thickness varies from ca. 50 m in proximal regions to 19m at Northern Boundary Rd.

Pumice of the Reporoa Boundary Unit is virtually identical in composition to that of the underlying basal tephras and consists predominantly of a single white/yellow/pink pumice type, locally up to 81 mm in length, but commonly 3-5 cm.

Lithics (predominantly andesite and ignimbrite; Chapter 5) are rare and commonly less than 5 cm. Large Rangitaiki ignimbrite-like lithics (up to 51 mm) are present at Maungahekeke Valley, and may represent incorporated or accidental lithics from the underlying Rangitaiki Ignimbrite. Lithic fragment lithotypes are consistent with a dominantly vent-derived source (see Chapter 5). RBU is locally fumarolically altered where overlain by lag breccia, which gives the unit a red or pink appearance. Basal exposures contain disseminated accretionary lapilli, and ubiquitously altered rhyolite and ignimbrite lithics similar to underlying basal tephras. The RBU matrix consists of glass shards, crystals, and lithic and pumice clasts. Pumice contain conspicuous biotite within vesicles of presumed vapour-phase origin. No internal stratigraphy is recognisable, preventing correlation from site to site. Graphic logs illustrating variation within RBU are illustrated in Fig 3.4a, and grainsize variations are illustrated in Fig 3.4b.

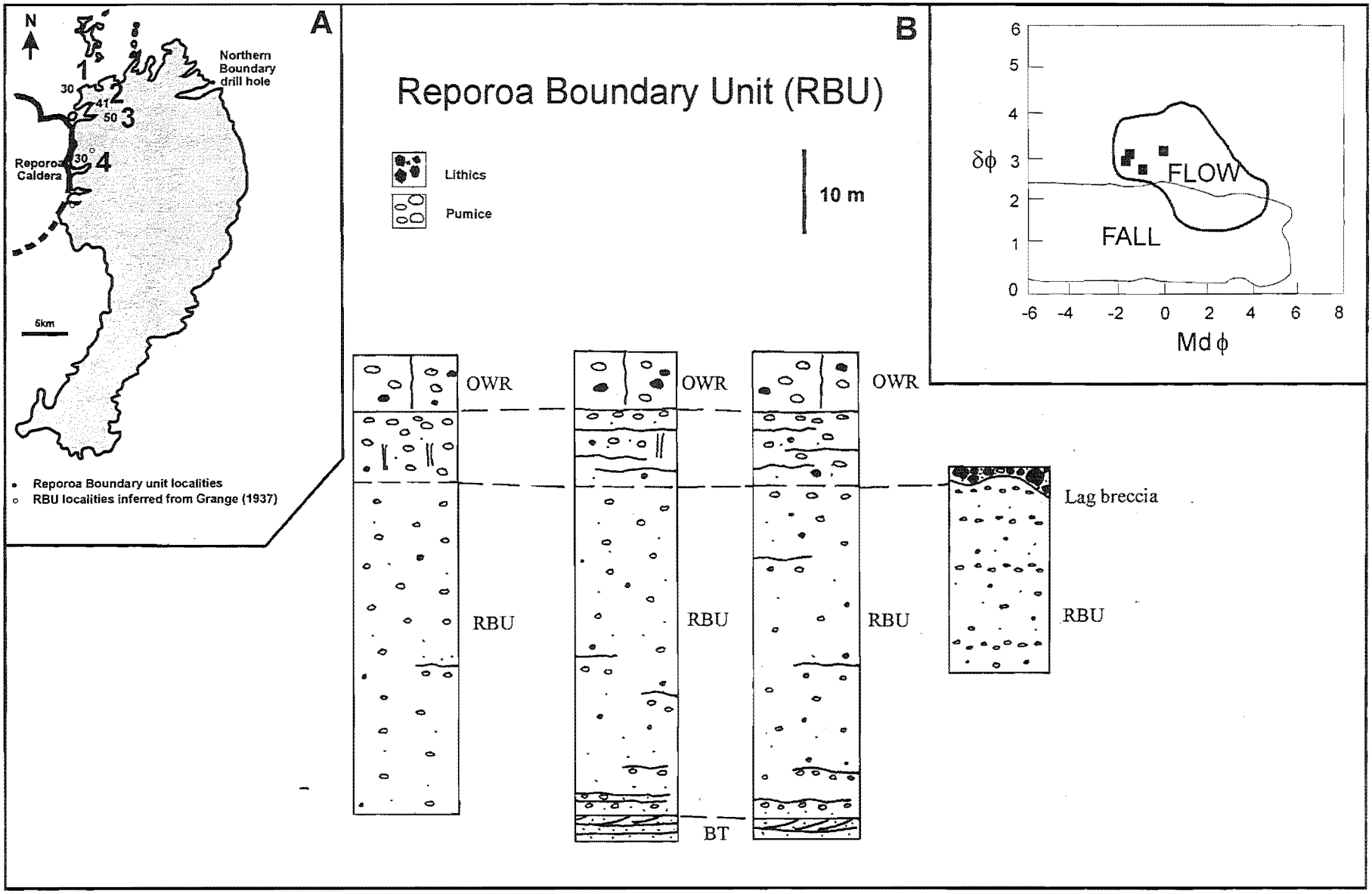

Figure 3.4 Stratigraphic logs of the Reporoa Boundary Unit (RBU), maximum lithic distribution, and granulometric variation.

M_L and M_P and lithic content suggest a poorly defined vent location in the northern part of Reporoa Caldera (Fig 3.4). The vent site is inferred to be similar in location to the underlying basal tephras. Limited exposure prevents assessment of vent migration or accurate vent location during basal tephra and RBU eruption.

Cessation of eruption of RBU was evidently brought about by the sudden inception of caldera collapse, and transition to climactic or ring vent phase.

3.6.3 Lag breccia and transition zone

In proximal localities the transition from RBU to the overlying OWR unit (see below) is marked by up to 45m+ of lithic breccia. The lithic breccia is compositionally zoned from a RBU-like matrix to OWR-like matrix, is locally interbedded with ignimbrite, and contains abundant gas segregation structures which suggest a co-ignimbrite lag breccia origin. The lag breccia unit fines rapidly from the topographic caldera margin, and is present as lithic-rich ignimbrites at sections 2-3 km from the caldera. At these localities the underlying RBU grades into OWR. At some localities the transition is marked by flow unit boundaries, whereas at Old Waiotapu Rd the transition is within a flow unit. The interval between RBU and OWR *senso stricto* in medial localities is termed the transition zone. This is recognised in the field by the incoming of abundant lithic types, variable pumice chemistry, and a colour transition from yellow (typical of underlying RBU) to black (typical of overlying OWR). Aspects of the proximal stratigraphic interval marking the transition from RBU and OWR are outlined in detail in Chapter 4.

3.6.4 Old Waiotapu Road unit (OWR)

Martin (1961) describe this unit (formerly termed kg_1; Healy et al. 1964; Nairn 1989) as a quartz-poor lightly welded dark grey to black pumice tuff containing light grey pumice fragments. Martin defined the type section as along Old Waiotapu Rd (U16/085108).

OWR is a pumice- and lithic-rich pyroclastic flow deposit, extensively exposed adjacent to Reporoa Caldera, and in medial sections in river valleys cut into the Kaingaroa Plateau. The unit is a prominent cliff-forming unit along the Kaingaroa Scarp and

valleys eroded headward into it, but is very poorly exposed away from proximal areas due to its partially-welded nature. The presence of OWR in Murupara drill holes suggests distribution is similar to the upper ignimbrite unit.

The OWR unit is a classical 'sandy black' ignimbrite with distinctive grey, highly vesicular (< 70 % vesicles) black and grey-black mingled pumices locally up to 30 cm in length set in a black/brown/grey commonly vitric matrix . A 'sandy-black' ignimbrite is herein defined as a pyroclastic flow deposit which is vitric, <1/16 mm fines poor, dark grey and generally pumice-rich. Rare yellow ('RBU-like' pumices)-grey mingled pumices are present at some localities. Plagioclase-phyric andesite lithics are abundant, with a variety of subordinate plutonic, andesitic, and ignimbritic lithic types. Lithic types are similar to the lag breccia and transition zone (see Chapter 5), except in medial-distal areas (e.g. 'Kaingaroa') where the lithic assemblage is dominated in basal sections by incorporated or accidental rounded greywacke lithics (Chapter 5). OWR matrix consists of brown and grey T and Y shaped glass shards. Welded ignimbrite specimens all exhibit 'classical' vitroclastic texture (Fig 3.5a; Cas and Wright 1987, Fig 3.27, pg 52). The predominance of brown-coloured shards suggests the brown/black pumice is dominant (c.f. grey) but preferentially fragmented during transport and deposition.

The unit is partially-welded in proximal regions, with a notable dark grey colouration and distinctive pseudo-eutaxitic texture formed by collapse of highly vesicular black pumices. In medial regions the unit is densely welded (Fig 3.5b), and resembles classical grey lenticulites with a prominent eutaxitic texture.

The interval between OWR and WIU (Webb ignimbrite unit; see below) is only exposed at a single locality (V17/222003) where it is a brown-coloured non-welded ignimbrite with intermediate characteristics. The presence of similar pumice and lithic types (notably unusual gabbroic and metavolcanic lithics) suggests the WIU is part of the same eruption, and not a separate ignimbrite.

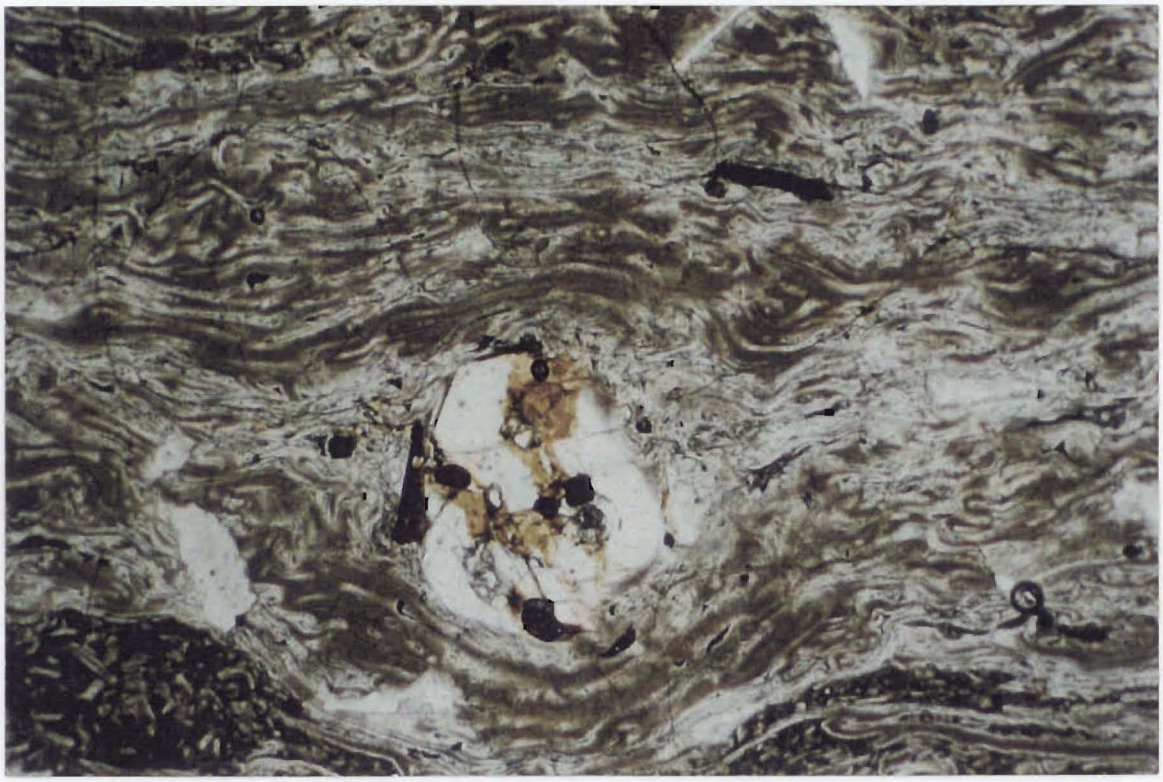

Figure 3.5a. Vitroclastic texture in Old Waiotapu Rd unit.

Figure 3.5b. Densely welded OWR near Kaingaroa township.

3.6.5 Webb ignimbrite unit (WIU)

Martin (1961) distinguished the upper Kaingaroa Ignimbrite units as a fine-grained pinkish, welded vitric tuff containing sparse relict pumice lenticules, and suggested a type locality at the quarry on Webb Rd, northeast of Kaingaroa township.

The WIU unit is poorly exposed north-west and west of Reporoa Caldera commonly present as pink-grey vapour-phase indurated ignimbrite blocks on rolling hillsides (e.g. Waikite Valley Rd; Fig 3.6a). East of Reporoa Caldera WIU outcrops discontinuously as the capping unit atop hills (Fig 3.6b) on the Kaingaroa Plateau (e.g. Putunoa), as semi-continuous outcrop along river valleys cut in the Kaingaroa Plateau surface (e.g. Main Gully Rd), as roadside exposures (Fig 3.6c) or aggregate quarries (Figs 3.6d; 3.7) .

The WIU is the plateau-capping unit, poorly exposed near source possibly due to ease of erosion of partially welded proximal facies. WIU is a pumice or fiamme-poor commonly densely welded lenticulite with a well developed eutaxitic texture. The unit is commonly devitrified, and vapour phase altered in its upper part. WIU forms a strong cliff forming unit in Rerewhakaaitu area, and in valleys cut into the Kaingaroa Plateau. Vapour-phase altered ignimbrite is commonly cavernous weathered reflecting the friable nature of the altered pumices. Locally in the Rerewhakaitu region vapour-phase altered ignimbrite is indurated, forming a distinctive bench beneath the upper welded zone.

The unit exhibits limited variation in thickness and little facies variation, probably due to emplacement onto limited paleotopography. WIU is slightly thicker and more densely-welded in medial sections, and exhibits a prominent hackly fracture in medial densely-welded zones.

The ignimbrite shows variable colours (e.g. white, grey, pink, red, purple and brown) related to degree of welding and vapour-phase alteration. Pumice fragments are rare but of two broad types, a white-grey variety and a highly vesicular silky grey variety. Lithic types are similar to the underlying OWR unit, including distinctive gabbroic and metavolcanic lithics. The presence of these rare lithic lithotypes and sparse M_L data suggest the same source as the underlying OWR unit (Fig 3.8).

Both OWR and WIU exhibit limited circumcaldera variation in contrast to other large scale ignimbrites (e.g. Bishop Tuff; Hildreth 1979). This is interpreted to reflect the near uniform mineralogy and geochemistry (Chapter 7), and eruption, emplacement and depositional processes (Chapter 4).

3.6.6 Intracaldera

Intracaldera Kaingaroa Ignimbrite was described by Nairn et al (1994) in the RP1 geothermal exploration drill hole, drilled to 1337 m depth near Opaheke, and thin sections of RP1 drill core were re-examined during this study. The drill hole consists of 1250m of lacustrine sediments, rhyolitic lavas and possible epiclastic Kaingaroa Ignimbrite. The drill hole encountered a welded tuff at 1250 m depth, and bottomed out at 1337 m in the same unit (Table 3.1). Hydrothermal alteration within the cores is intense, and the majority of primary phenocrysts are replaced.

The welded tuff is lithic-rich and has a moderate crystal content composed of plagioclase and chlorite pseudomorphs (after pyroxene?) and subordinate quartz. Rare spherulitic masses resemble relic pumice, while the matrix contains remnant vitroclastic texture with abundant lithics of altered andesite and crystal-rich quartzose ignimbrites.

The altered andesites contain altered plagioclase and chlorite pseudomorphs (after pyroxene ?) set in a matrix of plagioclase microlites. The crystal-rich ignimbrite lithic mineralogy is distinctive of the Whakamaru-group ignimbrites.

The welded tuff is distinct from Kaingaroa outflow sheets in terms of crystal proportions, but the presence of andesite lithics, a plagioclase and pyroxene dominated mineral assemblage, inferred stratigraphic position (i.e. younger than 0.36-0.3 Ma Whakamaru-group ignimbrites which are present as a lithic type) and structural position (within inferred source caldera) suggest a correlation with the Kaingaroa Ignimbrite. Lipman (1984) reports that the majority of intracaldera ignimbrites are markedly different to their outflow correlatives, notably in crystal and lithic abundance, and this is considered to be the situation at Reporoa. The 87 m of drilled welded tuff is therefore interpreted as intracaldera Kaingaroa Ignimbrite, and provides a minimum intracaldera thickness.

Figure 3.6a. Vapour-phase altered WIU outcrops on the crests of hills in the Waikite Valley area.

Figure 3.6b. Welded WIU outcrop in recently deforested terrain in the Northern Boundary Rd area.

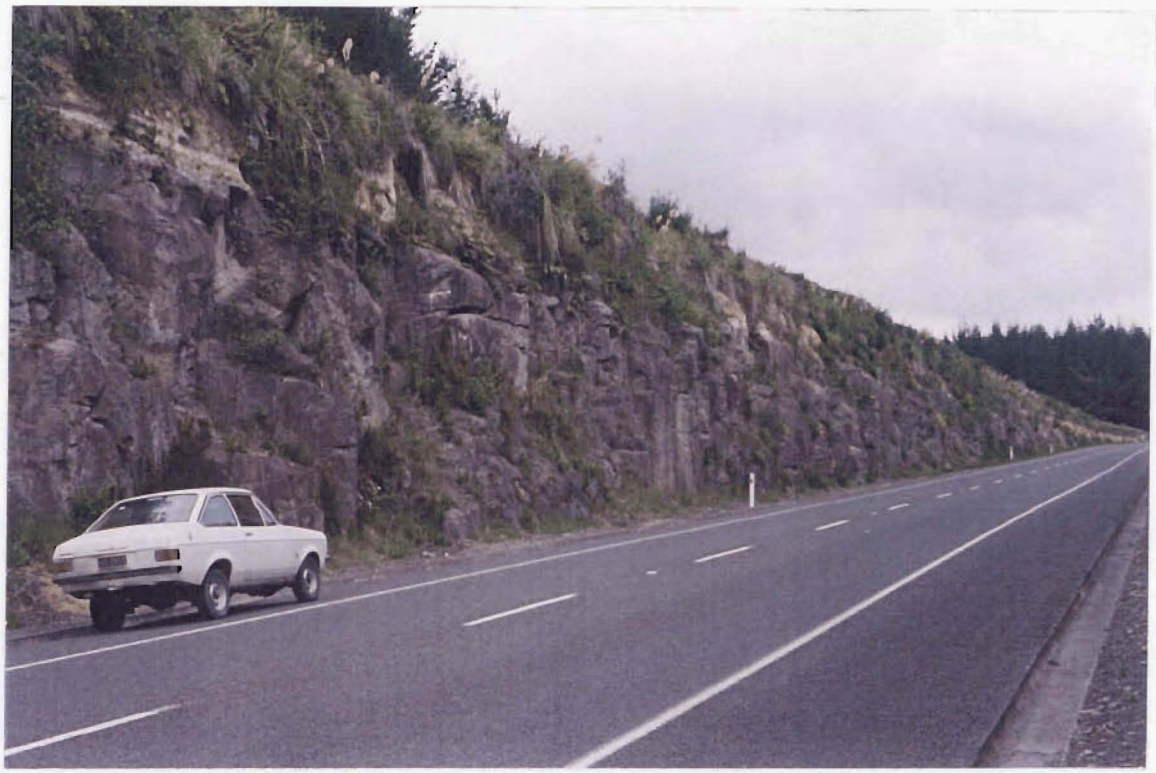

Figure 3.6c Densely welded WIU along State highway 38 on the road to Murupara.

Figure 3.6d Webb quarry, the type section of the upper unit of the Kaingaroa Ignimbrite (WIU).

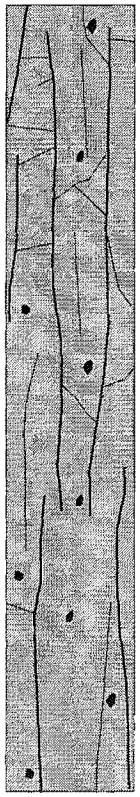

Pink/grey vapour-phase altered and devitrified, welded ignimbrite.
Very rare small highly flattened lenticles (aspect ratio ca. 8:1).
Strongly jointed and lithic-poor. Prominent axiolitic texture.

Buff densely-welded, strongly devitrified ignimbrite.
Small highly flattened lenticles (Aspect ratio 8:1).
Strongly jointed and lithic-poor.
Prominent spherulitic pumice and oxidised lithics.

Brown-grey partially-welded/compacted devitrified ignimbrite.
Rare small lenticles, weakly jointed,
moderate lithic content with prominent oxidised andesite lithics.
Trace contents of xenocrystic biotite.

Webb quarry: WIU

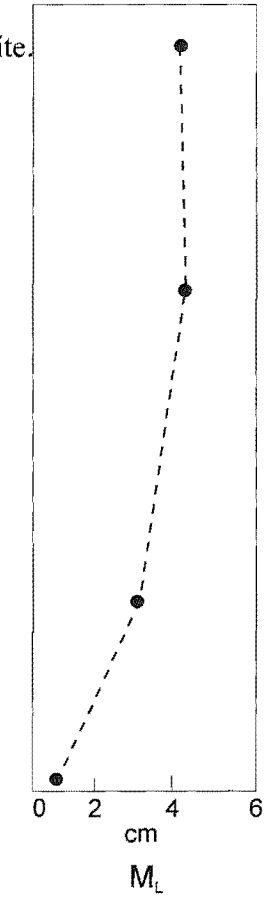

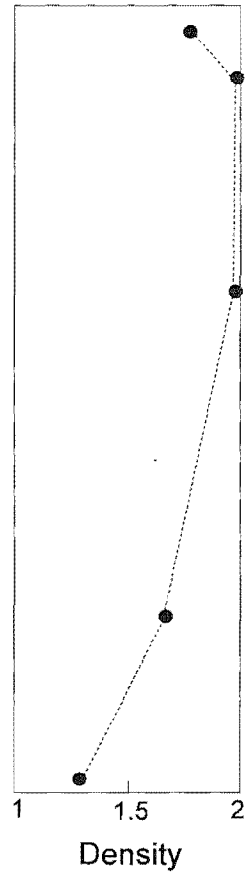

Figure 3.7. Graphic log of a section through WIU at Webb quarry. Entire section is 12m thick.

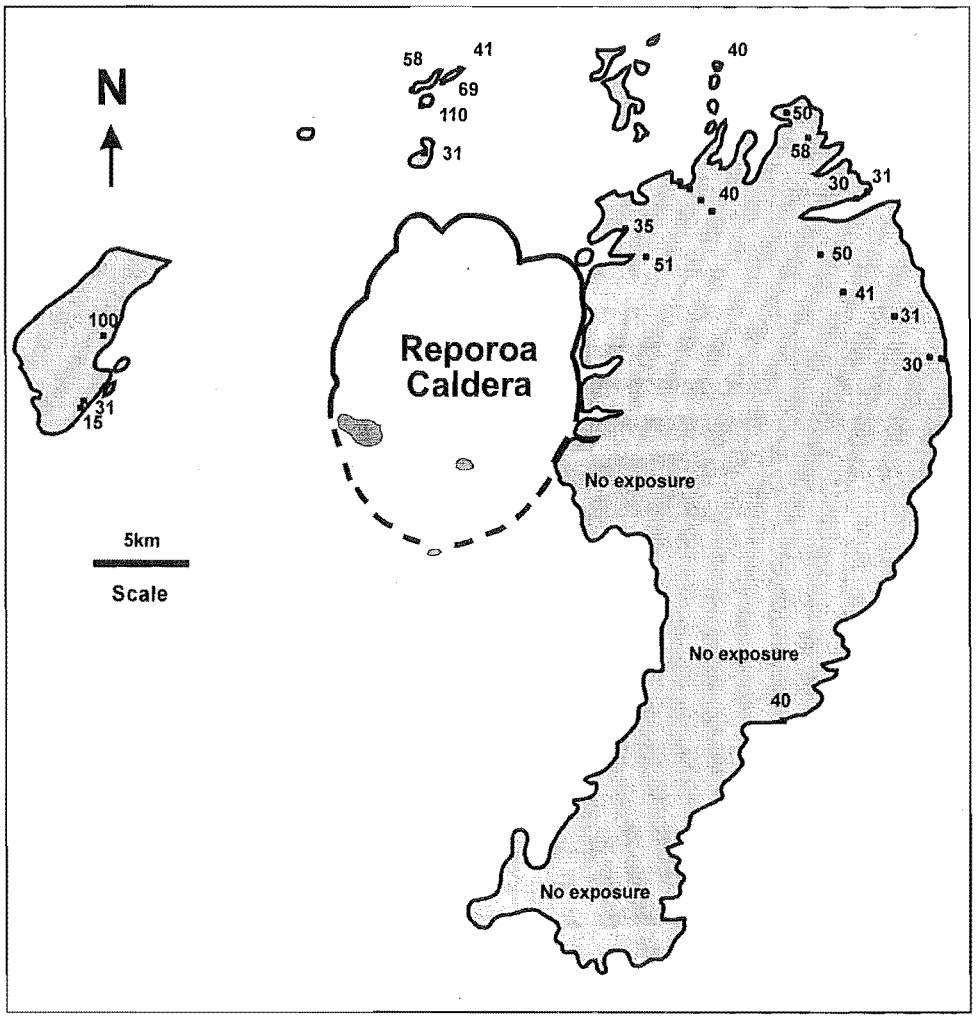

Figure 3.8. Maxium lithic distribution within the Webb ignimbrite unit (WIU). Despite the scarity of exposures and data a central Reporoa source is suggested.

Depth (m)	Thickness (m)	Unit
0-305	305	Recent tephra, alluvium and lacustrine sediments
305-645	340	Quartz-phyric rhyolite lava
645-835	190	Quartz-free rhyolite lavas and breccias
835-1250	415	Tuffaceous sediments and primary pyroclastics (possibly reworked Kaingaroa Ignimbrite)
1250-1337	>87	Intracaldera Kaingaroa Ignimbrite

Table 3.1 RP1 stratigraphy. Depth is below ground level which is 298 m above sea level (adapted from Nairn et al. 1994).

3.6.7 Kaingaroa Ignimbrite in other drill holes

Healy (unpublished letter on IGNS files, 1961) recorded up to 30m of a sandy-black ignimbrite overlying Whakamaru-group ignimbrites in drill holes 19 and 22 south of Murupara. The ignimbrite is dark-grey compacted to non-welded ignimbrite which correlates with the OWR unit. In addition over 10 m of compacted to partially-welded OWR-like ignimbrite was noted in drill hole 24, and 30 m in drill hole 20. M_L is ca. 50 mm.

Nairn (1984) reported 50m of welded Kaingaroa Ignimbrite in the Northern Boundary drill holes (V16/191115; V16/196112), underlain by basal tephras and Onuku Pyroclastics. Drill cores were not accessible during the course of this study.

Bignall et al (1996) correlates hydrothermally altered rocks in Broadlands drill core, with the Kaingaroa Ignimbrite. Present day distribution is consistent with original flows travelling south towards the current site of Broadlands geothermal field. C.P. Wood (pers comm 1994) suggests that the Kaingaroa Ignimbrite should be present in other drill cores, possibly unidentified within the Waiora Formation.

Wood (1994b) correlated the Kaingaroa Ignimbrite with a fine-grained sandy-black ignimbrite present within the Waiora Formation in the Wairakei drill holes. A single

sample was analysed by EPMA (CORE; Appendix D). The presence of zoned Fe-rich orthopyroxenes (En_{45-29}), and obsidian and greywacke lithics suggest the ignimbrite is distinct from the Kaingaroa and other known 'sandy-black' ignimbrites (e.g. Rangatira Point, Pokai, Kawerau).

3.6.8 Reworked deposits

Reworked Kaingaroa Ignimbrite deposits and channels cut into the upper surface of the Kaingaroa Ignimbrite are locally preserved in the Rerewhakaitu region. Two distinct facies are preserved. Facies A contains abundant slab-shaped clasts of vapour-phase altered Kaingaroa Ignimbrite, derived from the underlying WIU. The welded ignimbrite clasts are imbricated, within a decimetre to 50 cm planar to cross bedded sequence. The base of the deposit is commonly scoured (gullies up to 1m in depth) into the underlying indurated vapour-phase altered Kaingaroa Ignimbrite (WIU). Facies A is attributed to small localised alluvial channel deposits, with scour and fill and channel lag deposits.

Facies B consists of massive to sparsely bedded poorly sorted gravel composed of slab-shaped clasts of WIU. Facies B is interpreted to be of debris flow origin. The base of the Kaingaroa Ignimbrite is not exposed in the Rerewhakaitu area, but the abundance of spectacular gas segregation pipes (e.g. State Highway 38; V17/124110) suggests the Kaingaroa pyroclastic flows may have been water saturated at the time of emplacement, and reflect passage across pre-Kaingaroa alluvial systems. The gas segregation pipes could represent local steam vents. Lithics derived from river gravels are present as 'incorporated' or accidental lithics in both units in some medial localites (Chapter 5). The Kaingaroa Ignimbrite is inferred to rest on river gravels. Evidence of shallow alluvial systems is also suggested from minor variations in thickness and welding variation (see below). The 'reworked' ignimbrite facies atop the Kaingaroa Ignimbrite are typical following moderate voluminous ignimbrite eruptions, where the drainage network is destroyed, and possibly re-established post-eruption (Sparks et al. 1985).

3.7 Welding and secondary recrystallisation zonation

Welding is defined as the post-depositional sintering of shards and pumice under a compactional load (Ross and Smith 1961). Three welding facies are distinguished: non-

welded, partially welded and densely welded; transitions between which are gradational. Welding zones are defined on three criteria: density (g/cm^3), pumice attenuation, and shard deformation in thin section; Parameters are outlined in Table 3.2. The variable vesicularity of Kaingaroa pumices prevents meaningful interpretation of pumice aspect ratios.

Devitrification and *vapour phase* are the two main types of secondary crystallisation: Glass is metastable and will readily undergo post-eruptive crystallisation of alkali feldspar and cristobalite, particularly in densely welded sections of ignimbrites. Vapour phase crystallisation is the growth of crystals within pore spaces under the influence of a vapour phase. The main products are alkali feldspar, tridymite and cristobalite. Vapour originates from water liberated during devitrification, and by heating of meteoric water penetrating the deposit, and crystallisation tends to be concentrated in porous upper parts of ignimbrites. The results of both processes are very similar in pumices of partially-welded units.

Four secondary crystallisation types are defined with respect to the Kaingaroa Ignimbrite:

1. Incipient devitrification. Minor growth of cryptocrystalline aggregates of cristobalite and alkali feldspar within matrix glass. Not detectable in hand specimen.
2. Axiolitic. Parallel fibrous intergrowths crystallising inwards from margins of a shard and meeting at a central discontinuity marked by a dark line.
3. Spherulitic. Spherulitic replacement of either pumice fragments or matrix. Observable in hand specimen, in particular coarse spherulitic replacement of pumice or fiamme. Intense spherulitic devitrification may obscure original matrix vitroclastic texture.
4. Vapour phase. Fibrous intergrowths infilling pores within pumice fragments and matrix interstices, which often produces soft woody friable pumice fragments in hand specimen.

This section summarises bulk density and petrographic evidence of welding and crystallisation variations in the Kaingaroa Ignimbrite. The Kaingaroa Ignimbrite exhibits a standard compound unit, with an upper vapour-phase crystallisation zone, and devitrified zones in zones of dense-welding, typical of large ignimbrites (Smith 1960).

Fig 3.9 schematically illustrates thickness variations relative to paleotopography, from proximal to distal regions. The three welding zones superimposed on these thickness variations are empirically defined as having densities of >1.8, < 1.8 >1.3, and < 1.3 g/cm^3, respectively. The lower unit is non-welded throughout and restricted to proximal regions, whereas the middle and upper unit thicken gradually and increase in welding grade towards the central plateau, and thin towards distal regions. A combination of petrographic criteria e.g. compression of glass shards around phenocrysts and lithics, and fiamme aspect ratios suggest samples with densties greater than 1.8 g/cm^3 could be considered as densely welded. The limited exposure and hence limited density and crystallisation profiles prevents production of detailed fence diagrams (e.g. Briggs 1976; Bailey and Carr 1994), and interpolation of lateral variations away from the east-west axis. Distribution, and thickness data suggest southward and northward thinning of units away from source, as predicted for most ignimbrites (Smith 1960).

Welding facies	Density	Pumice deformation	Shard deformation	Jointing
Non-	> 1.3	None	None	None
Partially-	1.3-1.8	Slight to strong	Slight to mod.	Several metres-1m spacing
Densely-	1.8 <	Strong	Strong	ca.1m spacing

Table 3.2 Summary of welding facies definition for the Kaingaroa Ignimbrite.

The lower unit (RBU) is non-welded throughout, and the middle OWR unit is non-welded to partially welded at all but central Kaingaroa Plateau exposures. The increase in thickness and welding degree is accompanied by change in colour to light grey and decreased joint spacing. The upper unit (WIU) is partially welded in lithic-rich proximal regions, and densely welded in medial regions. Colour varies from light brown to grey, and joint spacing from several metres to 1 m. Upper vapour phase altered WIU shows a variety of colours including grey, white, pink, and red.

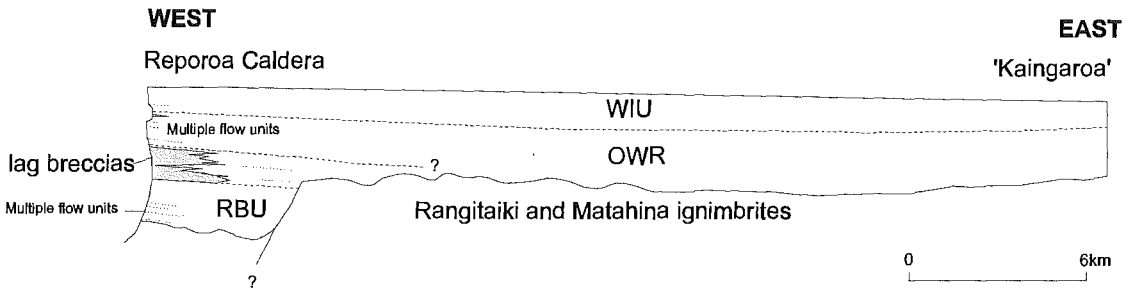

Figure 3.9. Schematic cross section showing thickness variations with stratigraphy and distance from Reporoa Caldera. The vertical scale is greatly exaggerated.

The middle OWR unit exhibits incipient devitrification in thick welded sections e.g. Main Gully Rd, whereas the WIU is commonly devitrified, and exhibits an upper vapour phase zone, as is common in most ignimbrites. No effort has been made to delineate crystallisation zones due to the limited exposure, difficulty in assigning zones based on field criteria, and gradational transitions between facies.

A notable feature of welding variation is the increase in welding (and thickness) away from source, in the centre of the Kaingaroa Plateau. Bailey and Carr (1994) detailed an increase in thickness and welding away from source in the Matahina Ignimbrite, which they considered consistent with ponding of the Matahina pyroclastic flows along the range front. The variation in thickness and welding described here is interpreted as due to pyroclastic flows ponding in a broad lowland in central Kaingaroa Plateau, possibly a broad paleo-Rangitaiki River (alluvial) basin.

An unusual feature is the presence of a vapour-phase zone beneath (and above) welded and devitrified WIU in the Rerewhakaitu area. The Rerewhakaitu area exhibits two cliff-forming units in the WIU, a standard welded and devitrified zone with upper vapour-phase zone, and a lower vapour-phase zone. Both vapour-phase zones are lithified. Vapour-phase crystallisation is commonly attributed to vapour derived from devitrification, and therefore is commonly described in upper parts of ignimbrites. Ross and Smith (1961) highlight a similar example and attribute the lower vapour-phase zone to vapour being squeezed out downwards during compaction, and subsequently being

trapped by the welded zone. An alternative hypothesis is that vapour is derived from an external source, such as ground water. The localised presence of reworked (alluvial?) ignimbrite atop the Kaingaroa succession in the Rerewhakaaitu area, and small thickness variations attributed to paleo-alluvial channels suggest a history of alluvial systems, especially in the Rerewhakaaitu region, consistent with thickness and welding variation.

CHAPTER FOUR

Kaingaroa Ignimbrite:

Proximal lag facies and lateral variation

4.1 Introduction

The Kaingaroa Ignimbrite displays striking facies variation from proximal to medial localities. Adjacent to the eastern edge of Reporoa Caldera the Kaingaroa Ignimbrite exhibits a distinctive proximal facies, dominated by coarse-grained breccias rich in accessory lithic fragments, locally interbedded with ignimbrite. This lithic breccias grade laterally into Kaingaroa Ignimbrite (sensu stricto), and locally is intimately associated with it. The lithic breccias display the same compositional and colour zonation as the Kaingaroa Ignimbrite$_{s.s.}$ and hence are deduced to have been deposited coincidentally with pyroclastic flow emplacement. The vertical variation in colour is the key to unraveling stratigraphic complexities and providing constraints on depositional facies.

These lithic breccias were originally interpreted as andesitic gravels (Grange 1937) or river gravels, tills and debris flows (Huka Group; Grindley 1959) but Nairn et al. (1994) consider them to be a co-ignimbrite lag breccia or lithic lag breccia (sensu Druitt and Sparks 1982), because of the association with the Kaingaroa Ignimbrite, similar lithic contents, presence of gas segregation structures and similarities with documented lag breccias. Co-ignimbrite lag breccias are classically interpreted to be due to proximal sedimentation of the coarsest and densest components that are too dense and large to be transported by the parent pyroclastic flow(s).

The main objectives of the chapter are to report stratigraphic and volcanological analyses of lithic breccias and other proximal ignimbrite facies of the Kaingaroa Ignimbrite, and describe the lateral transition to medial facies vertically zoned ignimbrite in order to provide insights into mechanisms of deposition. Details of the stratigraphic interval enclosed by the RBU (Reporoa Boundary Unit) and OWR (Old Waiotapu Rd unit) are also described here in more detail.

Despite the poor exposure it is believed that combined lithic componentry, pumice chemistry and stratigraphic logs provide adequate constraints on three dimensional lithofacies association.

A flow unit is defined as the deposit from a single pyroclastic flow. Boundaries are commonly marked by distinct grain size breaks such as pumice or lithic concentration zones, and interbedded units. Such boundaries may not reflect a separate depositional unit but rather variations in current steadiness during incremental deposition. For the purposes of description discrete packages are termed flow units.

4.2 Stratigraphy, distribution and general character

The RBU-OWR interval includes a complex array of lithic breccias and intercalated ignimbrites. This interval can be divided into 4 recognisable sub-units defined on the basis of texture, geochemistry and stratigraphic position. Within each sub-unit are recognisable lithofacies variations, ascribed on the basis of sedimentary structure and textural variations.

(1) Lithic breccia which grades laterally into a grey-yellow gradational colour-zoned ignimbrite termed the transition zone (TZ).

(2) Tan-coloured transition ignimbrite (TTI) is present only at Butchers Boundary Rd, but is inferred to represent part of the transition zone.

(3) Brown-coloured pumice-rich transition ignimbrite (BTI), which grades laterally into either lag breccia or OWR, and marks a stratigraphic break between lower and upper lithic breccia units.

(4) Bleb-bearing welded lithic-rich ignimbrite (Tokiaminga subunit).

The most conspicuous feature of the proximal facies is the presence of lithic breccias (up to 45 m+ thick), which are poorly exposed in forestry road cuts along the eastern margin of Reporoa Caldera, adjacent to the well defined topographic caldera scarp (Fig

4.1). The breccias extend as far as ca.2 km from the eastern topographic caldera rim, and are not present at Maungahekeke Valley and Riehana Rd 3 km from the rim.

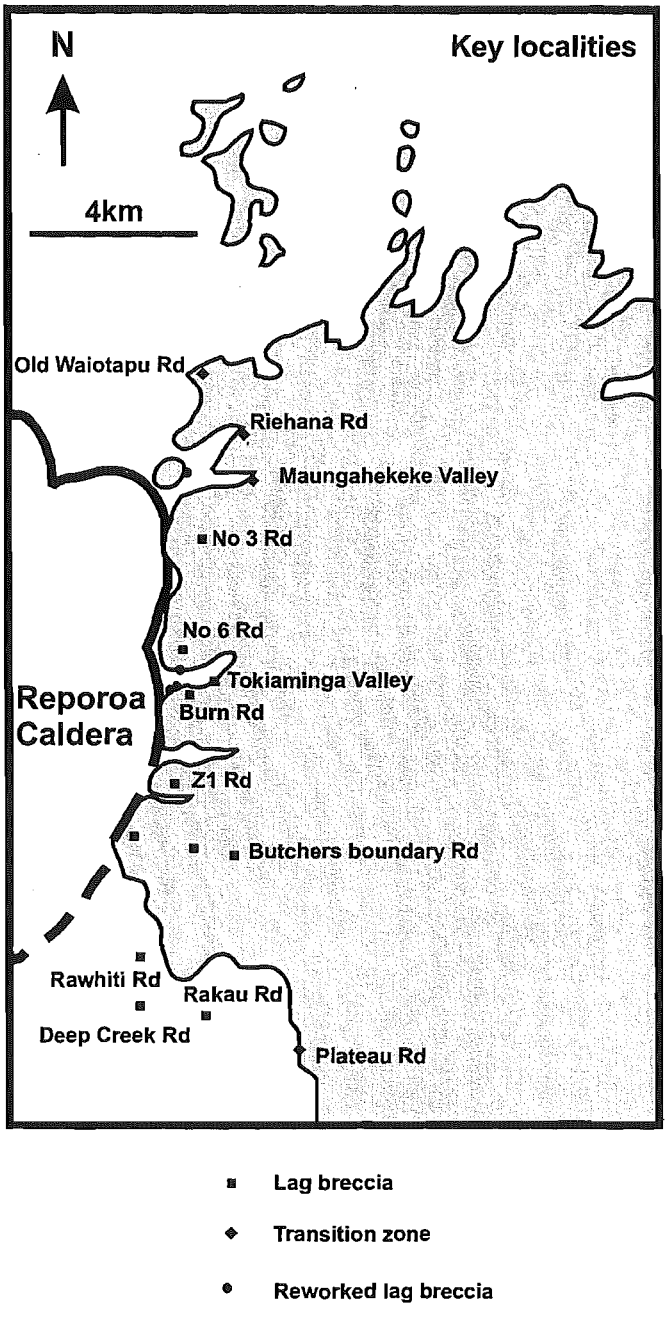

Figure 4.1 Lag breccia and transition zone localities discussed in text. Note also reworked lag breccia localities.

No exposures of lithic breccias have been located west and south of Reporoa Caldera, and only a single poorly exposed outcrop of reworked lithic breccia has been documented at Shilts Farm north of Reporoa Caldera.

The base of the lithic breccias is exposed only on No 6 Rd, but field relations indicate that the breccias thin outwards from greater than 45 m at No 6 Rd to ca.30 cm at Butchers Boundary Rd. The poor exposure precludes assessment of thickness variation relative to topography.

Good exposures of the lithic breccias occur at No 6 Rd (Fig 4.2), Burn Rd (Fig 4.3) and at Butchers Boundary Rd Quarry, where it is coarse-grained, rich in accessory lithic fragments, with subordinate rounded pumice, clast- and rarely matrix-supported, and grades vertically upwards from a yellow pumice-poor lithic rich breccia to a grey-black pumice moderately-rich lithic-rich breccia. The variation in matrix and pumice colour is mimicked within the laterally equivalent ignimbrite termed the transition zone (Chapter 3 and below). The upwards increase in fines reflects a changing juvenile component and incoming of black/brown blocky shards and grey pumice type. The presence of black/brown glass shards and lack of a black pumice type is interpreted to be due to abrasion during transport.

Matrix% is variable but where present is composed of sand-sized lithic fragments, crystals and subordinate vitric ash and is locally fumarolically altered. The lack of fines (i.e. fines depletion) is noteworthy.

Lithic fragments are abundant in all deposits, locally up to 4.5 m in length (Fig 4.5), commonly tens of cm to 1 m in size. The breccias are heterolithologic, with angular to subangular lithic clasts which include andesite lavas, welded ignimbrites, gabbros, granophyre, rhyolites, baked soil, meta-volcanics, meta-sediments and sediments (Chapter 5 and 6). Numerous lithics exhibit outer weathering rinds and/or hydrothermally/fumarolically altered interiors, and rare clasts crumble easily when handled. Some lithics have breadcrusted outer surfaces. Details of lithic morphology are outlined below.

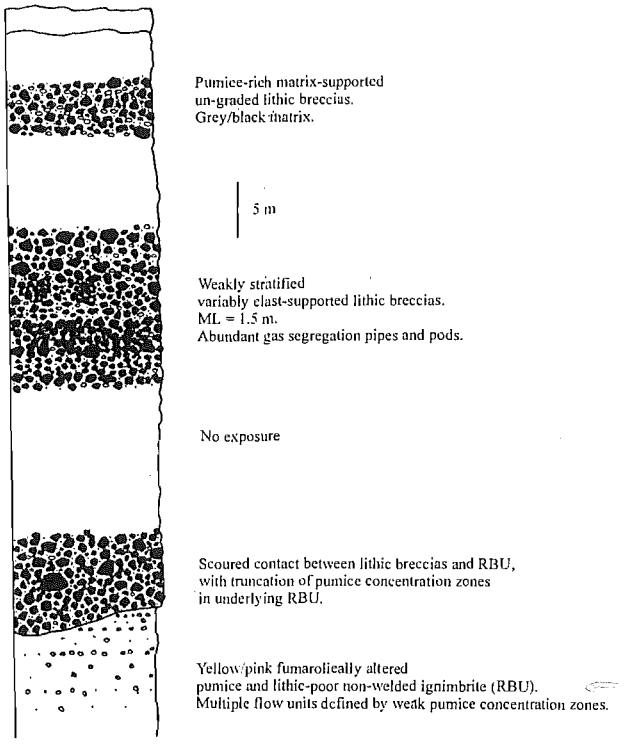

Figure 4.2. Stratigraphic log of lithic breccias along No 6 Rd

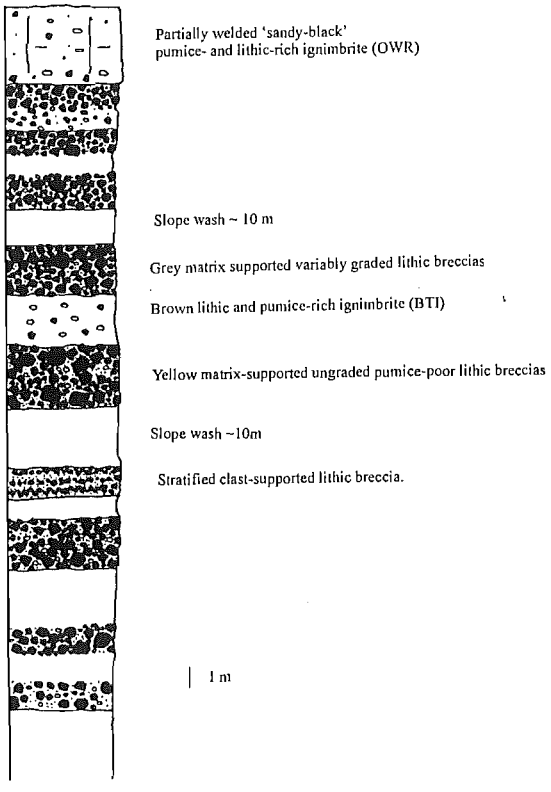

Figure 4.3. Stratigraphic log of lithic breccias and intercalated ignimbrite along Burn Rd

Figure 4.4. Weakly stratified proximal facies lithic breccias at Butchers Boundary Rd quarry

Figure 4.5 Maximum lithic, a 4.5 m Waiotapu Ignimbrite lithic at Butchers Boundary Rd quarry.

Pumices are locally present within interstitial areas (Fig 4.6), are ubiquitously well rounded, rarely exceed lapilli size (Mp = 60 mm) and are commonly fumarolically altered or visibly hydrated. M_L generally exceeds that of pumice in the same exposure by a factor of 10 to 30.

The breccias are generally massive to weakly normal graded in 'ultra' proximal localities (Fig 4.6a), with weakly developed sub-horizontal stratification defined by clasts of similar grain size. Flow unit boundaries are indistinct, but locally defined by weak stratification and truncation of gas segregation pipes. No grading of pumice is present and fine grained pumiceous basal layers, such as those found on Santorini (Druitt and Sparks 1982). The top of the lithic breccias are observed only at Burn Rd, where the breccias grade upwards into the overlying OWR. The base of the lithic breccias was only observed at a single locality (No 6 Rd) where the lithic breccias rests on an erosion surface on the underlying RBU unit (Fig 4.7).

The lithic breccias exhibit variable matrix support (Fig 4.6b), locally with an open framework. Gas segregation pipes and pods are present at all localities but are prominent within the quarry on Butchers Boundary Rd and in more distal localities further east along the road (Fig 4.8). Two broad gas segregation structures are noted: pipe-like and pod-like. Both structures are fines depleted, and contain small lapilli-sized pumice and lithics. The pipes are commonly truncated by weak stratification, defined by clasts of similar size.

An unusual fine grained well-stratified and sorted lithic breccia lithofacies is present on Burn Rd. No contacts are observed with other lithic breccias exposed along Burn Rd. The poor exposure also prevents assessment of geometry of the lithofacies. The fine-grained breccia is moderately sorted, fines-depleted, pumice-poor and lithic-rich and clast-supported in a matrix composed of sand-sized lithic fragments. Lithic and pumice types resemble those of enclosing units. The most striking feature of the breccia is its well stratified nature. Stratification is defined by lithic clasts of similar clast size and fluctuates on a lapilli-sized 2 cm to 5 cm scale. No internal grading or impact sags are present within the unit.

Figure 4.6a Weakly developed normal grading and stratification within lithic breccias, No 6 Rd.

Figure 4.6b. Matrix-supported lithic breccias, with abundant lithics and subordinate yellow crystal-poor pumices.

Figure 4.7. Sharp erosive boundary between the lithic breccias and underlying Reporoa Boundary Unit (RBU), along No 6 Rd. At this locality the lithic breccias have scoured considerable relief and locally truncate weak pumice concentration zones in the underlying non-welded RBU.

Figure 4.8. Fines-depleted gas segregation pods and pipes (G) within the lithic breccias along Butchers Boundary Rd.

The presence of angular lithic fragments, fumarolic matrix and lithics, homogeneous pumice type and similar compositional characteristics to other lithic breccias suggests the unit is primary.

The presence of abundant gas segregation pods and pipes, localised welding (e.g. Tokiaminga valley), and fumarolically altered matrix (e.g. No 6 Rd) indicate the lithic breccias were deposited at high temperature, and suggest the lithic breccias are primary pyroclastic deposits, distinct from lithic-rich lahars (Duncan et al. 1996), and alluvial gravels.

Two types of compositional zonation are observed in the lithic breccias; Vertical zonation in colour defined by a transition from a yellow-light brown (locally pink) matrix and pumice type upwards into a black matrix and grey pumice type. Accompanying the transition is an upwards increase in pumice abundance. A similar vertical zonation in colour is observed in medial facies ignimbrite. The vertical colour transition resembles the transition from RBU-like upwards to OWR-like.

The colour zonation is not accompanied by a concomittant change in pumice chemistry (Chapter 7), although the transition from RBU to the lag breccia is marked by the incoming of diverse pumice types, and variation in chemical composition.

Reworked lithic breccias occur at six sites (Fig 4.1) including three sites along the banks of the Tokiaminga stream. They are well stratified, commonly matrix supported, interbedded with recent tephras and paleosols, and commonly contain either well rounded lithic fragments and a clay-rich matrix, or tabular imbricated lithic fragments and ash matrix. Lithic componentry on the reworked lithic breccias confirms the lithic components are similar to lithic breccias$_{s.s.}$. At Deep Creek Rd a thin layer of clast-supported lithic fragments, with interstitial brown clay overlies a Rangitaiki Ignimbrite undulatory landscape. The lack of pumice and presence of clay matrix suggests the deposit is secondary, and it is interpreted as a remnant of lag breccia, with the matrix winnowed away. The undulatory Rangitaiki Ignimbrite surface is well exposed in the Deep Creek Rd-Rawhite Rd area.

4.3 Lateral variation

At Rawhiti Rd the lithic breccias are bedded, each bed being either reversely or normally graded with respect to lithics (Fig 4.9, 4.10). Pumice and matrix are similar to RBU and lower lithic breccias. At least 8 beds are present at this locality. Contacts between the beds are diffuse, and gas segregation pipes are rare. The base of the succession is not exposed but it is presumed to lie directly on the undulatory Rangitaiki Ignimbrite surface.

At the most eastern exposure along Butchers Boundary Rd, TTI is overlain by OWR (Fig 4.11). The contact is sharp, sub-horizontal and marked by a sharp colour change and the presence of a lithic concentration zone (Fig 4.12). Lithics within OWR are normally graded. The TTI is pumice-rich and lithic-poor and contains abundant gas segregation pipes, none of which cross the TTI-OWR contact. Despite the poor exposure of TTI the lithic concentration zone is considered to represent the lateral equivalent of the upper lithic breccias.

At more distal localities the lithic breccias are interbedded with fine-grained lithic- and pumice-rich ignimbrites, exhibit variable grading of lithics (normal, reverse or ungraded), and have prominent gas segregation pipes and pods typical of gas fluidisation (Wilson 1980; Druitt 1995).

In general field relations suggest the lithic breccias grade vertically and laterally from Reporoa Caldera, and the Kaingaroa Ignimbrite$_{s.s.}$ represents the lateral medial facies equivalent.

Intercalated within the lithic breccias are two distinct ignimbrite subunits:

Tan transition ignimbrite (TTI)

A pumice-rich ignimbrite outcrops beneath OWR on Butchers Boundary Rd. TTI is pumice-rich, with similar pumice chemistry and lithic componentry to the transition zone, and OWR unit. The prominent feature of the unit is abundant gas segregation pipes enriched in pumice and depleted in fines. Pipes are locally up to 1.5 m in length. No grading or stratification is present.

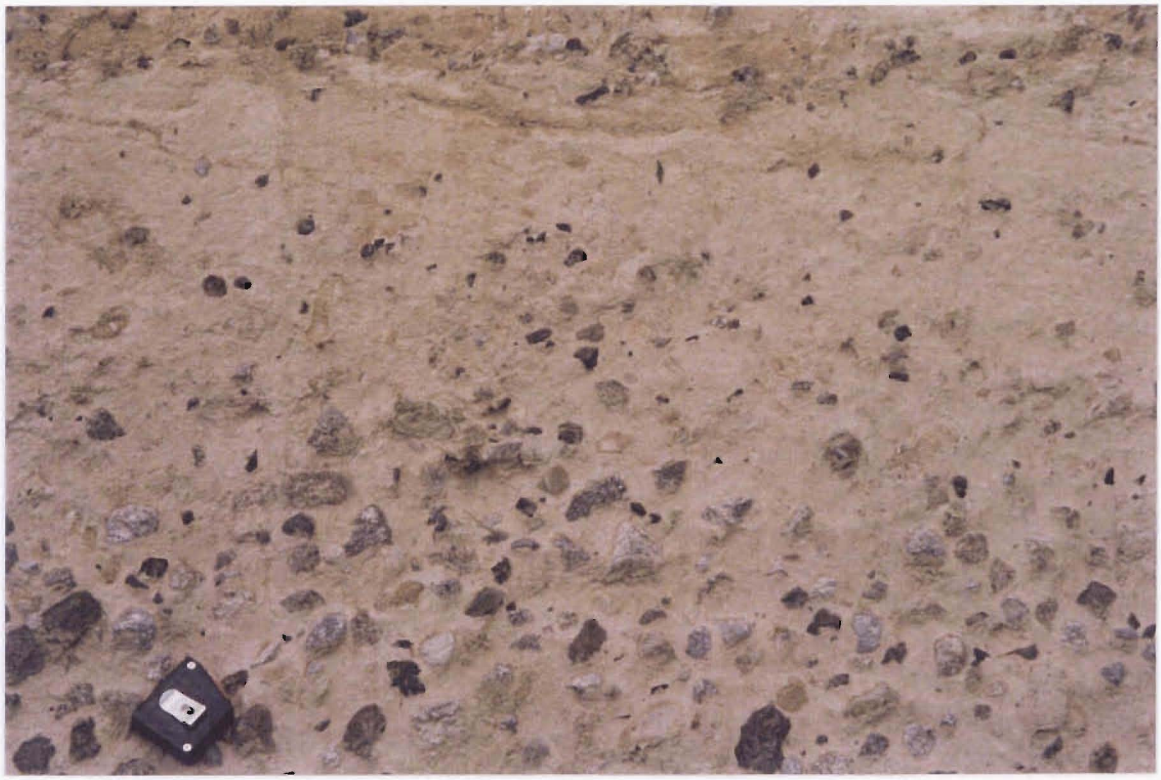

Figure 4.9. Normal graded lithic breccia unit, Rawhiti Rd.

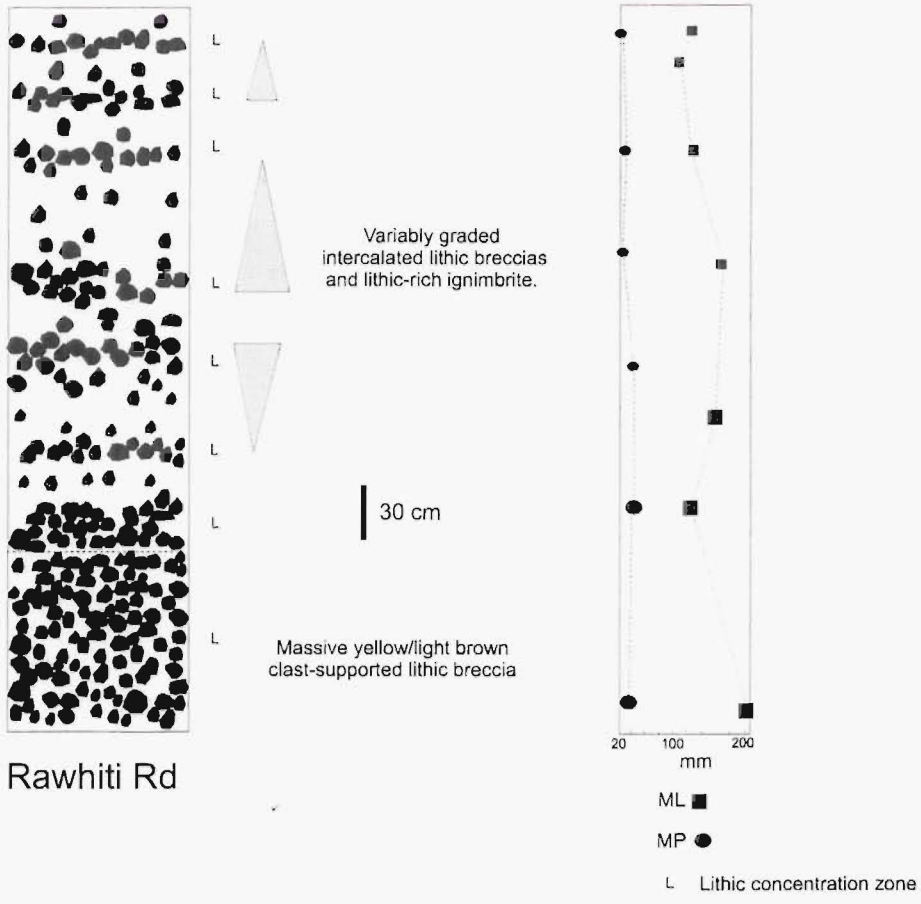

Figure 4.10. Graphic log of Rawhiti Rd section.

Figure 4.11. Butchers Boundary Rd (east). Pumice-rich tan-coloured ignimbrite (TTI) is overlain by the partially-welded 'sandy-black' Old Waiotapu Rd ignimbrite unit (OWR), with a well defined lithic concentration at the contact and normal grading of lithics.

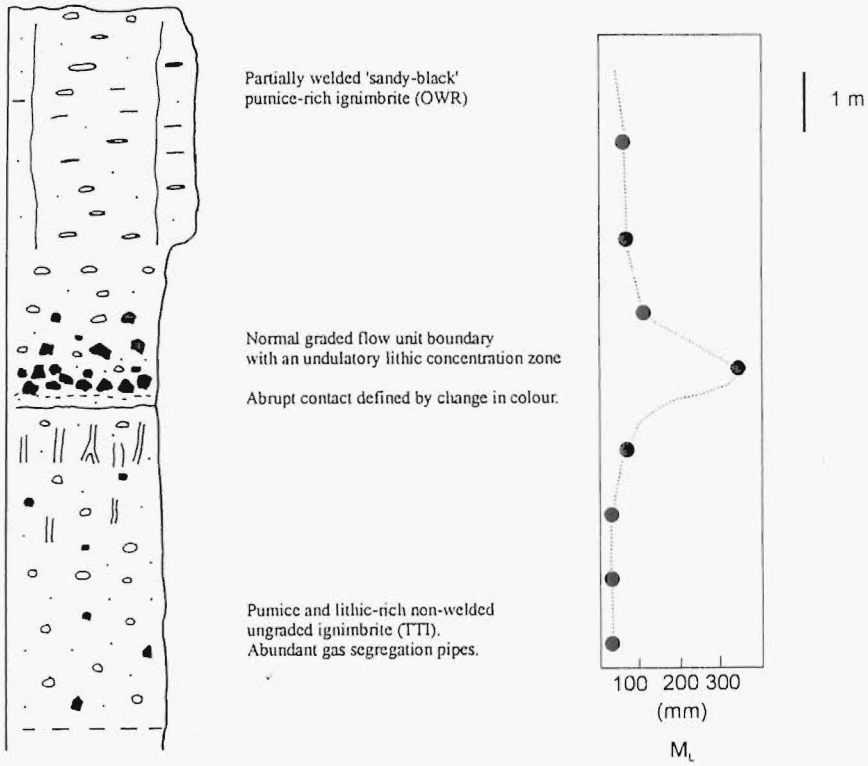

Figure 4.12. Graphic log of Butchers Boundary Rd (east) section.

The unit is overlain in sharp planar contact by lithic-rich OWR. TTI is probably a localised lateral variation of lag breccia and transition zone ignimbrite.

Brown transition ignimbrite (BTI)

The BTI is an unconsolidated, poorly sorted pumice-rich deposit which has features typical of ignimbrite (Sparks 1976). BTI is exposed at two localities, in roadside exposure on No. 3 and No. 6 roads, along the eastern margin of Reporoa Caldera, and overlying basal tephras at Plateau Rd. BTI is unusually dark (chocolate) brown in colour, pumice-rich and relatively lithic-poor. No grading or stratification is present. The lower boundary is commonly planar, and the upper boundary is either diffuse e.g. Burn Rd or erosive e.g. No 3 Rd. BTI is present at a similar stratigraphic interval and is of broadly similar thickness at all localities but there is insufficient outcrop to infer lateral variations in thickness or facies. The presence of brown pumice-rich transitional facies within the transition zone (see below) suggests this unit represents a fundamental change in magma composition and eruptive dynamics.

At medial localities (beyond 2 km from the topographic caldera margin) no lithic breccias are exposed and the RBU passes up into the overlying OWR. The contact is gradational over a height interval of 2-6 m and rarely coincides with a grain size break. This interval is termed the transition zone.

The *transition zone* exhibits variable grain size characteristics e.g. at some localities there is faint stratification, presence of diffuse lithic concentration zones and pumice concentration zones which are interpreted to represent numerous flow units e.g. Maungahekeke Valley. At other localities there are no observable grain size variations and the interval or transition zone is interpreted as a single flow unit (e.g. Old Waiotapu Rd; Figs 4.13,4.14).

The transition zone is a typical pumiceous (pumice-rich) poorly sorted ignimbrite. It is difficult to detect at more distal localities where it is marked by increased lithic content, presence of abundant gas segregation pipes and diversity of lithic types (c.f. underlying RBU; Chapter 5). Similar transition zones have been described in the Acatlan Ignimbrite (Wright and Walker 1981; Branney and Kokelaar 1997) and climactic ignimbrite at Mt Mazama (Druitt and Bacon 1986).

Figure 4.13. Transition zone from RBU-like to OWR-like facies, Old Waiotapu Rd.

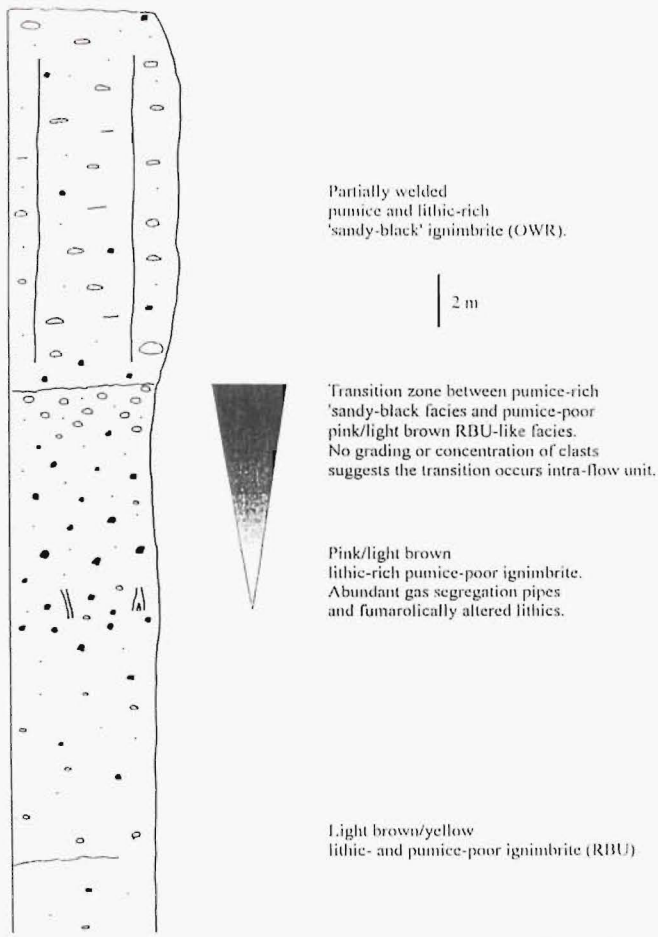

Figure 4.14. Graphic log of Old Waiotapu Rd section.

The presence of localised facies variation and grain size discontinuities (e.g. pumice concentration zones) near or within broad scoured channels, and weak stratification defined by pumice-rich layers, suggest variations in flow steadiness beneath an aggrading flow due to interaction with topography, or indicate deposition from numerous passing flow units.

At more distal localities e.g. Maungahakeke Valley, the transition zone contains prominent pumice concentration zones, reverse grading of pumice, normal grading of lithics, and no layer 2a deposits. Basal contacts with underlying units are commonly erosive, and are interpreted as scours into the underlying ignimbrites.

OWR overlies the lithic breccias in proximal localities and the transition zone in medial localities. OWR exhibits limited facies variation, and is generally a massive poorly-sorted deposit. Well defined flow unit boundaries were observed within 3 km of the topographic caldera margin defined by pumice and lithic concentration zones. Fine grained basal layers (layer 2a; sensu Sparks et al. 1973) are poorly developed or absent even in proximal localities. On the whole the ignimbrite is rather structureless. The simple medial facies stratigraphy is attributed to emplacement onto flat topography (levelled by preceeding RBU and transition zone eruptives), suggestive of a relatively low velocity of emplacement (Chapter 3). At more distal localities the incoming of abundant rounded greywacke lithics at the base of the unit suggests incorporation of lithics from alluvial gravels (Chapter 5).

4.4 Tokiaminga Valley

An unusual lithofacies or subunit of the Kaingaroa Ignimbrite is a welded fines-depleted tan-coloured lithic-rich ignimbrite which exhibits similar mineralogy and pumice chemistry to OWR but with less evolved dacitic fiamme/blebs (69 % SiO_2; low Rb/Sr; Chapter 7). The unit is exposed only in semicontinuous cliffs along the recently deforested valley walls of Tokiaminga Valley (Fig 4.15) lying stratigraphically above $OWR_{s.s.}$, >50 m of lag breccia, and the RBU. WIU (upper ignimbrite) is not exposed in this area but is inferred to overly the Tokiaminga valley subunit.

The unit is welded throughout, and varies in thickness from 6 m to 2 m. The base of the unit is not exposed but irregular ignimbritic foliation (eutaxitic texture) and dip and strike of lithic breccia horizons suggest an irregular base. The unit is not exposed further east of Tokiaminga Valley, but may extend beneath the Kaingaroa Plateau. The localised exposure of the unit might reflect sectorial or lobe emplacement of the unit along the eastern caldera perimeter.

The dominant thickness of the unit is made up of partially-welded (locally case-hardened), weakly jointed ignimbrite, which varies from a sandy-black (OWR-like) unit at its base, to a tan coloured unit at its exposed top. There is little density varies with stratigraphic height, and lateral distance from the topographic caldera margin. The exception is within prominent matrix-supported lithic breccia horizons prominent along the southern margin of Tokiaminga Valley. The thickness of the lithic breccia horizon varies with distance from the topographic caldera rim but is up to 30 cm thick (Fig 4.15). The lithic breccia horizons vary from 30 cm to 5 cm thick, and are notable for the high degree of welding in contrast to the underlying lithic breccias and the presence of dacitic fiamme/blebs. Representative columnar sections for the southern part of the valley are shown in Figure 4.15b. The maximum lithic clast (M_L) decreases with lateral distance from the topographic caldera margin. The boundaries between the lithic horizon and ignimbrite are locally sharp but commonly diffuse. Locally the horizon changes from a single lithic-rich horizon to anastomosing thin lithic-rich horizons commonly only a single clast in thickness. Lithic breccia horizon tends to be continuous for several metres, and have a lenticular geometry. Internally the lithic breccia are ungraded, and exhibit no structure except for a prominent and locally excellently exposed lithic preferred orientation, defined by long axis of prolate lithics (and concordant with long axes of blebs). Lithic preferred orientation is approximately perpendicular to the topographic caldera margin, consistent with inferred source direction.

A notable feature of the lithic breccia horizons is the partial welding indicated by eutaxitic texture within the matrix. The lithic breccias are unusually pumice (fiamme) rich (and fines depleted), and locally contain abundant dacitic blebs or dacite-rhyolite mingled fiamme. The presence of welding is anomalous and in contrast to the

underlying non-welded lithic breccias. The indurated nature of these deposits precluded granulometric analysis.

Lithics exhibit similar morphological variation to lithic breccias; breadcrusted lithics are notably abundant, and gabbroic (Fig 4.16a) and metavolcanic lithics are conspicuous (Chapter 5).

An unusual feature of the breccias is the presence of weakly pumiceous juvenile components which exhibit features suggesting they deformed plastically during emplacement and/or welding (Fig 4.16b). These clasts are termed blebs (sensu Freundt and Schmincke 1992a). They resemble fiamme but exhibit localised sharp angular edges and diffuse boundaries. Blebs are ubiquitously mingled with typical Kaingaroa pumices/fiamme and the presence of diffuse contacts and mingling indicate they are juvenile components. Despite an extensive search blebs were not found in non-welded ignimbrite.

The lithic breccias exhibit a high degree of welding considering their lithic content. In addition the lithics show prominent evidence of retention of heat e.g. breadcrusting. This is attributed to the presence of abundant dacitic components i.e. localised higher temperature magma and hence more effective heat retention.

The Tokiaminga subunit is interpreted as a localised unit probably derived from a low fountaining column adjacent to the caldera rim, and hence a localised vent and flow. This is consistent with the eruption of high temperature material and eviceration of lithics of deep provenance only at this location. The presence of lithic breccias within the Tokiaminga subunit indicates further collapse occurred between the climactic phase represented by the lithic breccias$_{s.s.}$ and the WIU.

4.5 Lithic morphology and componentry

Lithic fragments range in size from <1 mm to 4.5 m in diameter. The majority of lithics are angular to subangular, with rare well rounded 'greywacke' lithic fragments, reflecting their inferred gravel provenance. Details of lithic componentry and petrology are outlined in Chapter 5 and 6.

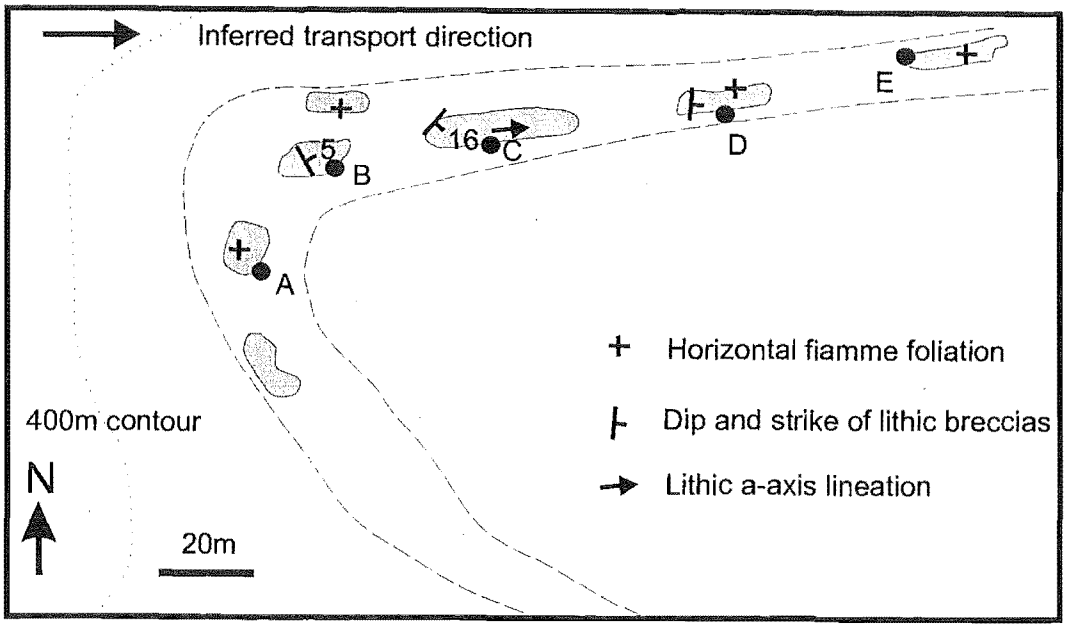

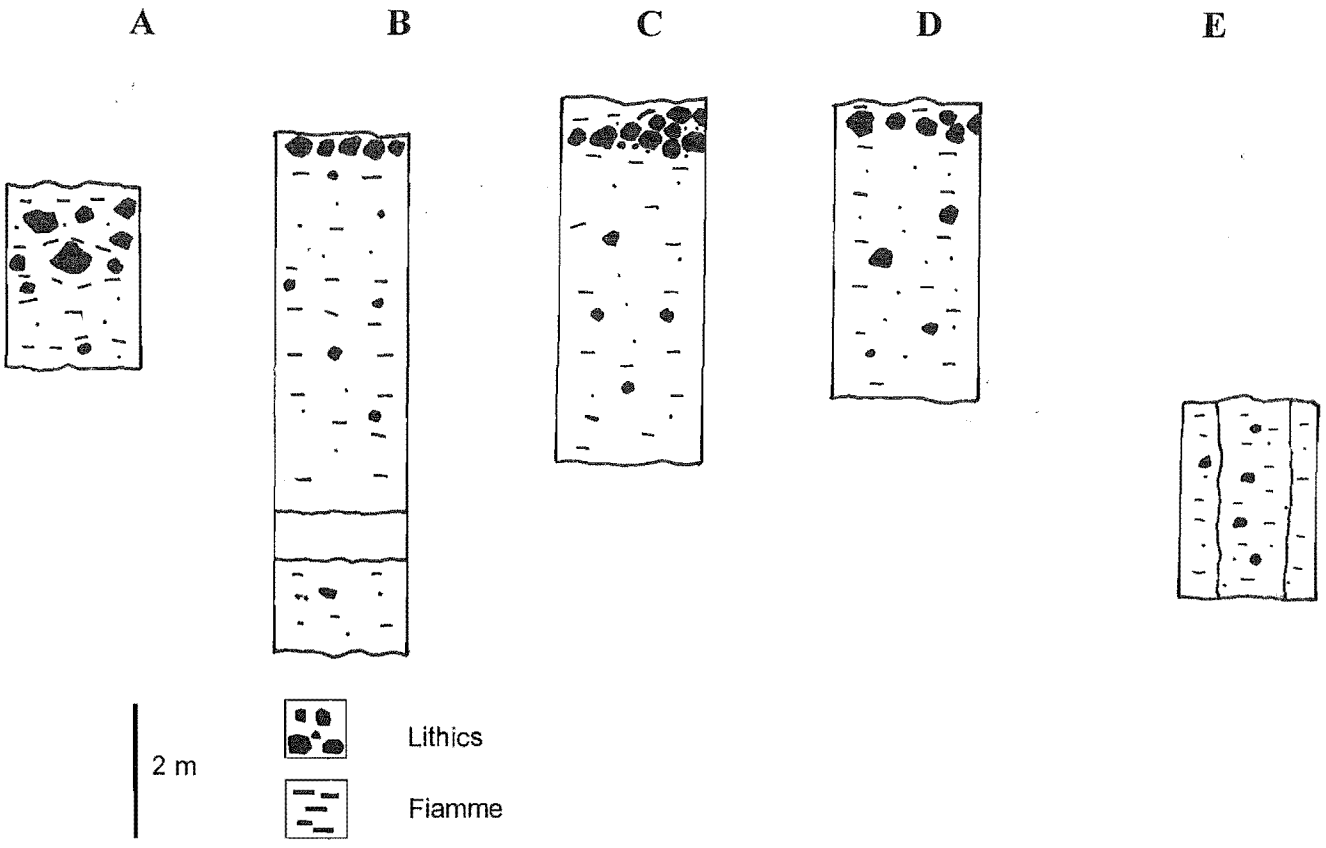

Figure 4.15. Schematic outcrop map of Tokiaminga Valley and graphic logs illustrating variation within the sub-unit.

Figure 4.16a. Leucogabbroic lithic fragment within the welded Tokiaminga subunit.

Figure 4.16b Hornblende two-pyroxene dacitic bleb in the Tokiaminga subunit. Note the mingling with rhyolitic fiamme/pumice and localised sharp margins.

This section outlines aspects of lithic morphology pertinent to proximal facies interpretation.

Lithics are commonly heat spalled, with an inner rounded ('spalled') zone of unaltered to weakly altered rock surrounded by a concentrically outer cracked zone of iron-stained rock. Heat spalling is commonly displayed in andesite lithics. Breadcrusted lithics are present in some ultra-proximal localities and in the high temperature welded Tokiaminga subunit. Lithics are intricately cracked, commonly in a hexagonal pattern (especially common in hydrothermal altered lithics), resembling textures characteristic of breadcrust bombs. Both heat spalled and breadcrusted lithics have been commonly reported in proximal lag breccias (e.g. Druitt and Bacon 1986), and interpeted to reflect thermal contraction of lithics, incorporated at varying temperature and P_{H2O}. Rare lithic blocks are radially jointed, with pervasive intense fracturing, that extend throughout the lithic. These blocks disintegrate when removed from the outcrop. All these features suggest many of the blocks were hot on entrainment.

Lithics exhibit variations in shape reflecting variations in entrainment and deposition processes and temperature and nature of the lithic protoliths. Lithics vary in shape from commonly equant to rarely prolate. A very rare bladed (Zingg 1935) or platy (Sneed and Folk 1958) rhyolite lithic was sampled at Butchers Boundary Rd. The presence of this lithic is notable for the intact angular edges, high aspect ratio $D_s/D_i = 0.025$, and fragile nature. The platy lithic is overlain by large lithic fragments which lie undisturbed on the fragile platy lithic. Similar lithic shapes have been observed in the Rotoiti lag breccia (personal observation). The presence of fragile and platy morphology lithics implies surprisingly gentle emplacement, in stark contrast to depositional facies that indicate a turbulent, highly fluidised and locally erosive environment (see below).

Gabbroic lithics commonly exhibit cataclastic margins or internal domains, which probably reflect either entrainment or pre-eruptive provenance processes.

Many of the lithics are altered, reflecting provenance alteration (Chapter 6), or post (or syn-) eruptive fumarolic activity. An unusual feature of many plagioclase-phyric andesite lithics is what is commonly referred to as 'inside-out weathering' (Suggate and

Watters 1991). Andesite lithics exhibit weathered cores, with abundant iron oxides within vesicles; outer shells are unaltered.

Many of the altered tuff and soil lithics crumble on removal from the outcrop, and could not have survived impact from airfall deposition. A rapid drop in percentage and size of friable lithologies with distance from the caldera margin (chapter 5) indicates abrasion and disaggregation of these lithologies. Similar friable lithics have been reported in other proximal facies (e.g. Taupo; Chernet 1987).

4.6 Grain size and granulometric variation

Six samples of lithic breccia and ignimbrite were sieved according to the methods outlined in Walker (1971). Due to the extreme grain size variation, and difficulties in including large clasts in granulometric analyses, and in order to compare with other lag breccias, grain size analyses were carried out in a similar fashion to Nairn et al (1994). Granulometric data from Nairn et al (1994) is also included in the following section. The aims of granulometry (outlined above) was to compare sorting rather than absolute clast size. As a result errors associated with removing or not sampling large clast sizes is considered unimportant to conclusions. A separate lithic componentry technique, analogous to techniques used in classical sedimentology is outlined in Chapter 5.

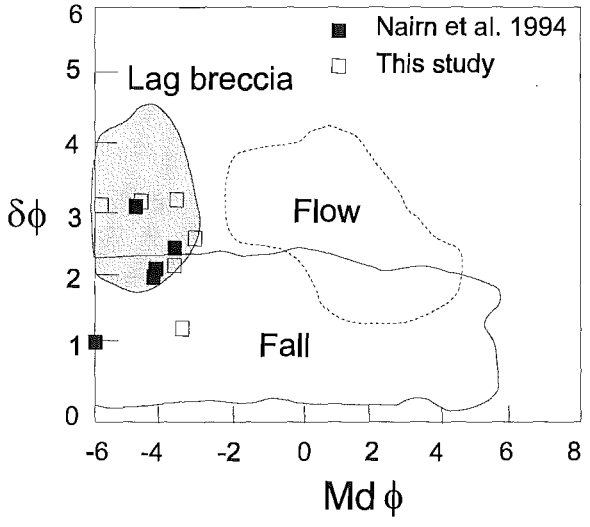

Figure 4.17 Granulometric variation in lithic breccias intercalated with the Kaingaroa Ignimbrite. Flow and fall fields after Walker (1971) and lag breccias field after Walker (1985) and Druitt et al (1996).

The breccias are very coarse (median diameter -5.98-2.9) and poorly sorted (Fig 4.17). All lithic breccias plot outside the pyroclastic flow field of Walker (1971) and overlap with the field of lag breccias of Walker (1985) and Druitt et al (1996). The stratified facies falls in the fall field of Walker (1971), reflecting its finer grainsize, better sorting and extreme fines depletion.

4.7 Ignimbrite source

Delineating source vents is difficult in TVZ due to tectonic and volcanic overprinting. Source can be constrained by using a number of methods: Maximum lithic size (M_L), anisotropy of magnetic susceptibility (AMS) (e.g. Fisher et al. 1993), clast preferred orientation (e.g. Potter and Oberthal 1987), proximal lag breccia facies (e.g. Wright and Walker 1977, Walker 1985), and key lithic clast types (e.g. Cole et al. submitted). Nairn et al (1994) considered the source of the Kaingaroa Ignimbrite to be Reporoa Caldera, based on the presence of proximal facies lag breccias along the eastern rim, and this is supported by the evidence in this thesis.

$M_L$decreases from 2066 mm at Butchers Boundary Rd quarry to 50 mm eastwards at Maungahekeke Valley. M_L is defined as the average of the long axis diameter of the three largest clasts at any locality. M_L distances refer to distance from the topographic caldera boundary (Fig 4.18).

An interesting feature of M_L distribution is a marked inflection point at ca. 2-4 km (Fig 4.19). Similar inflection points were noted in lithic breccia-ignimbrite transitions by Druitt and Bacon (1986) and intepreted as either an artifact of sampling (i.e. poor exposure at intermediate localities) or marking the transition from the turbulent and expanded collapsing column to the deflating pyroclastic flow. M_L values in the lithic breccia exceed those in the intercalated ignimbrite at the same distance from the caldera rim.

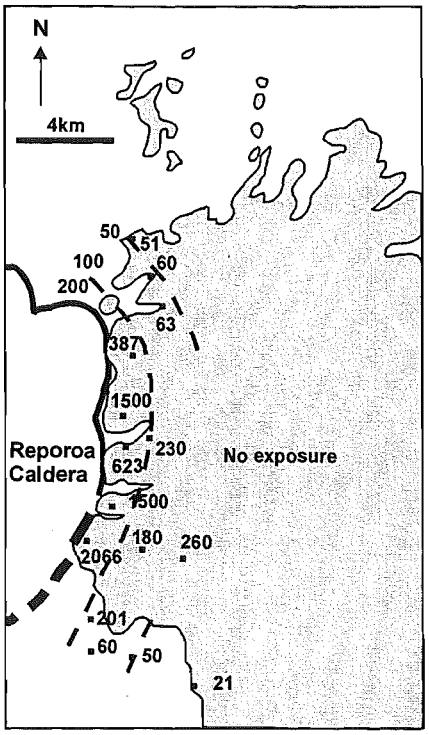

Figure 4.18a. Maximum lithic variation in proximal facies Kaingaroa Ignimbrite (including lithic breccias and intercalated ignimbrite) and lateral equivalent transition zone.

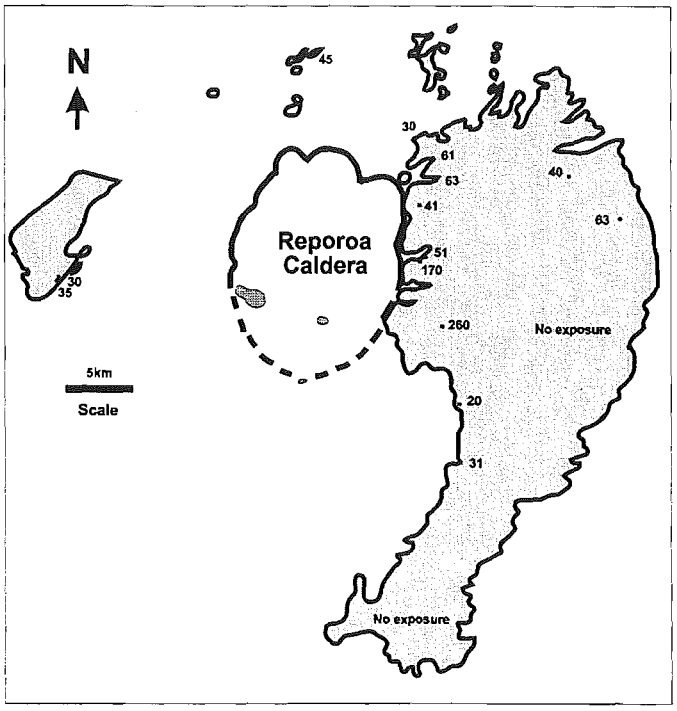

Figure 4.18b. Maximum lithic variation in the Old Waiotapu Rd unit (OWR) suggestive of a Reporoa Caldera source.

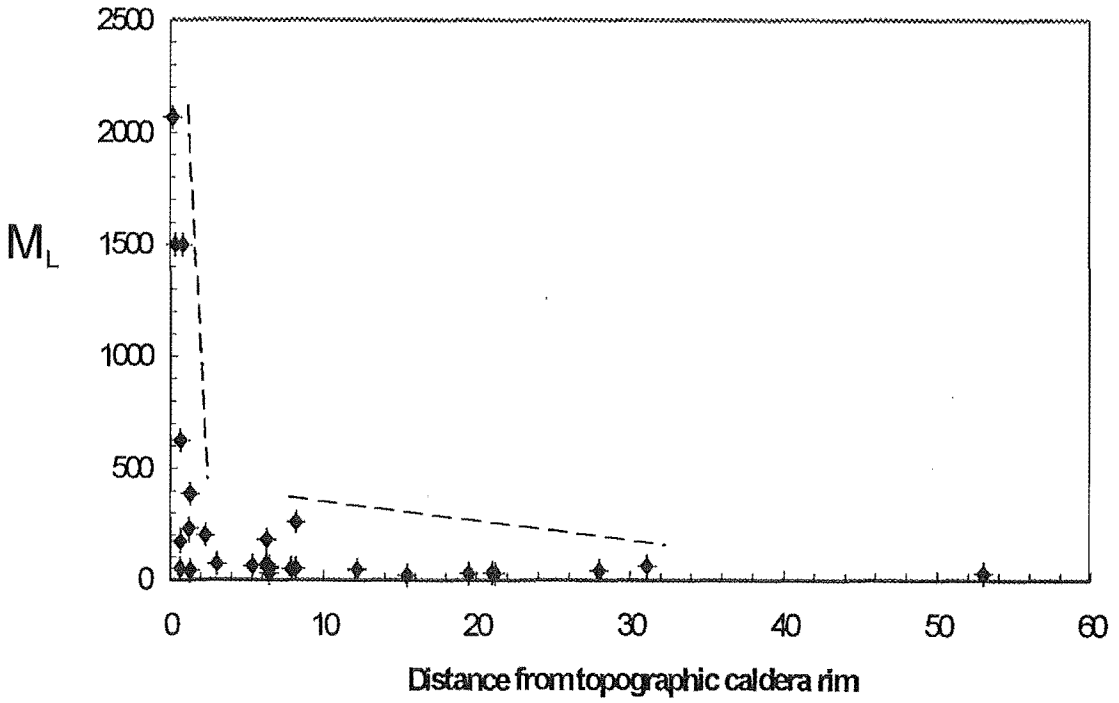

Figure 4.19. Variation in maximum lithic with distance from caldera rim. Note the inflection point and rapid drop in lithic size from the caldera rim.

4.8 Discussion

4.8.1 Pyroclastic flow depositional mechanisms

The subject of ignimbrites has traditionally provoked the debate among geologists, from the early discussions of their origin (e.g. Marshall 1935; Steiner 1960; Smith 1960; Ross and Smith 1961) to models of pyroclastic flow transport and deposition (e.g. Fisher 1966; Sparks 1976; Branney and Kokelaar 1992). Modern debate centres on the mechanisms by which pyroclastic flows travel and eventually become emplaced:

Fisher (1966) proposed that ignimbrites were deposited from turbulent pyroclastic flows. The seminal work of Sparks et al (1973) and Sparks (1976) concluded that many ignimbrites were the product of pyroclastic flows that were emplaced in a manner similar to debris flows (i.e. *en masse*). Sparks (1976) pointed out that many sedimentological features of ignimbrites (poor sorting, reverse grading of pumice, and fine grained basal layers) are similar to those found in deposits from other high-concentration gravity flows e.g. debris flows.

Wilson (1985) recognised complex facies variation in the low-aspect ratio Taupo Ignimbrite. He proposed a model that included different depositional regimes within a moving pyroclastic flow; valley-confined deposits came from the body of the flow (valley ponded ignimbrite; VPI) whereas interaction of the flow tail with topography generated ignimbrite veneer deposits (IVD). IVD are inferred to represent a fraction of the total flow that passes a given depositional site, with incremental or layer by layer deposition.

Branney and Kokelaar (1992) have recently questioned the '*en masse*' emplacement of pyroclastic flows. They propose a model of progressive aggradation from a density stratified pyroclastic flow.

It now appears possible that ignimbrites are generated by a continuum of pyroclastic flows, from highly concentrated plug flows that deposit *en masse* (Palladino and Valentine 1995; analogous to high yield strength mud flows) to high-speed types emplaced under dilute, highly turbulent conditions (analogous to turbidity currents; Druitt 1996). The existing depositional models of pyroclastic flows represent two ends of a spectrum in which ignimbrites are interpreted as either frozen remnants of the moving flow or as fractional parts of the flow as it passed any depositional point. Pyroclastic flows may therefore contain distinct transport and depositional systems (sensu Fisher 1990). In addition the transport and depositional systems may change in a single flow due to variations in flow steadiness and uniformity e.g. interaction with topography and varying eruption conditions (Kneller and Branney 1995; Fisher 1995).

The problem in interpreting mechanism of transport and deposition is that deposits record depositional processes and not necessarily directly the properties of a particulate current. As such ignimbrite characteristics may provide information only about conditions immediately prior to deposition.

4.8.2 Interpretation of proximal facies

Any model for emplacement of Kaingaroa lag breccia needs to account for:

A) Lack of impact sags, basal layer (layer 2a; terminology of Sparks et al. 1973) and ground layer, and presence of scouring of underlying deposits.

B) Unusual lithofacies association, in particular well sorted and stratified facies.

C) Intercalation with lenses of ignimbritic facies.

D) Presence of gas segregation pods and pipes (indicating extreme fluidisation), fumarolically altered matrix, fumarolically altered and breadcrusted lithics (indicating hot emplacement).

E) Presence of poorly indurated lithics (e.g. mudstone, baked soil and tuffs) which would not have survived falling from any appreciable height.

F) Similarities to published descriptions of lag breccias (e.g. Cape Riva, Druitt and Sparks 1982; Crater Lake, Druitt and Bacon 1986).

G) Lateral transition to lithic concentration zones in ignimbrites (lateral equivalent of layer 2bl), and abrupt M_L transition at 2-3 km from the topographic caldera rim. In particular Rawhiti Rd section which is a package of intercalated lithic breccias and lithic-rich ignimbrites with variable grading, and no layer 2a or 3 deposits.

H) Vertical compositional zonation (colour and chemistry) similar to Kaingaroa $Ignimbrite_{s.s.}$.

I) Change in eruption dynamics from energetic eruption and deposition of lag breccia to low energy ignimbrite emplacement (e.g. OWR). Proximal to medial facies variation in apparent eruption energy.

J) Pumice-rich nature of Tokiaminga subunit and upper 'sandy black' facies.

The complex and spatial variation in facies are typical of proximal pyroclastic flow deposits described elsewhere e.g. Druitt and Sparks (1982). Field and granulometric

characteristics are consistent with a co-ignimbrite lag origin and model of Druitt and Bacon (1986).

4.8.3 Constraints on transport and deposition, and implications for proximal ignimbrite emplacement

Evidence of lateral emplacement

The lithic breccias are demonstrably deposited by a flow mechanism. They grade laterally into ignimbrites that thicken into topographic lows and exhibit no impact sags in the underlying units, but scouring of intercalated or underlying ignimbrites is common. The presence of friable and platy lithics suggests gentle emplacement and argues against a direct fall mechanism.

Pumice and lithic abrasion

Flowing particulate systems are inherently grain abrasive. Pyroclasts in ignimbrites undergo attrition in the vent and a second major phase of abrasion during high energy proximal flow (Freundt and Schmincke 1992b) and minimal abrasion during low energy transport. The presence of shattered lithics, sand-sized lithic fragments, well rounded pumices, lack of black fragile highly-vesicular pumices in the lag breccias is a priori evidence of clast attrition during transport. This is consistent with attrition during transport during turbulent proximal high energy flowage. A remarkable feature is the presence of friable, incompetent and platy lithics, which, interestingly suggest surprising gentle emplacement.

Emplacement

The criteria outlined above i.e. coarse lithic-rich nature, extreme fluidisation, presence of incompetent lithics, similar compositional zonation to ignimbrite facies, and intercalation with ignimbrite facies indicates that these lithic breccias are co-ignimbrite lag breccias formed in the proximal turbulent zone (see below).

The structureless nature implies rapid and continuous accumulation in proximal localities. The presence of subtle multiple grading and sorting variations with compositional changes suggest deposition was sustained for some period of time rather than having been virtually instantaneous.

Of particular concern in pyroclastic studies is the discrimination of deposits that represent the product of discrete flows. Stacks of thin flow units have been regarded as problematic because each layer was regarded as recording a discrete single flow (e.g. Sparks 1976). Branney and Kokelaar (1992) suggest a sustained variable current which constitutes just one discrete event can account for these successions i.e. the weak stratification in the proximal facies could reflect continuous streaming of pyroclastic flow(s) rather than a number of flows.

Interaction between flow and fall ?

The stratified lithic breccia lithofacies is enigmatic in that there are no indicators of lateral transport and it exhibits similar grain size to fall deposits (i.e. sorting). In contrast the presence of abraded pumices, small pumices (i.e. not of pneumatolytic equivalence) and sand-sized lithic matrix suggests abrasion during high energy turbulent flowage similar to enclosing lag breccias. The presence of the fumarolic altered matrix and pumice suggests the unit is primary i.e. not alluvial or colluvial.

Erosive capability of the pyroclastic flows

Pyroclastic flows are known to be erosive in near-vent situations (Druitt and Bacon 1986; Fierstein and Hildreth 1992). The proximal facies of the Kaingaroa Ignimbrite is locally partly channelised into its own deposits e.g. scouring of lithic breccias into underlying RBU at No 6 Rd, and into intercalated BTI at No 3 Rd; scouring of transition zone into underlying RBU at Maungahekeke Valley. The lithic breccias appear to fill broad channels in the underlying ignimbrite, scoured by the lithic-rich flows that deposited the lag breccias. These erosional channels are infilled with the overlying unit. The presence of scours is additional evidence of the turbulent nature of the proximal zone.

The turbulence that produces scouring cannot be topographically induced, as described for other energetic proximal flows or proximal veneer deposits (Roobol et al 1987, Fierstein and Hildreth 1992, Cole et al. 1993). Turbulence is inherent in eruptive dynamics of proximal facies.

Origin of welded lithic breccias

Welding is rarely described in lithic breccias associated with ignimbrites due to the cooling effect of incorporation of lithics (Eichelberger and Koch 1979). Druitt et al (1996) describes thick lens of welded ignimbrite within Cape Riva lithic breccias on Santorini. They cite this as evidence that both facies were generated contemporaneously.

Deflation zone or proximal turbulent zone concept

Several lines of evidence suggest that the proximal zone of pyroclastic flows is a turbulent, high energy, highly fluidised environment inherent in pyroclastic flow generation. Walker (1985) termed this area the deflation zone. Because of the role of deflation in pyroclastic flow deposition (Branney and Kokelaar 1992) the term deflation zone is replaced by 'proximal turbulent zone' in this thesis.

The incoming (in a vertical section) of lag breccia marks an abrupt change in lithic content and diversity of lithic types both laterally and vertically and therefore signals a fundamental change in eruptive dynamics e.g. vent multiplicity, widening, reaming of lithics from the conduit and vent, and evisceration and syn-eruptive mingling of diverse pumice types, thought to represent caldera collapse.

The presence of intercalated ignimbrites, e.g. BTI, within the proximal facies argues for minor variations in eruptive dynamics i.e. waning of the eruption or hiatus or fluctuation in eruptive vigour. The transition from yellow to black pumice occurs at this stratigraphic interval and is thought to mark a fundamental change in composition, possible reflecting a change in oxygen fugacity.

The rapid transition from thick lithic breccias to ignimbrite and corresponding drop off in M_L variation is thought to represent evidence of this proximal turbulent zone.

Extreme variations in paleotopography are suggested by rolling landscape in Rawhite Rd-Deep Creek Rd area, inferred basin in Rangitaiki ignimbrite adjacent to the eastern caldera margin suggested by the presence of dry valleys, and thickness variations (Chapter 2). The rapid drop off in M_L and transition from proximal facies lithic breccias

to ignimbrite occurs within this basin, which suggests the drop off is eruption dynamics related.

The presence of intercalated ignimbrites is considerd to be due to variation in eruptive power and resultant width of the proximal turbulent zone. e.g. any given near-vent site may at times lie outside the zone and other time lie inside it. When it lies outside ignimbrite will be deposited; when it lies inside a lithic breccia will be deposited instead, providing that coarse dense ejecta are available. Thus the alternation of ignimbrite and lithic breccia records the variation in width of the proximal turbulent zone, reflecting variation in eruptive vigour and discharge rate.

Proximal to medial transition in flow energy

The contrasting proximal and medial facies is thought to reflect variation in fluidisation and flow steadiness due to variations in paleotopography and processes inherent to column collapse dynamics. Medial facies deposits are inferred to have been deposited on flat topography (smoothed by preceding RBU eruptives).

CHAPTER FIVE

Lithic component analysis

5.1 Introduction

During pyroclastic eruptions, lithic fragments may be incorporated into the magma from the vent walls, the lower conduit walls, even from the environs of the magma chamber, and brought rapidly to the surface.

Three types of lithic fragments commonly occur in large scale ignimbrites:
1) Wall rock (or accessory) lithics: Fragments of country rock dislodged from the vent, conduit walls, and magma chamber walls during explosive eruptions.
2) Accidental or incorporated lithics: Fragments eroded or collected from the substrate by pyroclastic flows.
3) Cognate lithics: Juvenile fragments derived from solidified parts of the erupting magma.

Detailed studies of lithic fragments can provide information on eruptive and depositional processes (e.g. Suzuki-Kamata 1988, Buesch 1992), vent evolution (e.g. Hildreth and Mahood 1986; Suzuki-Kamata et al. 1993; Wilson and Hildreth in press), sub-caldera geology (e.g. Suzuki-Kamata et al. 1993; Cole et al. submitted), the nature of the subvolcanic basement (Eichelberger and Koch 1979), nature of magma:hydrothermal interface (Wood 1994c), and the nature of thermal metamorphic and pyrometamorphic processes (Wood 1994c; Wood and Browne 1996).

Most lithic fragments observed in TVZ ignimbrites are rhyolite and andesite lavas, welded ignimbrites, and volcaniclastic sediments, reflecting the great thickness of Quaternary volcanic fill in central TVZ and the relatively shallow depths from which vent-derived lithics are being excavated during caldera-forming eruptions. A small but significant proportion of the lithics are plutonic and metamorphic rocks derived from deeper crustal levels. Ewart and Cole (1967) and Brown et al (1995; submitted) reported numerous granitoid and dolerite lithics, and concluded they represent the cognate equivalents of TVZ rhyolites and high alumina basalts. In the Ngatamariki geothermal

drill holes an altered quartz-diorite was drilled to 2200m (Browne et al. 1992). Other reported intermediate-basic plutonic lithics/xenoliths have been reported from andesitic centres and include gabbros and diorites (e.g. Burt et al. 1996); interpreted as subvolcanic equivalents of TVZ andesitic eruptives.

Lithic fragments range in size from <1mm to 4.5 m in diameter, and in density from <1.61 (g/cm^3) for friable tuffs to 2.80 (g/cm^3) for andesites and 'greywacke'. Lithics in the Kaingaroa Ignimbrite are predominantly accessory (wall rock) derived from the vent or conduit.

5.2 Lithic component analysis methodology

Evolution of vent geometry can be deduced by quantitative component analysis of lithic fragments in large scale ignimbrites. The method depends on recognising distinct groups of lithic fragments in the ignimbrite and being able to relate them to stratigraphic position, geographic location, or depth of origin (lithic provenance). Similar methods have been applied by Hildreth and Mahood (1986), Suzuki-Kamata et al (1993), Rosi et al (1996), and Lee (1996) to deduce vent evolution (migration) and assess sub-caldera geology.

The methodology of lithic componentry comprises:

A) Recognising lithic types, and relating them to geographic location, stratigraphic position or depth of lithic provenance, in order to assess vent evolution and change in depth of lithic provenance (combined with whole pumice chemistry; Chapter 7) during the Kaingaroa Ignimbrite eruption.

B) Brief petrography and geochemistry of lithic lithotypes, for purposes of correlation and characterisation, and to ascertain sub-caldera geology or stratigraphy, in particular the nature of the sub-volcanic basement.

The aim of this chapter is to introduce the methodology and data, Chapter 6 describes the petrology of lithics, and Chapter 9 discusses combined interpretation of lithic componentry and whole pumice geochemical data in a combined eruptive model.

Approximately 23 000 lithics were collected from locations along the caldera rim at variable azimuthal intervals controlled by the limited exposure. In addition lithics were sampled at numerous medial sections to further characterise lithic distribution in azimuthally poorly controlled areas, and to test for incorporation of lithics by pyroclastic flows. Figs 5.1-5.4 illustrate proximal variations in lithic types, and Appendix B presents lithic componentry data excluding lithic counts from welded medial sections.

Lithic fragments in the basal tephras were collected from three locations (Fig 5.1); in the Reporoa boundary unit (RBU) at 4 (Fig 5.2, 5.3), in the lag breccia and OWR unit at 18 (Fig 5.4), and upper Webb unit (WIU) at 12 localities. To check for vertical variation in lithic componentry in the basal tephras, samples were taken from 6 horizons on Riehana Rd (Fig 5.3), and to check for vertical variation in lag breccia, samples were taken from 8 horizons on Burn Rd (Fig 5.4).

Proportions of lithic clast types at each site were determined by counting the number of clasts in each category, as opposed to determining weight proportions (e.g Chernet 1987). One hundred lithic fragments >30 mm diameter were sampled at each site from the basal tephras and RBU, two hundred lithic fragments > 30 mm within the transition zone, OWR and WIU units and four hundred lithic fragments, >50 mm, from each facies variation of the lag breccia. The larger number of samples studied in the lag breccia was due to the heterogenous nature of lithotypes (revealed by reconnaissance lithic analysis), size of lithics, and exposure.

Sampling method follows Howard (1993), and is broadly similar to that employed by Suzuki-Kamata et al (1993). The technique involved counting each individual clast greater than a lower clast size (eg >50 mm in lag breccia), within a 2 m by 1 m area until the sample size was obtained (eg n = 400 in lag breccia). In order to test reproducibility random samples of lithic fragments were taken from stratigraphically equivalent sites (commonly 2 m apart), and compared.

Identification of subtle differences in volcanic lithology beyond grouping lithics into more readily discriminated types, such as granitic, sedimentary and metamorphic rocks (as is commonly the case in classical glacial or alluvial sedimentological studies) poses

a major challenge. As a result reconnaissance study of lithic types was undertaken in May 1993, together with visiting units present within the Reporoa Caldera area. This was to gain appreciation of the regional geology and to understand facies variations, so common in areas of abundant vertical and lateral variations in geology such as central TVZ. Reference samples were studied petrographically and brief geochemistry was undertaken to characterise lithologies. Reference samples were also compared with thesis collections of ignimbrites and lithic fragments (e.g. Keall 1988).

Samples were washed and broken open to reveal fresh faces, then examined with a hand lens and/or binocular microscope. The number of plagioclase-pyroxene-phyric andesite (PPA) and Waiotapu Ignimbrite (WAI), were tallied because they were easy to recognise, and the remainder of samples were taken back to the lab. Thin sections were made when classification by hand lens examination was difficult. Samples were split into variations, and after original examination divided into 18 types. Original categories included all recognisable lithologic variations. It was soon recognised that the data were divided into too many lithotype variations. Samples from stratigraphically equivalent units were grouped, e.g. Rangitaiki, Paeroa and Te Kopia were added together to form WHAK (Whakamaru-group ignimbrites).

The 18 lithic types consist of 12 varieties of volcanic rocks; 3 sedimentary, 1 plutonic or subvolcanic, and 2 low-grade metamorphic rocks. Categories were compared with the stratigraphy established in Chapter 2, including general geology of Reporoa region, and the Waiotapu drill holes.

5.3 Lithic entrainment assumptions

Different rock types have inherently different capacities to form gravel-sized fragments, and particles can be selectively destroyed. In addition clasts maybe recycled from conglomerates, ignimbrites or lag breccias. The major factor in influencing lithic selection is abrasion during entrainment and transport. Pyroclastic flows selectively abrade lithics, leaving resistant lithologies, as is commonly reported in glacial and alluvial gravel componentry (e.g. Abbott and Peterson 1978). In addition the ignimbrite may have incorporated lithics from the substrate during the passage of the flow. By

studying proximal facies, these effects were minimised in this study, although selective abrasion cannot be ruled out with friable lithologies.

Assumptions made in lithic componentry analysis are that conduits remain near vertical and that units are not preferentially selected i.e. abrading of least resistant clasts.

5.4 Uncertainites

There are numerous uncertainities associated with any attempt at quantitative study of lithic componentry. Some of these uncertainites require assumptions, others adaptation of the method of sampling to reduce bias or increase precision. A 'counting of clasts' method was chosen in preference to 'weight %' method because:

1. It avoids problems with mechanical sample collection, splitting and sieving.
2. Volume % is dependant on particle size. Larger clasts are more likely to be counted than smaller ones.
3. Practical identification requires a minimum clast size and the lag breccia contains exceptionally large clast sizes.
4. The method is easier to apply, especially in detailed studies and in welded ignimbrites.
5. Granulometric methods are weak at large grain sizes.

Assumptions made are:

1. That the stratigraphy established in Chapter 2 is representative of the Reporoa Caldera area.
2. Error associated with clast identification is negligible (Perfect accuracy is impossible even if every clast was thin sectioned. The error is reduced by reconnaissance analysis and thin sections of uncertain samples).
3. Minimum clast size chosen doesn't exclude a lithic type preferentially comminuted to a smaller clast size.

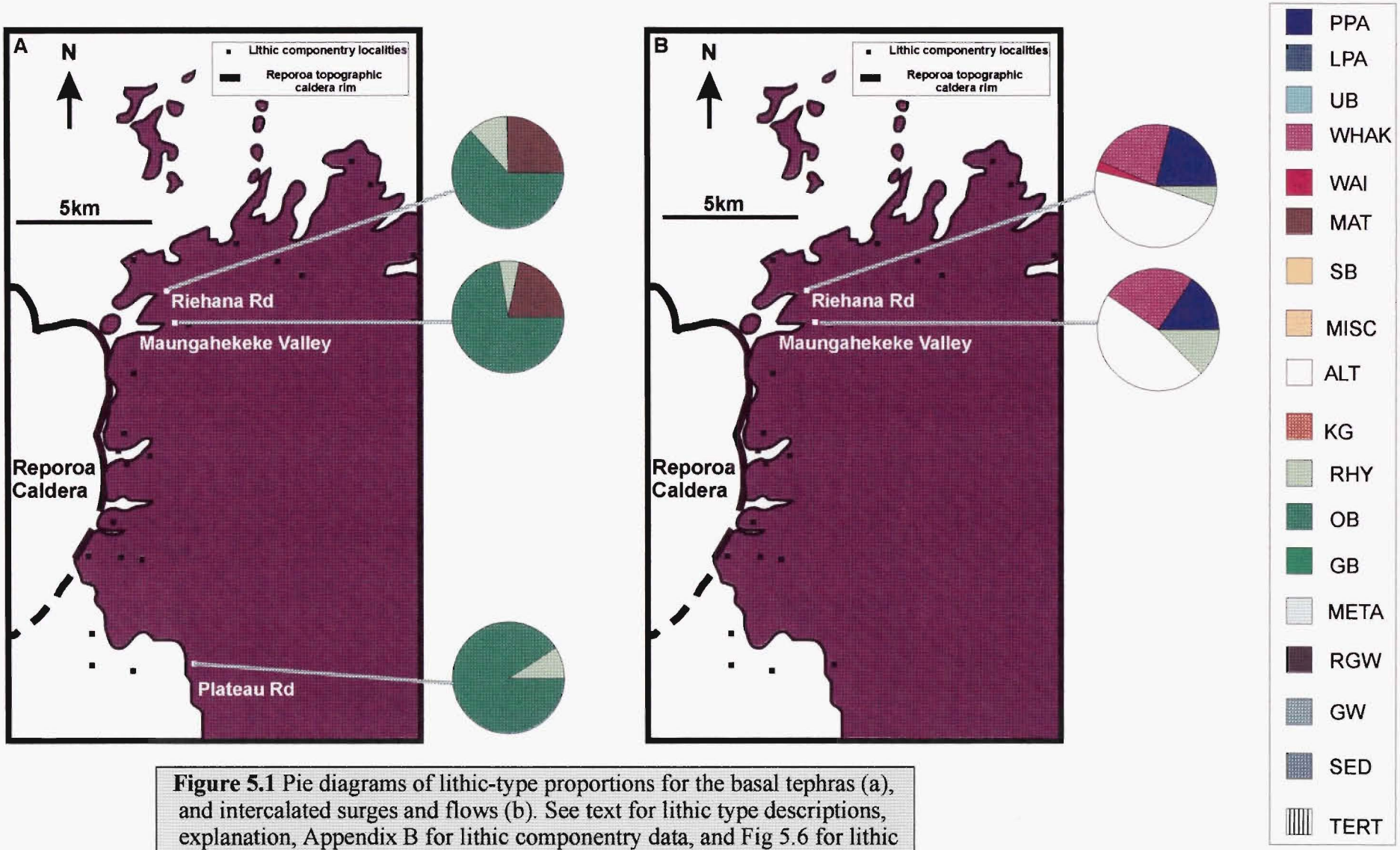

Figure 5.1 Pie diagrams of lithic-type proportions for the basal tephras (a), and intercalated surges and flows (b). See text for lithic type descriptions, explanation, Appendix B for lithic componentry data, and Fig 5.6 for lithic distribution summary. Pre-Kaingaroa geology is summarized in Fig 2.6.

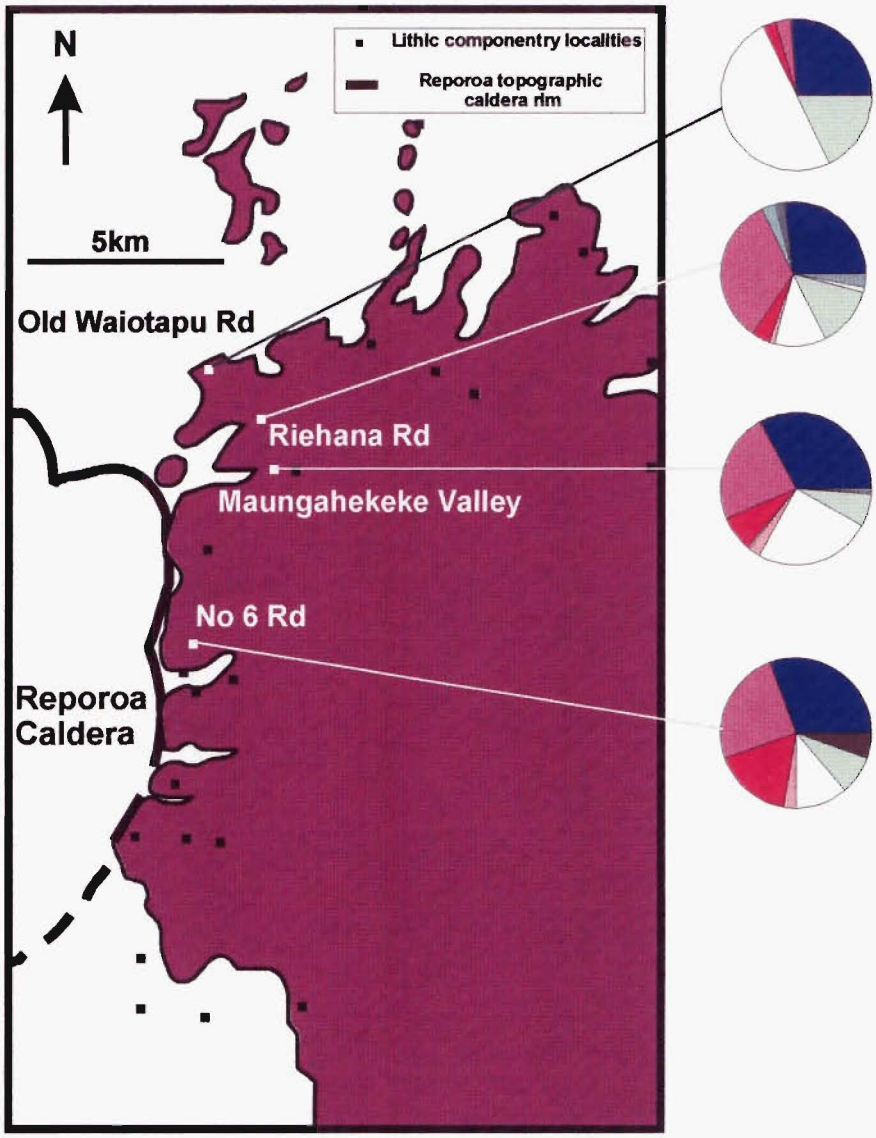

Figure 5.2 Pie diagrams of lithic-type distribution for Reporoa Boundary unit (RBU). Symbols as in Fig 5.1.

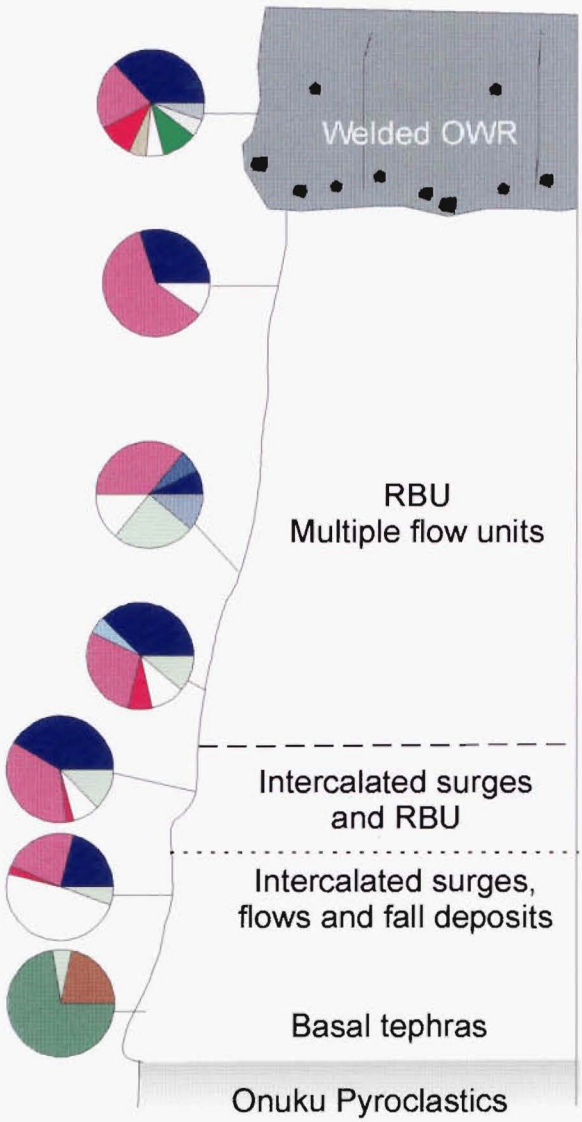

Figure 5.3 Pie diagrams of lithic-type distribution for horizons within the basal tephras, Reporoa Boundary ignimbrite unit (RBU), and Old Waiotapu Rd ignimbrite unit (OWR) at Riehana Rd. See Figure 5.1 for definition of abbreviations and symbols.

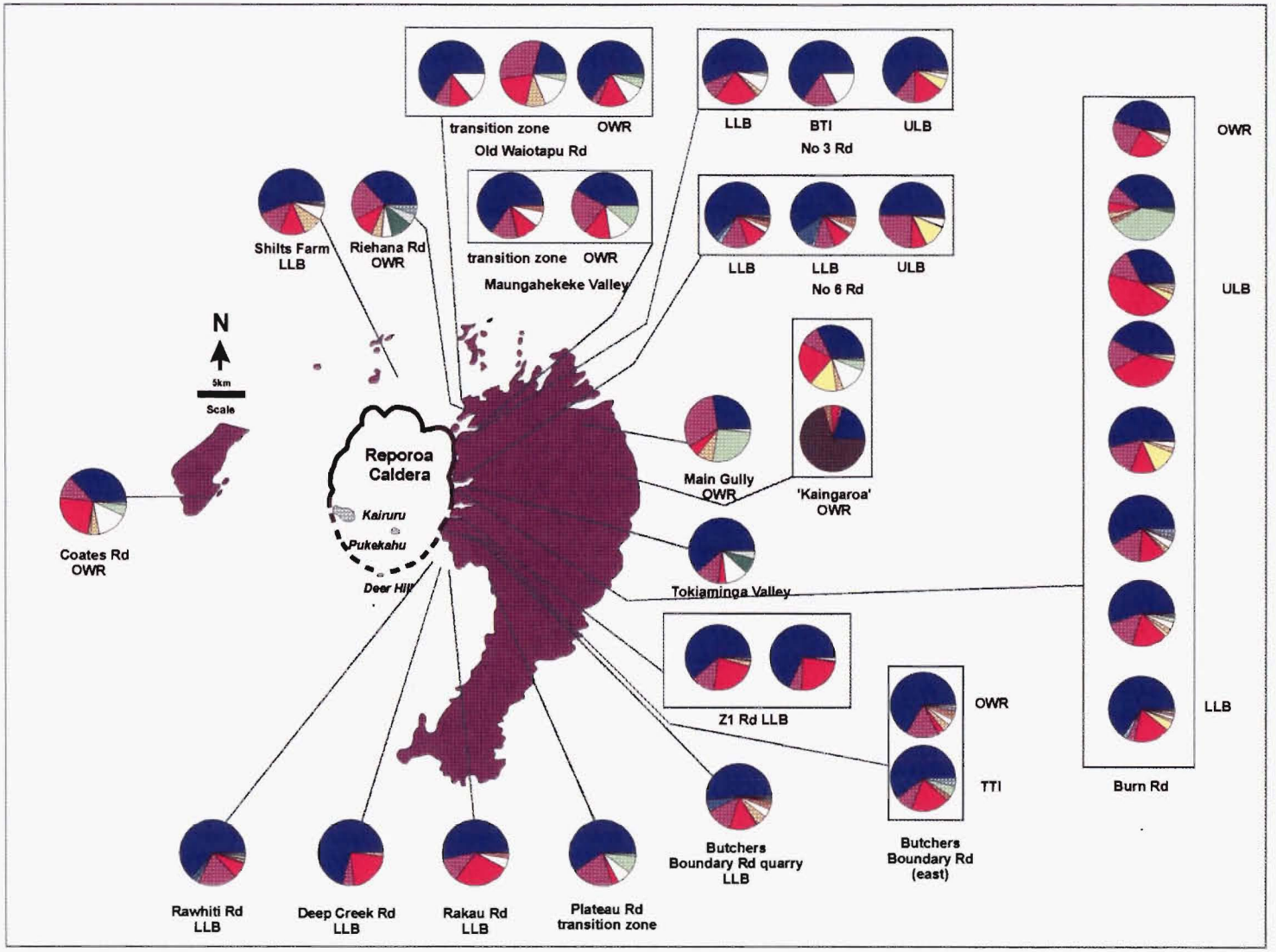

Figure 5.4 Lithic componetry variation in lag breccia, transition zone and OWR deposits. An enlargement of this diagram is presented in the map pocket.

5.5 Description and occurrence of lithic types

The description and distribution of the 18 types of lithic fragments are described below. Detailed petrography and geochemistry is presented in Chapter 6.

5.5.1 Andesites

Lithic types in the Kaingaroa Ignimbrite are dominated by andesite:

Type 1: Plagioclase-pyroxene-phyric (PPA); grey to green phenocryst-rich basaltic andesites and andesites. Plagioclase is the dominant phenocryst phase with subordinate orthopyroxene and augite. PPA is the dominant lithic component in the Kaingaroa Ignimbrite, and is ubiquitous at all sections in the RBU, lag breccia, OWR and WIU. PPA is locally present in the basal tephras in surges and flows, and shows weak azimuthal variation in abundance around the caldera, which may reflect thickness variations. Similar material to PPA was encountered in the Waiotapu drill holes (Ngakoro Andesite; Hedenquist 1983). Nairn et al (1994) correlated andesite lithics in the Kaingaroa Ignimbrite with the Ngakoro Andesite, a package of plagioclase-phyric andesite lavas present in the Waiotapu drill holes underlying the 0.7 Ma Waiotapu Ignimbrite, and suggested that the andesite lithics represent a sampling of a subcaldera andesite stratovolcano that thins to the north. Included in this group are rare microdiorites. Soengkono and Hochstein (1996) suggested that a reversely magnetised andesite body is present to the north and east of Reporoa Caldera (Chapter 2). This rock body is correlated with reversely magnetised rocks beneath Reporoa Caldera, dominantly the pre-0.7 Ma PPA andesite volcano and its lateral equivalent Ngakoro Andesite.

Type 2: Large pyroxene-phyric andesite (LPA); green-coloured andesite with large pyroxene phenocrysts up to 5 mm in length. LPA is found in RBU and the lag breccia and OWR unit in south-eastern and eastern localities. No similar material outcrops or is present in drill holes surrounding Reporoa Caldera. The unit is inferred to represent a localised dome or series of lava flows submerged beneath Reporoa Caldera. Included in this group are rare light-green augite-quartz-plagioclase-orthopyroxene-phyric dacites

(Chapter 6). The green dacites have similar distribution suggesting similar pre-eruptive distribution.

Type 3: Uralitised basaltic andesites (UB) have abundant plagioclase and augite phenocrysts, with variable contents of uralitised pyroxene phenocrysts in an altered matrix. The unit is a distinctive green colour, but broadly resembles an altered version of PPA. UB is rarely present in RBU and the lag breccia and OWR units, along the eastern margin of Reporoa Caldera, with a restricted sectorial or lobe-like distribution that may reflect a tracer unit for point source or lobe emplacement or variable depth of fragmentation, or variable provenance thickness (see below). The mafic nature of the unit (high Cr and Ni; Chapter 6) and dissimilar alteration may represent altered less evolved equivalents of PPA or separate possibly older andesite eruptives. UB exhibits similar alteration style to gabbroic lithics, suggesting pre-eruption spatial association. UB is a useful indicator of deep lithic provenance. Included in this group are a rare group of altered augite-phyric phenocryst-poor dacites present only in south-eastern localities.

5.5.2 Welded ignimbrites

Welded ignimbrites make up the majority of the remainder of lithic types and include:

Type 4: Whakamaru-group ignimbrites (WHAK) including the grey-white-pink crystal-rich quartzose 0.34-0.32 Ma Rangitaiki, Te Whaiti and Paeroa ignimbrites, and the black-brown crystal-rich Te Kopia Ignimbrite. WHAK occurs commonly in the OWR, WIU and lag breccia, and is a dominant component in the RBU and basal tephra surges and flows. WHAK is locally present as incorporated lithics picked up from the underlying substrate (e.g. RBU at Maungahekeke Valley). Whakamaru-group ignimbrites outcrop extensively around Reporoa Caldera. Distribution of Whakamaru-group ignimbrites is antithetic e.g. Te Kopia and Paeroa, and Rangitaiki ignimbrites do not outcrop in the same section, and their distributions are limited to the west and east of Reporoa Caldera. Te Kopia, Paeroa and Rangitaiki ignimbrite lithics are commonly present together in the Kaingaroa Ignimbrite, suggesting extensive pre-Kaingaroa distribution. Variation in these three components within Kaingaroa eruptives is interpreted to reflect variations in depth of lithic provenance (see below).

Type 5: Waiotapu Ignimbrite (WAI) is a purple-grey, crystal-poor, densely-welded lenticulite which occurs in OWR, WIU and lag breccia units. WAI is a minor component in basal tephras surges and early RBU flow units, and displays strong azimuthal variation around Reporoa Caldera in OWR, WIU, and lag breccia units, which is inferred to represent thickness variations probably related to a complex pre-Waiotapu paleotopography (c.f. Ritchie 1996). WAI is present above PPA in the Waiotapu drill holes, and also outcrops in the north-west of Reporoa Caldera along the Ngapouri Ridge. WAI is inferred to have ponded against the Kaingaroa Fault and be absent to the east of Reporoa Caldera.

Type 6: Matahina Ignimbrite (MAT) is a pink welded crystal-poor obsidian lithic-rich hornblende-bearing ignimbrite, that is a common lithic component in the basal tephras, and a very rare component in the lag breccia. MAT is correlated with the 0.28 Ma Matahina Ignimbrite that outcrops to the west and east of Reporoa Caldera. The unit forms the upper ignimbrite in the pre-Kaingaroa stratigraphy and is conspicuous by its absence (or limited percentage) in most units of the Kaingaroa Ignimbrite.

Type 7: Miscellaneous 'sandy black' (SB) ignimbrites including distinctive black to grey crystal-poor partially welded ignimbrites that resemble each other in hand specimen. SB includes at least 4 distinct ignimbrites which include a grey 'salt n pepper' crystal-poor altered ignimbrite correlated with unit A, an ignimbrite that outcrops to the northwest of Reporoa Caldera, underlying Waiotapu Ignimbrite, and Unit X (which contains clasts of Akatarewa A ignimbrite). A similar unit termed Akatarewa A was encountered in the Waiotapu drill holes. Other varieties include rhyolite-lithic-rich, and crystal and pumice-rich black partially-welded vitric varieties. Both units have no identified correlatives in the Reporoa area. The most abundant and conspicuous lithic type is a crystal-poor grey partially-welded vitric ignimbrite, with abundant andesite lithics, which is only present within the upper lag breccia. The unit resembles the OWR ignimbrite unit. All sandy black ignimbrite lithics are restricted to the lag breccia, their absence in ignimbrite units, possibly a function of disaggregation and comminution during transport and deposition. The incoming of this lithic type is illustrated in Fig 5.6, marked by a dramatic increase in SB above the middle lag breccia or BTI unit. Type 4 SB is believed to be derived from BTI.

Type 8: Miscellaneous welded ignimbrites (MISC) include at least two units that have no identified correlatives, and may represent pre-Waiotapu ignimbrites represented in the Waiotapu drill holes, or units present within the 'hotch potch' Waiora Formation. The degree of alteration within the drill cores, and limited previous work on the Waiora Formation limits further correlation. The abundance of Type A ignimbrites in northern localities e.g. Shilts Farm is consistent with the presence of pre-Waiotapu ignimbrites near the surface in northern Reporoa Caldera.

Type 9: Altered ignimbrites/rhyolites (ALT) include all rhyolite-looking lithics that are altered beyond confident identification and correlation. The alteration state is variable, ranging from yellow, ochre or red friable lithologies to indurated hematitic-stained or clay-rich ignimbritic units. This category is not considered to represent a particular unit, or represent increasing depth of lithic provenance, but rather variable alteration due to either pre- or post-eruption fumarolic or hydrothermal alteration. ALT is a common component in the basal tephra surges and flows, and the Reporoa boundary unit, and is here interpreted to represent samples from a localised shallow hydrothermal system.

Type 10: Kaingaroa-like (KG) consists of partially to densely welded, locally vitrophyric lithic-rich ignimbrites with similar lithic content, mineralogy, and geochemistry to Kaingaroa Ignimbrite. KG is present only in the lag breccia and OWR units in southeastern localities, and does not correlate with known ignimbrites and is interpreted as earlier Kaingaroa Ignimbrite (welded proximal Reporoa Boundary unit) incorporated during caldera collapse.

5.5.3 Rhyolites

Type 11: Miscellaneous rhyolites (RHY) including four dominant rhyolites: 1) Crystal-rich rhyolite petrographically similar to Trig 8566. This unit is found in all units at numerous localities suggesting more extensive distribution of Trig 8566-type rhyolites. The presence of crystal-rich rhyolite lithics at northern sites is consistent with the presence of a crystal-rich rhyolite at Trig 8566. 2) Crystal-poor obsidian/rhyolite with similar mineralogy to Kaingaroa Ignimbrite, which was found only at Butchers Boundary Rd Quarry and eastern localities. Rare samples were sampled in RBU at the eastern localities. This unit is inferred to represent a precursor rhyolite "leaked" from

the Kaingaroa magma system. 3) Mafic inclusion-bearing crystal-rich rhyodacite, which were sampled only at Butchers Boundary Rd Quarry. 4) Weakly altered crystal-poor quartz-free rhyolites.

Type 12: Juvenile Kaingaroa obsidian (OB) is black to grey rhyodacitic obsidian, which exhibits similar mineralogy and chemistry (Chapter 7). OB is present only in the basal tephras, and is interpreted to represent dense juvenile component within the Kaingaroa magma system.

5.5.4 Plutonics

Plutonics in the Kaingaroa Ignimbrite are dominated by a suite of gabbros.

Type 13: Gabbro (GB), which include a suite of leuco-gabbros, dolerites, gabbroic porphyries and altered gabbros. GB is not exposed around Reporoa Caldera, and is a unique lithology in TVZ ignimbrites. GB exhibits similar mineralogy, notably pyroxene Fe/Mg ratios consistent with derivation from basaltic andesite liquids, and is considered the subvolcanic equivalent of UB. GB is restricted to the lag breccia, OWR, and WIU along the eastern margin of Reporoa Caldera. The presence of GB is considered a useful index of deep lithic provenance. Many of the blocks contain amorphous aluminosilicate replacement of plagioclase cores, related to low-temperature fumarolic activity or chemical weathering. A single granophyre was sampled during reconnaissance field work (Chapter 6) but was not sampled during lithic componentry.

5.5.5 Metavolcanics/hornfels

Type 14: Metavolcanic lithics (META) include a suite of epidote-zoisite-titanite-andalusite-bearing meta-rhyolites, tourmaline-bearing meta-rhyolites and tourmalinite. The lithics are considered to represent a variable suite of rhyolites that have been variably metasomatised adjacent to the Kaingaroa magma system. META is rare in the lag breccia and OWR unit, and relatively common in the Webb unit (WIU). Intensely altered rocks such as META do not outcrop in the Reporoa Caldera area or TVZ, but have been noted as lithics in other large scale ignimbrites in the TVZ (personal

observation). META occur as lithics within juvenile pumices suggesting deep entrainment from the magma fragmentation level.

5.5.6 Gravels

Type 15: Rounded greywacke lithics (RGW) include well rounded, very well indurated greywacke, and intact 'greywacke' conglomerate lithics which occur in the lag breccia, OWR and WIU units. RGW are correlated with greywacke-dominated gravels commonly observed underlying Matahina Ignimbrite northwest of Reporoa Caldera (Lukes Farm Formation; Bailey and Carr 1994), underlying Kaingaroa Ignimbrite in Murupara drill holes, and intersected in Broadlands drill hole (Waikora Formation; Browne 1971). RGW is interpreted either as deep seated greywacke-dominated gravels, underlying Reporoa Caldera, or in medial localities as incorporated lithics picked up locally from streams on the Kaingaroa Plateau.

5.5.7 Greywacke

Type 16: "Greywacke" (GW) lithics are angular well indurated group of low-grade metasediments that include 'greywacke and argillite', hornfels, jasper, and sub-greenschist facies slates. The unit exhibits similar provenance petrography and geochemistry to Torlesse terrane metasedimentary basement that outcrops extensively in the ranges to the east of TVZ, and in scattered drill holes and outliers to the north, south and west of Reporoa Caldera. The unit is interpreted to represent the basement of the Reporoa area. GW is present only in the lag breccia, OWR and WIU.

5.5.8 Sediments

Type 17: Sediments (SED) includes sedimentary rocks and non-welded tuffs, baked soil, and other unconsolidated material of volcanogenic or associated origin (e.g. diatomite). SED occurs exclusively in proximal exposures of the lag breccia, their limited presence in other units is controlled by comminution processes rather than reflecting the nature of the source. Diatomites and mudstones are correlated with lacustrine sediments, which common outcrop intermittently throughout TVZ. The Reporoa area exhibits evidence of basinal topography and lacustrine sedimentation

intermittently throughout its geological and recent history. Lacustrine sediments are commonly interbedded with large-scale welded ignimbrites.

Non-welded tuffs are variable in mineralogy, and alteration. Many are crystal-poor and are tentatively correlated with the Waiora Formation which outcrops to the west of Reporoa Caldera, which is inferred to underlie Reporoa Caldera, and the Kaingaroa Plateau. Baked soil is a conspicuous lithic present at Butchers Boundary Rd Quarry.

Type 18: Tertiary sediments (TERT) form rare lithic components in the lag breccia. They are distinguished from SED, based on induration and non-volcanic components. Carbonaceous mudstones and rare sandstones are correlated with Tertiary sediments which unconformably overlie Waipapa and Torlesse basement to the west and east of TVZ, and inferred to underlie at least the western and eastern margins of TVZ. The lack of TERT in OWR and WIU is inferred to be due to disaggregation during transport and deposition.

5.6 Lithic componentry synopsis (Fig 5.5)

The main aim of lithic componentry was to correlate lithic types with pre-caldera units exposed in the caldera walls and to determine depth of lithic provenance (i.e. the inferred depth of source of the lithic lithology). The objective of the lithic componentry study was, using variation in lithic components and depth of lithic provenance, to asceratin aspects of vent evolution during the Kaingaroa Ignimbrite eruption.

5.6.1 Onset of eruption, basal tephras, and transition to Reporoa Boundary unit phase

Basal tephra lithics are of two broad types; accessory i.e. rhyolite and cognate i.e. dense juvenile obsidian. Many of the intercalated fall and surge horizons contain lithic assemblages dominated by accessory lithologies, with a trace of juvenile obsidian, whereas some units are dominated by purely juvenile obsidian; this is interpreted to represent variation between open vent activity, in which the magma is vesiculating to form pumice, and the conduit walls are exposed and eroded, and closed vent activity, in which magma-water interaction occurs through fragmenting lava (Wilson 1993b).

Wilson (1993b) describes similar variation in vent activity at Taupo 'volcano', and concludes that there is a correlation between eruption size and the lithic assemblage; a similar situation exists within the basal tephras of the Kaingaroa eruption, where smaller magnitude deposits are dominated by juvenile obsidian, whereas larger fall, surge, and flow deposits are dominated by accessory lithics, interpreted to reflect variable magma:water ratio during basal tephra eruption.

The earliest Kaingaroa eruptives contain an accessory lithic assemblage dominated by precursor rhyolites, weakly altered rhyolites of unknown provenance and Matahina Ignimbrite. These lithologies are interpreted as shallow derived volcanic rock types. The uniform proportions of lithic fragments at different sites suggests eruption from a single vent. Surges and flow deposits within the upper parts of the basal tephras mark the incoming of andesite (PPA) and Whakamaru-group ignimbrites (WHAK), dominantly the Rangitaiki Ignimbrite, and only limited evidence of magma: water interaction (limited juvenile obsidian, homogenous pumice types, accretionary lapilli are limited or absence, and coarse pumiceous grain size; contrasting the fine-grained nature of underlying deposits). The different rock types in the upper part of the basal tephras could reflect vent migration i.e. opening of a new vent, or vent flaring and deepening. The intercalation of fall, surge and flow deposits suggests no time interval break between the basal tephras and RBU. Vertical variation in lithic types within the basal tephras and overlying RBU is illustrated in Fig 5.3.

The RBU contains similar lithic types to the underlying basal tephras, consistent with eruption from the same vent. Later RBU flows contain Te Kopia and Waiotapu ignimbrite lithics (older and deeper units within the pre-Kaingaroa stratigraphy; see Chapter 2), and an increased andesite: Rangitaiki Ignimbrite ratio suggest deepening of lithic provenance as the RBU phase of the Kaingaroa eruption continued. At certain medial localities large and abundant Rangitaiki Ignimbrite and rounded greywacke lithics suggest possibility of localised incorporation of underlying substrate by the RBU pyroclastic flows. Similar lithic types within RBU (c.f. basal tephras) is consistent with a similar source vent. The location of this vent is not possible due to limited M_L data, and/or lack of distinctive tracer lithic lithologies, (c.f. Hildreth and Mahood 1986; Wilson and Hildreth in press).

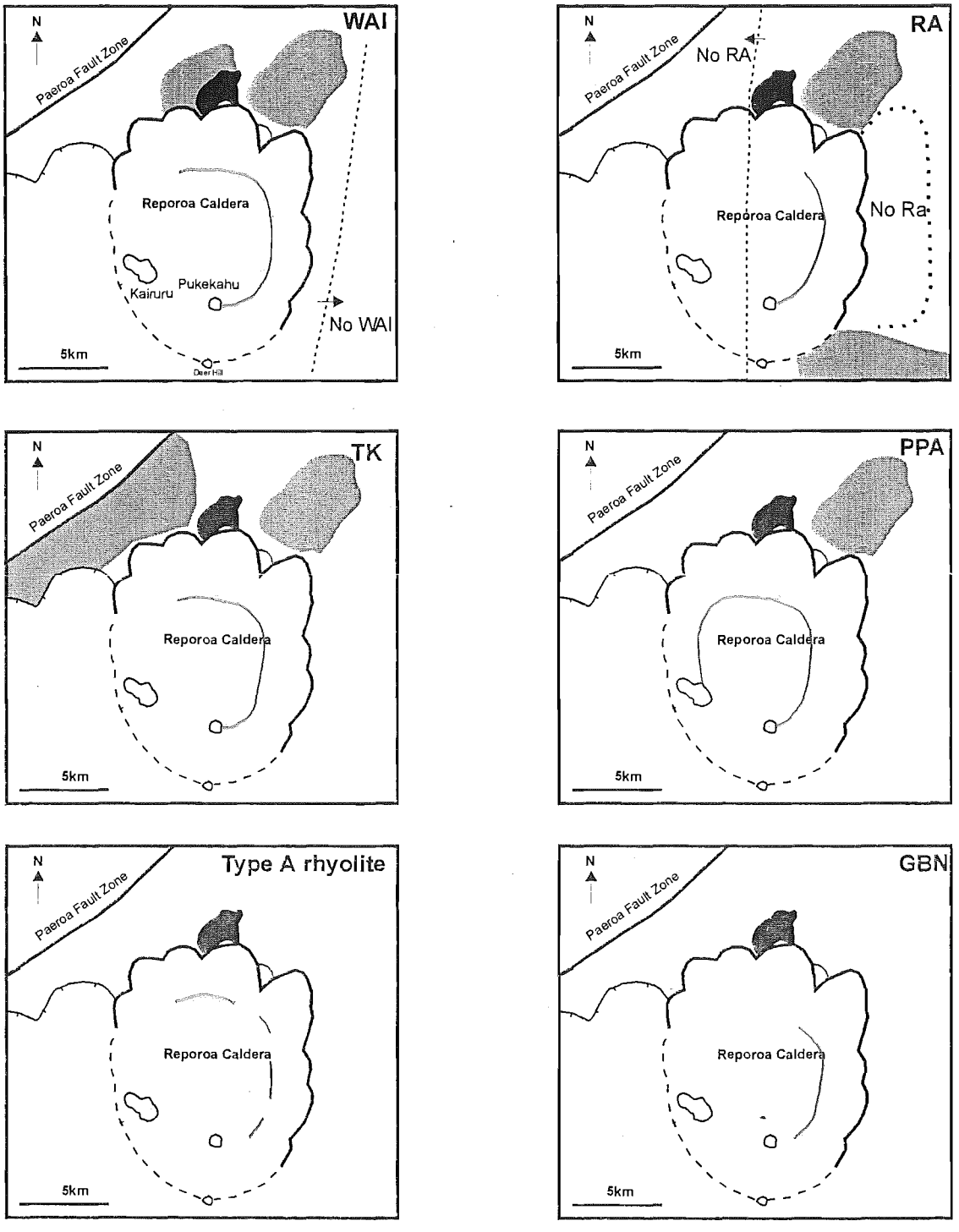

Fig 5.5 a Schematic illustrations of distribution of lithic types, correlation with pre-Kaingaroa geology, and paleogeographic interpretations. Dark grey shading denotes approximate outcrop and inferred distribution from drill hole information. The extent of the light grey line within Reporoa Caldera refers to inferred circumcaldera distribution of the lithology based on lithic distribution. Abbreviations as in Figure 5.1. plus Ra = Rangitaiki, TK = Te Kopia, Pa = Paeroa.

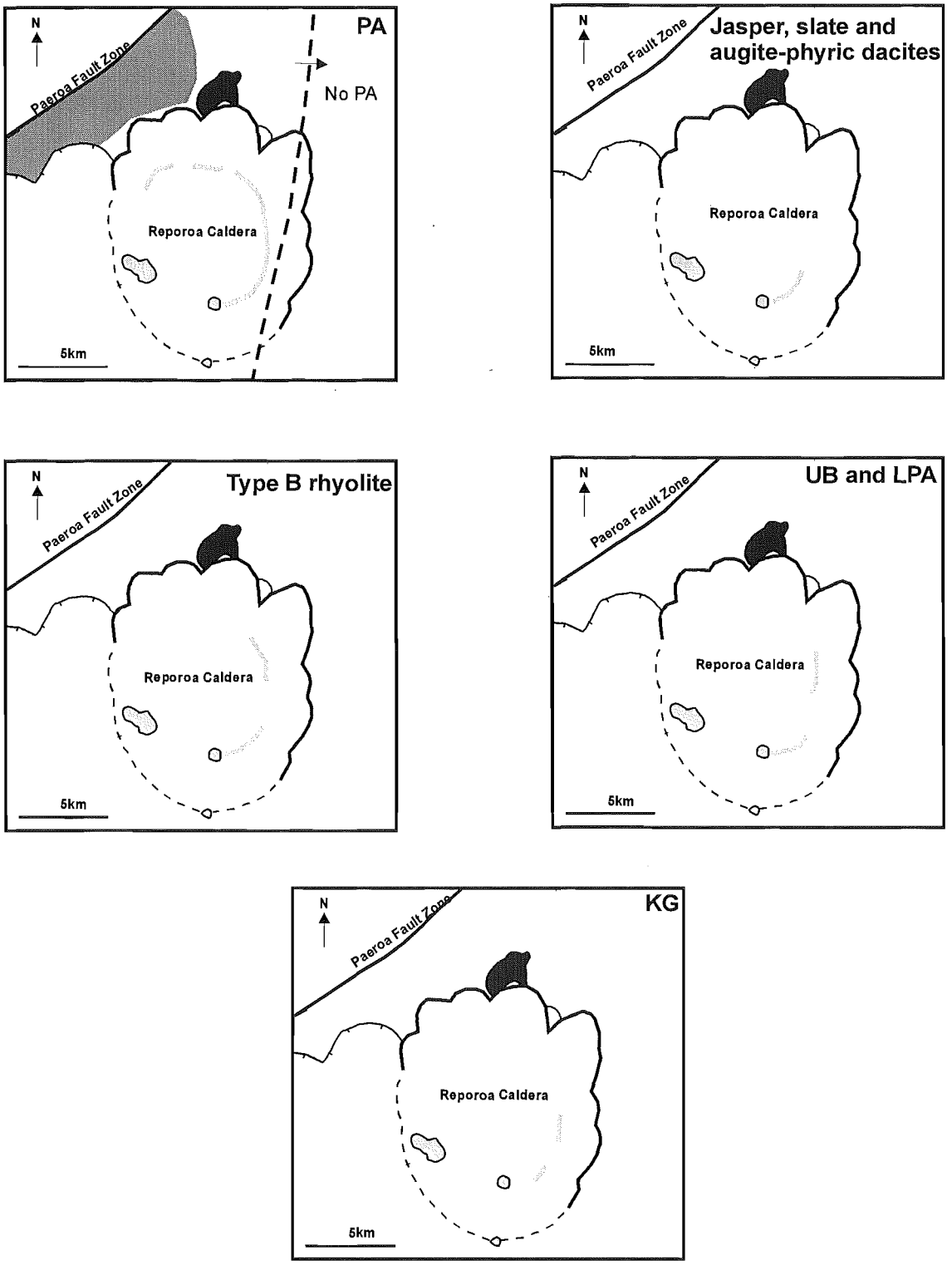

Fig 5.5 b Schematic illustrations of distribution of lithic types, correlation with pre-Kaingaroa geology, and paleogeographic interpretations.

Comparison with similar size caldera-forming eruptions e.g. Santorini, and Crater Lake, suggest pre-caldera products were erupted from a point source, with limited vent migration, in contrast to the complex vent migration described at Long Valley and Taupo 'calderas' by Colin Wilson and co-workers. The minor variation in lithic components does not require that the RBU opened a new vent, because the uppermost part of the basal tephras is interstratified with the RBU.

The lithic types within the basal tephras and RBU are weakly hydrothermally altered, suggesting the localised presence of a shallow hydrothermal system. The limited presence of low temperature altered lithics within later eruptive phases suggests the system was shallow and destroyed by caldera collapse.

5.6.2 Transition to lag breccia and Old Waiotapu Rd phase i.e. caldera collapse

The transition to the lag breccia or transition zone is marked in the field by an abrupt change in lithic content, types and abundance, which indicates a rapid and dramatic change in vent and eruption dynamics. In proximal regions the lag breccia marks the incoming of a diversity of lithic types including a variety of andesites, ignimbrites, 'greywacke' basement, plutonics, and metavolcanics. Asymmetric variation in these lithic types (Fig 5.4) is inconsistent with a similar vent site to the underlying Kaingaroa deposits, and is suggestive of either multiple vents or eruption from ring fractures. Evidence for ring fracture eruption, vent migration and eruption dynamics is discussed in Chapter 9 with reference to lithic componentry, field and geochemical data. The limited outcrop along the western margins of Reporoa Caldera prevents detailed assessment of circumcaldera variation in lithic types. Reconnaissance data and lithic componentry from near Coates Rd suggests lower PPA: ignimbrite and increased abundance of miscellaneous ignimbrite lithics, consistent with minor circumcaldera variation in pre-Kaingaroa geology. Despite an extensive search no gabbroic lithics were sampled. Circumcaldera variation in andesite: ignimbrite suggests extensive eastern distribution of the pre-Kaingaroa andesite volcano, consistent with magnetic and gravity data (Soengkono and Hochstein 1996).

The presence of increased WAI:WHAK and PPA:WHAK and deep level gabbros, metavolcanics, 'greywacke' and slates is consistent with a deeper level of lithic provenance during this phase. A fundamental change in lithic types is recorded at the BTI-upper lag breccia boundary. This boundary records the incoming of OWR-like ignimbrite lithics, and a marked change in pumice type and colour (Chapter 9). The Tokiaminga sub-unit contains notably higher contents of gabbros and metavolcanics consistent with a deeper level of provenance.

Medial facies lithic componentry

The majority of lithic types are vent-derived. At medial localities, the predominance of rounded greywacke lithics at the base of OWR at certain localities e.g. Kaingaroa, suggests incorporation of river or stream material by the pyroclastic flows. In addition medial localities do not contain friable lithologies such as baked soil and non-welded tuffs, indicating disaggregation of these rock types within the pyroclastic flow with distance, as would be expected.

WIU lithic componentry

Lithic types in the WIU closely match that of the underlying OWR, and a similar source is inferred. Notable variations include the incoming of greater proportions of metavolcanics, 'greywacke' and gabbroic lithics suggestive of a deeper level of lithic provenance. Samples from medial facies are too small to subdivide into lithic types assigned from coarser clasts from proximal exposures, though it is possible to broadly categorize these samples. Limited sample sites prevents detailed assessment of lithic variation.

A variety of lithics within the Kaingaroa Ignimbrite are similar to rocks exposed in the caldera walls. Details of the correlations are outlined in Chapter 6. Detailed lithic componentry of the Kaingaroa Ignimbrite has revealed the dominance of three components, PPA, WHAK, and WAI. The dominant lithic component (PPA) is not exposed, and the majority of lithic components are derived from planar ignimbrite units with non unique sectorial distribution. Variation within minor components is observed, but of limited statistical value, in terms of comparison. The *presence* of these minor components is considered important, rather than their absolute percentage. Despite these shortcoming, an artifact of the voluminous, and complex stratigraphy of central TVZ,

lithic componentry has revealed features of changing depth of fragmentation, and deepening of lithic provenance during vent evolution and the transition from single vent to ring vent or a caldera-forming phase.

CHAPTER SIX

Lithic petrology:

A window into subcaldera geology

6.1 Introduction

Previous studies of lithics from ignimbrites in the TVZ are limited to MSc theses by Chernet (1987; Taupo Ignimbrite) and Krippner (1996; Mangakino-centre ignimbrites). As part of a large FRST program, Brown et al (submitted) and Cole et al (submitted) report a variety of lithic types from large scale ignimbrites in the TVZ, varieties not reported in the Kaingaroa Ignimbrite include diorites (Orakonui, Mamaku), high alumina dolerites (Atiamuri, Rangitaiki, and Rangatira Point ignimbrites), and high-Mg andesite (Oruanui Ignimbrite).

Unique lithic types in the Kaingaroa Ignimbrite include gabbros (and unusual variants such as hornblendite), tourmaline-bearing metavolcanics (including tourmalinite), and slate. Rare reported lithologies include diatomite (a relatively common rock type in the TVZ), jasper, and baked soil (presumably a common lithotype, but preservation potential is limited in ignimbrites due to breakage during flow or entrainment).

This chapter documents petrologic data on lithic types to ascertain sub-caldera geology. Aspects of lithic petrology briefly outlined in Chapter 5, with reference to correlation are repeated and expanded here for continuity.

6.2 Andesites

Andesite is the dominant lithic component in the Kaingaroa Ignimbrite forming up to ca. 60 % at some sites. The predominance of andesite lithics is unusual in ignimbrites of similar age.

6.2.1 Field appearance and description

Previous work on andesite lithics in the Kaingaroa Ignimbrite was largely limited to reconnaissance petrography and a single XRF analysis (Nairn 1981).

Andesite lithics are variably grey-green, commonly exhibit weathered rims or cores, and are locally altered to smectitic clays and hematite, which give the rocks a yellow-red appearance in hand specimen. Andesite lithics are predominantly angular, with very rare well rounded altered varieties (e.g. KA83) probably being derived from gravels. Many of the andesite lithics within the lag breccia exhibit evidence of heat spalling (Chapter 4) indicating they were relatively hot on entrainment.

6.2.2 Petrography

The andesite lavas in the Kaingaroa Ignimbrite are principally grey-green basaltic andesites, with subordinate andesites and dacites. About 75 % of sampled lava lithics are basaltic-andesite, in contrast to many TVZ andesite volcanoes (e.g. Ruapehu; Graham and Hackett 1987). All the andesite lithics are porphyritic containing 22% to 45% phenocrysts of plagioclase, two pyroxenes, and subordinate Fe oxides, together with rare quartz, hornblende, and olivine in some samples. Three distinct andesitic lava lithic types were identified in hand specimen during lithic component analysis: PPA (plagioclase-phyric andesites), LPA (Large pyroxene-phyric andesites), and UB (uralitised basaltic andesites). PPA is sub-divided into two types based on mineral assemblages and corresponding distinctive chemistry and UB into two types based on petrography. An additional two andesite types were identified during reconnaissance analysis, but were not sampled during lithic componentry (see Chapter 5). Lithic clots are common, especially in strongly porphyritic lithic samples; textures vary from hypidomorphic granular to equigranular, with varying proportions of pyroxene and plagioclase.

Twenty eight andesitic/dacitic lithics were chosen for petrography and 25 of these were analysed for major and trace elements by XRF, 3 were chosen for reconnaissance microprobe analysis and 4 for REE analysis by ICP/MS. Detailed description of mineralogical and geochemical methods are presented in Appendix D and E. Seven

andesite types are recognised based on petrographic, mineralogical and geochemical criteria.

Plagioclase-pyroxene-phyric andesites (PPA)

Type 1: Plagioclase-phyric andesites

Dark grey, commonly vesicular plagioclase-phyric andesites are a common lithic type in the Kaingaroa Ignimbrite. Plagioclase (An_{82-61}) is the dominant phenocryst phase, commonly forming 40% of phenocrysts. Zoning is ubiquitous and consists of various combinations of oscillatory, reverse and normal. Plagioclase (up to 3 mm in length) displays three dominant habits; sieved, melt-inclusion-rich (i.e honeycomb) and clear. Skeletal morphologies are common. Plagioclase is locally altered to an amorphous aluminosilicate, which is discussed in detail in section 6.6 below. As in all andesitic lithics, plagioclase distribution is polymodal and can be classified into 3 size populations: phenocrysts, microphenocryst and groundmass. Phenocrysts are frequently mantled by clear sodic plagioclase, similar to groundmass feldspars.

Orthopyroxene and rare augite are markedly subordinate phases, locally forming 1% of some samples. Orthopyroxene occurs as pale green to colourless phenocrysts up to 2mm in length, which are commonly rimmed by euhedral or fine-grained augite. Augite is rarely present as a phenocryst phase, but is the dominant pyroxene in the groundmass. Fe-Ti oxides are ubiquitously present as microphenocrysts. Groundmass texture is variable, exhibiting intersertal, intergranular, hyalopilitic, subophitic and pilotaxitic textures. A single sample (KA92) exhibits an intimately mingled microlite-rich and microlite-free glassy matrix.

Type 2: Plagioclase-pyroxene andesites

Grey, commonly vesicular, plagioclase and pyroxene-phyric (type 2) andesites exhibit characteristics intermediate between plagioclase-phyric andesites and Type 3 plagioclase-augite-phyric andesites described below. Type 2 andesites are petrographically distinguished from Type 1 andesites, by the presence and/or increased abundance of augite. Plagioclase is the dominant phenocryst phase with subordinate orthopyroxene, augite and Fe/Ti oxides. Lithic clots of anorthositic and pyroxenitic composition are abundant, and many samples are coarsely vesicular (vesicles up to 7 mm in diameter). Plagioclase (up to 2 mm in length) varies markedly from 12-35%, and

crystals exhibit marked textural variation including sieved, clear, and melt-inclusion-rich varieties. Plagioclase is commonly euhedral, but sieved varieties are frequently corroded. Orthopyroxene is the dominant pyroxene, expecially in andesites $_{(s.s.)}$ and is locally rimmed by augite. Quartz is a rare phase, locally present as rounded resorbed xenocrysts in andesites, marginally rimmed by oxides. Olivine is a rare commonly oxidised phenocryst phase in less evolved varieties. Matrix texture varies from intergranular to hyalopilitic.

Large pyroxene-phyric andesite (LPA)

Type 3: Plagioclase-augite-phyric andesites

Type 3 andesites are green pyroxene and plagioclase-phyric andesites with conspicuous large pyroxene phenocrysts, and abundant pyroxene ± plagioclase lithic clots. These andesites are texturally and compositionally distinct from other andesite types, containing abundant pyroxene (up to 12%), either as abundant lithic clots or large 6 mm augite phenocrysts. Plagioclase (An_{80-65}) is the dominant phenocryst phase, with subordinate augite, the dominant pyroxene, orthopyroxene, and Fe/Ti oxides. Matrix texture varies from intergranular to intersertal.

Uralitised basaltic andesite (UB)

Type 4: Uralitised pyroxene-plagioclase-phyric basaltic andesites

Green-grey uralitised basaltic andesites contain phenocrysts of plagioclase (up to 30%), augite (up to 20%), and microphenocrysts of Fe-oxides and plagioclase. Plagioclase is ubiquitously weakly oscillatory zoned, notably calcic (An_{85-65}), and pervasively saussuritised, with strongly altered An-rich cores. Augite phenocrysts (up to 4 mm) are either totally pseudomorphed or marginally replaced by granular to fibrous actinolitic amphibole, chlorite, and rarely biotite. No orthopyroxene or olivine was observed in Type 4 andesites. Feldspathic and pyroxenitic lithic clots and quartzite xenoliths are relatively common. Matrix consists of highly altered plagioclase, Fe oxides and amphibole in an intergranular texture. Petrographic features of uralitised basaltic andesites (i.e calcic-rich plagioclase, abundance of pyroxene, lack of orthopyroxene, and uralitisation of augite) are similar to leucogabbro lithics described below.

Type 5: Augite-phyric dacite

Rare samples of altered augite-phyric dacite were sampled from Butchers Boundary Quarry, and are light grey, vesicular, phenocryst-poor dacites (> 6% phenocrysts), with conspicuous augite phenocrysts. Plagioclase and augite are the dominant phenocrysts with subordinate orthopyroxene and Fe-Ti oxides, and conspicuous accessory apatite. Plagioclase (labradorite) forms phenocrysts up to 5 mm in length, often within glomeroporphyritic clusters with augite and orthopyroxene (up to 0.5 mm in diameter). Plagioclase commonly shows sieve texture, and is weakly but complexly zoned. The matrix has an altered felsitic texture.

Type 6: Quartz-augite-phyric dacite

A single green quartz-augite-phyric dacite lithic (KA156) was sampled from Butchers Boundary Rd, during reconnaissance lithic sampling. The light green pumiceous dacite exhibits a complicated mineral assemblage indicative of disequilibrium. KA156 is coarsely porphyritic with phenocrysts of plagioclase, augite, orthopyroxene, quartz and accessory Fe oxides, apatite, biotite and olivine. Groundmass comprises plagioclase, pyroxene, Fe oxides and is vitrophyric to pilotaxitic. Feldspathic and pyroxene-rich lithic clots up to 7 mm in diameter are abundant. Plagioclase is the dominant phenocryst phase, and has three distinct characteristics; sieved, melt-inclusion-rich and clear, with sieved plagioclase occuring both in cores and mantles. Melt inclusion-rich plagioclase contains abundant melt inclusions either along a zone or throughout the core and mantle. Zoning is variable with large An% variation across resorbed complex zones. Plagioclase are rimmed by thin sodic zones, with similar compositions to groundmass microlites. Overall plagioclase texture is of multiple populations of plagioclase incorporated prior to groundmass crystallisation. Pyroxenes are zoned, and locally skeletal, quartz is ubiquitously rounded and resorbed, and biotite is present as small oxidised microphenocrysts. Feldspathic lithic clots are locally sieved, with thin clear sodic zones, and feldspar-rich microlite-rich zones external to the lithic clot, adjacent to thin clear plagioclase zone. The complex multiple phenocryst assemblage and abundant disequilibrium phenocryst indicate a role of magma mixing between a silicic end member (biotite + plagioclase + quartz) and less evolved (basaltic andesite?) end member (olivine + augite + plagioclase $\pm$ orthopyroxene). The lack of appropriate end member lithic types precludes further assessment.

Type 7: Hornblende-phyric andesite

A single hornblende-phyric andesite lithic was sampled from Rawhiti Rd during reconnaissance sampling. This is pink, hematite-stained with conspicuous green hornblende, pyroxene and plagioclase phenocrysts. Green pleochroic hornblende (up to 5 mm in length) is the most abundant mafic phenocryst phase forming up to 5% of the rock, with subordinate augite. Mafic minerals are marginally oxidised, and altered to hematite along fractures. Plagioclase (andesine) is commonly fractured and embayed, and may exhibit sieve texture. Rounded, fractured quartz phenocrysts are rare, and are interpreted as xenocrysts. Very altered Fe/Ti oxides are present as microphenocrysts. Matrix is heterogeneous, with spherulitic patches, abundant lithics or xenoliths (andesite, microdiorite, rhyolite and dacite), and localised microlite-rich areas. The lack of any fragmental textures, e.g. vitroclastic texture, and localised abundance of microlites suggests the sample is an inclusion-rich lava, but the altered nature of the sample precludes more detailed assessment.

6.2.3 Mineralogy

Plagioclase

Plagioclase is the most abundant phenocryst phase, and the only feldspar in the andesite lithics. Plagioclase values quoted are a combination of extinction angle optic methods (e.g. Michel Levy) and microprobe (Appendix D). Plagioclase compositions within the andesite lithics commonly contain calcic-cores (bytownite) and normal oscillatory zoned to sodic rims (andesine or labradorite). All plagioclase phenocrysts have low Or.

Pyroxene

Pyroxene are present in all andesite lithics, and are classified (Appendix D) according to Morimoto (1988). Orthopyroxene is the dominant phenocryst phase, whereas augite is the usual groundmass phase. Pigeonite was identified in a single andesite sample (KA 9A).

6.2.4 Geochemistry

Whole rock XRF was undertaken on unaltered samples to characterise the chemical variation within the suite of lithic samples, and to compare with TVZ andesite lavas exposed at the surface.

Major and trace elements

Major and trace element compositions of the andesite lavas are presented in Table 6.1. Compositions define a medium-K calc-alkaline suite, similar to common orogenic andesite lavas (Gill 1981). SiO_2 contents of the lavas range from 53 to 66 wt% with a compositional gap between 61 and 66 wt% (Fig 6.1). For the suite as a whole CaO, Fe_2O_3, MgO, MnO, TiO_2 and V decrease, and K_2O, Rb, and Ba increase with increasing SiO_2 (Fig 6.2). Despite its incipient alteration the Ngakoro Andesite sample of Hedenquist (1983) is geochemically (and petrographically) similar to andesites reported here, and is considered the lateral equivalent, as suggested by Nairn et al (1994).

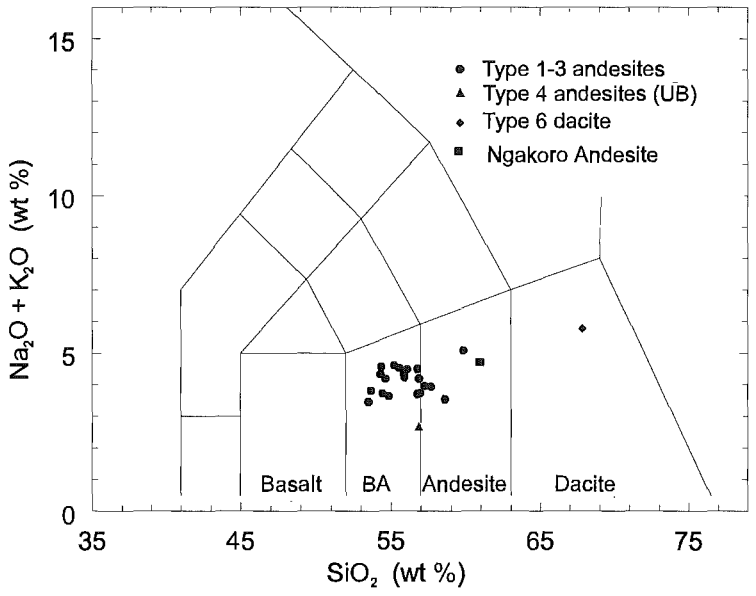

Figure 6.1 TAS classification of andesite lithics illustrating the broad range in compositions and compositional gaps.

The andesite lithics have typical arc signatures on MORB-normalised spidergrams (Fig 6.3), with large ion lithophile elements (LILE) enriched relative to high field strength elements and with a prominent negative Nb anomaly.

Plagioclase-phyric andesites are distinguished by high Al, Ca and low Cr, Ni, Mg and Mn content, reflecting the abundance of plagioclase, while Type 2 andesites exhibit intermediate characteristics. Type 3 lavas have high Cr, Ni, Mg, and low REE and Y, and low Ti, Sr and Al at a given SiO_2 content, and high Mn and Fe at a given SiO_2 content (compared with Type 1 lavas), reflecting the abundance of pyroxene, and their less evolved nature. Type 4 uralitised basaltic andesites are broadly similar to Type 3, with notable lower Na, K, Hf, and higher Rb, Ni, Cr, Ca, Zn, and Mn, possibly reflecting their less evolved and altered nature (e.g. High Zn). Type 6 dacites have high Cr and Ni for their SiO_2 contents, and high Rb/Sr and Ba reflecting their obvious mixed mineralogy.

The majority of samples do not fall within a single field of Ruapehu andesite types (Graham and Hackett 1987); however Kaingaroa plagioclase-phyric and plagioclase-pyroxene-phyric andesites broadly parallel Ruapehu type 1 and 2 lavas, albeit with lower SiO_2 than reported at Ruapehu. Type 6 quartz-augite phyric dacites are broadly similar to Tauhara dacites.

Rare Earth Elements

The rare earth element (REE) patterns of basaltic andesite lithics are charcterised by enrichment in light rare earth elements relative to heavy rare earth elements (Fig 6.4), and show no Eu anomaly, indicating either no plagioclase fractionation or that conditions were sufficiently oxidising that all the Eu is in 3+ form. Alternatively the negative anomaly may be masked by plagioclase accumulation, as possibly suggested by the high Al and Sr in Type 1 andesites. KA3 has a slight positive Eu anomalies, which may reflect plagioclase accumulation or enrichment, and sample KA83 exhibits a small negative Eu anomaly. The single dacite (KA156) exhibits a prominent negative Eu anomaly, indicating a role of plagioclase fractionation in dacite or end member genesis. REE patterns are consistent with mixing of evolved rhyolite, and basaltic or basaltic andesite magmas. Type 4 uralitised basaltic andesites exhibit similar REE contents and patterns to leuco-gabbroic lithics and are discussed in detail below.

Sample Name	KA3	KA92	KA84	KA194	KA428c	KA156
Rock Type	andesite	andesite	andesite	LPA	UB	dacite
Type	1	1	2	3	4	6
XRF						
SiO_2	54.36	53.08	54.08	56.56	56.29	65.51
TiO_2	0.93	0.99	0.93	0.69	0.69	0.39
Al_2O_3	19.74	20.51	17.40	17.15	17.29	15.07
Fe_2O_3*	8.49	8.66	10.03	8.01	7.71	3.68
MnO	0.13	0.14	0.17	0.15	0.24	0.07
MgO	2.87	2.74	4.69	4.60	4.33	2.49
CaO	8.71	8.81	7.56	7.62	9.70	3.72
Na_2O	3.18	2.75	2.29	2.69	2.09	2.81
K_2O	1.38	1.02	1.28	1.22	0.52	2.78
P_2O_5	0.19	0.18	0.16	0.12	0.11	0.06
LOI	0.30	0.97	1.20	0.07	0.84	2.04
Total	100.28	99.84	99.79	98.88	99.81	98.63
Cr	17	15	23	42	82	60
Ni	8	9	9	12	33	13
V	203	224	236	185	182	81
Pb	13	12	7	8	14	14
Zn	72	79	83	72	247	51
Rb	44	36	50	44	60	104
Ba	348	319	386	353	351	657
Sr	409	412	352	245	266	155
Ga	17	19	23	18	17	16
Nb	2	4	2	5	5	5
Zr	135	134	121	97	100	98
Y	26	21	25	19	20	23
Th	7	6	4	4	2	10
La	18	16	25	5	7	16
Ce	29	32	32	18	20	38
Nd	31	23	28	17	10	23
ICP-MS						
La	16.3	13.8	24.5			20.5
Ce	32.7	32	31.9			42.6
Nd	19.9	17	27.7			16.6
Sm	4.9	4.1	5.9			3.2
Eu	1.78	1.38	1.59			0.73
Gd	5	4.2	5.6			3.2
Dy	4.4	4.1	5.2			3.3
Er	2.9	2.4	2.7			2.1
Yb	2.7	2.4	2.3			2.2
Lu	0.8	0.4	0.3			0.4
Hf	3.3	3.3	3.2			3.1
Ta	1.4	1.2	1.1			0.8
Th	4.74	4.99	4.75			11.3
U	1.55	1.12	1.08			2.38

Table 6.1. Representative XRF and ICP-MS analyses of andesite lithics within the Kaingaroa Ignimbrite

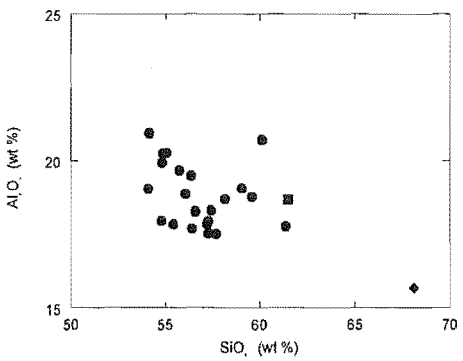

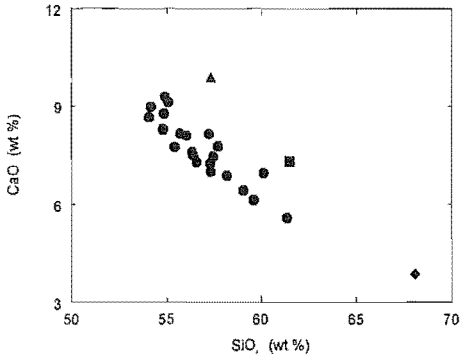

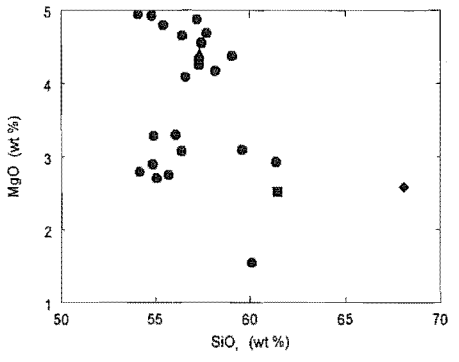

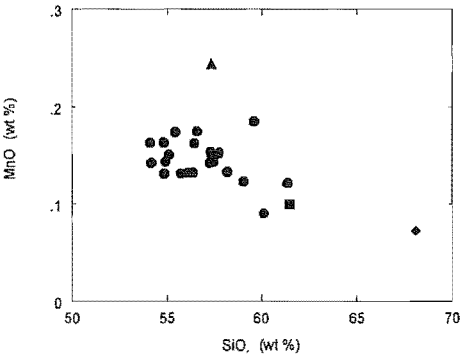

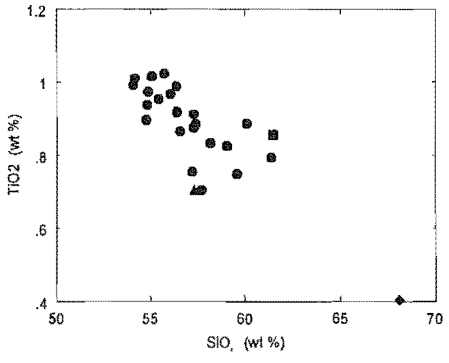

Figure 6.2a. Selected major element variation diagrams illustrating chemical variation within the suite of andesite lithics in the Kaingaroa Ignimbrite. Symbols as in Fig 6.1.

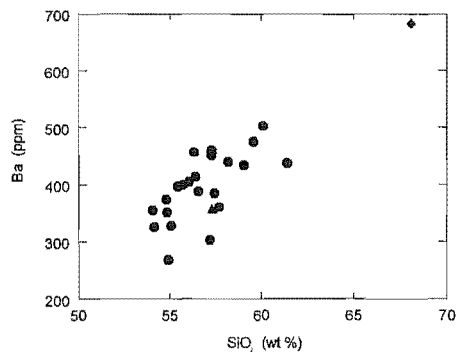

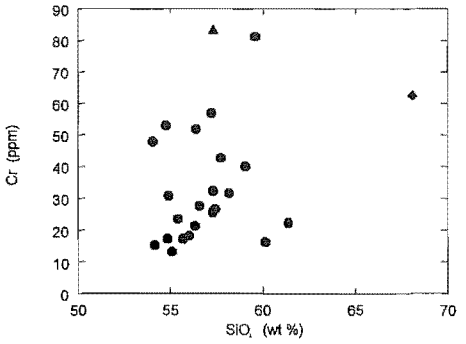

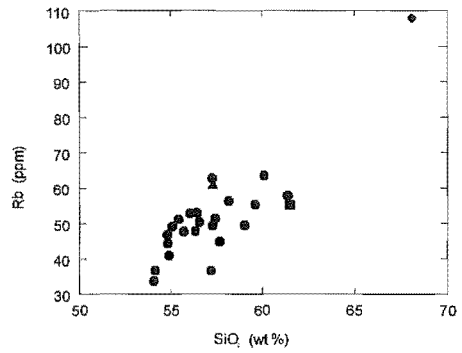

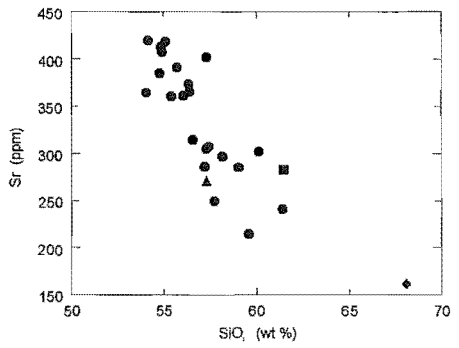

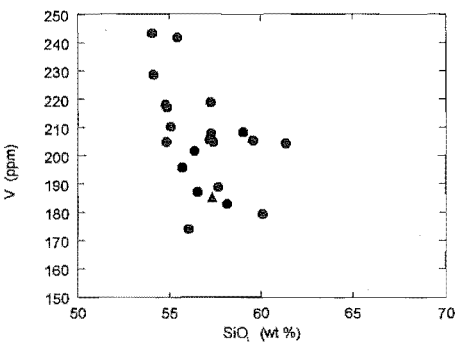

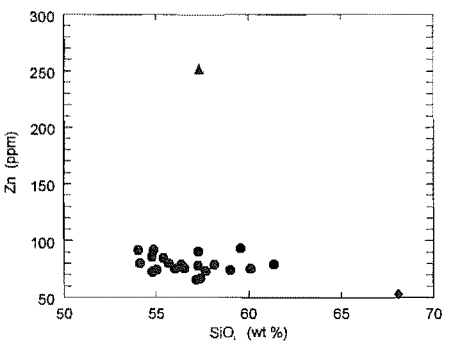

Figure 6.2b Selected trace element variations illustrating chemical variation within the andesite lithics in the Kaingaroa Ignimbrite.

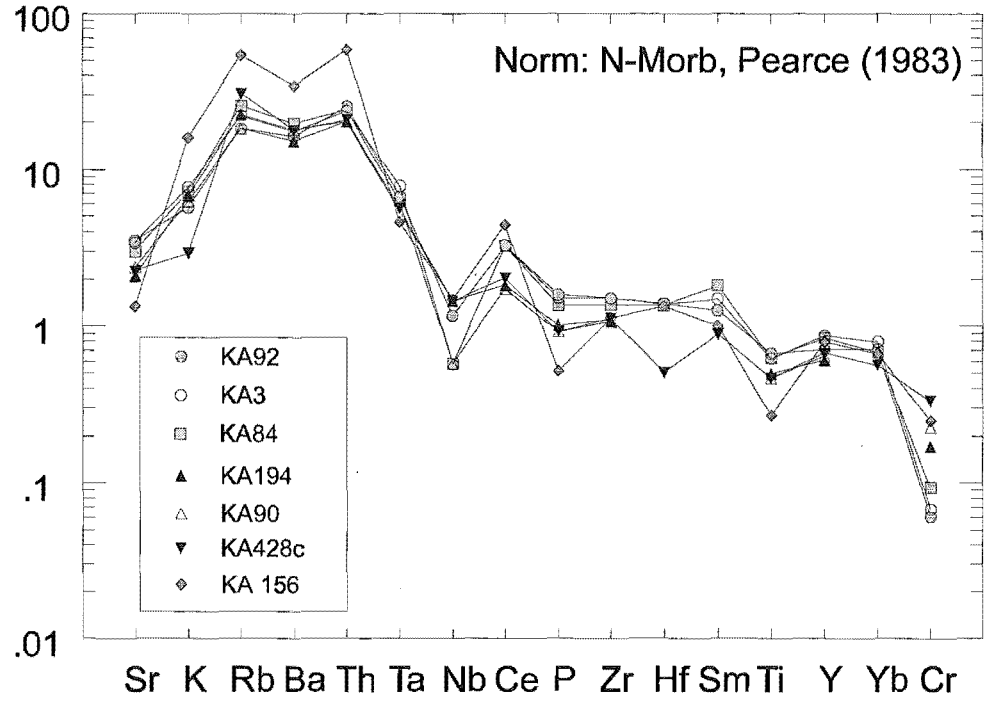

Figure 6.3 Morb-normalised multi-element plot illustrating variation in andesite types, with standard subduction-related enrichment in LILE, depletion in HFS and negative Nb anomaly.

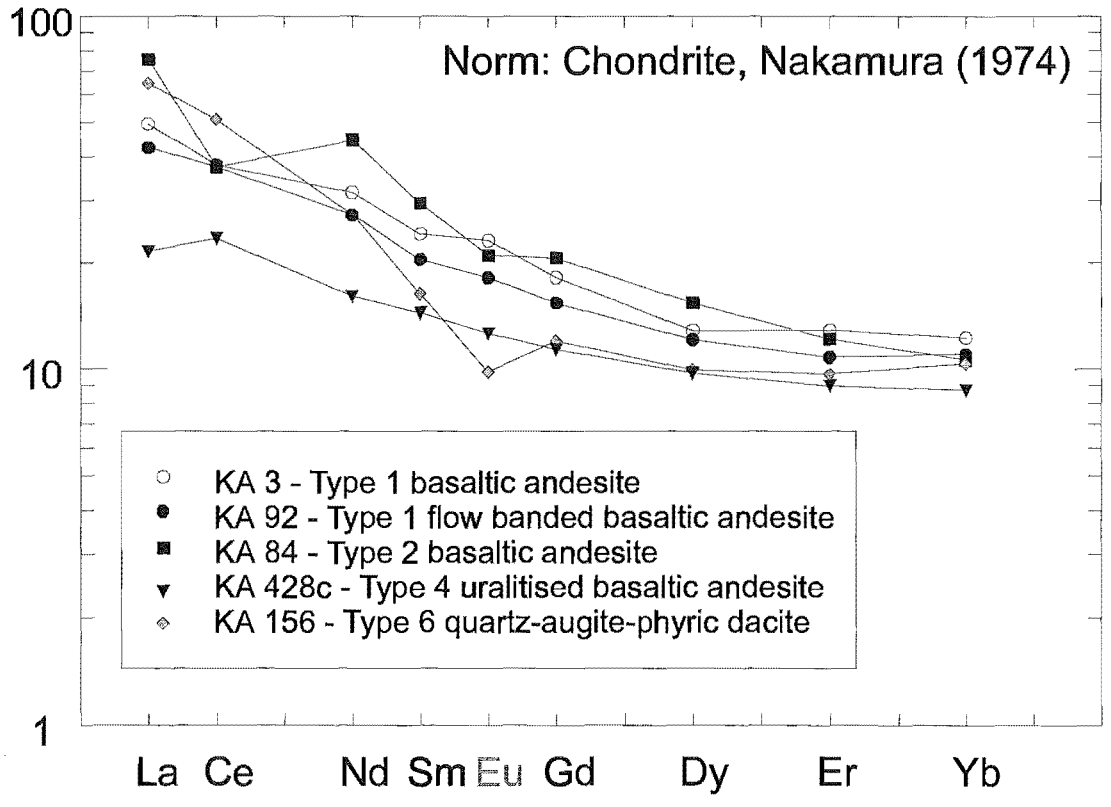

Figure 6.4 Chrondrite-normalised REE diagram illustrating chaotic REE patterns of basaltic andesite lithics and KA 156 (quartz-augite-phyric dacite).

REE analyses are limited for TVZ andesites. Cole et al (1983) reported REE analyses for TVZ andesites, noting limited or no Eu anomalies in basaltic andesites from Ruapehu and Tongariro, and prominent negative Eu anomalies in more evolved andesites, consistent with plagioclase fractionation.

6.2.5 Discussion

Despite the diversity of andesite types, the majority of lithics are inferred to have been derived from a single volcano, analogous to the diverse compositions exhibited by the large southern andesitic stratovolcanoes e.g. Ruapehu. LPA exhibits sectorial distribution as inferred from lithic component analysis (Chapter 5), possibly reflecting a localised centre on the volcano or dome. The origin of UB or Type 4 andesites is equivocal due their pervasive uralitisation and less evolved chemistry, and is discussed below in relation to the leuco-gabbroic lithics.

Although andesite lithics within the Kaingaroa Ignimbrite have broadly similar calc-alkaline medium K 'orogenic arc-type' andesite chemistry, they are geochemically different from other reported TVZ lavas. Plagioclase-phyric andesites have been reported from Rotokawa and Ruapehu, but are more evolved. The presence of petrographically and texturally similar plagioclase-phyric lavas at Reporoa suggests similar processes of 'enrichment in plagioclase' are present across the andesitic spectrum. TVZ andesites are modelled as fractionated high alumina basalts with simultaneous assimilation of Torlesse 'greywacke' basement (Graham et al. 1995). Variation between andesite types is attributed to variable amount of assimilant, and/or crystallisation, mineral accumulation, and variation in fractionating assemblage, with additional textural modification due to prolonged plagioclase crystallisation, re-entrainment and recharge. Aspects of this textural variation, and its relationship to leuco-gabbroic lithics and a model of feldspathic accumulation are discussed in Section 6.6.

In addition the abundance of disequilibrium textures (e.g. sieved plagioclase, rounded quartz, reaction rims, and two plagioclase populations) in andesite lithics suggests magma mixing was a common process operating within the magma system, as has been advocated at numerous andesitic volcanic centres (e.g. Motuhora; Burt et al. 1996). The

petrography and geochemistry of the quartz-augite-phyric dacite is broadly similar to Tauhara dacite, and a similar origin is inferred. The presence of andesitic lavas at Reporoa is inferred to represent sampling of a large volcano destroyed during caldera collapse. Remants of this volcano are preserved within the Waiotapu drill holes and have been identified along the northern and eastern margins by gravity and magnetic studies (Soengkono and Hochstein 1996).

6.3 Welded ignimbrites

Welded ignimbrites are a common lithic type in the Kaingaroa Ignimbrite and include a variety of mineralogical and lithological variations. Twenty eight ignimbrite lithics were thin sectioned to characterise lithologies and correlate with stratigraphy established in Chapter 2. In addition welded ignimbrite variations were noted from whole-rock Kaingaroa Ignimbrite thin sections.

6.3.1 Whakamaru-group ignimbrites (WHAK)

WHAK encompasses a broad variety of lithic types which are correlated with the diverse Whakamaru-group eruptives. Grey-white-pink, crystal-rich, quartzose, densely-welded ignimbrites are a common lithic type in all ignimbrite units of the Kaingaroa Ignimbrite. They form two broad compositions; a crystal-rich, quartzose, biotite-sanidine-bearing ignimbrite, and a quartzose crystal-rich hornblende-orthopyroxene-bearing ignimbrite. A wide degree of welding, density, and textures is present across these two types. These lithotypes are correlated with the 0.34-0.32 Ma Rangitaiki and Paeroa ignimbrites which outcrop all around Reporoa Caldera. A black to buff densely-welded crystal-rich hornblende-bearing ignimbrite is ubiquitously present in the lag breccia, OWR and WIU units and locally present in the Reporoa Boundary unit. This lithotype is correlated with the 0.34 Ma Te Kopia Ignimbrite, which outcrops west of Reporoa Caldera at the base of the Paeroa Fault scarp, and has been correlated in the Ngatamariki and Broadlands drill holes.

Representative thin sections of Paeroa and Rangitaiki ignimbrites were examined during the course of this study. Both ignimbrites exhibit similar broad characteristics including crystal-rich (up to 32% crystals), variation in colour from grey (common) to pink to

white, with abundant andesitic and crystal-rich ignimbrite lithic fragments, and partially to densely welded, commonly lenticulitic. Plagioclase, sanidine and quartz are the dominant crystal types in the Paeroa Ignimbrite, with subordinant biotite, Fe/Ti oxides, and rare orthopyroxene. Rangitaki Ignimbrite contains up to 32% crystals of plagioclase, quartz, orthopyroxene, hornblende, and Fe/Ti oxides (Table 6.2). Plagioclase (andesine; up to 4 mm in length) forms large oscillatory or patchy zoned, commonly resorbed crystals, locally with allanite, zircon and Fe/Ti oxide inclusions, and quartz forms large (up to 7 mm) bipyramidal, fractured, and embayed crystals, typical of Whakamaru-group eruptives. Orthopyroxene and green pleochroic hornblende (up to 1.5 mm in length) are locally oxidised, and commonly fractured. Matrix texture is generally vitroclastic, but varies from vitric to spherulitic and/or axiolitic, to vapour-phase altered.

Field no.	*Plag*	*Qtz*	*Opyx*	*Amph*	*Biot*	*San*	*Fe/Ti*	*Crystal %*	*Corr*
KA79	14.8	14	0	0	0.8	5.2	0.2	35	Pa
KA78	16	11	1	0.4	0	3	0.8	32.2	Ra
KA4	15	5	2	3	0.8	tr	1	26.8	Ra
KA86	27	15	4	3	0.2	tr	1	48.2	TK

Table 6.2 Modal analyses of selected Whakamaru-group ignimbrite lithics. Plag=plagioclase; qtz=quartz; opyx=orthopyroxene; amph= amphibole; biot=biotite; san= sanidine; Fe/Ti =Fe/Ti oxides; Corr=correlation; Pa=Paeroa; Ra=Rangitaiki; TK= Te Kopia.

Seven thin sections of Te Kopia Ignimbrite were examined in this study, due to the variable welding states and colour variations, and the resemblance to rhyolites of the majority of specimens. All samples exhibit similar mineralogy (Table 6.2), and are correlated with the lower and middle member of the Te Kopia Ignimbrite, exposed along the base of the Paeroa Fault scarp to the west of Reporoa Caldera. Plagioclase is the dominant crystal phase, forming fractured subhedral oscillatory zoned crystals up to 3 mm. Quartz commonly forms euhedral crystals up to 2.5 mm, with subordinate green pleochroic euhedral hornblende, orthopyroxene, and Fe/Ti oxides. Matrices vary within

samples from spherulitic or axiolitic replacement of vitroclastic texture, to complete spherulitic replacement of vitroclastic texture (these specimens resemble rhyolite lavas). Remnant brown or white fiamme are locally present, and very rare samples are vitric. The degree of welding varies from densely welded to vitrophyric. Lithic fragments include phenocryst-poor andesite lava, 'greywacke' and rhyolite.

6.3.2 Waiotapu Ignimbrite

A grey-purple, densely-welded crystal-poor lenticulite is the dominant welded-ignimbrite lithic in the Kaingaroa Ignimbrite, forming prominent lithic blocks up to 3 m at Butchers Boundary Rd Quarry. Two broad types are present; grey and purple/red. Plagioclase is the dominant phenocryst type forming oscillatory zoned crystals up to 3 mm in length, locally forming glomeroporphyritic clusters with orthopyroxene and Fe/Ti oxides. Orthopyroxene, oxidised Fe/Ti oxides and hornblende are present in trace amounts. The matrix is ubiquitously vapour phase altered and devitrified with prominent spherulitic pumice/fiamme and axiolitic devitrification of vitroclastic texture groundmass. Locally the groundmass is overprinted by cryptocrystalline devitrification products. Lithophysae up to 5 cm in diameter are locally present in lithic blocks. Attenuation of pumices/fiamme and shards suggest all blocks are densely welded. The crystal-poor nature, extreme devitrification and vapour phase alteration, colouration, mineralogy, hackly fracture, presence of lithophysae, and lithic-poor nature indicate this ignimbrite lithic type is the distinctive Waiotapu Ignimbrite, which outcrops north of Reporoa Caldera.

6.3.3 Matahina Ignimbrite

A pink crystal-poor/moderate, pumice-rich, 'Matahina-like' ignimbrite is present as a rare lithic type within surges and early flows of the basal tephra unit. Plagioclase is the dominant crystal phase with subordinate quartz, orthopyroxene, Fe/Ti oxides and hornblende. A notable feature of the ignimbrite is the abundance of obsidian, brown rhyolite lithics and vitric matrix. The similar mineralogy and lithic content suggests the lithics are Matahina Ignimbrite, commonly exposed around Reporoa Caldera (Bailey and Carr 1994; Chapter 2).

6.3.4 'Sandy black' ignimbrites

'Sandy-black' crystal-poor ignimbrite lithics comprise a small percentage of lithic lithotypes in the Kaingaroa Ignimbrite. A number of varieties are present (A,B,C,D), the most common being a partially-welded andesite-lithic rich ignimbrite. The lithics contain similar mineralogy and lithic types to the Kaingaroa OWR unit, but Type A and B lithics occur in the lag breccia beneath the 'sandy black' OWR, and are therefore not correlatives of OWR as proposed below for Type C.

Type A resembles a grey vitric ignimbrite locally mapped as Akatarewa ignimbrite in the Waikite region. Type B was sampled from lower lag breccia at Rawhiti Rd, and is a vitric crystal- and lithic-poor ignimbrite. Plagioclase is the dominant phenocryst phase with subordinate orthopyroxene and Fe/Ti oxides. Very rare rhyolite lithics are present. Unfortunately the mineral assemblage and lithic content is common in TVZ, particular in the 0.24-0.22 Ma ignimbrites, so further work is required to correlate this unit.

Type C 'sandy black' ignimbrite lithics are partially welded to compacted, vitric, pumice- and lithic-rich. Plagioclase is the dominant phenocryst type with subordinate orthopyroxene and Fe/Ti oxides. Lithic fragments include andesite, Paeroa Ignimbrite and rhyolite, and pumice fragments include grey and brown varieties. The presence of similar mineralogy and lithic types suggests a correlation with the OWR unit.

A fourth distinctive 'sandy black' ignimbrite (Type D) was sampled at Burn Rd within the Brown transition ignimbrite unit (BTI). Specimen KA 188A is a partially welded brown-black crystal-poor ignimbrite with abundant spherulitic crystal-poor rhyolite lithics, and locally orange pumices. Plagioclase is the dominant phenocryst phase, with subordinate orthopyroxene, augite, hornblende, Fe/Ti oxides, and prominent apatite and zircon. As with types A and B the presence of this lithic beneath the OWR unit indicates this is not a correlative of OWR. The presence of hornblende-rich crystal-poor rhyolite lithics and crystal-poor augite-bearing mineralogy is similar to Pokai Ignimbrite, but as noted above numerous ignimbrites in TVZ exhibit broadly similar mineralogy. As outlined in chapters 3 and 9, correlation of sandy black ignimbrites in TVZ has been frought with numerous mis-correlations, due to the presence of numerous mineralogically similar units at a similar stratigraphic interval. A firm correlation would

require mineralogical and/or geochemical evidence. Type D ignimbrite is not correlated with any unit present within the Reporoa area.

6.3.5 Miscellaneous ignimbrites

Some ignimbrites have no known correlative; two varieties are listed below:

Type 1 miscellaneous ignimbrites is a brown-buff partially-welded hornblende-bearing vitric crystal-moderate ignimbrite, with a plagioclase + amphibole + orthopyroxene + Fe/Ti oxides ± quartz mineralogy. Lithic fragments are predominantly rhyolite with subordinate dacite and andesite. This ignimbrite has no known correlative.

Type 2 is a pink/orange well indurated altered ignimbrite locally cut by quartz veins, with a plagioclase + biotite aggregates (orthopyroxene) + quartz assemblage. Lithics are ubiquitously rhyolite. The altered nature of this unit suggests a transition between this lithic type and metavolcanics described below.

6.3.6 Kaingaroa-like ignimbrite

A conspicuous tan lithic-rich partially welded to densely-welded vitrophyric ignimbrite lithic is present at numerous sites in the lag breccia. The distinctive petrography, mineralogy and lithic assemblage is indicative of the Kaingaroa Ignimbrite. The unit is interpreted to represent proximal early flows of the Reporoa Boundary Unit (RBU). Details of mineralogy and geochemistry are presented in Chapter 7.

6.4 Rhyolites

Rhyolite lithics show a great diversity of textures and crystal percentage. A number of types are present including blue, black, grey and pink, crystal-rich and poor, flow banded and spherulitic varieties. Rhyolite lithics within the Kaingaroa Ignimbrite are divided into four common varieties. Type A: a crystal-rich, quartzose, devitrified spherulitic rhyolite, Type B: a crystal-poor vitric rhyolite/obsidian, Type C: a crystal-rich mafic-inclusion-rich quartzose rhyodacite, and Type D a weakly altered crystal-poor rhyolite. Table 6.3 presents modal analyses of selected rhyolite lithics.

Type A rhyolites are crystal-rich (up to 25%) quartzose rhyolites which petrographically resemble Trig 8566 rhyolite dome. Crystal-rich rhyolites are relatively rare in the Reporoa area, but the occurrence of this lithic type at numerous sites suggests pre-0.23Ma extensive distribution of crystal-rich rhyolites.

Type B rhyolites consists of up to 6% phenocrysts of; plagioclase (3%), quartz (2%), orthopyroxene (1%), and Fe/Ti oxides (tr). Plagioclase (andesine-oligoclase) up to 2 mm in diameter typically occurs as single, discrete, oscillatory zoned, commonly fractured phenocrysts, with rare glomeroporphyritic aggregates. Plagioclase commonly contains Fe/Ti oxide and melt inclusions. Ubiquitously fractured and broken quartz phenocrysts up to 0.5 mm in diameter typically form 'porphyroclasts' in the flow banded matrix. Orthopyroxene occurs as commonly oxidised phenocrysts up to 0.5 mm, which commonly contain Fe/Ti oxide inclusions. Flow banding in the matrix is defined by flow aligned microlites, and localised brecciated phenocryst zones. Two samples were thin sectioned (KA14, KA201B), and both exhibit similar mineralogy to the Kaingaroa Ignimbrite. A single sample was analysed for XRF, which geochemically resembles pumice analyses from the Kaingaroa Ignimbrite. The rhyolite/obsidians are texturally distinct from juvenile obsidian (see below) and are interpreted as precursor 'Kaingaroa' rhyolites leaked from the Kaingaroa magma system. This point is further assessed in Chapter 7.

Type C rhyodacite lithics form a common lithic type at Butchers Boundary Rd Quarry where they contain numerous aphyric microdioritic inclusions up to 3 cm in diameter. Petrographically the lithic type contains up to 25% phenocrysts of plagioclase, quartz, Fe/Ti oxides, and biotite. Plagioclase feldspar phenocrysts up to 3 mm in length are commonly complexly oscillatory zoned and sieved, with abundant apatite and melt inclusions. Plagioclase is locally present as glomeroporphyritic aggregates. Quartz forms large (up to 4 mm) anhedral commonly embayed phenocrysts. Fe/Ti oxides are locally abundant and commonly oxidised. Brown pleochroic biotite forms up to 1%. Type C rhyolites petrographically and geochemically resemble 0.34-0.32 Ma crystal-rich rhyolites and ignimbrites (Appendix E).

Type D rhyolites are crystal-poor (up to 10% phenocrysts) plagioclase-orthopyroxene-phyric rhyolites. A notable feature of this rhyolite type is the incipiently altered felsitic

matrix, and oxidised orthopyroxenes which suggest a transition from rhyolites described here to meta-rhyolites discussed below. The crystal-poor plagioclase-orthopyroxene quartz-free nature is suggestive of Kaingaroa-like rhyolites, and of numerous other rhyolite and ignimbrites between 0.24-0.22 Ma (see Chapter 9). Geochemical analyses of all rhyolite samples are presented in Appendix E.

Field No	*Plag*	*Qtz*	*Opyx*	*Biot*	*Fe/Ti*	*Matrix*	*Type*
KA 14	3	2	1.1	0	tr	93.9	B
KA 11	22.5	2.8	0	0.2	4.0	70.5	C
KA 241A	9.1	0	0.8	0	tr	90.1	D

Table 6.3 Modal analyses for selected rhyolite lithics from the Kaingaroa Ignimbrite. Abbreviations as in Table 6.2.

6.5 Obsidian

Obsidian lithics in the Kaingaroa Ignimbrite range from vitrophyric ignimbrite to glassy rhyolite lavas. A detailed description of juvenile obsidian is presented in Chapter 7.

6.6 Leuco-gabbros

Nairn et al (1994) first reported diorite lithics in the Kaingaroa Ignimbrite. These blocks are now reinterpreted as leuco-gabbros. The blocks form up to ca. 1% of lithic ejecta in the proximal lag breccia facies.

The aim of detailed study of the gabbroic lithics was: to investigate variations in the composition of primary or magmatic minerals; to record the occurrence and distribution of secondary (most hydrous and oxide mineral grains) minerals; to characterise the whole rock geochemistry to compare with plutonic lithics identified in the TVZ by previous workers, and identify possible parental magma compositions.

Gabbroic lithics were collected from 13 localities, dominantly from the proximal lag facies. The majority of samples are from Butchers Boundary Quarry, which is

interpreted as the most proximal lag breccia site, as M_L exceeds 4 m. Despite a thorough search no gabbroic lithics were recovered from sites along the western boundary of Reporoa Caldera.

A total of 18 gabbroic lithics was collected for thin sectioning, 10 of these were chosen for whole rock XRF analysis, 3 for REE, and 3 for microprobe analysis.

6.6.1 Field appearance and occurrence

Gabbroic lithic fragments range in size from a few cm to blocks up to 30 cm in diameter, and occur in the WIU and OWR ignimbrite units, and proximal lag facies, along the eastern margin of Reporoa Caldera.

In hand specimen the blocks are angular to subrounded, coarse to medium grained leucocratic (colour index = 18-25%) gabbros (Fig 6.5a) with rare porphyritic mesocratic (colour index = 33%) samples. The blocks are intensely fractured and cut by quartz and amphibole veins. No phase layering is evident on hand specimen scale. Rare blocks exhibit mafic and pegmatitic clots. The lithics show evidence of heat spalling, breadcrusting and prismatic joint patterns that suggest the blocks were hot when ejected.

Disaggregated gabbroic lithics are common and occur in all stages of development. At proximal localities e.g. Butchers Boundary Rd Quarry, gabbroic lithics are dense and intact, while at more distal localities e.g. Old Waiotapu Rd, the blocks are intensely fractured and granular, and break up into individual crystals. At distal localities e.g. Main Gully Rd only xenocrysts of calcic plagioclase and fibrous amphibole are present. These features reflect particulate transport and depositional processes and not lithic entrainment processes.

6.6.2 Petrography and mineral chemistry

Texturally the gabbroic rocks are coarse grained, with an average grain size of 3 cm, and a well developed ophitic texture. Subordinate gabbroic porphyries and dolerites exhibit intergranular and subophitic groundmasses. The gabbros are leuco-gabbros and relic orthopyroxene : augite : olivine ratios suggest variation from olivine leuco-gabbros to

leuco-gabbronorites (Le Maitre 1989). Medium grained and porphyritic lithologies classify as dolerites and gabbroic porphyries.

The principal mineral phases in the gabbros are dominated by plagioclase feldspar, augite, and orthopyroxene, with minor olivine, magnetite, and accessory apatite. The lithic blocks exhibit variations in modal olivine, orthopyroxene and augite, and mafic mineral percent. All samples are extensively altered with secondary minerals including fibrous actinolite and cummingtonite, chlorite, biotite, titanite, epidote, stilpnomelane, hematite, tourmaline, carbonate, talc and Fe/Ti oxides. Olivine-free samples contain rare quartz and granophyric and micrographic intergrowths. Gabbroic lithics exhibit minor variations in grain size (Table 6.4). Modal percentages of mafic minerals for selected samples are presented in Table 6.5.

Plagioclase

Plagioclase is the dominant mineral phase comprising up to 82% of some samples, and forming crystals of varying size, commonly up to 4 mm. Plagioclase 'phenocrysts' in porphyry samples are up to 8 mm in length, and plagioclase exhibit a complex array of textures. These include skeletal growth habit, presence of devitrified melt-inclusions and abundant pyroxene, amphibole, and opaque mineral inclusions (Fig 6.5b), complex oscillatory zoning involving marked dissolution unconformities and marked changes in An % (up to 15%), patchy sodic zoning (An_{59-61}), with locally in excess of 51 observable distinct zones. Three distinct plagioclase textural types are commonly observed; clear, honeycomb, and a distinctive sieve-textured type, which contains an amorphous material and is discussed further below. Clear and honeycomb plagioclase types resemble classical feldspar textures in andesites (Tsuchiyama 1985; Kawamoto 1992). Honeycomb plagioclase contains large melt inclusions and sodic zones, whereas clear plagioclase lacks devitrified melt inclusions. Devitrified melt inclusions (with their long axis parallel to host plagioclase crystal) are restricted to the calcic plagioclase core, with localised sodic zones which impart a heterogenous composition to the core. An inclusion-free sodic rim similar to 'groundmass' and clear feldspar surrounds the mantle and plagioclase core. Similar textures were observed in the andesite lithics. An origin to that invoked by Kawamoto (1992) is advocated here; i.e. skeletal growth under supercooling conditions. Two samples were probed in detail for representative plagioclase compositions (Appendix D). KA173, a coarse-grained leuco-gabbronorite

exhibits three plagioclase sizes, similar to andesitic volcanics. Large plagioclase crystals are zoned from An_{79-72}, similar to microphenocryst compositions. Small (up to 1 mm) crystals are andesine in composition (An_{48}) and exhibit minimal zoning. Rare large crystals are zoned from An_{79-48}. KA386P, a medium grained leuco-gabbroic porphyry exhibits similar plagioclase crystal size variation, and is zoned from An_{82-61}, similar to weakly zoned 'groundmass' compositions (An_{62-65}). Plagioclase textures and compositional variation suggest a complex history of skeletal growth, disequilibrium conditions, variation in P-T conditions, probably reflecting mixing, and a prolonged history of growth and mafic magma replenishment, which is discussed further below.

Pyroxene

Pyroxene is rare as cores (Fig 6.5c) mantled by fibrous green-brown pleochroic amphibole and/or chlorite, and rare relics of co-existing augite and orthopyroxene have been analysed in two specimens (Fig 6.6). Pyroxenes are classified after Morimoto (1989). KA173 contains clinopyroxene ($Wo_{41}En_{34.4}Fs_{24.6}$) associated with Fe-rich orthopyroxene (En_{47}) relics. KA386P contains Mg-rich orthopyroxene (En_{68}) and augite ($Wo_{44.7}En_{34.4}Fs_{18.2}$). There is insufficient pyroxene relics to assess extent of the compositional variation. Rare gabbroic lithic samples (e.g. KA6) contain bleb and rod-like exsolution lamellae of augite within orthopyroxene and vice versa. KA157A contains a complex intergrowth of plagioclase and pyroxene, similar to as described by Schubert (1977, 1979), and Obata (1980). Pyroxene is rarely euhedral and dominantly present within interstices. Rare euhedral skeletal pyroxene is present within the 'groundmass' of porphyry samples. Pyroxene locally forms anhedral clusters reminiscent of glomeroporphyritic aggregates in volcanic samples.

Olivine

Rare relics of rounded, fractured, incipiently-altered olivine are present in two samples. Olivine is more commonly totally pseudomorphed by talc, Fe/Ti oxides and chlorite (Fig 6.5c). No primary olivine was present within probed samples.

Apatite

Apatite is ubiquitous in gabbroic lithics as small sub-mm inclusions within plagioclase. Apatite is locally abundant in some samples and forms euhedral inclusions up to 0.5 mm in secondary amphibole e.g. KA173.

colour index

Sample no	C.I.	Primary minerals	Texture	Classification	Alteration minerals	AA
KA6	27	Pl+aug+opyx+mgt+(ol?)	Coarse, ophitic	leuco-gabbronorite	Act+cumm+biot+chl+Fe ox+ tit	
KA7	27	Pl+pyx+mgt	Coarse, ophitic	leuco-gabbro	Act+cumm+chl+Fe/Ti ox+biot	
KA17	28	Pl+pyx+mgt+qtz	Coarse, ophitic	leuco-gabbro	Act+cumm+biot+chl+Fe/Ti ox+lim+hem	tr
KA73	27	Pl+pyx+mgt	Coarse, ophitic	leuco-gabbro	Act+cumm+chl+Fe/Ti ox+talc	
KA82	20	Pl+pyx+mgt+qtz	Coarse, ophitic	leuco-gabbro	Act+cumm+biot+chl+Fe ox	tr
KA157A	29	Pl+opyx+aug+mgt+qtz	Medium, intergranular, subophitic	dolerite	Act+cumm+biot+chl+Fe ox	
KA173	24	Pl+opyx+aug+qtz+mgt	Coarse, ophitic	leuco-gabbronorite	Act+cumm+biot+chl+Fe/Ti ox +epid	1
KA194AII	22	Pl+aug+opyx+ol+mgt	Porphyritic, subophitic matrix	olivine leucogabbroic porphyry	Marginal act+cumm+biot+chl +Fe/Ti ox+talc+serp	
KA201A	28	Pl+pyx+mgt	Coarse, ophitic	leuco-gabbro	Act+cumm+biot+chl+Fe/Ti ox	2
KA386P	33	Pl+aug+ol+opyx+mgt+qtz	Porphyritic, intergranular-subophitic matrix	olivine leucogabbroic porphyry	Act+cumm+chl+talc+biot	1
KA421	30	Pl+aug+opyx+ol+mgt	Medium, ophitic	dolerite	Act+cumm+biot+chl+Fe ox+talc+stipn+lim+epid	tr
KA428A	29	Pl+pyx+mgt	Medium, subophitic-ophitic	dolerite	Act+cumm+biot+chl+Fe ox	1
KA428B	27	Pl+pyx+mgt	Coarse, ophitic	leuco-gabbro	Act+cumm+chl	
KA428D	22	Pl+pyx+mgt	Coarse, ophitic	leuco-gabbro	Act+cumm+biot+chl+Fe ox	
KA428E	21	Pl+pyx+mgt	Coarse, ophitic	leuco-gabbro	Act+cumm+biot+chl+Fe ox	
KA428F	29	Pl+pyx+mgt		leuco-gabbroic porphyry	Act+cumm+biot+chl+Fe ox	
KA438A	23	Pl+pyx+mgt+qtz	Coarse, ophitic	leuco-gabbro	Act+cumm+chl	1
KA443	33	Pl+pyx+mgt		dolerite	Act+cumm+ abundant biot+hem+chl+Fe ox	tr

Table 6.4 Descriptions of gabbroic lithic samples. Pl=plagioclase; aug=augite; opyx=orthopyroxene; mgt=magnetite; ol=olivine; qtz=quartz; act=actinolite; cumm=cummingtonite ;biot=biotite; chl=chlorite; Fe/Ti ox=Fe/ti oxides; tit=titanite; lim=limonite; hem=hematite; talc=talc; epid=epidote;serp=serpentine; stipn=stipnomelane.

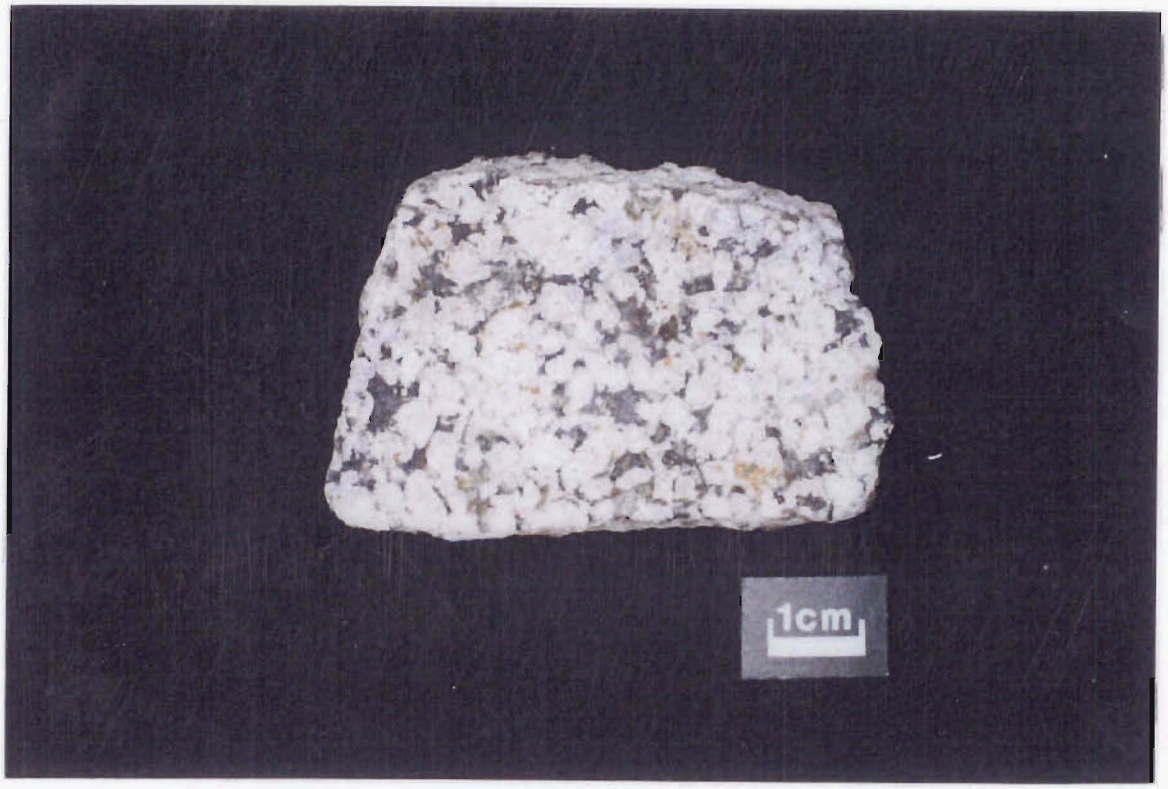

Figure 6.5a Leucogabbroic lithic hand specimen illustrating plagioclase-rich nature.

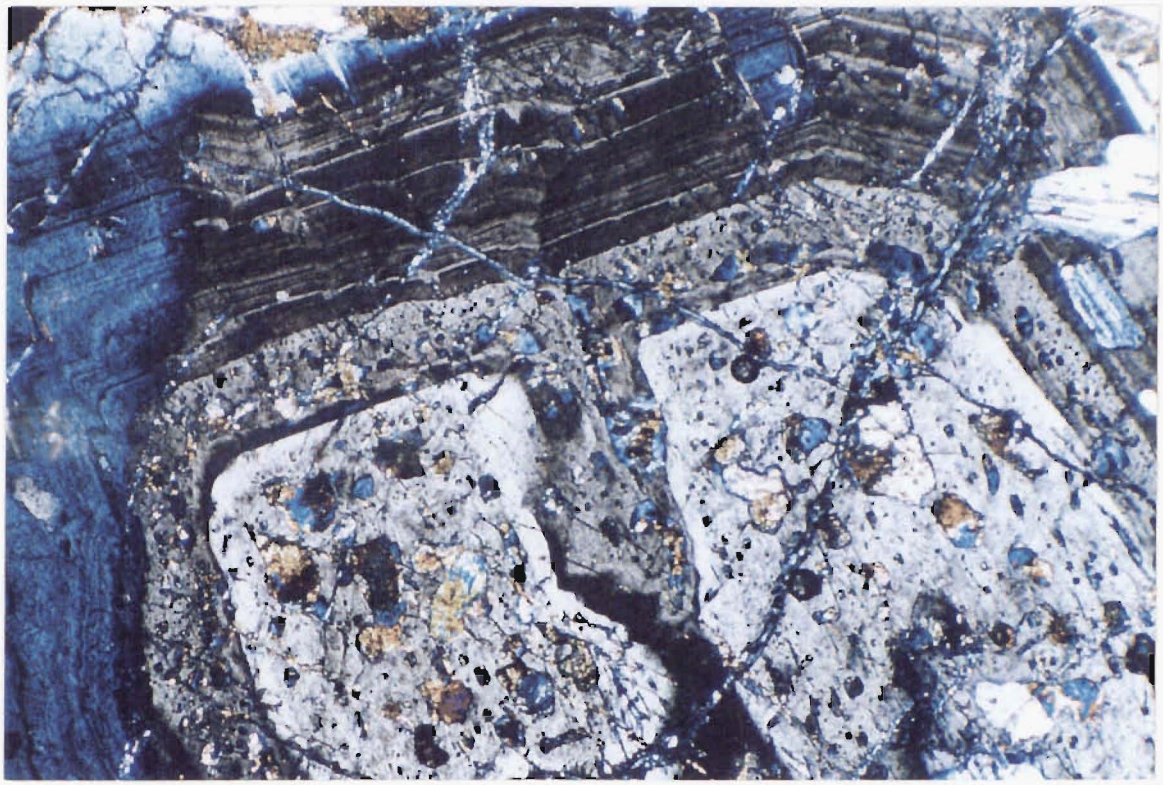

Figure 6.5b Complexly zoned and inclusion-rich calcic plagioclase within a leucogabbroic lithic. Field of view is 2 mm.

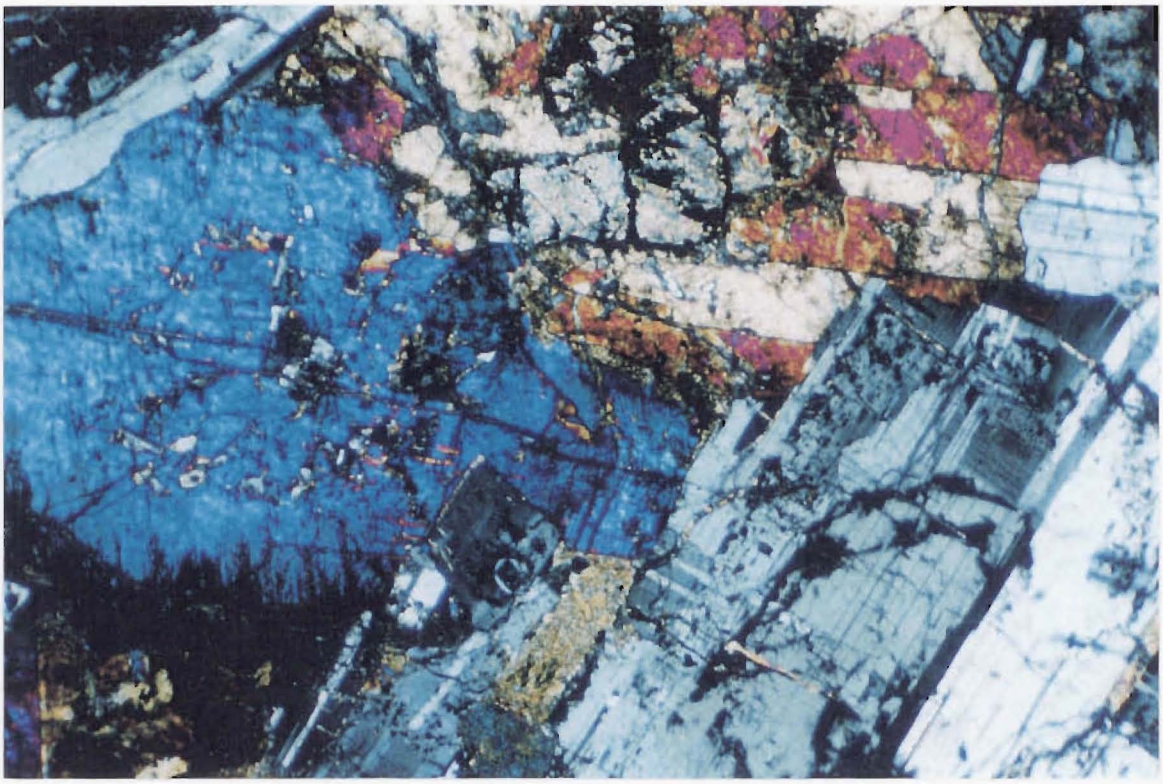

Figure 6.5c Marginal uralitisation of augite and total pseudomorphing of olivine by talc and Fe oxides in a weakly altered leucogabbroic lithic fragment. Field of view is 2 mm.

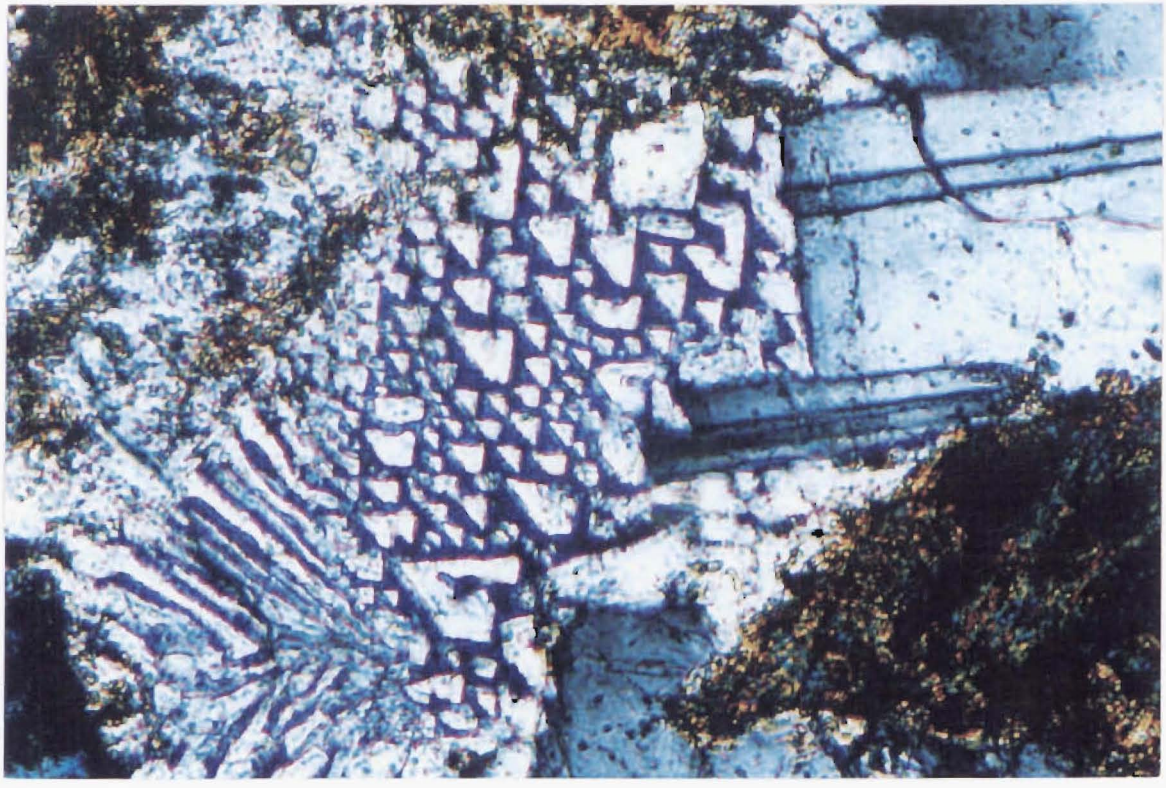

Figure 6.5d Micrographic intergrowth in a quartz-bearing leuco-gabbroic lithic. Field of view is 0.5 mm.

Sample no.	Pl	Opyx	Aug	Ol	amph +chl+talc+biot	Mgt	qtz
KA194AII	62.7	14.8	3.7	tr	17.0	1.3	0.1
KA386P	62.0	inf	4.3	inf	27.9	0.6	0.2
KA173	24.9	0.2	tr	0	23.6	tr	1.4
KA73	72.4	inf	inf	inf	27	0.5	0
KA6	72.7	0.20.1	0.3	inf?	25.9	0.7	0
KA82	78.4	tr	tr	0	20.1	1.5	tr

Table 6.5. Modal analyses of selected gabbroic lithics in the Kaingaroa Ignimbrite. Mineral abbreviations as in Table 6.4. In addition: tr = trace contents i.e. not detected during point count analysis; inf = mineral inferred from secondary mineral assemblage.

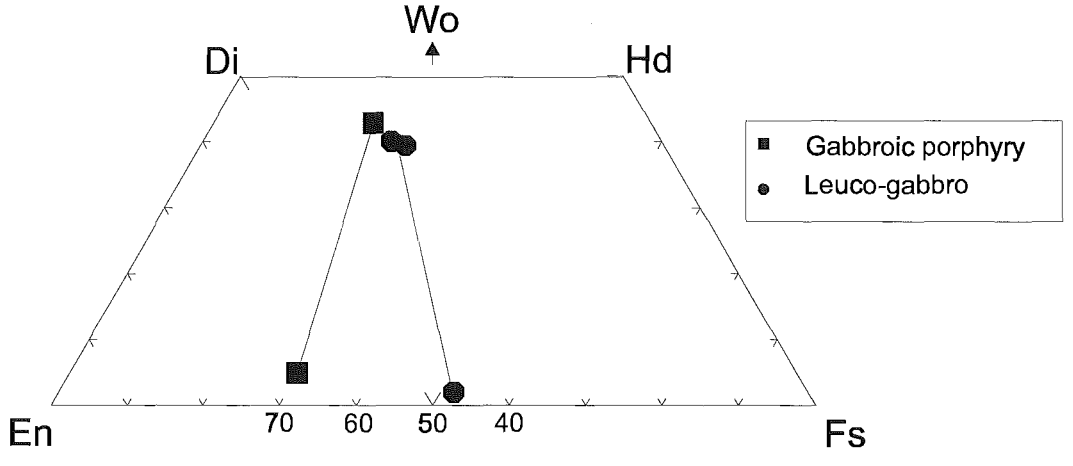

Figure 6.6. Pyroxene compositions in leuco-gabbroic lithics, classified after Morimoto (1989).

The presence of complex oscillatory zoned plagioclase, honeycomb plagioclase, granophyric texture (Fig 6.5d), and skeletal growth habits suggests the gabbroic lithics are samples of a sub-volcanic pluton or complex. The homogeneity of the dominant leuco-gabbroic lithologies and their inferred extensive distribution along the eastern margin of Reporoa Caldera suggests sampling of a single extensive intrusive (complex?) along the eastern margin of Reporoa Caldera. The variation in olivine and pyroxene modal% and pyroxene chemistry is interpreted to represent large scale

layering or zoning within the pluton or intrusive complex. Finer grained varieties are interpreted as margins of this complex or dike lithologies.

6.6.3 Geochemistry

If whole rock geochemical data are to be used to determine evolution of the gabbros, the basic requirement is that secondary alteration should not involve chemical transfer over distances greater than the size of the analysed specimen. All thin sections show evidence of secondary mafic mineral replacement, and this alteration could have lead to mobility of some major and trace elements. It is important to clarify the effects of this alteration on chemical composition.

Examples of unusual element enrichments in highly fractured samples include:

1) High K and Rb in KA173. In thin section this sample exhibits extensive secondary biotite, which may reflect K and Rb metasomatism.

2) Unusual high Ba in KA17 and the lack of a secondary Ba-rich mineral phase suggests the order of magnitude increase in Ba may be attributable to metasomatism.

3) High Zn in KA6, 173 and 428D.
The presence of secondary hydrous mafic silicates, anomalous variations in Th, K, Rb, Ba, and Ce suggests it is unlikely alteration was isochemical. In addition numerous samples exhibit aluminosilicate alteration of plagioclase. Despite this, immobile elements such as Zr, V, and Y show little variation between weakly altered and altered samples, and the majority of major and trace elements display coherent trends consistent with whole rock petrography and mineralogy.

Whole-rock compositions of the gabbroic rocks are given in Table 6.6. The gabbroic rocks have only a small range of SiO_2 (49-51 wt%), high Al_2O_3 (19.94-24.93 wt%), and a range in MgO (4-7 wt%). Gabbros are broadly calc-alkaline, and cluster as basalts in the TAS classification of volcanic rocks (Fig 6.7). Most of the gabbroic samples exhibit chemistry that probably does not represent *liquid* compositions. Evidence for this includes (1) High modal % plagioclase (up to 82%); (2) Whole-rock major and trace

element compositions that does not resemble typical magmatic arc lavas e.g. very high Al_2O_3, CaO, Sr (Fig 6.8) and positive europium anomaly (Eu/Eu*= 1.2-1.3). Rare finer-grained gabbroic porphyry and dolerites, interpreted as marginal facies, are interpreted to represent near magmatic compositions (liquid + crystals). These samples exhibit higher REE contents, higher MgO and a small negative Eu anomaly.

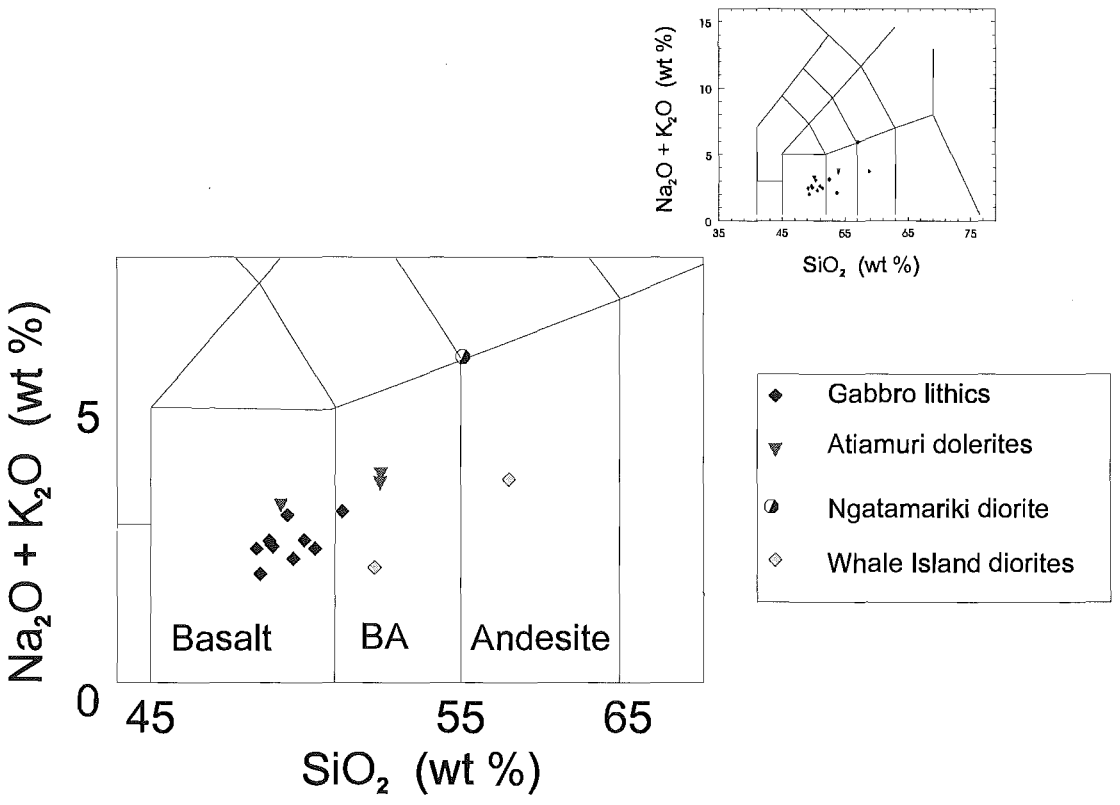

Figure 6.7. TAS classification of leucogabbroic lithics and associated intermediate and mafic plutonics in the TVZ (after Le Maitre 1989). Atiamuri data from Brown (1994), Ngatamariki data from Browne et al (1992) and Whale Island data from Burt et al (1996).

Sample Name	*KA6*	*KA82*	*KA173*	*KA194A11*	*KA428a*	*KA428d*
Rock Type	GB	GB	GB	GB	GB	GB
XRF						
SiO_2	48.26	49.05	51.58	50.32	49.48	49.68
TiO_2	0.33	0.33	0.34	0.46	0.42	0.41
Al_2O_3	22.17	24.93	20.97	22.74	20.25	23.17
Fe_2O_3*	6.43	4.96	6.13	6.02	7.02	6.36
MnO	0.12	0.08	0.12	0.12	0.11	0.12
MgO	5.12	3.98	5.41	4.01	5.89	4.49
CaO	13.24	12.77	10.65	13.14	11.26	13.14
Na_2O	2.21	2.35	2.56	2.62	2.24	2.29
K_2O	0.21	0.16	0.53	0.45	0.30	0.32
P_2O_5	0.05	0.03	0.03	0.04	0.05	0.04
LOI	0.52	1.55	1.93	0.58	1.72	0.42
Total	98.65	100.19	100.26	100.49	98.74	100.45
Cr	148	80	91	56	224	90
Ni	21	14	16	12	24	18
V	122	126	105	144	134	157
Pb	13	6	15	4	16	19
Zn	112	49	120	44	96	111
Rb	39	9	87	85	11	90
Ba	101	180	443	136	528	119
Sr	376	407	332	393	363	414
Ga	18	24	20	20	18	20
Nb	2	2	2	2	0	2
Zr	31	37	41	38	6	31
Y	6	19	8	7	13	6
Th	1	2	1	1	1	1
La	5	5	5	5	8	5
Ce	8	5	7	5	7	11
Nd	10	10	10	10	12	10
ICP-MS						
La			5.13	4.55	11	
Ce			11.8	10.4	10.7	
Nd			6.7	5.9	14.2	
Sm			1.7	1.4	3.1	
Eu			0.74	0.66	0.96	
Gd			1.7	1.6	3.1	
Dy			1.8	1.7	3.1	
Er			1	0.9	1.6	
Yb			1	0.8	1.5	
Lu			0.2	0.1	0.2	
Hf			0.3	0.6	0.4	
Ta			1.3	0.8	0.9	
Th			1.6	0.9	1.17	
U			0.27	0.11	0.31	

Table 6.6. Representative XRF and ICP-MS analyses of leucogabbroic lithics

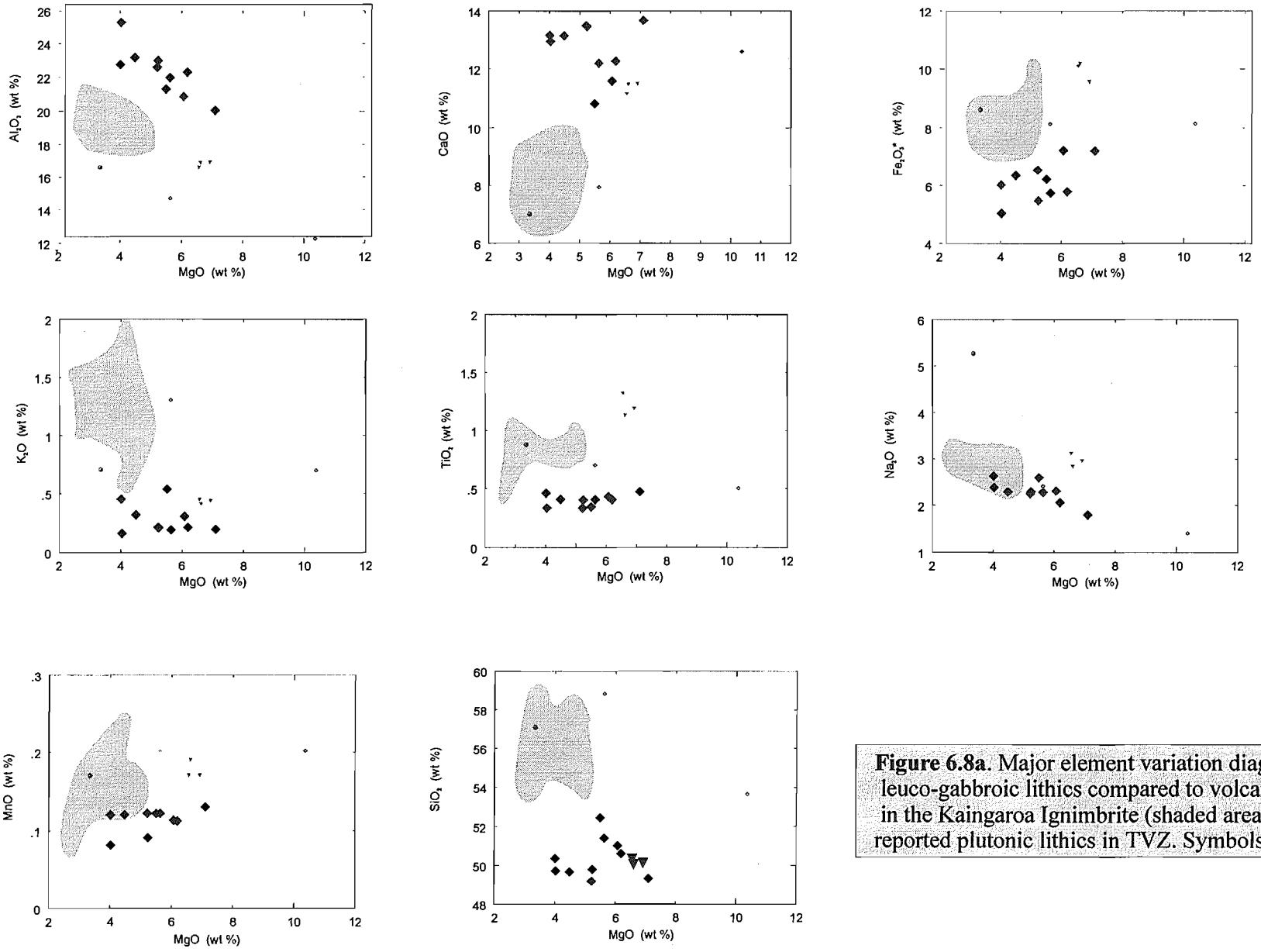

Figure 6.8a. Major element variation diagrams of leuco-gabbroic lithics compared to volcanic lithics in the Kaingaroa Ignimbrite (shaded area), and other reported plutonic lithics in TVZ. Symbols as in Fig 6.9.

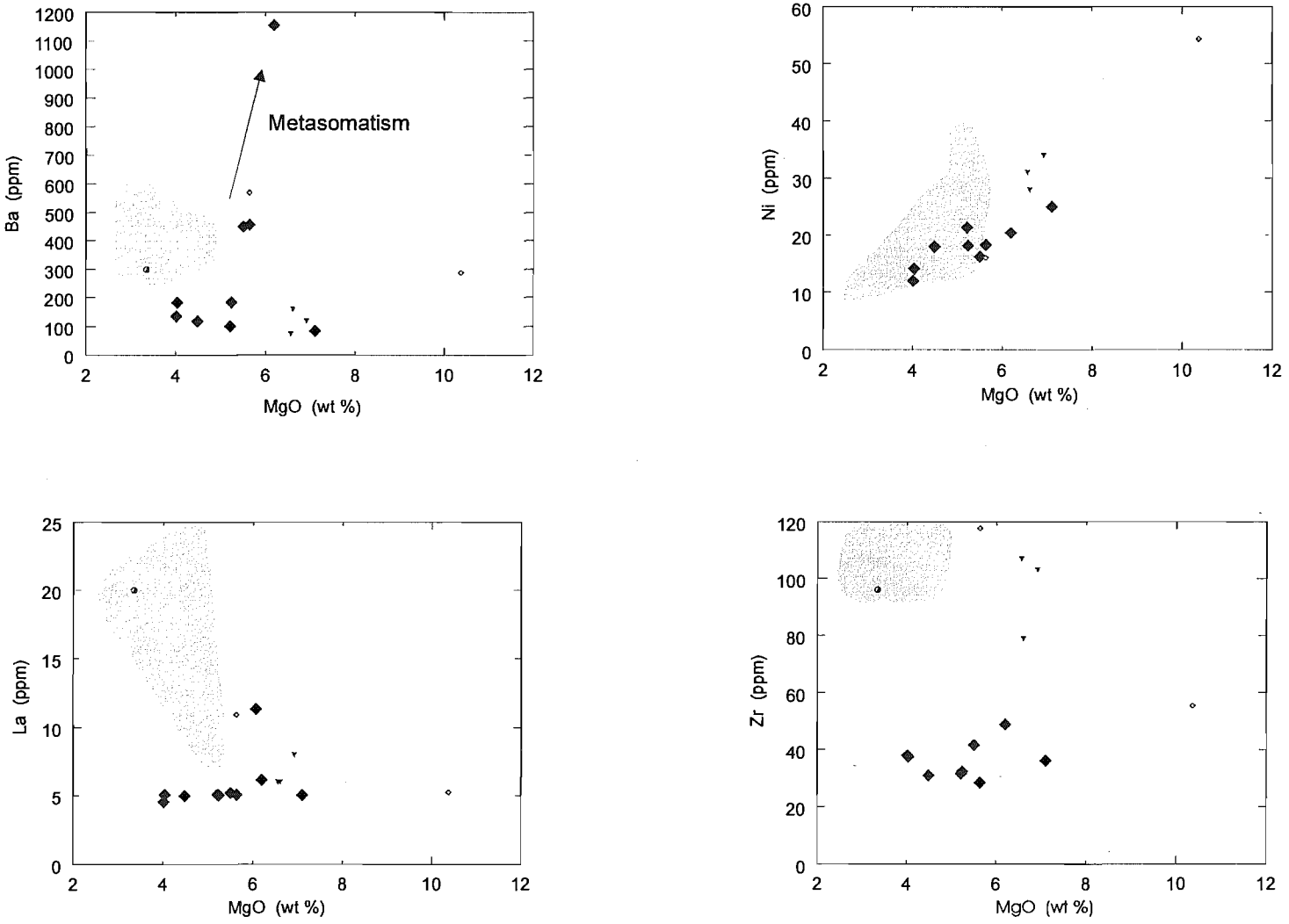

Figure 6.8b. Selected trace element variation diagrams of leuco-gabbroic lithics. Symbols as in Fig 6.8a.

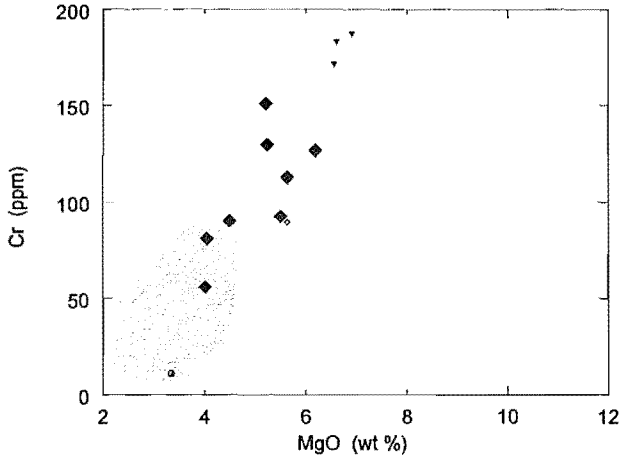

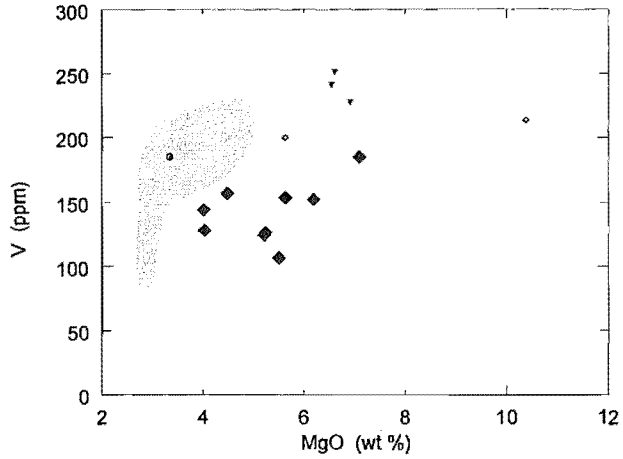

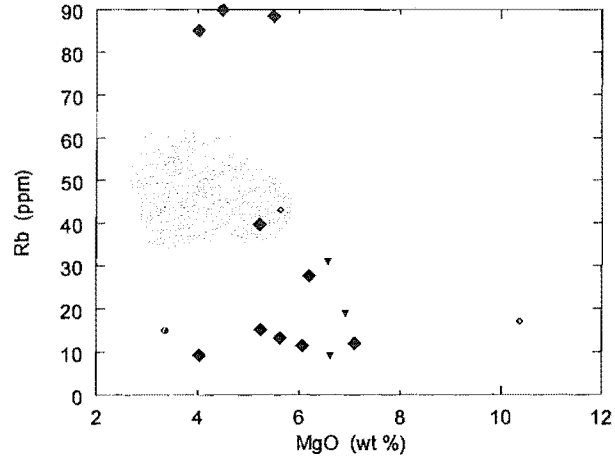

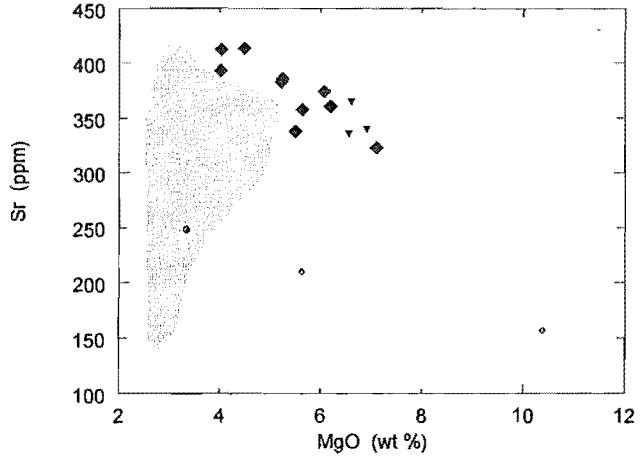

Figure 6.8c. Selected trace element variation diagrams of leuco-gabbroic lithics. Symbols as in Fig 6.8a.

Systematic trends on variation diagrams reflect variations in modal mineralogy, i.e. variable plagioclase: mafic ratios, variable orthopyroxene : augite ratios, and the presence of olivine. Figure 6.8 shows that with decreasing MgO content: Al_2O_3, Na_2O increases, CaO and Fe_2O_3 remain constant or gradually decrease, and SiO_2, TiO_2, K_2O and MnO remain constant. Trace elements exhibit more marked variation (Fig 6.8); Ni, Cr, and V show marked variations and decrease with decreasing Mg content, reflecting the abundance and fractionation of olivine and augite in Mg-rich samples. Zr shows no variation with Mg content, but is markedly low compared with other TVZ compositions, notably medium-grained dolerite KA428A (6 ppm), and Sr increases with decreasing Mg content reflecting the abundance of plagioclase. La show bimodal compositions reflecting the LREE enriched nature of the dolerites. Some variations in Ce content reflect alteration as illustrated by negative Ce anomalies in REE plots; in addition high Ce coupled with high P_2O_5 in some samples suggest cumulus apatite.

Rare Earth Elements

The chrondrite-normalized REE patterns of gabbroic rocks (Fig 6.9) show enrichment of the light elements (LREE). Total REE abundances increase with increasing MgO content. The REE abundances are higher for dolerite than for gabbroic $rocks_{s.s}$.

Gabbros exhibit a pronounced Eu anomaly (Eu/Eu* = 1.2-1.3), whereas the dolerites exhibit a small negative anomaly. The dolerite sample has similar chemistry to a uralitised andesite lithics.

6.6.4 Parental compositions and petrological evolution

The main aim of studying high level intrusives is to determine their parental composition, and/or possible extrusive equivalent. The classical approach to estimating parental compositions of mafic intrusions has been to sample chilled margins or associated dikes. This method is subject to error in complex open system intrusions involving multiple replenishment episodes as suggested by the complex plagioclase textures in the gabbroic lithics in the Kaingaroa Ignimbrite. A common approach in such cases is to infer parental composition from major-element mineral data.

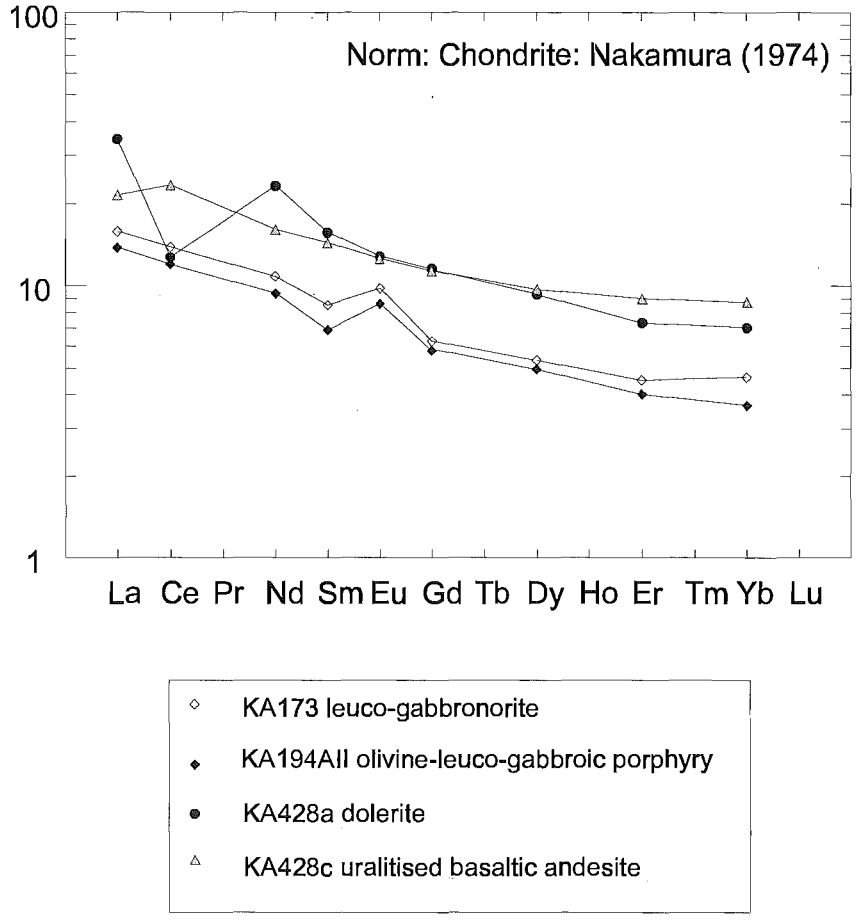

Figure 6.9. Chrondrite normalised rare earth element patterns for leuco-gabbroic lithics.

The most likely origin for these gabbros are they are fragments of a:

1) Pre-Pleistocene pluton surrounding the Reporoa area
2) Pre-existing TVZ subvolcanic pluton

Evidence supporting a sub-volcanic TVZ origin, probably related to uralitised basaltic-andesite lithics in the Kaingaroa Ignimbrite are:

A) Mg/(Mg/Fe) ratios of ferromagnesian minerals are appropriate for equilibrium with liquids having Fe/Mg ratios like basaltic andesite lithics in the Kaingaroa Ignimbrite,

B) Similar magmatic temperatures, mineralogy and broadly similar chemistry to the basaltic andesite lithics, notably the uralitised high Cr, Ni, Mg basaltic andesites,
C) Similar alteration which indicates pre-eruptive spatial association,
D) Spatial association with basaltic andesite lithics i.e. sampled together during the Kaingaroa Ignimbrite eruption, and
E) Medium-grained dolerites exhibit similar mineralogical, trace element and REE contents to UB which suggest they may represent approximates of parental magmas.

The low Mg numbers and Mg content of pyroxene indicates the gabbros were not derived from primary magmas. Comparison with high alumina basalts and low alumina basaltic andesites suggests the gabbros were probably derived from a magma with intermediate characteristics.

The TVZ is characterised by three distinct mafic magma types: high magnesian andesite (HMA), high alumina basalt (HAB), and low alumina basaltic andesite (LAB). The precise nature of primary mafic melts in TVZ is unknown due to limited near primary magmatic compositions, and general debate over primary magmas in arc environments. Discussion of primary magmas is beyond the scope of this thesis; but the gabbroic lithics in the Kaingaroa Ignimbrite were derived from magma(s) less evolved than the basaltic andesites in the Kaingaroa Ignimbrite, probably similar to dolerite and uralitised basaltic andesite lithics. Similar compositions are not exposed at the surface, and further work may shed light on the evolution and/or relationship of HAB to LAB (e.g. Graham et al. 1995).

Gabbroic lithics described here are distinct from other reported intermediate-mafic plutonics in the TVZ (Figs 6.7, 6.8). The Ngatamariki diorite, despite its obvious altered state (i.e high Na, Pb, Zn) is more evolved (e.g lower MgO, Cr), and could be considered the subvolcanic equivalent of TVZ andesites. Brown (1994) describes high alumina dolerite lithics from Atiamuri, which exhibit characteristics similar to high alumina basalts in TVZ.

The plagioclase-rich nature, high Sr, Ca, Al, positive Eu anomaly and depletion in K are suggestive of plagioclase accumulation, relative to the doleritic and andesitic lithics. In light of continuing debate over the method of plagioclase accumulation an alternative

hypothesis is discussed here. The model is based on continual and prolonged plagioclase resorption and growth, as advocated by numerous workers for plagioclase-phyric andesites, gabbros associated with anorthosite complexes, deep level arc-related leuco-gabbroic complexes, and leuco-gabbros in general (e.g. Blundy and Shimizu 1991). Plagioclase textures in the gabbroic lithics exhibit a variety of textures and compositions. All of the zoning patterns are broadly normal, because the most sodic composition occurs at the crystal margin. Oscillatory zoning is marked by two notable An% jumps, a calcic spike and a sudden decrease in An content, which correspond to complex resorption features within the plagioclase mantles. The cores of all gabbroic samples are calcic, suggestive of derivation from basaltic parent as described above. In contrast the evolution of plagioclase compositions towards the rim suggests the crystals have experienced changing P-T, i.e. disequilibrium conditions. Some crystals exhibit marked chemical discontinuities suggesting a crystallisation hiatus and/or a period of resorption. The simplest explanation is mixing of plagioclase in more (i.e. recharge) and less evolved melts.

Blundy and Shimizu (1991) propose that crystals displaying continuous zoning patterns represent crystals *retained* in the magma throughout its evolution, whereas crystals exhibiting hiatus or resorption textures have a complex history involving *re-entrainment*, and record the influx of less evolved magma. Small variations in An% are unlikely to represent mixing, but rather changes in pressure, water fugacity and temperature, but large jumps (e.g. 15 An%) suggest mixing. The implication for gabbros described here, is of a complex history of recharge from less evolved ('basaltic') magma into a crystallising, fractionating chamber. Plagioclase recycling is indicated by variation in oscillatory zoning patterns, suggesting that not all plagioclase have not undergone the same evolution. This method has been advocated as creating alumina-enriched magmas such as plagioclase-phyric andesites or ultra-phyric andesites (e.g. Komor et al. 1987; Cullen et al. 1989). Such rocks are 'crypto-cumulates', preserving 'geochemical evidence of accumulation' i.e. enrichment of element abundant in plagioclase, (Ca, Al, Sr, Eu) but textural evidence of complex magma processes involving recharge and fractionation, common processes in andesitic magma systems. Further work is required on plagioclase trace element variation to quantify any textural model for evolution of the gabbros.

6.6.5 Secondary deformation and alteration

Deformation textures

Numerous samples exhibit extensive fracturing, and/or are cut by biotite, chlorite, quartz, Fe-oxide, adularia or actinolite veins. Rare samples show evidence of localised patches of cataclasis, with sericitised fragments of plagioclase set in a sericite matrix. This may reflect deformation during alteration or entrainment during the Kaingaroa Ignimbrite eruption.

Secondary mafic minerals

All samples exhibit secondary alteration of ferromagnesian minerals, and rarely of plagioclase:

Augite is present as rare relics with marginal alteration of Fe/Ti oxides and fine grained amphibole along cleavage, and grain boundaries. Commonly augite is pseudomorphed by fibrous randomly or variably orientated actinolite, or rarely as granular actinolite i.e. uralitisation (Fig 6.5c). Orthopyroxene is variably altered to cummingtonite, chlorite and biotite in similar specimens. Biotite is present in small amounts in some samples, either associated with titaniferous magnetite or associated with chlorite and/or amphibole. Olivine alteration varies from replacement by chlorite or serpentine along margins and internal cracks within the olivine to total replacement by talc, fine-grained opaques, carbonate, and chlorite (Fig 6.5c). All of the above minerals are associated with varying amounts of opaque minerals, interpreted to represent oxidation of ferromagnesian minerals to iron oxides. Titaniferous magnetite is present either as isolated grains replacing calcic plagioclase interiors, within thin veins associated with epidote and/or quartz, and as marginally altered primary magmatic mineral, altered to maghemite. Titanite is locally present associated with chlorite or magnetite. Limonite is commonly present along fractures, locally forming spherulitic patches.

Plagioclase is rarely altered (except to an amorphous aluminosilcate as discussed below), but locally is saussuritised (fine grained sericite and clusters of sub mm epidote) in cataclastic domains. Epidote is locally present within veins, but no carbonate minerals are associated with either alteration of mafic minerals or plagioclase.

Rare gabbroic lithic samples contain fine-grained, sub-mm, blue-green pleochroic tourmaline associated with (pseudomorphing?) plagioclase feldspar, interpreted to represent a tertiary alteration event, similar to observed in associated metavolcanics described below.

Alteration comprises a complex secondary mineral assemblage interpreted as high temperature hydrothermal alteration or deuteric alteration at P-T analogous to approximately greenschist facies conditions (inferred due to presence of abundant chlorite, actinolite and biotite). This alteration event is similar to observed in numerous basic intrusions (e.g. Rhum; Housden et al. 1996; Skaergaard, Bird et al. 1988), and is inferred to represent deuteric alteration accompanying or postdating magmatic intrusion, prior to juxtaposition adjacent to the Kaingaroa magma system and evisceration during eruption.

Amorphous aluminosilicate alteration

Nine of 18 gabbroic lithics sampled show variable degrees of plagioclase alteration. The alteration occurs in three textural associations: sieved plagioclase, isolated pockets, and veins, where brown to yellow or pink, amorphous material occurs in plagioclase cores, individual zones, along cleavage, and in patchy zones (Figs 6.10, 6.11), and occasionally along two separate zones. In highly altered samples e.g. KA201AI small plagioclase crystals are almost totally replaced, whereas larger plagioclase may exhibit minor replacement along thin mantle zones. The degree of alteration mimics the degree of intensity of fracturing and hematitic staining. A similar style of alteration is observed in many plagioclase-phyric andesite lithics.

Amorphous material is dominantly isotropic, resembling glass, but is locally weakly birefringent, and exhibits a distinctive halloysite-like chemistry (Table 6.7). Sample KA421 exhibits fine-grained phyllosilicates associated with highly brecciated domains, which are intimately associated with the brown isotropic amorphous aluminosilicate.

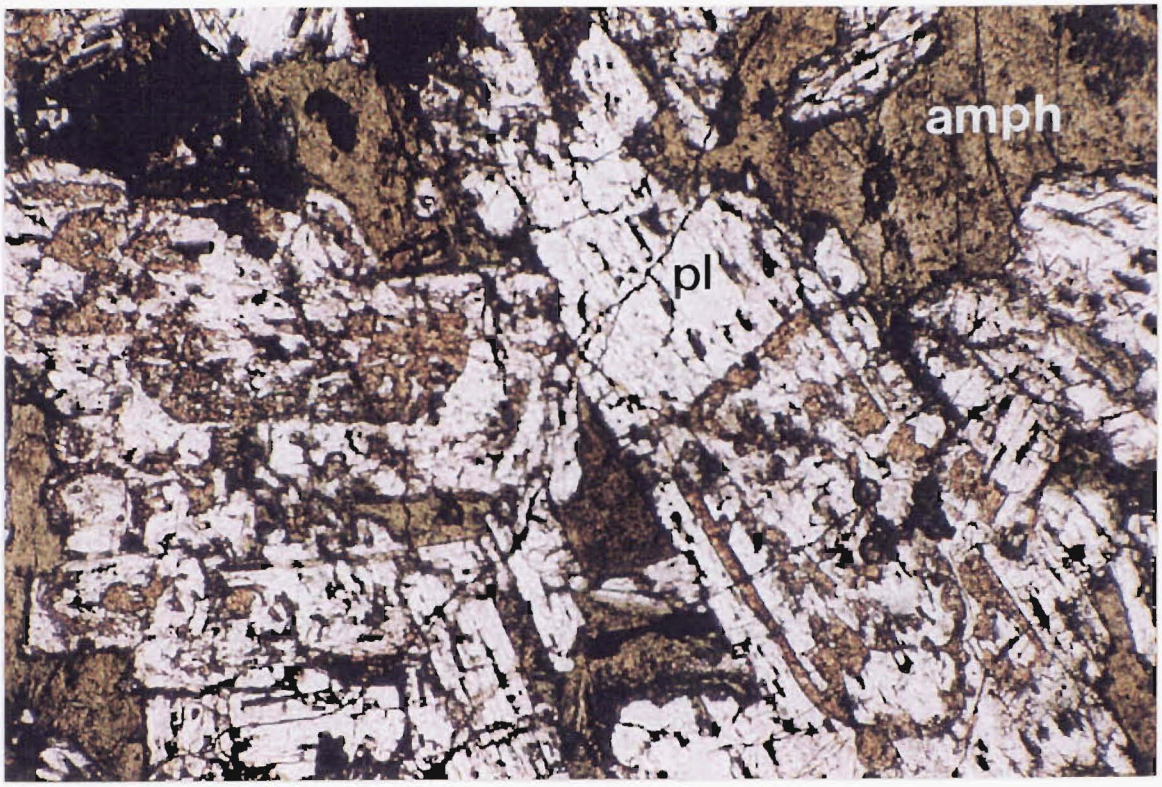

Figure 6.10a. General texture of altered leucogabbroic lithic illustrating presence of brown amorphous aluminosilicate material within 'sieve-textured' plagioclase. Field of view is 7 mm.

Figure 6.10b. Brown amorphous aluminosilicate replacing plagioclase feldspar margins and core in an altered leucogabbroic lithic. Field of view is 2 mm.

SiO_2	46.14	42.30	44.79	45.72	44.93	44.39	44.21
Al_2O_3	39.96	37.54	36.59	38.05	37.70	37.24	35.16
TiO_2	0.03	0.02	0.07	0.07	0.10	0.12	0.05
FeO	0.73	1.68	1.99	0.91	0.94	1.6	1.15
MnO	0.13	nd	nd	0.04	0.04	0.02	0.03
MgO	0.03	nd	0.03	nd	nd	0.04	0.03
CaO	0.35	0.16	0.32	0.36	0.42	0.32	0.35
Na_2O	0.05	0.09	0.08	0.02	0.11	0.22	0.06
K_2O	0.17	0.23	0.19	0.23	0.25	0.32	0.31
Total	87.59	82.01	84.06	85.39	84.50	84.27	81.34

Note: (1-7) amorphous aluminosilicate, nd = not detected.

Table 6.7 Amorphous aluminosilicate compositions in sample KA386P.

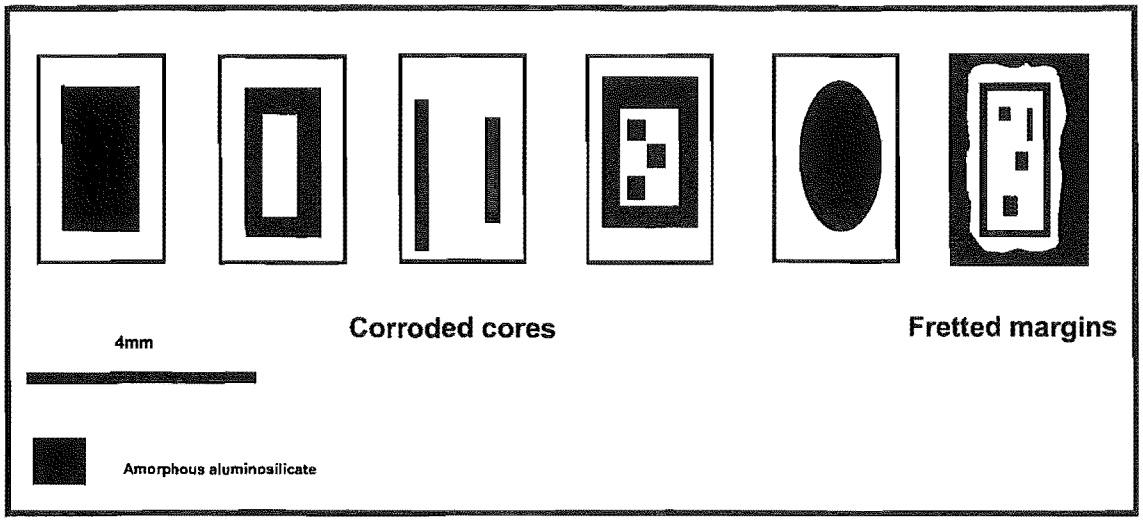

Figure 6.11 Textural occurences of amorphous aluminosilicate alteration of plagioclase in leucogabbroic lithics

	Rim	*Mantle*	*AA edge*	*AA middle*	*AA core*
SiO_2	54.31	52.75	50.32	45.87	47.61
Al_2O_3	29.3	29.04	41.49	38.41	35.37
TiO_2	0.04	0.00	0.00	0.03	0.03
FeO	0.56	0.64	1.09	1.32	2.68
MnO	0.00	0.00	0.00	0.00	0.00
MgO	0.06	0.03	0.05	0.04	0.06
CaO	12.66	12.80	0.10	0.10	0.11
Na_2O	4.33	3.87	0.15	0.14	0.09
K_2O	0.30	0.64	0.91	0.76	0.77
Total	101.56	99.78	94.10	86.67	86.72

Table 6.8 KA201AI transect across calcic plagioclase (1-2) and amorphous aluminosilicate (AA; 3-5). Cation totals of plagioclase are presented in Appendix D.

To determine the nature of the amorphous material, microprobe traverses were undertaken across two samples; KA386P and KA201AI. Analyses were conducted under conditions outlined in Appendix C, except to avoid Na diffusion within the sample during analysis, the amorphous material was analysed with a beam diameter of 30-μm.

Sample KA386P is zoned from An_{82-61}. The amorphous aluminosilicate is present in trace amounts along a thin zone within the feldspar mantle, and is flanked by calcic plagioclase (An_{83} and An_{68}). This mantle zone is frequently replaced by the amorphous material, and hence gives no clues as to the replaced composition. The composition is tentatively assumed to be intermediate between An_{83} and An_{68}, as is the case in preserved unaltered examples.

The second sample KA201AI contains approximately 2% amorphous material within cores, sodic zones, mantles, and rarely replacing rims. Preserved mantle and rim data suggest plagioclase is normally zoned from a calcic core to An_{61} rim. Transect compositions are presented in Table 6.8.

The transects across individual plagioclase crystals suggests the amorphous material is near homogeneous. Microprobe analysis totals are low (ca. 84-87), interpreted to reflect the abundance of water, and/or possibly other volatiles (e.g. Cl), and may represent variation in temperature controlled dissolution (Casey et al. 1991). The presence of amorphous aluminosilicate within cores of plagioclase suggest the result of weathering rather than deuteric alteration, as secondary chlorite and amphibole are unaltered.

Similar styles of alteration were noted in granitoids and gabbros by Snetsinger (1967), Okumura (1985) and Habteselassie et al (1996), which they attributed to chemical weathering. Considering the original range in inferred core compositions from unaltered specimens, alteration has resulted in depletion in CaO, alkalis, and the introduction of water, and possibly Cl. Ca and alkalis are inferred to have been removed by the vapour or fluid. Alteration is inferred to have occurred or propagated along planes of weakness i.e. zones and cleavage. Spilde et al (1993) noted amorphous aluminosilicate within plagioclase cores associated with amorphous silica in andesite pumice, adjacent to fumaroles. They interpret the amorphous material as due to low temperature dissolution of calcic plagioclase, similar to that advocated by Snetsinger and Okamura. Spidle et al (1993) consider the dissolution of feldspar as due to fumarolic alteration by chloride-rich vapour; in addition noting greater degree of replacement at zones further from the fumarole, at lower temperatures. They also note preferential destruction of anorthitic-rich plagioclase to albitic.

The amorphous aluminosilicate replacement of calcic plagioclase occurs in altered lithic clasts found adjacent to unaltered lithics. This precludes an insitu weathering origin post eruption. Alteration is interpreted to be due to hydrous metasomatism, and fumarolic leaching, post deuteric alteration (which resulted in alteration of mafic minerals) and prior to eruption. The abundance of amorphous aluminosilicate alteration within andesites and gabbroic lithics in welded ignimbrites sections, suggests a similar process may occur during welding, perhaps analogous to the pervasive replacement of mafic silicate phenocrysts by clay minerals, observed in devitrified welded ignimbrites by Smith (1960) and Stimac et al (1996). The presence of halloysite suggests alteration occurred at low temperatures e.g. $>100^{o}$ C as halloysite transforms to kaolinite above 110^{o}C (Hurst and Kunkle 1985).

6.7 Granophyre

A leucocratic (colour index= 2%) medium grained, porphyritic, granophyre lithic was sampled at Butchers Boundary Rd Quarry. The granitoid fragment is a holocrystalline porphyritic biotite granophyre, composed of > 75% granophyric intergrowth.
Plagioclase(An_{38-12}) and quartz are the dominant phenocryst types with subordinate biotite, which is commonly replaced by biotite (± chlorite) aggregates. Accessory minerals include titanite, zircon, apatite, ilmenite and magnetite.

Granophyric intergrowths are common suggesting rapid subsolvus crystallisation at shallow crustal levels or the release of volatiles during volcanic eruptions. The presence of complexly zoned phenocrysts and granophyric intergrowths suggest a subvolcanic environment of crystallisation. Similar secondary minerals suggest a possible spatial association with the metavolcanics (see below). The limited presence of granophyre lithics, despite a detailed lithic componentry study, and specific search for plutonic lithics, suggests that the lithic may represent either a recycled lithic from a pre-Kaingaroa ignimbrite, or sample of a intrusion of limited size. The presence of rhyolite domes in the area and rhyolite lithics in the Kaingaroa Ignimbrite indicates localised rhyolitic magmatism in the Reporoa region. Brown et al (submitted) summarised the petrology and geochemistry of granitoid lithics in the TVZ. These included numerous granophyre lithics that petrographically resemble the Kaingaroa granophyre. The lithic was too small for chemical analysis.

6.8 Metavolcanics

6.8.1 Introduction

A variety of altered hornfelsic meta-rhyolite lithics was sampled during lithic componentry, and include tourmaline-bearing metavolcanics and tourmalinites.

Tourmaline is a common accessory mineral in a variety of rock types and mineral deposits, but the most common association is with granitic rocks and their associated pegmatites and metasomatic aureoles. Tourmaline-bearing rocks that contain in excess of 20% tourmaline are termed *tourmalinites* (Slack 1996). Tourmaline-rich rocks have

been reported in New Zealand by Black (1971) on Cuvier Island, where they are associated with the hydrothermal aureole of a diorite intrusion. The presence of tourmaline is interpreted as due to boron metasomatism (tourmalinization) during late stages of magmatism. Black (1971) found that tourmalines inherited their composition partly from their host rocks, and partly from metasomatising solutions.

This section describes the metavolcanics, in particular the first reported occurrence of tourmaline-bearing metavolcanics and tourmalinites in the Taupo Volcanic Zone. The metavolcanic lithics form up to 5% of lithic ejecta in the lag breccia, OWR and WIU ignimbrite units, but are difficult to identify as they closely resemble rhyolites. The coarsened groundmass of many samples was interpreted as plutonic in origin (tonalite) by Nairn et al (1994). Meta-rhyolite is the most common metavolcanic lithotype and these may contain tourmaline, with one block composed of 70% tourmaline. Three distinct alteration types are identified within the metavolcanic lithics:

6.8.2 Biotite-zoisite-epidote-andalusite-bearing meta-rhyolites

Texturally the rocks are porphyritic with variable phenocryst totals and populations. They are crystal-rich (up to 40% phenocrysts) and contain embayed and fractured quartz, fresh to incipiently sericitised oscillatory zoned plagioclase feldspar (An_{45-32}), and fresh to kaolinitised sanidine phenocrysts in a recrystallised felsitic to granoblastic quartz ($\pm$ feldspar) matrix. Mafic minerals are pseudomorphed by biotite ($\pm$ epidote) aggregates. Biotite is locally present as circular aggregates, interpreted to represent amgydales. Secondary minerals include biotite, chlorite, epidote, zoisite, titanite, andalusite, magnetite, ilmenite, and maghemite. All samples are cut by quartz veins. Similar compositions have been as lithic types in numerous TVZ ignimbrites by the author.

The majority of biotite-zoisite-epidote-andalusite-bearing meta-rhyolites were too small for geochemical analysis. A single lithic was analysed for major and trace elements by XRF. The sample (KA91) exhibits broadly rhyolitic chemistry (Appendix E). The presence of epidote and zoisite and alteration state of feldspars suggests extensive element mobility, illustrated by high Ca, Sr, and low Rb, Ba and K. Despite the high Zn content (225 ppm), sphalerite or other Zn-bearing ore minerals were not detected.

6.8.3 Tourmaline-bearing meta-rhyolites

Tourmaline-bearing samples superficially resemble biotite-zoisite-epidote-andalusite-bearing meta-rhyolites, but notably contain blue-green to green-brown pleochroic tourmaline, either associated with biotite aggregates or pseudomorphing feldspar. The mineral is commonly colour zoned and occurs as xenoblastic radiating or spherulitic aggregates filling vugs (Fig 6.12), and replacing plagioclase feldspar. Rarely tourmaline occurs as microcrystalline trains in the matrix or microlite-like needles emanating from biotite aggregates, and is locally altered to iron oxides. The impression is of tourmalinization superimposing on biotite replacement of feldspar. The tourmalinisation is a late stage process that obliterates the original texture of the rock. The presence of phenocrysts, oscillatory zoned plagioclase, amgydales and secondary coarsened felsitic texture indicate a volcanic protolith. The groundmass of some samples, whose original nature could have been glassy, contains irregular lenticular quartzose patches suggestive of pseudomorphed fiamme or pumice, and an ignimbritic origin.

6.8.4 Tourmalinite

One medium grained rock consists of almost pure euhedral-subhedral blue-green pleochroic tourmaline prisms (tourmalinite), with interstitial fine-grained biotite. The texture is hypidiomorphic granular, with no layering, and no remnant textures or minerals to suggest a protolith. The similar tourmaline composition (Fig 6.13, Table 6.9) and alteration mineralogy suggest a metavolcanic protolith, and spatial association with the metavolcanic lithics.

6.8.5 Tourmaline chemistry

Tourmaline is a complex borosilicate with the general formula of $XY_3Z_6(BO_3)_3$ - $Si_6O_{18}(F, OH)_4$. The Z site is typically occupied by Al, whereas the Y site can be occupied by a variety of cations (e.g. Ti, Fe, Mg, Mn, Li and Al). The X site usually contains Na, but may be replaced by Ca, Mg, and K. Several solid solutions exist in tourmaline, depending on substitutions in the various sites. Most tourmalines belong to one of two solid solutions: schorl (Fe-rich)- dravite (Mg-rich), and schorl (Fe-rich)-elbaite (Li-rich).

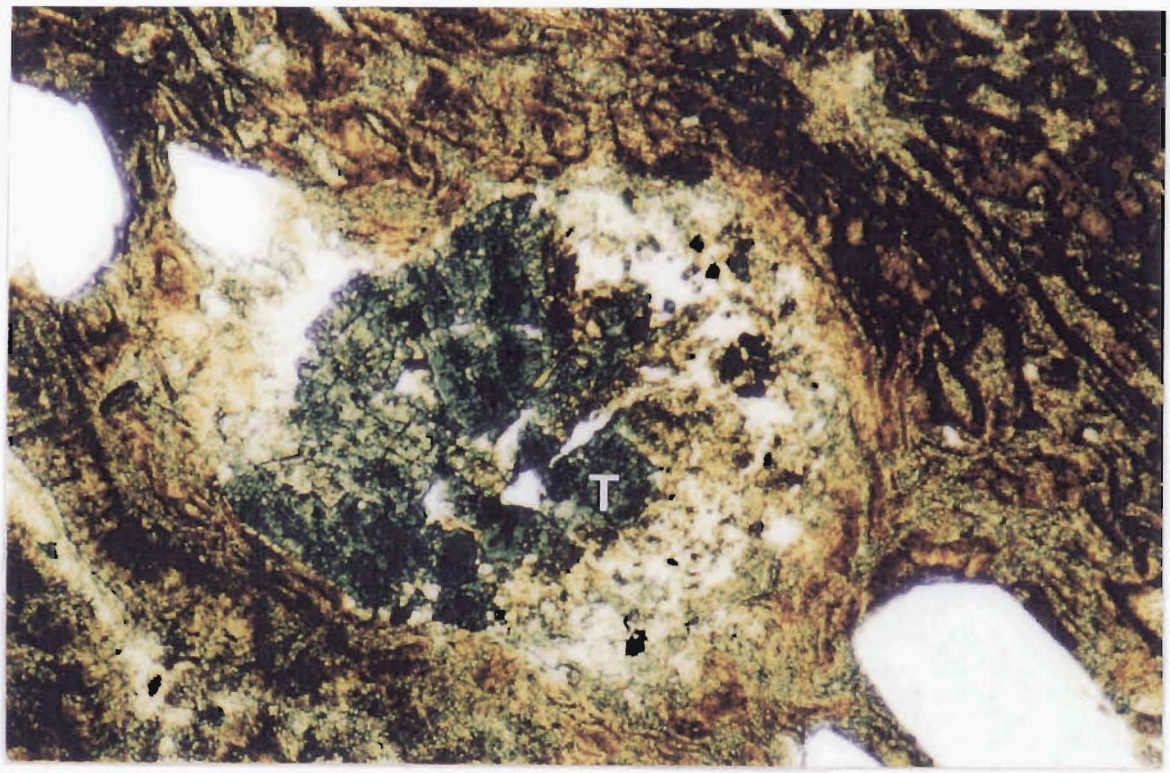

Figure 6.12a. Blue-green pleochroic tourmaline-rich lithic fragment within welded Kaingaroa ignimbrite, Main Gully Rd. Field of view is 2mm.

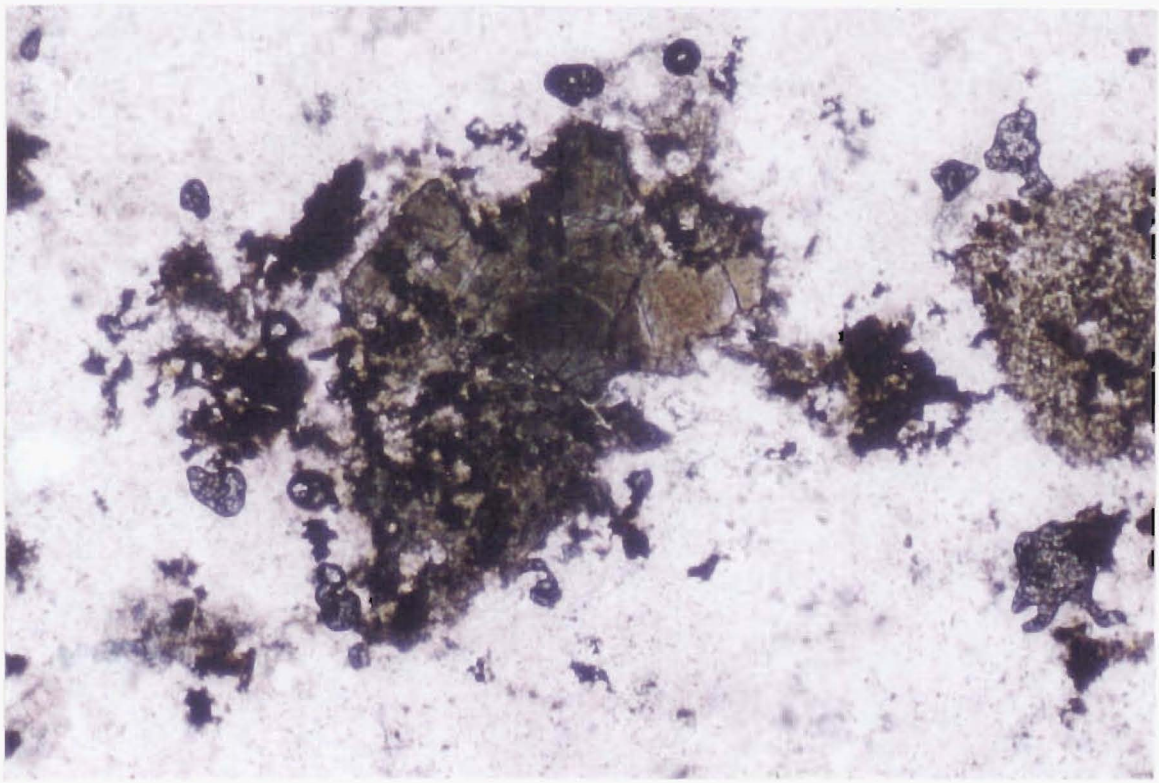

Figure 6.12b. Spherulitic aggregates of zoned blue-green pleochroic tourmaline replacing biotite aggrgates and plagioclase in a meta-rhyolite lithic. Field of view is 4mm.

	KA46 Sm tourm	KA430 Core				Rim
SiO_2	36.888	36.176	36.347	35.81	36.32	36.238
Al_2O_3	36.066	36.019	36.317	35.977	36.02	36.006
TiO_2	0.092	0.091	0.119	0.135	0.119	0.126
FeO	6.25	5.877	5.978	5.915	6.123	4.237
MnO	0	0	0	0	0	0.023
MgO	4.813	5.088	4.964	4.964	4.966	4.927
CaO	1.346	1.44	1.295	1.413	1.45	1.47
Na_2O	1.478	1.478	1.429	1.428	1.488	1.39
K_2O	0.092	0.097	0.079	0.091	0.143	0.075
Total	87.0292	86.2695	86.5301	85.7372	86.6326	84.4976
Oxygen	29	29	29	29	29	29
B	3.000	3.000	3.000	3.000	3.000	3.000
Si	6.9912	6.9153	6.9209	6.8897	6.9244	6.9966
Al	8.056	8.1148	8.15	8.1577	8.0934	8.1932
Ti	0.0132	0.0132	0.0171	0.0196	0.0171	0.0183
Fe	0.9906	0.9395	0.9519	0.9518	0.9762	0.6842
Mn	0	0	0	0	0	0.0038
Mg	1.3599	1.4501	1.4091	1.4238	1.4116	1.4181
Ca	0.2734	0.295	0.2642	0.2913	0.2962	0.3042
Na	0.5431	0.5478	0.5276	0.5328	0.5501	0.5206
K	0.0224	0.0238	0.0192	0.0224	0.0349	0.0185
Total	21.2502	21.2998	21.2604	21.2894	21.3042	21.158

Table 6.9. Tourmaline analyses from tourmalinite (KA46) and meta-rhyolite lithic (KA430). All Fe as FeO. In the absence of accurate analyses, B is assumed to have a stoichiometric value of 3.000, and normalisation of cations on the basis of 29 oxygens, following the recommendations of Henry and Dutrow (1996).

During formation tourmaline is highly influenced by its chemical environment. Numerous workers have reported that tourmaline compositions closely reflect the bulk composition of the rock in which they were formed (e.g. Black 1971; Henry and Guidotti 1985). Henry and Guidotti (1985) demonstrated that tourmalines from different geological environments have characteristic compositions. In general, tourmaline from granitic environments tend to trend towards the schorl end member, whereas tourmalines associated with massive sulphide deposits generally approach dravitic compositions. Tourmalines from the meta-rhyolite lithics are classified according to Henry and Guidotti (Fig 6.13; Table 6.9). Tourmalines in meta-rhyolite lithics exhibit compositions suggesting they are intermediate between schorl and dravite. Similar compositions have been noted by Fiersmans and Paepe (1982) and Cavaretta et al (1992) in meta-silicic volcanic rocks. Additional factors influencing chemistry may include redox conditions, temperature and pH of the fluid (Slack and Coad 1989). Protolith compositions for all metavolcanics in the Kaingaroa Ignimbrite are interpreted to be silicic volcanics and variations in tourmaline composition are assumed to be related to external (e.g. temperature) or fluid chemical variations. Tourmaline was also noted in leucogabbroic lithic fragments (Section 6.6) but was not analysed. The presence of tourmaline in hydrothermally altered gabbros suggests probable pre-eruption spatial association with meta-rhyolites. Holgate (1977) noted tourmaline as sporadic clots in altered gabbros, associated with albitised plagioclase and actinolite, a similar mineral assemblage to altered gabbros described in Section 6.6.

Boron is a relatively mobile element, and the abundance of tourmaline in volcanic deposits indicates a high activity of boron in hydrothermal or metasomatic fluids. The presence of tourmaline in TVZ is notable, as tourmaline is commonly asociated with a wide range of precious metal deposits e.g. Au, Ag, Zn, U, Mo.

Tourmaline has not previously been reported in the TVZ, but is reported in hydrothermal systems in the Philippines associated with andesitic volcanics by Reynes and Giggenbach (1992), who note tourmaline in 'magmatic' wells (i.e. wells that encounter magmatic-hydrothermal fluids) associated with rocks exhibiting contact metamorphism grading into high temperature hydrothermal alteration. Reynes and Giggenbach (1992) advocate temperatures in excess of 200°C, and probably between 300 and 500°C. Temperatures for formation of biotite-zoisite-epidote-magnetite meta-

rhyolites of 350°C + are suggested by the coexistence of secondary biotite and magnetite, and the presence of epidote indicates > 250°C (C.P.Wood pers comm 1996).

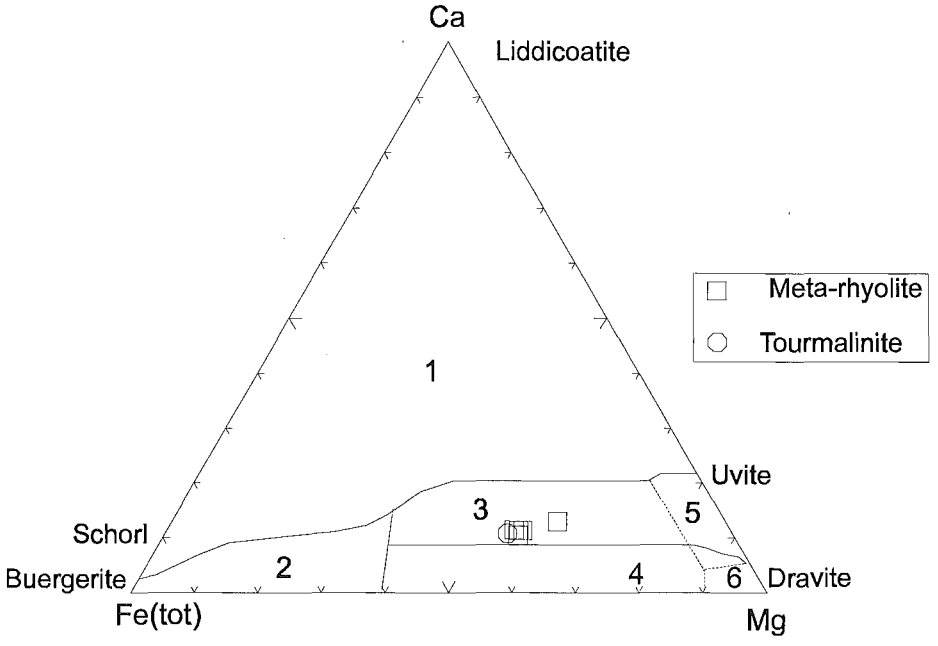

Figure 6.13. Tourmaline analyses classified after Henry and Guidotti (1985). The majority of analyses are intermediate between schorl and dravite in composition.

6.8.6 Discussion

Lateral and vertical trends or zones of alteration are commonly associated with hydrothermally altered areas, especially magmatic metasomatic zones. Petrographic evidence suggests alteration of metavolcanics was followed by, or superimposed on tourmalinization. The three alteration types described above are inferred to represent alteration or metasomatic zones (facies) formed around the Kaingaroa magma system. The presence of kaolinitised and albitised felspar, tourmaline and abundant secondary hydrous phases suggests extensive mobility of K, Na, B, and H_2O. The biotite-zoisite-epidote-andalusite-bearing meta-rhyolites exhibit quartz-sericite alteration facies, and coarsened matrices suggestive of contact metamorphism and metasomatism. Temperatures in excess of 350 °C are indicated by the presence of magnetite, biotite and epidote. The replacement of biotite by tourmaline suggests tourmalinitisation is an overprinting or tertiary process possibly related to separate period of

metamorphism/metasomatism. A more likely scenario is that the incoming of tourmaline reflects progressive metasomatism due to a change in fluid temperature, pH, or oxidation conditions. A single tourmalinite sample suggests a possible third zone, where boron metasomatism is pervasive. Similar zonation in alteration facies has been commonly described adjacent to plutons (e.g. Bajwah et al. 1995; London et al. 1996), and in tourmaline-bearing silicic volcanic clasts (e.g. Fiersmans and Paepe 1982).

The presence of metavolcanic lithics within juvenile pumices suggests metavolcanic lithics were present at or near magma fragmentation level, consistent with an inferred position, adjacent to the Kaingaroa magma system. The metavolcanic blocks are inferred to be related to a minor metasomatic reaction, and not a pervasive and extensive hydrothermal system, analogous to the extensive geothermal systems present at the surface e.g. Waiotapu.

6.9 "Greywacke" (GW)

GW comprises a diverse group of angular low-grade metasedimentary lithics, including variably altered highly indurated feldslitharenites, argillites, sub-greenschist facies slates, hornfels, and jasper. Five thin sections of 'greywacke' and slate lithics were analysed. Four samples were low-grade and medium-grained sandstones, and therefore provenance could be interpreted. All four samples contained abundant quartz, feldspar, and rock fragments, and classify as feldslitharenites (Folk et al. 1970). In addition the matrices consist of muscovite, chlorite and pumpellyite within the groundmass. Sample KA 200a exhibits decussate micas suggesting a weak contact metamorphic overprint. The development of pressure solution seams and presence of pumpellyite indicates all samples are low grade, probably prehnite-pumpellyite facies. The presence of trachyitic and spherulitic-rhyolitic rock fragments, and granophyre rock fragments and microcline suggests a volcanic and plutonic provenance. Possible correlative basement lithologies (i.e. Waipapa and Torlesse) exhibit dominantly volcanic and plutonic provenances respectively. Therefore to assess likely provenance a sample was analysed for major and trace elements by XRF (Appendix E), and exhibit Torlesse-like composition (Mortimer 1995). GW is correlated with the low-grade quartzofeldspathic Torlesse terrane basement, based on similar chemistry, and petrography.

A single meta-greywacke sample was examined. KA201A is a fine-grained slate with well defined lattice- and shape preferred orientation of quartz and micas. The presence of stilpnomelane, abundant pressure solution seams, quartzose and micaeous domains suggests sub-greenschist facies. Slates are inferred to represent higher grade Torlesse-like basement.

The presence of inferred Torlesse metasediments beneath Reporoa Caldera, further corroborates Mortimer's (1995) proposal that Torlesse metasediments underlie most of TVZ.

6.10 Sediments and tuffs (SED)

SED includes a variety of weakly consolidated to friable lithologies, which are commonly present only in proximal sections. Included in this category are baked soils, volcanic sediments and breccias, non-welded ignimbrites or pumice breccias, and diatomites.

Two low-density light brown-grey lithologies were classified as diatomite during field lithic descriptions, which subsequent thin section (KA188) and SEM analysis revealed to include two different lithologies; altered silicic tuff and diatomite.

CHAPTER SEVEN

Kaingaroa Magma System

7.1 Introduction

Whole pumices in silicic ignimbrites are considered to represent quenched fragments of vesiculated and disrupted magma, and as such are perceived as instantaneous samples of the pre-eruption magma chamber/system. Systematic compositional and mineralogical gradients within ignimbrites provides unequivocal evidence of chemical and thermal zonation in their magma chambers. Compositional zonation can be recognised as systematic changes in bulk major- and trace- element chemistry (and often isotopic ratios), phenocryst content and mineralogy, and volatile content (Lipman 1967; Smith 1979; Hildreth 1979, 1981). Large chemical, thermal, and volatile gradients are common features of some magma bodies, especially smaller scale examples, particularly in alkaline compositions (Wolff et al. 1990). Large silicic systems are more commonly homogenous or only weakly zoned (e.g. Fish Canyon Tuff; Whitney and Stormer 1985), and were termed 'monotonous' by Hildreth (1981) and De Silva (1991).

Previous work on TVZ ignimbrites noted the lack of significant compositional zonation (Dunbar et al. 1989; Smith 1989; Hochstein et al 1993), especially in recent rhyolitic eruptives from Okataina and Taupo caldera complexes. Briggs et al (1993) described chemical variation in Mangakino-derived ignimbrites and attributed the existence of zonation to lower heat flow and lower level of tectonic activity in western TVZ. Brown (1994) documented extensive thermal, mineralogical and chemical zonation in the Whakamaru-group ignimbrites of TVZ. These eruptives are notable for their large volume, high crystal content, abundance of quartz, hydroxyl-bearing mafic phenocrysts, and presence of sanidine, suggestive of extensive fractionation of large volumes of magma.

Magmatic processes in silicic magma chambers in central TVZ are poorly understood, despite numerous recent studies (e.g. Briggs et al. 1993, Karhunen 1993, Brown 1994; Sutton et al. 1995). Unresolved topics include:

A) Styles of compositional zonation, continuous (Briggs et al. 1993) or stepwise (Brown 1994).

B) Replenishment dynamics and timing i.e. recharge, and subsequent magma mixing.

C) Evisceration of multiple magma chambers (Sutton et al. 1995).

D) Relationships between magma composition, eruptive dynamics and caldera collapse

Aspects of the Kaingaroa magma system addressed here are:

1. Mineralogical and chemical variation of pumices, and pre and post-caldera rhyolites.
2. Development of the compositional variation and role of syn-eruptive mingling.
3. Evolution of the Kaingaroa magma system, and implications of styles of compositional variation or zoning in TVZ ignimbrites.

Aspects of petrological comparison with other TVZ ignimbrites and petrogenesis of rhyolites in the TVZ are outlined and discussed in Chapter 9.

Previous work on the petrology of the Kaingaroa Ignimbrite is limited to a single pumice XRF analysis in Nairn (1981), and reconnaissance glass shard chemistry by Black et al (1996).

Pumices were sampled from *all* non-welded ignimbrite sections, in particular samples were collected systematically from a vertical section through Reporoa Boundary Unit (RBU), transition zone and OWR at Old Waiotapu Rd, and a section through lag breccia and OWR at Burn Rd. Numerous pumice clasts were sampled from the same horizon (where possible) to check for heterogeneous pumice compositions, and evidence of syn-eruptive mingling. Due to the welded nature of Kaingaroa Ignimbrite (in particular WIU), pumice samples were mainly from non-welded basal and upper sections. Although pumices are present in the upper parts of WIU, they are extremely vapour-phase altered and unsuitable for sampling and chemical analysis. Locations where relatively fresh pumices from WIU can be extracted are restricted to lower transition zones between OWR and WIU, and a single sample from beneath the lower vapour-phase zone at Putunoa hill. The rarity of basal tephra and RBU samples is due to extremely poor exposure and the small grain size of these units. Pumices analyses are presented for basal tephras (8), Reporoa Boundary Unit (13), transition zone and lag breccia (37), Old Waiotapu Rd unit (31), and Webb ignimbrite unit (4). 29 pumices

were thin sectioned, and all pumices examined under the binocular microscope to determine pumice petrography. Modal analyses were calculated by weight% where possible, because of the difficulties of retaining crystals in pumices during thin section preparation, and hence the possible large errors in point counting. 93 samples were analysed for major and trace elements by XRF, and a further subset for mineral chemistry (EPMA), REE and selected trace elements (INAA) and isotopes (Appendix D and E). Samples with high LOI and Al_2O_3 contain kaolinite and meta-halloysite, formed from hydration of glass (Appendix E), and were removed from the dataset (Appendix E). Representative analyses of Kaingaroa pumices are presented in Table 7.1.

Three post-caldera rhyolites exposed at the surface within the Reporoa area have been identified (Kairuru, Pukekahu, and Deer Hill; Chapter 2). Kairuru and Pukekahu rhyolite domes were each sampled for petrography, mineral chemistry and chemistry, and Kairuru dome also for isotope analysis. The analysis of Deer Hill rhyolite dome is from Brown (1994).

Two distinctive 'Kaingaroa-like' obsidian and rhyolite lithic fragments were also identified during lithic componentry (Chapter 5 and 6). A single dense juvenile obsidian lithic and Kaingaroa-like rhyolite lava lithic were sampled for petrography and geochemistry. In addition an inferred welded 'Kaingaroa-like' ignimbrite lithic with similar lithic content and phenocryst phases was analysed by EPMA, in order to confirm correlation with Kaingaroa Ignimbrite (see Chapter 5 and 6).

7.2 Magmatic components

7.2.1 Pumice

The Kaingaroa Ignimbrite consists of pumice, variably coloured due to variations in glass iron oxidation state and vesicularity rather than mineralogical and chemical variation (see below). Three broad pumice colours are identified: A) highly vesicular white or yellow pumice, which is present as the only pumice type in the basal tephras, RBU, and lower transition zone, and rarely as an mingled component in OWR; B) grey pumice and C) black pumice, both present only in the upper transition zone or lag

breccia, OWR and WIU. The bulk of the pumices sampled and discussed herein consist of glass, free of any post-magmatic alteration (see Appendix E).

Moderately vesiculated white/yellow or grey pumice are sub-aphyric to porphyritic, contain 0.6-3.5 wt% (commonly < 1%) phenocrysts of, in order of decreasing abundance, euhedral plagioclase feldspar, orthopyroxene, Fe/Ti oxides, and very rare hornblende and augite. This is a typical mineralogical assemblage for Quaternary ignimbrites and rhyolites from the Taupo Volcanic Zone (Ewart et al. 1975). Apatite and zircon are present as accessory phases. Biotite and quartz were identified in whole rock ignimbrite, but due to their absence in pumices are inferred to be xenocrystic and derived from disaggregation of Whakamaru-group ignimbrites. Fe/Ti oxides also occur as inclusions within plagioclase and orthopyroxene. Magnetite is more abundant than ilmenite. Phenocrysts are commonly present as 4-6mm clots giving the pumice a glomeroporphyritic texture.

Highly vesicular black pumices are a rare type present only in the OWR unit and upper transition zone. Glass shards in matrices of whole rock ignimbrite suggest black pumices were more abundant than grey, but were preferentially fragmented and disaggregated (due to their highly vesicular nature) during eruption and emplacement. Black pumices exhibit the same mineralogy, major, trace element (including REE) and isotopic composition as grey pumices. Similar colour variation, not attributable to chemical variation, has been outlined by Briggs et al (1993), Karhunen (1993), and Druitt et al (1996). Black pumices are notably more vesicular (80-90 vol%), crystal-poor, and contain dark brown/black high SiO_2 rhyolitic glass. Powdered forms of black pumices and their high vesicularity suggests colour variation is *partly* attributable to bubble wall reflection. Cashman (net communication) attributes black pumice colouration to very small sub-100 angstrom microlites, which reflect variations in oxidation state of iron.

Rare pumice samples contain occasional xenoliths of hydrothermally-altered and spherulitic rhyolite, and hornblende-bearing altered 'Rangitaiki-like' ignimbrite, especially in basal tephra pumices. This is consistent with shallow magma fragmentation level within Whakamaru-group ignimbrites (Chapter 5).

A single bleb was chiselled from the welded Tokiaminga Valley facies (Chapter 4). Blebs (1-60 mm) resemble fiamme, but exhibit localised sharp angular edges suggesting aspects of brittle behaviour during emplacement (Chapter 4). The presence of fluidal (plastically deformed) boundaries and mingling with Kaingaroa pumices $_{s.s.}$ indicates the blebs are juvenile. All samples exhibit oxidised rims and are surrounded by bleached matrices. Only one sample was analysed, because of abundant mingling of other pumice types and small size of many samples.

Blebs are weakly vesicular, with 0.1 wt% phenocrysts of euhedral plagioclase, orthopyroxene, augite, hornblende, Fe/Ti oxides. Apatite is present as an accessory phase. Fe/Ti oxides also occur as inclusions in pyroxene and plagioclase. Phenocrysts of plagioclase and pyroxene range in size up to 1.5mm in length. Acicular green-pleochroic hornblende has rims altered to opacite. Both hornblende and augite are markedly more abundant than Kaingaroa pumices$_{s.s.}$. Magnetite is very rare and commonly oxidised. Non-vesicular domains within the bleb are composed of brown-coloured, locally perlitic, cracked glass. The blebs do not resemble vitrophyric ignimbrites, pumices, or fiamme. The presence of mingled pumice and bleb and evidence of heat retention, suggest the blebs are juvenile. They are inferred to represent recycled pyroclasts, possibly derived from earlier eruption products during the Kaingaroa eruption.

Black-red coloured obsidians comprise up to 90% of dense components (i.e. lithics and obsidian) in the basal tephras. The obsidians are frequently conchoidally fractured, perlitic cracked, transluscent, locally pumiceous, and contain ca.10 vol% phenocrysts of plagioclase, orthopyroxene, Fe/Ti oxides, hornblende and accessory zircon and apatite. They have similar mineralogy and phenocryst clots to Kaingaroa pumices. Well aligned microphenocrysts of plagioclase and pyroxene define a flow fabric. Some obsidians exhibit ignimbritic textures such as fiamme and fractured phenocryst domains, suggesting they may represent densely-welded vitrophyric ignimbrites. Basal tephra pumices exhibit rare transitional pumices which grade into obsidian i.e. banding defined by variation in vesicularity, colour and density. Obsidian fragments in the basal tephras are interpreted as a dense juvenile component.

7.2.2 Precursor rhyolite lithics

Crystal-poor obsidian lithics were identified in the lag breccia during lithic componentry. These blocks exhibit similar mineralogy to the Kaingaroa Ignimbrite pumices i.e. plagioclase, orthopyroxene and Fe/Ti oxides. Groundmass is ubiquitously vitric, and locally perlitic cracked.

7.2.3 Post-caldera rhyolite domes

Post-caldera rhyolite domes were analysed to assess their role in evolution of the Kaingaroa magma system, especially following a major caldera-forming eruption. The field characteristics and petrography of Kairuru, Pukekahu, Deer Hill were outlined in Chapter 2, and are summarised here with respect to the Kaingaroa pumices.

Pukekahu rhyolite dome contains (2.5 vol%) of plagioclase, orthopyroxene, Fe/Ti oxides and hornblende. Deer Hill is petrographically similar with 6 vol% plagioclase, orthopyroxene, augite, Fe/Ti oxides phenocrysts. Both rhyolite domes are mineralogically similar to the Kaingaroa Ignimbrite. Kairuru is petrographically distinct with 10-11 vol% phenocrysts of plagioclase, quartz, orthopyroxene and Fe/Ti oxides.

7.2.4 Kaingaroa-like ignimbrite lithic

Light brown-yellow andesite and ignimbrite lithic-rich ignimbrite lithic fragments are a common lithic-type in the Kaingaroa Ignimbrite, notably in the lag breccia (Chapter 5). The lithic blocks vary from massive to breadcrusted, frequently conchoidal-fractured, and exhibit similar mineralogy and lithic types to the Kaingaroa Ignimbrite, notably the RBU.

The blocks are texturally variable but distinct from RBU, exhibiting a wide variation in welding from densely welded to partially welded to compacted non-welded. All samples are vitric; the densely welded blocks are notable for their extreme degree of welding illustrated by highly flattened fiamme, and a perlitic cracked- highly compressed vitroclastic matrix. Some of these are breadcrusted and resemble high-grade vitrophyric ignimbrites. All samples are pumice- and lithic-rich, and texturally distinct both in terms

of matrix texture and pumice and lithic abundance to the RBU. This may be a function of degree of welding, and reflect the proximal nature of the samples.

A number of samples were thin sectioned to assess variation in mineral content or texture, and compared mineralogically with the Kaingaroa Ignimbrite. All the samples are mineralogically similar and are interpreted to represent samples through a single complexly welded ignimbrite unit. Crystal content of sampled lithics vary from 5 to 15 vol%.

Plagioclase is the dominant phenocryst phase, with subordinate orthopyroxene, Fe/Ti oxides, hornblende, quartz and augite. Augite and quartz are locally demonstrably xenocrysts derived from fragmentation of ignimbrite and andesite lithics. The occurrence of vitric matrix and glassy fiamme indicates that these lithics were formed by quenching of hot fragments. Breadcrusting suggests exsolution of volatiles after the clasts were ejected from the conduit.

The lithics are interpreted as fragments of proximal lithic-rich pumice-rich ignimbrite that was broken up and ejected by vent widening during caldera collapse. Many of the densely welded vitrophyric blocks may represent ignimbrite agglutinated within the conduit, which was later rejected, when they were still at magmatic temperature. Similar 'cognate' lithic blocks have been reported in many large scale caldera-forming ignimbrites e.g. Campanian Ignimbrite (Rosi et al. 1996).

7.3 Mineral and glass chemistry

7.3.1 Plagioclase

Plagioclase (up to 2 mm in length); the dominant phenocryst, occurs as euhedral to subhedral, often fractured phenocrysts, commonly with inclusions of glass, apatite and Fe/Ti oxides. Glomeroporphyritic aggregates with pyroxene are common. Plagioclase is ubiquitously normally oscillatory zoned from An_{49-26}. Microprobe analyses of plagioclase are presented in Appendix D. Plagioclase exhibits limited compositional variation both within the pumices and in Kaingaroa-like ignimbrite lithics. Anomalously An-rich plagioclase crystals within the Kaingaroa-like ignimbrite lithics are considered

xenocrystic, derived from disaggregated andesite lithic fragments, based on similar mineral composition (Chapter 6), absence from pumices, and local evidence of disaggregated andesite lithics. Plagioclase compositional variation with pumice chemistry is summarised in Table 9.3.

7.3.2 Pyroxene

Orthopyroxene is the dominant pyroxene in Kaingaroa pumices, with very rare augite present in some mineral separates, and as an abundant phase in the less evolved dacitic bleb (KA386f). The small bleb size of KA386f did not provide sufficient sample for a mineral separate, and augite was not analysed in the pumice sample, but identified optically from X-Z sections with inclined extinction, high birefringence, biaxial +ve interference figure with moderate 2V.

Weakly green-brown pleochroic orthopyroxene occurs as subhedral to anhedral rounded and fractured prisms up to 2 mm in length, commonly with Fe/Ti oxide and apatite inclusions, and rarely with zircon and glass inclusions. Microprobe analyses are presented in Appendix D and illustrated in Fig 7.1a, relative to pumice chemical variation described below. Orthopyroxenes range from En_{51-40} in composition similar to typical orthopyroxene values in TVZ rhyolites (Ewart et al. 1975). Pyroxene exhibits weak variation becoming more Fe rich in more evolved compositions. Normal zoning is weakly developed. Insufficient data are available to speculate on the extent of the zonation. The Kaingaroa-like ignimbrite lithic (Fig 7.1) exhibits similar orthopyroxene chemistry and limited zonation (En_{49-45}). Mg-rich orthopyroxenes (En_{58}) and augite are considered to be derived from disaggregated andesite lithic fragments (as with calcic-plagioclase above). Post-caldera rhyolites (Fig 7.1) exhibit variable orthopyroxene chemistry. Orthopyroxene in Pukekahu rhyolite dome is similar to Kaingaroa pumices (En_{50-43}), whereas Kairuru orthopyroxenes are more Fe-rich (ca.En_{37}), consistent with its more evolved composition. Pyroxene compositional variation with pumice chemistry is summarised in Table 7.3.

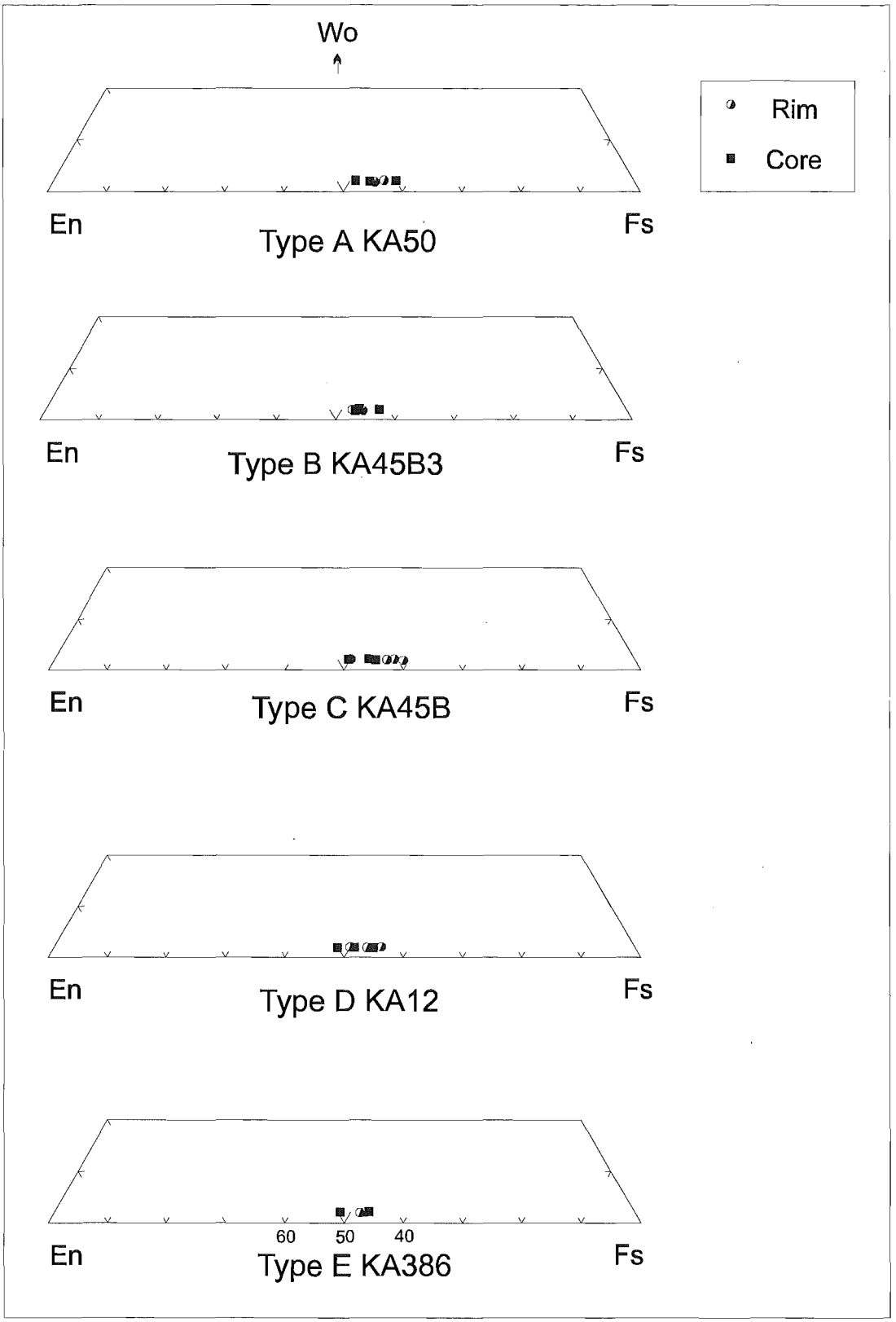

Figure 7.1a. Orthopyroxene variation in Kaingaroa pumices, relative to pumice types defined below.

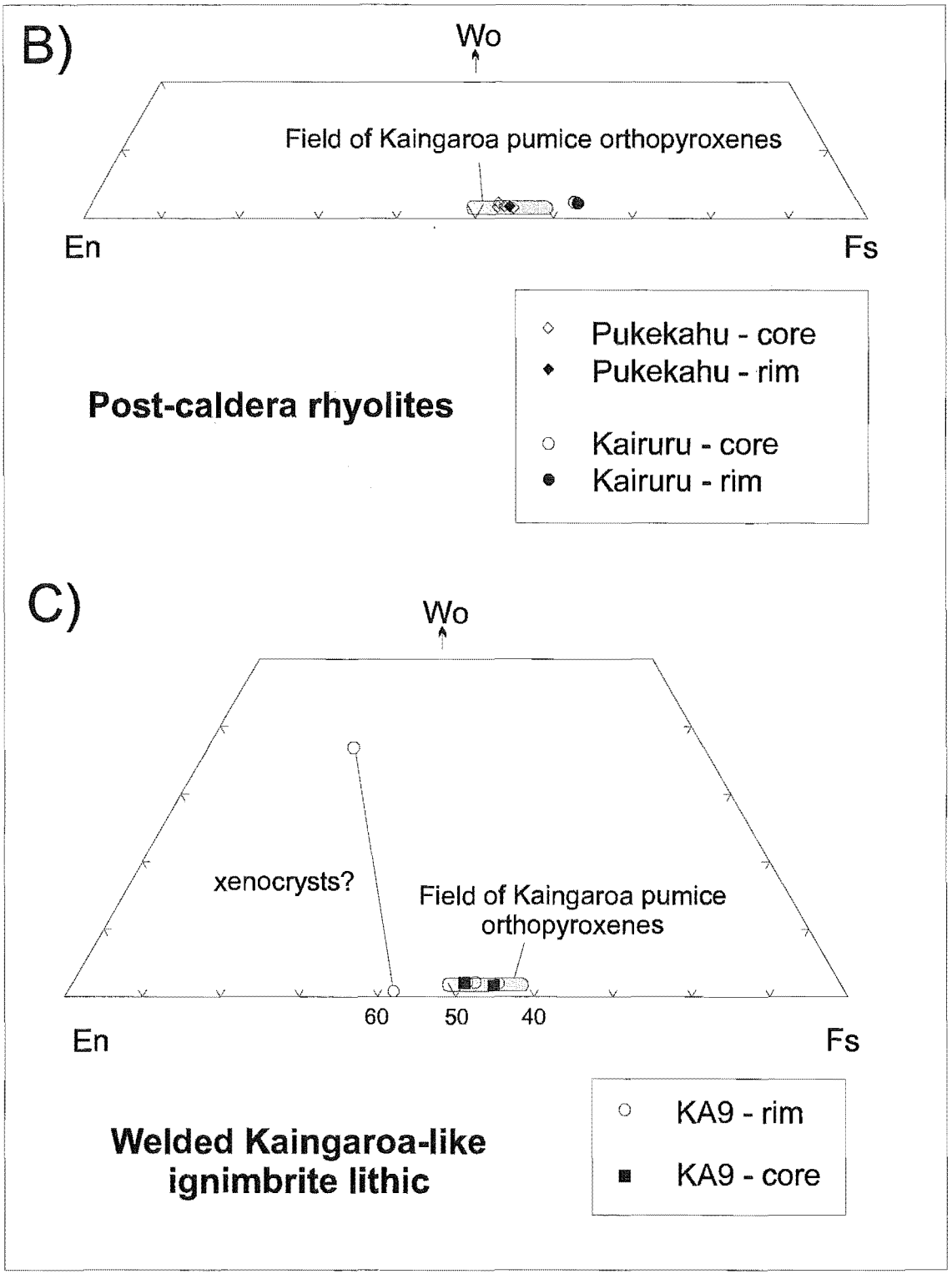

Figure 7.1b. Orthopyroxene compositions in post-caldera rhyolite domes, compared with Kaingaroa pumice orthopyroxenes.

Figure 7.1c. Pyroxenes in Kaingaroa-like ignimbrite lithics, illustrating similarity to Kaingaroa pumice pyroxenes, and xenocrysts derived from disaggregated andesite lithics.

7.3.3 Hornblende and accessory phases

Hornblende (up to 0.5 mm in length) was detected in some thin sections but was not present in analysed pumice mineral separates. Apatite and zircon are ubiquitous accessory phases, commonly as inclusions in plagioclase, within all pumices, Kaingaroa-like ignimbrite lithics, and post-caldera rhyolites.

7.3.4 Fe/Ti oxides

All Kaingaroa pumices contain magnetite and subordinate ilmenite (Appendix D). Due to heterogeneous alteration magnetite was not analysed in KA386f.

Fe/Ti oxide geothermometry is probably the most accurate means of determining temperature in high level silicic magma systems. Where possible co-existing magnetite and ilmenite inclusions in pyroxene or plagioclase have been analysed, which unambiguously represent equilibrium pairs. A secondary test of partitioning between Mg and Mn (Bacon and Hirschmann 1988) was applied to test for equilibrium. Fresh Fe/Ti oxides that exhibited no evidence of exsolving were analysed, and analyses are presented in Appendix D. Iron-titanium oxide temperatures vary from 816°C for Type A pumice to 820°C for a Type D pumice using the geothermometer of Buddington and Lindsley (1964) and refinements of Anderson and Lindsley (1985). Oxygen fugacity determined from Fe/Ti oxides varies from approximately log fO_2 of -13.378 in Type A pumice to -13.169 in Type D pumice, consistent with the orthopyroxene as the dominant mafic phenocryst. Total temperature range for Kaingaroa pumices is illustrated in Table 7.3 (802-820°C). Despite the limited data the calculated equilibrium temperatures suggest derivation from a near homogeneous system, with no observable temperature gradient.

7.3.5 Glass

The glass of pumice clasts is homogenous high-silica rhyolite (ca.77% SiO_2, anhydrous; Appendix D). Black et al (1996) also note the limited compositional variation exhibited by glass shards in the Kaingaroa Ignimbrite. Similar homogeneous glass compositions were reported in the crystal-poor Pokai Ignimbrite by Karhunen (1993) and Mangakino

ignimbrites by Briggs et al (1993), despite whole pumice chemical variation (see below). All post-caldera rhyolites exhibit devitrified matrices.

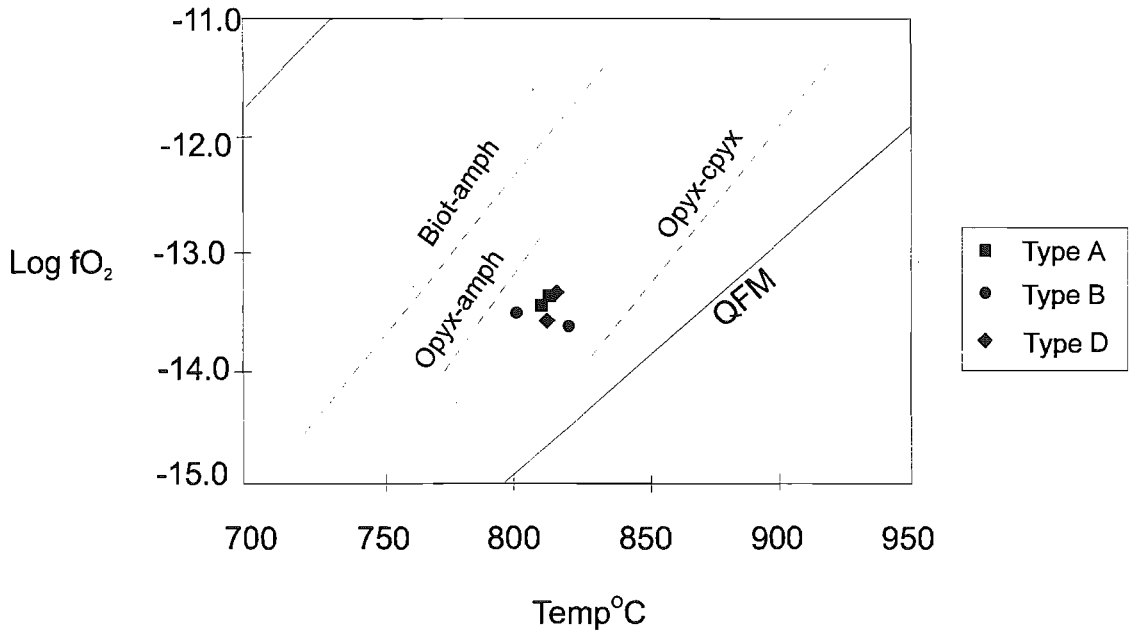

Figure 7.2 Plot of magmatic temperature and oxygen fugacity variation within Kaingaroa pumices as determined from coexisitng magnetite/ilmenite pairs. QFM, Biot-Amph, Opyx-Cpyx are oxygen fugacity buffer curves for dacitic and rhyolitic compostions (Carmichael 1967).

7.3.6 Water content

Water content is estimated by comparison of observed mineral assemblage with published experimental phase equilibria (e.g. Naney 1983). Naney (1983) determined the stability fields of ferromagnesian minerals in synthetic granitic and granodioritic melts, with varying pressure, temperature, and water content and comparison with his data, the presence of orthopyroxene and temperature between 802-820°C in the Kaingaroa Ignimbrite suggests a water content of <2.5 wt%. This is considered very approximate, as Naney's experiments involved an alkali feldspar-bearing assemblage. The paucity and small grain size of hornblende is consistent with water content of <4-6% (Rutherford and Devine 1988; Geschwind and Rutherford 1992; Rutherford 1993), at or near the stability limit of hornblende. This is also compatible with the limited grain size and low abundance of hornblende in the Kaingaroa-like ignimbrite lithic, type E bleb, and Pukekahu rhyolite dome (i.e. <4-6%).

Another indirect method for assessing volatile content in the Kaingaroa pumices is variation in loss on ignition (LOI). LOI incorporates both magmatic volatiles, and volatiles added during alteration and hydration. Unfortunately all pumices are partly-hydrated, thus variation in LOI in Kaingaroa pumices can be attributed to variable hydration, and not directly to any volatile gradient. No volatile gradient can be inferred from the available data. Pressure is difficult to estimate on mineralogical grounds in the Kaingaroa magma system due to the limited presence of hornblende and lack of two feldspars.

7.4 Geochemistry

All Kaingaroa Ignimbrite pumices are subalkalic, vary in composition from dacite to rhyolite (Fig 7.3), and are metaluminous to peraluminous (Fig 7.4). Major oxides of all samples are quoted and illustrated on an anhydrous basis to permit comparison of variably hydrated samples (see Appendix E).

All pumices and rhyolites plot in the volcanic arc granite (VAG) field of Pearce et al (1984), illustrating the near homogeneous composition, and a similarity to other subduction-related rhyolites/granitoids (Fig 7.5).

Pumice types in most ignimbrites can be grouped according to chemical variation, mineralogy and crystal content (e.g. Grunder and Mahood 1988; Boden 1989; Orsi et al. 1995; Streck and Grunder 1997). Chemical variations in such systems, exhibit stepwise variation with clear compositional gaps, interpreted to represent stepwise compositional zonation in the pre-eruptive magma chamber. Five pumice types are identified in the Kaingaroa Ignimbrite from the geochemical variation of Rb and Sr (Fig 7.6, Fig 7.7):

Type A: High Rb/Sr rhyolite; Plag + opyx + Fe/Ti oxides (only found in single airfall horizon)

Type B: Plag + opyx + Fe/Ti oxides

Type C: Plag + opyx + Fe/Ti oxides $\pm$ aug

Type D: Plag + opyx + Fe/Ti oxides $\pm$ amph $\pm$ aug

Type E: Low Rb/Sr dacite; Plag + opyx + aug + amph + Fe/Ti oxides (bleb present only at Tokiaminga Valley)

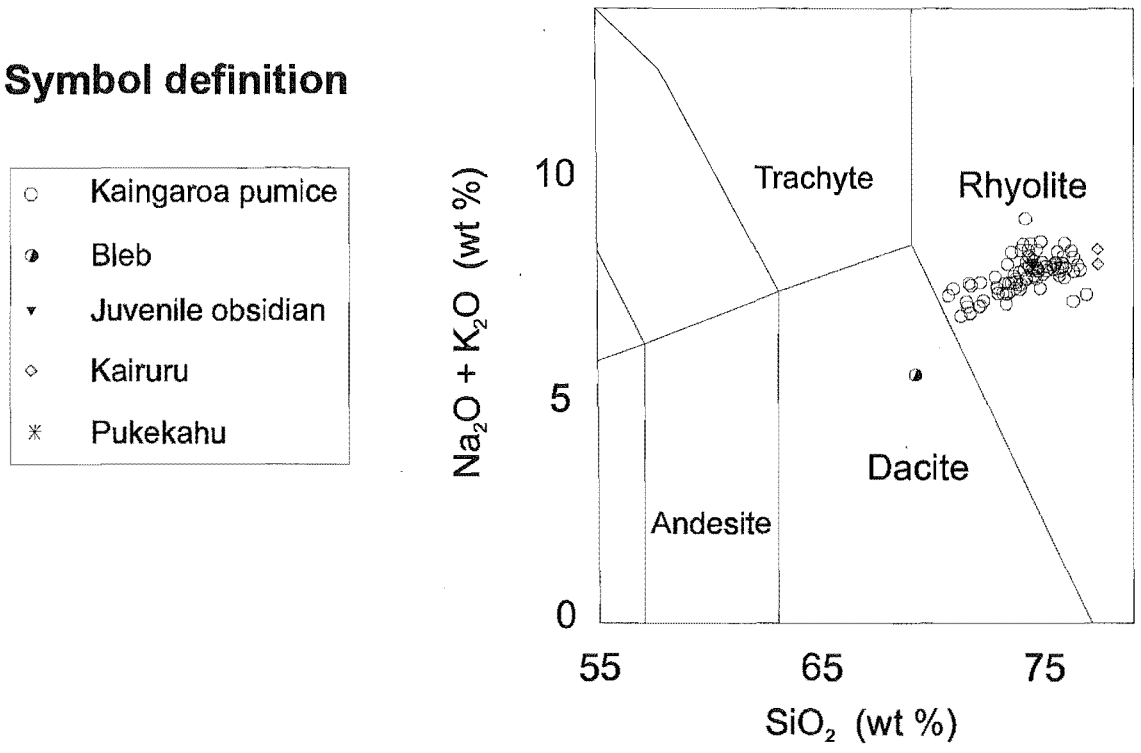

Figure 7.3 TAS classification of Kaingaroa pumices (after Le Maitre 1989). The majority of pumices are rhyolitic with a single dacitic bleb.

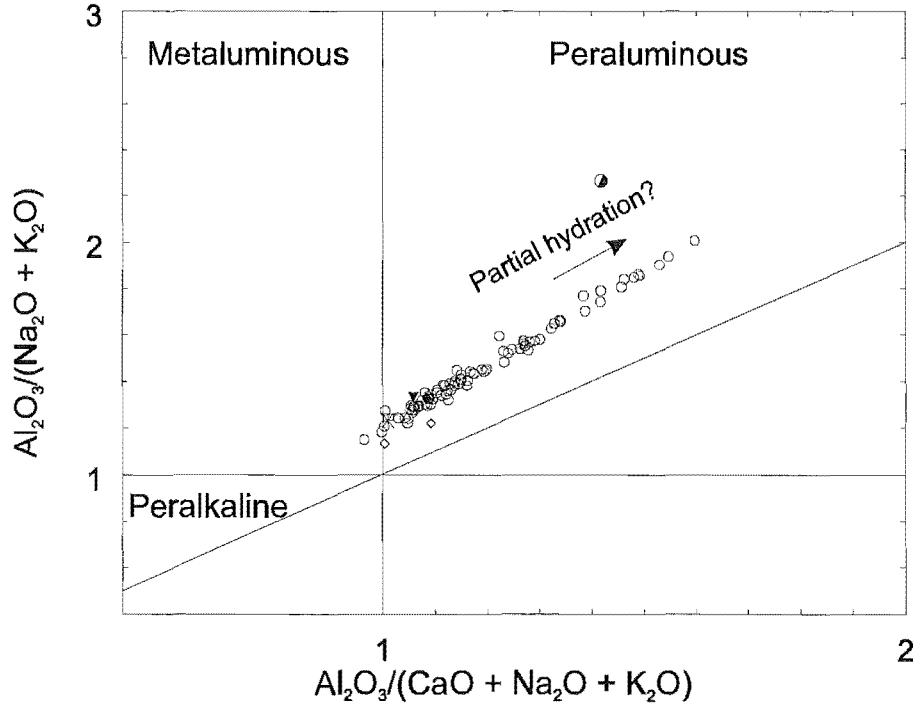

Figure 7.4 ASI variation in Kaingaroa pumices and post-caldera rhyolites. Symbols as in Fig 7.3.

Two of these 'groups' (A and E) are defined by single analyses, and localised distribution, but they represent distinct compositions that are chemically different from the majority of Kaingaroa pumices, and represent end-members (or distinct compositions) in the Kaingaroa magma system. Both pumices are considered juvenile components because they are mingled with other Kaingaroa pumices. Type B, C, D form the majority of pumices in the Kaingaroa Ignimbrite, and represent a continuum from less (D; high Sr/Rb) to more (B; low Sr/Rb) evolved compositions. These three types are arbitrarily divided in terms of Rb/Sr to allow for assessment of chemical variation with stratigraphy (Fig 7.7). The consistency of the variation is valid in all variation plots (Fig 7.8). Scatter is attributed to hydration, analytical error and minor variation in crystal content (see Appendix E). The chemical variation in the Kaingaroa magma system is not stepwise, with the possible exception of the single analyses of types A and E. Pumice types do not exhibit corresponding crystal content or mineralogical variation, and show only minor mineral chemical variation (section 7.3 and below). Interpretation of this variation and implications for zonation style are discussed below.

Inferences on the volumes of pumices types are poorly constrained due to the limited exposure, and inability to identify different pumice types in the field. Types C and D are interpreted to represent the dominant pumice types of the Kaingaroa Ignimbrite, as they are dominant in the large OWR and WIU units. Type A (KA50) is present at a single horizon in the basal tephras (Chapter 3) and E blebs are present only in the Tokiaminga Valley facies (Chapter 4). Type B pumices are only in the basal tephras and RBU, and interpreted to be subordinate to types C and D.

Juvenile obsidian and rhyolite lithics are similar to Type C pumices and considered to be quenched samples of the Kaingaroa magma chamber.

Post-caldera rhyolite domes exhibit a diverse range of chemical compositions (Fig 7.9). Deer Hill rhyolite exhibits distinct trace element compositions (e.g. low Rb) inconsistent with a simple relationship to the Kaingaroa magma system by crystal fractionation (Fig 7.9). Pukekahu is broadly similar to the Kaingaroa Ignimbrite Type C, whereas Kairuru rhyolite exhibits similar trace element chemistry to the Kaingaroa Ignimbrite albeit more evolved (e.g. higher Rb/Sr).

7.4.1 Major and trace elements

Major and trace element variation diagrams of bulk pumice are shown in Fig 7.8. Pumices of the Kaingaroa Ignimbrite range between 71% and 76% SiO_2; the single sampled bleb is broadly dacitic in composition (69% SiO_2). Rb content ranges from 76 to 128 ppm and is used as an index of differentiation (see Appendix E). With increasing Rb content, K_2O increases and Ba and Y increase slightly, as would be expected from their overall incompatible behaviour with respect to the observed phenocryst phases. Sr, Ca, Al_2O_3, Fe_2O_3, Zn decrease, consistent with minor fractionation of the observed phenocryst phases e.g. plagioclase and Fe/Ti oxides. Na_2O exhibits limited or no variation, and MgO, MnO, Ni, Cr, V are close to detection limits and trends are difficult to identify. Zr, and Th exhibit similar low consentrations in Type E bleb, but decrease with increasing Rb in type D-A pumices consistent with zircon fractionation in evolved rhyolitic compositions. Type E is distinct in terms of trace element composition from types A-D, notably low Rb/Sr, Ca, Sr, Fe_2O_3, and Zn, consistent with its less evolved dacitic composition. The crystal-poor mineralogy and isotopic composition (see below) suggest Type E blebs are unrelated to the Kaingaroa pumices$_{s.s.}$, by simple crystal fractionation.

Juvenile obsidian, and type B rhyolite lithics exhibit similar trace element chemistry to Kaingaroa pumices (Fig 7.9). Post-caldera rhyolites exhibit variable trace element chemistry. The low Rb/Sr content of Deer Hill rhyolite dome is inconsistent with a simple relationship to the Kaingaroa magma system. Pukekahu exhibits similar trace element chemistry to Kaingaroa pumices. Kairuru rhyolite is a high silica rhyolite with high Rb/Sr, and is more evolved than Kaingaroa pumices.

Variations in trace element composition of Kaingaroa magma components are illustrated in spider diagrams normalised to primitive mantle in Fig 7.10a.

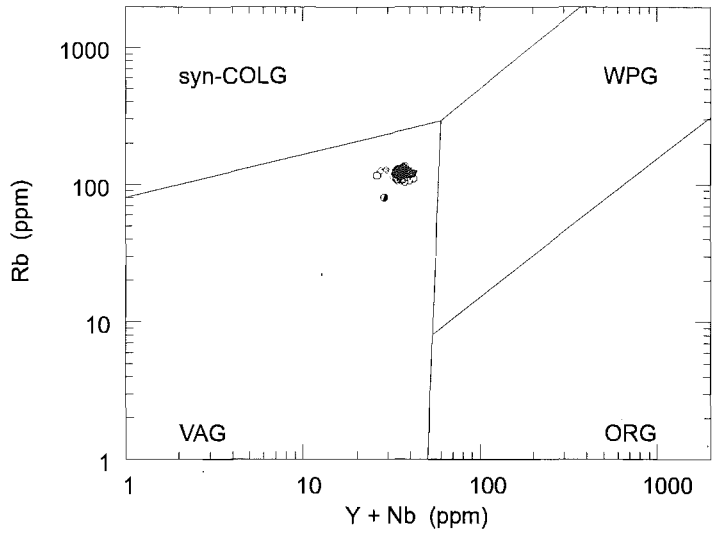

Figure 7.5 Tectonic discrimination diagram (after Pearce et al. 1984) illustrating Volcanic arc granitoid-like composition (VAG) of Kaingaroa pumices. ORG = Ocean ridge granitoid, WPG = within plate granitoid, syn-COLG = syn-collision granitoid.

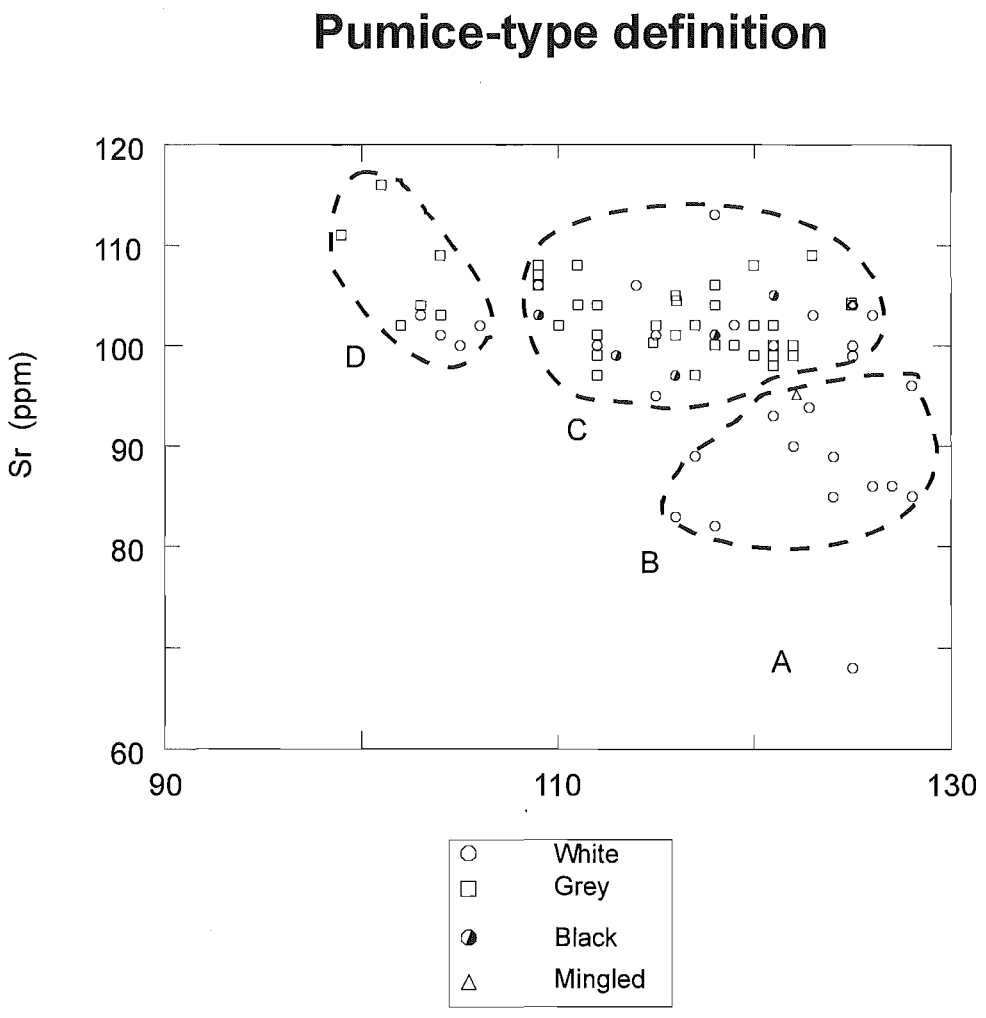

Figure 7.6 Rb-Sr variation diagram illustrating pumice type definition, and variation of pumice colour with chemistry.

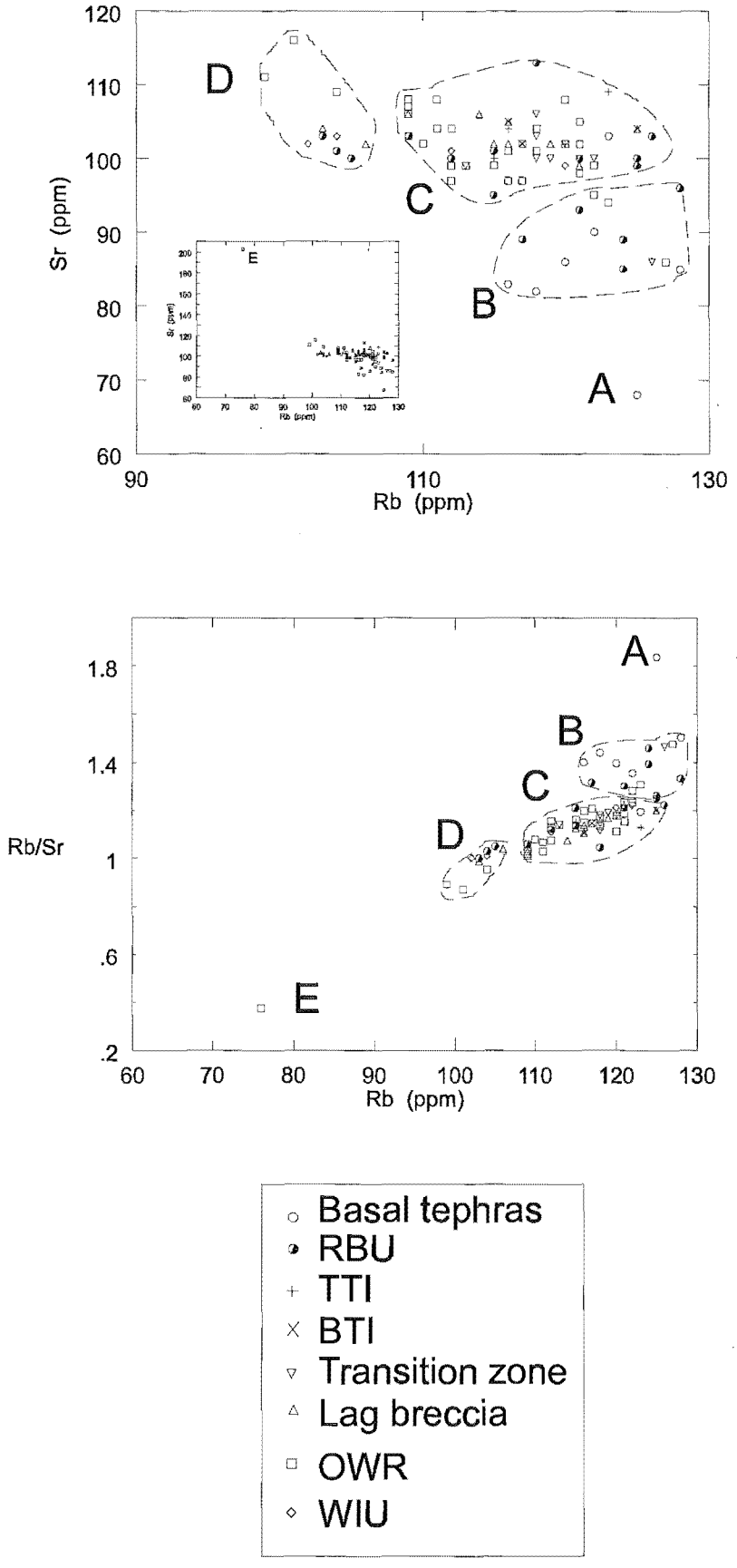

Figure 7.7 Pumice type definition and variation of pumice type with stratigraphic unit.

Sample Name	*KA50*	*KA45B3*	*KA45B*	*KA53*	*KA45A*	*KA25*	*KA377*	*KA269C*	*KA386f*	*KA42*
Rock Type	Pumice	Pumice	Pumice	Pumice	Pumice	Pumice	Pumice	Pumice	Bleb	Rhyolite
Unit	BT	OWR	OWR	BT	OWR	LLB	WIU	WIU	TOK	KAR
Pumice type	A	B	C	C	C	D	D	D	E	
XRF										
SiO_2	72.99	74.23	72.55	72.77	71.32	69.23	68.53	67.85	65.56	76.68
TiO_2	0.16	0.17	0.20	0.23	0.22	0.25	0.24	0.26	0.68	0.15
Al_2O_3	12.72	12.68	12.90	13.04	13.62	15.09	16.33	17.19	15.89	12.27
Fe_2O_3*	1.51	1.47	1.75	1.73	1.84	3.07	2.22	2.43	4.41	1.28
MnO	0.06	0.05	0.05	0.06	0.05	0.06	0.06	0.06	0.08	0.03
MgO	0.15	0.13	0.18	0.22	0.20	0.21	0.21	0.10	0.74	0.09
CaO	0.93	1.03	1.16	1.24	1.18	1.19	1.20	1.21	2.33	0.76
Na_2O	3.42	3.68	3.62	3.67	4.02	3.80	3.92	3.34	2.83	4.21
K_2O	3.70	3.85	3.71	3.56	3.55	3.11	2.90	2.84	2.15	3.62
P_2O_5	0.02	0.03	0.03	0.03	0.08	0.03	0.03	0.02	0.18	0.03
LOI	4.26	2.95	2.48	3.73	3.04	4.13	4.40	3.95	4.83	0.68
Total	0.00	0.00	0.00	0.00	0.00	0.00	0.00	0.00	0.00	0.00
Cr	3	4	4	3	4	5	4	5	5	3
Ni	5	5	5	4	5	8	3	3	6	3
V	9	9	12	10	10	11	10	12	34	11
Pb	16	15	12	15	14	14	17	20	24	16
Zn	49	32	33	44	29	52	59	50	134	29
Rb	125	127	122	123	116	109	104	102	76	125
Ba	767	770	754	739	825	759	806	844	555	719
Sr	68	86	99	103	101	103	103	102	203	62
Ga	20	17	14	21	16	14	18	20	18	13
Nb	8	5	8	5	9	9	9	9	8	8
Zr	135	156	175	176	187	202	230	246	170	117
Y	28	31	27	27	31	25	23	25	19	19
Th	15	13	13	15	14	13	11	17	11	12
La	29	31	29	27	27	22	19	29	16	25
Ce	68	59	58	57	66	67	54	75	47	55
INAA										
La	25.63	25.69	26.75					26.12	17.60	
Ce	55.50	56.10	53.50					63.20	39.10	
Sm	4.65	4.55	4.77					4.46	3.86	
Eu	0.69	0.73	0.77					0.82	0.97	
Tb	0.71	0.70	0.77					0.68	0.58	
Yb	2.99	2.94	3.01					2.92	2.05	
Lu	0.423	0.386	0.474					0.433	0.313	
Hf	4.89	5.03	5.98					7.39	5.05	
Ta	0.74	0.75	0.73					0.94	0.61	
Th	13	13	13					16	10	
U	3	3	3					3	2	
87Sr/86Sr	.705567/17	.705707/29	.705827/28	.705658/22	.705751/51	.705832/23	.705784/18		.706251/21	.705416/37
143Nd/144Nd	.512700/10	.512679/11	.512672/11	.512694/10	.512678/11	.512676/12	.512672/9		.512623/12	.512721/14

Table 7.1. Representative XRF, INAA, and Sr and Nd isotopic analyses of Kaingaroa Ignimbrite pumices. Only selected INAA analyses are shown. Details in Appendix E.

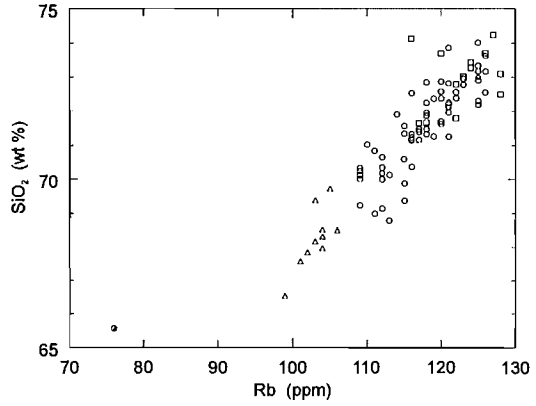

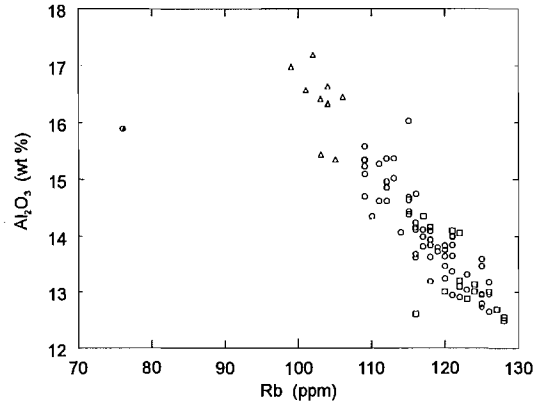

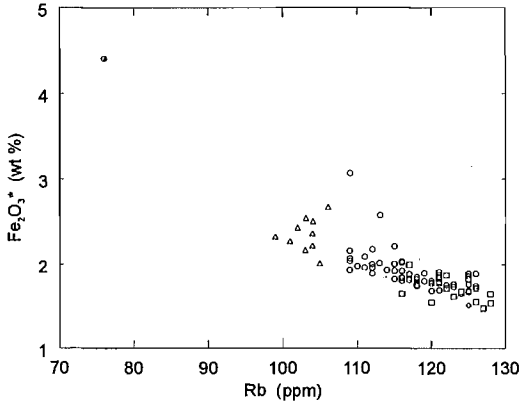

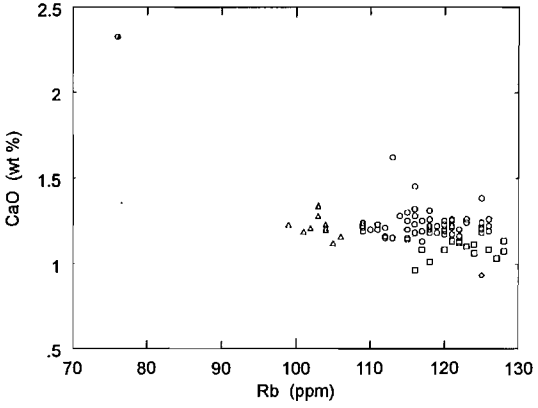

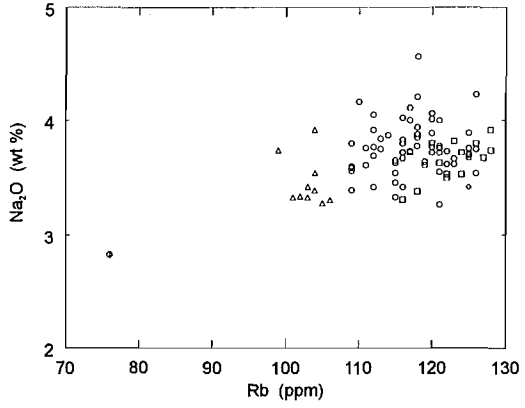

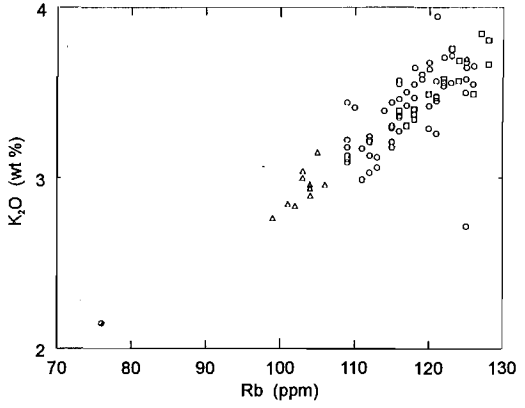

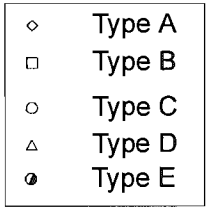

Figure 7.8a. Major element variation diagrams of Kaingaroa Ignimbrite pumices. Symbols as defined in Figs 7.6, 7.7.

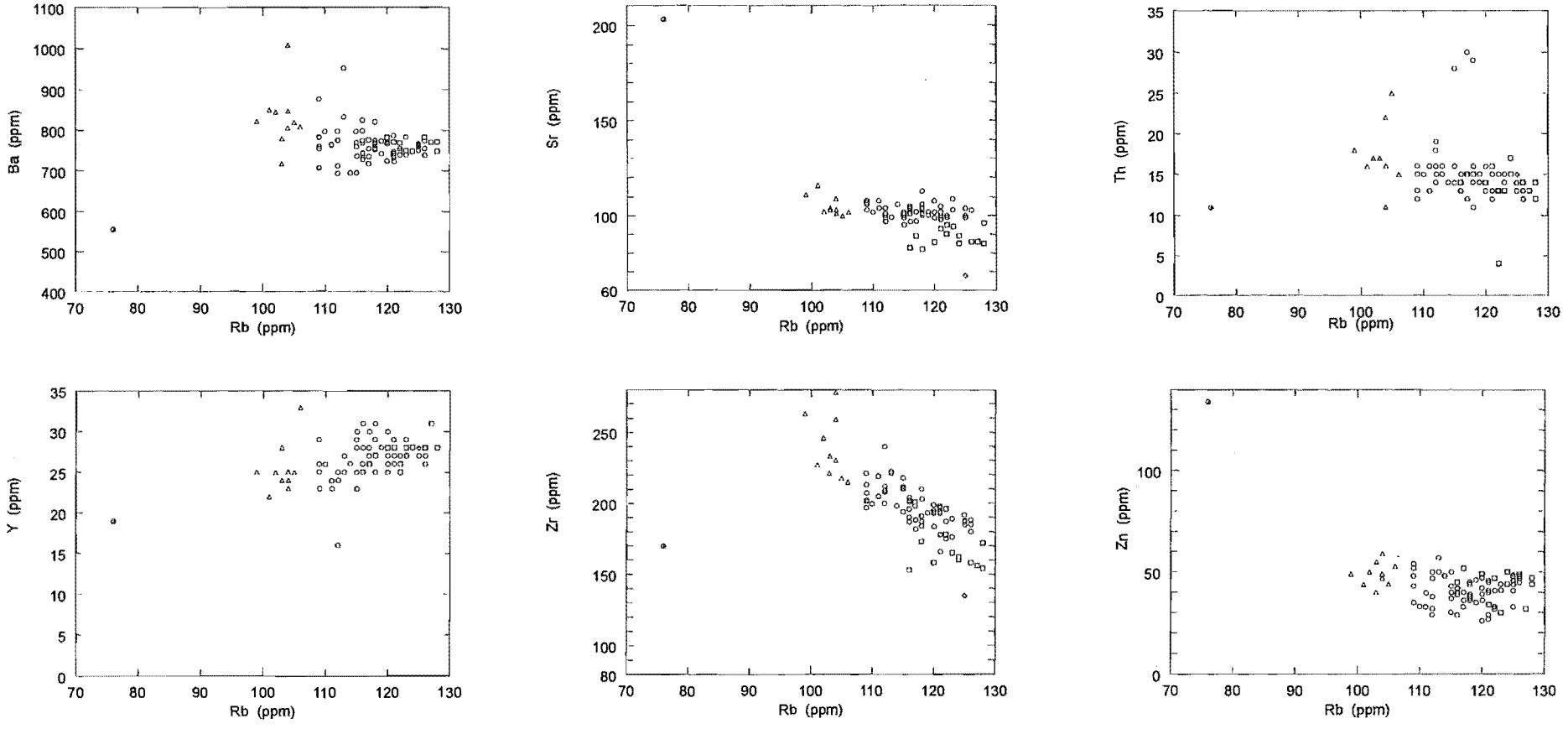

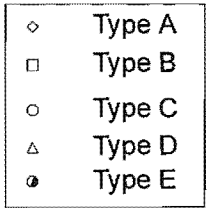

Figure 7.8b. Selected trace element variation diagrams of Kaingaroa Ignimbrite pumices. Symbols as defined in Figs 7.8a

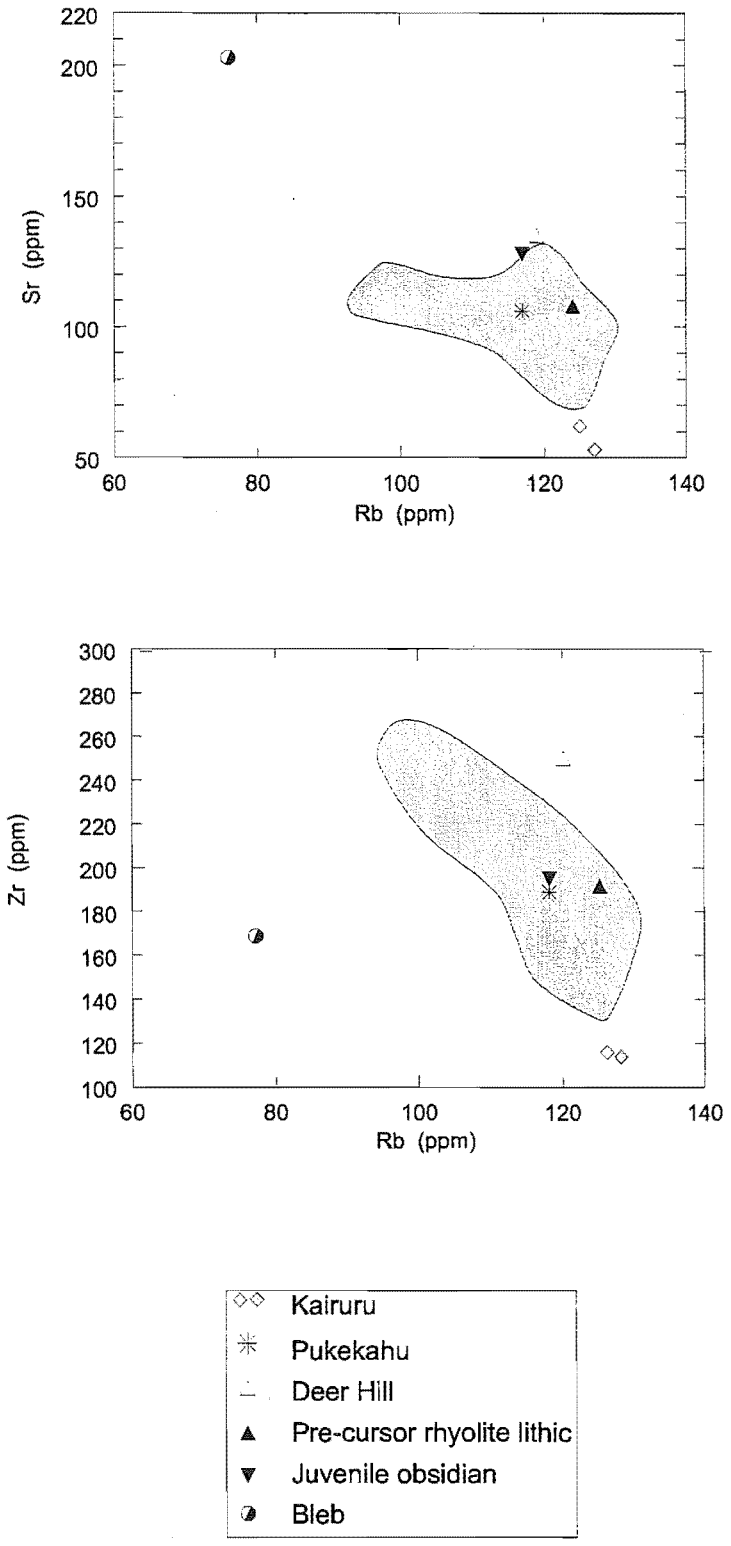

Figure 7.9 Selected variation diagrams of post-caldera rhyolites, and Kaingaroa-like lithics illustrating relationship to Kaingaroa pumices.

Variations in trace element composition of Kawerau magma components is also illustrated in multi-element plots compared with ocean-ridge granite (ORG; Fig 7.10b). Pearce et al (1984) calculated a hypothetical granitoid composition as a residual liquid after 75% crystal fractionation of average N-MORB. This calculation attempted to produce a model granitic (rhyolitic) liquid, with no crustal interaction. Any deviation from a flat pattern is interpreted to reflect a more complex magma genesis.

All patterns exhibit high LILE/HFSE and negative Nb depletion, characteristic of subduction-related magmas (Wilson 1989). Kaingaroa pumices show a weak depletion in Sr and Ti reflecting fractionation of plagioclase and mafic minerals. There is a general uniform depletion in Sr and Ti between less and most evolved pumice types, and a general uniform enrichment in incompatible elements between less and more evolved pumice types, consistent with the inferred plagioclase, Fe/Ti oxides and orthopyroxene fractionating assemblage. Post-caldera rhyolites are more depleted in Sr and Ti (Fig 7.10c) reflecting their more evolved compositions.

7.4.2 Rare Earth Elements (REE)

Rare earth element analyses of five samples were determined by INAA and are reported in Appendix E and Table 7.2. Kaingaroa pumices are characterised by light rare earth element (LREE) enrichment and a relatively flat heavy rare earth (HREE) pattern,and a prominent negative Eu anomaly (Fig 7.11), similar to that observed in other TVZ rhyolites (e.g. Brown 1994).

The increasing negative Eu anomaly with increasing Rb/Sr is suggestive of plagioclase fractionation. Type E is LREE enriched albeit with lower LREE content compared with Kaingaroa pumices$_{s.s.}$, relatively flat HREE, but weakly HREE depleted compared with Kaingaroa pumices$_{s.s.}$, and a weak negative Eu anomaly, characteristics consistent with its less evolved nature. The weak negative Eu anomaly is consistent with limited plagioclase fractionation. Details of the origin of magma components are discussed below.

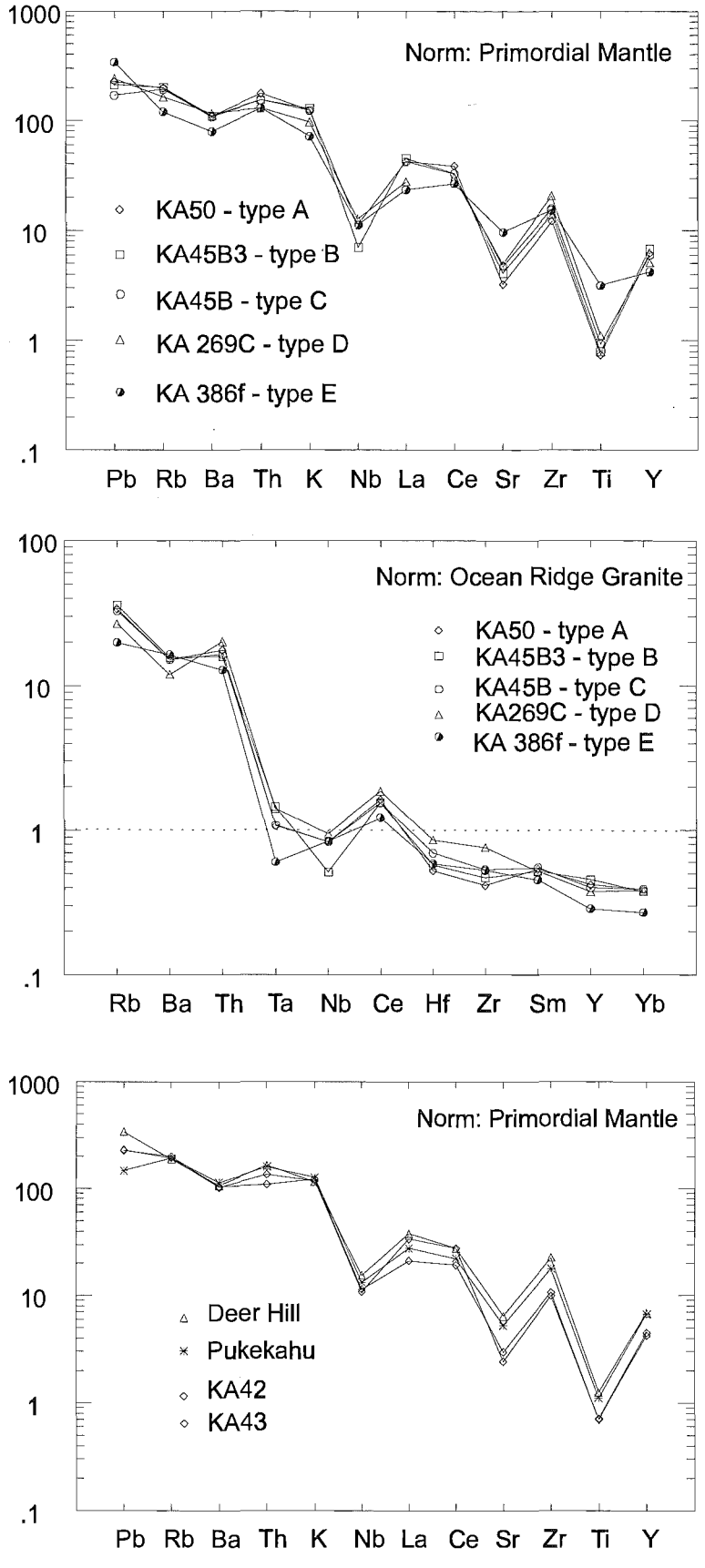

Figure 7.10 Multielement plots illustrating variation within Kaingaroa pumices and post-caldera rhyolites. Primordial mantle values from Sun and McDonough (1989).

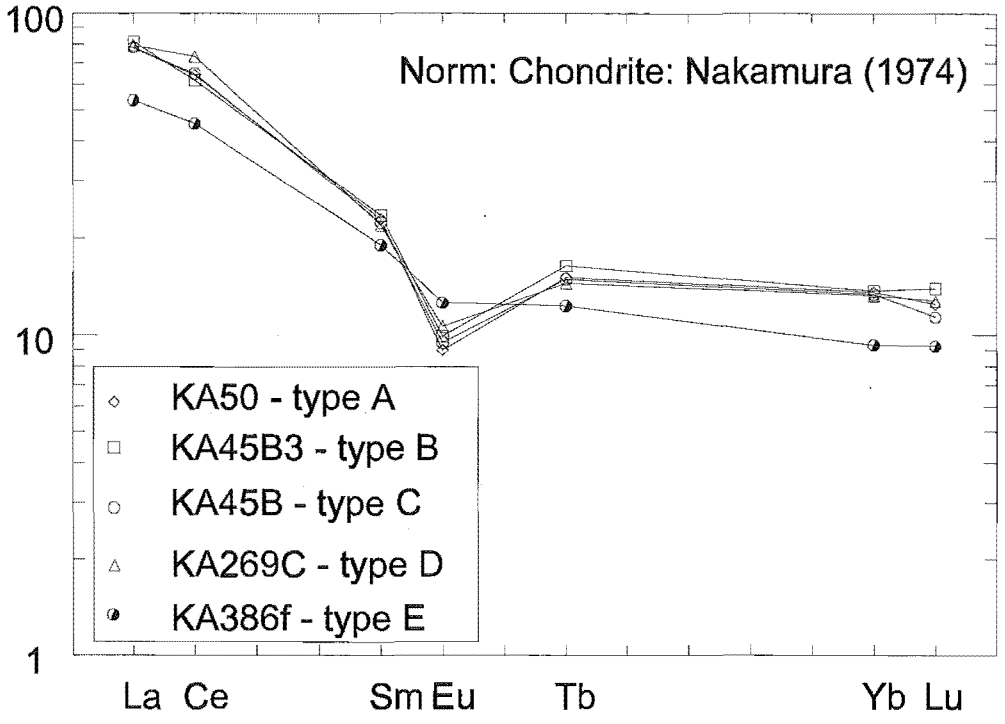

Figure 7.11 Chrondrite-normalised rare earth element plot illustrating variation within Kaingaroa pumices. Note the low REE content and limited negative Eu anomaly of Type E.

7.4.3 Sr and Nd isotopes

Sr and Nd isotopes of 8 Kaingaroa pumices, and one post-caldera rhyolite (Kairuru) were analysed to assess isotopic variations within the Kaingaroa magma system. Analyses and methods are reported in Appendix E. In addition, McCulloch et al (1993) report Sr and Nd isotopic ratios for Pukekahu rhyolite dome.

Pumices exhibit a limited range in $^{87}Sr/^{86}Sr$ (0.70557-0.70625) and $^{143}Nd/^{144}Nd$ (0.51262-0.51270; Fig 7.12). These values are within ranges for other TVZ ignimbrites (Blake et al. 1992; Briggs et al. 1993; Sutton et al. 1995). $^{143}Nd/^{144}Nd$ isotopic ratios correlate inversely with $^{87}Sr/^{86}Sr$ (Fig 7.12a). Despite the overall range in isotopic values there are analytically significant variations between magma components which suggest isotopic heterogeneity in the pre-eruptive Kaingaroa magma system. Type, B, C, and D pumices have a very narrow range in $^{87}Sr/^{86}Sr$ (0.70566-0.70583) and $^{143}Nd/^{144}Nd$ (0.51267-0.51269), supporting their near homogeneous trace element and REE

chemistry (Fig 7.12b,c). Type A pumice (high Rb/Sr; evolved high silica rhyolite) exhibits less radiogenic $^{87}Sr/^{86}Sr$ (0.70557), and high $^{143}Nd/^{144}Nd$ (0.51270), but is within error of Kaingaroa pumices and consistent with a simple relationship to types B, C, and D by crystal fractionation. Fig 7.12 illustrates the variation in radiogenic isotopic ratios with Rb.

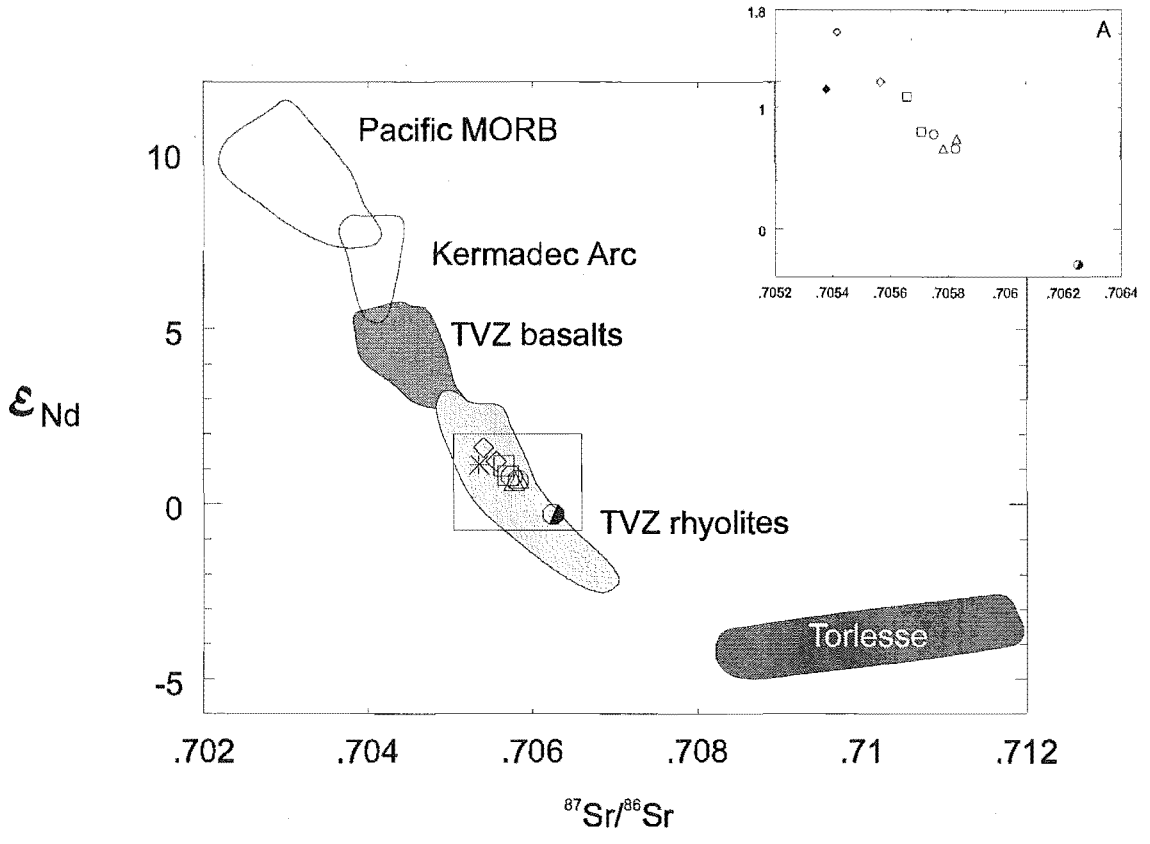

Figure 7.12a $^{143}Nd/^{144}Nd$ and $^{87}Sr/^{86}Sr$ isotopic variation in Kaingaroa pumices compared to Pacific Morb (Ito et al. 1987), Kermedec Arc (Ewart and Hawksworth 1987), TVZ basalts (Gamble et al. 1993), and Torlesse (Mc Culloch et al 1993). Symbols as in Fig 7.11.

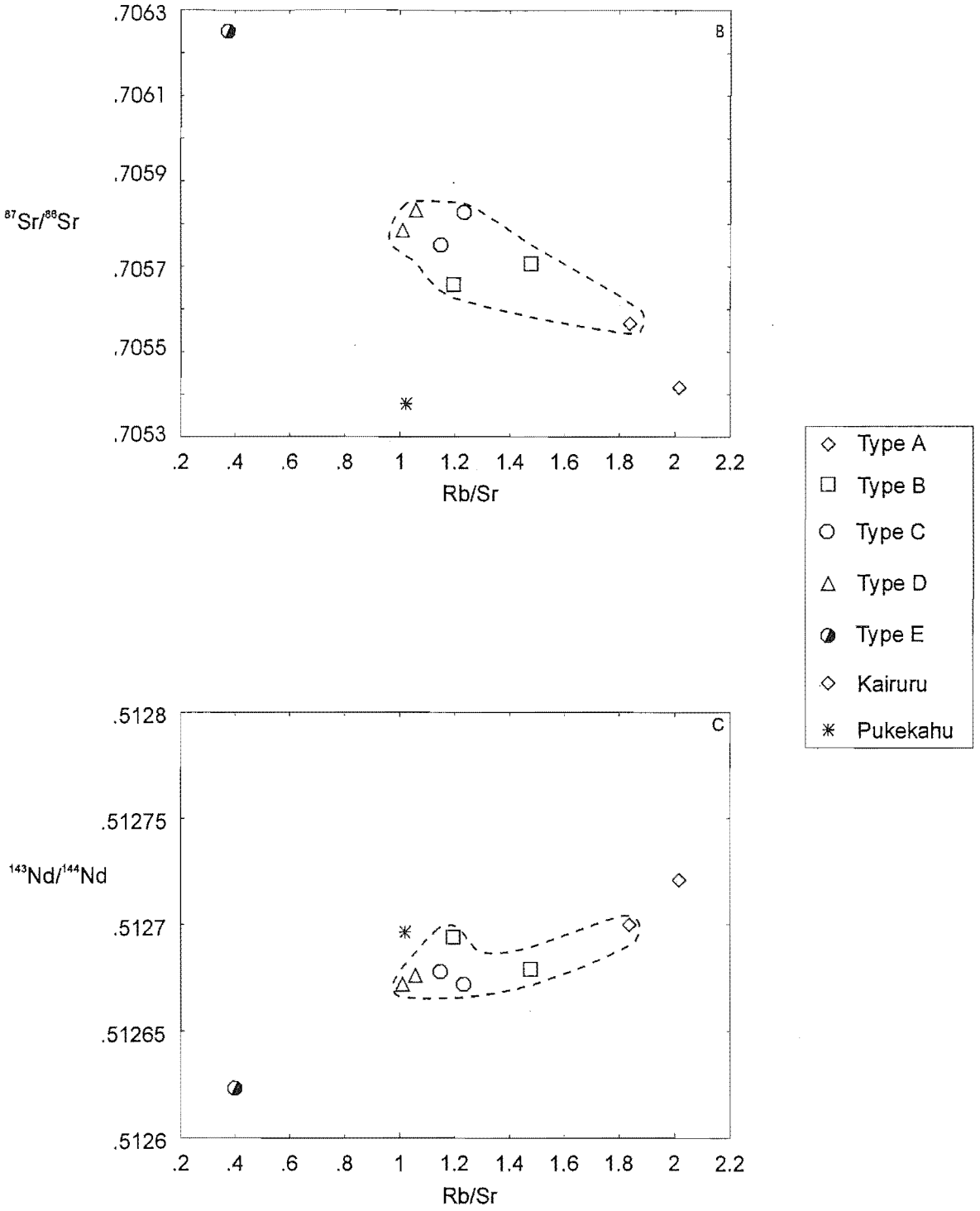

Figure 7.12b Apparent reverse $^{87}Sr/^{86}Sr$ isotopic zonation in the Kaingaroa Ignimbrite pumices defined by the end-member Type E bleb (more radiogenic) and less radiogenic post-caldera rhyolites.

Figure 7.12c. $^{143}Nd/^{144}Nd$ isotopic varition in Kaingaroa pumices. Symbols as in Fig 7.11.

Many ignimbrites are zoned in radiogenic isotope composition indicating roofward assimilation in the pre-eruptive magma chamber (e.g. Johnston 1989; Riciputi et al. 1995; Civetta et al. 1997). This is precluded by the lower $^{87}Sr/^{86}Sr$ ratios of Type A (which are beyond analytical error), and negative trend between $^{87}Sr/^{86}Sr$ and Rb (Fig 7.12b,c). The overall zonation in radiogenic isotopes observed in the Kaingaroa magma components suggests decreasing $^{87}Sr/^{86}Sr$ and increasing $^{143}Nd/^{144}Nd$ with differentiation, the opposite of commonly observed isotopic zonation in silicic magma systems.

Negative correlations between $^{87}Sr/^{86}Sr$ and Rb (i.e. reverse zonation) has been documented by Duffield and Ruiz (1992), who illustrated a negative correlation between $^{87}Sr/^{86}Sr$ and Rb in the Taylor Creek rhyolites which they attribute to variable contamination with Precambrian upper crust. Their inference is based on the dubious assumption that all the rhyolites were derived from the same temporally and spatially associated magma chamber.

The reverse zonation in radiogenic isotopes within the Kaingaroa magma system is attributed to open system processes. Type E is notably more radiogenic ($^{87}Sr/^{86}Sr$ = 0.70623; $^{143}Nd/^{144}Nd$ = 0.51262) and is at the radiogenic end of reported TVZ volcanics (Blake et al. 1992; Brown 1994; Graham et al 1995). Type E (low Rb/Sr; less evolved dacite) radiogenic isotopic ratios are also inconsistent with simple crystal fractionation processes or roofward assimilation (Fig 7.12b,c). Post-caldera rhyolites also exhibit distinct isotopic values (Fig 7.12), precluding a simple crystal fractionation or AFC relationship. Distinct isotopic values are commonly reported in post-caldera rhyolites (e.g. Brown 1994) and are interpreted to represent distinct magma batches. Both Type E and post-caldera rhyolites exhibit radiogenic isotope compositions significantly greater than that explainable by analytical uncertainties.

Palacz and Wolff (1989) suggest that whole rock Sr-isotopic variations may be inconsistent with purely magmatic processes. They attribute high $^{87}Sr/^{86}Sr$ values to interaction with hydrothermal fluids. Post-eruptive alteration of isotopic values reported here are rejected on the following grounds:

1) The negative correlation of $^{87}Sr/^{86}Sr$ with Rb (or SiO_2) suggests interaction with low $^{87}Sr/^{86}Sr$ fluids, or selective assimilation.

2) Pumice samples are petrographically and chemically free of alteration (except for partial hydration).

3) It is considered unlikely that the magma components could reflect variably contaminated magma, especially considering the coupled $^{87}Sr/^{86}Sr$ and $^{143}Nd/^{144}Nd$ values.

The distinct isotopic compositions of pumice Type E, and post-caldera rhyolites preclude a simple magmatic relationship to Kaingaroa pumices$_{s.s.}$ i.e. crystal fractionation or AFC, and suggest derivation from distinct magma batches. The pre-eruptive configuration of these compositions is discussed below.

7.4.4 Chemostratigraphy

A tacit assumption of many arguments related to zonation in ignimbrites is that magma chambers are tapped from the top down i.e. lower most portions of the erupted sequence are derived from the upper parts of the magma chamber, and overlying products are derived from successively deeper levels. Hence the observed stratigraphic sequence is the inverse of compositional gradients in the magma reservoir. The degree and nature of compositional zonation in the ignimbrite is a function of withdrawal dynamics (Blake 1980; Blake and Ivey 1986) and pre-existing topography (Valentine et al. 1992).

Plots of geochemical parameters versus stratigraphic units and height are summarised in Fig 7.13. The data show that the Kaingaroa Ignimbrite varies in composition, but there are no systematic trends with stratigraphic height in the ignimbrite. Generalisations concerning variation with chemistry with stratigraphic unit are outlined below:

The stratigraphic sequence consists of the basal tephras, which have been arbitrarily divided into two sub-groups (Chapter 3 and 5) based on depositional style and lithic components. The early basal tephras consist of fall horizons intercalated with surge deposits, whereas later basal tephras consist of dominantly surge and flow deposits, with an increased diversity of lithic types. At the base of the Kaingaroa stratigraphic sequence the basal tephras contain pumice types A, B, and rare C. Type A pumice is restricted to a single plinian-style fall deposit (unit B). Type B is predominant.

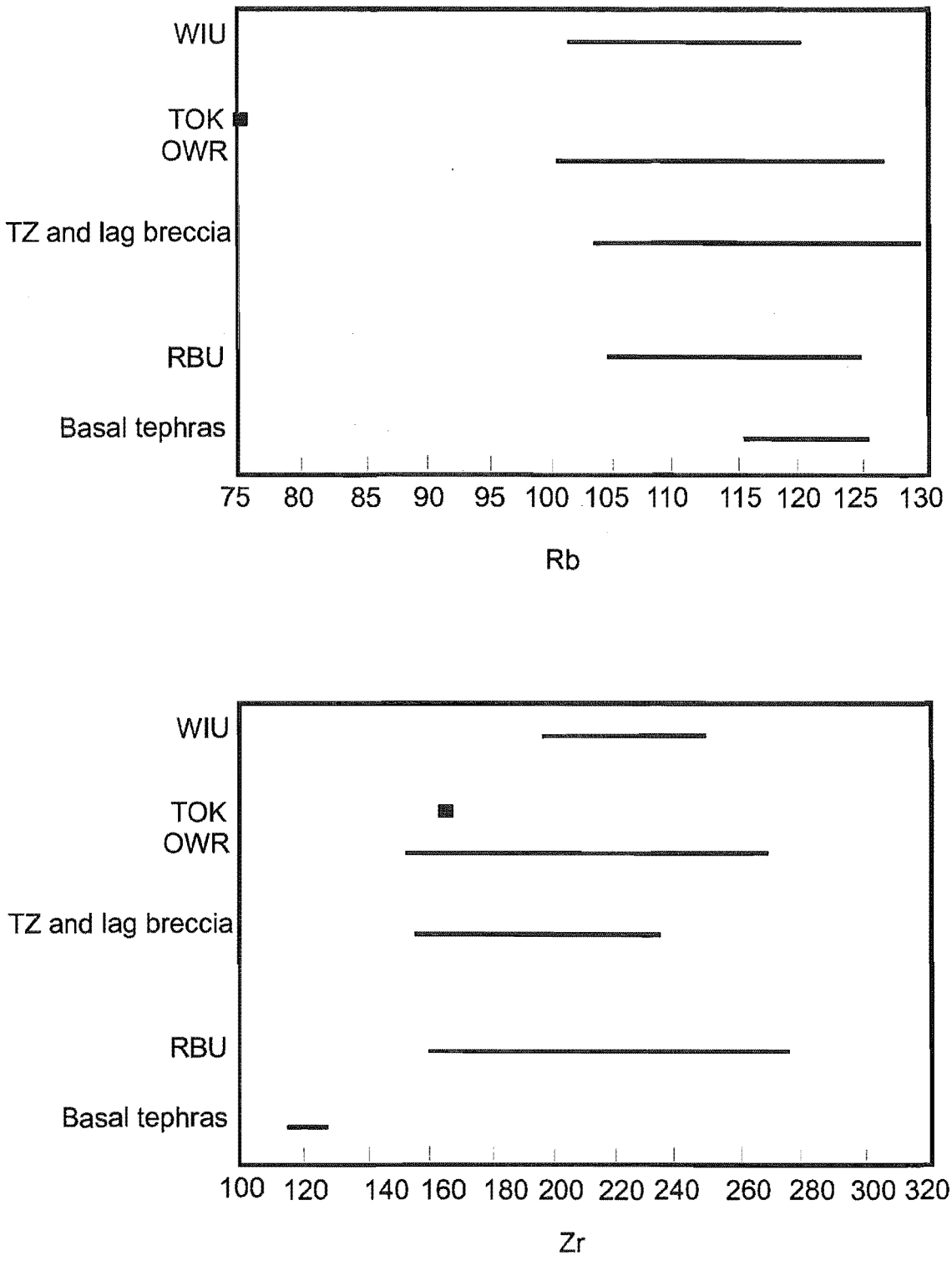

Figure 7.13. Combined Rb and Zr values for Kaingaroa pumices versus stratigraphic unit and idealised stratigraphic height. Bars denote variation within each stratigraphic unit. Box denotes bleb sample.

RBU is the lower ignimbrite unit, and is marked by its limited distribution adjacent to the eastern caldera scarp. RBU contains pumice types B, C, and D, though predominantly of Type B.

A marked change in vent conditions is marked by the presence of the vertically colour zoned co-ignimbrite lag breccia in proximal regions, and lateral equivalent vertically colour zoned transition zone in medial regions. The increase in lithic types, abundance, and size is interpreted to coincide with a marked change in vent conditions, magma discharge, and eruptive dynamics i.e. caldera collapse. Pumice types C and D were erupted at this stratigraphic interval, and commonly coexist at the same stratigraphic height. Tokiaminga Valley facies is anomalous, as it contains additional Type E blebs.

OWR i.e. middle ignimbrite contains pumice types C and D (commonly coexisting at the same stratigraphic height), similar to the lag breccia. A notable feature of OWR pumice compositions is the lack of Type B pumice. The presence of mingled pumices provides evidence of syn-eruptive mingling of magma types during the eruption.

WIU, the upper ignimbrite unit is a widespread lenticulite. WIU pumice data are limited but includes Type C, and abundant Type D, consistent with tapping of the less evolved compositions of a progressively tapped chamber. The important conclusion is that pumices with similar compositions to those erupted at the inception of the Kaingaroa eruption were also deposited at the end of the eruption.

Theoretical, field and geochemical studies of magma withdrawal during eruption indicate that magma from different depths within the chamber may erupt simultaneously and that the resultant ignimbrite stratigraphy does not therefore represent the inverse of the magma chamber stratigraphy (e.g. Blake 1981; Blake and Ivey 1986; Schuraytz et al. 1989; Briggs et al 1993). Thus the compositional zonation can be obliterated by syn-eruptive mingling, either in the conduit (during evacuation) or resultant flow. The chemical variation of the Kaingaroa pumices is consistent with progressive tapping of a weakly zoned magma chamber, with syn-eruption of magma compositions, notably at the basal tephra-RBU, and RBU-lag breccia eruptive stages. Eruption of Type E is not consistent with this model and is discussed below.

7.5 Origin of magma components

The pumice compositional data, together with mineralogical and temperature variation can be used to re-construct pre-eruptive magma configuration.

Kaingaroa pumices, blebs, obsidian, and post-caldera rhyolites exhibit limited variation in terms of mineralogy, major and trace elements (including REE), and isotopic composition. This variation is expressed in terms of three distinct compositional entities:

A) Kaingaroa pumices, obsidian, and precursor rhyolite lithics, interpreted to represent samples of a large volume weakly-thermally and compositionally zoned chamber.

B) Isotopically distinct Type E blebs, which exhibit trace element and mineralogical variation consistent with possible parental compositions of Kaingaroa pumices, but are isotopically distinct, suggestive of distinctive magma batch.

C) Mineralogical, chemical and isotopically distinct post-caldera rhyolites.

As noted in Chapter 3, all samples of the Kaingaroa Ignimbrite are thought to represent samples from a single eruption, due to the lack of intervening paleosols, similar chemical composition of components, similar lithic types etc. As such the magma components of the Kaingaroa magma system are discussed below in terms of their genetic relationship, pre-eruptive configuration, and evolution during the Kaingaroa Ignimbrite eruption.

The term 'system' is defined herein as the configuration of magma beneath Reporoa Caldera, without any implication of geometry.

Differentiation mechanisms in rhyolitic systems include: 1) Partial melting of a protolith and/or crystal fractionation of parental composition; 2) Ascent and high level emplacement; and 3) High level magma system processes e.g. crystal fractionation, thermogravitational diffusion. Added to these mechanisms may be wall rock assimilation and magma mixing; both of which are not exclusive to any particular

evolutionary stage, nor are they mutually exclusive. Smith (1979) and Macdonald et al (1992) consider magma mixing is probably ubiquitous in silicic systems. Aspects of the high level processes interpreted to be responsible for the compositional variability of the Kaingaroa magma components are discussed here; Mechanisms 1 and 2 are considered petrogenetic processes, and are discussed in Chapter 9.

The main processes thought to be operative specifically in silicic magma systems are crystal-liquid fractionation, magma mixing, wall-rock assimilation, and thermogravitational diffusion (TGD). Elucidation of the role of these processes was an important topic of debate in the early 1980's (Michael 1983; Hildreth 1983). It is now generally accepted that crystal fractionation is the most common mechanism of zonation or variation (Michael 1983; Baker and McBirney 1985; Macdonald et al. 1992; De Silva and Wolff 1995). Recent chemical and mineralogic studies of large silicic systems has outlined evidence of two additional open system controls on magma system chemical variation or zonation:

A) Magma mixing between two rhyolitic magmas of similar chemistry (e.g. De Silva 1991; Hervig and Dunbar 1992; Stimac et al. 1996; Stimac in press), or dissimilar chemistry (e.g. Cambray et al. 1995).

B) Evisceration of multiple magma chambers (e.g. Briggs et al. 1993; Sutton et al. 1995).

The chemical variation among pumice fragments is continuous, and chemical trends in the Kaingaroa Ignimbrite pumices are qualitatively consistent with crystal fractionation. Fig 7.14 illustrates simple vector models of crystal fractionation assuming subtraction of observed phenocryst phases. Crystal fractionation of observed phenocrysts and proportions can generally account for observed trends (Fig 7.14; Table 7.2). Rb and Sr are strongly fractionated from each other during plagioclase crystallisation and Rb/Sr is therefore a sensitive indicator of plagioclase fractionation. The systematic increase of Rb/Sr with Rb (or SiO_2) in pumices types A through D suggest the magmas have undergone plagioclase-dominated fractionation from a Type D parent and this is supported by enrichment of REE and systematic decrease in Eu/Eu^* from Type A to D.

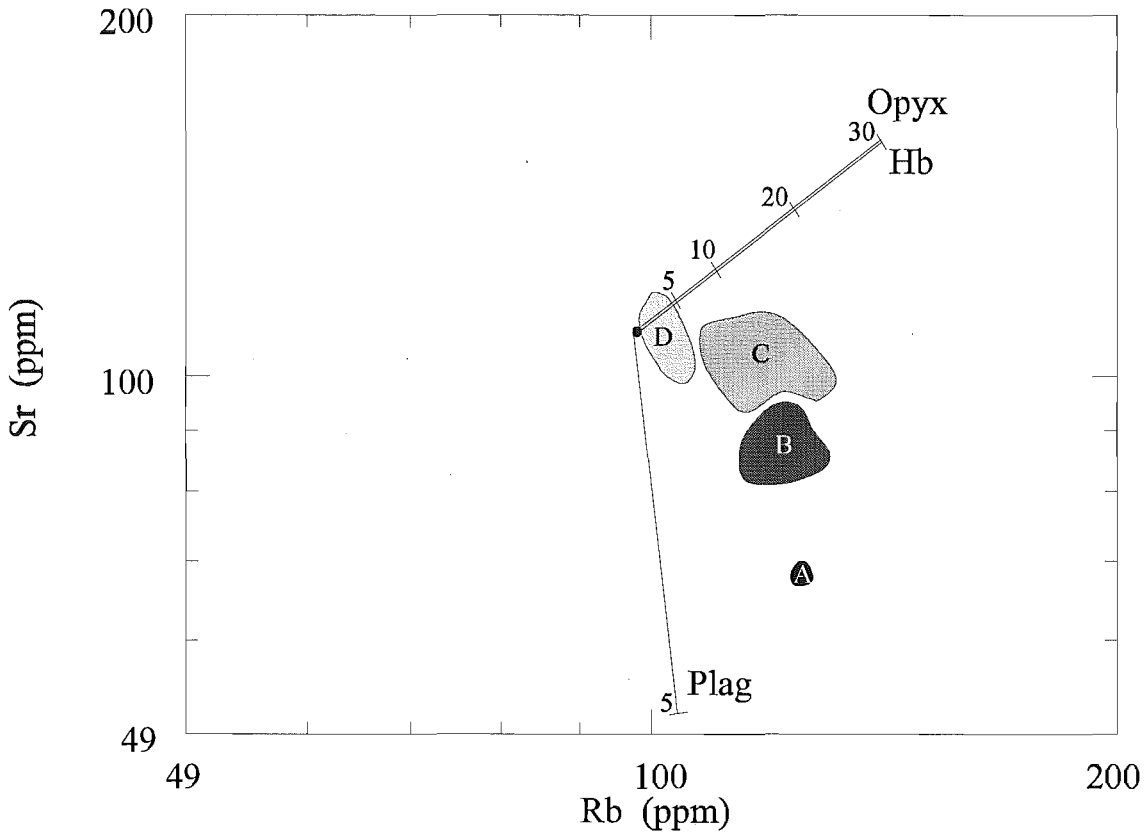

Figure 7.14 Simple vector model illlustrating role of plagioclase as dominant fractionating mineral in Kaingaroa magma system. Partition coefficients and model assumptions outlined in Table 7.2. Pumice fields refer to pumice types defined in Figs 7.6, 7.7.

Vector modelling example

Partition coefficients for rhyolitic liquids

	Opyx	*Plag*	*Hb*
Rb	0.003	0.105	0.014
Sr	0.009	15.633	0.022

Partition coefficients from Arth (1976) and Nash and Creecraft (1985)

Initial composition: Rb 99; Sr 111 Type D pumice KA 175D.

Using Rayleigh fractionation modelling

$$C_L/C_O = F^{(D-1)}$$

C_L = wt% of trace element
C_O = wt% of trace element of parent liquid
F = Fraction of melt remaining
D = Distribution coefficient

	Opyx	*Plag*	*Hb*
5%			
Rb	104.2	103.7	104.1
Sr	116.8	52.4	116.7
10%			
Rb	109.9	108.8	109.8
Sr	123.2	23.8	123.0
20%			
Rb	123.7	120.9	123.4
Sr	138.5	4.2	138.1
30%			
Rb	141.3	136.2	140.7
Sr	158.1	0.6	157.3

Table 7.2 Vector model tabulation, partition coefficients and assumptions used in calculating Fig 7.14.

The systematic decrease in Fe, Ti, and Zr, also suggests fractionation of ferromagnesian minerals and zircon. $^{87}Sr/^{86}Sr$ and $^{143}Nd/^{144}Nd$ isotopic ratios exhibit limited variation consistent with derivation of types A-D by crystal fractionation.

The origin of type E magma is less clear. Type E bleb has dissimilar mineralogy and trace element chemistry to Kaingaroa pumices $_{s.s.}$ consistent with its less evolved dacitic composition. Type E is rejected as a parental composition to the Kaingaroa magma chamber, due to anomalously high $^{87}Sr/^{86}Sr$ and low $^{143}Nd/^{144}Nd$.

No 'a priori' evidence of mixing has been recognised in the Kaingaroa Ignimbrite pumices, in contrast to the Pokai Ignimbrite (Karhunen 1993) which exhibits multiple phenocryst populations, and Whakamaru Ignimbrite which exhibits mingled and mixed 'dacitic' pumices (Brown 1994). Mingled pumices (rhyolite-rhyolite) have been observed in the Kaingaroa Ignimbrite, but are interpreted as evidence of syn-eruptive mingling.

Similar mineralogy and trace element chemistry suggests the juvenile obsidian sampled from the basal tephras and obsidian/rhyolite lithics sampled from the lag breccia are juvenile magmatic components within the Kaingaroa magma system. Both lithics exhibit similar trace element chemistry to Type C magma, and their origin is discussed as such. The obsidian lithics are considered to represent non-vesicular components, which are partially degassed, quenched primary magma. They are interpreted as fragmented material welded onto conduit walls. Similar obsidian has been reported by Hildreth and Mahood (1986), Suzuki-Kamata et al (1993) and Dunbar and Kyle (1992). Obsidian/rhyolite lithics are considered evidence of small scale effusive precursor rhyolite domes erupted ('leaked') from the Kaingaroa magma system prior to the climactic Kaingaroa Ignimbrite eruption, which were quarried by caldera collapse.

Kairuru, and Pukekahu are isotopically distinct from the Kaingaroa Ignimbrite, precluding an origin by simple crystal-fractionation or AFC of Kaingaroa-like magma. Deer Hill rhyolite exhibits dissimilar trace element chemistry also precluding a simple relationship to Kaingaroa magma system. This suggests the post-caldera rhyolites are not geochemically related to the Kaingaroa magma system and represent separate magma batches, as inferred for the Western Dome Belt rhyolites, which are post-

Whakamaru-group ignimbrites (Brown 1994). Mineralogical and chemical variation in Kaingaroa magma components is summarised in Table 9.3.

In conclusion, the origin of magma components can best be explained by a combination of crystal fractionation and syn-eruptive mingling of a two discrete magmas. Post-caldera rhyolites are interpreted to represent additional discrete magma batches.

7.6 Kaingaroa magma system

A model of the magmatic system beneath Reporoa Caldera prior to the Kaingaroa eruption must account for the following features:

1. a relatively shallow ca. 100-200 km^3 magma.
2. the existence of a large volume of near homogeneous rhyolite magma.
3. weak chemical and mineralogical zonation.
4. presence of a less-evolved dacitic composition of isotopically distinct composition. within a unit with sectorial distribution, and inferred localised source.
5. eruption of an evolved composition only at a single fall horizon.
6. no evidence of hybridisation (mixing).
7. syn-eruptive mingling of pumice types during caldera collapse.
8. geochemically distinct post-caldera rhyolites.

The proposed magma chamber model is illustrated in Fig 7.15. based on probable densities, and allowing for approximate magmatic volumes outlined above and Chapter 3. The lateral dimensions of the chamber are based on structural caldera boundaries, and inferred coin-like geometry of TVZ magma chambers (Blake et al. 1992, Blake pers comm 1994; see below).

Kaingaroa pumices types A, B, C, D exhibit weak variations in mineralogy and trace element chemistry, and limited isotopic variation consistent with derivation from a weakly zoned magma chamber. Homogeneous temperature estimates, water content, and glass chemistry suggest a vigorous convecting magma system. The juvenile obsidian lithics are interpreted as degassed(?) dense juvenile samples from the magma chamber, and Kaingaroa-like rhyolite/obsidian lithics exhibit similar mineralogy and

chemistry which suggest they are pre-climactic eruption leaks from the Kaingaroa magma system. Origin of the compositional diversity of the Kaingaroa pumices is attributable to weak plagioclase-dominated fractionation, with no assimilation of Torlesse crust.

Type E magmas appear to be unrelated to Kaingaroa pumices $_{s.s.}$ by crystal fractionation or AFC, and therefore are interpreted as distinct magma batches that were incorporated into the eruption. The similarity in crystal content, mineralogy, and trace element chemistry suggest they may have been derived from similar sources and/or followed similar petrogenetic pathways e.g. plagioclase-dominated fractionation. The spatial relationships of these distinct compositions is not clear.

Late addition of silicic magma with similar compositions to the resident magma has been documented for many other large scale ignimbrites e.g. Bishop Tuff (Hervig and Dunbar 1992), Topopah Spring Tuff (Schuraytz et al. 1989) and Neapolitan Yellow Tuff (Orsi et al. 1995). Origin of compositional zonation in ignimbrites has been a topic of debate throughout the 1970's, 80's and 90's, with increasing evidence that this zonation reflects a combination of closed-system crystal fractionation processes and open system mixing.

Hervig and Dunbar (1992) explain the chemical variation in the Bandelier and Bishop 'ignimbrites' by a combination of crystal fractionation and mixing of a second rhyolite. In both magma systems, the additional magma is markedly subordinate in volume, hotter, less fractionated, and interpreted to be derived from a similar source to the bulk of the magma system. Hervig and Dunbar (1992) advocate mixing of the less-evolved component into the base of the chamber. Alternatively Briggs et al (1993) and Sutton et al (1995) suggest that batches of magma may be derived from different sources and erupted simultaneously.

Contemporaneous extraction and magma mingling with Kaingaroa pumices$_{s.s.}$ unequivocally indicates Type E blebs were juvenile components associated with the pre-eruptive Kaingaroa magma system. The lack of mixed compositions, limited sectorial emplacement, and stratigraphic position (in relation to an assumed progressively withdrawn chamber) is difficult to reconcile with co-existence in the same magma

chamber. Type E is interpreted to represent samples of a discrete small volume (<< 1 vol%) magma batch incorporated during caldera collapse. The limited volume suggests either a small chamber or probably a dike-like body.

An added implication of sampling of less evolved compositions (though volumetrically insignificant) is that they represent weakly fractionated magmas, possibly from similar sources to the main body, and thus possibly still preserve evidence of their parentage. This point is discussed in Chapter 9.

The eruption of Type A magma is restricted to a single airfall horizon, suggesting vent migration during basal tephra eruption, which tapped a distinct zone, possibly a more evolved cupola or apophysis .

7.7 Implications for eruptive dynamics and caldera collapse

Chemical and isotopic data from the proximal and medial Kaingaroa Ignimbrite indicate the eruption began with evisceration of evolved magma, followed by the simultaneous tapping of various portions of the magma chamber, and ended with eruption of less evolved compositions. The eruption of types A and E record localised anomalies in this eruptive sequence.

The basal tephra eruption began with a single vent phase that drained only the evolved part of the magma chamber. Transition to column collapse and pyroclastic flow eruption probably marks the propagation of the single vent and activation of discrete fractures along the eastern margin of Reporoa Caldera, as suggested by the distribution of lower Reporoa boundary unit (RBU). This phase of the eruption completely drained the evolved part of the magma system (Type B). The lag breccias and OWR mark the onset of caldera collapse leading to complex evacuation and syn-eruptive mingling of different composition magmas. The localised eruption of Type E dacite with Kaingaroa $pumices_{s.s.}$ reflects tapping of multiple magma batches. Late collapse relating to the eruption and deposition of WIU reflects evisceration of the least evolved portions of the magma system.

Magma component	*Mineralogy*	*Plag*	*Pyx*	*Temp*	*Rb*	*$^{87}Sr/^{86}Sr$ isotopes*
A	Plag+opyx+Fe/Ti ox	An_{32-26}	En_{49-41}	814-816°C	125	0.70557
B	Plag+opyx+Fe/Ti ox	An_{34-32}	En_{47-43}	801-812°C	109-128	0.70566-0.70571
C	Plag+opyx+Fe/Ti ox+aug	An_{49-32}	En_{46-40}	-	109-126	0.70575-0.70583
D	Plag+opyx+Fe/Ti ox±amph±aug	An_{42-32}	En_{51-45}	811-820°C	95-109	0.70578-0.70583
E	Plag+opyx+aug+amph+Fe/Ti ox	An_{47-28}	En_{51-47}	-	76	0.70625
Kg-like lithic	Plag+opyx+Fe/Ti ox+amph+qtz+aug	An_{40-30}	En_{49-45}	-	-	-
Pukekahu rhyolite	Plag+opyx+Fe/Ti ox+amph	An_{57-26}	En_{50-43}	-	117	-
Kairuru rhyolite	Plag+qtz+opyx+Fe/Ti ox	-	En_{37}	-	125-127	0.70542
Juvenile obsidian	Plag+opyx+Fe/Ti ox+amph	-	-	-	117	-
Rhyolite lithic	Plag+opyx+Fe/Ti ox	-	-	-	124	-

Table 7.3 Mineralogical and chemical variation of Kaingaroa magma components.

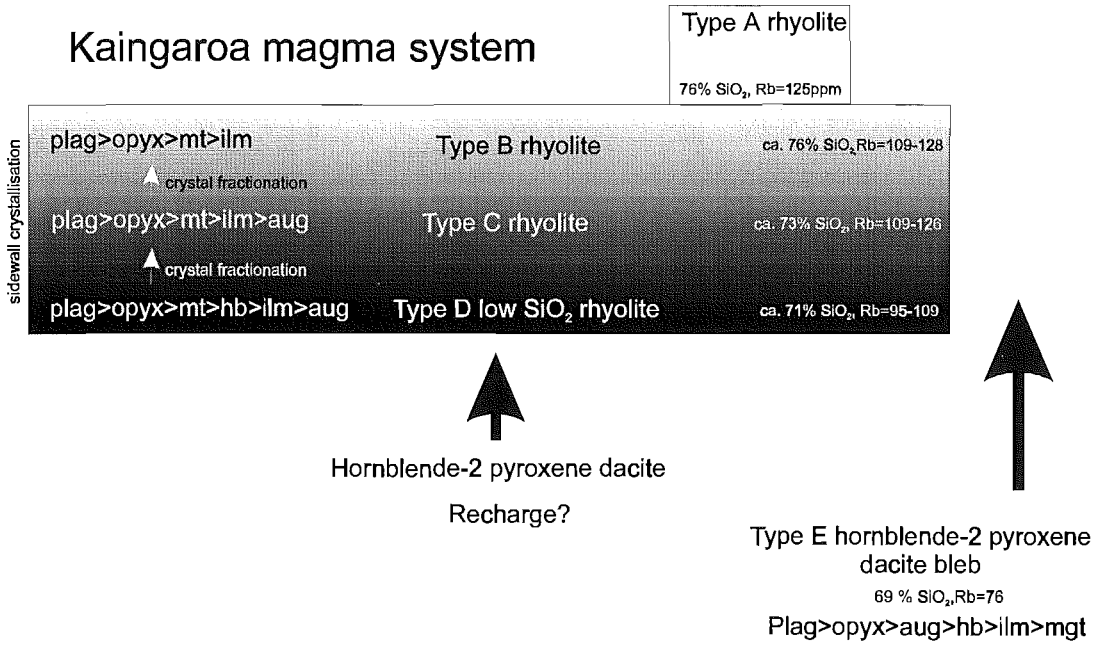

Figure 7.15 Kaingaroa magma system model

7.8 Zonation in TVZ ignimbrites

Ignimbrites exhibit a spectrum of zonation styles (De Silva 1991); a function of numerous variables including stress and thermal regimes, crustal composition, crystallisation history, magma chamber geometry, parental magma composition, eruptive dynamics, and pre-eruptive configuration.

There has become an increasing awareness of limited zonation in some ignimbrites (e.g. Whitney and Stormer 1985). These so called monotonous ignimbrites have been documented worldwide (De Silva 1991). Homogenous or weakly-zoned ignimbrites were originally recognised by Smith (1979) and Hildreth (1981). Smith (1979) considered homogenous ignimbrites represent eruptions that tapped only a homogenous layer within a large zoned chamber. Smith and Shaw (1975) considered only ca. 10% by volume of a magma chamber is ever evacuated during eruption. De Silva (1991) suggests homogenous ignimbrites represent eruption from homogenous chambers i.e. chambers that have been thoroughly mixed by convection. Recent workers e.g. Bacon and Druitt (1988) and Blake et al (1992) advocate eruption of almost the entire chamber. Homogenous or monotonous ignimbrites are now generally excepted as eruptions from homogenised chambers.

Taupo Volcanic Zone ignimbrites have been traditionally thought of as homogenous (Dunbar et al. 1989; Hochstein et al. 1993), but recent trace element and isotopic chemistry has illustrated the trace element variation within of Mangakino-derived ignimbrites (Briggs et al. 1993), and the Pokai and Whakamaru-group ignimbrites (Karhunen 1993; Brown 1994). Aspects of this variation, and implications of zonation patterns are addressed here.

Details of the extent of compositional zonation in TVZ ignimbrites has been hampered by limited data, and data largely restricted to Taupo and Okataina caldera complexes (e.g. Dunbar et al. 1989; Smith 1989; Hochstein et al. 1993). Briggs et al (1993) documented compositional variability in Mangakino-derived ignimbrites, illustrated by two types of zonation:

Type A zonation (e.g. Ongatiti Ignimbrite) is manifest as variation in trace element chemistry, with no compositional gaps, and limited mineralogical and shard chemical or thermal variation.

Type B zonation (e.g. Ahuroa Ignimbrite) is documented by two discrete trace element and isotopic compositional groups, separated by a large compositional gap. The two groups cannot be related by simple crystal fractionation.

Briggs et al. (1993) suggests Type A represents eruption of weakly zoned magma, and Type B may represent eruption of two discrete bodies. The majority of TVZ ignimbrites exhibit homogeneous glass shard chemistry (Karhunen 1993; Briggs et al. 1993; Black et al. 1996, this study), thought to reflect the lack of (or limited) zonation in their magma system, despite whole pumice chemical variations. Zonation in TVZ ignimbrites is thus manifest in a variety of forms. A spectrum of zonation styles and configurations are recognised:

Homogenous e.g. Taupo (Dunbar et al. 1989; Sutton et al. 1995)
Weak zonation e.g. Kaingaroa (this study)
Strong zonation e.g. Whakamaru (Brown 1994)
Rhyolite-rhyolite mixing e.g. Matahina (Carr 1984)
Multiple systems e.g. Ahuroa (Briggs et al. 1993), Kaingaroa (this study)

The dominance of TVZ ignimbrites which exhibit weak or no zonation is likely to be a function of variable convections rate and energies (Orsi et al. 1995). Exceptions to this can be explained by open system processes, e.g. evisceration of two separate components either from the same chamber, or from two or more discrete chambers. This can be related to the high heat flow, speed of magma generation in central TVZ, and inferred magma chamber geometry.

De Silva (1991) concludes that the main process in magma chamber zonation is heat transfer relating to magma chamber geometry. Magma chambers are thought to represent a continuum from coin-shaped (sill-like) to column-shaped bodies (pipe-like; De Silva 1991; De Silva and Wolff 1995). Blake et al (1992) and Blake (pers comm 1994) interprets TVZ magma chambers as high aspect-ratio thin coin-like bodies. The

implications of eruption from coin-shaped chambers on development of compositional zonation in TVZ magmas is that high aspect ratio chambers suggest more surface area to interact with, resulting in prolonged convection and hence prevention of crystallisation. This is further accentuated by the high heat flow within central TVZ. Thermal constraints require smaller volume chambers be more equant, without crystallising. Therefore minor *in situ* zonation can be explained by variations in magma chamber shape and configuration. Apophyses or cupolas in granitoids (and magma chambers?) are typically more equant, of smaller surface area, and hence exhibit more evolved magma. Thus a weakly zoned large chamber may develop an apophysis of more evolved zoned magma (e.g. Type A?; De Silva and Wolff 1995).

Thus a general relationship can be advocated between the high heat flow in central TVZ, high aspect ratio chambers, and the resultant lack of (or limited) *in situ* chemical differentiation in magma chambers. High heat flow in central TVZ promotes continued supply of heat to a greater surface area, promoting convection. Recharge of further rhyolitic magma provides additional heat flow, chemical variation, and may possibly play a role in eruption triggering.

I would suggest that zonation of TVZ ignimbrite is not a function of age or geographic location i.e. not restricted to Mangakino (Briggs et al 1993) or older TVZ ignimbrites (Karhunen 1993), but is present throughout TVZ eruptives, albeit weakly developed and a function of open system processes. The central TVZ is a unique window into a high heat flow environment, with resultant speed of magma and magma chamber generation, and prevention of insitu chemical differentiation, with the exception of the spectacular Whakamaru-group eruptives.

Central TVZ ignimbrites are thus examples of homogenous or weakly-zoned eruptives. Exceptions are noteworthy (e.g. Whakamaru), and probably represent culmination of prolonging periods of magmatic (and tectonic?) quiescence, and/or spatial and temporal evolution of heat flow in central TVZ.

CHAPTER EIGHT
Kawerau ignimbrite

8.1 Introduction

Nairn (1981) mapped the unit outcropping within the Puhipuhi Basin and near Kawerau as the Kaingaroa Ignimbrite and subsequent authors have adopted this interpretation (e.g. Bailey and Carr 1994; Nairn et al. 1994).

Reconnaissance study in the area in late 1993 however revealed the unit contained a number of features inconsistent with either the Kaingaroa Ignimbrite or ignimbrites of similar age and stratigraphic position. It is here informally called Kawerau ignimbrite (new name) and is exposed at two localities in the north-eastern part of TVZ: 1) near Kawerau, and 2) Puhipuhi Basin (Figs 8.1, 8.2).

The aim of this chapter is to report the presence of a newly discovered ignimbrite, correlate and compare the Kawerau ignimbrite with other TVZ ignimbrites, and to briefly investigate compositional variation. A notable feature of the Kawerau ignimbrite petrology is anomalously high Zr, Zn and Hf, and the presence of vapour-phase alkali amphibole, biotite and manganoan-fayalite.

8.2 Age and stratigraphic relations

Kohn (in Nairn 1989) obtained a fission track age of 0.24 Ma $\pm$ 0.005 Ma from a non-welded sandy-black ignimbrite at V16/292318, which is consistent with its stratigraphic position overlying the Whakamaru-group ignimbrites (0.34-0.32 Ma) and Matahina Ignimbrite (0.28 Ma), and beneath the Mamaku Ignimbrite (0.22 Ma) and Rotoiti Breccia (0.06 Ma).

8.3 Lithology and distribution

The Kawerau ignimbrite is composed of two units that locally grade into each other: a lower non-partially welded 'sandy-black' ignimbrite and an upper non-welded, tan/buff pumice-poor ignimbrite. The type section is proposed as a road side outcrop on State Highway 30 (V15/343448; Fig 8.3), where 60 m Kawerau ignimbrite is well exposed in a recently cleared roadcut. The outcrop illustrates the relationship between the lower and upper units. The lower sandy-black/brown unit grades up into the tan/buff pumice-poor unit, with no observable contact or grading of lithics, and subtle grading of pumice abundance. Both units are non-welded. M_P locally exceeds 30 cm, with rare outsized pumices up to 70 cm in diameter. The upper unit is well exposed around Kawerau, underlying Rotoiti Breccia, which infills valleys cut in Kawerau ignimbrite (Nairn 1981). Here the upper unit is a non-welded, brown-orange pumice-rich ignimbrite with localised 50 cm thick fines-depleted pumice concentration zones, and M_P exceeding 250 mm. Lithics are generally less than 10 mm and dominantly rhyolite.

Both units are exposed in Puhipuhi Basin (Fig 8.2), an 8 km diameter basin on the eastern margin of Okataina caldera complex. The basin has little topographic expression as it has been largely infilled by the Kawerau ignimbrite (to a depth of ca. 120 m) and the Puhipuhi massif, a small dacite lava dome and adjacent area of uplifted and deformed lacustrine sediments and pyroclastics which have been intruded by the dacite lavas (Nairn 1981, 1989). Puhipuhi Basin is interpreted as a marginal slump block or subsidiary embayment related to Matahina caldera collapse (0.28 Ma), which may be due to synchronous collapse along regional faults during caldera collapse.

The Kawerau ignimbrite forms a dissected plateau remnant within the basin at approximately 200 masl (50 m higher than the basin rim; Nairn 1981). Both units are exposed in clear felled knolls, forestry roads and cliffs adjacent to the Tarawera River, with best exposures along Tarawera Rd at V16/288343 (Fig 8.4) and V16/293348. Nowhere is the base of the ignimbrite exposed, but steep sided valley walls that cut into the plateau have flat bases suggesting that the erosional base level was lower than the present basin floor (Nairn 1981). The lower unit is a non- to partially welded pumice-rich sandy-black/brown ignimbrite with two distinct pumice types: orange/pink or vesicular black rhyolite and a rare chocolate brown dacite. All pumices are crystal-poor.

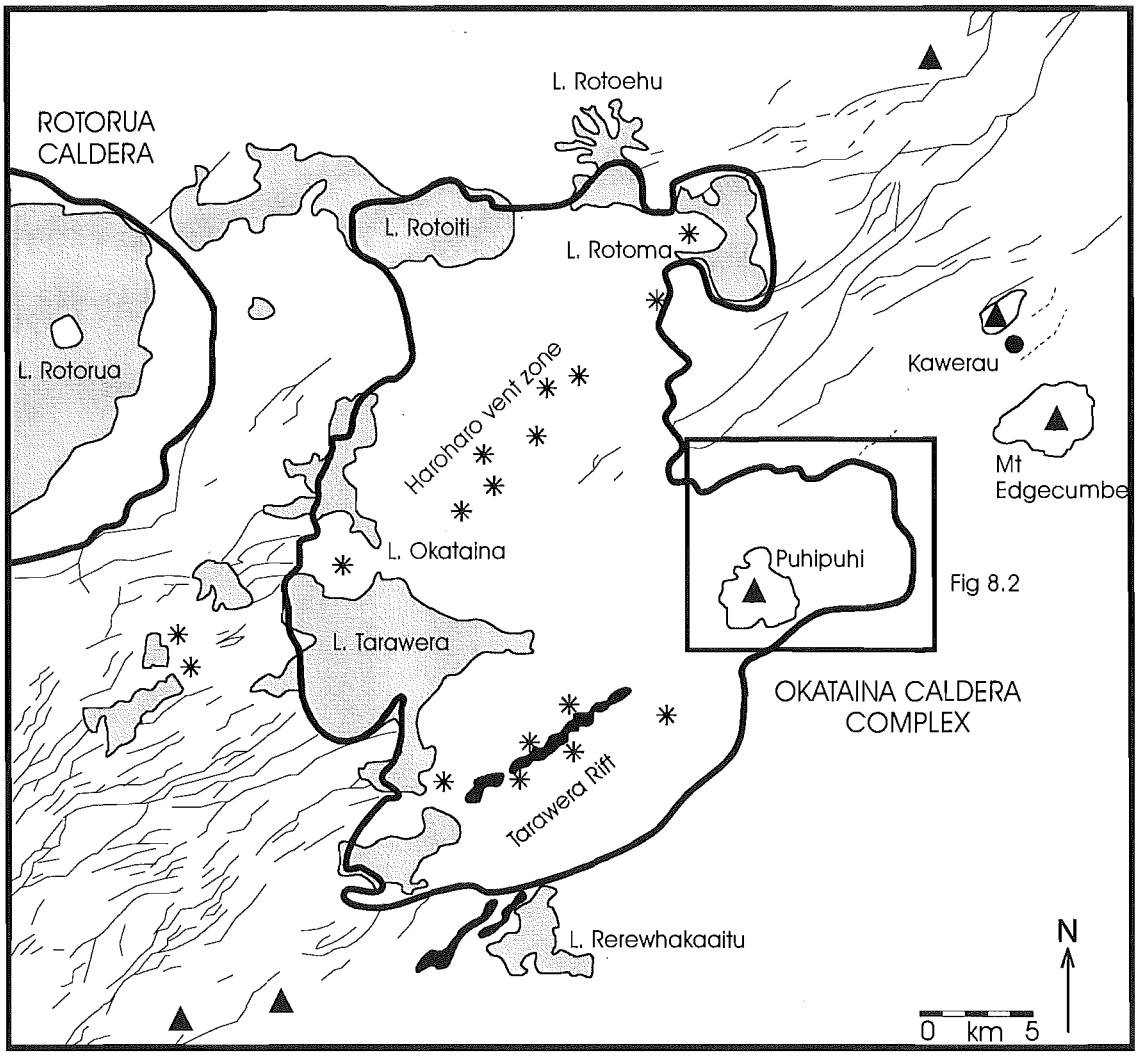

Figure 8.1 Location of Puhipuhi Basin (box) relative to Okataina caldera complex. Detailed distribution of the Kawerau ignimbrite within Puhipuhi Basin is illustrated in Figure 8.2. M_L data are insufficient to construct meaningful contours but broadly coarsen towards an inferred source in the Okataina caldera complex region.

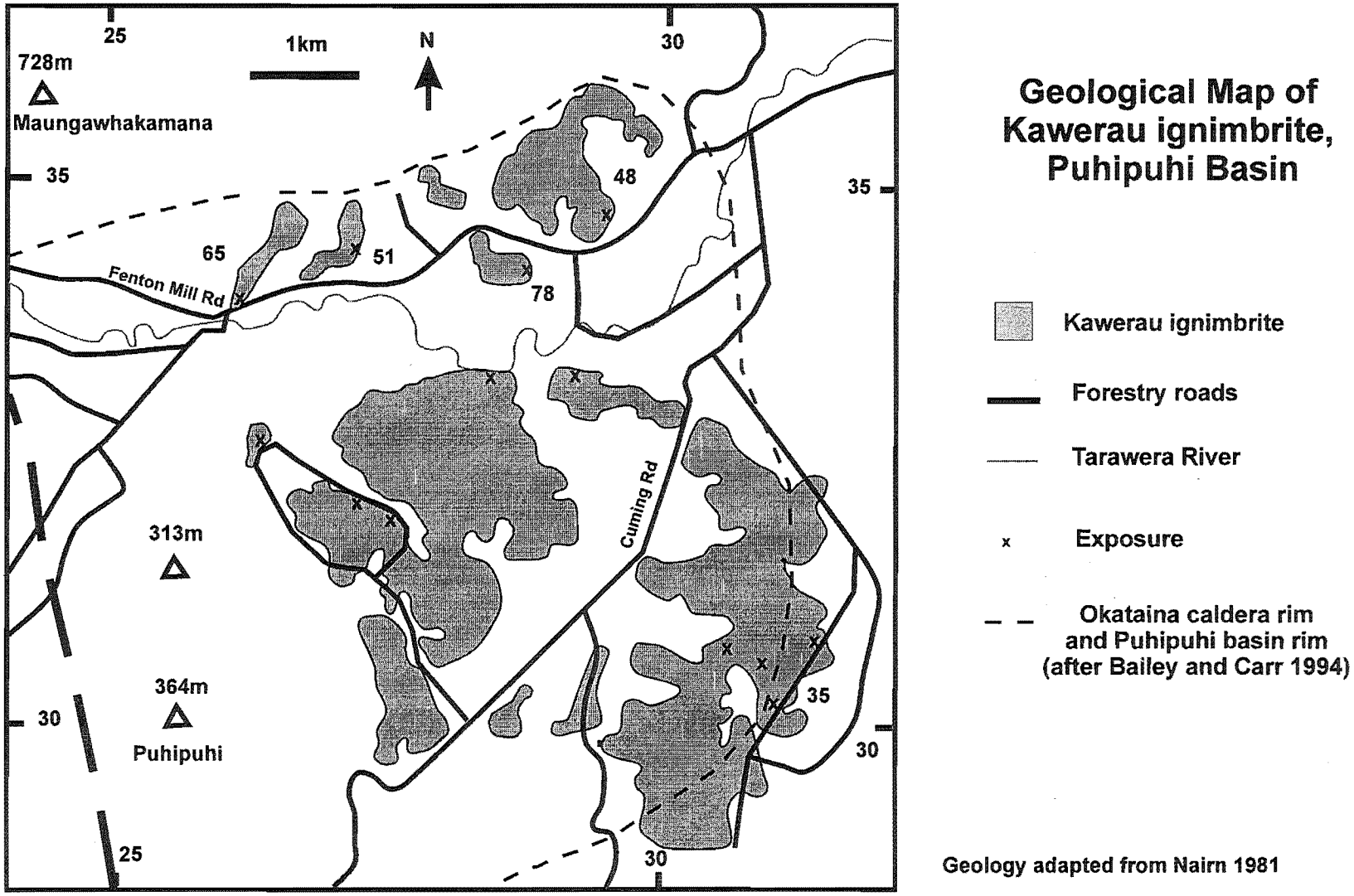

Figure 8.2. Geological map of Puhipuhi Basin illustrating distribution of the Kawerau ignimbrite and maximum lithic data.

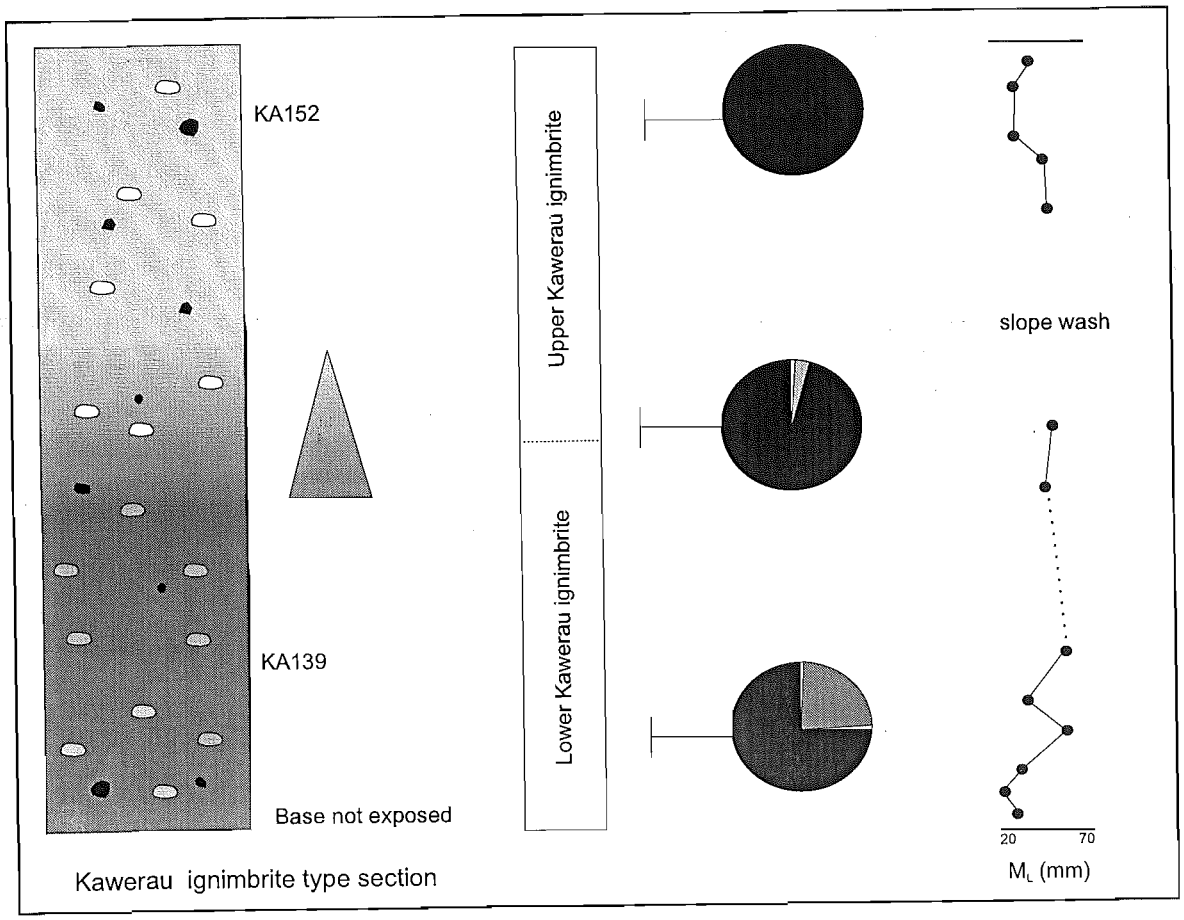

Figure 8.3 Graphic log through the type section of the Kawerau ignimbrite, north-east of Kawerau. Pie diagrams illustrate the composition of lithic assemblages in the ignimbrite.

The unit is relatively coarse-grained with M_P locally exceeding 194 mm, and M_L locally reaching 78 mm. A single dacite lithic of 161 mm was found at V16/292318.

The ignimbrite is vitric throughout, with no signs of devitrification, although it is commonly silica case hardened, and contains conspicuous bladed fayalite of vapour phase origin (Fig 8.5). Locally within the basin the ignimbrite is partially welded with widely spaced vertical cooling joints (4-6 m spacing).

In thin section the welded sandy-black ignimbrite exhibits typical vitroclastic texture. Plagioclase is the dominant phenocryst phase, with subordinate acicular green-brown hornblende (dominant mafic), orthopyroxene, apatite, zircon and Fe/Ti oxides. Mineral separates reveal trace contents of augite and titanite. No variation in mineral content with stratigraphic interval was observed.

8.4 Lithic fragments

Lithic fragments were collected from seven localities within Puhipuhi Basin and near Kawerau, and percentages determined using methods outlined in Chapter 5. Lithics are predominantly flow-banded, porphyritic hornblende-bearing rhyolite, with subordinate basalt, Matahina-like ignimbrite, obsidian, and a distinctive phenocryst-poor dacite (Fig 8.3). Lithics are generally angular and range in size up to 161 mm in Puhipuhi Basin with dacites generally the largest lithics.

The dacite lithic type is phenocryst-poor (5-10%) and contains plagioclase + orthopyroxene + augite in a fine grained groundmass, composed of devitrified glass and swallow tail plagioclase microlites (which locally form a pilotaxitic texture). Plagioclase (An_{45-40}) is oscillatory zoned, forms phenocrysts up to 3 mm, and contains abundant apatite needles and melt inclusions. Rare crystals show sieve texture. The lithic type is widely dispersed within the lower sandy-black ignimbrite within Puhipuhi Basin, and is correlated on the basis of petrography with the Puhipuhi dacite, exposed in western Puhipuhi Basin. The correlation confirms Nairn's (1981, 1989) inference that the dacite is older than the sandy-black ignimbrite and constrains the source of the ignimbrite.

Figure 8.4 Partially welded lower 'sandy-black' unit of the Kawerau ignimbrite within Puhipuhi Basin.

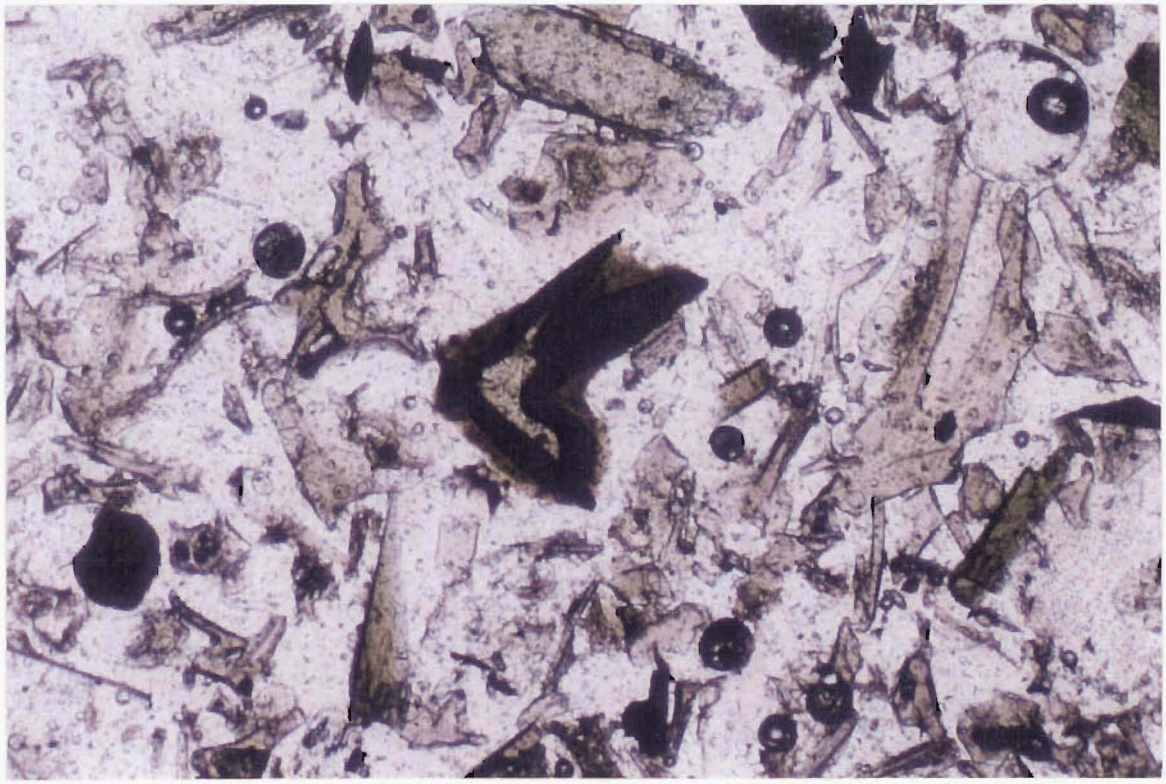

Figure 8.5 Bladed manganoan fayalite (of inferred vapour-phase origin) within a mineral separate. The rim is oxidised and coated with limonite. Field of view is 7 mm.

8.5 Kawerau magma system

Magmatic components of the Kawerau ignimbrite are divided into two types: Type A orange, grey or black high-silica rhyolite pumice, and Type B chocolate brown dacitic pumice. There is a compositional gap between ca. 69% and 74% SiO_2. Pumices of Type B comprise less than 1 vol% of the erupted products.

8.5.1 Petrography

Type A pumice

The phenocryst contents of pumices were measured by panning methods (see Appendix E). These estimates yield 5-8 wt% crystals. All high silica rhyolitic pumices contain the phenocryst assemblage plagioclase + hornblende + orthopyroxene + Fe/Ti oxides. Apatite and zircon are present as accessory minerals. Phenocrysts are commonly present as glomeroporphyritic clusters. Plagioclase forms subhedral oscillatory zoned phenocrysts up to 2 mm in length, which are commonly fractured in whole rock specimens. Hornblende occurs as green pleochroic euhedral acicular prisms up to 3.5 mm in length, and as rare inclusions in pyroxene. Orthopyroxene occurs as colourless-light brown subhedral to euhedral phenocrysts up to 2 mm in length. Magnetite and ilmenite occurs as euhedral inclusions in orthopyroxene (and more rarely plagioclase and hornblende) phenocrysts. Apatite occurs as acicular needles typically < 0.1 mm within plagioclase phenocrysts. Zircon is found as tiny prismatic inclusions within orthopyroxene. Matrix glass is clear and highly vesiculated.

Type B pumice

The phenocryst content of Type B pumices yield an estimate of 1-2 wt% crystals, composed of plagioclase + augite + hornblende + orthopyroxene + Fe/Ti oxides. Titanite, zircon and apatite are present as accessory minerals. Type B pumices are notable for the presence of augite and their crystal poorer nature (c.f. Type A). Plagioclase, orthopyroxene and hornblende exhibit similar size and crystal habit as in Type A pumices. Augite occurs as green-pleochroic subhedral prisms up to 2 mm. Titanite is present as disseminated small (up to 0.5 mm) anhedral crystals, and apatite as acicular needle inclusions in Fe/Ti oxides and plagioclase. Matrix glass is brown and poorly vesicular (c.f. Type A). No banded (i.e. mingled) pumices were observed.

8.5.2 Mineral compositions

Phenocrysts from Kawerau pumices were analysed by EPMA. Representative analyses are given in Table 8.1.

Most plagioclase phenocrysts in both pumice types are normally oscillatory zoned. Type A pumice plagioclase phenocrysts are zoned from An_{41-28}, whereas Type B pumices are normally zoned from An_{48-36} (Fig 8.6, Table 8.1), and notably more calcic, reflecting their more mafic composition and association with Mg-rich orthopyroxene and augite (see below).

Hornblende is the most abundant mafic phenocryst in both pumice types, and is notable as hornblende-rich crystal-poor rhyolites are uncommon in units of similar age or in the TVZ as a whole. Type A pumices contain magnesio-hornblende, typical of many TVZ ignimbrites (Ewart et al. 1975; Briggs et al. 1993) whereas Type B pumices contain tsckermatic-hornblende (classified after Leake 1978), again consistent with its more mafic composition. Hornblendes exhibit limited zonation (Appendix D). The stability of amphibole in rhyolitic magmas requires from 4-6 wt% H_2O (Rutherford and Devine 1988; Geschwind and Rutherford 1992; Rutherford 1993).

Pyroxene is subordinate to hornblende in both pumice types. Orthopyroxene (En_{60-56}) is the only pyroxene phenocryst phase in Type A pumices. Type B pumice exhibit notably Mg-rich orthopyroxene (En_{65}) coexisting with Fe-richer orthopyroxene (En_{42}) and augite ($Wo_{41.7}En_{42.7}Fs_{15.6}$ - $Wo_{41.9}En_{41.3}Fs_{16.8}$; Fig 8.7, Table 8.1; Appendix D). Most pyroxene phenocrysts show limited zonation. Pyroxene chemistry is notably distinct from Kaingaroa Ignimbrite pyroxenes, notably the presence of Mg-rich orthopyroxene and augite in Type B pumices (Fig 8.5). Augite has been reported in a few TVZ ignimbrites as a very rare and subordinate phase, but no analyses have been published.

Magnetite is the predominant Fe/Ti oxide with subordinate ilmenite. Where possible co-existing magnetite and ilmenite inclusions in pyroxene or plagioclase have been analysed, which unambiguously represent equilibrium pairs. A secondary test of partitioning between Mg and Mn (Bacon and Hirschmann 1988) was applied to test for equilibrium.

Sample no.	*KA114*	*KA114*	*KA110*	*KA110*	*KA114*	*KA114*	*KA114*	*KA114*	*KA110*	*KA110*	*KA114*	*KA114*	*KA110*	*KA110*
Pumice type	B	B	A	A	B	B	B	B	A	A	B	B	A	A
Analysis no	419	420	524	525	433	434	440	441	532	533	426	427	539	540
	plag	plag	plag	plag	cpyx	cpyx	opyx	opyx	opyx	opyx	hb	hb	hb	hb
	core	rim	core	rim	core	rim	core	rim	core	rim	core	rim	core	rim
SiO_2	59.63	57.76	61.45	58.13	52.61	51.45	51.79	52.62	50.83	51.85	43.00	43.03	46.41	47.94
Al_2O_3	25.50	25.76	23.72	25.91	1.44	2.03	0.46	0.49	0.34	0.38	9.61	9.40	6.89	5.94
TiO_2	0.00	0.06	0.00	0.00	0.41	0.49	0.15	0.10	0.11	0.09	3.07	3.07	1.59	1.44
FeO	0.24	0.17	0.18	0.14	9.34	9.61	24.81	24.40	23.52	24.57	4.98	6.42	4.22	2.98
MnO	0.00	0.02	0.00	0.00	0.61	0.61	2.37	2.30	2.17	2.34	0.28	0.19	0.66	0.68
MgO	0.00	0.03	0.00	0.00	15.25	14.18	20.55	20.32	20.14	20.48	13.96	13.94	14.59	15.04
CaO	7.95	8.78	5.30	8.12	20.68	19.38	0.83	0.83	0.80	0.79	10.45	11.08	10.51	10.32
Na_2O	6.83	5.20	7.13	6.23	0.30	0.33	0.00	0.05	0.00	0.00	2.29	2.16	1.60	1.44
K_2O	0.26	0.25	0.38	0.17	0.00	0.00	0.00	0.01	0.00	0.00	0.39	0.37	0.31	0.20
Fe_2O_3*											8.32	7.08	9.59	11.85
Total	100.40	98.01	98.15	98.70	100.64	98.07	100.96	101.13	97.91	100.49	97.19	97.45	97.31	99.02
Oxygen	32	32	32	32	6	6	6	6	6	6	23	23	23	23
Si	10.611	10.505	11.059	10.507	1.950	1.954	1.955	1.975	1.970	1.964	6.344	6.352	6.797	6.892
Al	5.347	5.521	5.031	5.520	0.063	0.091	0.020	0.022	0.015	0.017	1.670	1.635	1.189	1.007
Ti	0.000	0.008	0.000	0.000	0.011	0.014	0.004	0.003	0.003	0.003	0.341	0.341	0.175	0.156
Fe	0.035	0.026	0.027	0.021	0.289	0.305	0.784	0.766	0.762	0.778	0.614	0.793	0.517	0.358
Mn	0.000	0.003	0.000	0.000	0.019	0.020	0.076	0.073	0.071	0.075	0.035	0.023	0.082	0.083
Mg	0.000	0.007	0.000	0.000	0.842	0.803	1.157	1.137	1.164	1.157	3.071	3.069	3.185	3.223
Ca	1.515	1.710	1.021	1.572	0.821	0.789	0.034	0.033	0.033	0.032	1.653	1.752	1.650	1.589
Na	2.355	1.833	2.489	2.184	0.022	0.024	0.000	0.003	0.000	0.000	0.656	0.617	0.456	0.401
K	0.059	0.058	0.088	0.039	0.000	0.000	0.000	0.001	0.000	0.000	0.074	0.069	0.057	0.037
Fe^{3+}											0.924	0.787	1.057	1.281
Total	19.922	19.671	19.714	19.844	4.018	3.999	4.030	4.013	4.019	4.025	15.382	15.439	15.163	15.027

Table 8.1. Representative plagioclase, pyroxene and amphibole analyses from Kawerau ignimbrite pumices.

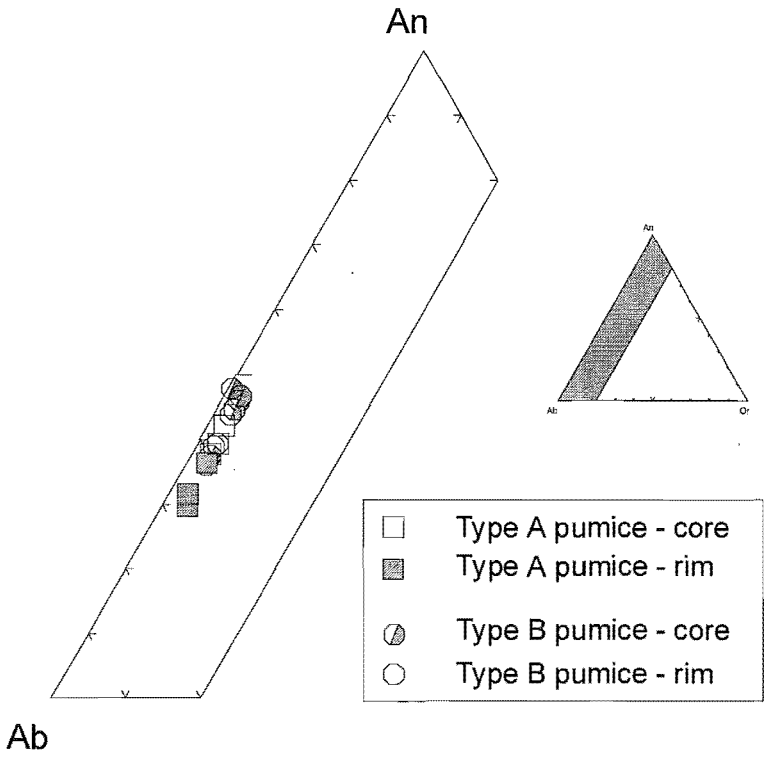

Figure 8.6 Plagioclase phenocryst compositions (mol %) in the Kawerau pumices.

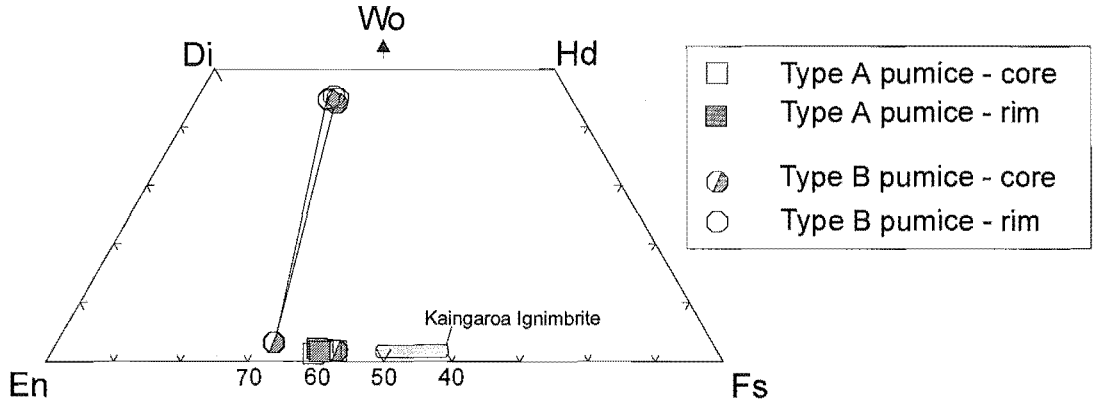

Figure 8.7 Pyroxene quadrilateral showing compositions of clinopyroxenes with tielines to co-existing orthopyroxenes in Type B pumices, and orthopyroxenes in Type A pumices, compared with pyroxene compositions in Kaingaroa Ignimbrite.

Fresh Fe/Ti oxides that exhibited no evidence of exsolving were analysed, and analyses are presented in Appendix D. Iron-titanium oxide temperatures are 777°C for one Type A sample using the geothermometer of Buddington and Lindsley (1964) and refinements of Anderson and Lindsley (1985). Oxygen fugacity determined from Fe/Ti oxides is approximately log fo_2 of - 13.889 in Type A pumices, consistent with the hornblende-pyroxene mineral assemblage. No magnetite was identified in Type B pumices.

8.5.3 Whole pumice compositions

Pumices were collected from two representative sections within Puhipuhi Basin and near Kawerau (Fig 8.2). Analytical methods are outlined in Appendix E. The pumices vary from calc-alkaline dacite to rhyolite, and from metaluminous to weakly peraluminous, with the exception of sample KA119, which is strongly peraluminous due to hydration (high Al_2O_3 and LOI). Pumices from the Kawerau ignimbrite exhibit significant variation in major and trace elements e.g. SiO_2: 67-76% (Fig 8.8); Rb: 65 - 91 ppm; Zr: 193 - 718 ppm; Table 8.2, Figure 8.9). Two distinct pumice types are identified based on dissimilar SiO_2, Fe, Ti, Ca, Zr, and Zn contents, which correspond to pumice types identified on field and petrographic criteria. Insufficient data are present to ascertain variations within pumice types.

Petrography and pumice chemistry indicate two magmatic components in the Kawerau magma system. It is unclear whether the compositional gap reflects the real absence of magma within this compositional range or a sampling gap. Trace element concentrations exhibit slight variations on variation diagrams (Fig 8.9) indicating there may be compositional gradients within individual pumice types. Further detailed work is required on the pumice chemistry of this unit.

The Kawerau ignimbrite pumices as a whole exhibit anomalously high Zr, Zn and Hf, and Na, Ga for their SiO_2 content compared with other TVZ rhyolites. Type B pumice in particular exhibits very high Zr, Hf and Zn, similar to levels in weakly peralkaline and including the highest abundances reported in subalkalic rhyolites/dacites of any affinity (Macdonald et al. 1992) e.g. Zr abundance is ca. 400ppm higher than for reported TVZ rhyolites.

Sample Name	*KA110*	*KA114*	*KA119*	*KA139*	*KA152*
Pumice Type	A	B	B	A	A
XRF					
SiO_2	71.60	66.60	63.73	72.29	73.19
TiO_2	0.28	0.59	0.61	0.29	0.21
Al_2O_3	13.93	15.09	17.19	13.60	12.98
Fe_2O_3*	1.69	3.20	3.61	1.65	1.51
MnO	0.09	0.12	0.12	0.09	0.09
MgO	0.30	0.86	0.48	0.50	0.21
CaO	1.43	2.69	2.16	1.43	1.29
Na_2O	4.41	4.48	4.04	4.34	4.29
K_2O	2.62	2.18	1.98	2.65	2.79
P_2O_5	0.05	0.14	0.12	0.05	0.03
LOI	2.87	3.26	5.36	2.16	2.64
Total	99.27	99.21	99.39	99.05	99.23
Cr	3	3	3	3	7
Ni	3	3	3	3	4
V	7	12	11	7	11
Pb	15	19	21	14	13
Zn	58	148	386	54	48
Rb	81	67	61	84	88
Ba	778	648	620	833	877
Sr	137	219	198	135	121
Ga	16	16	20	14	14
Nb	9	8	9	9	9
Zr	244	622	675	241	221
Y	34	42	40	37	33
Th	9	6	7	8	8
La	23	24	19	26	21
Ce	69	60	61	59	67
INAA					
Sc	5.92	15.29			
As	3.10	3.20			
Br	4.70	5.50			
Sb	0.13	0.17			
Cs	2.87	2.55			
La	23.87	23.70			
Ce	54.00	53.80			
Sm	5.37	6.79			
Eu	1.14	1.74			
Tb	0.87	1.17			
Yb	3.63	4.64			
Lu	0.561	0.707			
Hf	7.15	13.31			
Ta	0.66	0.63			
Th	8	7			
U	2	2			

Table 8.2 Representative XRF and INAA analyses of Kawerau pumices

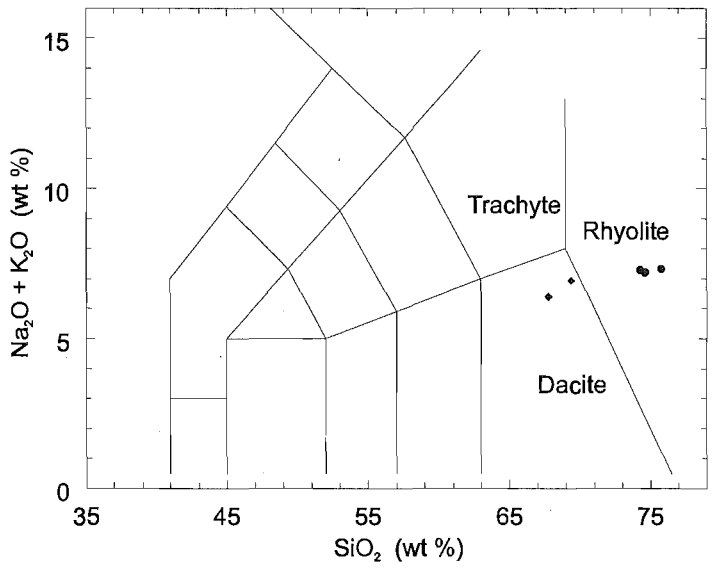

Figure 8.8 TAS classification of Kawerau pumices (after Le Maitre 1989).

Two samples one from each type were analysed for a further selection of elements (including REE) by INAA (Table 8.2). Kawerau pumices are notably higher in total REE content than other TVZ rhyolites e.g. Kaingaroa Ignimbrite (Fig 8.10).

Both samples are LREE-enriched and have flat HREE profiles (Fig 8.10). The difference in MREE and HREE between types A and B is generally considered typical of amphibole removal (Fig 8.10b). Both pumice types exhibit negative Eu anomalies, reflecting varying degrees of plagioclase fractionation, retention of plagioclase in the source, or oxidation of Eu^{2+} to Eu^{3+}. Eu anomalies do not increase systematically with decreasing Sr and Eu, as would be expected if plagioclase were the only fractionating phase. Partition coefficients of ca.2 for Eu in plagioclase (e.g. Arth 1976; Nash and Crecraft 1985) indicate plagioclase fractionation will lead to Eu depletion and larger Eu anomalies. Increasing Eu with increasing MREE and LREE suggests plagioclase fractionation was subordinate to hornblende. Flat HREE patterns indicate garnet was not stable in the source region; this is typical of all reported TVZ rhyolites (Chapter 7, 9).

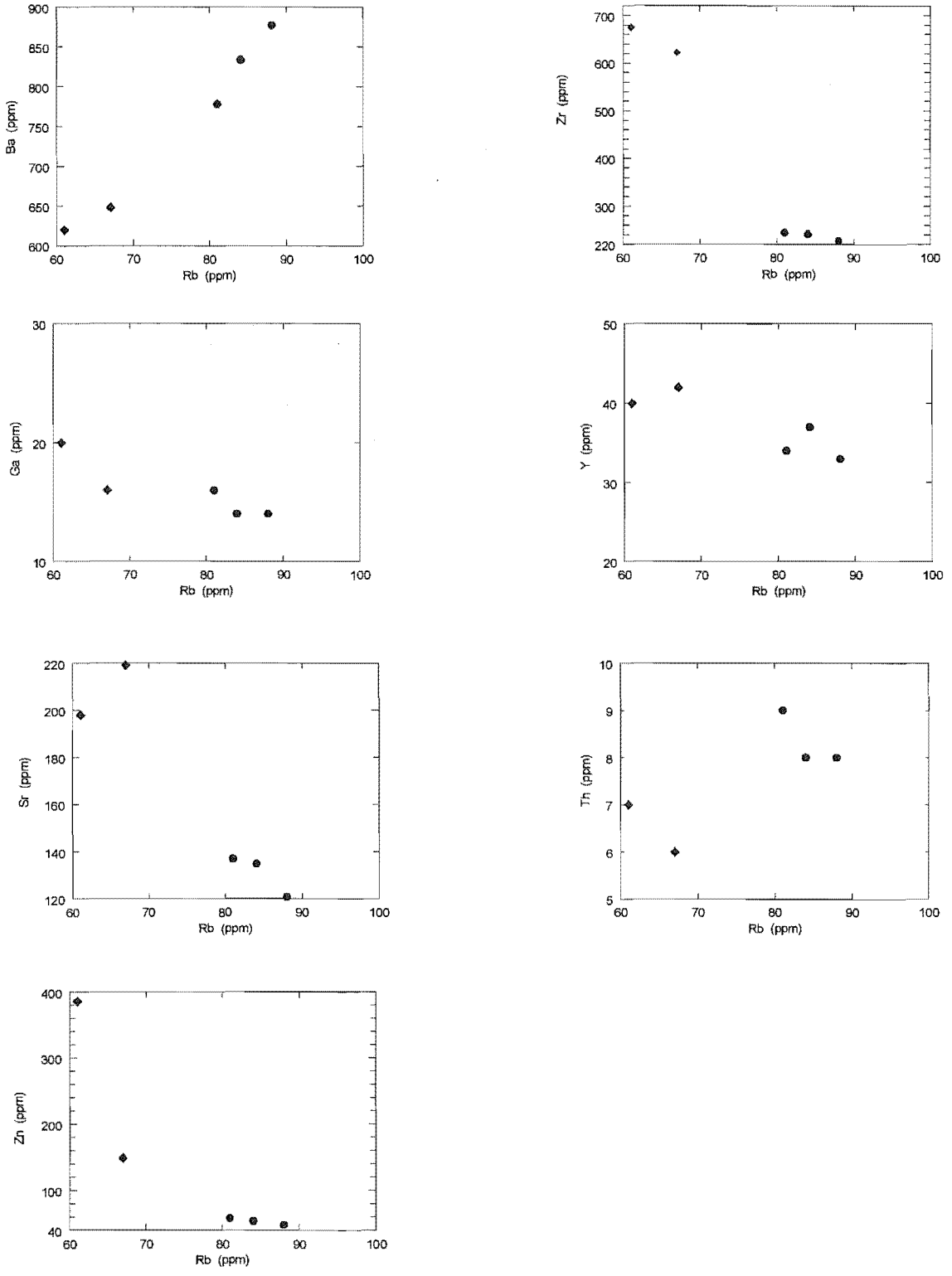

Figure 8.9 Selected major and trace element variation diagrams of Kawerau ignimbrite pumices illustrating two distinct pumice types. Note the anomalously high Zr, Zn and moderately high Na, Ga content of Kawerau Type B pumices in comparison to Type A pumices and Kaingaroa Ignimbrite pumice chemistry.

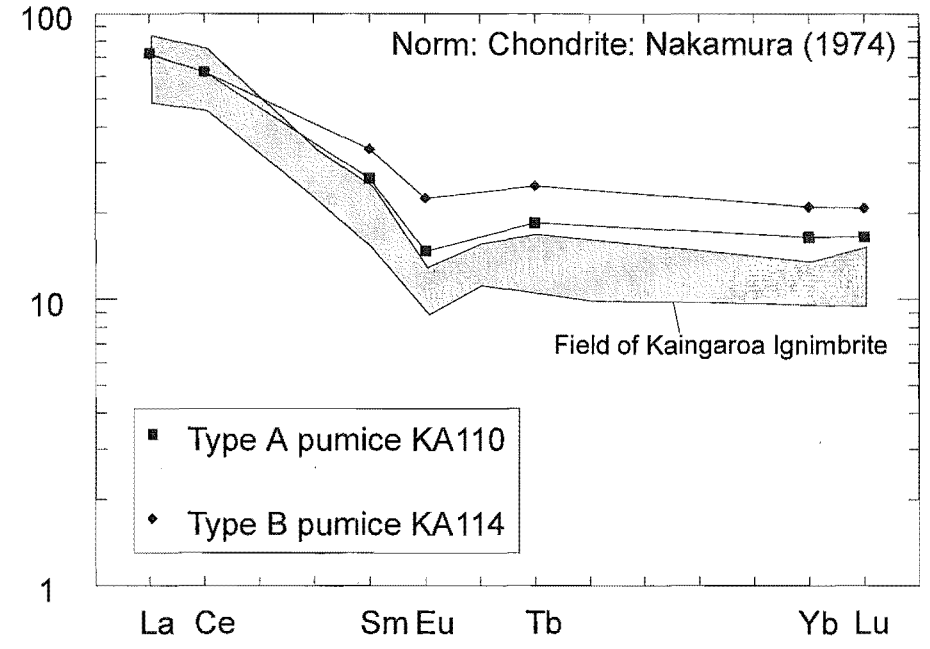

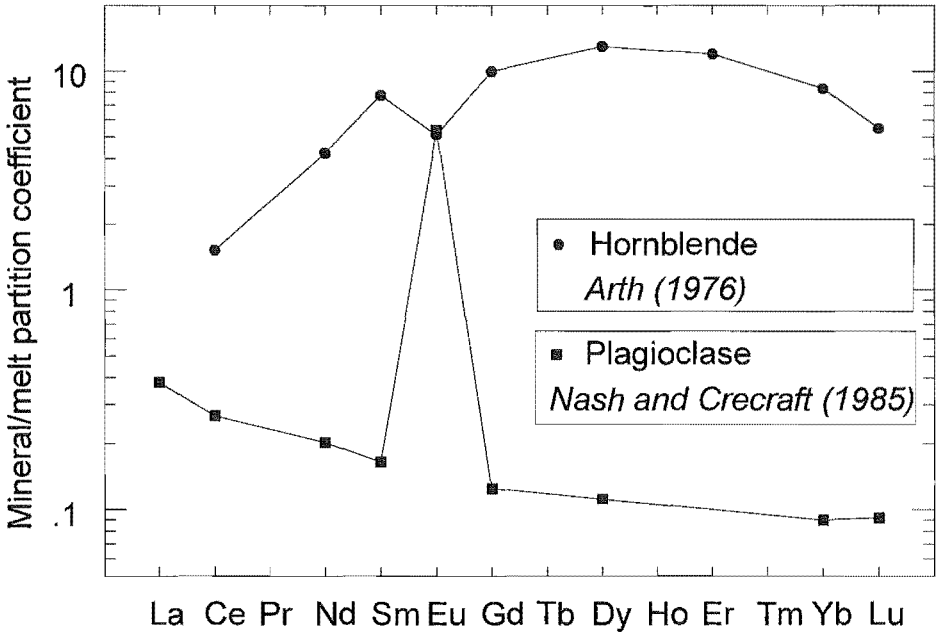

Figure 8.10a Chrondrite-normalised Rare Earth Element data of Kawerau ignimbrite pumices, illustrating high REE content compared with other TVZ rhyolites (e.g. Kaingaroa Ignimbrite). LREE enrichment and depletion in MREE and HREE between Type B and A pumices is consistent with a component of amphibole fractionation. Note the negative Eu anomalies even in Type B dacitic pumices. Type B pumices exhibits similar Eu/Eu^* values to Type A suggestive of limited plagioclase fractionation.

Fig 8.10b Mineral partition coefficients for hornblende in rhyolites illustrating MREE enrichment.

Major, trace, and REE variation is consistent with a relationship between pumice types due to fractionation of hornblende, and subordinate plagioclase, Fe/Ti oxides and pyroxene. Further work is required on the relationship between pumice types. The Kawerau magma system represents a rare case of amphibole-dominated fractionation in TVZ rhyolites (Chapter 9).

8.6 Vapour-phase manganoan fayalite, sodic amphibole, and biotite

Whole-rock and pumice samples are vitric at all stratigraphic intervals at sampled localities, apart from the presence of fine-grained drusy infills of fayalite, sodic amphibole and rare biotite and tridymite. Tridymite and biotite are commonly reported vapour phase products whereas amphibole and fayalite are rarely reported vapour phase products (Smith 1960), and warrant further discussion.

8.6.1 Manganoan fayalite

Iddings (1888) describes almost pure Fe-rich fayalite within lithophysae; opaque black crystals about 2mm in length with a metallic lustre occasionally with brilliant irridescent colours, mostly reds. Crystals are tabular or flattened and are coated with ferric oxide. Fayalite in Kawerau ignimbrite pumices occurs as petrographically similar bladed honey-coloured euhedral six-sided crystals, commonly in radiating aggregates, with an altered black metallic lustre, nearly opaque mineraloid mantle and limonite rims (Fig 8.5). A notable feature of fayalite crystals is high Mn content and lack of Mg.

Fayalite has been reported in New Zealand at Taupo volcano by Ewart et al (1975) and Sutton (1995) as a primary phase in distinctive metaluminous rhyolites collectively termed 'South eastern domes', at Motuoapa and Echo Cliffs (Fa_{11-16}; Sutton 1995), and on Mayor Island in peralkaline pantellerites (Fa_{24}; Buck et al. 1981). In both cases fayalite is associated with Fe-rich pyroxenes. Grapes et al (1993) and Shepherd (1991) report analyses of fine-grained fayalite (Fig 8.11) as a vapour-phase product at Ngongotaha rhyolite dome, Rotorua, associated with sodic amphiboles, biotite, tridymite, and osumulite.

This section details an occurrence of manganoan fayalite as a vapour-phase mineral in the Kawerau ignimbrite, and is the first reported occurrence of manganoan fayalite as a vapour phase product, although end-member fayalite is a commonly observed vapour-phase mineral. Fayalites were identified in pumice mineral separates during reconnaissance petrography and mineral identification. Subsequent petrographic identification of whole rock and pumice sections revealed that fayalite is present in small quantities as oxidised bladed opaque-like crystals within vesicles. Chemical analyses of olivine crystals are reported in Table 8.3 and illustrated in Fig 8.11. The samples cluster as manganoan fayalites ($Fa_{93.9}Fo_0Te_{6.1}$ - $Fa_{92.3}Fo_{0.1}Te_{7.6}$), with high Mn and low Mg content. Altered rims give consistently low totals, probably due to oxidation of FeO to Fe_2O_3, but exhibit similar Fe/Mg/Mn ratios (Fig 8.9). Similar alteration rims are described in primary magmatic Mn-bearing fayalite by Mahood (1981) and Janeczek (1989). Samples from Type A pumices are ubiquitously pervasively oxidised (Fig 8.11; Table 8.3).

Manganoan fayalite is a member of the Fe_2SiO_4 (Fayalite)-Mn_2SiO_4 (Tephroite) solid solution series, which is a common phase in iron-manganese ore deposits, and has occasionally been reported in the literature as a primary igneous phase in rhyolitic ignimbrites (Mills and Rose 1991). Deer et al. (1982) suggested that many of the reported fayalite samples in igneous rocks are probably Mn-bearing.

Results are similar to reported primary igneous phases in the Bandelier Tuff (Warshaw and Smith 1988), but distinctly Mn-rich and Mg-poor compared with vapour-phase fayalite analyses reported from Ngongotaha (Shepherd 1991; Grapes et al. 1993), and fayalite phenocrysts in Taupo rhyolites (Sutton 1995). Petrography and mineral chemistry are broadly similar to manganoan fayalite in the Ammonian Tanks Member of the Timber Mountain Tuff (i.e. Mg-poor; Mills and Rose 1991). Mills and Rose (1991) noted that the fayalites were only identified in mineral separates, and exhibited radiating, bladed, fragile, crystal habits (Fig 4 of Mills and Rose 1991) unlikely to have survived transport within a pyroclastic flow. The origin advocated by Mills and Rose (1991) as primary magmatic phases is possible given co-existing mineral phases, and magma chemistry but considered unlikely given crystal habit and occurrence. Briggs et al (1993) reports ferrosilite ($En_{96.6}$; Fig 8.11) crystals, co-existing with En_{50-60} orthopyroxene phenocrysts (Briggs pers comm 1996) within the Ongatiti Ignimbrite.

Sample no.	KA114	KA114	KA114	KA114	KA114	KA114	KA114	KA114	KA114	KA114	KA114	KA110
Analysis no.	412	413	414	415	416	418	423	424	425	428	429	543
	r	c	r	r	c	r	c	r	r	c	r	c
SiO_2	30.03	28.00	30.77	30.46	27.91	29.78	28.15	28.01	28.31	28.36	29.02	29.62
TiO_2	0.10	0.00	0.45	0.13	0.00	0.03	0.00	0.00	0.00	0.00	0.04	0.00
Al_2O_3	0.04	0.00	0.05	0.06	0.03	0.00	0.00	0.05	0.00	0.00	0.00	0.00
FeO	62.15	68.06	59.23	59.83	67.42	62.25	69.40	67.56	68.81	67.64	65.20	59.78
MnO	5.08	5.18	4.70	4.44	4.89	4.54	4.57	4.78	4.45	4.70	4.76	5.29
MgO	0.03	0.00	0.04	0.21	0.00	0.00	0.00	0.00	0.00	0.00	0.00	0.14
CaO	0.05	0.00	0.13	0.06	0.04	0.04	0.02	0.02	0.03	0.00	0.03	0.07
Na_2O	0.00	0.00	0.00	0.00	0.00	0.05	0.00	0.00	0.00	0.00	0.00	0.00
K_2O	0.01	0.00	0.04	0.02	0.00	0.07	0.00	0.00	0.00	0.00	0.00	0.00
Total	97.49	101.24	95.42	95.21	100.29	96.76	102.14	100.42	101.59	100.71	99.05	94.91
Oxygen	4	4	4	4	4	4	4	4	4	4	4	4
Si	1.029	0.955	1.060	1.055	0.959	1.030	0.952	0.960	0.960	0.967	0.995	1.039
Al	0.004	0.000	0.018	0.005	0.000	0.001	0.000	0.000	0.000	0.000	0.002	0.000
Ti	0.001	0.000	0.001	0.002	0.001	0.000	0.000	0.001	0.000	0.000	0.000	0.000
Fe	1.782	1.941	1.706	1.734	1.937	1.801	1.964	1.937	1.951	1.929	1.869	1.754
Mn	0.148	0.150	0.137	0.130	0.142	0.133	0.131	0.139	0.128	0.136	0.138	0.157
Mg	0.002	0.000	0.002	0.011	0.000	0.000	0.000	0.000	0.000	0.000	0.000	0.008
Ca	0.002	0.000	0.005	0.002	0.001	0.001	0.001	0.001	0.001	0.000	0.001	0.003
Na	0.000	0.000	0.000	0.000	0.000	0.003	0.000	0.000	0.000	0.000	0.000	0.000
K	0.001	0.000	0.002	0.001	0.000	0.003	0.000	0.000	0.000	0.000	0.000	0.000
Total	2.968	3.045	2.931	2.941	3.040	2.972	3.048	3.038	3.040	3.033	3.005	2.961
Fa	92.28	92.85	92.46	92.48	93.16	93.12	93.75	93.32	93.86	93.42	93.11	91.41
Fo	0.08	0	0.12	0.56	0	0	0	0	0	0	0	0.39
Te	7.64	7.15	7.42	6.96	6.84	6.88	6.25	6.68	6.14	6.58	6.89	8.2

Table 8.3. Manganoan fayalite analyses.

Briggs et al (1993) suggested a xenocrystic origin, possibly as a metastable high temperature vapour-phase mineral.

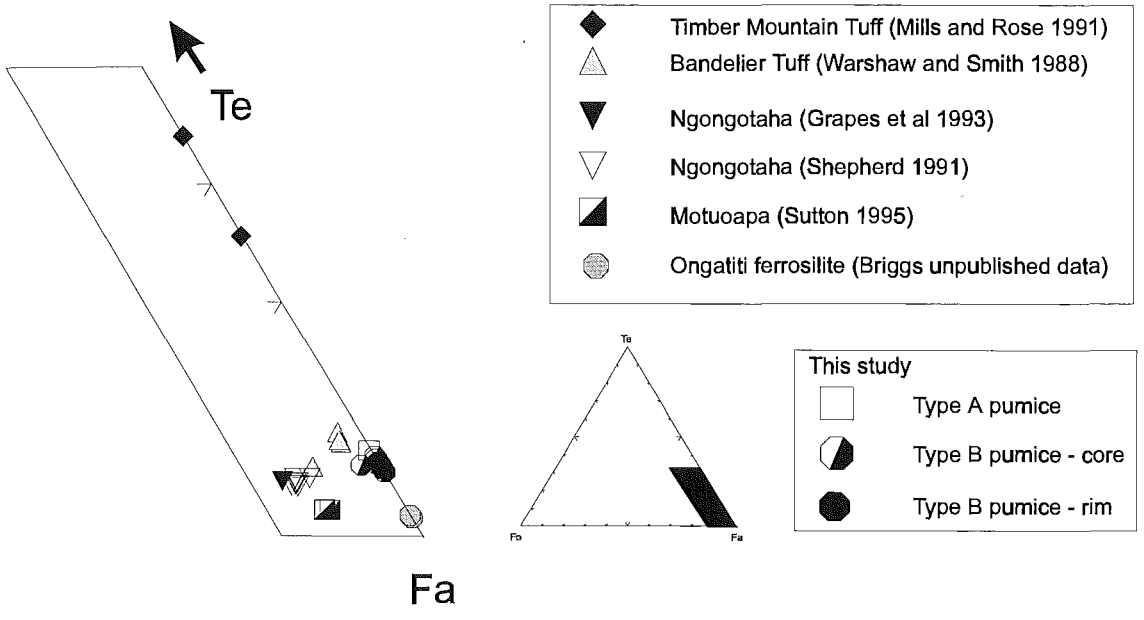

Figure 8.11 Composition of fayalite crystals from the Kawerau ignimbrite plotted in terms of Fe, Mg, and Mn, and compared with fayalite analyses from Ngongotaha, Motuoapa, Bandelier Tuff, and manganoan fayalites or knebelites from the Timber Mountain Tuff. Ferrosilites (orthopyroxenes) reported by Briggs et al (1993; unpublished data) are also shown for comparison.

8.6.2 Sodic amphiboles and biotite

Dark brown katophoritic prismatic amphibole and biotite were observed in the porous groundmass of whole rock specimens and infilling vesicles in Type B pumices. Amphibole occurs as very small pleochroic crystals present within vesicles and located observed nucleated on pyroxene and plagioclase phenocrysts and lithics. Biotite is rarely present as small prismatic brown crystals. Both minerals are easily confused with the abundant limonite which rims fayalites, and goethite/limonite disseminated throughout the groundmass. No microprobe analyses were undertaken, due to the small size. Similar composition amphiboles and biotite were reported co-exisiting with Mn-rich fayalite in Ngongotaha rhyolite lithophysae.

The presence of manganoan fayalites, sodic amphiboles and biotite in the Kawerau ignimbrite are attributed to formation from a high temperature halogen-rich gas phase. This halogen-rich vapour phase origin is further supported by the high Br (and probably Cl and F) content of Kawerau pumices (4-5 ppm; Table 8.2). Br contents average 2-3 ppm in rhyolites, and high Br contents are ubiquitously associated with high Cl (Shinonaga et al. 1994).

Stimac et al (1996) report a diverse suite of minerals (e.g. zircon, titanite, apatite etc) deposited from vapour during the eruption and post emplacement of the Bandelier Tuff, New Mexico. Stimac et al (1996) conclude that the minerals could have grown directly from pre- or syn-eruptive magmatic vapours. The abundance of volatiles including halogens in evolved caps of silicic magma bodies, suggests a significant amount of halogens could be released during eruption. These volatiles could be partitioned into the vapour phase and deposited on glassy tephra. The partially to non-welded nature of the Kawerau ignimbrite would of allowed free travel of vapour, resulting in pervasive albeit incipient (i.e. trace contents of vapour phase crystals c.f. classic vapour-phase altered ignimbrites) vapour-phase alteration.

Manganoan fayalite and ferrosilite are both metastable at surface pressures, and interpreted to be derived from alkaline, halogen-rich, high temperature vapours.

8.7 Ignimbrite source

The predominance of rhyolite, ignimbrite and dacite lithic types in the Kawerau ignimbrite of the Puhipuhi Basin, suggests that the lithics may be locally derived (i.e. incorporated by the pyroclastic flow). An additional possibility is that the lithic distribution, lithic types and coarsening of M_L to the west is consistent with a western source in the Okataina caldera complex region. The presence of similar lithic types at all localities and sparse M_L data suggest a Okataina caldera complex source. Distribution, M_L, lithic types and chemistry are inconsistent with a Kapenga, Rotorua or Reporoa source, and with correlation with ignimbrites of similar mineralogy, chemistry, age and stratigraphic position.

8.8 Correlation

Three other ignimbrite of similar age and stratigraphic position to the Kawerau ignimbrite have similar field characteristics. Table 8.4 outlines the similarities and differences between the Rangatira Point ignimbrite, Kaingaroa Ignimbrite and Pokai Ignimbrite. The distinctive hornblende-rich mineralogy, dissimilar chemistry, M_L and lithic type distribution suggest the Kawerau ignimbrite is distinct from known ignimbrites, and represents a newly recognised caldera-forming ignimbrite, within period IIIb of Houghton et al (1995) timescale, from the Okataina caldera complex.

The original mis-correlation of the Kawerau ignimbrite (and history of miscorrelation of other sandy-black ignimbrites) highlights the need for integrated field mapping, petrographic, mineral chemistry and whole-pumice chemical studies in correlating ignimbrites which are similar in field characteristics.

8.9 Reconstructed stratigraphy of Puhipuhi Basin-Kawerau area

The recognition of a new ignimbrite in the Puhipuhi Basin-Kawerau region alters currently accepted models of stratigraphy and eruptive history of the region, and adds complexity to the eruptive history of Okataina caldera complex. The early history (0.32 Ma-0.24 Ma) of Okataina caldera complex can be divided in three main periods, each marked by the eruption of a caldera-forming ignimbrite.

A) 0.34-0.32 Ma ? Eruption of the quartz-biotite ignimbrite during large scale volcano-tectonic event throughout the entire TVZ, forming the Whakamaru-group ignimbrites. This event changed the entire nature of the TVZ, and forms the boundary between the Wilson et al (1995a) old and young TVZ.

The interval between 0.32 and 0.28 Ma is poorly preserved but was dominated by numerous small scale rhyolitic eruptives (Nairn 1989) and periods of rhyolite dome effusive activity.

	Pokai Karhunen (1993).	***Rangatira Point*** Sutton (1990); Cole et al (submitted).	***Kaingaroa*** (this study).	***Kawerau*** (this study).
Description	Lower orange/brown unit with white and orange pumices, grading up into upper 'sandy-black' unit with orange and brown/black pumices	Lower brown lithic-rich unit. Upper 'sandy-black' pumice-rich ignimbrite. Non-partially welded.	Lower tan pumice-poor unit passing up into 'sandy-black' pumice-rich ignimbrite which passes up into pink/grey densely welded lenticulite	Lower 'sandy-black' unit passing up into buff ignimbrite.
Mineralogy/ opyx:hb	Plag + opyx + hb + Fe/Ti oxides ± qtz opyx > hb	Plag + opyx + Fe/Ti oxides + hb + qtz ± aug opyx > hb	Plag + opyx + Fe/Ti oxides + hb opyx >>> hb	Plag + hb + opyx + Fe/Ti oxides + augite ± titanite hb>>opyx
SiO_2 (anhydrous)	70-77%	71-76	71-76	67-76 % (n=5)
Rb	89-140	126-136	76-128	61-88
Zr	106-306	150-193	170-246	221-675
Lithics	Rhyolite, Pokai-like ignimbrite and rare 'greywacke'	Rhyolite, Rangatira-like ignimbrites, and rare dolerite and dacite.	Andesite with subordinate Whakamaru-group ignimbrites, Waiotapu Ignimbrite, greywacke and leucogabbro.	Rhyolite, dacite, and Matahina Ignimbrite
Crystal %	Poor	5-7%	1-3.5 wt%	1-7 wt%
Stratigraphic position	Overlies Whakamaru-group ignimbrites and Chimp ignimbrite. Overlain by Mamaku and Ohakuri ignimbrites	Overlies Whakamaru-group ignimbrites.	Overlies Whakamaru-group, Matahina, and Chimp ignimbrites. Overlain by Earthquake Flat Breccia.	Overlies Whakamaru-group and Matahina ignimbrites. Overlain by Rotoiti Breccia.
Age	0.28-0.22 Ma	ca. 0.22 Ma	0.23 Ma (Ar/Ar)	0.24 Ma (Fission track)
Source	Kapenga?	Taupo	Reporoa	Okataina

Table 8.4. Comparision of 'sand-black' ignimbrite of similar stratigraphic position to Kawerau ignimbrite.

B) 0.28 Ma eruption of the Matahina Ignimbrite from a source within the southern part of Haroharo/Okataina caldera complex (Bailey and Carr 1994), accompanied by shallow synchronous collapse along regional faults to form Puhipuhi Basin and other embayments.

During the period between 0.28 Ma and 0.24 Ma lacustrine sedimentation occurred within Puhipuhi Basin (and Okataina caldera complex?), there was intrusion of the Puhipuhi dacite, and numerous small scale dominantly rhyolitic eruptives (Onuku Pyroclastics; Nairn 1989). A large basin, only marginally infilled by pyroclastic, tectonic and effusive activity, would provide ideal conditions for ponding of a large scale ignimbrite that was erupted between 0.28-0.24 Ma. No large scale ignimbrites are known of this age within the region.

C) 0.24 Ma eruption of the Kawerau ignimbrite from a Okataina caldera complex source. Inferred caldera collapse?

A detailed study of the evolution of rhyolitic eruptives between 0.34 Ma and 0.24 Ma would reveal interesting spatial and temporal evolution of a rapidly changing magma system(s), as has been recently documented by Sutton et al (1995) at Taupo volcano. A fundamental difference between the centres is the preservation of older eruptives, which are all weakly compositionally zoned. This has numerous implications for the rate of formation of compositional zonation, spatial arrangement of large rhyolitic chambers, and replenishment processes, following climactic caldera-forming events. A detailed study of the eruptives of the Okataina caldera complex is beyond the scope of this thesis.

8.10 Discussion: Origin of compositional diversity

A model of the Kawerau magmatic system must account for the following features:

1. Inferred volume (ca. 50 km^3 + ?) of magma.
2. Compositional and inferred thermal zonation, including presence of subordinate, more mafic dacite.

3. Lack of mingling or mixing of pumice types.
4. Type B pumice exhibits anomalously high Zr, Zn, Hf, Ga, REE, Zr/Nb, and slightly higher Na, Y, Cr, Fe, Ti, Mg, Al, Ca, compared with Type A.
5. Post or syn-eruptive high temperature halogen-rich vapour-phase.

Mineral chemistry and whole pumice chemistry indicate significant compositional variation or zonation within the Kawerau magma system. Two pumice or magma types are identified. The anomalous trace element chemistry and large compositional gap is inferred to represent eruption of two distinct compositions. Further isotopic work is required to confirm this hypothesis (c.f. Chapter 7 Kaingaroa Ignimbrite). The lack of mixing between the two pumice types and large thermal and compositional gap between the two compositions suggests the two compositions could represent a situation analogous to the Kaingaroa magma system (i.e. syn-eruptive mingling of a separate distinct magma chamber). The dacitic component is markedly subordinate in volume, and could represent either a separate zone or a separate chamber or recharge of less evolved dacitic/rhyolitic material into or adjacent to the magma system. The strong negative Eu anomaly is in marked contrast to other dacites associated with rhyolites in the TVZ (Chapter 7,9), and suggests a diversity of source compositions or petrogenetic pathways in 'rhyolite petrogenesis'.

The anomalously high Zr and Zn contents of pumices in the Kawerau ignimbrite could be due to addition of Zr and Zn-bearing vapour-phase minerals; Zr is compatible in sodic amphiboles, and Zn in fayalites and amphiboles (Ewart and Griffin 1994). The presence of these minerals as vapour-phase products throughout the ignimbrite, in both pumice types, suggests alteration is an unlikely cause of the anomalous trace element chemistry. An alternative possibility is that Zr contents could reflect alteration and mobility. Zirconium is regarded as an immobile element, and is classically used to classify tectonic setting in altered or metamorphosed mafic igneous rocks (e.g. Pearce and Cann 1973). Rubin et al (1993) demonstrated that Zr is mobile under certain hydrothermal conditions, e.g. breakdown of zircon-bearing silicates but this situation does not apply in the Kawerau ignimbrite. It is therefore concluded that the Zr (and Zn and Hf) contents are representative of the original magma composition.

The extreme values of Zr, Zn and Hf are inconsistent with the bulk chemistry and mineral content of the Type B pumices, and are suggestive of an alkalic parentage. This anomalous chemistry cannot be explained by fractionation of the current mineral assemblage; published partition coefficients for Zr in plagioclase, orthopyroxene, and Fe/Ti oxides are all too low. Two published values for Zr in hornblende suggest that Zr is can be compatible or incompatible (Watson 1979; Watson and Harrison 1983; Ewart and Griffin 1994), but the growing literature on the subject suggests Zr is compatible in sodic pyroxene and amphiboles (e.g. Rubin et al.1993), but in most non-alkalic magmas Zr concentration is controlled by zircon. Trace amounts of zircon is present in Kawerau ignimbrite pumices generally as inclusions in orthopyroxene and plagioclase. Watson and Harrison (1983) demonstrated that Zr concentration and saturation is attributed to the presence of excess alkalis and high halogen contents with excess alkali over aluminium increasing the solubility of Zr and prevents zircon crystallisation, thereby concentrating Zr in the liquid phase. The Zr (and Hf) levels in the Kawerau ignimbrite are consistent with a high temperature origin (Watson and Harrison 1983), typical of peralkaline magmas, but the low alkali content, and mineral chemistry of the sample indicates the ignimbrite is clearly calc-alkaline.

A detailed discussion on the petrogenesis of the Kawerau magma system is beyond the scope of this thesis or data presented, but a number of interesting points can be raised regarding the anomalous chemistry. Three possible origins of the anomalous trace element chemistry are briefly considered:

A) Derivation from an alkalic magma, with alkali-loss
B) Mixing of an alkaline high Zr, Zn, Hf magma and a calc alkaline magma
C) Unusual source or parent magma

Alkali-loss has been well documented in peralkaline rhyolites. Degassing of halogen-rich vapour complexed with alkalies, removes alkalies from the system, resulting in a normative corundum, peraluminous magma (Wiesneth and Eichelberger 1994). The presence of typical calc-alkaline dacite/rhyolite mineral assemblage and low Ba, Nb, and other HFSE (except Zr) contents in the Kawerau pumices is suggestive of a calc-alkaline parentage.

Dorais et al (1991) advocate mixing of an alkaline trachytic magma with a calc-alkaline rhyolite to explain the anomalous trace element chemistry of peraluminous calc-alkaline dacite pumices in the Carpenter Ridge Tuff, San Juan volcanic field, Colorado. Carpenter Ridge dacites also exhibit anomalously high Zr (600-900 ppm), but also contain very high Ba and a positive Eu anomaly. The Kawerau pumices exhibit certain trace elements consistent with an alkaline parentage e.g. Zr, Hf, Zn, Br (and inferred Cl), and other trace elements consistent with a calc-alkaline parentage. No alkaline compositions have been reported in TVZ, although peralkaline compositions exist at Mayor Island volcano to the northwest (Weaver et al. 1990), and ignimbrites with 'A-type' affinities have been recorded in TVZ (Chapter 9). The tectonic setting of Mayor Island is controversial, but it is likely the localised uprising of asthenopheric (OIB) magma is due to coincidental extension along the Havre Trough (Cole 1978) and cross faulting within the North Island Shear Belt (Cole 1990) and therefore unique. The Kawerau pumices exhibit no evidence of unusual mineral compositions which might suggest a complex origin.

The third possibility involves derivation from an unusual source. Few of the minerals present are likely to alter the Zr/Nb significantly during fractionation; hence derivation of high Zr and low Nb contents is not considered possible by crystal fractionation of known mineral assemblages utilising published experimental work and partition coefficients. Other TVZ rhyolites exhibit similar anomalous Zr:Zn, albeit at lower but still unusual Zr contents. Details of comparison with other rhyolites and source constraints are discussed in Chapter 9.

Further work is required on Kawerau pumice chemistry, including a detailed study of accessory minerals, glass compositions, isotopic variation, and determination of partition coefficients for the mineral assemblage, particularly for Zr and Zn. Literature values quoted for partition coefficients are both rare and contradictory, and probably not applicable to Kawerau pumices due to the contradictory evidence of temperature and chemical composition; both important controls on partition coefficients.

CHAPTER NINE
Discussion

The purpose of the chapter is to provide:

A) A brief synopsis and discussion of eruptive stratigraphy, lithic componentry and pumice chemistry into an eruptive model.
B) Recognition and implications of recently discovered temporal clustering of units.
C) Constraints on petrogenesis of rhyolites and suggest future work

9.1 Eruptive model

Aspects of field geology, lithic componentry and pumice mineralogy and chemistry have been outlined and briefly discussed in the preceding chapters. This section aims to synthesize the data presented in terms of pre-Kaingaroa erosional and depositional environment; sub-caldera geology, vent evolution during the 0.23 Ma Kaingaroa Ignimbrite eruption and implications for caldera formation and structure.

9.1.1 Erosion and depositional environment

Three domains can be identified within the study area: Reporoa Caldera, Te Weta Block, and Kaingaroa Plateau. Each domain has differing aspects of the pre-Kaingaroa Ignimbrite topography and environment in which the Kaingaroa Ignimbrite was eventually emplaced.

The Reporoa Caldera paleotopography is inferred from the presence of pre-existing scarps, arroyos and ignimbrite distribution and is discussed below with relation to caldera structure.

The Te Weta block, to the west of Reporoa Caldera is within the Taupo fault belt, one of the most intensely faulted areas of New Zealand (Wood 1994a). The Kaingaroa Ignimbrite appears to have infilled a complex paleotopographic surface cut into the Paeroa ignimbrite although exposure is poor. Distribution of the Kaingaroa Ignimbrite

in this area is strongly controlled by normal faulting. On the Kaingaroa Plateau where the Kaingaroa Ignimbrite pyroclastic flows passed over a relatively flat topography, away from Reporoa Caldera with minor undulations typical of alluvial channels, weakly undulatory Rangitaiki and Matahina ignimbrite surfaces, and localised irregular 'greywacke' basement relief (e.g. Pekepeke Hill). The current Kaingaroa Ignimbrite distribution pattern on the plateau is controlled by welded portions of WIU. The presence of 30m + thickness of Kaingaroa Ignimbrite in the Murupara drill holes further to the east suggests the pyroclastic flows reached at least Murupara and probably the ranges to the east, but resultant deposits have subsequently been eroded away.

Welding and thickness variations suggest the Kaingaroa Ignimbrite thickens and increases in welding grade in central Kaingaroa Plateau, coinciding with the abundance of N-S aligned gas segregation structures. The amount of reworking in this area suggests the Kaingaroa pyroclastic flows passed over a shallow alluvial basin. Minor thickness variations may represent ponding in interfluves and small channels. The limited charcoal fragments in the Kaingaroa Ignimbrite suggest there was limited vegetation present.

9.1.2 Vent evolution

Details of vent evolution during the Kaingaroa eruption and eruptive dynamics utilises discussions on field geology (Chapter 3), lithic componentry (Chapter 5) and pumice chemistry (Chapter 7). Figs 9.1-9.3 summarise possible eruptive and vent evolution models for the Kaingaroa Ignimbrite.

Single vent phase

The eruption of the basal tephras is inferred to represent eruption from a single vent. Alternations in eruptive style were probably due to variable magma:water interaction, although as unit B is a 'dry' plinian style unit containing type A pumice, it suggests the vent migrated during the early single vent phase eruptives as documented by Smith and Houghton (1996) at Taupo, and Nairn et al (1995) at Rabaul. An initial phreatomagmatic eruption is inferred to have occurred in a lake-filled basin and continued into the initial RBU period when the water supply was exhausted, and eruptive style reverted to magmatic activity.

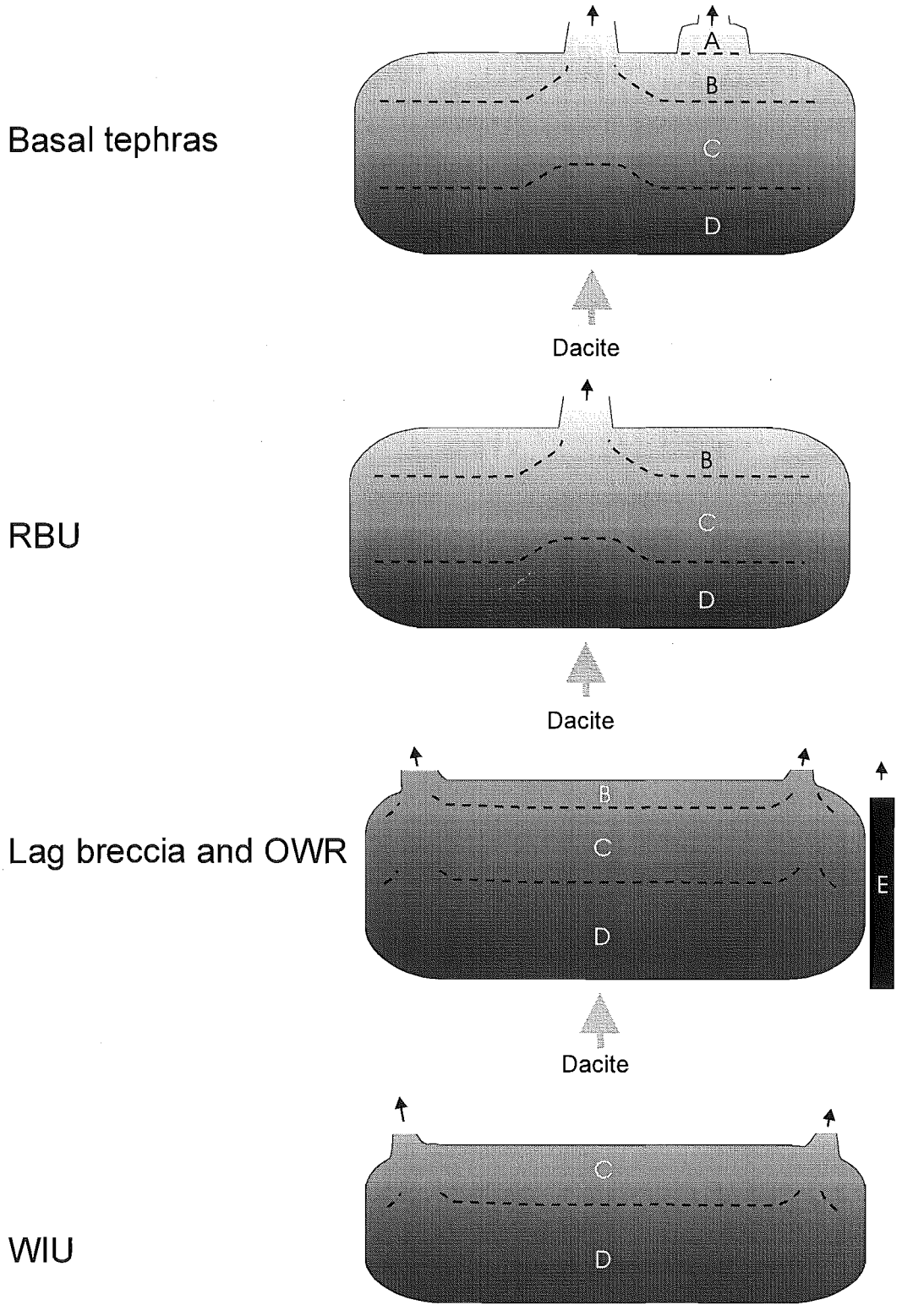

Figure 9.1 Magma system eruption model.

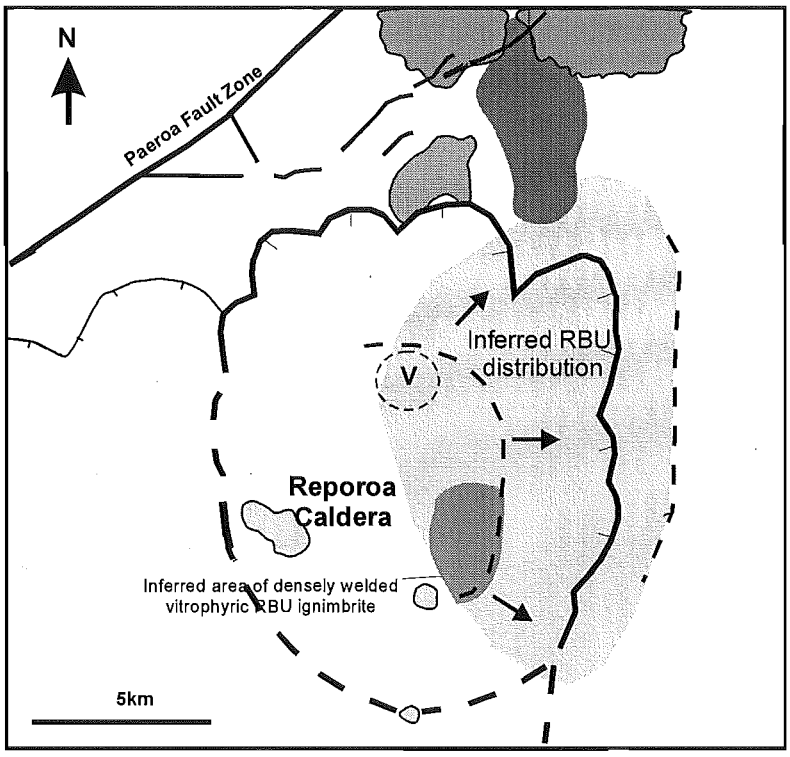

Figure 9.2 Inferred vent activity during the emplacement of the Reporoa Boundary Unit (RBU)

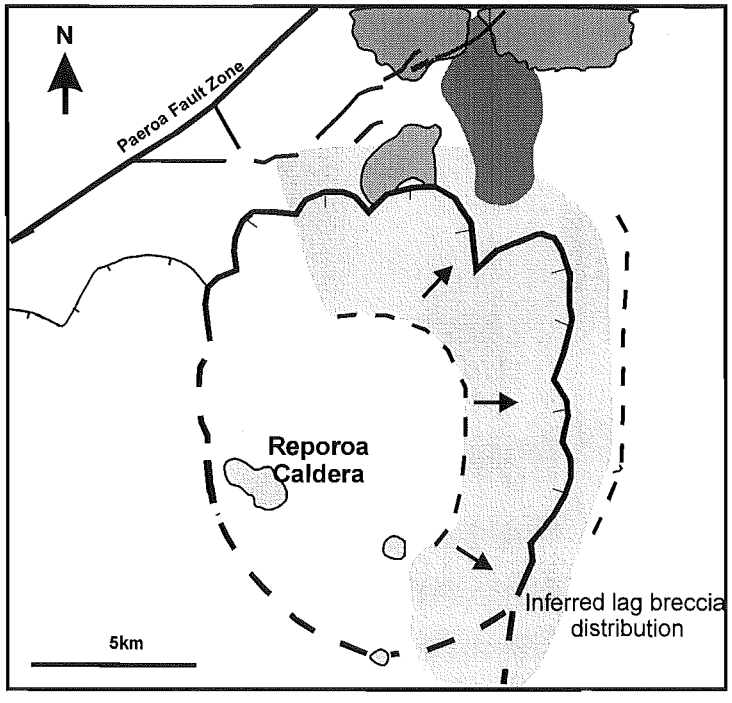

Figure 9.3 Inferred vent activity during emplacement of the lag breccia

Reporoa Basin has contained a lake intermittently throughout its geological and recent history, as evidenced by the lacustrine sediments of the Huka Group intercalated with rhyolites in RP1 drill hole (Chapter 3) and surficial lacustrine sediments in the modern Reporoa Caldera. Reporoa Basin was also a lake following the 1800y. B.P. Taupo eruption.

The transition to surge and pyroclastic flow eruptions reflects collapse or marginal collapse of the eruption column. The presence of andesite and welded ignimbrite lithics suggest deepening of the lithic provenance and increase in magma discharge, possibly due to vent widening. Eruption of the RBU pyroclastic flows marks column collapse and the accompanying increase in lithic abundance and diversity of lithic types may mark the onset of incipient caldera collapse. The distribution of the RBU is largely controlled by paleotopography, with pyroclastic flows infilling a basin developed in the Rangitaiki Ignimbrite (Fig 9.2).

Ring vent

The transition to ring-vent or multiple vents is marked in the field by the sudden transition to the presencce of lag breccias, an increase in lithic types and size, and incoming of a diversity of pumice types. A deep level of lithic provenance is suggested by the presence of low-grade metasedimentary basement and plutonic lithics.

Collapse initially took place along the northern and eastern edge of Reporoa Caldera as suggested by the distribution of the Kaingaroa Ignimbrite and presence of proximal facies (Fig 9.3). The eruption of the widely distributed OWR and WIU suggest both caldera collapse and radial emplacement.

The Tokiaminga valley subunit is interpeted to represent localised collapse and sectorial emplacement of the unit. This eruptive episode tapped two discrete magma batches including one of a high temperature dacitic composition. The resultant lithic breccias are anomalously welded, thought to reflect this higher temperature juvenile component.

The OWR-WIU contact is gradational where exposed, indicating that both units form part of a single eruptive episode. There is no exposure in proximal regions and further collapse may have accompanied the eruption of WIU, which is locally densely welded

with a hackly fracture and resembles a typical medium-high grade ignimbrite. The degree of welding and extreme pumice aspect ratios suggest the pyroclastic flows did not mix much with the atmosphere, as the emplacement temperatures (as suggested by the degree of welding) are ca.100°C below the inferred magmatic temperatures.

9.1.3 Subcaldera geology

One of the main objectives of detailed lithic componentry is that it provides a window into the upper crustal compositions quarried during caldera collapse. In silicic provinces such as TVZ, which are poorly exposed and exhibit complex stratigraphy and overprinting by later tectonism and volcanism, lithics provide another geological tool in delineating ignimbrite distribution, establishing caldera extent, and providing further constraints on ignimbrite stratigraphy. In addition many lithics within TVZ ignimbrites provide information on units not exposed at the surface.

Andesite is the dominant lithic type in the Kaingaroa Ignimbrite. A diversity of andesite types are present including rare hornblende-phyric varieties and uralitised high Cr, Ni variants which have undergone heterogeneous greenschist facies alteration. Associated with these uralitised andesites are leuco-gabbros, which exhibit complex secondary mineral assemblages including pervasive uralitisation and tourmalinisation. Superimposed on this alteration is fumarolic leaching of plagioclase, which has resulted in amorphous aluminosilicate replacement of calcic plagioclase cores. The leuco-gabbros are related to the altered andesites and are not cognate margins of the Kaingaroa magma system.

The diversity of andesite types is thought to represent 'quarrying' of a single volcano during the eruption. Distribution of andesite lithics and andesite:ignimbrite lithic ratios suggest collapse took place entirely within this andesite volcano. The position of the andesite is further corroborated by magnetic and gravity data (Soengkono and Hochstein 1996), and consistent with northward thinning of the unit towards the Waiotapu drill holes where the distal correlative of the andesite lithic (Ngakoro Andesite) is present in drill holes.

The distribution of leuco-gabbro lithics suggest the pluton or complex was present along the eastern margin of the structural caldera boundary. The incoming of this unit in the lag breccia and OWR is thought to reflect a further deepening of lithic provenance.

Numerous welded ignimbrite were documented in Chapters 5 and 6. Many have been correlated with the caldera walls. The abundance of Te Kopia and Paeroa ignimbrite lithics in the Kaingaroa Ignimbrite suggest more extensive distribution than is present in the Paeroa Scarp area. An interesting feature of the 'extended' distribution is the apparent antithetic distribution of the Paeroa and Rangitaiki ignimbrites, a feature common amongst the Whakamaru-group ignimbrites (Brown 1994). Further methodical work is required to document the extent, and lateral and stratigraphic variation in the Whakamaru-group eruptives, in this area.

A variety of meta-rhyolite and meta-ignimbrite lithics include complexly metasomatised zoned country rock adjacent to the Kaingaroa magma chamber, which was fragmented during caldera collapse. The presence of these lithics within pumice suggest the units were abundant at the magma fragmentation level. The presence of tourmaline and tourmalinites is the first documented case in TVZ, and testifies to the localised metasomatic and pneumatolytic alteration adjacent to large silicic magma bodies in TVZ.

The presence of 'greywacke' and slates are the only samples of basement incorporated by the Kaingaroa Ignimbrite eruption, consistent with the known basement terranes in the TVZ (Mortimer 1995), and the position of Reporoa Caldera along the eastern margin of TVZ.

9.1.4 Caldera structure and evolution

TVZ 'calderas' exhibit a variety of structures due to differing roles of downsag and regional tectonic influence and overprint. The Reporoa Caldera is morphologically simple and exhibits no evidence of downsag, although a more complex origin maybe masked by its morphological youthfulness (c.f. Branney 1995). The caldera exhibits no tectonic influence despite being flanked on it western flank by the Taupo fault belt and eastern flank by the eastern margin of TVZ.

Delineation of calderas remains an outstanding problem in TVZ geology. Difficulties encountered in determing caldera location include:

1) Complexity of stratigraphy, due to interaction of positive- and negative- relief-forming features.
2) Burial by later volcanic products and superposition of regional structures.

The Reporoa Caldera is superficially simple but numerous structures in the Reporoa area may reveal aspects of a complex pre-Kaingaroa structure:

The Waiora Formation to the southwest of Reporoa Caldera is worthy of further study. The unit contains a sequence of pervasively altered crystal-poor pumice-rich ignimbrite and intercalated silicified sandstones (Lloyd 1972; Keall 1988), suggestive of an intracaldera association. The extent of this unit and overlap with the post-Kaingaroa Kairuru rhyolite massif (Soengkono and Hochstein 1996), suggest an intermittant basinal history southwest of Reporoa Caldera. It is unclear whether this basin is tectonic in origin, or related to caldera collapse or synchronous with caldera collapse. The presence of scarps in the Paeroa-Range ignimbrites in this area also indicate pre-Kaingaroa basins southwest of Reporoa Caldera.

Along the eastern flanks of Reporoa Caldera the RBU appears to infill a basin defined by the presence of arroyos at the eastern extent of RBU distribution and by the lack of Rangitaiki ignimbrite. This basin may represent eastern demarcation of the Kaingaroa Fault, or a pre-existing caldera scarp.

9.2 Period IIIb ignimbrites

Ignimbrites are the main products of rhyolitic volcanism in central TVZ. The stratigraphy of these widespread ignimbrite units is difficult to decipher due to poor exposure, and structural, erosional and volcanic overprinting. Despite ongoing regional mapping studies and reconnaissance geochronology and geochemistry, this stratigraphy remains poorly understood. The problem is compounded by the lithological similarity of many units (which has led to mis-correlations), the rarity of sections which expose more than one unit, and the antithetic distribution of many ignimbrites.

The difficulty of ignimbrite correlation in TVZ is exemplified by the Kaingaroa Ignimbrite, which superficially resembles, and has been mis-correlated with, many of the units in the same stratigraphic interval (see Chapter 3). Ignimbrite correlation relies on integration of field, petrologic, paleomagnetic and geochronologic studies (Hildreth and Mahood 1985; Best et al. 1995). In particular, TVZ ignimbrites are usefully correlated on variations in mineral chemistry, crystal content, useful index minerals (e.g. sanidine in the Whakamaru Ignimbrite), mafic mineral ratios, pumice chemistry, lithic contents, and where possible paleomagnetism and geochronology.

High precision Ar/Ar dating has established periods of clustering of ignimbritic volcanism (Houghton et al. 1995). Period IIIb (Fig 9.4) represents the time between 0.28 Ma and 0.15 Ma, a period that encloses both the Kaingaroa and Kawerau ignimbrites. Five caldera-forming ignimbrites are known to have been erupted during this period: Kaingaroa, Matahina, Kawerau, Mamaku (and Mokai), Ohakuri, with additional smaller scale ignimbrites (e.g. Kawakawa; Sutton 1995; Cole et al. submitted), rhyolitic domes and small volume tephras. Several recently described ignimbrite units also fall within this stratigraphic interval but have yet to be dated or are the subject of an ongoing dating programme (Houghton pers comm 1996, 1997) e.g. Pokai and Chimp (Karhunen 1993), Hongis Bluff (Lowther et al. 1996), Matata (Wilson 1980), Rangatira Point (Cole et al. submitted), Murupara Gorge (Martin and Lewis 1963), Rautawiri Breccia (Brown 1994), welded ignimbrite of Wairakei drill hole (this study), Waiora 1 (Grindley 1965; Wood 1994b), Maroa-derived ignimbrites e.g. Orakonui, Pukeahua, Korotai, Tawiri, Atiamuri (Houghton et al. 1995;Wilson pers comm 1996), and numerous uncorrelated units present within the Waiora Formation in geothermal drill holes (Wood 1994b). The productivity of this period of ignimbritic volcanism is borne out by the distal tephra record (Manning in press), where numerous large tephra deposits are preserved between the distal Matahina and Mamaku units.

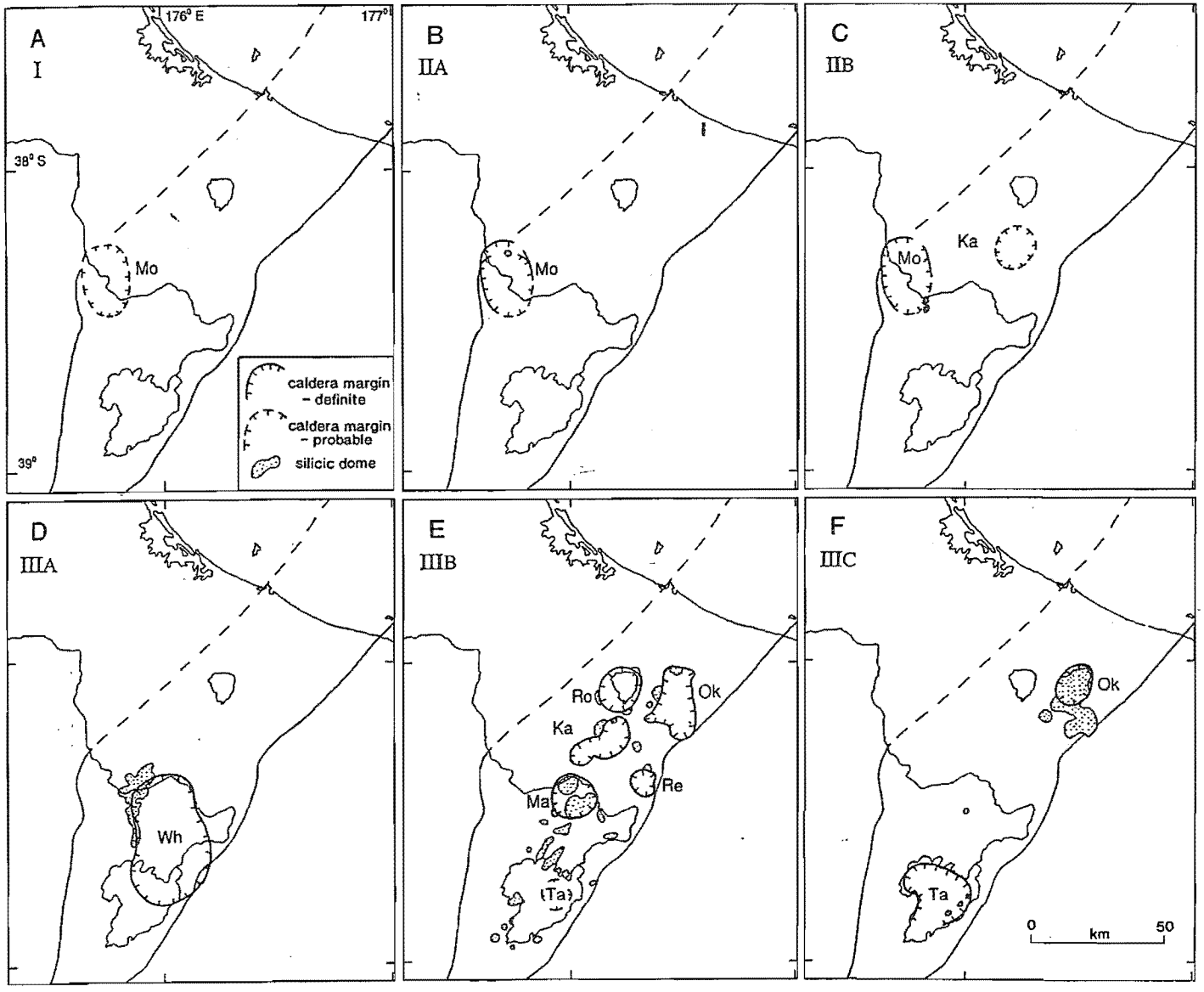

Figure 9.4. Series of maps illustrating 'calderas' active during eruptive periods (After Houghton et al. 1995). A: I (1.68-1.53 m.y.). B:IIA (1.21-0.89 m.y.). C: IIB (0.77-0.68 m.y.). D: IIIA (0.34-0.32 m.y.). E. IIIB (0.28-ca. 0.15 m.y.). F. IIIC (0.0065 m.y.-present). Mo-Mangakino, Ka-Kapenga, Wh-Whakamaru, Ma-Maroa, Ok-Okataina, Re-Reporoa, Ro-Rotorua, Ta-Taupo.

Most of these units are poorly exposed, poorly preserved and are of unknown size. Source areas or calderas remain to be delineated, and may have been overprinted by tectonism and subsequent volcanism. It is beyond the scope of this thesis to introduce the field geology and petrology of these units, but they are the subject of ongoing research. A brief comparision of data of many of the units outlined is presented here.

The Kaingaroa and Kawerau ignimbrites exhibit compositional variation similar to the majority of Period IIIb ignimbrites (Fig 9.5), many of which contain a subordinate volume of less evolved pumice. These less evolved dacitic compositions are interpreted as samples from a subordinate magma or magma chamber (Chapter 7). Major, trace element, trace element ratios (e.g. Zr:Zn) and isotopic chemistry are very similar for the units and indeed for TVZ rhyolites in general. Variable trace element chemistry, illustrated by the coeval dacites, suggests variable sources and that the magmas evolved along similar petrogenetic pathways. Details of petrogenesis are discussed below.

It is proposed here that the 0.28-0.15 Ma period records a clustering of caldera-forming ignimbritic volcanism, of comparable volume to the period recorded by the Whakamaru-group ignimbrites (ca. 1000 km^3+), but involving many sources from all of the recognised 'young TVZ' calderas. The extent of this interval or period is poorly defined due to poor exposure and limited study of units, but both the deposits and caldera delineation is the subject of ongoing research.

Structural data and new Ar/Ar dates suggest that the Mamaku and Kaingaroa ignimbrites are cut by major faults that delineate the margins of the Taupo fault belt (Horohoro and Paeroa faults). Thus there appears to have been a major period of faulting and tectonism postdating or accompanying several major ignimbrite eruptions within this period. The implication is a period of magma genesis on a regional scale which may have accompanied a major period of tectonism within TVZ. The question arises as to what role extension or tectonism plays in ignimbritic volcanism (i.e. initiation of magmatism, emplacement and eruption triggering)? The role of extension is widely demonstrated in emplacement of silicic bodies (e.g. Hutton and Reavy 1992), but largely equivocal in eruption triggering (e.g. Cambray et al. 1995). The relationship between tectonism and volcanism has been demonstrated within TVZ by the association of caldera structures and regional faults (e.g. Cole et al. 1996), and volcanism whose

lineaments define the same NNE 'TVZ structural trend' (e.g. 10ka Tongariro eruptives; Nairn et al. pers comm 1996; 1886 ka Tarawera, Cole 1990). Is it possible to distinguish between a caldera-forming event which generates faults whose orientations are controlled by the regional structural trend or volcanism generated by seismic activity along regional structures (i.e. seismic pumping)?

The eastern margin of TVZ, marked by the Kaingaroa fault, can be demonstrated to have been a fundamental structural feature in TVZ evolution since at least in the last 700ka. The fault marks the eastern edge of TVZ, and has provided a barrier to large scale ignimbrites (e.g. Waiotapu) and locus of eruptive vents of unusual magmatism and volcanism (e.g. adakites at Rolles Peak; andesitic ignimbrites at Rautawiri). Geophysical research along the eastern margin of TVZ has demonstrated a large offset of the basement greywacke (e.g. Stagpoole 1994). Ongoing volcanological studies and geophysical research (Bibby pers comm 1996) suggests much of the eastern margin are nested calderas probably related to clustering of ignimbrite volcanism during period IIIb.

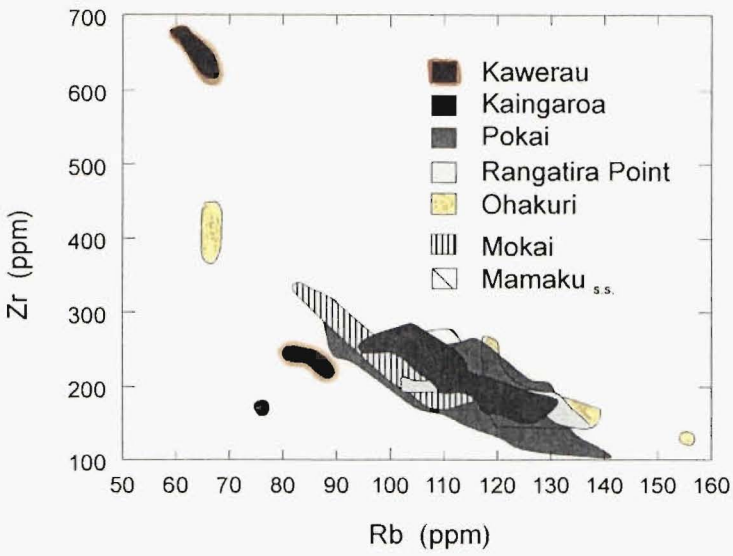

Figure 9.5 Variation in trace element chemistry of ignimbrites erupted in the similar stratigraphic period as the Kaingaroa Ignimbrite. Data from Weaver and Houghton (unpublished data), Karhunen (1993), Cole et al (submitted), this study.

Rotorua, Okataina, Reporoa, Maroa and Taupo 'calderas' have largely formed since 280 ka and portions of the caldera margins are recognisable modern topographic features. Much of the geomorphic relief of TVZ was formed during this period and has overprinted evidence of the structures formed during the Whakamaru period. The failure to recognise structures relating to other units within this period is largely due to overprinting by tectonism and or volcanism. Geophysical determination of 'caldera' structures in the Kapenga and Taupo-Reporoa basin region record remnant evidence of the calderas formed during this period and subsequently overprinted.

9.3 Petrogenetic constraints

"The polemic stems from lines of evidence which permit equivocal interpretation of results" Smith and Gamble (1993)

Petrogenesis of large-scale rhyolitic provinces remains a controversial topic in igneous petrology. Rhyolites from large rhyolitic provinces have been ascribed to differentiation of mantle-derived magmas (e.g. Smith et al. 1996) or lower crustal anatexis (e.g. Pankhurst and Rapela 1995). Numerous provinces have had both models proposed e.g. Sierra Madre Occidental, Mexico (Cameron et al. 1980; Ruiz et al. 1988). Much of the evidence for origin of rhyolites is circumstantial, and evidence for either model is equivocal. This section outlines the problem and debate with relevance to central TVZ.

9.3.1 Basement

Basement lithologies along the eastern edge of TVZ are of particular interest in assessing the various crustal components likely to have been involved as essential constituents or incidental contaminants in rhyolitic magma genesis. Three principal elements have been identified by previous workers:

1) Torlesse metasedimentary basement
2) Granulite (unknown geographic extent)
3) Unknown diopside normative meta-igneous lower crust

9.3.2 Previous work

Previous petrological work on the origin of TVZ rhyolites (Graham et al. 1995 and references within) has established the following models:

A) Crustal anatexis of Torlesse or Waipapa 'greywacke' basement (Reid 1983)

The lack of intermediate compositions, lack of evidence of complementary cumulate material and dominance of high Si compositions have led most workers to the conclusion that the rhyolite magmas were not directly derived from associated basalts. A widely proposed source material has been the 'greywacke' basement or their metamorphosed lower crustal equivalents but isotopic work precludes the direct melting of 'greywacke' metasediments because:

1) Low $\delta^{18}O$ contents of the rhyolitesis not possible by direct partial melting of either Torlesse or Waipapa greywacke (Blattner and Reid 1982).

2) Experimental work by Conrad et al (1988) point out that TVZ rhyolites are metaluminous to weakly peraluminous, whereas partial melts of the sedimentary basement would be peraluminous; their experimental results suggest that a more likely source is a di-normative meta-igneous source.

3) Differences in radiogenic Pb and Sr composition of Torlesse 'greywacke' compared to TVZ rhyolites preclude direct partial melting of observed basement lithologies, but Graham et al (1992) suggest Torlesse is probably an important contaminant. TVZ rhyolites contain very limited zircon inheritance (e.g. Lindsay et al. 1995) suggesting minimal assimilation or direct melting of metasedimentary basement. Lindsay et al (1995) suggest probable derivation from zircon-poor intermediate composition lower crust.

B) Assimilation and fractionation of high alumina basalt (e.g. McCulloch et al. 1994)

McCulloch et al (1994) proposed that mantle derived basalts pond near the base of the crust, incorporate 15-25% of 'Torlesse-like' metasediments by bulk assimilation, and subsequently undergo closed system fractionation to produce rhyolitic compositions. This model is refuted by most workers (e.g. Graham et al. 1995) due to the lack of

intermediate compositions, lack of evidence of definitive associated cumulate material, and because it does not explain the compositional bimodality of central TVZ.

C) Crustal anatexis of andesitic-dacitic lower crust basement (e.g. Conrad et al. 1988; Graham et al. 1992).

TVZ rhyolites are remarkably similar isotopically to TVZ intermediate volcanics, exposed dominantly in the southern and northern part of TVZ. Graham et al (1995) suggests two possible source rocks:

1) Buried 'early' TVZ andesites, chemically and isotopically similar to contemporary TVZ andesites, or southern extension of Coromandel Volcanic zone andesites. Further work is required on the presence of pre-2 Ma andesites in the central TVZ area, and on Coromandel Volcanics. Early andesite volcanics in the central TVZ region is currently a research focus of the University of Canterbury.

2) Granulitic lower crust, similar to that sampled by Graham et al (1990) as xenoliths in Ruapehu lavas. These xenoliths are isotopically different to TVZ rhyolites precluding their source by direct partial melting. Further work is required on these xenoliths and their extent.

Briggs et al (1993) highlighted from REE studies on Mangakino ignimbrites a possible unusual plagioclase-rich source (anorthositic or gabbroic anorthositic) for the Ahuroa Ignimbrite, and with the Marshall A ignimbrite a positive Eu anomaly and MREE depletion suggestive of amphibole (and possibly plagioclase) in the source, indicating possible amphibolitic source lithologies. The presence of plagioclase-rich anorthositic and amphibolitic lithologies are very common in lower crustal arcs.

Various lines of circumstantial evidence can be used to advance models of partial melting of an unknown meta-igneous crust. Possible arguements for partial melting are generally arguments against fractionation or AFC e.g. lack of intermediate derivatives. The chemical and isotopic homogeneity of TVZ rhyolites was considered strong evidence of large scale melting of a lower crustal source (e.g. Hochstein et al. 1993), but there is evidence for heterogeneity in possible source compositions as outlined in section 9.2 and discussed below.

9.3.3 Constraints on source

The majority of TVZ high silica rhyolites exhibit similar trace element and isotopic compositions, suggesting a near homogenous protolith. The variations may be attributable to melting under different pressures and temperatures or reflect derivation from distinct sources.

Clearly the rhyolites of TVZ have undergone significant crystal fractionation involving plagioclase-rich extracts. Nicholls et al (1992) considered that compositions which have high silica contents (ca. 75% SiO_2) probably represent fractionated compositions. The presence of negative Eu anomalies (contrasting with coeval dacites) suggest this is the case. The coeval dacites may represent closer approximations to primary 'crustal' melts; these dacites (or low SiO_2 rhyolites) generally exhibit no or limited Eu anomaly (Brown 1994; this study) and high normative An contents (Nicholls et al. 1992).

Despite the similar chemistry exhibited by their high silica derivatives the dacites identified in this study have variable trace element compositions, best illustrated by variation in Zr vs Rb and REE. Three end members with high Zr, moderate Zr and low Zr respectively are identified. These end-members exhibit differing REE contents and Eu variations. The distinct compositions of these possible primary melts and their convergence on fractionated high SiO_2 rhyolites (Fig 9.5) suggests TVZ dacites follow similar plagioclase-dominated fractionation paths converging on high silica rhyolite compositions. Rare amphibole-dominated fractionation e.g. Kawerau (this study) and sanidine fractionation e.g. Whakamaru (Brown 1994) is responsible for additional variants.

9.3.4 Rhyolitic suites

In central TVZ, at least three distinct rhyolitic suites are identified suggesting either minor variations in source or degree or depth of melting. Different trace element suites have been identified at Mangakino (Briggs et al. 1993), that maybe related to plagioclase-rich sources, and a further distinct suite is identified from this study (Kawerau ignimbrite; Chapter 8). Other possible variants of this suite are outlined below.

Rhyolites with A-type affinities

Three unusual rhyolites reported in this study include the Marshall, Ohakuri and Kawerau ignimbrites (Fig 9.6). The Marshall ignimbrite exhibits element abundances typical of A-type granitoids e.g. high HFSE (Zr, Nb, Ga/Al_2O_3; Eby 1990, 1992; Fig 9.9). Both Ohakuri and Kawerau magmas are anomalous and exhibit characteristics typical of both arc-related subalkaline and alkaline rhyolites. On tectonic discrimination diagrams the Marshall ignimbrite plots in the WPG (within plate granitoid) field (Pearce et al. 1984) and A-type field of Whalen et al (1987). The Ohakuri and Kawerau ignimbrite exhibit elemental abundances consistent with A-type designation but are distinct on tectonic discrimination plots, reflecting their unusual and variable trace element chemistry (e.g. high Zr but low Nb; Fig 9.6). The presence of the negative Nb anomaly in multi-element plots probably reflects a source characteristic. Negative Nb anomalies are a common feature of arc-related volcanics, or rhyolites which have been derived from a crustal source, which itself was derived from an arc-related crust. This may explain the unusual high Zr:Nb of the Ohakuri and Kawerau ignimbrites. i.e. abundance of HFSE consistent with A-type rhyolites and low Nb consistent with subduction related or typical arc-related rhyolites. Macdonald et al. (1992) report similar rhyolites which are chemically transitional between typical oceanic extensional and active continental margin rhyolites, and exhibit high Hf, Zr, Y, Ta, and REE.

Origin of A-type granites/rhyolites is currently one of the most debated topics in the field of igneous petrology. Numerous models have been put forward to explain their genesis e.g. fractionation of mafic magma vs partial melting of lower crustal sources. Several compositions have been assigned for this protolith: (1) felsic crust that was already melt depleted from a previous anatectic event (Collins et al. 1982); (2) tonalitic (Creaser et al. 1991, Weaver et al. 1992); (3) partially dehyroxylated and F-enriched by a previous high-grade metamorphic event (Skjerkie and Johnston 1992). This debate results from the fact that A-type granitoids/rhyolites represent a diverse group of petrogenetically distinct silicic lithologies (Eby 1990;1992).

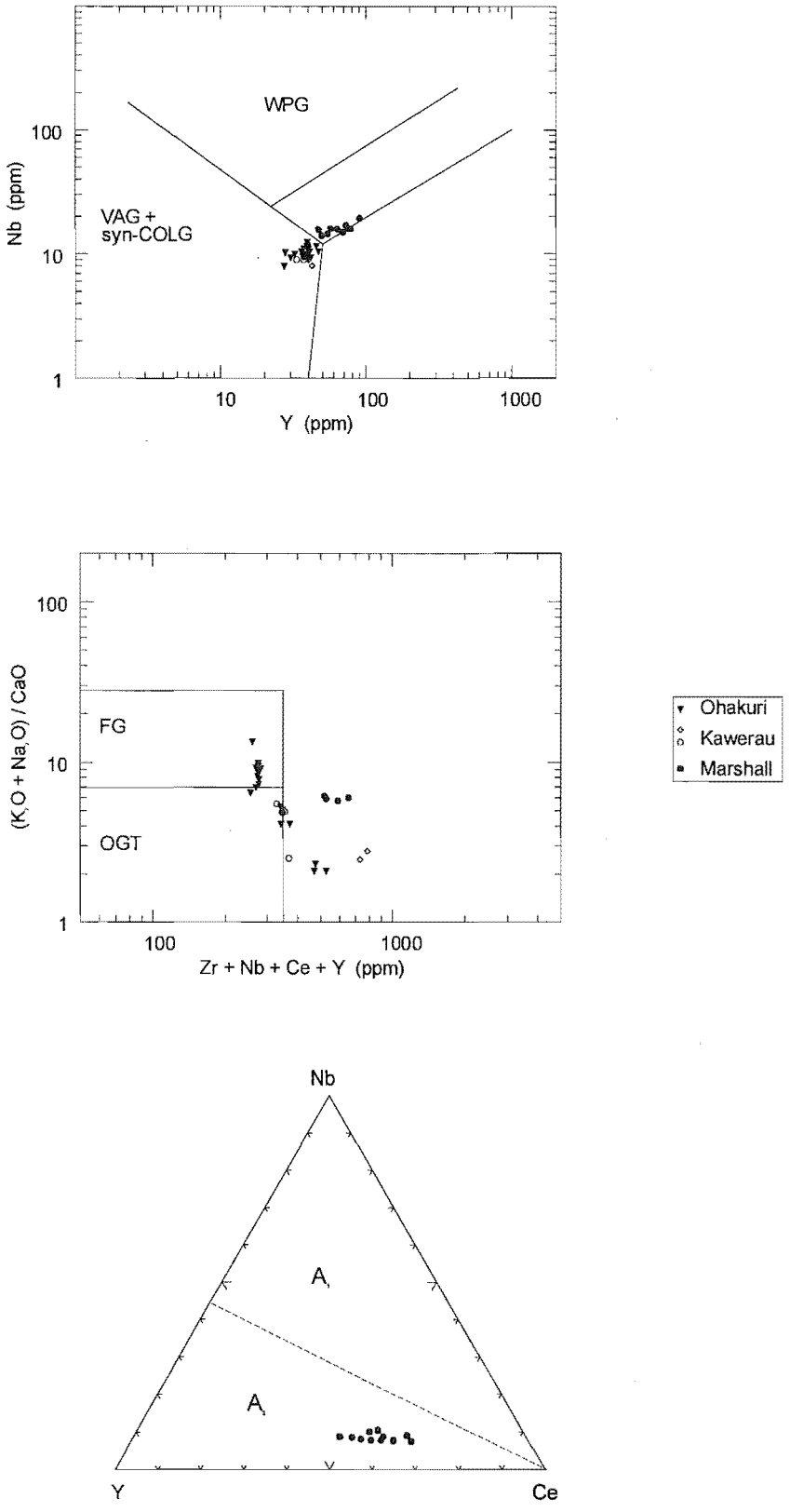

Figure 9.6 Tectonic discrimination diagrams (after Pearce et al. 1984), Whalen et al (1987), and Eby (1992) of rhyolites in the TVZ with A-type affinites. Black circles = Marshall ignimbrite; Triangles = Ohakuri (Weaver and Houghton unpublished data); Grey circles (Type A) and diamonds (Type B) = Kawerau (this study).

A-type granitoids/rhyolites were divided by Eby (1992) into types A_1 (alkaline association with trace element chracteristics of ocean island basalts) and A_2 (orogenic association with trace element chracteristics of continental crust and island arc basalts). The Marshall ignimbrite exhibits typical type A_2 compositions, consistent with the negative Nb anomaly and lack of association with alkalic basalts. Although A-type rhyolites are typically interpreted to represent anorogenic tectonic setting, the A_2 group contains rhyolites/granitoids thought to be emplaced in a variety of tectonic settings. The arc-related environment of the TVZ is clearly subduction-related, although debate continues on the nature of the arc (Cole 1990; Wilson et al. 1995a). It is unclear whether TVZ exhibits a distinct arc and back arc or is a rare example of a extensional arc. The large volumes of rhyolite, small recurrence interval, extreme heat flow, and rapid extension rates are similar to measurements on oceanic islands, where asthenospheric mantle upwelling provides a heat source. Hochstein et al (1993) discount the role of asthenospheric magma in TVZ, and Smith and Gamble (1993) concur that an asthenospheric plume would be difficult to accommodate within the subduction zone setting. The origin of heat flow in TVZ remains equivocal (Simmons and Weaver 1995).

Extensive melting of the lower crust implies high thermal gradients and injection of voluminous mantle-derived magmas, the probable scenario within central TVZ. Distinct alkalic and subalkaline silicic suites in arc-related environments has been documented in numerous granitoid studies (e.g. Eby 1990) but is less commonly documented in modern arc environments.

9.3.5 Nature of sources?

It is possible to speculate about variations, but what constraints can we put on the nature of sources? Can any TVZ rhyolites be traced to particular source-rock compositions?

The source of TVZ rhyolites is at best poorly constrained, due to the lack of information about the lower crust. As such it is important to determine whether any of the rhyolites are sufficiently unmixed, unevolved and uncontaminated to provide information about specific source lithologies. An origin by partial melting of lower crust has many attractive features but much supporting evidence is still required on its extent and

nature. Clearly it is impossible to solve a problem with two rather crucial unknowns (nature of source and/or nature of the assimilant).

Despite these reservations it is possible that any magma erupted from a TVZ magma system may represent an isotopically (and possibly chemically) unmodified extract from a source domain. This is in contrast to complex rhyolite fields, e.g. Yellowstone, in which complex processes of source mixing, basaltic magma influx and mixing, and contamination obscure isotopic, let alone chemical fingerprints of source (Hildreth et al. 1991). SHRIMP analysis by Lindsay et al (1995) suggests TVZ rhyolitic source is comparatively zircon-free (i.e. distinctly mafic) or that melting was at such a high temperature that source zircon were assimilated (which also suggests mafic input).

Basalt involvement in rhyolite genesis, at least as a thermal component, can hardly be doubted, due to extraordinarily high heat flow, mantle-derived $^{3}He/^{4}He$ ratios, high fluxes of CO_2 in geothermal springs (Giggenbach 1995), and circumstantial evidence as a mingled component. This evidence suggest basalts are probably involved as a component in petrogenesis. It can not be ruled out that rhyolites (or dacites) represent mixtures of lower crustal melts and basalt.

9.3.6 Future work

The source of TVZ rhyolites will remain equivocal due to lack of information about the role of primary mafic magma and nature of the lower crust. Further work is required to constrain the nature of the lower crust (the missing variable or key to constraining AFC or crustal melting models). Further xenoliths studies are required to elucidate the nature and extent of the lower crust. The reconnaissance SHRIMP work of Lindsay et al (1995) detected little zircon inheritance in TVZ rhyolites. These results are clearly remarkable and unexpected, as they restrict possible crustal sources and limit the amount of assimilation in modelling. I would suggest further SHRIMP work remains a primary objective in TVZ rhyolite petrogenetic studies, especially as the lithologies utilised by Lindsay et al (1995) were rather restricted.

A fruitful possible avenue of research continues to be the documentation of coeval dacites (Briggs et al. 1993; Brown 1994; this study). These compositions are clearly less

evolved and can be demonstrated to represent parental compositions to the rhyolites. These dacites exhibit variable trace element compositions illustrating compositional diversity of less evolved melts in central TVZ, in contrast to the homogeneity illustrated by high silica rhyolite chemistry.

CHAPTER TEN
Conclusions

- Reporoa Caldera is a simple monogenetic structure which collapsed during the Kaingaroa Ignimbrite eruption. It remains the only simple monogenetic caldera in TVZ. Complex paleotopography in the Reporoa area is revealed by the presence of arroyos, thickness variations, complex pre-Kaingaroa ignimbrite surface topography, pre-Kaingaroa arcuate scarps. The nature of the Waiora Formation also suggest the area has undergone a complex history, with possible preceding caldera-forming events. The Kaingaroa Fault to the east marks a fundamental boundary in TVZ (eastern edge) which has provide the focus for a variety of magma compositions, a barrier to large ignimbrites, and a regional structural weakness during caldera collapse. The identification of ignimbrites south of Kaingaroa Forest and reconnaissance geophysics (Bibby pers comm 1996) suggest the Taupo-Reporoa basin may be a complex of nested calderas.

- The Kaingaroa Ignimbrite has a complex internal stratigraphy illustrated by a complex basal tephra sequence with intercalated fall, surge and flow deposits and three ignimbrite units which have strikingly proximal to medial facies transitions.

- Welding and thickness variations in the extensive OWR and WIU units suggests gradual thickening towards the centre of Kaingaroa Plateau. The presence of this pre-Kaingaroa basin could be alluvial in origin based on inferred geometry, localised abundance of gas segregation structures, unusual vapour-phase zonation patterns, smaller scale thickness variations (consistent with ponding in alluvial interfluves), and the presence of reworked Kaingaroa deposits of alluvial origin lying stratigraphically above the WIU (indicating possible re-establishment of pre-Kaingaroa stream systems).

- Detailed lithic componentry studies reveal changes in lithic diversity and abundance between stratigraphic units, marking changes in vent conditions, and increasing depth of lithic provenance and hence inferred fragmentation level.

- The Reporoa sub-caldera geology is dominated by an andesitic volcano and it's leuco-gabbroic subvolcanic roots, with intercalated welded ignimbrites, rare low-grade metasedimentary basement and meta-rhyolites. Gabbros and meta-rhyolite lithics contain complex secondary mineral assemblages suggesting multiple periods of alteration/metasomatism, including amorphous aluminosilicate replacement of calcic plagioclase, in leucogabbros and andesites, and tourmalinisation of meta-rhyolites and meta-ignimbrites.

- Pumice chemistry reveals a near homogeneous magma chamber, from which magma was progressively tapped during the eruption. Syn-eruptive mingling and evisceration of multiple magma batches occurred during the climactic caldera collapse phase.

- Dramatic changes in pumice chemistry and eruptive style suggest possible vent migration during basal tephra eruption as has been documented at other TVZ rhyolitic 'calderas'.

- The Kaingaroa Ignimbrite has been mis-correlated with the Matahina, Mamaku, and Rangatira Point ignimbrites, and three new units described in this thesis: Kawerau ignimbrite, Wheao sheet, and the welded 'sandy-black' ignimbrite of Wairakei drill holes. Identification of these units has resulted in major revisions to the regional stratigraphy. It is clear that despite numerous international publications on ignimbrite correlation the TVZ poses its own challenges, not the least of which is the poor exposure and the limited stratigraphic sections that document multiple units. A major reason for the mis-correlation in the Kaingaroa case is its distinctive (though not unique) black colouring. Reconnaissance field and chemical data is presented for these new units. Kawerau ignimbrite remains an enigma, largely because of the anomalous Zr, Hf and Zn contents suggestive of a relationship to peralkaline rhyolites, and the presence of unusual manganoan fayalite of vapour-phase origin. Identification of these units and other intermediate size ignimbrite in the stratigraphic

interval post-Whakamaru-group ignimbrite and pre-Mamaku require further careful documentation; the implications are of a temporal clustering of units sourced from throughout TVZ.

Acknowledgements

Firstly I'd like to thank my supervisors Professor Jim Cole, Associate Professor Steve Weaver, and Dr Ian Nairn (GNS Wairakei). In particular I would like to thank Jim, as principal supervisor, for his support, and for instilling in me that a Phd was more than a thesis. Thanks go to Steve who battled with the entire thesis at a very late stage, and for advice on all things geochemical, and especially for finding the financial means for isotopic data.

To the lads at GNS, Drs Ian Nairn, Peter Wood, Bruce Houghton, and Colin Wilson, a big cheers for discussions. Peter allowed access to thin sections of RP1 drill hole, and we had numerous discussions both on ignimbrite stratigraphy and distribution, and petrological matters relating to the gabbroic lithics and those tourmaline-bearing meta-rhyolites.

Thank you Dr Shelley ('D.S.') for petrographic advice, trusting me with your petrology classes, and for instilling in me a need to question both my own and others scientific logic.

Cheers to the other members of staff at the University of Canterbury: Jarg Pettinga for his impeccable taste, and advice on all matters aesthetic. Dave McKinnon assisted in SEM observation of diatomite and altered silicic tuff lithics. Steve Brown for generating those XRF numbers, and XRD plots, Kerry Swanson for help with photography, and especially Rob Spiers who made so many thin sections.

I would like to thank all those who I had discussions with: Hugh Bibby, Stu ('PC) Brown, Rod Burt, George Guthrie, Craig Jones, Mitsuhiro Nakagawa, Jens Richnow, Richard Smith, Supri Soengkono and Simon Ward to name a few. Cheers to Phil Kyle for INAA analyses, Tod Waight who ran the isotope analyses, Stu Brown who assisted with Mg:Mn partitioning of Fe/Ti oxides, and Yosuke Kawachi for microprobe assistance.

ECNZ allowed access to Wairakei drill core. John Gamble allowed access to Victoria theses and rock collections, so vital to lithic componentry correlation. Forestcorp allowed access to the Kaingaroa forest, and numerous farmers allowed access to their land.

I wish to acknowledge the financial support of the Mason Trust, and a University of Canterbury doctoral scholarship.

Although not directly related to this thesis, my conference trip to the IAVCEI and IUGG meeting in Boulder, Colorado, allowed presentation of ideas within this thesis, and thus contributed greatly to the overall picture. I acknowledge financial support from the Royal Society of New Zealand Canterbury branch, Royal Society of New Zealand 'Young Scientists Fund', IAVCEI, Mason Trust, and my ever increasing student loan.

On a personal note I would like to say a special thanks to:

Those who kept me from my work, and from my play, in the last year: Rach, Al, Rod, Mark, Richie J, Jezza, Jen and Jane (the 'jelly' twins), and Rhys. Cheers for pulling me through the tough times.

'The late night lads' i.e. Jezza and Ed.

My roomie Mark, for setting the work ethics, and for 'help!' with computers.

Jane and Harriet who battled with the entire 'semi-finished' thesis at the eleventh hour.

My parents and sis, not only for these last three years, but for all my time at varsity. My thesis field work gave me a chance to visit places where I was born and grew up; a chance to see places no longer in my memories.

A special mention needs to be made here to Christine and Jim who kept me going for months, with those little chats, dinners, and the 'Coke'. They then let me stay during those difficult last couple of months. I dont know what else to say other than thanks.

Final thanks go to Sarah for keeping me sane (and insane).

I can't go through the entire thesis without saying something about the car thefts, 48 dozen eggs, 12583 e-mails. To all those who kept me sane through all this in the last few weeks I say cheers……

Cheers….Groundhog day is finally over.

References

Abbott, P.L., and Peterson, G.L. 1978. Effects of abrasion and durability on conglomerate clast populations- examples from Cretaceous and Eocene conglomerates of the San Diego area, California. J. Sedimentary Petrology 48:31-42.

Anderson, D.J., and Lindsley, D.H. 1988. Internally consistent solution models for Fe-Mg-Mn-Ti oxides: Fe/Ti oxides. American Mineralogist 73: 714-726.

Arth, J.L. 1976. Behaviour of trace elements during magmatic processes - a summary of theoretical models and their applications. J. Res. U.S. Geol. Surv. 4: 41-47.

Bacon, C.R., and Druitt, T.H. 1988. Compositional evolution of the zoned calc-alkaline magma chamber of mount Mazama, Crater Lake, Oregon. Contributions to Mineralogy and Petrology 98: 224-256.

Bacon, C.R., and Hirschmann, M.M. 1988 Mg/Mn partioning as a test for equilibrium between Fe/Ti oxides. American Mineralogist. 73: 57-61.

Bailey, R.A. and Carr, R.G. 1994. Physical geology and eruptive history of the Matahina Ignimbrite, Taupo Volcanic Zone, North Island, New Zealand. N.Z.J. Geol. Geophys 37: 319-344.

Baker, B.H., and McBirney, A.R. 1985. Liquid fractionation. Part III: geochemistry of zoned magmas and the compositional effects of liquid fractionation. Journal of Volcanology and Geothermal Research 24: 55-81.

Bajwah, Z.U., Whie, A.J.R., Kwak, T.A.P., and Price, R.C. 1995. The Renison granite, northwestern Tasmania: A petrological, geochemical and fluid inclusion study of hydrothermal alteration. Economic Geology 90: 1663-1675.

Beck, A.C. and Robertson, E.I. 1955. Chapter II Geology and Geophysics. In Geothermal steam power in New Zealand. DSIR Bulletin 117: 15-19.

Best, M.G., Christiansen, E.H., Deino, A.L., Gromme, C.S., and Tingey, D.G. 1995. Correlation and emplacement of a large, zoned, discontinously exposed ash flow sheet: the 40Ar/39Ar chronology, paleomagnetism, and petrology of the Pahranagat Formation, Nevada. Journal of Geophysical Research 100: 24593-24609.

Bibby, H.M., Caldwell, T.G., Davey, F.J., and Webb, T.H. 1995. Geophysical evidence of the structure of the Taupo Volcanic Zone and its hydrothermal circulation. Journal of Volcanology and Geothermal Research 68:29-58.

Bignall, G., Browne, P.R.L., and Kyle, P.R. 1996. Geochemical characterisation of hydrothermally altered ignimbrites in active geothermal fields from the central Taupo Volcanic Zone, New Zealand. Journal of Volcanology and Geothermal Research 73: 79-97.

Bird, D.K., Manning, C.E., and Rose, N.M. 1988. Hydrothermal alteration of Tertiary layered gabbros, East Greenland. American Journal of Science 288: 405-457.

Black, P.M., 1971. Tourmalines from Cuvier Island, New Zealand. Mineralogical Magazine 38: 374-376.

Black, T.M., Shane, P.A.R., Westgate, J.A., and Froggatt, P.C. 1996. Chronological and palaeomagnetic constraints on widespread welded ignimbrites of the Taupo volcanic Zone, New Zealand. Bulletin of Volcanology 58: 226-238.

Blake, S.,1981. Eruptions from zoned magma chambers. Journal of the Geological Society of London 138: 281-287.

Blake, S., and Ivey, G.N. 1986. Density and viscosity gradients in zoned magma chambers, and their influence on withdrawal dynamics. Journal of Volcanology and Geothermal Research 30: 201-230.

Blake, S., Wilson, C.J.N., Smith, I.E.M. and Walker, G.P.L. 1992. Petrology and dynamics of the Waimihia mixed magma eruption, Taupo Volcano, New Zealand. Journal of the Geological Society of London 149: 193-207.

Blattner, P., and Reid, F. W. 1982. The origin of lavas and ignimbrites of the Taupo Volcanic Zone, New Zealand, in light of oxygen isotope data. Geochimica et Cosmochimica Acta 46: 1417-1429.

Blundy, J.D., and Shimizu, N. 1991. Trace element evidence for plagioclase recycling in calc-alkaline magmas. Earth and Planetary Science Letters 102: 178-197.

Boden, D.R. 1989. Evidence for step-function zoning of magma and eruptive dynamics, Toquima caldera complex, Nevada. Journal of Volcanology and Geothermal Research 37: 39-57.

Branney, M.J. 1995. Downsag and extension at calderas: new perspectives on collapse geometries from ice-melt, mining, and volcanic subsidence. Bulletin of Volcanology 57: 303-318.

Branney, M.J., and Kokelaar, P. 1992. A reappraisal of ignimbrite emplacement: progressive aggradation and changes from particulate to non-particulate flow during emplacement of high-grade ignimbrite. Bulletin of Volcanology 54: 504-520.

Branney, M.J., and Kokelaar, P. 1997. Giant bed from a sustained catastrophic density current flowing over topography: Acatlan ignimbrite, Mexico. Geology 25: 115-118.

Briggs, N.D.1976. Welding and crystallisation zonation in Whakamaru Ignimbrite, central North Island, New Zealand. N. Z. J.Geol. Geophys 19:189-212.

Briggs, R.M., Gifford, M.G., Moyle, A.R., Taylor, S.R., Norman, M.D., Houghton, B.F. and Wilson, C.J.N. 1993. Geochemical zoning and eruptive mixing in ignimbrites from Mangakino volcano, Taupo Volcanic Zone, New Zealand. Journal of Volcanology and Geothermal Research., 56: 175-203.

Brown, S.J.A.1994. Geology and geochemistry of the Whakamaru group ignimbrites, and associated rhyolite domes, Taupo Volcanic Zone, New Zealand. Unpublished Ph.D thesis, University of Canterbury, Christchurch.

Brown, S.J.A., Cole, J.W., Beresford, S.W., and Shelley, D.,1995. The nature of subvolcanic magma reservoirs in central Taupo Volcanic Zone, New Zealand as evidenced by lithic fragments in large volume ignimbrites. IUGG XXI General Assembly, Boulder, Colorado Abstract :A445.

Brown, S.J.A.., Burt, R.M., Cole, J.W., Krippner, S., Price, R. and Cartwright, R. submitted to Chemical Geology. The Origin of plutonic lithics in large volume ignimbrites, Taupo Volcanic Zone, New Zealand: Evidence from petrographic, geochemical and isotopic data.

Browne, P.R.L.1971. Petrological logs of drillholes, Broadlands geothermal field 87 pgs. Report/New Zealand Geological Survey 52.

Browne, P.R.L., Graham, I.J., Parker. R.J. and Wood, C.P. 1992. Subsurface andesite lavas and plutonic rocks in the Rotokawa and Ngatamariki geothermal systems, Taupo Volcanic Zone, New Zealand. Journal of Volcanology and Geothermal Research., 51: 199-215.

Buddington, A.F., and Lindsley, D.H. 1964. Iron-Titanium oxide minerals and synthetic equivalents. Journal of Petrology 5: 310-357.

Buck, M.D., Briggs, R.M., and Nelson, C.S. 1981. Pyroclastic deposits and volcanic history of Mayor Island. New Zealand Journal of Geology and Geophysics 24: 449-467.

Buesch, D.C. 1992. Incorporation and redistribution of locally derived lithic fragments within a pyroclastic flow. Geol. Soc. Am. Bull 104: 1193-1207.

Burt, R.M., Cole, J.W., and Vroon, P.Z. 1996. Volcanic geology and geochemistry of Motuhora (Whale Island), Bay of Islands, New Zealand. New Zealand Journal of Geology and Geophysics 39: 559-575.

Cambray, F.W., Vogel, T.A., and Mills Jr, J.G. 1995. Origin of compositional heterogeneities in tuffs of the Timber Mountain Group: the relationship between magma batches and magma transfer and emplacement in an extensional environment. Journal of Geophysical Research 100: 15793-15805.

Cameron, M., Bagby, W.C., and Cameron, K.L. 1980. Petrogenesis of voluminous mid-Tertiary ignimbrites of the Sierra Madre Occidental, Chihuahua, Mexico. Contributions to Mineralogy and Petrology 74: 271-284.

Carmichael, I.S.E. 1967. The iron-titanium oxides of salic volcanic rocks and their associated ferromagnesian silicates. Contributions to Mineralogy and Petrology 14: 36-64.

Carr, R.G., 1984. The Matahina Ignimbrite: its evolution including its eruption and post-depositional changes. Unpublished Ph.D. thesis, Auckland University, Auckland, New Zealand.

Cas, R.A.F., and Wright, J.V. 1987. Volcanic Successions, modern and ancient. Unwin Hyman, London, 528 pgs.

Casey, W.H., Westrich, H.R., and Holden, G.R. 1991. Dissolution rates of plagioclase at pH = 2 and 3. American Mineralogist 76: 211-217.

Cavaretta, G., Puxeddu, M., Franceschelli., Pandeli, E., and Valori, A. 1992. Tourmalinites from hydrothermal systems related to Permian rift magmatism of the Hercynian Saalian phase in Tuscany (Italy). In: Miles (ed). Water-rock Interaction, Rotterdam. 141-144.

Chernet, T. 1987. Lithic inclusions in the Taupo Pumice Formation. Unpublished M.Sc thesis, Victoria University, Wellington.

Civetta, L., Orsi, G., Pappalardo, L., Fisher, R.V., Heiken, G., and Ort, M. 1997. Geochemical zoning, mingling, eruptive dynamics and depositional processes- the Campanian Ignimbrite, Campi Flegrei caldera, Italy. Journal of Volcanology and Geothermal Research 75: 183-219.

Cole, J.W. 1978. Tectonic setting of Mayor Island volcano. New Zealand Journal of Geology and Geophysics 21: 645-647

Cole, J.W., 1990. Structural control and origin of volcanism in the Taupo Volcanic Zone, New Zealand. Bulletin of Volcanology 52: 445-459.

Cole, J.W., Cashman, K.V., and Rankin, P.C. 1983. Rare-earth element geochemistry and the origin of andesites and basalts of the Taupo Volcanic Zone, New Zealand. Chemical Geology 38: 255-274.

Cole, J.W., Beresford, S.W., Burt, R.M., and Ritchie, A.B.H. 1996. Location and terminology of 'caldera' structures in the Taupo Volcanic Zone. Geological Society of New Zealand Miscellaneous Publication 91A: 53.

Cole, J.W., Brown, S.J.A., Burt, R.M., Beresford, S.W., and Wilson, C.JN. Submitted to Journal of Volcanology and Geothermal Research. Lithic types in ignimbrites as a guide to the evolution of a volcanic centre, Taupo, New Zealand.

Cole, P., Guest, J.E., and Duncan, A.M. 1993. The emplacement of intermediate volume ignimbrites: a case study from Roccamonfina volcano, southern Italy. Bulletin of Volcanology 55: 467-480.

Collins, W.J., Beams, S.D., White, A.J.R., and Chappell, B.W. 1982. Nature and origin of A-type granites with particular reference to south-eastern Australia. Contributions to Mineralogy and Petrology 80: 189-200.

Conrad, W.K., Nicholls, I.A., and Wall, V.J. 1988. Water-saturated and undersaturated melting of metaluminous and peraluminous crustal compositions at 10kb: evidence for the origin of silicic magmas in the Taupo Volcanic Zone, New Zealand, and other occurences. Journal of Petrology 29: 765-803.

Creaser, R.A., Price, R.C., and Wormald, R.J. 1991. A-type granites revisited: assessment of a residual source model. Geology 19: 163-166.

Cullen, A.B., Vicenzi, E., and McBirney, A.R. 1989. Plagioclase-ultraphyric basalts of Galapagos Archipelago. Journal of Volcanology and Geothermal Research 37: 325-337.

Deer, W.A., Howie, R.A., and Zussman, J. 1982. Olivine group. In Rock forming minerals, Vol 1A: Orthosilicates (2nd edition), Longman, London, 375pgs.

De Silva, S.L. 1991. Styles of zoning in central Andean ignimbrites; insights into magma chamber processes. Geological Society of America Special Paper 265: 217-231.

De Silva, S.L., and Wolff, J.A. 1995. Zoned magma chambers: the influence of magma chamber geometry on sidewall convective fractionation. Journal of Volcanology and Geothermal Research 65: 111-118.

Dorais, M.J., Whitney, J.A., and Stormer Jr, J.C. 1991. Mineralogical constraints on the petrogenesis of trachytic inclusions, Carpenter Ridge Tuff, central San Juan volcanic field, Colorado. Contributions to Mineralogy and Petrology 107: 219-230.

Droop, G.T.R. 1987. A general equation for estimating Fe (super 3+) concentrations in ferromagnesian silicates and oxides from microprobe analyses, using stoichiometric criteria. Mineralogical Magazine 51: 431-435.

Druitt, T.H. 1995. Settling behaviour of concentrated dispersions and some volcanological applications. Journal of Volcanology and Geothermal Research 65: 27-39.

Druitt, T.H. 1996. Turbulent times at Taupo. Nature 381: 476-477.

Druitt, T.H., and Sparks, R.S.J.1982. A proximal ignimbrite facies on Santorini, Greece. Journal of Volcanology and Geothermal Research 13: 147-171.

Druitt, T.H., and Bacon, C.R. 1986. Lithic breccia and ignimbrite erupted during the collapse of Crater Lake caldera, Oregon. Journal of Volcanology and Geothermal Research 29: 1-32.

Druitt, T., Lanphere, M., and Vougioukalakis, G. 1996. Santorini: guide and excursions. IAVCEI commission on explosive volcanism fieldguide. 88 pgs.

Duffield, W.A., and Ruiz, J. 1992. Compositional gradients in large reservoirs of silicic magma as evidenced by ignimbrites versus Taylor Creek rhyolite lava domes. Contributions to Mineralogy and Petrology 110: 192-210.

Dunbar, N.W., and Kyle, P.R. 1992. Volatile contents of obsidian clasts in tephra from the Taupo Volcanic Zone, New Zealand; implications to eruptive processes. Journal of Volcanology and Geothermal Research 49: 127-145.

Dunbar, N.W., Kyle, P.R. and Wilson, C.J.N. 1989. Evidence for limited zonation in silicic magma systems, Taupo Volcanic Zone, New Zealand. Geology 17: 134-236.

Duncan, A.M., Cole, P.D., Guest, J.E., Chester, D.K. 1996. Transport and emplacement mechanisms of mass-flow deposits on Monte Vulture volcano, Basilicata, southern Italy. Geological Society Special Publication 110:237-247.

Eby, G.N. 1990. The A-type granitoids: a review of their occurrence and chemical characteristics and speculations on their petrogenesis: Lithos 26: 115-134.

Eby, G.N. 1992. Chemical subdivision of the A-type granitoids: petrogenetic and tectonic implications. Geology 20: 641-644.

Eichelberger, J.C., and Koch, F.G. 1979. Lithic fragments in the Bandelier tuff, Jemez mountains, New Mexico. Journal of Volcanology and Geothermal Research., 5: 115-134.

Ewart, A., 1968. The petrography of the central North Island rhyolitic lavas. Part 2-Regional petrography including notes on associated ash flow pumice deposits. N.Z.J. Geol. Geophys. 11: 478-545.

Ewart, A., and Cole, J.W. 1967. Textural and mineralogical significance of the granitic xenoliths from the Central Volcanic region, North Island, New Zealand. N.Z.J. Geol. Geophys. 10: 31-54.

Ewart, A., and Griffin, W.L. 1994. Application of proton-microprobe data to trace-element partitioning in volcanic rocks. Chemical Geology 117: 251-284.

Ewart, A., and Hawkworth, C.J. 1987. The Pleistocene-Recent Tonga-Kermadec Arc lavas; interpretation of new isotopic and rare earth data in terms of depleted mantle source model. Journal of Petrology 28: 495-530.

Ewart, A., Hildreth, W., and Carmichael, I.S.E. 1975. Quaternary Acid magma in New Zealand. Contributions to Mineralogy and Petrology 51: 1-27.

Fiersmans, M., and De Paepe, P. 1982. Genesis of tourmalinites from Belgium: petrographic and chemical evidence. Mineralogical Magazine 46: 95-102.

Fierstein, J., and Hildreth, W. 1992. The plinian eruptions of 1912 at Novarupta, Katmai National Park, Alaska: Bulletin of Volcanology 54: 646-684

Fisher, R.V. 1966. Mechanism of deposition from pyroclastic flows. American Journal of Science 264: 350-363.

Fisher, R.V. 1990. Transport and deposition of a pyroclastic surge across an area of high relief: The 18 May 1980 eruption of Mount St Helens, Washington. Geol. Soc. Am. Bull. 102: 1038-1054.

Fisher, R.V. 1995. Decoupling of pyroclastic currents: hazards assessments. Journal of Volcanology and Geothermal Research 66: 257-263.

Fisher, R.V., Orsi, G., Ort, M., Heiken, G. 1993. Mobility of a large-volume pyroclastic flow-emplacement of the Campanian ignimbrite, Italy. Journal of Volcanology and Geothermal Research 56: 205-220.

Folk, R.L., Andrews, P.B., and Lewis, D.W. 1970. Detrital sedimentary rock classification and nomenclature for use in New Zealand: N.Z.J. Geology and Geophysics 13: 937-968.

Freundt, A., and Schmincke, H.U. 1992a. Mixing of rhyolite, trachyte and basalt magma erupted from a vertically and laterally zoned reservoir, composite flow P1, Gran Canaria, Contributions to Mineralogy and Petrology 112: 1-19.

Freundt, A., and Schmincke, H.U. 1992b. Abrasion in pyroclastic flows. Geologische Rundschau 81/2: 383-389.

Froggatt, P.C. 1983. Toward a comprehensive Upper Quaternary tephra and ignimbrite stratigraphy in New Zealand using electron microprobe analysis of glass shards. Quaternary Research 19: 188-200.

Gamble, J.A., Smith, I.E.M., McCulloch, M.T., Graham, I.J., and Kokelaar, B.P. 1993. The geochemistry of basalts from the Taupo Volcanic Zone and Kermadec Island Arc, S.W. Pacific. Journal of Volcanology and Geothermal Research 54: 265-290.

Geschwind, C.H., and Rutherford, M.J. 1992. Cummingtonite and the evolution of the Mount St Helens magma system: an experimental study. Geology 20: 1011-1014.

Gill, J.B. 1981. Orogenic andesites and plate tectonics. Springer, Berlin.

Giggenbach, W.F. 1995. Variations in the chemical and isotopic composition of fluids discharged from the Taupo Volcanic Zone. Journal of Volcanology and Geothermal Research 68: 89-116.

Graham, I.J. and Hackett, W.R. 1987. Petrology of calc-alkaline lavas from Ruapehu volcano and related vents, Taupo Volcanic Zone, New Zealand. Journal of Petrology 28: 531-567.

Graham, I.J., Blattner, P. and McCulloch, M.T. 1990. Meta-igneous granulite xenoliths from Mount Ruapehu, New Zealand: fragments of altered oceanic crust? Contributions to Mineralogy and Petrology 105: 650-661.

Graham, I.J., Gulson, B.L., Hedenquist, J.W. and Mizon, K. 1992. Petrogenesis of late Cenozoic volcanic rocks from the Taupo Volcanic Zone, New Zealand, in light of new lead isotope data. Geochim. Cosmochim. Acta., 56: 2797-2819.

Graham, I.J., Cole, J.W., Briggs, R.M., Gamble, J.A., and Smith, I.E.M. 1995. Petrology and petrogenesis of volcanic rocks from the Taupo Volcanic Zone, New Zealand: a review. Journal of Volcanology and Geothermal Research 68: 59-87.

Grange, L.I. 1937. The geology of the Rotorua-Taupo subdivision, Rotorua and Kaimanawa divisions. New Zealand Geol. Surv. Bull 37. 138 pages.

Grapes, R., Thornton, J., and Howard, D. 1993. Vug minerals in rhyolite, Hendersons Quarry, Mount Ngongotaha. Geological Society of New Zealand Miscellaneous Publication 79A: 76.

Grindley, G.W. 1959. Sheet N85, Waiotapu. Geological Map of New Zealand 1:63360. Department of Scientific and Industrial Research, Wellington, New Zealand.

Grindley, G.W., Mumme, T.C., and Kohn, B. 1994. Stratigraphy, paleomagnetism, geochronology and structure of silicic volcanic rocks, Waiotapu/Paeroa Range area. Geothermics 23: 473-499.

Grunder, A.L., and Mahood, G.A. 1988. Physical and chemical models of zoned silicic magmas: the Loma Seca Tuff and Calabozos Caldera, Southern Andes. Journal of Petrology 29: 831-867.

Habteselassie, M.M., Mathison, C.I., and Gilkes, R.J. 1996. Vanadium in magnetite gabbros and its behaviour during lateritic weathering, Winimurra complex, Western Australia. Australian Journal of Earth Sciences 43: 555-566.

Healy, J. 1992. Central Volcanic Region. In. Landforms of New Zealand. Soons, J., and Selby, M. 256-286.

Healy, J., Schofield, J.C. and Thompson, B.N. 1964. Sheet 5 Rotorua; Geological Map of New Zealand 1: 250,000. Department of Scientific and Industrial Research, Wellington, New Zealand.

Hedenquist, J.W., 1983. Waiotapu, New Zealand: the geochemical evolution and mineralization of an active hydrothermal system. Unpublished Ph.D. thesis, University of Auckland, Auckland, New Zealand.

Henry, D.J., and Dutrow, B.L. 1996. Metamorphic tourmaline and its petrologic applications. In: Grew, E.S., and Anovitz, L.M. (eds) Boron: mineralogy, petrology and geochemsitry. Reviews in Mineralogy 33: 503-557.

Henry, D.J. and Guidotti, C.V. 1985. Tourmaline as a petrogenetic indicator mineral: an example from the staurolite-grade metapelites of NW Maine. American Mineralogist 70: 1-15.

Hervig, R.L., and Dunbar, N.W. 1992. Causes of chemical zoning in the Bishop (California) and Bandelier (New Mexico) magma chambers. Earth Planet. Sci. Lett 11: 97-108.

Hildreth, W. 1979. The Bishop Tuff: Evidence for the origin of compostional zonation in silicic magma chambers. In: C.E. Chapin, and W.E. Elston (Eds), ash Flow Tuffs. Geological Society of America Special Paper 180: 43-84.

Hildreth, W., 1981. Gradients in silicic magma chambers: implications for lithospheric magmatism. Journal of Geophysical Research 86: 10153-10192.

Hildreth, W. 1983 Comment on 'chemical differentiation of the Bishop Tuff and other high-silica magmas through crystallization processes. Geology 11: 622-623.

Hildreth, W., and Mahood, G.A. 1985. Correlation of ash-flow tuffs. Geological Society of America Bulletin 96: 968-974.

Hildreth, W., and Mahood, G.A. 1986. Ring fracture eruption of the Bishop Tuff. Geological Society of America Bulletin 97: 396-403.

Hildreth, W., Halliday, A.N., and Christiansen, R.L. 1991. Isotopic and chemical evidence concerning the genesis and contamination of basaltic and rhyolitic magma beneath the Yellowstone Plateau Volcanic Field. Journal of Petrology 32: 63-138.

Hochstein, M.P., Smith, I.E.M., Regenauer-lieb, K. and Ehara, S. 1993. Geochemistry and heat transfer processes in Quaternary rhyolitic systems of the Taupo Volcanic Zone, New Zealand. Tectonophysics., 223: 213-235.

Holgate, M. 1977. Tourmaline from amphibolitised gabbro at Hanter hill, Radnorshire. Mineralogical Magazine 41: 124-127.

Houghton, B.F., Wilson, C.J.N., McWilliams, M.O., Lanphere, M.A., Weaver, S.D., Briggs, R., and Pringle, M.S. 1995. Chronology and dynamics of a large silicic magma system; central Taupo volcanic zone, New Zealand. Geology 23: 13-16.

Housden, J., O'Reilly, W., and Day, S.J. 1996. Variations in magnetic properties of unit 10, eastern layered intrusion, Isle of Rhum, Scotland: implications for patterns of high temperature hydrothermal alteration. Transactions of the Royal Society of Edinburgh: Earth Sciences 86: 91-112.

Howard, J. L. 1993. The statistics of counting clasts in rudites: a review, with examples from the upper Palaeogene of southern California, USA. Sedimentology 40: 157-174.

Hunt,T.M., and Glover, R,B. 1994. Waimangu, Waiotapu, and Waikite geothermal systems, New Zealand. Geothermics 23: 373-661.

Hunt, T.M., Glover, R.B., and Wood, C.P. 1994. Waimangu, Waiotapu, and Waikite geothermal systems, New Zealand; background and history. Geothermics 23: 379-400.

Hurst, V.J.,and Kunkle, A.C. 1985. Dehydroxylation, rehydroxylation, and stability of kaolinite. Clays and Clay Minerals 33: 1-14.

Hutton, D.H.W., and Reavy, R.J. 1992. Strike slip tectonics and granite petrogenesis. Tectonics 11: 960-967.

Iddings, J.P. 1888. Obsidian cliff, Yellowstone National Park. Department of the Interior, U.S. Geological Survey. 285pgs.

Ito, E., White, W.M., and Goepal, C. 1987. The O, Sr, Nd and Pb isotope geochemistry of MORB. Chemical Geology 62: 157-176.

Janeczek, J. 1989. Manganoan fayalite and products of its alteration from the Strzegom pegmatites, Poland. Mineralogical Magazine 53: 315-325.

Johnson, C.M. 1989. Isotopic zonation in silicic magma chambers. Geology 17: 1136-1139.

Karhunen, R.A. 1993. The Pokai and Chimp Ignimbrites of NW Taupo Volcanic Zone. Unpublished Ph.D. thesis, University of Canterbury, Christchurch, New Zealand.

Kawamoto, T. 1992. Dusty and honeycomb plagioclase: indicators of processes in the Uchino stratified magma chamber, Izu Peninsula, Japan. Journal of Volcanology and Geothermal Research 49: 191-208.

Keall, J.M. 1988. Volcanology and ignimbrite stratigraphy along the Paeroa Fault, Taupo Volcanic Zone. Unpublished M.Sc. thesis, Victoria University, Wellington, New Zealand.

Kneller, B.C., and Branney, M.J. 1995. Sustained high-density turbidity currents and the deposition of thick massive sands. Sedimentology 42: 607-616.

Komor, S.C., Elthon, D., and Casey, J.F. 1987. Petrology of a leucogabbroic interval within basal layered gabbros at North Arm Mountain, Bay of Islands Ophiolite. Contributions to Mineralogy and Petrology 95: 278-300.

Krippner, S.J. 1996. Petrology and geochemistry of lithic ejecta sampled from Mangakino volcanic centre-derived ignimbrites, Taupo Volcanic Zone, New Zealand. Unpublished MSc thesis, Waikato University, Hamilton.

Leake, B.E. 1978. Nomenclature of amphiboles. American Mineralogist 63: 1023-1052.

Lee, I. W. 1996. Component analysis of lag breccia in the youngest Toya pyroclastic flow deposit; southwest Hokkaido, Japan. Bull. Volcanol. Soc. Japan 41: 31-34.

Le Maitre, R.W. (ed) 1989. A classification of igneous rocks and glossary of terms. Blackwell, Oxford.

Lindsay, J.M., Williams, I.S., Ireland, T.R., Black, P.M., and Smith, I.E.M. 1995. Zircon ages in young rhyolites and zircon age distributions in greywacke terranes, North Island, New Zealand. Geological Society of New Zealand Miscellaneous Publication 81A: 138.

Lipman, P.W. 1965. Chemical comparison of glassy and crystalline volcanic rocks. U.S. Geological Survey Bull. 1201: 1-24.

Lipman, P.W. 1967. Mineral and chemical variations within an ash-flow sheet from Aso Caldera, southwestern Japan. Contributions to Mineralogy and Petrology 16: 300-327.

Lipman, P.W. 1984 . The roots of ash flow calderas in western North America: windows into the tops of granitic batholiths. Journal of Geophysical Research 89: 8801-8841.

Lipman, P.W. Submitted to Bulletin of Volcanology. Subsidence of ash-flow calderas: relation to caldera size and magma-chamber geometry.

Lloyd, E.F. 1972. Geology and hot springs of Orakeikorako. N.Z. Geological Survey Bulletin 85.

London, D., Morgan VI, G.B., and Wolf, M.B. 1996. Boron in granitic rocks and their contact aureoles. In: Grew, E.S., and Anovitz, L.M. (eds) Boron: mineralogy, petrology and geochemsitry. Reviews in Mineralogy 33: 299-330.

Lowther, K.J., Briggs, R.M., and Lowe, K.J. 1996. Quaternary geology and tephrostratigraphy of the north-eastern Rotorua region. Geological Society of New Zealand Miscellaneous Publication 91A: 114.

McCulloch, M.Y., Kyser, T.K., Woodhead, J.D., and Kinsley, L. 1994. Pb-Sr-Nd-O isotopic constraints on the origin of rhyolites from the Taupo Volcanic Zone of New Zealand: evidence for assimilation followed by fractionation from basalt. Contributions to Mineralogy and Petrology 115: 303-312.

Macdonald, R., Smith, R.L., and Thomas, J.E. 1992. Chemistry of subalkalic obsidians. U.S. Geol. Surv. Prof. Pap. 1523: 214pp.

Mahood, G.A. 1981. Chemical evolution of a Pleistocene rhyolitic center: Sierra La Primavera, Jalisco, Mexico. Contributions to Mineralogy and Petrology 77: 129-149.

Manning, D.A. 1995. The Chimp Ignimbrite; a widespread and chemically distinctive late Pleistocene ignimbrite. Geological Society of New Zealand Miscellaneous Publication 81A: 141.

Manning, D in press. Middle to late Pleistocene tephrostratigraphy of the eastern Bay of Plenty. Quaternary International.

Marshall, P. 1935. Acid rocks of the Taupo-Rotorua Volcanic District. Transactions of the Royal Society of New Zealand 64: 323-366.

Martin, R.C., 1961. Stratigraphy and structural outline of the Taupo Volcanic Zone. N.Z. J. Geol. Geophys. 2: 449-478.

Martin, R.C., and Lewis, J.F. 1963. Nature of glass in New Zealand ignimbrites. Nature 197: 1166-1167.

Maas, R., and Mc Culloch, M.T. 1991. The provenance of Archean clastic metasediments in the Narryer Gneiss Complex, Western Australia: trace element geochemistry, Nd isotopes, and U-Pre-Baton ages for detritial zircons. Geochimica et Cosmochimica Acta 55: 1915-1932.

Michael, P.J. 1983. Reply on 'Chemical differentiation of the Bishop Tuff and other high silica magma through crystallization processes'. Geology 11: 623-624.

Mills Jr, J.G., and Rose, T.P. 1991. Manganoan fayalite: A new occurrence in rhyolitic ash-flow tuff, southwestern Nevada, U.S.A. American Mineralogist 76: 288-292.

Modriniak, N., and Studt, F.E. 1959. Geological structure and volcanism of the Taupo-Tarawera district. N.Z.J. Geol. Geophys., 2:654-684.

Morimoto, N. 1989. Nomenclature of pyroxenes. Canadian Mineralogist 27: 143-156.

Mortimer, N. 1995. Origin of the Torlesse terrane and coeval rocks, North Island, New Zealand. International Geology Review 36: 891-910.

Nairn, I.A., 1973. Geology of the Waimangu Geothermal Mapping Project Area, Central Volcanic Region, New Zealand. Report Open File. Unpublished. NZ Geological Survey, Rotorua.

Nairn, I.A., 1981. Some studies of the geology, volcanic history, and geothermal resources of the Okataina volcanic centre, Taupo Volcanic Zone, New Zealand. Unpublished Ph.D. thesis, Victoria University, Wellington, New Zealand.

Nairn, I.A. 1984. Stratigraphic drillholes at Rerewhakaitu. Unpublished NZGS preliminary report. 6 pgs.

Nairn, I.A., 1989. Sheet V16AC Tarawera; Geological Map of New Zealand 1: 50,000. Department of Scientific and Industrial Research, Wellington, New Zealand.

Nairn, I.A., and Hull, A.G. 1985. Post-1800 years displacements on the Paeroa Fault Zone, Taupo Volcanic Zone, New Zealand. New Zealand Geological Survey Record 8, research notes: 135-142.

Nairn, I.A., Wood, C.P., and Bailey, R.A. 1994. The Reporoa Caldera, Taupo Volcanic Zone: source of the Kaingaroa Ignimbrites. Bulletin of Volcanology 56: 529-537.

Nairn, I.A., McKee, C.O., Talai, B., and Wood, C.P. 1995. Geology and eruptive history of the Rabaul Caldera area, Papua New Guinea. Journal of Volcanology and Geothermal Research 69: 255-284.

Nakamura, N. 1974. Determination of REE, Ba, Fe, Mg, Na and K in carbonaceous and ordinary chrondrites. Geochimica et Cosmochimica Acta 38: 757-775.

Naney, M.T. 1983. Phase equilibria of rock-forming ferromagnesian silicates in granitic systems. America Journal of Science 283: 993-1033.

Nash, W.P., and Crecraft, H.R. 1985. Partition coefficients for trace elements in silicic magmas. Geochimca et Cosmochimica Acta 49: 2309-2322.

Nicholls, I.A., Oba, T., and Conrad,W.K. 1992. The nature of primary rhyolitic magmas involved in crustal evolution: evidence from an experimental study of cummingtonite-bearing rhyolites, Taupo Volcanic Zone, New Zealand. Geochimca et Cosmochimica Acta 56: 955-962.

Norrish, K., and Hutton, J.T. 1969. An accurate X-ray spectrographic method for the analysis of a wide range of geological samples. Geochimica et Cosmochimica Acta 33: 431-453.

Obata, M. 1980. The Ronda peridotite; garnet-, spinel-, and plagioclase-lherzolite facies and the P-T trajectories of a high-temperature mantle intrusion. Journal of Petrology 21: 533-572.

Okumura, S. 1985. Neoformation of allophane and gibbsite from plagioclase during weathering process of gabbro. Journal of Geosciences, Osaka City University 28: 85-103.

Orsi, G., Civetta, L., Antonio, M.D., Di Girolamo, P., Piochi, M. 1995. Step-filling and development of a three-layer magma chamber: the Neapolitan Yellow Tuff case history. Journal of Volcanology and Geothermal Research 67: 291-312.

Palacz, Z.A., and Wolff, J.A. 1989. Strontium, neodymium and lead isotope characteristics of the Granadilla Pumice, Tenerife: a study of the causes of strontium isotope disequilibrium in felsic pyroclastic deposits. Geological Society Special publication 42: 147-159.

Palladino, D.M., and Valentine, G.A. 1995. Coarse-tail vertical and lateral grading in pyroclastic flow deposits of the Latera Volcanic Complex (Vulsini, central Italy): origin and implications for flow dynamics. Journal of Volcanology and Geothermal Research 69: 343-364.

Pain, C.F., and Pullar, W.A. 1975. Chronology of 'paleosurfaces' and present land surfaces in the Reporoa Basin, North Island, New Zealand. N.Z. J. Sci., 18: 313-322.

Pankhurst, R.J., and Rapela, C.R. 1995. Production of Jurassic rhyolite by anatexis of the lower crust of Patagonia. Earth and Planetary Science Letters 134: 23-36.

Pearce, J.A., and Cann, J.R. 1973. tectonic setting of basic rocks determined using trace element geochemistry analyses. Earth and Planetary Sciences Letters 12: 339-349.

Pearce, J.A., Harris, N.B.W., Tindle, A.G. 1984. Trace element discrimination diagrams for the tectonic interpretation of granitic rocks. Journal of Petrology 25: 956-983.

Potter, D.B., and Oberthal, C.M. 1987. Vent sites and flow directions of the Otowi ash flows (lower Bandelier Tuff), New Mexico. Geological Society of America Bulletin 98: 66-76.

Reid, F.W. 1983. Origin of the rhyolitic rocks of the Taupo volcanic Zone, Journal of Volcanology and Geothermal Research 15: 315-338.

Reid, F.W., and Cole, J.W. 1983. Origin of dacites of Taupo Volcanic Zone, New Zealand. Journal of Volcanology and Geothermal Research 18: 191-214.

Reynes, A.G., and Giggenbach, W.F. 1992. Petrology and fluid chemistry of magmatic-hydrothermal systems in the Philippines. In: Kharaka and Maest (eds). Water-Rock interaction, Rotterdam. 1341-1344.

Riciputi, L.R., Johnson, C.M., Sawyer, D.A., and Lipman, P.W. 1995. Crustal and magmatic evolution in a large multicyclic caldera complex: isotopic evidence from the central San Juan volcanic field. Journal of Volcanology and Geothermal Research 67: 1-28.

Risk, G.F., Caldwell, T.G., and Bibby, H.M. 1994. Deep resistivity surveys in the Waiotapu-Waikite-Reporoa region, New Zealand. Geothermics 23: 423-443.

Ritchie, A.B.H. 1996. Volcanic geology and geochemistry of Waiotapu Ignimbrite, Taupo Volcanic Zone, New Zealand. Unpublished MSc thesis, University of Canterbury, Christchurch.

Rogan, N. 1982. A geophysical study of the Taupo volcanic zone, New Zealand. Journal of Geophysical Research B 87: 4073-4088.

Roobol, M.J., Smith, A.L., and Wright, J.V. 1987. Lithic breccias in pyroclastic flow deposits on St.Kitts, West Indies. Bulletin of Volcanology 49: 694-707.

Rosi, M., Vezzoli, L., Aleotti, L., and De Censi, M. 1996. Interaction between caldera collapse and eruptive dynamics during the Campanian Ignimbrite eruption, Phlegrean Fields, Italy. Bulletin of Volcanology 57: 541-544.

Ross, C.S., and Smith, R.L. 1961. Ash flow tuffs; their origin, geologic relations, and identification. U.S. Geological Survey professional paper 366: 81 p.

Rubin, J.N., Henry, C.D., and Price, J.G. 1993. The mobility of zirconium and other "immobile" elements during hydrothermal alteration. Chemical Geology 110: 29-47.

Ruiz, J., Patchett, P.J., and Arculus, R.J. 1988. Nd-Sr isotopic composition of lower crustal xenoliths- evidence for the origin of mid-Tertiary felsic volcanics in Mexico. Contributions to Mineralogy and Petrology 99: 36-43.

Rutherford, M.J.1993. Experimental petrology applied to volcanic processes. EOS 74: 49, 55.

Rutherford, M.J., and Devine, J.D. 1988. The May 18, 1980 eruption of Mount St. Helens 3. Stability and chemistry of amphibole in the magma chamber. J. Geophys. Res 93: 11949-11959.

Schubert, W. 1977 Reaktionen im alpinotypen Peridotitmassiv von Ronda (Spanien) und seinen partiellen Schmelzprodukten. Contributions to Mineralogy and Petrology 62: 205-220.

Schubert, W. 1979. Ca-tschermakitic orthopyroxene from the Ronda peridotite, Spain. Neues Jahrbuch fuer Mineralogie. Monatshefte 5: 210-216.

Schumacher, R., and Mues-Schumacher, U. 1996. The Kizilkaya ignimbrite-an unusual low-aspect-ratio ignimbrite from Cappadocia, central Turkey. Journal of Volcanology and Geothermal Research 70:107-121.

Schuraytz, B., Vogel, T.A., and Younker, L.W. 1989. Evidence for dynamic withdrawal from a layered magma body: The Topopah Spring Tuff, south-western Nevada. Journal of Geophysical Research 94: 5925-5942.

Self, S. 1983. Large-scale phreatomagmatic silicic volcanism, a case study from New Zealand: Journal of Volcanology and Geothermal Research 17: 433-469.

Shepherd 1991. Volcanology and petrology of the post-caldera rhyolitic domes, Rotorua volcanic centre. Unpublished B.Sc (hons) thesis. Victoria University of Wellington.

Shinonaga, T., Ebihara, M., Nakahara, H., Tomura, K., and Heumann, K.G. 1994. Cl, Br and I in igneous standard rocks. Chemical Geology 115: 213-225.

Simmons, S.F., and Weaver, S.D. 1995. Preface. Taupo Volcanic Zone, New Zealand special issue. Journal of Volcanology and Geothermal Research 68:vii.

Skjerklie, K.P., and Johnston, A.D. 1992. Vapor-absent melting at 10 kbar of a biotite- and amphibole-bearing tonalitic gneiss; implications for the generation of A-type granites. Geology 20: 263-266.

Slack, J.F. 1996. Tourmaline associations with hydrothermal ore deposits In: Grew, E.S., and Anovitz, L.M. (eds) Boron: mineralogy, petrology and geochemsitry. Reviews in Mineralogy 33: 559-643.

Slack, J.F., and Coad, P.R. 1989. Multiple hydrothermal and metamorphic events in the Kidd Creek volcanogenic massive sulphide deposit, Timming, Ontario: evidence from tourmalines and chlorites. Canadian Journal of Earth Sciences 26: 694-715.

Smith, I.E.M. 1989. Magma chamber processes beneath large rhyolitic volcanoes of the Taupo Volcanic Zone, New Zealand. I.A.V.C.E.I., Abstract volume, New Mexico Bureau of Mining and Mineral Resources Bulletin 131: 248.

Smith, I.E.M., and Gamble, J.A. 1993. Northland and Taupo Zone volcanism, North Island, New Zealand. IAVCEI Field Trip Guide C6, Canberra, 35pgs.

Smith. R.D., Cameron, K.L., McDowell, F.W., Niemeyer, S., and Sampson, D.E. 1996. Generation of voluminous silicic magmas and formation of mid-Cenozoic crust beneath north-central Mexico: evidence from ignimbrites, associated lavas, deep crustal granulites, and mantle pyroxenites. Contributions to Mineralogy and Petrology 123: 375-389.

Smith, R.L., 1960. Ash flows. Geological Society of America Bulletin 71: 795-841.

Smith, R.L. 1979. Ash flow magmatism. In: C.E. Chapin and W.E. Elston (eds). Ash Flow Tuffs, Geological Society of America Special Paper 180.

Smith, R.L., and Shaw, H.R. 1975. Igneous-related geothermal systems. U.S. Geological Survey Circular. Assessment of geothermal resources of the United States: 58-83.

Smith, R.T., and Houghton, B.F. 1996. Vent migration and changing eruptive style during the 1800a Taupo eruption: new evidence from the Hatepe and Rotongaio phreatoplinian ashes. Bulletin of Volcanology 57: 432-439.

Sneed, E.D., and Folk, R.L. 1958. Pebbles in the lower Colorado River, Texas, a study in particle morphogenesis. Journal of Geology 66: 114-150.

Snetsinger, K.G. 1967. High alumina allophane as a weathering product of plagioclase. American Mineralogist 52: 254-262.

Soengkono, S., and Hochstein, M.P. 1996. Interpretation of magnetic anomalies over the Reporoa geothermal field, Taupo Volcanic Zone, New Zealand. Proceedings 18th NZ Geothermal Workshop: 243-248.

Sparks, R.S.J.1976. Grainsize variations in ignimbrites and implications for the transport of pyroclastic flows. Sedimentology 23: 147-188.

Sparks, R.S.J., Self, S., and Walker, G.P.L. 1973. Products of ignimbrite eruptions. Geology 1: 115-118.

Sparks, R.S.J., Francis, P.W., Hamer, R.D., Pankhurst, R.J., O'Callaghan, L.O., Thorpe, R.S., and Page, R. 1985. Ignimbrites of the Cerro Galan Caldera, NW Argentina. Journal of Volcanology and Geothermal Research 24: 205-248.

Spidle, M.N., Brearley, A.J., and Papike, J.J. 1993. Alteration of plagioclase and pyroxene phenocrysts in a fissure fumarole, Valley of Ten Thousand Smokes, Alaska. American Mineralogist 78: 1066-1081.

Stagpoole, V.M. 1994. Interpretation of refraction seismic and gravity data across the eastern margin of the Taupo Volcanic Zone, New Zealand. Geothermics 23: 501- 510.

Steiner, A. 1960. Origin of ignimbrites of the North Island, New Zealand: a new petrogenetic concept. N.Z. Geological Survey Bulletin 68.

Steiner, A.1963. The rocks penetrated by drillholes in the Waiotapu thermal area, and their hydrothermal alteration. DSIR Bulletin 155: 26-34.

Stimac, J. in press. Hornblende dacite pumice in the Tshirege Member of the Bandelier Tuff: implications for magma chamber and eruptive processes. New Mexico. Geol. Soc. Guidebook 47th Field Conference, Sept 25-28.

Stimac, J., Hickmott, D., Abell, R., Larocque, A.C.L., Broxton, D., Gardner, J., Chipera, S., Wolff, J., and Gauerke, E. 1996. Redistribution of Pb and other volatile trace metals during eruption, devitrification, and vapor-phase crystallization of the Bandelier Tuff, New Mexico. Journal of Volcanology and Geothermal Research 73: 245-266.

Streck, M.L., and Grunder, A.L. 1995. Crystallization and welding variations in a widespread ignimbrite sheet; the Rattlesnake tuff, eastern Oregon, USA. Bulletin of Volcanology 57: 151-169.

Streck, M.L., and Grunder, A.L. 1997. Compositional gradients and gaps in high-silica rhyolites of the Rattlesnake Tuff, Oregon. Journal of Petrology 38: 133-163.

Sun, S.S., and McDonough, W.F. 1989. Chemical and isotopic systematics of oceanic basalts: implications for mantle compositions and processes. in A.D. Saunders and M.J. Norry (eds) Magmatism in the Ocean Basins. Geol. Soc. London. Spec. Pub. 42: 313-345.

Suggate, R.P., and Watters, W.A. 1991. "Inside-out weathering" of boulders in glacial outwash gravel. New Zealand Journal of Geology and Geophysics 34: 93-97.

Sutton, A.N., Blake, S., and Wilson, C.J.N. 1995. An outline geochemistry of rhyolitic eruptives from Taupo volcanic centre, New Zealand. Journal of Volcanology and Geothermal Research 68: 153-175.

Sutton, R. 1990. The geology, petrography and geochemistry of the area surrounding Rangatira Point, northeast Lake Taupo, New Zealand. Unpublished B.Sc (hons) thesis, Victoria University, Wellington.

Suzuki-Kamata, K. 1988. The ground layer of Ata pyroclastic flow deposit, southwestern Japan - evidence for the capture of lithic fragments. Bulletin of Volcanology 50: 119-129.

Suzuki-Kamata, K., Kamata, H., and Bacon, C.R. 1993. Evolution of the caldera-forming eruption at Crater Lake, Oregon, indicated by component analysis of lithic fragments. Journal of Geophysical Research 98: 14059-14074.

Tanaka, H., Turner, G.M., Houghton, B.F., Tachibana, T., Kono, M., and McWilliams, M.O. 1996. Palaeomagnetism and chronology of the central Taupo Volcanic Zone, New Zealand. Geophys. J. Int.124: 919-934.

Tsuchiyama, A. 1985. Dissolution kinetics of plagioclase in the melt of the system diopside-albite-anorthite, and the origin of dusty plagioclase in andesites. Contributions to Mineralogy and Petrology 89: 1-16.

Valentine, G.A., Wohletz, K.H., and Kieffer, S.W. 1992. Effects of topography on facies and compositional zonation in caldera related ignimbrites. Geological Society of America Bulletin 104: 154-165.

Walker, G.P.L. 1971. Grain-size characteristics of pyroclastic deposits. Journal of Geology 79: 696-714.

Walker, G.P.L., 1985. Origin of coarse lithic breccias near ignimbrite source vents. Journal of Volcanology and Geothermal Research., 25: 157-171.

Warshaw, C.M., and Smith, R.L. 1988. Pyroxenes and fayalites in the Bandelier Tuff, New Mexico: temperatures and comparision with other rhyolites. American Mineralogist 73: 1025-1037.

Watson, E.B. 1979. Zircon saturation in felsic liquids: experimental results and applications to trace element geochemistry. Contributions to Mineralogy and Petrology 70: 407-419.

Watson, E.B., and Harrison, T.M. 1983. Zircon saturation revisited: temperature and composition effects in a variety of crustal magma types. Earth and Planetary Science Letters 64: 295-304.

Weaver, S.D., Gibson, S.L., Houghton, B.F., and Wilson, C.J.N. 1990. Mobility of rare earth and other elements during the crystallisation of peralkaline silicic glasses. Journal of Volcanology and Geothermal Research 43: 57-70.

Weaver, S.D., Adams, C.J., Pankhurst, R.J., and Gibson, I.L. 1992. Granites of Edward VII Peninsula, Marie Byrd Land: anorogenic magmatism related to Antarctic-New Zealand rifting. Transactions of the Royal Society of Edinburgh: Earth Sciences 83:281-290.

Wiesneth, D.W., and Eichelberger, J.C. 1994. Migration of alkalis in melt during crystallization of rhyolite lava. Eos, transactions, American Geophysical Union 75: 44.

Whalen, J.B., Currie, K.L., and Chappell, B.W. 1987. A-type granites: geochemical characteristics, discrimination and petrogenesis. Contributions to Mineralogy and Petrology 95: 407-419.

Whitney, J.A., and Stormer Jr., J.C. 1985. Mineralogy, petrology, and magmatic conditions from Fish Canyon Tuff, central San Juan Volcanic Field, Colorado. Journal of Petrology 26: 726-762.

Wilson, C.J.N. 1980. The role of fluidisation in the emplacement of pyroclastic flows: an experimental approach. Journal of Volcanology and Geothermal Research 8: 231-249.

Wilson, C.J.N. 1985. The Taupo eruption. New Zealand II. The Taupo Ignimbrite. Philos. Trans. R. Soc. London. Ser. A. 314: 229-310.

Wilson, C.J.N. 1986. Pyroclastic flows and ignimbrites. Scientific Prog., Oxford 70: 171-207.

Wilson, C.J.N. 1993a Lecture 9: Ignimbrites. In: Houghton and McPhie (eds) IAVCEI short course notes. 17 pgs.

Wilson, C.J.N. 1993b. Stratigraphy, chronology, styles and dynamics of late Quaternary eruptions from Taupo volcano, New Zealand. Philosophical Transactions of Royal Society of London 343-205-306.

Wilson, C.J.N. 1994. Ash-fall deposits from large-scale phreatomagmatic volcanism: limitations of available eruption-column models. U.S. Geological Survey Bulletin 2047: 93-99.

Wilson, C.J.N. 1996. Taupo's atypical arc. Nature 379:27-28

Wilson, C.J.N., and Hildreth, W. in press. The Bishop Tuff: new insights from eruptive stratigraphy. Journal of Geology.

Wilson, C.J.N., Rogan, A.M., Smith, I.E.M., Northey, D.J., Nairn, I.A. and Houghton, B.F. 1984. Caldera volcanoes of the Taupo Volcanic Zone, New Zealand. Journal of Geophysical Research 89: 8463-8484.

Wilson, C.J.N., Houghton, B.F., and Lloyd, E.F. 1986. Volcanic history and evolution of the Maroa-Taupo area, central North Island. Bulletin/Royal Society of New Zealand 23: 194-223.

Wilson, C.J.N., Switsur, V.R., and Ward, A.P. 1988. A new ^{14}C age for the Oruanui (Wairakei) eruption, New Zealand. Geological Magazine 125: 297-300.

Wilson, C.J.N., Houghton, B.F., McWilliams, M.O., Lanphere, M.A., Weaver, S.D., and Briggs, R.M. 1995a. Volcanic and structural evolution of Taupo Volcanic Zone, New Zealand; a review. Journal of Volcanology and Geothermal Research 68: 1-28.

Wilson, C.J.N., Houghton, B.F., Kamp, P.J.J., and McWilliams, M.O. 1995b. An exceptionally widespread ignimbrite with implications for pyroclastic flow emplacement. Nature 378: 605-607.

Wilson, M. 1989. Igneous petrogenesis. Harper Colins Academic. London. 466pgs.

Wolff, J.A. 1985. The effect of explosive eruption processes on geochemical patterns within pyroclastic deposits. Journal of Volcanology and Geothermal Research 26: 189-201.

Wolff, J.A., Worner, G., and Blake, S. 1990. Gradients in physical parameters in zoned felsic magma bodies: implications for evolution and eruptive withdrawal. Journal of Volcanology and Geothermal Research 43: 37-55.

Wood, C.P. 1994a Aspects of the geology of Waimangu, Waiotapu, Waikite and Reporoa geothermal areas, Taupo Volcanic Zone, New Zealand. Geothermics 23: 401-421.

Wood, C.P.1994b. The Waiora Formation geothermal aquifer, Taupo Volcanic Zone, New Zealand. Proceedings 16th New Zealand Geothermal Workshop, Geothermal Institute, University of Auckland:121-126.

Wood, C.P. 1994c. Mineralogy at the magma-hydrothermal system interface in andesite volcanoes, New Zealand. Geology 22; 75-78.

Wood, C.P. 1995. Calderas and geothermal systems in the Taupo Volcanic Zone, New Zealand. Proceedings of the world geothermal congress 1995 (Vol 2): 1331-1336.

Wood, C.P., and Browne, P.R.L. 1996. Chlorine-rich pyrometamorphic magma at White Island volcano, New Zealand. Journal of Volcanology and Geothermal Research 72: 21-35.

Wright, J.V., and Walker, G.P.L. 1977. The ignimbrite source problem: significance of a co-ignimbrite lag-fall deposit. Geology 5: 729-732.

Wright, J.V., and Walker, G.P.L. 1981 .Eruption, transport and deposition of ignimbrite: a case study from Mexico. Journal of Volcanology and Geothermal Research 9: 111-131.

Zielenski, R.A., Lipman, P.W., and Millard Jr, H.T. 1977. Minor-element abundances in obsidian, perlite, and felsite of calc-alkalic rhyolites. American Mineralogist 62: 426-437.

Zingg, T. 1935. Beitrage zur Schotteranalyse: Schweiz. Mineralog. Petrog. Mitt 15:21-29.

Appendix A

Wheao sheet

The Wheao sheet was identified by Dr R.G. Martin (unpublished letters in IGNS files) and J. Healy (unpublished letter in IGNS files) as a grey-pink-purplish fine-grained vitric welded lenticulite overlying purplish Rangitaiki Ignimbrite near Wheao dam. The Wheao sheet, resembles the 0.23 Ma Kaingaroa Ignimbrite, but is distinct in having no andesite lithics. Nowhere can the relationship between the Wheao sheet and Kaingaroa Ignimbrite be identified. Healy noted that the lenticulite also resembles the Matahina Ignimbrite in appearance, while Wilson et al (1984) identified the unit as the upper Kaingaroa Ignimbrite unit (kg_2; WIU, this study) and noted an underlying plinian airfall deposit. This was cited as evidence for the Kaingaroa Ignimbrite being two separate eruptions. In regional maps it was however included in the Rangitaiki Ignimbrite (Healy et al. 1964).

The Wheao sheet occurs in the area near the Wheao and Flaxy dams, upstream of the junction between the Wheao and Rangitaiki rivers. Near Wheao and Flaxy dams it consists of a purple-orange lenticulite, with a non-welded base, and locally a stratified plinian fall deposit, unconformably overlying an erosion surface developed on purplish altered crystal-rich Rangitaiki Ignimbrite. The Wheao sheet overlies the 0.36-0.3 Ma Whakamaru-group ignimbrites.

Figure 1 is a graphic log of the stratigraphy of the Wheao sheet in the Wheao-Flaxy dam area. The basal tephras contain a single white phenocryst-poor (2-3 vol%) pumice type. Oscillatory zoned plagioclase (andesine) is the dominant phenocryst with subordinate brown pleochroic orthopyroxene, quartz and Fe/Ti oxides. Rare glomerocrysts of plagioclase and orthopyroxene are present in some samples. The non-welded base of the sheet consists of a crystal-poor (7-12%) vitric ignimbrite with rhyolitic orange/brown pumice. The matrix has a prominent vitroclastic texture, and no signs of devitrification or vapour-phase alteration. Plagioclase is the dominant phenocryst phase with subordinate orthopyroxene, quartz, Fe/Ti oxides and very rare green-brown hornblende, augite, and xenocrystic biotite.

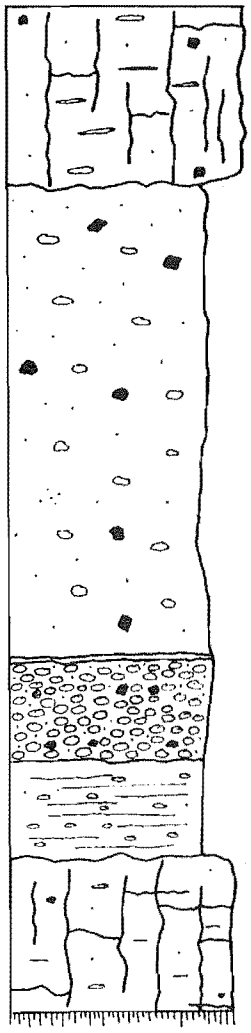

Partially-densely welded purple/orange lenticulite. abundant closley spaced jpoints (1-1.5 m spacing). Crystal- and pumice-poor. Strongly devitrified with prominent axiolitic and spherulitic texture e.g. KA10).

Sharp clay-rich welding break.

Massive non-welded orange/brown lithic-poor ignimbrite. ML = 24 mm; MP = 4 mm.

Non-stratified lithic- and pumice-rich airfall deposit. Abundant obsidian and rhyolite lithics.

Stratified fine-grained airfall deposit. MP = 20 mm.

Locally undulating unconformable contact. No paleosol.

Grey-partially-densely welded crystal-rich quartzose Rangitaiki Ignimbrite

Figure 1. Graphic log of representative section of Wheao sheet near Wheao dam.

Welded sections of the sheet exhibit similar mineralogy, but the matrix shows is strongly devitrified, with prominant axiolitic and localised spherulitic replacement of glass shards, and spherulitic replacement of pumices. Fe/Ti oxides and mafic minerals are altered to hematite and limonite.

Two distinct pumice types, two each from the plinian airfall, and orange non-welded base of the ignimbrite were sampled from the Wheao sheet near Wheao dam for pumice chemistry. All samples exhibit similar mineralogy and chemistry. Samples from the basal tephras (e.g. KA67a and b) exhibit slightly more evolved compositions (e.g. higher Rb/Sr). Pumice XRF analyses are presented in Appendix E.

Lithics sampled from both sites consist predominantly of vesiculated and bladed obsidian lithics, rhyolite, an unknown ignimbrite and a Whakamaru group-like ignimbrite.

The unit exhibits different field, petrographic and geochemical characteristics (Table 1) to the Kaingaroa Ignimbrite but has a similar mineralogy and geochemistry (Fig 2; Table 1), to the Matahina Ignimbrite (Table 1,2). The presence of vesiculated obsidian lithics and similar stratigraphic position also suggest a correlation with the Matahina Ignimbrite.

The Matahina Ignimbrite$_{s.s.}$ has not been dated by Ar/Ar (age quoted in Houghton et al. (1995) is from the Wheao sheet locality). Kohn (in Nairn 1989) reports a zircon fission track age of 0.28 Ma for the Matahina Ignimbrite, similar to the 0.28 Ma age reported by Houghton et al (1995) for the Wheao sheet.

The Matahina Ignimbrite has not been mapped or noted south of Murupara (Bailey and Carr 1994; Bailey pers comm 1993). Bailey (pers comm 1993) suggests the distribution of the Wheao sheet in the Wheao dam region is consistent with Matahina pyroclastic flows having ponded along the Wheao fault scarp, just as did along the Waiohau scarp to the north (Bailey and Carr 1994), this might also explain the unexpectedly greater degree of welding.

A number of miscellaneous welded ignimbrite units have been identified on the southern Kaingaroa Plateau (this study; unpublished reconnaissance mapping Brown

and Beresford 1992-1994). Further work is required on the miscellaneous ignimbrites of southern Kaingaroa Plateau, including correlation of these units with known ignimbrites and identification of new units with distinct sources (Taupo-Reporoa basin?).

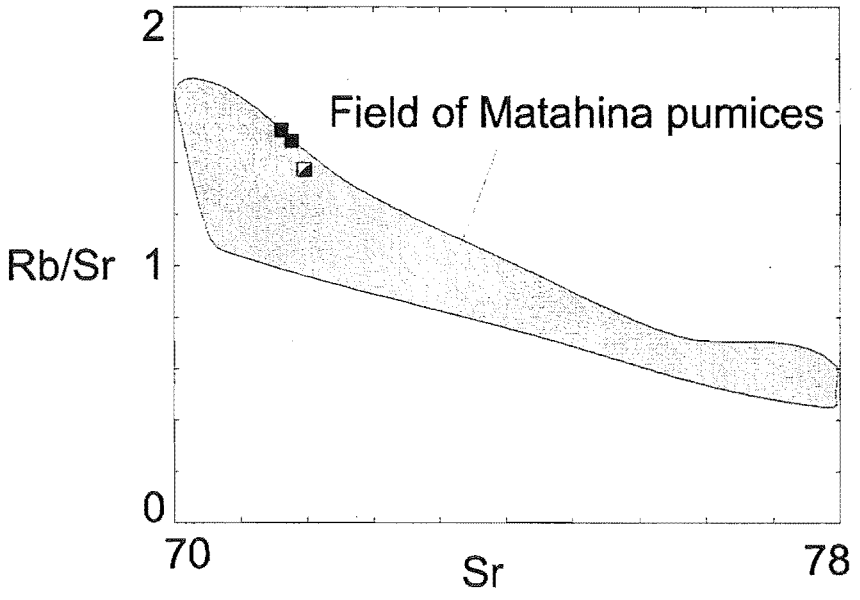

Figure 2. Variation diagram of Wheao sheet pumices illustrating similar chemistry to Matahina Ignimbrite pumices. Matahina Ignimbrite field from Carr (1984).

Table 2	*Wheao sheet*	*Kaingaroa Ignimbrite*	*Matahina Ignimbrite*
Field description and stratigraphy	Basal plinian tephra overlain by non-partially welded purple-orange lenticulite.	Basal tephras, and three ignimbrite members. Upper ignimbrite unit superfically resembles Matahina and Mamaku ignimbrites.	Basal plinian tephra and three welded ignimbrite members
Vapour-phase alteration and devitrification	Extensively devitrified and vapour-phase altered. Well developed axiolitic texture	Middle unit incipiently devitrified Upper unit extensively devitrified, and locally vapour phase altered. Poorly developed axiolitic texture	Extensive devitrification. Upper unit displays extreme vapour-phase alteration.
Mineralogy	Plag + opyx + hb + Fe/Ti oxides $\pm$ augite + xenocrystic biot. opyx > hb	Plag + opyx + Fe/ti oxides $\pm$ hb $\pm$ qtz. opyx >>>hb.	Plag + qtz + hb + opyx + fe/Ti oxides $\pm$ aug. opyx > hb.
Crystal %	2-3% (pumice); 7-12% (ignimbrite)	0.1-3.5% (pumice)	4-16%
SiO_2	74.02-75.22; n=4	69-76%	74-76 %
Rb	122-130	76-128	84-141
Lithic content	Vesiculated and bladed obsidian, rhyolite, unknown ignimbrite, Whakamaru-group ignimbrite	Andesite, Whakamaru-group ignimbrites, Waiotapu Ignimbrite, rare greywacke, gabbro, greywacke and rhyolite.	Vesiculated and bladed obsidian, vitrophyre. Rare granite?
Age	0.28 Ma (Ar/Ar)	0.23 Ma (Ar/Ar)	0.28 Ma (Fission track)
Stratigraphic position	Overlies Whakamaru-group ignimbrites	Overlies Matahina and Whakamaru-group ignimbrites	Overlies Whakamaru-group ignimbrites

Table 2. Comparision of Wheao sheet with Kaingaroa and Matahina ignimbrites. Data from this study, Carr (1984) and Bailey and Carr (1994).

Appendix B

Lithic Componentry data

Lithic type	*PPA*	*LPA*	*UB*	*WHAK*	*WAI*	*MAT*	*SB*	*MISC*	*ALT*	*KG*	*RHY*	*OB*	*GB*	*META*	*RGW*	*GW*	*SED*	*TERT*	*n=*
Basal Tephras																			
Riehana Rd	-	-	-	-	-	21.7	-	-	-	-	5.8	72.5	-	-	-	-	-	-	89
Plateau Rd	-	-	-	-	-	-	-	-	-	-	9.0	91.0	-	-	-	-	-	-	100
M. Valley	-	-	-	-	-	25.4	-	-	-	-	11.3	63.4	-	-	-	-	-	-	71
upper Basal Tephras																			
Riehana Rd	21.1	-	-	22.4	2.6	-	-	-	48.7	-	5.3	-	-	-	-	-	-	-	86
M. Valley	15.6	-	-	25.0		-	-	-	46.9	-	12.5	-	-	-	-	-	-	-	96
RBU																			
No6 Rd	30.6	-	-	25.0	16.7	-	-	2.8	11.1	-	8.3	-	-	-	5.6	-	-	-	72
OWR	26.6	-	-	2.9	2.9	-	-	-	50.0	-	17.6	-	-	-	-	-	-	-	68
M. Valley	33.0	-	-	23.5	7.5	-	0.5	2.5	25.0	-	7.0	-	-	-	-	0.5	0.5	-	100
Riehana Rd	27.1	2.1	3.1	33.3	4.2	-	-	1.1	11.5	-	13.5	-	-	1.0	-	-	3.1	-	96
Lower lag breccia																			
BB Rd quarry	51.6	5.6	-	13.1	13.8	0.3	-	5.3	4.1	3.4	0.9	-	0.6	-	-	-	0.6	0.6	396
BB Rd west	45.1	14.0		12.8	13.1			1.8	8.1	1.8	0.3		1.2	0.3		0.6	0.9		385
BB Rd (east) (TTI)	60.5		-	9.4	19.6	-		-	-	2.6	5.1	-	-	-	-	2.8	-	-	200
Burn Rd	55.7	-	-	14.6	17.6	-	1.6	2.4	3.7	-	2.4	-	-	-	0.4	0.8	0.8	-	406
Burn Rd	64.1	0.5	4.0	3.8	17.6	-	4.0	1.0	2.0	1.0	1.0	-	-	-	0.5	0.5	-	-	386
Burn Rd	57.8	-	0.4	15.5	13.6	-	0.8	1.8	3.9	0.4	0.8	-	-	-	0.4	1.9	2.7	-	514
Rawhiti Rd	63.7	2.6	1.6	19.2	7.8	-	0.5	1.0	0.5	-	1.1	-	1.0	-	-	1.0	-	-	393
Deep Creek Rd	70.7	-	-	5.9	21.8	-	-	1.6	-	-	-	-	-	-	-	-	-	-	388
Shilts Farm	56.0	-	-	12.8	12.8	-	-	9.6	6.4	-	0.8	-	-	-	0.8	-	-	0.8	250
No 3 Rd	56.3	-	-	8.1	22.3	-	0.8	2.1	8.1	-	1.5	-	-	-	-	-	0.8	-	335
No 3 Rd (BTI)	65.2	-	-	17.4	-	-	-	-	17.4	-	-	-	-	-	-	-	-	-	115
Z1Rd	68.2	-	-	6.2	23.4	0.3	-	0.3	1.6	-	-	-	-	-	-	-	-	-	395
Z1 Rd	61.0	-	-	11.5	22.4	-	-	3.3	0.4	-	-	-	-	-	0.4	1.0	-	-	354
No 6 Rd	61.5	2.7	2.5	13.3	10.5	-	-	0.3	2.9	2.7	0.8	-	-	-	1.6	1.2	-	-	445
No 6 Rd	59.5	9.8	1.2	9.9	9.2	-	-	0.8	3.3	4.6	1.2	-	0.3	-	-	-	0.3	-	338
M. Valley (TZ)	64.9	-	-	13.8	10.6	-	-	-	7.4	3.3	-	-	-	-	-	-	-	-	194
Rakau Rd	53.5	-	-	11.2	27.3	-	-	-	5.3	2.7	-	-	-	-	-	-	-	-	387
Old Waiotapu Rd (TZ)	65.7	-	-	8.3	11.2	-	0.7	-	14.1	-	-	-	-	-	-	-	-	-	277

Lithic type	*PPA*	*LPA*	*UB*	*WHAK*	*WAI*	*MAT*	*SB*	*MISC*	*ALT*	*KG*	*RHY*	*OB*	*GB*	*META*	*RGW*	*GW*	*SED*	*TERT*	*Total*
Upper lag breccia .																			
Burn Rd	32.6	-	-	13.4	44.5	-	3.8	2.5	1.3	-	1.3	-	-	-	0.6	-	-	-	391
Burn Rd	42.9	-	-	15.5	37.9	-	1.7	-	1.7	-	0.3	-	-	-	-	-	-	-	403
Burn Rd	53.9	-	-	15.8	11.9	-	11.8	2.6	3.0	-	0.3	-	-	-	-	-	0.7	-	430
No 3 Rd	64.0	-	-	10.3	15.3	-	5.7	-	2.7	-	0.2	-	-	1.2	0.2	0.2	-	-	406
No 6 Rd	50.0	-	-	24.1	8.3	-	11.3	0.5	4.2	-	0.3	-	-	-	0.9	0.2	0.2	-	424
Old Waiotapu Rd (TZ)	20.8	-	-	32.0	18.9	-	-	9.4	15.0	-	3.9	-	-	-	-	-	-	-	103
Plateau Rd (TZ)	59.3	-	-	20.3	3.4	-	-	-	6.8	-	8.5	-	-	-	-	1.7	-	-	99
OWR																			
Burn Rd	45.8	-	-	21.6	21.6	-	-	2.3	4.3	1.1	1.1	-	1.1	-	1.1	-	-	-	83
Burn Rd	38.9	-	-	8.3	5.5	-	-	2.8	-	2.8	38.9	-	2.8	-	-	-	-	-	108
Old Waiotapu Rd	64.8	-	-	3.7	14.8	-	-	-	9.3	-	5.6	-	1.8	-	-	-	-	-	54
M. Valley	42.0	-	-	22.6	12.8	-	-	-	11.3	-	11.3	-	-	-	-	-	-	-	92
Main Gully Rd	28.4	-	-	31.6	6.0	-	-	6.0	-	-	26.0	-	-	2.0	-	-	-	-	106
BB Rd (east)	67.0	-	-	16.0	3.0	-	-	4.0	3.0	4.0	-	-	-	-	-	-	2.0	1.0	100
Coates Rd	37.0	-	-	11.0	24.7	-	1.4	4.1	15.0	-	5.4	-	-	-	-	1.4	-	-	106
Tokiaminga valley	61.5	-	-	11.5	3.9	-	-	-	11.6	-	-	-	7.6	3.9	-	-	-	-	104
Riehana Rd	36.8	-	-	21.0	10.5	-	-	5.3	5.3	-	-	-	10.5	5.3	-	5.3	-	-	76
Kaingaroa'	20.0	-	-	2.0	4.0	-	-	-	-	4.0	-	-	-	-	70.0	-	-	-	100
Kaingaroa'	40.0	-	-	6.0	28.0	-	-	4.0	18.0	-	4.0	-	-	-	-	-	-	-	100
WIU																			
S.H.38 (east)	22.9	-	-	4.8	39.8	-	-	-	25.3	-	-	-	-	-	-	7.2	-	-	83
S.H. 38 (west)	54.0	-	-	10.0	16.0	-	-	2.0	14.0	-	2.0	-	-	-	-	2.0	-	-	100
S.H.38 (west)	53.0	-	-	7.0	24.0	-	-	-	2.0	14.0		-	-	-	-	-	-	-	100
Putunoa	53.8	-	-	28.5	7.7	-	-	-	2.5	5.0	-	-	-	-	-	2.5	-	-	78
Waikite Valley Rd	12.5	-	6.2	18.9	6.0	-	-	-	-	-	31.3	-	-	-	6.2	-	18.9	-	32

APPENDIX C

Sample numbers and localities

Grid references from NZMS 260 series 1:50 000 sheets.
ts = thin section, xrf = xrf major and trace element analysis, min = electron microprobe analysis, icp-ms = inducted couple plasma mass spectrometry, inaa = instrumental neutron activation analysis, iso = Nd and Sr isotope analysis.
All samples tabulated below are from the Kaingaroa Ignimbrite, unless stated.

Field #	Description	Grid Ref	Analyses
KA3	Plagioclase-phyric andesite lithic	No 6 Rd; U17/072045	ts, xrf, icp/ms
KA4	Rangitaiki ignimbrite lithic	No 6 Rd; U17/072045	ts
KA6	Gabbro lithic	B.B. Rd quarry; U17/062999	ts, xrf?
KA7	Gabbro lithic	B.B. Rd quarry; U17/062999	ts
KA8	Kg-like ignimbrite lithic	B.B. Rd quarry; U17/062999	ts
KA9	Kg-like ignimbrite lithic	B.B. Rd quarry; U17/062999	ts, min
KA10	Wheao ignimbrite	Wheao dam; V18/205793	ts
KA11	Rhyodacite lithic	B.B. Rd quarry; U17/062999	ts
KA12	White/yellow pumice	B.B. Rd quarry; U17/062999	min, xrf
KA13c	plagioclase-phyric andesite lithic	B.B. Rd quarry; U17/062999	xrf
KA14	obsidian lithic	B.B. Rd quarry; U17/062999	ts, xrf
KA15	plagioclase-phyric andesite lithic	B.B. Rd quarry; U17/062999	ts
KA16	Waiotapu ignimbrite lithic	B.B. Rd quarry; U17/062999	ts
KA17	oxidised gabbro lithic	B.B. Rd quarry; U17/062999	ts, xrf
KA18	coarsely vesicular andesite lithic	B.B. Rd quarry; U17/062999	ts
KA19	medium grained andesite lithic	B.B. Rd quarry; U17/062999	ts
KA22	Te Kopia ignimbrite-like lithic	B.B. Rd quarry; U17/062999	ts
KA23a	white/yellow pumice	Old Waiotapu Rd; U16/085108	ts, xrf
KA23b	white/yellow pumice (Silky)	Old Waiotapu Rd; U16/085108	ts, xrf
KA24	plagioclase-phyric andesite lithic	B.B. Rd quarry; U17/062999	xrf
KA25	pumice	B.B. Rd quarry; U17/062999	xrf, iso
KA28	plagioclase-phyric andesite lithic	Webb Quarry; V17/194053	xrf
KA29	WIU	Webb Quarry; V17/194053	ts
KA30	WIU	Webb Quarry; V17/194053	ts
KA31	vapour-phase altered WIU	Webb Quarry; V17/194053	ts
KA36	pumice	Old Waiotapu Rd; U16/085108	xrf
KA37	white pumice	Old Waiotapu Rd; U16/085108	ts, xrf
KA38	grey pumice	Old Waiotapu Rd; U16/085108	xrf

KA39	grey pumice	Old Waiotapu Rd; U16/085108	xrf
KA40a	grey pumice	Old Waiotapu Rd; U16/085108	ts
KA40b	grey/black pumice	Old Waiotapu Rd; U16/085108	ts
KA40c	black pumice	Old Waiotapu Rd; U16/085108	ts
KA42	Kairuru rhyolite	Kairuru	ts, min, xrf, iso
KA43	Kairuru rhyolite	Kairuru	ts
KA44a	grey pumice	Old Waiotapu Rd; U16/085108	ts, xrf
KA44b	grey pumice	Old Waiotapu Rd; U16/085108	ts, xrf
KA44c	grey/black pumice	Old Waiotapu Rd; U16/085108	ts, xrf
KA44d	grey/black pumice	Old Waiotapu Rd; U16/085108	ts
KA44e	black pumice	Old Waiotapu Rd; U16/085108	ts, xrf
KA45a	grey pumice	Old Waiotapu Rd; U16/085108	ts, xrf, iso
KA45b	grey pumice	Old Waiotapu Rd; U16/085108	ts, min, xrf, inaa, iso
KA45b3	yellow pumice	Old Waiotapu Rd; U16/085108	ts, min, xrf, inaa, iso
KA45bc	yellow/greypumice	Old Waiotapu Rd; U16/085108	ts, xrf
KA45c	black pumice	Old Waiotapu Rd; U16/085108	ts, xrf
KA45d	grey/black pumice	Old Waiotapu Rd; U16/085108	ts, xrf
KA45e	grey/black pumice	Old Waiotapu Rd; U16/085108	ts
KA45f	grey/black pumice	Old Waiotapu Rd; U16/085108	ts, xrf
KA46	WIU and tourmalinite lithic	Main Gully Rd; V17/195070	ts
KA48a	grey pumice	Old Waiotapu Rd; U16/085108	ts, xrf
KA48b	black pumice	Old Waiotapu Rd; U16/085108	ts, xrf
KA48c	grey/black pumice	Old Waiotapu Rd; U16/085108	ts, xrf
KA49a	grey pumice	Old Waiotapu Rd; U16/085108	ts, xrf
KA49b	grey pumice	Old Waiotapu Rd; U16/085108	ts, xrf
KA50	white pumice	Reihana Rd; U17/0910998	ts, xrf, min, iso
KA50m	streaked pumice	Reihana Rd; U17/0910998	xrf
KA51	white pumice	Reihana Rd; U17/0910998	ts, xrf
KA53	white pumice	Reihana Rd; U17/0910998	ts, xrf, iso
KA53B	white pumice	Reihana Rd; U17/0910998	xrf

KA56	yellow pumice	Reihana Rd; U17/0910998	xrf
KA57	white pumice	Reihana Rd; U17/0910998	ts
KA63	pumice	Reihana Rd; U17/0910998	xrf
KA64	Wheao ignimbrite	Wheao dam; V18/205793	ts
KA67	white pumice	Reihana Rd; U17/0910998	ts
KA68	Wheao ignimbrite	Flaxy dam; V18/193765	ts
KA71	pumice	No 6 Rd; U17/072045	xrf
KA72	pumice	No 6 Rd; U17/072045	xrf
KA73	gabbroic lithic	B.B. Rd quarry; U17/062999	ts
KA74	andesite lithic	B.B. Rd quarry; U17/062999	ts
KA75	Paeroa/Rangitaki ignimbrite lithic?	B.B. Rd quarry; U17/062999	ts
KA77	andesite lithic	B.B. Rd quarry; U17/062999	ts
KA78	Paeroa ignimbrite lithic	B.B. Rd quarry; U17/062999	ts
KA78b	Paeroa ignimbrite lithic	B.B. Rd quarry; U17/062999	ts
KA79	Rangitaiki ignimbrite lithic	B.B. Rd quarry; U17/062999	ts
KA80	andesite lithic	B.B. Rd quarry; U17/062999	ts
KA81	andesite lithic	B.B. Rd quarry; U17/062999	ts
KA82	gabbro lithic	B.B. Rd quarry; U17/062999	ts
KA83	oxidised andesite lithic	B.B. Rd quarry; U17/062999	ts
KA84	andesite lithic with elongate vesicles	B.B. Rd quarry; U17/062999	ts, xrf, icp-ms
KA85	weathered andesite lithic	B.B. Rd quarry; U17/062999	ts
KA86	Te Kopia ignimbrite lithic	B.B. Rd quarry; U17/062999	ts
KA87A	miscellaneous ignimbrite lithic	B.B. Rd quarry; U17/062999	ts
KA88	Kg-like ignimbrite lithic	B.B. Rd quarry; U17/062999	ts
KA90	andesite lithic	B.B. Rd quarry; U17/062999	ts
KA91	meta-rhyolite lithic	B.B. Rd quarry; U17/062999	ts
KA92	flow-banded basaltic andesite	B.B. Rd quarry; U17/062999	ts, xrf, icp-ms
KA93	coarsely vesicular andesite lithic	B.B. Rd quarry; U17/062999	ts
KA94	andesite lithic	B.B. Rd quarry; U17/062999	xrf
KA96	andesite lithic	B.B. Rd quarry; U17/062999	ts

KA97	juvenile obsidian	Reihana Rd; U17/0910998	ts
KA98	andesite lithic	B.B. Rd quarry; U17/062999	ts
KA99	Waiotapu ignimbrite lithic	B.B. Rd quarry; U17/062999	ts
KA100	miscellaneous ignimbrite lithic	B.B. Rd quarry; U17/062999	ts
KA101	andesite lithic	B.B. Rd quarry; U17/062999	ts
KA110	Kawerau ignimbrite grey pumice type	Tarawera Rd; V16/288343	min, xrf, inaa
KA114	Kawerau ignimbrite brown pumice type	Tarawera Rd; V16/288343	ts, min, xrf, inaa
KA115	Kawerau ignimbrite	Tarawera Rd; V16/288343	ts
KA118	Dacitic lithic (Kawerau ignimbrite)	Tarawera Rd; V16/288343	ts
KA156a	quartz-augite phyric dacite	B.B. Rd quarry; U17/062999	ts, xrf, icp-ms
KA156$	hydrothermally altered coarsely porphyritic andesite	B.B. Rd quarry; U17/062999	ts
KA156b	quartz-augite phyric dacite	B.B. Rd quarry; U17/062999	ts
KA157a	intensely veined gabbro lithic	B.B. Rd quarry; U17/062999	ts
KA173	gabbro lithic	B.B. Rd quarry; U17/062999	ts, min, xrf, icp-ms
KA175B	grey pumice	Burn Rd; U17/075034	xrf
KA175BL	vesicular black pumice	Burn Rd; U17/075034	xrf
KA175C	pumice	Burn Rd; U17/075034	xrf
KA175D	pumice	Burn Rd; U17/075034	xrf
KA177A	pumice	Burn Rd; U17/075034	xrf
KA177B	pumice	Burn Rd; U17/075034	xrf
KA177C	pumice	Burn Rd; U17/075034	xrf
KA182	sandy-black ignimbrite lithic	Burn Rd; U17/075034	ts
KA185	sandy-black ignimbrite lithic	Burn Rd; U17/075034	ts
KA185I	sandy-black ignimbrite lithic	Burn Rd; U17/075034	ts
KA186A	grey pumice	Burn Rd; U17/075034	xrf
KA188A	grey pumice	Burn Rd; U17/075034	xrf
KA188B	grey pumice	Burn Rd; U17/075034	xrf
KA188C	grey pumice	Burn Rd; U17/075034	xrf
KA188	sandy-black ignimbrite lithic	Burn Rd; U17/075034	ts

KA188ai	sandy-black ignimbrite lithic	Burn Rd; U17/075034	ts
KA188bi	sandy-black ignimbrite lithic	Burn Rd; U17/075034	ts
KA194	meta-rhyolite lithic	BB. Rd (west); U17/092998	ts
KA194aI	gabbro lithic	BB. Rd (west); U17/092998	ts, icp-ms
KA194b	andesite lithic (LPA)	BB. Rd (west); U17/092998	ts
KA197	pumice	BB. Rd (west); U17/092998	xrf
KA199	pumice	Rawhiti Rd;U17/065984	xrf
KA200a	greywacke lithic	Rawhiti Rd;U17/065984	ts
KA200a	sandy-black ignimbrite	Rawhiti Rd;U17/065984	ts
KA200b	altered hornblende-phyric andesite	Rawhiti Rd;U17/065984	ts
KA200b	greywacke lithic	Rawhiti Rd;U17/065984	ts
KA200c	greywacke lithic	Rawhiti Rd;U17/065984	ts
KA201a	greywacke lithic	Rawhiti Rd;U17/065984	ts
KA201aI	gabbro lithic	Rawhiti Rd;U17/065984	ts, min
KA201b	obsidian lithic	Rawhiti Rd;U17/065984	ts
KA201c	miscellaneous ignimbrite lithic	Rawhiti Rd;U17/065984	ts
KA220	altered Whakamaru-group ignimbrite lithic	Shilts Farm; U16/999111	ts
KA230	pumice	No 3 Rd; U17/079071	xrf
KA230A	pumice	No 3 Rd; U17/079071	xrf
KA233A	pumice	No 3 Rd; U17/079071	xrf
KA233B	pumice	No 3 Rd; U17/079071	xrf
KA238	WIU	State Highway 38; V17/214002	ts
KA240	WIU	State Highway 38; V17/214002	ts
KA241a	meta-rhyolite lithic	No 6 Rd; U17/072045	ts
KA242	pumice	No 6 Rd; U17/072045	xrf
KA243a	meta-rhyolite lithic	No 6 Rd; U17/072045	ts
KA244	pumice	No 6 Rd; U17/072045	xrf
KA245a	Kg-like ignimbrite lithic	No 6 Rd; U17/072045	ts
KA245b	Kg-like ignimbrite lithic	No 6 Rd; U17/072045	ts
KA246A	pumice	No 6 Rd; U17/072045	xrf

KA246B	pumice	No 6 Rd; U17/072045	xrf
KA251a	juvenile obsidian	Reihana Rd; U17/0910998	ts, xrf
KA251B	Matahina-like ignimbrite lithic	Reihana Rd; U17/0910998	ts
KA263	pumice	Plateau Rd; V17/109935	xrf
KA265	Transition zone ignimbrite	Plateau Rd; V17/109935	ts
KA269A	grey pumice	State Highway 38; V17/222003	xrf
KA269B	grey pumice	State Highway 38; V17/222003	xrf
KA269C	grey pumice	State Highway 38; V17/222003	xrf
KA273	WIU	Maungahekeke Valley; U17/ 0990857	ts
KA275	uralitised basaltic andesite (UB)	M.Valley; U17/0990857	ts
KA276	pumice	M.Valley; U17/0990857	xrf
KA282	pumice	M.Valley; U17/0990857	xrf
KA285	pumice	M.Valley; U17/0990857	xrf
KA291	pumice	M.Valley; U17/0990857	xrf
KA294	OWR	M.Valley; U17/0990857	ts
KA296	OWR	M.Valley; U17/0990857	ts
KA297	OWR	M.Valley; U17/0990857	ts
KA300	OWR	M.Valley; U17/0990857	ts
KA301	OWR	M.Valley; U17/0990857	ts
KA302	OWR	M.Valley; U17/0990857	ts
KA303	WIU	'Lindane'; V16/169132	ts
KA306	WIU	'Lindane'; V16/169132	ts
KA307	OWR	Main Gully Rd; V17/195070	ts
KA309	OWR	Main Gully Rd; V17/195070	ts
KA310	OWR	Main Gully Rd; V17/195070	ts
KA311	OWR	Main Gully Rd; V17/195070	ts
KA313	OWR	Main Gully Rd; V17/195070	ts
KA316	WIU	Main Gully Rd; V17/195070	ts
KA317	WIU	Main Gully Rd; V17/195070	ts

KA330BL	vesicular black pumice	B.B. Rd (east); V17/101995	xrf
KA331A	pumice	B.B. Rd (east); V17/101995	xrf
KA332A	pumice	B.B. Rd (east); V17/101995	xrf
KA332B	pumice	B.B. Rd (east); V17/101995	xrf
KA333A	pumice	B.B. Rd (east); V17/101995	xrf
KA333B	pumice	B.B. Rd (east); V17/101995	
KA334	OWR	B.B. Rd (east); V17/101995	ts
KA338a	WIU	State Highway 38; V16/120114	ts
KA338ai	ignimbrite lithic?	State Highway 38; V16/120114	ts
KA338b	altered andesite lithic	State Highway 38; V16/120114	ts
KA345	WIU	Ngatamawahine valley; V16/ 197112	ts
KA347	WIU	N. valley; V16/197112	ts
KA350	partially welded WIU	N. valley; V16/197112	ts
KA352A	pumice	Coates Rd; U17/865023	xrf
KA352C	pumice	Coates Rd; U17/865023	xrf
KA354A	pumice	M.Valley; U17/0990857	xrf
KA354B	pumice	M.Valley; U17/0990857	xrf
KA354C	pumice	M.Valley; U17/0990857	xrf
KA356B	pumice	M.Valley; U17/0990857	xrf
KA358	pumice	M.Valley; U17/0990857	xrf
KA360	pumice	M.Valley; U17/0990857	xrf
KA362A	pumice	M.Valley; U17/0990857	xrf
KA362B	pumice	M.Valley; U17/0990857	xrf
KA362C	pumice	M.Valley; U17/0990857	xrf
KA366	pumice	M.Valley; U17/0990857	xrf
KA370	WIU	Webb Quarry; V17/194053	ts
KA371	WIU	Putunoa; V16/125157	ts
KA377	pumice	Putunoa; V16/125157	xrf, iso

KA385	Tokiaminga subunit	Tokiaminga valley; U17/ 082019	ts
KA386f	dacitic bleb	T. valley; U17/082019	ts, min, xrf, inaa, iso
KA386p	gabbroic lithic	T. valley; U17/082019	ts, min
KA387	Pukekahu rhyolite	Pukekahu;	ts, min, xrf
KA415	pumice	Reihana Rd; U17/0910998	xrf
KA415B2	pumice	Reihana Rd; U17/0910998	xrf
KA416	pumice	Reihana Rd; U17/0910998	xrf
KA417A	pumice	Reihana Rd; U17/0910998	xrf
KA417B	pumice	Reihana Rd; U17/0910998	xrf
KA421	gabbro lithic	Reihana Rd; U17/0910998	ts
KA421B	grey pumice	Reihana Rd; U17/0910998	xrf
KA428a	gabbro lithic	B.B. Rd quarry; U17/062999	ts
KA428b	gabbro lithic	B.B. Rd quarry; U17/062999	ts, icp-ms
KA428c	uralitised basalitic andesite lithic (UB)	B.B. Rd quarry; U17/062999	ts, min, xrf, icp-ms
KA428d	gabbro lithic	B.B. Rd quarry; U17/062999	ts
KA428e	gabbro lithic	B.B. Rd quarry; U17/062999	ts
KA428f	gabbro lithic	B.B. Rd quarry; U17/062999	ts
KA430	tourmaline-bearing meta-rhyolite lithic	Waimahunga Rd; V17/159895	ts, min
KA438	gabbro lithic	B.B. Rd quarry; U17/062999	ts
KA438	granophyre lithic	B.B. Rd quarry; U17/062999	ts
KA439	Terrace Rd basalt	Terrace Rd; U16/087115	ts
KA440	Waikokomuku andesite	U16/080133	ts
KA443	gabbro lithic	T. valley; U17/082019	ts
DAC	augite-phyric dacite	B.B. Rd quarry; U17/062999	ts
RA1	Rangatira Point ignimbrite	Rangatira Point; U18/724698	ts
CORE	welded ignimbrite of Wairakei drill hole		ts, min

Appendix D

Electron microprobe data

Mineral and glass analyses were undertaken by electron microprobe (EMPA) at the University of Otago. Samples were analysed using a JEOL 8600 'Superprobe' operating with an accelerating voltage of 15kV and an electron current of 20nA. Data were reduced on line using standard ZAF correction procedures modified by Kawachi and Trinder (unpublished data 1993). Typical lower limits of detection (wt%) were: SiO_2=0.07, TiO_2=0.07, Al_2O_3=0.05, FeO=0.12, MnO=0.10, MgO=0.05, Na_2O=0.08, K_2O=0.03. The electron beam was typically 1-3um in diameter for mineral spot analyses, but was widened for analysis of volcanic glass and amphibole. During analysis of glass the electron beam was widened to 50um and the sample moved slowly to reduce the effects of alkali migration. In addition the count time was reduced following the recommendations of Froggatt (1983).

EPMA was undertaken on a representative suite of pumice and lithic samples. Due to the crystal-poor nature of Kaingaroa pumices, mineral mounts were prepared for pumice samples, using standard panning, magnetic separation, and polished thin sections techniques. Polished thin sections were prepared by Rob Spiers, University of Canterbury.

Magnetite are recalculated on the basis of 32 oxygens, ilmenite = 6, pyroxene = 6, olivine = 4, amphibole = 23+2OH, tourmaline = 29, and feldspar = 32. Total Fe is FeO. Fe_2O_3 was recalculated for Fe/Ti oxide and amphibole analyses following the recommendations and methods of Droop (1987). EMP data were manipulated using PETMIN software.

Microprobe data are listed according to mineral type in the following tables:

D.1 Kaingaroa pumices and rhyolites

a) Plagioclase

b) Pyroxene

c) Fe/Ti oxides

d) Glass

D.2 Kaingaroa gabbro lithics

D.3 Kaingaroa andesite lithics

D.4 Kaingaroa meta-rhyolite lithics

D.5 Kawerau pumices

D.6 Welded ignimbrite of Wairakei drill hole

Appendix D.1a. Kaingaroa plagioclase

Sample no	KA12	KA12	KA12	KA12	KA12	KA12	KA45b3	KA45b3	KA45b3	KA45b3	KA45b	KA45b	KA45b
Analysis no	474	475	476	477	490	491	390	391	392	393	501	502	503
	c	r	c	r	c	r	c	r	c	r	c	c	r
SiO_2	57.59	60.75	60.89	60.69	61.74	60.95	60.86	61.67	61.72	61.58	62.69	62.86	62.60
Al_2O_3	26.37	24.54	24.76	24.84	24.36	23.82	25.20	24.97	25.30	24.43	25.16	24.56	25.00
TiO_2	0.00	0.02	0.00	0.00	0.00	0.00	0.00	0.00	0.00	0.00	0.00	0.00	0.02
FeO	0.22	0.15	0.12	0.19	0.14	0.22	0.16	0.13	0.15	0.18	0.14	0.13	0.14
MnO	0.00	0.00	0.00	0.00	0.00	0.00	0.00	0.00	0.00	0.00	0.00	0.00	0.00
MgO	0.00	0.00	0.00	0.00	0.00	0.00	0.00	0.00	0.00	0.00	0.00	0.00	0.00
CaO	8.84	7.15	6.45	7.08	6.46	6.33	7.16	6.76	6.73	6.95	6.18	6.24	6.48
Na_2O	6.30	7.18	7.31	7.21	7.27	7.50	7.28	7.54	7.52	7.34	7.40	6.81	7.33
K_2O	0.31	0.45	0.32	0.35	0.38	0.41	0.42	0.49	0.46	0.46	0.48	0.54	0.49
Total	99.63	100.24	99.85	100.36	100.34	99.22	101.08	101.57	101.87	100.94	102.05	101.13	102.06
Oxygen	32	32	32	32	32	32	32	32	32	32	32	32	32
Si	10.368	10.803	10.834	10.775	10.924	10.926	10.736	10.816	10.787	10.866	10.899	10.999	10.892
Al	5.595	5.142	5.193	5.197	5.079	5.034	5.239	5.162	5.212	5.081	5.155	5.066	5.126
Ti	0.000	0.003	0.000	0.000	0.000	0.000	0.000	0.000	0.000	0.000	0.000	0.000	0.003
Fe	0.033	0.023	0.018	0.028	0.020	0.032	0.024	0.020	0.022	0.026	0.020	0.020	0.021
Mn	0.000	0.000	0.000	0.000	0.000	0.000	0.000	0.000	0.000	0.000	0.000	0.000	0.000
Mg	0.000	0.000	0.000	0.000	0.000	0.000	0.000	0.000	0.000	0.000	0.000	0.000	0.000
Ca	1.705	1.362	1.229	1.346	1.224	1.215	1.353	1.270	1.260	1.313	1.150	1.169	1.208
Na	2.199	2.474	2.521	2.483	2.493	2.607	2.491	2.563	2.549	2.511	2.496	2.310	2.473
K	0.072	0.103	0.072	0.079	0.085	0.093	0.094	0.109	0.103	0.104	0.106	0.120	0.109
Total	19.970	19.911	19.867	19.907	19.825	19.907	19.937	19.940	19.933	19.902	19.825	19.683	19.833
An	42.88	34.58	32.15	34.44	32.20	31.03	34.34	32.22	32.20	33.42	30.66	32.49	31.87
Ab	55.88	62.81	65.97	63.54	65.57	66.59	63.26	65.01	65.17	63.93	66.52	64.18	65.24
Or	1.80	2.61	1.88	2.02	2.23	2.37	2.40	2.77	2.63	2.65	2.81	3.33	2.88

Appendix D.1a. Kaingaroa plagioclase

Sample no	KA45b	KA45b	KA45b	KA386	KA386	KA386	KA386	KA386	KA386	KA386	KA386	KA50	KA50
Analysis no	504	505	506	457	458	459	460	466	467	471	472	400	401
	r	c	r	c	r	c	r	c	r	c	r	c	r
SiO_2	60.77	58.69	55.74	57.72	60.01	62.13	62.37	59.56	59.96	61.84	62.14	62.39	62.14
Al_2O_3	24.79	25.53	26.92	26.30	25.50	24.71	24.20	25.19	25.58	24.83	24.36	24.00	24.49
TiO_2	0.00	0.00	0.00	0.00	0.00	0.02	0.00	0.04	0.00	0.00	0.02	0.00	0.04
FeO	0.14	0.25	0.24	0.16	0.18	0.11	0.11	0.17	0.24	0.24	0.17	0.17	0.14
MnO	0.02	0.00	0.00	0.00	0.00	0.00	0.00	0.00	0.02	0.00	0.00	0.03	0.00
MgO	0.00	0.00	0.00	0.00	0.00	0.00	0.00	0.00	0.00	0.00	0.00	0.00	0.00
CaO	6.82	8.03	10.02	8.55	7.61	5.92	5.98	7.11	7.71	6.65	5.71	5.44	6.23
Na_2O	6.99	6.49	5.57	6.06	6.86	7.58	7.64	7.09	6.88	7.47	7.68	7.88	7.63
K_2O	0.43	0.37	0.22	0.28	0.40	0.45	0.48	0.34	0.40	0.49	0.42	0.45	0.53
Total	99.96	99.35	98.72	99.07	100.57	100.92	100.78	99.50	100.79	101.51	100.51	100.35	101.21
Oxygen	32	32	32	32	32	32	32	32	32	32	32	32	32
Si	10.812	10.560	10.161	10.419	10.650	10.921	10.983	10.674	10.627	10.846	10.965	11.023	10.915
Al	5.198	5.413	5.783	5.595	5.334	5.119	5.022	5.320	5.343	5.132	5.066	4.997	5.071
Ti	0.000	0.000	0.000	0.000	0.000	0.003	0.000	0.006	0.000	0.000	0.003	0.000	0.005
Fe	0.020	0.037	0.037	0.025	0.027	0.017	0.016	0.026	0.036	0.035	0.026	0.025	0.020
Mn	0.003	0.000	0.000	0.000	0.000	0.000	0.000	0.000	0.004	0.000	0.000	0.004	0.000
Mg	0.000	0.000	0.000	0.000	0.000	0.000	0.000	0.000	0.000	0.000	0.000	0.000	0.000
Ca	1.300	1.547	1.957	1.653	1.447	1.114	1.128	1.365	1.464	1.249	1.079	1.029	1.173
Na	2.412	2.266	1.970	2.121	2.361	2.584	2.607	2.464	2.364	2.540	2.627	2.700	2.599
K	0.098	0.085	0.052	0.064	0.091	0.100	0.107	0.077	0.090	0.110	0.095	0.101	0.120
Total	19.844	19.909	19.959	19.876	19.909	19.858	19.863	19.931	19.928	19.912	19.860	19.880	19.904
An	34.12	39.69	49.19	43.08	37.11	29.34	29.37	34.95	37.37	32.04	28.39	26.87	30.14
Ab	63.30	58.12	49.51	55.26	60.56	68.02	67.84	63.09	60.34	65.15	69.11	70.48	66.78
Or	2.58	2.19	1.29	1.65	2.33	2.64	2.79	1.96	2.29	2.81	2.50	2.64	3.07

Appendix D.1a. Kaingaroa plagioclase

Sample no	KA50	KA50	KA9	KA9	KA9	KA9	KA9	KA9	KA387	KA387	KA387	KA387	KA387
Analysis no	402	403	187	188	189	190	191	192	83	79	80	81	94
	c	r	c	r	c	r	c	r	c	c	r	c	c
SiO_2	61.00	61.21	60.90	63.01	62.54	61.97	61.65	62.23	59.17	60.33	63.51	59.17	54.00
Al_2O_3	24.67	24.46	25.24	24.46	23.53	23.89	24.45	24.32	27.45	26.01	24.45	27.34	29.65
TiO_2	0.03	0.00	0.00	0.00	0.00	0.00	0.03	0.00	0.00	0.03	0.02	0.04	0.00
FeO	0.15	0.19	0.27	0.24	0.23	0.21	0.19	0.23	0.29	0.25	0.17	0.33	0.23
MnO	0.00	0.00	0.00	0.00	0.00	0.00	0.00	0.00	0.00	0.00	0.00	0.00	0.00
MgO	0.00	0.00	0.00	0.00	0.00	0.00	0.00	0.00	0.00	0.00	0.00	0.02	0.00
CaO	6.63	6.55	7.88	6.48	5.64	6.43	6.83	6.37	8.76	7.85	5.22	8.57	12.16
Na_2O	7.28	7.36	6.31	6.77	6.87	6.90	6.56	6.66	5.67	6.24	7.55	5.75	4.86
K_2O	0.33	0.51	0.38	0.51	0.52	0.49	0.44	0.41	0.27	0.35	0.57	0.27	0.18
Total	100.09	100.28	100.98	101.47	99.34	99.87	100.15	100.22	101.61	101.05	101.50	101.49	101.06
Oxygen	32	32	32	32	32	32	32	32	32	32	32	32	32
Si	10.835	10.864	10.740	11.001	11.124	11.003	10.919	10.990	10.395	10.632	11.063	10.405	9.683
Al	5.163	5.117	5.246	5.032	4.933	4.999	5.103	5.063	5.683	5.403	5.020	5.666	6.266
Ti	0.004	0.000	0.000	0.000	0.000	0.000	0.004	0.000	0.000	0.004	0.003	0.005	0.000
Fe	0.022	0.028	0.040	0.035	0.035	0.031	0.028	0.034	0.043	0.036	0.025	0.049	0.034
Mn	0.000	0.000	0.000	0.000	0.000	0.000	0.000	0.000	0.000	0.000	0.000	0.000	0.000
Mg	0.000	0.000	0.000	0.000	0.000	0.000	0.000	0.000	0.000	0.000	0.000	0.006	0.000
Ca	1.262	1.245	1.489	1.213	1.074	1.223	1.297	1.206	1.648	1.482	0.975	1.615	2.336
Na	2.507	2.534	2.156	2.291	2.370	2.374	2.253	2.280	1.930	2.132	2.550	1.959	1.688
K	0.076	0.115	0.086	0.114	0.119	0.110	0.099	0.093	0.060	0.079	0.126	0.060	0.041
Total	19.870	19.902	19.759	19.686	19.654	19.740	19.702	19.665	19.758	19.768	19.762	19.766	20.048
An	32.83	31.97	39.91	33.53	30.14	32.99	35.54	33.70	45.30	40.13	26.71	44.44	57.47
Ab	65.20	65.08	57.79	63.32	66.52	64.04	61.74	63.70	53.05	57.73	69.84	53.91	41.53
Or	1.97	2.95	2.31	3.15	3.34	2.97	2.71	2.60	1.65	2.14	3.45	1.65	1.01

Appendix D.1a. Kaingaroa plagioclase

Sample no	KA387	KA387	KA387	KA387	KA387
Analysis no	97	98	99	100	102
	c	r	c	c	r
SiO_2	59.49	61.08	61.90	60.85	61.93
Al_2O_3	24.85	25.16	24.56	25.89	24.82
TiO_2	0.00	0.00	0.00	0.00	0.00
FeO	0.17	0.20	0.12	0.23	0.19
MnO	0.00	0.00	0.00	0.00	0.00
MgO	0.00	0.00	0.00	0.00	0.00
CaO	7.12	6.68	5.84	7.20	6.42
Na_2O	7.38	6.91	7.37	7.06	7.57
K_2O	0.34	0.40	0.44	0.37	0.49
Total	99.35	100.43	100.23	101.61	101.43
Oxygen	32	32	32	32	32
Si	10.691	10.804	10.943	10.672	10.862
Al	5.265	5.245	5.117	5.351	5.132
Ti	0.000	0.000	0.000	0.000	0.000
Fe	0.025	0.030	0.018	0.034	0.028
Mn	0.000	0.000	0.000	0.000	0.000
Mg	0.000	0.000	0.000	0.000	0.000
Ca	1.371	1.266	1.106	1.354	1.207
Na	2.572	2.368	2.525	2.402	2.576
K	0.078	0.091	0.100	0.082	0.110
Total	20.002	19.803	19.811	19.894	19.915
An	34.10	33.99	29.64	35.28	31.00
Ab	63.96	63.57	67.68	62.58	66.17
Or	1.94	2.44	2.68	2.14	2.83

Appendix D1.b. Kaingaroa pyroxene

Sample no	*KA12*	*KA12*	*KA12*	*KA12*	*KA12*	*KA12*	*KA45b3*	*KA45b3*	*KA45b3*	*KA45b3*	*KA45b3*	*KA45b3*	*KA45b3*
Analysis no	478	479	481	482	488	489	383	384	385	386	387	388	389
	c	r	c	r	c	r	c	r	r	c	r	c	r
SiO_2	51.42	50.75	51.69	51.48	50.93	50.50	50.88	51.25	51.15	51.45	51.39	51.04	51.48
Al_2O_3	0.30	0.24	0.33	0.38	0.19	0.23	0.22	0.18	0.13	0.22	0.23	0.28	0.19
TiO_2	0.12	0.13	0.08	0.09	0.11	0.07	0.20	0.07	0.09	0.10	0.09	0.10	0.08
FeO	29.26	30.74	28.17	29.51	31.35	31.48	30.53	31.98	30.34	31.02	30.67	30.36	30.12
MnO	1.75	1.74	1.88	0.96	1.75	1.86	1.35	1.77	1.85	1.64	1.15	1.16	1.64
MgO	16.97	16.38	18.36	17.65	16.02	15.13	16.63	15.77	15.64	16.45	16.41	16.41	16.76
CaO	0.99	0.98	0.99	1.10	0.99	1.04	0.94	1.05	0.90	1.12	1.05	0.99	1.00
Na_2O	0.00	0.00	0.00	0.00	0.00	0.00	0.00	0.00	0.00	0.00	0.00	0.00	0.00
K_2O	0.00	0.01	0.00	0.00	0.00	0.00	0.00	0.00	0.00	0.00	0.00	0.00	0.01
Total	100.81	100.97	101.51	101.17	101.34	100.31	100.77	102.06	100.10	102.00	100.99	100.33	101.29
Oxygen	6	6	6	6	6	6	6	6	6	6	6	6	6
Si	1.980	1.967	1.967	1.971	1.971	1.979	1.970	1.974	1.994	1.973	1.982	1.981	1.979
Al	0.014	0.011	0.015	0.017	0.009	0.011	0.010	0.008	0.006	0.010	0.010	0.013	0.008
Ti	0.003	0.004	0.002	0.003	0.003	0.002	0.006	0.002	0.003	0.003	0.003	0.003	0.002
Fe	0.942	0.997	0.897	0.945	1.015	1.032	0.989	1.030	0.989	0.995	0.990	0.985	0.969
Mn	0.057	0.057	0.060	0.031	0.057	0.062	0.044	0.058	0.061	0.053	0.038	0.038	0.054
Mg	0.974	0.947	1.042	1.007	0.924	0.884	0.960	0.905	0.909	0.940	0.944	0.949	0.961
Ca	0.041	0.041	0.041	0.045	0.041	0.044	0.039	0.043	0.037	0.046	0.043	0.041	0.041
Na	0.000	0.000	0.000	0.000	0.000	0.000	0.000	0.000	0.000	0.000	0.000	0.000	0.000
K	0.000	0.001	0.000	0.000	0.000	0.000	0.000	0.000	0.000	0.000	0.000	0.000	0.001
Total	4.010	4.024	4.023	4.018	4.021	4.013	4.019	4.020	4.000	4.020	4.010	4.010	4.015
En	48.36	46.38	51.08	49.66	45.36	43.74	47.25	44.46	45.52	46.22	46.85	47.15	47.46
Fs	49.62	51.63	46.93	48.12	52.62	54.10	50.83	53.42	52.61	51.53	51.00	50.82	50.50
Wo	2.02	1.99	1.99	2.22	2.02	2.16	1.92	2.12	1.87	2.25	2.15	2.04	2.04

Appendix D1.b. Kaingaroa pyroxene

Sample no	*KA45b3*	*KA45b3*	*KA45b*	*KA45b*	*KA45b*	*KA45b*	*KA45b*	*KA45b*	*KA45b*	*KA45b*	*KA386*	*KA386*	*KA386*
Analysis no	395	396	507	508	509	511	512	513	514	520	462	463	468
	c	c	c	r	r	r	c	r	r	c	c	c	c
SiO_2	50.33	50.35	49.54	48.29	49.30	49.38	50.18	50.21	49.40	48.12	50.65	51.17	50.43
Al_2O_3	0.23	0.26	0.33	0.17	0.10	0.23	0.44	0.35	0.26	0.23	0.38	0.29	0.39
TiO_2	0.13	0.09	0.10	0.06	0.09	0.17	0.12	0.09	0.09	0.09	0.09	0.12	0.11
FeO	32.48	32.49	30.26	32.79	32.29	31.79	28.55	28.47	30.00	33.29	31.00	30.42	27.59
MnO	1.60	1.06	1.70	1.89	1.81	1.65	1.61	1.56	1.77	1.66	1.05	1.73	0.99
MgO	14.97	14.97	15.18	13.53	14.18	14.70	17.30	16.93	15.78	13.51	16.30	16.48	17.66
CaO	1.03	1.01	0.96	0.92	1.02	0.99	1.08	1.01	1.09	1.07	1.13	1.07	1.07
Na_2O	0.00	0.00	0.00	0.00	0.00	0.00	0.00	0.00	0.00	0.02	0.00	0.00	0.00
K_2O	0.00	0.00	0.00	0.00	0.00	0.00	0.00	0.00	0.00	0.00	0.00	0.00	0.00
Total	100.77	100.23	98.08	97.64	98.79	98.92	99.28	98.62	98.39	97.98	100.61	101.27	98.24
Oxygen	6	6	6	6	6	6	6	6	6	6	6	6	6
Si	1.971	1.978	1.979	1.969	1.976	1.970	1.961	1.974	1.967	1.960	1.968	1.973	1.976
Al	0.010	0.012	0.016	0.008	0.005	0.011	0.020	0.016	0.012	0.011	0.018	0.013	0.018
Ti	0.004	0.003	0.003	0.002	0.003	0.005	0.003	0.003	0.003	0.003	0.003	0.003	0.003
Fe	1.064	1.067	1.011	1.118	1.082	1.061	0.933	0.936	0.999	1.134	1.007	0.981	0.904
Mn	0.053	0.035	0.058	0.065	0.062	0.056	0.053	0.052	0.060	0.057	0.034	0.056	0.033
Mg	0.874	0.876	0.904	0.822	0.847	0.874	1.008	0.992	0.937	0.820	0.944	0.947	1.032
Ca	0.043	0.042	0.041	0.040	0.044	0.042	0.045	0.042	0.046	0.047	0.047	0.044	0.045
Na	0.000	0.000	0.000	0.000	0.000	0.000	0.000	0.000	0.000	0.002	0.000	0.000	0.000
K	0.000	0.000	0.000	0.000	0.000	0.000	0.000	0.000	0.000	0.000	0.000	0.000	0.000
Total	4.020	4.014	4.011	4.025	4.019	4.019	4.025	4.016	4.024	4.033	4.021	4.018	4.011
En	42.97	43.36	44.90	40.20	41.64	42.99	49.42	49.06	45.89	39.85	46.45	46.69	51.24
Fs	54.90	54.55	53.06	57.84	56.21	54.92	48.36	48.85	51.84	57.89	51.24	51.12	46.53
Wo	2.13	2.09	2.04	1.96	2.15	2.09	2.22	2.09	2.27	2.26	2.31	2.18	2.22

Appendix D1.b. Kaingaroa pyroxene

Sample no	*KA386*	*KA50*	*KA50*	*KA50*	*KA50*	*KA50*	*KA50*	*KA50*	*KA50*	*KA50*	*KA9*	*KA9*	*KA9*
Analysis no	469	398	399	404	405	406	407	408	494	495	185	151	168
	r	c	r	c	r	r	c	r	c	r	c	c	c
SiO_2	51.13	50.95	50.46	50.05	48.56	50.19	50.50	50.39	51.41	51.06	51.87	52.61	50.46
Al_2O_3	0.28	0.24	0.21	0.25	0.36	0.21	0.40	0.27	0.14	0.22	0.38	0.31	0.16
TiO_2	0.10	0.08	0.09	0.13	0.14	0.07	0.12	0.11	0.10	0.12	0.13	0.07	0.09
FeO	30.15	31.02	30.91	33.49	30.46	32.30	29.89	30.95	28.50	31.48	27.97	24.42	30.46
MnO	1.64	1.78	1.72	1.81	1.52	1.77	1.44	1.92	1.72	1.69	1.55	1.79	1.69
MgO	16.83	16.12	16.00	14.48	15.67	15.16	17.14	15.48	17.41	15.71	16.52	21.08	15.19
CaO	1.04	0.99	1.02	1.08	1.10	1.09	1.11	0.93	1.07	1.02	1.05	0.43	0.97
Na_2O	0.00	0.00	0.00	0.00	0.00	0.00	0.00	0.00	0.00	0.00	0.15	0.18	0.32
K_2O	0.00	0.00	0.00	0.00	0.00	0.00	0.00	0.00	0.00	0.00	0.02	0.06	0.02
Total	101.17	101.18	100.41	101.29	97.81	100.80	100.59	100.05	100.35	101.31	99.66	100.95	99.37
Oxygen	6	6	6	6	6	6	6	6	6	6	6	6	6
Si	1.970	1.972	1.970	1.963	1.952	1.966	1.957	1.976	1.982	1.977	2.005	1.974	1.988
Al	0.013	0.011	0.010	0.012	0.017	0.010	0.018	0.012	0.006	0.010	0.017	0.014	0.008
Ti	0.003	0.002	0.003	0.004	0.004	0.002	0.003	0.003	0.003	0.003	0.004	0.002	0.003
Fe	0.971	1.004	1.009	1.098	1.024	1.058	0.969	1.015	0.919	1.019	0.904	0.766	1.004
Mn	0.053	0.058	0.057	0.060	0.052	0.059	0.047	0.064	0.056	0.056	0.051	0.057	0.057
Mg	0.967	0.931	0.931	0.846	0.939	0.885	0.990	0.905	1.001	0.907	0.952	1.179	0.892
Ca	0.043	0.041	0.042	0.045	0.047	0.046	0.046	0.039	0.044	0.042	0.044	0.017	0.041
Na	0.000	0.000	0.000	0.000	0.000	0.000	0.000	0.000	0.000	0.000	0.011	0.013	0.024
K	0.000	0.000	0.000	0.000	0.000	0.000	0.000	0.000	0.000	0.000	0.001	0.003	0.001
Total	4.021	4.020	4.022	4.028	4.035	4.027	4.031	4.015	4.012	4.015	3.989	4.025	4.017
En	47.52	45.75	45.66	41.28	45.53	43.22	48.25	44.74	49.54	44.81	48.80	58.40	44.73
Fs	50.37	52.24	52.26	56.51	52.17	54.54	49.51	53.33	48.27	53.10	48.95	40.76	53.21
Wo	2.10	2.01	2.08	2.21	2.30	2.23	2.25	1.92	2.18	2.09	2.26	0.84	2.06

Appendix D1.b. Kaingaroa pyroxene

Sample no	*KA9*	*KA9*	*KA9*	*KA9*	*KA387*	*KA387*	*KA387*	*KA387*	*KA387*	*KA42*	*KA42*	*KA42*
Analysis no	152	175	169	170	88	103	107	108	110	116	117	213
	r	c	c	r	c	c	c	r	c	c	r	c
SiO_2	50.57	52.19	50.89	50.55	51.25	50.40	49.75	49.97	49.82	49.50	49.68	49.36
Al_2O_3	0.29	1.76	0.23	0.40	0.50	0.25	0.20	0.23	0.25	0.12	0.16	0.17
TiO_2	0.10	0.57	0.15	0.12	0.12	0.08	0.06	0.08	0.06	0.07	0.08	0.09
FeO	30.82	10.42	28.94	28.44	29.87	27.75	29.68	30.11	30.79	34.63	35.00	32.99
MnO	1.67	0.26	1.28	1.09	1.45	1.53	1.78	1.70	1.39	2.09	2.15	2.15
MgO	15.81	15.53	16.33	17.03	16.44	17.36	15.87	15.68	15.72	12.72	12.62	12.09
CaO	0.87	17.92	1.07	1.05	1.10	1.02	0.85	0.85	0.76	1.17	1.11	1.10
Na_2O	0.25	0.48	0.23	0.16	0.00	0.03	0.00	0.02	0.00	0.18	0.16	0.13
K_2O	0.02	0.04	0.04	0.04	0.00	0.00	0.00	0.00	0.00	0.03	0.02	0.04
Total	100.40	99.16	99.16	98.88	100.74	98.41	98.19	98.64	98.79	100.50	100.99	98.12
Oxygen	6	6	6	6	6	6	6	6	6	6	6	6
Si	1.974	1.956	1.990	1.977	1.978	1.978	1.979	1.980	1.975	1.974	1.974	2.002
Al	0.013	0.078	0.011	0.019	0.023	0.011	0.009	0.011	0.012	0.006	0.008	0.008
Ti	0.003	0.016	0.004	0.004	0.004	0.002	0.002	0.002	0.002	0.002	0.002	0.003
Fe	1.006	0.326	0.946	0.931	0.964	0.911	0.987	0.998	1.021	1.155	1.163	1.119
Mn	0.055	0.008	0.042	0.036	0.047	0.051	0.060	0.057	0.047	0.071	0.072	0.074
Mg	0.920	0.868	0.952	0.993	0.946	1.016	0.941	0.926	0.929	0.756	0.747	0.731
Ca	0.036	0.720	0.045	0.044	0.046	0.043	0.036	0.036	0.032	0.050	0.047	0.048
Na	0.019	0.035	0.018	0.012	0.000	0.002	0.000	0.001	0.000	0.014	0.012	0.010
K	0.001	0.002	0.002	0.002	0.000	0.000	0.000	0.000	0.000	0.001	0.001	0.002
Total	4.027	4.008	4.010	4.017	4.007	4.015	4.015	4.013	4.017	4.029	4.027	3.997
En	45.61	45.16	47.96	49.55	47.23	50.27	46.49	45.91	45.79	37.20	36.82	37.07
Fs	52.60	17.38	49.77	48.25	50.47	47.60	51.73	52.31	52.64	60.33	60.87	60.50
Wo	1.78	37.46	2.27	2.20	2.30	2.13	1.78	1.78	1.58	2.46	2.32	2.43

Appendix D.1.c

Sample no	*KA12*	*KA12*	*KA12*	*KA12*	*KA12*	*KA386*	*KA386*	*KA45b*	*KA45b*	*KA45b*	*KA45b*	*KA45b3*	*KA45b3*
Analysis no	480	483	484	486	487	464	465	515	518	519	521	571	573
	mgt	ilm	ilm	ilm	ilm	ilm	ilm	ilm	ilm	mgt	mgt	mgt	ilm
SiO_2	0.00	0.00	0.00	0.00	0.00	0.00	0.00	0.00	0.00	0.03	0.00	0.05	0.00
Al_2O_3	1.41	0.07	0.06	0.06	0.05	0.04	0.05	0.06	0.06	1.24	1.05	0.89	0.04
TiO_2	11.23	49.32	49.22	47.90	48.79	49.44	49.10	47.95	48.21	10.34	11.88	18.87	49.33
MnO	0.50	1.38	1.18	1.12	1.12	1.30	1.22	1.16	1.24	0.63	0.43	0.63	1.34
MgO	0.58	1.43	1.27	1.20	1.17	1.17	1.26	1.32	1.06	0.46	0.47	0.52	1.21
CaO	0.03	0.02	0.00	0.05	0.00	0.00	0.02	0.00	0.00	0.00	0.00	0.00	0.00
Na_2O	0.00	0.00	0.00	0.00	0.00	0.00	0.00	0.00	0.00	0.00	0.00	0.00	0.00
K_2O	0.00	0.00	0.00	0.00	0.00	0.00	0.00	0.01	0.00	0.00	0.00	0.00	0.00
Droop recalc													
Fe_2O_3	46.23	10.38	8.22	11.04	9.97	9.95	10.01	10.55	9.57	47.88	44.14	31.20	9.71
FeO	40.40	40.39	40.81	39.74	40.66	41.06	40.66	39.56	40.21	39.63	40.70	47.16	40.86
Total	100.37	103.00	100.76	101.10	101.77	102.96	102.32	100.60	100.35	100.21	98.68	99.33	102.48
Oxygen	32	6	6	6	6	6	6	6	6	32	32	32	6
Si	0.000	0.000	0.000	0.000	0.000	0.000	0.000	0.000	0.000	0.008	0.000	0.016	0.000
Al	0.497	0.004	0.004	0.004	0.003	0.002	0.003	0.003	0.004	0.441	0.379	0.315	0.002
Ti	2.534	1.808	1.844	1.792	1.813	1.816	1.814	1.801	1.818	2.344	2.733	4.284	1.820
Fe^{2+}	10.137	1.646	1.700	1.653	1.680	1.677	1.670	1.652	1.686	9.985	10.405	11.902	1.676
Fe^{3+}	10.436	0.381	0.308	0.413	0.371	0.366	0.370	0.396	0.361	10.855	10.155	7.085	0.358
Mn	0.128	0.057	0.050	0.047	0.047	0.054	0.051	0.049	0.053	0.160	0.112	0.162	0.056
Mg	0.258	0.104	0.094	0.089	0.086	0.085	0.092	0.099	0.079	0.207	0.216	0.236	0.089
Ca	0.011	0.001	0.000	0.003	0.000	0.000	0.001	0.000	0.000	0.000	0.000	0.000	0.000
Na	0.000	0.000	0.000	0.000	0.000	0.000	0.000	0.000	0.000	0.000	0.000	0.000	0.000
K	0.000	0.000	0.000	0.000	0.000	0.000	0.000	0.001	0.000	0.000	0.000	0.000	0.000
Total	24	4	4	4	4	4	4	4	4	24	24	24	4

Appendix D.1.c

Sample no	*KA45b3*	*KA50*	*KA50*	*KA50*	*KA50*
Analysis no	574	497	498	499	500
	ilm	ilm	ilm	mgt	mgt
SiO_2	0.00	1.15	0.00	0.05	0.00
Al_2O_3	0.08	0.07	0.08	1.17	1.06
TiO_2	49.38	44.95	48.41	11.65	11.51
MnO	1.44	0.88	1.19	0.70	0.73
MgO	1.18	1.68	1.19	0.57	0.41
CaO	0.00	0.04	0.04	0.00	0.00
Na_2O	0.00	0.00	0.00	0.00	0.00
K_2O	0.00	0.00	0.00	0.00	0.00
Droop recalc					
Fe_2O_3	10.15	12.85	10.53	46.20	46.49
FeO	40.85	37.88	40.18	40.96	40.89
Total	103.07	99.49	101.61	101.29	101.09
Oxygen	6	6	6	32	32
Si	0.000	0.058	0.000	0.015	0.000
Al	0.004	0.004	0.005	0.411	0.375
Ti	1.812	1.697	1.802	2.607	2.587
Fe^{2+}	1.666	1.590	1.662	10.192	10.218
Fe^{3+}	0.372	0.486	0.392	10.345	10.452
Mn	0.060	0.037	0.050	0.176	0.185
Mg	0.086	0.125	0.088	0.254	0.184
Ca	0.000	0.002	0.002	0.000	0.000
Na	0.000	0.000	0.000	0.000	0.000
K	0.000	0.000	0.000	0.000	0.000
Total	4	4	4	24	24

Sample no	*KA45b*	*KA45b*	*KA9*	*KA9*	*KA386*	*KA386*
Analysis no	274	269	177	178	461	470
SiO_2	75.51	75.52	75.83	75.78	77.39	78.49
Al_2O_3	11.34	11.28	11.27	11.42	11.67	12.39
TiO_2	0.19	0.11	0.15	0.14	0.13	0.16
FeO	0.60	0.97	1.19	1.22	1.18	0.53
MnO	0.15	0.05	0.05	0.00	0.02	0.00
MgO	0.02	0.04	0.12	0.10	0.09	0.07
CaO	0.65	0.58	0.85	0.88	0.76	0.85
Na_2O	3.52	3.31	4.81	4.51	2.91	1.99
K_2O	3.75	3.93	3.81	4.21	3.71	3.53
Total	95.72	95.79	98.08	98.25	97.87	98.01

Appendix D.2.

Plagioclase													
Sample no	***KA173***	***KA173***	***KA173***	***KA173***	***KA173***	***KA173***	***KA173***	***KA173***	***KA173***	***KA173***	***KA173***	***KA173***	***KA173***
Analysis no.	1	2	7	8	10	20	21	22	23	24	25	28	29
	r	c	c	r	r	r	c	r	m	m	c	r	c
SiO_2	48.79	47.56	48.74	47.84	57.22	50.58	49.56	49.93	51.10	49.05	50.55	50.16	50.75
Al_2O_3	30.92	31.92	32.53	32.45	28.07	31.70	31.51	32.52	31.92	32.94	31.64	32.42	31.09
TiO_2	0.07	0.00	0.04	0.00	0.05	0.03	0.03	0.02	0.03	0.03	0.04	0.02	0.05
FeO	0.66	0.71	0.55	0.69	0.49	0.64	0.71	0.61	0.68	0.59	0.66	0.67	0.64
MnO	0.00	0.00	0.00	0.00	0.00	0.00	0.00	0.00	0.02	0.00	0.00	0.00	0.00
MgO	0.06	0.02	0.00	0.02	0.00	0.03	0.00	0.02	0.02	0.00	0.00	0.04	0.04
CaO	14.68	15.84	16.01	15.60	9.93	14.90	15.63	15.61	14.87	16.14	15.29	15.63	14.91
Na_2O	3.09	2.26	2.33	2.68	5.83	2.96	2.83	2.67	3.19	2.45	2.96	2.87	3.20
K_2O	0.12	0.04	0.07	0.08	0.25	0.10	0.09	0.09	0.09	0.07	0.11	0.07	0.10
Total	98.38	98.34	100.27	99.38	101.83	100.94	100.37	101.48	101.89	101.27	101.25	101.88	100.78
Oxygen	32	32	32	32	32	32	32	32	32	32	32	32	32
Si	9.189	8.882	8.914	8.847	10.116	9.159	9.062	9.012	9.168	8.888	9.140	9.025	9.213
Al	6.788	7.025	7.013	7.073	5.848	6.765	6.789	6.917	6.750	7.036	6.744	6.875	6.653
Ti	0.010	0.000	0.006	0.000	0.007	0.004	0.004	0.003	0.004	0.004	0.005	0.003	0.006
Fe	0.102	0.110	0.084	0.107	0.072	0.096	0.109	0.092	0.101	0.089	0.101	0.100	0.097
Mn	0.000	0.000	0.000	0.000	0.000	0.000	0.000	0.000	0.000	0.000	0.000	0.000	0.000
Mg	0.017	0.006	0.000	0.007	0.000	0.007	0.000	0.005	0.005	0.000	0.000	0.011	0.010
Ca	2.931	3.169	3.136	3.092	1.881	2.891	3.062	3.019	2.858	3.133	2.962	3.013	2.899
Na	1.115	0.817	0.825	0.962	1.999	1.040	1.005	0.935	1.109	0.862	1.036	1.000	1.128
K	0.028	0.010	0.016	0.020	0.055	0.022	0.021	0.022	0.021	0.015	0.025	0.017	0.023
Total	20.079	20.020	19.994	20.107	19.979	19.985	20.052	20.005	20.018	20.028	20.014	20.044	20.030
An	71.94	79.30	78.85	75.90	47.80	73.13	74.90	75.93	71.66	78.13	73.63	74.76	71.58
Ab	27.37	20.45	20.74	23.61	50.80	26.31	24.58	23.52	27.81	21.50	25.75	24.81	27.85
Or	0.69	0.25	0.40	0.49	1.40	0.56	0.51	0.55	0.53	0.37	0.62	0.42	0.57

Appendix D.2.

Sample no	*KA201A1*	*KA201A1*	*KA386P*	*KA386P*	*KA386P*	*KA386P*	*KA386P*	*KA386P*	*KA386P*	*KA386P*	*KA386P*	*KA386P*	*KA386P*
Analysis no.	560	561	41	45	46	47	48	49	50	51	52	53	54
	r	r	r	c	r	c	r	c	r	r	m	m	Na-zone
SiO_2	54.31	52.75	68.05	53.16	53.45	52.70	51.92	52.89	53.96	53.16	51.59	48.01	54.29
Al_2O_3	29.30	29.04	26.57	30.38	29.30	30.10	30.96	29.95	29.95	29.67	31.38	33.24	29.37
TiO_2	0.04	0.00	0.00	0.05	0.05	0.07	0.04	0.05	0.08	0.06	0.03	0.00	0.06
FeO	0.56	0.64	0.21	0.52	0.55	0.47	0.41	0.45	0.44	0.51	0.46	0.52	0.49
MnO	0.00	0.00	0.03	0.00	0.02	0.00	0.00	0.04	0.00	0.00	0.02	0.00	0.00
MgO	0.06	0.03	0.00	0.04	0.02	0.04	0.00	0.00	0.00	0.06	0.05	0.04	0.07
CaO	12.66	12.80	5.83	13.36	12.92	12.73	13.82	12.94	12.66	12.72	14.28	16.84	12.01
Na_2O	4.33	3.87	0.69	3.83	4.00	4.24	3.49	4.02	4.12	4.27	3.51	1.93	4.30
K_2O	0.30	0.64	0.17	0.26	0.27	0.31	0.19	0.26	0.19	0.31	0.27	0.11	0.31
Total	101.56	99.78	101.55	101.61	100.55	100.66	100.84	100.60	101.41	100.75	101.60	100.68	100.89
Oxygen	32	32	32	32	32	32	32	32	32	32	32	32	32
Si	9.709	9.629	11.444	9.514	9.655	9.521	9.372	9.555	9.645	9.593	9.272	8.767	9.742
Al	6.174	6.248	5.265	6.408	6.237	6.409	6.585	6.376	6.309	6.311	6.646	7.153	6.211
Ti	0.005	0.000	0.000	0.006	0.007	0.009	0.006	0.007	0.011	0.007	0.004	0.000	0.007
Fe	0.084	0.098	0.030	0.079	0.083	0.070	0.062	0.068	0.065	0.077	0.069	0.079	0.074
Mn	0.000	0.000	0.004	0.000	0.000	0.000	0.000	0.006	0.000	0.000	0.003	0.000	0.000
Mg	0.017	0.009	0.000	0.012	0.006	0.011	0.000	0.000	0.000	0.015	0.013	0.010	0.018
Ca	2.424	2.503	1.050	2.562	2.500	2.465	2.672	2.505	2.424	2.459	2.750	3.294	2.310
Na	1.502	1.370	0.223	1.329	1.400	1.487	1.223	1.408	1.429	1.493	1.224	0.683	1.495
K	0.068	0.149	0.036	0.060	0.061	0.071	0.044	0.059	0.044	0.072	0.061	0.026	0.071
Total	19.984	20.006	18.054	19.970	19.950	20.044	19.963	19.984	19.927	20.026	20.043	20.011	19.928
An	60.69	62.23	80.21	64.84	63.12	61.27	67.83	63.07	62.20	61.11	68.15	82.29	59.60
Ab	37.60	34.07	17.04	33.64	35.34	36.96	31.05	35.45	36.67	37.10	30.33	17.06	38.57
Or	1.71	3.70	2.75	1.52	1.54	1.76	1.12	1.49	1.13	1.79	1.51	0.65	1.83

Appendix D.2.

										Pyroxene			
Sample no	***KA386P***	***KA386P***	***KA386P***	***KA386P***	***KA386P***	***KA386P***	***KA386P***	***KA386P***	***KA386P***	***Sample no.***	***KA173***	***KA173***	***KA173***
Analysis no.	55	56	57	58	59	60	61	62	63	Analysis no.	13	15	27
	c	c	r	r	m	r	r	m	m		r	c	c
SiO_2	47.79	56.47	52.46	61.70	52.90	57.45	53.26	48.09	50.35	SiO_2	52.33	52.90	51.42
Al_2O_3	32.57	28.39	30.26	25.61	30.07	27.70	30.08	31.80	31.76	Al_2O_3	2.09	0.47	0.06
TiO_2	0.00	0.05	0.09	0.00	0.02	0.06	0.04	0.06	0.02	TiO_2	0.16	0.12	0.07
FeO	0.58	0.43	0.39	0.25	0.50	0.41	0.42	0.46	0.46	FeO	14.11	13.19	30.41
MnO	0.00	0.00	0.00	0.00	0.00	0.00	0.00	0.00	0.00	MnO	0.64	0.65	1.13
MgO	0.07	0.03	0.00	0.00	0.06	0.00	0.03	0.00	0.03	MgO	11.58	12.61	16.48
CaO	16.98	10.42	13.09	6.99	12.93	9.93	12.78	15.79	14.37	CaO	19.19	20.26	0.57
Na_2O	1.97	5.12	3.90	6.70	3.86	5.44	4.27	2.32	2.98	Na_2O	0.24	0.23	0.00
K_2O	0.07	0.37	0.18	0.59	0.27	0.41	0.26	0.12	0.15	K_2O	0.00	0.01	0.00
Total	100.02	101.27	100.38	101.85	100.61	101.40	101.14	98.65	100.11	Total	100.34	100.45	100.14
Oxygen	32	32	32	32	32	32	32	32	32	Oxygen	6	6	6
Si	8.795	10.041	9.495	10.775	9.550	10.186	9.566	8.941	9.171	Si	1.975	1.995	1.995
Al	7.064	5.949	6.455	5.270	6.397	5.788	6.368	6.968	6.817	Al	0.093	0.021	0.003
Ti	0.000	0.006	0.012	0.000	0.003	0.009	0.006	0.009	0.003	Ti	0.004	0.003	0.002
Fe	0.089	0.064	0.059	0.037	0.076	0.061	0.063	0.072	0.070	Fe	0.445	0.416	0.987
Mn	0.000	0.000	0.000	0.000	0.000	0.000	0.000	0.000	0.000	Mn	0.020	0.021	0.037
Mg	0.019	0.007	0.000	0.000	0.015	0.000	0.008	0.000	0.007	Mg	0.652	0.709	0.953
Ca	3.347	1.985	2.539	1.307	2.501	1.887	2.460	3.145	2.804	Ca	0.776	0.818	0.024
Na	0.703	1.765	1.370	2.269	1.352	1.871	1.487	0.837	1.052	Na	0.018	0.017	0.000
K	0.016	0.085	0.041	0.132	0.063	0.092	0.060	0.028	0.036	K	0.000	0.001	0.000
Total	20.032	19.903	19.971	19.791	19.956	19.989	20.018	19.999	19.961	Total	3.983	4.000	4.001
An	82.32	51.76	64.28	35.25	63.87	49.01	61.39	78.43	72.05	En	34.44	36.10	47.63
Ab	17.29	46.02	34.68	61.19	34.53	48.60	37.11	20.87	27.03	Fs	24.56	22.25	51.17
Or	0.39	2.22	1.04	3.56	1.61	2.39	1.50	0.70	0.92	Wo	40.99	41.65	1.20

Appendix D.2.

Sample no.	*KA386*	*KA386*
Analysis no.	44	64
	r	c
SiO_2	54.25	51.93
Al_2O_3	1.05	1.82
TiO_2	0.41	0.40
FeO	17.85	10.72
MnO	0.31	0.53
MgO	24.85	12.86
CaO	2.21	21.52
Na_2O	0.00	0.16
K_2O	0.00	0.02
Total	100.93	99.95
Oxygen	6	6
Si	1.966	1.954
Al	0.045	0.081
Ti	0.011	0.011
Fe	0.541	0.337
Mn	0.010	0.017
Mg	1.343	0.721
Ca	0.086	0.867
Na	0.000	0.012
K	0.000	0.001
Total	4.001	4.001
En	67.83	37.13
Fs	27.83	18.23
Wo	4.34	44.64

Appendix D.3.

Plagioclase											Pyroxene		
Sample no.	*KA428C*	*KA428C*	*KA428C*	*KA428C*	*KA9A*	*KA9A*	*KA9A*	*KA9A*	*KA9A*	*KA9A*	*Sample no.*	*KA9A*	*KA9A*
Analysis no.	567	568	569	570	195	198	199	200	201	202	Analysis no	159	160
	c	r	c	r	c	m	c	c	m	r		c	c
SiO_2	48.90	49.96	52.76	49.24	52.73	52.50	64.57	52.01	49.78	50.33	SiO_2	52.39	52.61
Al_2O_3	31.86	30.81	29.46	31.64	28.01	28.96	21.47	29.05	30.91	29.98	Al_2O_3	0.89	2.14
TiO_2	0.03	0.03	0.00	0.04	0.02	0.05	0.10	0.04	0.00	0.05	TiO_2	0.2	0.3
FeO	0.39	0.39	0.31	0.58	0.47	0.44	0.96	0.54	0.52	0.68	FeO	19.8	18.38
MnO	0.00	0.00	0.00	0.00	0.00	0.04	0.00	0.00	0.00	0.00	MnO	0.36	0.37
MgO	0.00	0.03	0.00	0.00	0.06	0.07	0.00	0.05	0.10	0.08	MgO	22.28	23.73
CaO	16.14	14.64	13.28	15.79	12.39	12.94	6.67	13.83	14.25	14.15	CaO	1.99	2.03
Na_2O	2.45	3.02	3.72	2.51	3.96	3.53	3.50	3.50	2.46	2.72	Na_2O	0.28	0.24
K_2O	0.12	0.19	0.28	0.14	0.38	0.34	1.09	0.30	0.15	0.20	K_2O	0.04	0.05
Total	99.88	99.08	99.81	99.93	98.03	98.88	98.58	99.32	98.17	98.20	Total	98.24	99.83
Oxygen	32	32	32	32	32	32	32	32	32	32	Oxygen	6	6
Si	8.981	9.212	9.599	9.035	9.761	9.638	11.504	9.843	9.233	9.344	Si	1.975	1.937
Al	6.896	6.696	6.317	6.842	6.112	6.267	4.509	6.480	6.756	6.560	Al	0.040	0.093
Ti	0.005	0.004	0.000	0.005	0.003	0.007	0.042	0.006	0.000	0.007	Ti	0.006	0.008
Fe	0.060	0.061	0.047	0.088	0.073	0.068	0.143	0.085	0.081	0.106	Fe	0.624	0.566
Mn	0.000	0.000	0.000	0.000	0.000	0.006	0.000	0.000	0.000	0.000	Mn	0.011	0.012
Mg	0.000	0.008	0.000	0.000	0.018	0.020	0.000	0.015	0.027	0.022	Mg	1.252	1.303
Ca	3.175	2.892	2.589	3.105	2.457	2.545	1.273	2.804	2.832	2.814	Ca	0.080	0.080
Na	0.871	1.080	1.313	0.893	1.421	1.257	1.210	1.284	0.886	0.980	Na	0.020	0.017
K	0.028	0.045	0.064	0.033	0.091	0.079	0.247	0.073	0.035	0.048	K	0.002	0.002
Total	20.016	19.998	19.931	20.002	19.936	19.889	18.928	20.589	19.850	19.882	Total	4.011	4.018
An	77.93	71.99	65.28	77.03	61.90	65.58	46.63	67.39	75.46	73.24	En	63.65	66.45
Ab	21.38	26.89	33.11	22.15	35.80	32.39	44.32	30.86	23.61	25.51	Fs	32.28	29.47
Or	0.69	1.12	1.61	0.82	2.29	2.04	9.05	1.75	0.93	1.25	Wo	4.07	4.08

Appendix D.3.

Sample no.	*KA9A*	*KA9A*	*KA9A*	*KA9A*	*KA9A*	*KA9A*	*KA428C*	*KA428C*	*KA29*	*KA29*	*KA29*
Analysis no	161	162	163	164	167	193	565	566	358	356	363
	c	c	c	r	c	c	c	r	r	c	c
SiO_2	53.71	50.78	53.02	53.42	51.73	53.15	51.61	52.75	50.83	50.35	50.7
Al_2O_3	0.78	1.84	1.21	1.26	1.64	1.69	4	1.48	2.13	3.61	2.34
TiO_2	0.15	0.51	0.33	0.35	0.36	0.21	0.49	0.33	0.46	0.59	0.42
FeO	18.7	12.83	19.58	18.63	23.43	18.02	9.53	9.93	10.69	11.81	11.47
MnO	0.37	0.26	0.31	0.38	0.34	0.43	0.27	0.85	0.23	0.26	0.35
MgO	24.07	12.87	22.8	23.24	17.95	23.12	14.82	15.36	14.65	14.03	14.88
CaO	1.86	18.45	1.94	1.8	3.46	1.6	18.54	18.33	21.42	20.98	19.85
Na_2O	0.22	0.76	0.24	0.2	0.19	0.16	0.13	0.34	0.38	0.35	0.42
K_2O	0.08	0.04	0.04	0.03	0.1	0.02	0.06	0.05	0.03	0.01	0.02
Total	99.95	98.33	99.46	99.32	99.19	98.4	99.44	99.4	100.82	101.98	100.45
Oxygen	6	6	6	6	6	6	6	6	6	6	6
Si	1.976	1.950	1.968	1.975	1.971	1.976	1.919	1.972	1.901	1.867	1.902
Al	0.034	0.083	0.053	0.055	0.074	0.074	0.175	0.065	0.094	0.158	0.104
Ti	0.004	0.015	0.009	0.010	0.010	0.006	0.014	0.009	0.013	0.017	0.012
Fe	0.575	0.412	0.608	0.576	0.746	0.560	0.296	0.310	0.334	0.366	0.360
Mn	0.011	0.008	0.010	0.012	0.011	0.014	0.009	0.027	0.007	0.008	0.011
Mg	1.320	0.737	1.262	1.281	1.019	1.281	0.821	0.856	0.817	0.775	0.832
Ca	0.073	0.759	0.077	0.071	0.141	0.064	0.739	0.734	0.858	0.833	0.798
Na	0.016	0.056	0.017	0.014	0.014	0.012	0.009	0.024	0.028	0.025	0.030
K	0.004	0.002	0.002	0.002	0.005	0.001	0.003	0.002	0.001	0.001	0.001
Total	4.013	4.023	4.006	3.996	3.991	3.987	3.985	4.000	4.054	4.050	4.050
En	66.7	38.47	64.49	66.03	53.16	66.75	44.02	44.42	40.53	39.1	41.58
Fs	29.61	21.92	31.58	30.31	39.49	29.91	16.35	17.49	16.91	18.87	18.54
Wo	3.69	39.61	3.93	3.66	7.36	3.34	39.62	38.09	42.56	42.03	39.88

Appendix D.4. Kaingaroa meta-rhyolite lithics: Tourmaline

Tourmaline						
Sample no	KA46	KA430	KA430	KA430	KA430	KA430
Analyses no	553	555	556	557	558	559
	c	c	c	m	m	r
SiO_2	36.888	36.176	36.347	35.81	36.32	36.238
Al_2O_3	36.066	36.019	36.317	35.977	36.02	36.006
TiO_2	0.092	0.091	0.119	0.135	0.119	0.126
FeO	6.25	5.877	5.978	5.915	6.123	4.237
MnO	0	0	0	0	0	0.023
MgO	4.813	5.088	4.964	4.964	4.966	4.927
CaO	1.346	1.44	1.295	1.413	1.45	1.47
Na_2O	1.478	1.478	1.429	1.428	1.488	1.39
K_2O	0.092	0.097	0.079	0.091	0.143	0.075
Total	87.0292	86.2695	86.5301	85.7372	86.6326	84.4976
Oxygen	29	29	29	29	29	29
B	3.000	3.000	3.000	3.000	3.000	3.000
Si	6.9912	6.9153	6.9209	6.8897	6.9244	6.9966
Al	8.056	8.1148	8.15	8.1577	8.0934	8.1932
Ti	0.0132	0.0132	0.0171	0.0196	0.0171	0.0183
Fe	0.9906	0.9395	0.9519	0.9518	0.9762	0.6842
Mn	0	0	0	0	0	0.0038
Mg	1.3599	1.4501	1.4091	1.4238	1.4116	1.4181
Ca	0.2734	0.295	0.2642	0.2913	0.2962	0.3042
Na	0.5431	0.5478	0.5276	0.5328	0.5501	0.5206
K	0.0224	0.0238	0.0192	0.0224	0.0349	0.0185
Total	21.2502	21.2998	21.2604	21.2894	21.3042	21.158

Appendix D.5. Kawerau ignimbrite

Plagioclase													
Sample no.	KA114	KA114	KA114	KA114	KA114	KA114	KA114	KA114	KA114	KA110	KA110	KA110	KA110
Analysis no	419	420	421	422	430	431	432	446	447	524	525	526	530
	c	r	c	r	c	m	r	c	r	c	r	r	c
SiO_2	59.63	57.76	59.97	60.03	57.36	57.44	57.61	57.24	59.09	61.45	58.13	58.40	59.33
Al_2O_3	25.50	25.76	25.40	25.35	26.61	26.53	26.92	26.65	25.76	23.72	25.91	24.76	24.98
TiO_2	0.00	0.06	0.00	0.02	0.02	0.03	0.06	0.00	0.00	0.00	0.00	0.00	0.00
FeO	0.24	0.17	0.21	0.28	0.26	0.27	0.40	0.28	0.12	0.18	0.14	0.24	0.32
MnO	0.00	0.02	0.00	0.00	0.00	0.00	0.00	0.04	0.00	0.00	0.00	0.02	0.00
MgO	0.00	0.03	0.00	0.00	0.02	0.02	0.02	0.00	0.00	0.00	0.00	0.00	0.00
CaO	7.95	8.78	7.21	7.45	9.34	8.97	8.69	9.70	7.88	5.30	8.12	7.32	7.05
Na_2O	6.83	5.20	7.17	6.95	6.03	6.15	6.19	6.09	6.93	7.13	6.23	6.78	6.95
K_2O	0.26	0.25	0.28	0.26	0.20	0.20	0.18	0.19	0.21	0.38	0.17	0.23	0.27
Total	100.40	98.01	100.25	100.35	99.84	99.60	100.08	100.20	99.97	98.15	98.70	97.77	98.90
Oxygen	32	32	32	32	32	32	32	32	32	32	32	32	32
Si	10.611	10.505	10.669	10.671	10.310	10.339	10.316	10.274	10.557	11.059	10.507	10.657	10.693
Al	5.347	5.521	5.326	5.311	5.638	5.628	5.681	5.637	5.424	5.031	5.520	5.326	5.305
Ti	0.000	0.008	0.000	0.003	0.003	0.004	0.008	0.000	0.000	0.000	0.000	0.000	0.000
Fe	0.035	0.026	0.031	0.042	0.040	0.040	0.060	0.042	0.018	0.027	0.021	0.037	0.048
Mn	0.000	0.003	0.000	0.000	0.000	0.000	0.000	0.006	0.000	0.000	0.000	0.003	0.000
Mg	0.000	0.007	0.000	0.000	0.005	0.006	0.007	0.000	0.000	0.000	0.000	0.000	0.000
Ca	1.515	1.710	1.374	1.418	1.799	1.730	1.668	1.866	1.508	1.021	1.572	1.432	1.362
Na	2.355	1.833	2.472	2.395	2.100	2.147	2.149	2.120	2.400	2.489	2.184	2.400	2.428
K	0.059	0.058	0.064	0.059	0.045	0.045	0.040	0.043	0.047	0.088	0.039	0.054	0.063
Total	19.922	19.671	19.937	19.898	19.941	19.939	19.930	19.989	19.954	19.714	19.844	19.908	19.900
An	38.56	47.50	35.14	36.63	45.60	44.10	43.24	46.31	38.12	28.38	41.42	36.85	35.35
Ab	59.95	50.91	63.22	61.86	53.25	54.75	55.72	52.63	60.68	69.19	57.56	61.77	63.02
Or	1.49	1.60	1.63	1.52	1.15	1.15	1.04	1.05	1.19	2.43	1.02	1.38	1.63

Appendix D.5. Kawerau ignimbrite

Pyroxene

Sample no.	KA110	KA110	KA110	KA110	Sample no.	KA114	KA114	KA114	KA114	KA114	KA114	KA114	KA114
Analysis no	531	547	548	549	Analysis no	433	434	435	436	440	441	448	449
	r	c	c	r		c	r	c	r	c	r	c	r
SiO_2	59.46	62.47	62.45	60.00	SiO_2	52.61	51.45	52.87	52.87	51.79	52.62	52.35	52.55
Al_2O_3	25.38	24.18	24.94	25.78	Al_2O_3	1.44	2.03	1.27	1.18	0.46	0.49	1.85	1.30
TiO_2	0.00	0.00	0.00	0.00	TiO_2	0.41	0.49	0.34	0.28	0.15	0.10	0.49	0.35
FeO	0.16	0.18	0.20	0.28	FeO	9.34	9.61	20.54	20.57	24.81	24.40	9.58	9.27
MnO	0.00	0.02	0.02	0.00	MnO	0.61	0.61	0.68	0.57	2.37	2.30	0.44	0.66
MgO	0.00	0.00	0.00	0.00	MgO	15.25	14.18	23.83	23.95	20.55	20.32	14.63	15.28
CaO	7.59	6.11	6.24	7.81	CaO	20.68	19.38	1.51	1.51	0.83	0.83	20.62	20.89
Na_2O	6.50	7.58	7.35	6.75	Na_2O	0.30	0.33	0.03	0.00	0.00	0.05	0.34	0.33
K_2O	0.28	0.37	0.34	0.26	K_2O	0.00	0.00	0.00	0.00	0.00	0.01	0.00	0.00
Total	99.37	100.91	101.54	100.88	Total	100.64	98.07	101.06	100.93	100.96	101.13	100.31	100.64
Oxygen	32	32	32	32	Oxygen	6	6	6	6	6	6	6	6
Si	10.657	10.985	10.908	10.614	Si	1.950	1.954	1.941	1.943	1.955	1.975	1.947	1.950
Al	5.361	5.011	5.134	5.375	Al	0.063	0.091	0.055	0.051	0.020	0.022	0.081	0.057
Ti	0.000	0.000	0.000	0.000	Ti	0.011	0.014	0.009	0.008	0.004	0.003	0.014	0.010
Fe	0.025	0.027	0.029	0.042	Fe	0.289	0.305	0.631	0.632	0.784	0.766	0.298	0.288
Mn	0.000	0.003	0.004	0.000	Mn	0.019	0.020	0.021	0.018	0.076	0.073	0.014	0.021
Mg	0.000	0.000	0.000	0.000	Mg	0.842	0.803	1.304	1.312	1.157	1.137	0.811	0.845
Ca	1.458	1.151	1.168	1.480	Ca	0.821	0.789	0.060	0.059	0.034	0.033	0.822	0.830
Na	2.260	2.584	2.489	2.317	Na	0.022	0.024	0.002	0.000	0.000	0.003	0.025	0.024
K	0.063	0.083	0.076	0.058	K	0.000	0.000	0.000	0.000	0.000	0.001	0.000	0.000
Total	19.824	19.843	19.807	19.886	Total	4.018	3.999	4.023	4.024	4.030	4.013	4.011	4.024
An	38.55	30.15	31.29	38.40	En	42.71	41.89	64.72	64.92	56.44	56.60	41.71	42.60
Ab	59.78	67.67	66.68	60.10	Fs	15.64	16.95	32.33	32.15	41.92	41.76	16.03	15.54
Or	1.67	2.17	2.04	1.50	Wo	41.65	41.16	2.95	2.93	1.64	1.65	42.26	41.86

Appendix D.5. Kawerau ignimbrite

Sample no.	KA114	KA110	KA110	KA110	KA110	KA110	KA110
Analysis no	450	532	533	534	535	537	538
	c	c	c	c	r	c	r
SiO_2	51.39	50.83	51.85	52.23	51.41	52.01	51.92
Al_2O_3	2.37	0.34	0.38	0.24	0.77	0.35	0.52
TiO_2	0.59	0.11	0.09	0.10	0.25	0.08	0.12
FeO	9.70	23.52	24.57	23.54	22.61	22.02	22.77
MnO	0.59	2.17	2.34	1.93	1.47	2.22	2.04
MgO	14.24	20.14	20.48	20.92	20.52	21.08	20.79
CaO	20.12	0.80	0.79	0.90	0.96	0.54	0.73
Na_2O	0.30	0.00	0.00	0.00	0.00	0.00	0.00
K_2O	0.00	0.00	0.00	0.00	0.00	0.00	0.00
Total	99.29	97.91	100.49	99.85	98.00	98.29	98.90
Oxygen	6	6	6	6	6	6	6
Si	1.933	1.970	1.964	1.977	1.973	1.987	1.978
Al	0.105	0.015	0.017	0.011	0.035	0.016	0.023
Ti	0.017	0.003	0.003	0.003	0.007	0.002	0.003
Fe	0.305	0.762	0.778	0.745	0.726	0.703	0.725
Mn	0.019	0.071	0.075	0.062	0.048	0.072	0.066
Mg	0.798	1.164	1.157	1.180	1.174	1.201	1.181
Ca	0.811	0.033	0.032	0.036	0.039	0.022	0.030
Na	0.022	0.000	0.000	0.000	0.000	0.000	0.000
K	0.000	0.000	0.000	0.000	0.000	0.000	0.000
Total	4.009	4.019	4.025	4.015	4.002	4.003	4.007
En	41.29	57.32	56.64	58.33	59.10	60.10	58.99
Fs	16.76	41.06	41.79	39.87	38.92	38.80	39.53
Wo	41.95	1.63	1.57	1.80	1.98	1.10	1.47

Amphibole

Sample no.	KA114	KA114	KA114	KA114	KA114
Analysis no.	426	427	437	438	439
	c	r	c	m	r
SiO_2	43.00	43.03	44.04	44.10	44.54
Al_2O_3	9.61	9.40	9.14	9.10	9.09
TiO_2	3.07	3.07	2.71	2.90	2.68
FeO	12.47	12.79	14.12	14.38	13.71
MnO	0.28	0.19	0.41	0.27	0.32
MgO	13.96	13.94	13.76	13.75	13.74
CaO	10.45	11.08	10.54	10.28	10.62
Na_2O	2.29	2.16	2.15	2.17	2.13
K_2O	0.39	0.37	0.34	0.36	0.29
Total	95.53	96.03	97.21	97.32	97.11
Droop recalc					
FeO	12.467	6.42	5.05	4.69	5.81
Fe_2O_3	8.32	7.08	10.08	10.78	8.78
Oxygen	23	23	23	23	23
Si	6.344	6.352	6.396	6.387	6.471
Al	1.670	1.635	1.564	1.554	1.556
Ti	0.341	0.341	0.296	0.315	0.292
Fe^{2+}	0.614	0.793	0.614	0.568	0.706
Fe^{3+}	0.924	0.787	1.101	1.174	0.960
Mn	0.035	0.023	0.050	0.033	0.039
Mg	3.071	3.069	2.978	2.969	2.976
Ca	1.65	1.75	1.64	1.59	1.65
Na	0.66	0.62	0.61	0.61	0.60
K	0.07	0.07	0.06	0.07	0.05
Total	15.382	15.439	15.310	15.272	15.305

Appendix D.5. Kawerau ignimbrite

			Fe/Ti oxides								Fayalite		
Sample no	KA110	KA110	Sample no	KA110	KA110	KA110	KA110	KA110	KA114	KA114	Sample no.	KA114	KA114
	539	540		515	518	536	545	546	442	443	Analysis no.	412	413
	c	r		ilm	ilm	ilm	mgt	mgt	ilm	ilm		r	c
SiO_2	46.41	47.94	SiO_2	0.00	0.00	0.00	0.00	0.00	0.00	0.00	SiO_2	30.03	28.00
Al_2O_3	6.89	5.94	Al_2O_3	0.22	0.23	0.06	0.06	0.09	1.54	1.11	Al_2O_3	0.10	0.00
TiO_2	1.59	1.44	TiO_2	41.81	41.68	47.92	48.21	44.17	8.39	8.91	TiO_2	0.04	0.00
FeO	12.85	13.64	FeO	52.02	53.60	49.02	48.82	50.66	84.66	83.50	FeO	62.15	68.06
MnO	0.66	0.68	MnO	0.83	0.84	1.16	1.24	1.46	1.06	0.78	MnO	5.08	5.18
MgO	14.59	15.04	MgO	2.25	2.89	1.32	1.06	1.86	0.86	0.99	MgO	0.03	0.00
CaO	10.51	10.32	CaO	0.00	0.02	0.00	0.00	0.01	0.00	0.00	CaO	0.05	0.00
Na_2O	1.60	1.44	Na_2O	0.00	0.00	0.00	0.00	0.00	0.00	0.00	Na_2O	0.00	0.00
K_2O	0.31	0.20	K_2O	0.00	0.00	0.01	0.00	0.00	0.00	0.00	K_2O	0.01	0.00
Total	95.39	96.64	Total	97.14	99.26	99.48	99.39	98.26	96.50	95.29	Total	97.49	101.24
Droop recalc			Droop recalc								Oxygen	4	4
FeO	9.59	11.85	FeO	39.56	40.21	34.91	37.26	37.34	32.76	31.47	Si	1.029	0.955
Fe_2O_3	4.22	2.98	Fe_2O_3	10.55	9.57	17.51	52.68	51.29	21.41	24.59	Al	0.004	0.000
Oxygen	23	23	Oxygen	6	6	6	32	32	6	6	Ti	0.001	0.000
Si	6.797	6.892	Si	0.000	0.000	0.000	0.000	0.000	0.000	0.000	Fe	1.782	1.941
Al	1.189	1.007	Al	0.003	0.004	0.006	0.536	0.393	0.013	0.013	Mn	0.148	0.150
Ti	0.175	0.156	Ti	1.801	1.818	1.667	1.867	2.012	1.587	1.539	Mg	0.002	0.000
Fe^{2+}	1.057	1.281	Fe^{2+}	1.652	1.686	1.465	9.221	9.371	1.383	1.292	Ca	0.002	0.000
Fe^{3+}	0.517	0.358	Fe^{3+}	0.396	0.361	0.661	11.731	11.583	0.813	0.908	Na	0.000	0.000
Mn	0.082	0.083	Mn	0.049	0.053	0.062	0.265	0.197	0.035	0.035	K	0.001	0.000
Mg	3.185	3.223	Mg	0.099	0.079	0.139	0.381	0.444	0.169	0.211	Total	2.968	3.045
Ca	1.65	1.59	Ca	0.00	0.00	0.00	0.00	0.00	0.00	0.00	Fa	92.28	92.85
Na	0.46	0.40	Na	0.00	0.00	0.00	0.00	0.00	0.00	0.00	Fo	0.08	0.00
K	0.06	0.04	K	0.00	0.00	0.00	0.00	0.00	0.00	0.00	Te	7.64	7.15
Total	15.163	15.027	Total	4	4	4	24	24	4	4			

Appendix D.5. Kawerau ignimbrite

Sample no.	KA114	KA114	KA114	KA114	KA114	KA114	KA114	KA114	KA114	KA110
Analysis no.	414	415	416	418	423	424	425	428	429	543
	r	r	c	r	c	r	r	c	r	c
SiO_2	30.77	30.46	27.91	29.78	28.15	28.01	28.31	28.36	29.02	29.62
Al_2O_3	0.45	0.13	0.00	0.03	0.00	0.00	0.00	0.00	0.04	0.00
TiO_2	0.05	0.06	0.03	0.00	0.00	0.05	0.00	0.00	0.00	0.00
FeO	59.23	59.83	67.42	62.25	69.40	67.56	68.81	67.64	65.20	59.78
MnO	4.70	4.44	4.89	4.54	4.57	4.78	4.45	4.70	4.76	5.29
MgO	0.04	0.21	0.00	0.00	0.00	0.00	0.00	0.00	0.00	0.14
CaO	0.13	0.06	0.04	0.04	0.02	0.02	0.03	0.00	0.03	0.07
Na_2O	0.00	0.00	0.00	0.05	0.00	0.00	0.00	0.00	0.00	0.00
K_2O	0.04	0.02	0.00	0.07	0.00	0.00	0.00	0.00	0.00	0.00
Total	95.42	95.21	100.29	96.76	102.14	100.42	101.59	100.71	99.05	94.91
Oxygen	4	4	4	4	4	4	4	4	4	4
Si	1.060	1.055	0.959	1.030	0.952	0.960	0.960	0.967	0.995	1.039
Al	0.018	0.005	0.000	0.001	0.000	0.000	0.000	0.000	0.002	0.000
Ti	0.001	0.002	0.001	0.000	0.000	0.001	0.000	0.000	0.000	0.000
Fe	1.706	1.734	1.937	1.801	1.964	1.937	1.951	1.929	1.869	1.754
Mn	0.137	0.130	0.142	0.133	0.131	0.139	0.128	0.136	0.138	0.157
Mg	0.002	0.011	0.000	0.000	0.000	0.000	0.000	0.000	0.000	0.008
Ca	0.005	0.002	0.001	0.001	0.001	0.001	0.001	0.000	0.001	0.003
Na	0.000	0.000	0.000	0.003	0.000	0.000	0.000	0.000	0.000	0.000
K	0.002	0.001	0.000	0.003	0.000	0.000	0.000	0.000	0.000	0.000
Total	2.931	2.941	3.040	2.972	3.048	3.038	3.040	3.033	3.005	2.961
Fa	92.46	92.48	93.16	93.12	93.75	93.32	93.86	93.42	93.11	91.41
Fo	0.12	0.56	0.00	0.00	0.00	0.00	0.00	0.00	0.00	0.39
Te	7.42	6.96	6.84	6.88	6.25	6.68	6.14	6.58	6.89	8.20

Appendix D.6. Welded ignimbrite of Wairakei drill holes

Sample no.	CORE	CORE	CORE	CORE	CORE	CORE	CORE	CORE	CORE	CORE	CORE	CORE
Mineral	opyx	opyx	opyx	opyx	opyx	opyx	plag	plag	plag	plag	glass	glass
Analysis no.	131	132	138	140	141	148	207	208	210	211	146	147
	c	r	c	r	c	c	c	r	c	r	brown	clear
SiO_2	49.92	47.83	48.11	48.79	48.28	50.60	64.04	64.24	62.25	64.23	76.58	76.58
Al_2O_3	0.92	0.38	0.63	0.10	0.23	1.16	23.72	24.42	25.44	23.87	11.48	10.91
TiO_2	0.26	0.15	0.21	0.08	0.09	0.48	0.00	0.00	0.00	0.00	0.05	0.03
FeO	30.53	37.45	34.27	38.42	39.05	34.84	0.19	0.27	0.16	0.20	1.13	1.20
MnO	1.05	1.49	1.49	1.73	1.65	1.98	0.00	0.00	0.02	0.00	0.00	0.04
MgO	14.97	10.22	12.13	10.07	9.68	10.17	0.00	0.00	0.00	0.00	0.00	0.05
CaO	1.08	1.04	1.84	1.11	1.16	0.95	5.71	6.05	7.21	4.97	0.45	0.50
Na_2O	0.00	0.00	0.00	0.00	0.00	0.17	6.33	6.49	6.47	6.82	6.53	4.84
K_2O	0.00	0.00	0.00	0.00	0.02	0.09	0.49	0.48	0.35	0.54	3.95	4.10
Total	98.73	98.57	98.69	100.28	100.16	100.15	100.47	101.96	101.90	100.61	100.18	98.23
Oxygen	6	6	6	6	6	6	32	32	32	32		
Si	1.974	1.972	1.955	1.982	1.973	2.014	11.215	11.113	10.835	11.226		
Al	0.043	0.019	0.030	0.005	0.011	0.055	4.895	4.980	5.219	4.917		
Ti	0.008	0.005	0.006	0.002	0.003	0.005	0.000	0.000	0.000	0.000		
Fe	1.010	1.292	1.165	1.306	1.334	1.160	0.028	0.039	0.023	0.029		
Mn	0.035	0.052	0.051	0.059	0.057	0.067	0.000	0.000	0.002	0.000		
Mg	0.882	0.629	0.735	0.610	0.590	0.603	0.000	0.000	0.000	0.000		
Ca	0.046	0.046	0.080	0.048	0.051	0.041	1.071	1.122	1.344	0.931		
Na	0.000	0.000	0.000	0.000	0.000	0.013	2.148	2.177	2.184	2.310		
K	0.000	0.000	0.000	0.000	0.001	0.005	0.109	0.106	0.078	0.119		
Total	3.997	4.014	4.023	4.013	4.020	3.962	19.466	19.539	19.686	19.531		
En	44.7	31.15	36.19	30.15	29.04	32.23	32.18	32.95	37.27	27.71		
Fs	52.97	66.57	59.87	67.47	68.45	65.58	64.54	63.94	60.57	68.75		
Wo	2.33	2.28	3.94	2.37	2.51	2.19	3.28	3.11	2.16	3.54		

Appendix E

Geochemical methods and data

Sample collection and preparation

Pumice

Samples of pumice, and not whole rock pyroclastic deposits have been analysed, to eliminate the effects of crystal concentration or depletion, presence of lithics, and sampling of multiple pumice types and hence magma compositions. Wherever possible clasts of > 4cm in length were selected, as pumices less than this size may no longer be representative of magmatic compositions, having preferentially lost crystals during syn-eruptive fragmentation, and/or cleaning (Wolff 1985). Individual pumices were chosen where possible, as combined pumices obscure possible compositional variation. Pumice samples are hence taken to be representative of the magma. Several pumice samples were collected from the same stratigraphic horizon and analysed in order to evaluate possible heterogeneity.

Matrix adhering to pumices was removed by washing in water and using a wire brush or toothbrush; they were then dried. Where possible only single non vapour-phase altered pumices were used for analysis. Pumice size and alteration in the Kaingaroa Ignimbrite was such that most pumices were unsuitable for analysis. Outer pink Fe-stained rims, where present, were removed, and a fraction of the sample retained for possible further detailed analysis (e.g. REE or isotopes). Samples were lightly crushed, and milled using a tungten carbide concentric ring mill, or in the case of small sample size, milled in a tungten carbide ball mill. The mill was thoroughly cleaned between samples.

Lithics and rhyolite domes

Dense rock samples for XRF included rhyolite domes, lithics within the Kaingaroa Ignimbrite, and a single bleb sample (KA386f). Samples were cleaned, coarsely crushed in a hydraulic ram, and a representative portion milled similar to that described above for pumice preparation.

XRF

Major and trace element analysis was carried out at the University of Canterbury following the general methods of Norrish and Hutton (1969). XRF trace elements were obtained using 30 or 50 mm (sample size dependent) pressed powder pellets, prepared from powdered rock and bound with 7% aqueous polyvinyl alcohol. Pressed pellets were irradiated using a 3kW Au tube (at 60kV, 45mA) for analysis of Zr, Nb, Ba, Ni, Cr, V, La, Ce, and Nd, and with a 3kW Mo tube (at 90kV, 30mA) for analysis of Rb, Sr, Y, Pb, Th, and Ga. Lithium tetraborate fusion beads were irradiated using a 3kW Sc tube (at 50kV, 50mA) for determination of major element concentrations. Analyses were carried out on a Philips PW 1400 X-Ray spectrometer. Estimates of XRF precision are presented in Weaver et al (1990). Regular calibrations of XRF made on a set of 35 international standards, and analyses were carried out by Stephen Brown. Only analyses with totals of 99.5 $\pm$ 1.0% were accepted. Major element analyses are hydrous in tables, but are recalculated anhydrous in all figures, and are quoted in the text. Total iron is given as Fe_2O_3.

ICP-MS and INAA

Rare earth elements, Th, U, Hf and Ta of gabbroic and andesitic lithics were determined by conventional ICP-MS (inductively coupled plasma mass spectrometry) techniques at Analabs, Perth, Western Australia. Approximately 0.5g of rock powder was made up to 50mL aliquots with a mixed acid digest and analysed by ICP-MS. Instrumental neutron activation analyses (INAA) of rhyolitic pumices were determined by Dr Phil Kyle at Department of Earth and Environmental Sciences, New Mexico Tech, Socorro, USA.

Use of XRF, ICP-MS and INAA analyses

XRF was undertaken on 140 samples; a further subset of 8 andesitic and gabbroic samples was analysed by ICP-MS for La, Ce, Nd, Sm, Eu, Gd, Dy, Yb, Lu, Th, Hf, Ta, U. Accessory minerals were not fully dissolved in their preparation but this is not believed to be a factor in gabbroic and andesitic samples, which appear to have no REE or Th-bearing accessory phases. A subset of 7 pumice samples were analysed by INAA for Sc, As, Br, Sb, Cs, La, Ce, Sm, Eu, Tb, Yb, Lu, Hf, Ta, Th, and U.

All tables of representative analyses quote both XRF and INAA (or ICP-MS) values where available. Variation diagrams present XRF data only; spiderplots present XRF and INAA/or ICP/MS for separate elements but XRF and INAA/or ICP/MS are not used for comparison. REE plots utilise INAA/or ICP/MS.

Isotopes

Twelve samples, representative of each pumice type, and a single gabbroic lithic and post-caldera rhyolite dome were chosen for Sr and Nd isotope analysis. Nd and Sr isotope ratios were determined at the TIMS laboratory at La Trobe University, Melbourne, by Dr Tod Waight. Isotope ratios were measured on a Finnigan MAT262 multi-collector mass spectrometer. Methods used during isotope dissolution and measurement were similar to those of Maas and McCulloch (1991).

Procedural blanks (dissolution, column chemistry, handling, loading etc) measured during the course of this work were 671pg for Sr and 332 pg for Nd. These are negligible relative to the sample sizes used and no blank corrections were applied to the data. Analyses of standards collected during this study are SRM987 of 0.710230 $\pm$ 70 (2 s.d.) and La Jolla Nd of 0.511860 $\pm$ 20 (2 s.d.). No age corrections were applied to this data. Raw ratios were corrected for instrumental mass fractionation using $^{143}Nd/^{144}Nd=0.7219$ and $^{87}Sr/^{86}Sr=8.3752$. $\varepsilon Nd = [(^{144}Nd/^{143}Nd$ sample/0.512638 (CHUR))-1] 104.

Is pumice chemistry really magma representative?

A common assumption with whole-pumice chemistry is that pumices are 'magma representative'. A number of features suggest there are numerous problems with this assumption.

A common problem in dealing with ignimbrites is that extractable pumice clasts are not always present throughout the ignimbrite. In addition pumice size in the Kaingaroa Ignimbrite are generally small (commonly > 5 cm), thus limiting sampling areas. Many analysed pumices were small, and pellet size etc is limited by the small amount of

resultant powder. As the sample size of the sample becomes larger, the true 'magmatic composition' of the magma is approached. The sample size in this study is considered representative due to the crystal-poor nature. Pumices commonly contain heterogenous glass compositions, some notably mingled, while small scale heterogeneity in phenocryst/glass ratio may occur because of glomeroporphyritic aggregates. No rhyolite-basaltic mingled clasts or basaltic pumices/scoria were observed in the Kaingaroa Ignimbrite. Recognisable mingled rhyolitic pumices were avoided during analysis, except where individual compositions could be extracted e.g. KA 45B and KA45B3.

All pumices encountered in this study were partially hydrated, and many weakly altered either due to hydration, clay replacement of glass or vapour phase alteration. Strongly altered samples were avoided during sampling, with the exception of pumices containing vapour-phase fayalite in the Kawerau ignimbrite, and two visibly altered (hydrated) pumice clasts (e.g. KA 199, 175B) which were sampled to assess possible effect of alteration on the closed sum affect and major element analyses, and mobility of alkalis and alkali earths. Altered samples are presented in Table E.2.

Low temperature ion exchange constants suggest that enrichment in H_2O and K_2O and a depletion in Na_2O will accompany interaction of glassy samples with meteoric water. Accompanying the hydration (illustrated by high LOI) is an increase in peraluminosity, and mobility or leaching of trace alkali and alkali earth elements (e.g. Ba), as has been noted by numerous other workers (e.g. Lipman 1965; Zielinski et al. 1977). High LOI contents artificially adjust major element totals, notably decreasing SiO_2, and increasing Al_2O_3 content, thus further accentuating the closed sum affect, and resulting in spurious trends on variation diagrams. The standard procedure in the literature is to normalise all major element totals to 100% i.e. recalculate all samples to anhydrous values, to compensate for variable degrees of hydration; this does not correct the problem, rather it normalises data for comparative purposes, thus recalculation to anhydrous values retains original element ratios, whether they are 'magmatic' or altered. To avoid secondary element mobility, all vapour-phase altered samples and samples containing even trace quantities of clay were removed from the sample set and are presented separately in Table E.2. Complete removal of altered samples is impossible, as all pumices are hydrated to some extent, and some scatter within variation plots may be explained by

weak variable hydration. To avoid the added problem of the closed sum affect (especially in rhyolitic compositions) limited petrogenetic or comparative value is put on major elements.

All samples with high LOI and Al_2O_3 and a representative suite of samples containing moderate to small contents of Al_2O_3 and LOI were analysed by XRD. XRD scans were run by Stephen Brown at the University of Canterbury, on a Philips PW 1729 X-Ray diffractometer, controlled by an IBM PC. XRD scans revealed presence of meta-halloysite and kaolinite in some samples, notably in samples containing greater than 18.5 % Al_2O_3 and LOI in excess of 5%.

A notable feature of the pumice chemistry of the Kaingaroa Ignimbrite is the weak zonation (as discussed in Chapter 7). Variation diagrams illustrate weak compositional zonation, and appreciable scatter. The scatter is attributed to a combination of analytical error, weak hydration, and effect of accessory minerals in crystal-poor pumices. The latter point is considered in more detail; The problem posed by accessory phases is that their modal abundances are extremely low, and are concentrated perhaps even restricted to inclusions in abundant phenocryst phases e.g. plagioclase and orthopyroxene. While it is likely on large scale that accessory phases are homogeneously distributed on the sale of the magma chamber, it is unlikely that they are homogenously distributed on the scale of individual pumice clasts. Accessory minerals are commonly hosts for large fractions of the trace element content of rhyolites and granitoids e.g Zr in zircon. As a result small variation in phenocryst content (and inclusions), can have more marked affect on certain trace element variation. Minor variations in LREE and Zr in analyses may be attributable to variable accessory phase content of pumices.

Indices of differentiation

SiO_2 is refuted as an index of differentiation due to the possibility of mobility of alkalis during hydration of pumices, and the resulting closed sum affect on major elements. Rb is used in all variation diagrams illustrating pumice chemical data, because it is incompatible in the mineral assemblage containing plagioclase + orthopyroxene + Fe/Ti oxides, and exhibits large variation which can not be attributed to accessory phase

variation. Rb is however mobile in aqueous solutions so only fresh unaltered samples are utilised in the thesis.

Data

E.1 Kaingaroa pumice XRF

E.2 Kaingaroa altered pumice XRF

E.3 Kaingaroa lithic XRF

E.4 Kawerau and Wheao XRF

E.5 Kaingaroa lithics ICP-MS

E.6 INAA

E.7 Isotopes

Appendix E.1. Kaingaroa XRF

Sample Name	*KA12*	*KA14*	*KA23A*	*KA23B*	*KA25*	*KA36*	*KA37*	*KA38*	*KA39*	*KA42*	*KA43*	*KA44A*	*KA44B*
Rock Type	Pumice	Lithic	Pumice	Pumice	Pumice	Pumice	Pumice	Pumice	Pumice	Rhyolite	Rhyolite	Pumice	Pumice
Unit	LLB	BT	TZ	TZ	LLB	RBU	RBU	OWR	OWR	KAR	KAR	OWR	OWR
Pumice type	D		C	B	D	D	B	C	C			C	C
SiO_2	70.00	74.82	68.79	73.68	69.23	69.72	73.26	70.64	70.32	76.68	76.59	71.32	71.02
TiO_2	0.26	0.21	0.27	0.19	0.25	0.28	0.16	0.24	0.24	0.15	0.16	0.22	0.21
Al_2O_3	15.35	12.89	15.37	13.00	15.09	15.35	13.00	14.85	14.70	12.27	12.54	13.19	14.36
Fe_2O_3*	2.16	1.81	2.58	1.54	3.07	2.01	1.65	1.89	1.93	1.28	1.40	1.78	1.98
MnO	0.06	0.05	0.06	0.05	0.06	0.06	0.06	0.06	0.06	0.03	0.03	0.05	0.06
MgO	0.19	0.17	0.50	0.17	0.21	0.16	0.19	0.16	0.17	0.09	0.07	0.19	0.20
CaO	1.24	1.30	1.62	1.08	1.19	1.12	1.06	1.16	1.24	0.76	0.66	1.22	1.20
Na_2O	3.39	4.06	3.84	3.80	3.80	3.28	3.72	3.69	3.58	4.21	3.83	4.57	4.16
K_2O	3.44	3.44	3.06	3.49	3.11	3.15	3.57	3.22	3.18	3.62	3.68	3.65	3.41
P_2O_5	0.04	0.04	0.04	0.03	0.03	0.02	0.02	0.03	0.03	0.03	0.02	0.03	0.03
LOI	3.77	0.52	4.11	2.74	4.13	3.40	2.28	4.21	3.70	0.68	1.18	3.39	3.45
Total	99.90	99.31	100.24	99.77	100.17	98.55	98.97	100.15	99.15	99.80	100.16	99.61	100.08
Cr	5	3	5	3	5	4	3	3	6	3	3	6	4
Ni	8	3	6	4	8	6	5	4	4	3	4	5	5
V	12	12	12	10	11	14	8	12	13	11	12	12	10
Pb	16	18	13	11	14	36	16	21	14	16	17	13	13
Zn	54	43	57	49	52	44	44	29	35	29	33	37	33
Rb	109	124	113	126	109	105	124	112	109	125	127	118	110
Ba	784	729	952	783	759	820	746	776	754	719	742	753	798
Sr	106	108	99	86	103	100	85	104	107	62	53	104	102
Ga	17	14	11	22	14	19	17	21	21	13	12	14	23
Nb	8	7	9	7	9	9	7	9	8	8	8	7	8
Zr	207	193	221	158	202	218	162	200	201	117	115	184	200
Y	29	27	25	28	25	25	28	25	26	19	21	25	26
Th	16	15	15	14	13	25	17	19	13	12	12	11	15
La	27	28	28	29	22	23	28	28	26	25	24	27	27
Ce	85	56	77	67	67	69	71	63	56	55	51	59	64

Appendix E.1. Kaingaroa XRF

Sample Name	*KA44C*	*KA44E*	*KA45A*	*KA45B*	*KA45B3*	*KA45BC*	*KA45C*	*KA45D*	*KA45E*	*KA45F*	*KA48A*	*KA48B*	*KA48C*
Rock Type	Pumice	Pumice	Pumice	Pumice	Pumice	Pumice	Pumice	Pumice	Pumice	Pumice	Pumice	Pumice	Pumice
Unit	OWR	OWR	OWR	OWR	OWR	OWR	OWR	OWR	OWR	OWR	TZ	TZ	TZ
Pumice type	C	C	C	C	B	B	C	C	C	C	C	C	
SiO_2	71.39	72.81	71.32	72.55	74.23	73.01	72.53	72.57	72.84	71.16	72.36	72.24	67.33
TiO_2	0.20	0.20	0.22	0.20	0.17	0.21	0.22	0.21	0.23	0.22	0.22	0.21	0.26
Al_2O_3	14.12	13.37	13.62	12.90	12.68	12.87	14.16	13.24	13.94	13.82	13.80	14.10	16.86
Fe_2O_3*	1.81	1.79	1.84	1.75	1.47	1.61	1.80	1.68	1.78	1.83	1.80	1.74	2.30
MnO	0.06	0.05	0.05	0.05	0.05	0.04	0.05	0.05	0.06	0.05	0.05	0.06	0.04
MgO	0.18	0.22	0.20	0.18	0.13	0.17	0.17	0.19	0.19	0.18	0.20	0.20	0.24
CaO	1.19	1.26	1.18	1.16	1.03	1.10	1.18	1.20	1.20	1.13	1.18	1.21	1.24
Na_2O	4.11	3.78	4.02	3.62	3.68	3.82	3.72	3.77	3.85	4.00	3.64	3.78	3.67
K_2O	3.50	3.45	3.55	3.71	3.85	3.76	3.36	3.49	3.47	3.42	3.58	3.34	3.04
P_2O_5	0.02	0.03	0.08	0.03	0.03	0.02	0.02	0.02	0.03	0.02	0.03	0.03	0.04
LOI	2.87	2.96	3.04	2.48	2.95	3.06	3.15	2.89	2.43	3.15	3.19	3.09	3.50
Total	99.45	99.92	99.12	98.63	100.27	99.67	100.36	99.31	100.02	98.98	100.05	100.00	98.52
Cr	3	3	4	4	4	4	8	5	4	7	5	7	
Ni	5	4	5	5	5	5	6	5	5	4	5	5	
V	12	9	10	12	9	12	11	10	10	11	11	13	
Pb	18	12	14	12	15	12	14	10	13	18	21	10	
Zn	36	45	29	33	32	30	39	26	39	33	35	45	
Rb	117	121	116	122	127	123	116	120	118	117	119	118	
Ba	754	731	825	754	770	748	799	724	820	734	773	767	
Sr	102	105	101	99	86	94	97	102	101	97	100	103	
Ga	20	17	16	14	17	15	19	13	14	13	17	14	
Nb	8	9	9	8	5	9	8	7	6	7	8	8	
Zr	188	178	187	175	156	165	190	184	187	182	193	187	
Y	30	26	31	27	31	28	31	25	29	27	28	27	
Th	30	15	14	13	13	13	14	14	29	12	15	16	
La	29	28	27	29	31	28	30	27	28	27	27	32	
Ce	62	58	66	58	59	66	65	51	58	58	66	55	

Appendix E.1. Kaingaroa XRF

Sample Name	*KA49A*	*KA49B*	*KA50*	*KA50M*	*KA51*	*KA53*	*KA53B*	*KA56*	*KA63*	*KA71*	*KA72*	*KA175B*	*KA175BL*
Rock Type	Pumice	Pumice	Pumice	Pumice	Pumice	Pumice	Pumice	Pumice	Pumice	Pumice	Pumice	Pumice	Pumice
Unit	OWR	OWR	BT	BT	BT	BT	BTI	RBU	BT	RBU	RBU	OWR	OWR
Pumice type	C	C	A	C	B	C	C	C	B	C	B	D	C
SiO_2	71.95	72.37	72.99	72.88	71.65	72.77	73.60	71.56	73.08	73.85	73.41	65.89	70.12
TiO_2	0.22	0.21	0.16	0.14	0.20	0.23	0.21	0.24	0.16	0.21	0.23	0.26	0.21
Al_2O_3	13.63	13.47	12.72	12.49	14.16	13.04	12.96	14.68	12.49	12.94	13.13	18.49	15.02
Fe_2O_3*	1.75	1.80	1.51	1.46	1.77	1.73	1.74	1.92	1.53	1.69	1.67	2.43	2.01
MnO	0.06	0.05	0.06	0.06	0.06	0.06	0.06	0.06	0.05	0.06	0.05	0.09	0.08
MgO	0.21	0.20	0.15	0.14	0.16	0.22	0.24	0.23	0.19	0.23	0.17	0.20	0.10
CaO	1.18	1.19	0.93	0.94	1.01	1.24	1.26	1.15	1.07	1.21	1.11	1.16	1.15
Na_2O	4.21	4.01	3.42	3.68	3.38	3.67	3.75	3.63	3.92	3.55	3.53	3.40	3.75
K_2O	3.55	3.64	3.70	3.85	3.40	3.56	3.55	3.29	3.81	3.57	3.69	2.66	3.12
P_2O_5	0.03	0.04	0.02	0.02	0.02	0.03	0.02	0.03	0.03	0.03	0.04	0.03	0.01
LOI	3.60	2.70	4.26	4.15	3.79	3.73	2.60	3.24	3.99	3.32	3.26	5.13	3.54
Total	100.39	99.68	99.92	99.81	99.60	100.28	99.99	100.03	100.32	100.66	100.29	99.74	99.11
Cr	5	6	3		3	3	3	3	3	3	3	3	8
Ni	5	4	5		5	4	3	4	5	4	5	6	5
V	13	11	9		10	10	11	11	10	10	10	12	10
Pb	17	14	16		22	15	14	16	16	15	14	11	16
Zn	38	39	49		44	44	45	50	44	40	50	50	50
Rb	118	120	125		118	123	126	115	128	121	124	95	113
Ba	751	725	767		754	739	754	798	771	723	747	1084	832
Sr	100	102	68		82	103	103	95	85	100	89	106	99
Ga	22	15	20		18	21	14	15	17	20	18	19	17
Nb	8	9	8		8	5	8	7	7	6	7	10	9
Zr	191	193	135		173	176	188	194	154	166	160	254	222
Y	31	27	28		27	27	26	28	28	29	28	24	27
Th	15	16	15		15	15	12	28	14	13	15	18	16
La	33	28	29		28	27	13	25	29	27	27	23	23
Ce	62	68	68		69	57	29	62	59	57	63	82	70

Appendix E.1. Kaingaroa XRF

Sample Name	*KA175C*	*KA175D*	*KA177A*	*KA177B*	*KA177C*	*KA186A*	*KA188A*	*KA188B*	*KA188C*	*KA189*	*KA191A*	*KA193*	*KA197*
Rock Type	Pumice	Pumice	Pumice	Pumice	Pumice	Pumice	Pumice	Pumice	Pumice	Pumice	Pumice	Pumice	Pumice
Unit	OWR	OWR	OWR	OWR	OWR	ULB	BTI	BTI	BTI	LLB	LLB	LLB	LLB
Pumice type	D	D	B	C	D	C	C	C	C	C	C	C	C
SiO_2	68.31	66.53	70.23	70.11	67.59	69.99	71.46	71.17	72.24	71.23	70.35	71.90	74.01
TiO_2	0.27	0.27	0.23	0.24	0.25	0.25	0.25	0.28	0.22	0.23	0.26	0.24	0.21
Al_2O_3	16.64	16.98	15.59	15.34	16.58	14.86	13.99	14.24	13.99	14.12	14.74	14.07	12.94
Fe_2O_3*	2.37	2.33	2.07	2.04	2.28	2.17	1.88	2.03	1.84	2.02	1.92	1.93	1.68
MnO	0.09	0.08	0.06	0.07	0.06	0.06	0.08	0.07	0.06	0.07	0.06	0.06	0.06
MgO	0.19	0.21	0.14	0.19	0.21	0.21	0.33	0.32	0.24	0.27	0.26	0.29	0.24
CaO	1.23	1.23	1.23	1.21	1.19	1.16	1.25	1.45	1.22	1.32	1.23	1.28	1.24
Na_2O	3.54	3.74	3.60	3.56	3.33	3.42	3.73	3.83	3.76	3.80	3.42	3.87	3.89
K_2O	2.94	2.77	3.22	3.13	2.85	3.24	3.30	3.27	3.48	3.35	3.46	3.39	2.72
P_2O_5	0.02	0.03	0.03	0.03	0.03	0.03	0.07	0.04	0.04	0.04	0.03	0.03	0.03
LOI	4.20	4.43	3.82	3.50	4.41	4.20	3.70	2.86	3.02	2.93	3.92	3.32	1.47
Total	99.80	98.60	100.22	99.42	98.78	99.59	100.04	99.56	100.11	99.38	99.65	100.38	98.49
Cr	3	3	7	7	4	7	3	3	4	8	7	5	3
Ni	3	3	4	4	5	6	5	4	4	6	7	6	4
V	9	9	11	10	12	17	11	12	11	14	15	14	11
Pb	22	18	15	16	19	9	16	16	13	6	16	12	16
Zn	49	49	48	48	44	38	40	42	41	40	45	48	44
Rb	104	99	109	109	101	112	117	116	121	116	116	114	125
Ba	846	821	877	782	850	712	717	743	736	732	728	694	763
Sr	109	111	108	106	116	97	102	105	100	105	102	106	104
Ga	18	19	16	16	18	16	15	17	14	16	17	15	15
Nb	10	10	9	9	10	8	9	8	7	7	8	7	8
Zr	259	263	221	213	227	208	198	202	194	201	204	198	187
Y	24	25	23	25	22	24	28	28	27	26	25	26	27
Th	16	18	16	15	16	14	15	15	12	13	14	14	13
La	25	25	21	23	22	20	25	25	25	23	24	21	24
Ce	92	87	67	66	60	64	68	69	58	57	67	67	60

Appendix E.1. Kaingaroa XRF

Sample Name	*KA230*	*KA230A*	*KA233A*	*KA233B*	*KA242*	*KA244*	*KA246A*	*KA246B*	*KA251*	*KA263*	*KA269A*	*KA269B*	*KA269C*
Rock Type	Pumice	Pumice	Pumice	Pumice	Pumice	Pumice	Pumice	Pumice	Pumice	Pumice	Pumice	Pumice	Pumice
Unit	ULB	ULB	BTI	BTI	LLB	ULB	ULB	ULB	BT	TZ	WIU	WIU	WIU
Pumice type	B	C	C	C	D	C	D	C	B	C	C	C	D
SiO_2	72.91	71.26	72.89	73.16	68.50	71.26	69.38	69.36	72.39	72.38	69.14	72.87	67.85
TiO_2	0.20	0.21	0.19	0.19	0.24	0.23	0.25	0.25	0.21	0.24	0.20	0.19	0.26
Al_2O_3	12.74	13.84	12.96	12.94	16.45	13.73	16.42	16.03	13.21	13.20	15.37	13.83	17.19
Fe_2O_3*	1.60	1.77	1.67	1.76	2.68	1.90	2.17	2.21	1.93	1.75	1.96	1.77	2.43
MnO	0.05	0.06	0.06	0.06	0.06	0.06	0.06	0.06	0.06	0.05	0.06	0.05	0.06
MgO	0.21	0.22	0.20	0.22	0.22	0.24	0.20	0.26	0.35	0.35	0.18	0.19	0.10
CaO	1.15	1.17	1.20	1.21	1.16	1.22	1.28	1.30	1.53	1.20	1.15	1.17	1.21
Na_2O	3.41	3.27	3.71	3.68	3.31	3.61	3.42	3.33	4.15	3.73	3.92	3.89	3.34
K_2O	3.91	3.95	3.65	3.68	2.96	3.61	3.04	3.21	3.28	3.54	3.03	3.29	2.84
P_2O_5	0.03	0.03	0.03	0.03	0.05	0.04	0.04	0.04	0.03	0.03	0.02	0.02	0.02
LOI	2.82	3.23	2.71	2.66	4.53	2.87	3.87	4.10	2.69	3.08	3.72	2.84	3.95
Total	99.03	99.01	99.27	99.59	100.16	98.77	100.13	100.15	99.83	99.55	98.75	100.11	99.25
Cr	3	3	3	5	9	4	3	3	3	3	6	3	5
Ni	3	3	3	3	8	6	6	6	3	3	3	4	3
V	11	11	12	10	24	14	12	15	13	9	11	9	12
Pb	9	10	10	12	18	9	10	5	17	16	16	16	20
Zn	25	27	33	33	53	46	40	37	45	41	47	47	50
Rb	130	121	125	125	106	119	103	115	117	122	112	120	102
Ba	751	742	760	750	809	741	717	736	709	739	774	770	844
Sr	99	99	104	104	102	102	104	102	128	100	101	99	102
Ga	14	15	14	15	18	15	18	17	16	15	17	15	20
Nb	7	8	7	6	7	7	10	8	7	8	9	8	9
Zr	179	197	187	188	215	193	233	218	196	187	212	195	246
Y	29	29	27	27	33	28	28	29	25	26	25	26	25
Th	15	12	13	14	15	14	17	16	12	15	16	13	17
La	23	22	26	23	22	25	22	22	20	24	23	24	29
Ce	67	59	57	52	82	69	75	68	52	65	59	54	75

Appendix E.1. Kaingaroa XRF

Sample Name	*KA276*	*KA282*	*KA285*	*KA291*	*KA330BL*	*KA331B*	*KA332A*	*KA332B*	*KA333A*	*KA333B*	*KA352 A*	*KA352C*	*KA354 A*
Rock Type	Pumice	Pumice	Pumice	Pumice	Pumice	Pumice	Pumice	Pumice	Pumice	Pumice	Pumice	Pumice	Pumice
Unit	RBU	RBU	RBU	RBU	TTI	TTI	TTI	TTI	TTI	TTI	OWR	OWR	OWR
Pumice type	C	B	C	B	C	C	C	C	C	C	C	C	C
SiO_2	72.54	72.48	73.32	71.64	70.32	71.14	71.61	69.87	72.29	72.95	71.96	72.12	70.17
TiO_2	0.23	0.15	0.22	0.21	0.22	0.21	0.23	0.20	0.21	0.24	0.20	0.26	0.23
Al_2O_3	12.65	12.54	13.59	14.36	15.23	13.68	13.76	14.39	13.47	13.32	14.01	13.65	14.62
Fe_2O_3*	1.71	1.64	1.82	1.99	2.07	1.83	1.80	1.82	1.86	1.76	1.79	1.91	2.00
MnO	0.07	0.05	0.05	0.06	0.06	0.06	0.07	0.06	0.06	0.06	0.05	0.06	0.05
MgO	0.20	0.19	0.23	0.23	0.14	0.32	0.28	0.30	0.32	0.25	0.17	0.25	0.21
CaO	1.19	1.13	1.18	1.08	1.22	1.28	1.23	1.25	1.38	1.26	1.14	1.25	1.16
Na_2O	3.54	3.74	3.89	3.72	3.59	3.67	4.06	3.46	3.70	3.62	3.72	4.00	4.05
K_2O	3.66	3.67	3.58	3.30	3.09	3.57	3.68	3.44	3.58	3.72	3.57	3.26	3.21
P_2O_5	0.06	0.02	0.03	0.02	0.04	0.02	0.03	0.03	0.03	0.02	0.03	0.02	0.02
LOI	2.78	2.93	2.06	3.39	4.14	3.67	3.45	4.09	2.58	2.75	2.92	2.95	3.75
Total	98.63	98.54	99.97	100.00	100.12	99.45	100.20	98.91	99.48	99.95	99.56	99.73	99.47
Cr	3	3	3	3	5	3	3	3	3	3	3	3	3
Ni	3	3	4	4	4	4	3	5	4	4	4	4	4
V	13	12	11	14	11	11	8	9	9	10	8	15	10
Pb	17	18	18	21	17	10	13	12	12	12	14	18	17
Zn	47	47	48	52	43	40	42	40	41	41	29	46	32
Rb	126	128	125	117	109	116	120	115	125	123	121	121	112
Ba	738	747	766	776	707	768	771	760	767	784	787	747	693
Sr	103	96	100	89	103	104	102	100	104	109	98	102	99
Ga	15	15	16	16	17	16	16	16	15	15	16	15	16
Nb	7	7	8	10	8	8	9	8	8	8	7	8	9
Zr	180	172	185	201	197	196	199	211	192	189	198	193	209
Y	28	28	27	26	23	28	30	30	27	29	27	27	25
Th	13	12	14	15	12	13	14	14	13	14	13	13	15
La	23	24	24	24	26	25	24	26	23	23	25	26	22
Ce	66	50	62	63	49	51	63	60	60	64	63	56	56

Appendix E.1. Kaingaroa XRF

Sample Name	***KA354B***	***KA354C***	***KA356A***	***KA356B***	***KA358A***	***KA358 B***	***KA360***	***KA362A***	***KA362B***	***KA362C***	***KA366***	***KA377***	***KA386f***
Rock Type	Pumice	Pumice	Pumice	Pumice	Pumice	Pumice	Pumice	Pumice	Pumice	Pumice	Pumice	Pumice	Bleb
Unit	OWR	OWR	OWR	OWR	TZ	TZ	TZ	RBU	TZ	TZ	RBU	WIU	TOK
Pumice type	C	C	B	C	C	B	D	D	C	C	C	D	E
SiO_2	71.34	70.84	71.78	71.69	71.86	72.19	68.17	67.97	70.59	71.46	70.34	68.53	65.56
TiO_2	0.23	0.22	0.22	0.20	0.27	0.17	0.26	0.30	0.19	0.23	0.24	0.24	0.68
Al_2O_3	14.64	14.62	14.05	13.64	14.17	14.10	15.44	16.34	14.44	13.84	14.96	16.33	15.89
Fe_2O_3*	2.00	1.96	1.87	1.78	1.82	1.87	2.55	2.51	2.00	1.85	2.18	2.22	4.41
MnO	0.06	0.08	0.05	0.06	0.07	0.06	0.09	0.08	0.06	0.05	0.06	0.06	0.08
MgO	0.30	0.21	0.18	0.20	0.23	0.21	0.45	0.24	0.24	0.26	0.22	0.21	0.74
CaO	1.14	1.20	1.13	1.25	1.26	1.13	1.34	1.21	1.20	1.31	1.21	1.20	2.33
Na_2O	3.65	3.76	3.53	3.72	3.88	3.63	3.33	3.39	3.54	3.94	3.77	3.92	2.83
K_2O	3.18	3.17	3.56	3.42	3.37	3.47	3.00	2.96	3.30	3.40	3.13	2.90	2.15
P_2O_5	0.03	0.03	0.03	0.02	0.08	0.02	0.03	0.04	0.04	0.03	0.02	0.03	0.18
LOI	3.77	3.26	2.89	2.88	3.28	3.25	3.91	5.09	4.38	3.17	4.03	4.40	4.83
Total	100.34	99.35	99.29	98.86	100.29	100.10	98.57	100.13	99.98	99.54	100.16	100.04	99.68
Cr	3	3	3	3	3	3	13	4	3	3	4	4	5
Ni	4	4	3	3	4	3	5	4	4	3	3	3	6
V	10	11	10	11	12	10	22	16	15	13	11	10	34
Pb	16	17	13	15	15	16	17	16	16	14	15	17	24
Zn	30	33	32	36	36	34	55	47	43	44	50	59	134
Rb	115	111	122	120	118	121	103	104	115	118	112	104	76
Ba	695	763	768	767	770	771	779	1008	770	775	798	806	555
Sr	99	104	95	108	106	93	103	101	101	113	100	103	203
Ga	18	16	16	16	15	16	17	18	16	16	17	18	18
Nb	9	9	9	7	8	9	8	10	8	7	9	9	8
Zr	212	219	196	194	210	198	221	278	210	203	240	230	170
Y	23	24	26	27	25	28	24	25	25	25	16	23	19
Th	16	16	13	13	14	16	17	22	16	14	18	11	11
La	21	22	25	24	22	25	19	22	22	20	24	19	16
Ce	76	69	66	60	72	67	89	143	79	64	80	54	47

Appendix E.1. Kaingaroa XRF

Sample Name	*KA387*	*KA415*	*KA415B2*	*KA416*	*KA417A*	*KA417B*	*KA421B*
Rock Type	Rhyolite	Pumice	Pumice	Pumice	Pumice	Pumice	Pumice
Unit	PUK	BT	BT	BT	RBU	RBU	OWR
Pumice type		B		B	C	C	C
SiO_2	71.27	72.78	74.22	74.13	72.18	73.15	68.99
TiO_2	0.23	0.22	0.14	0.21	0.21	0.19	0.24
Al_2O_3	13.46	13.10	12.57	12.60	12.78	13.18	15.27
Fe_2O_3*	1.79	1.71	1.37	1.64	1.89	1.89	2.09
MnO	0.05	0.06	0.05	0.06	0.07	0.07	0.06
MgO	0.28	0.13	0.17	0.11	0.19	0.19	0.13
CaO	1.26	1.12	1.13	0.96	1.20	1.22	1.23
Na_2O	3.76	3.50	3.56	3.31	3.76	4.23	3.61
K_2O	3.65	3.58	3.69	3.39	3.50	3.66	2.99
P_2O_5	0.02	0.02	0.02	0.03	0.03	0.02	0.03
LOI	2.83	4.16	3.46	3.74	2.81	2.23	4.24
Total	98.60	100.38	100.38	100.18	98.62	100.03	98.88
Cr	3	4		3	3	3	3
Ni	4	4		5	3	4	4
V	10	10		15	10	10	10
Pb	10	19		18	19	18	18
Zn	40	47		45	46	48	40
Rb	117	122		116	125	126	111
Ba	757	748		774	764	774	765
Sr	106	90		83	99	103	108
Ga	17	14		14	14	15	16
Nb	9	8		7	7	7	9
Zr	190	178		153	185	185	205
Y	29	25		25	27	27	23
Th	13	4		14	14	12	13
La	21	26		26	27	26	22
Ce	57	61		65	62	65	57

Appendix E.2. Altered Kaingaroa pumices XRF

Sample Name	*KA40A*	*KA186b*	*KA 175A*	*KA198*	*KA228A*	*KA199*	*KA27*
Rock Type	Pumice	Pumice	Pumice	Pumice	Pumice	Pumice	Pumice
SiO_2	65.97	64.88	67.00	66.33	66.03	64.23	62.08
TiO_2	0.25	0.32	0.25	0.27	0.31	0.27	0.33
Al_2O_3	18.75	18.35	17.78	18.14	18.11	19.39	20.58
Fe_2O_3*	2.05	3.01	2.14	2.43	2.20	2.60	3.08
MnO	0.05	0.05	0.07	0.08	0.07	0.10	0.06
MgO	0.11	0.24	0.19	0.12	0.25	0.13	0.23
CaO	0.96	0.94	1.15	0.87	1.44	1.19	1.09
Na_2O	3.18	2.90	3.29	3.06	3.25	3.54	3.21
K_2O	2.64	2.81	2.72	2.43	2.52	2.29	2.13
P_2O_5	0.03	0.03	0.02	0.02	0.03	0.02	0.03
LOI	5.38	6.01	5.08	6.07	4.60	5.58	6.60
Total	99.37	99.54	99.69	99.82	98.81	99.34	99.42
Cr	6	17	3	6	8	5	13
Ni	5	13	5	4	4	4	8
V	11	39	10	14	14	14	23
Pb	18	10	16	28	15	31	16
Zn	33	35	54	72	45	65	48
Rb	94	91	99	87	91	84	81
Ba	831	712	886	871	678	795	729
Sr	85	82	99	69	123	104	97
Ga	29	19	19	21	20	22	30
Nb	13	8	10	13	9	12	10
Zr	249	241	275	274	267	278	240
Y	23	21	27	27	24	24	20
Th	20	19	18	19	16	19	17
La	22	24	32	26	19	22	20
Ce	71	89	80	104	61	127	91

Appendix E.3. Kaingaroa lithics XRF

Sample Name	*KA11*	*KA241A*	*KA91*	*KA99*	*KA201*	*KA6*	*KA7*	*KA17*	*KA82*	*KA173*	*KA194A11*	*KA428b*
Rock Type	RHY	RHY	META	IGN	GW	GB	GB	GB	GB	GB	GB	GB
SiO_2	68.78	73.78	74.03	73.46	70.22	48.26	50.51	49.52	49.05	51.58	50.32	49.29
TiO_2	0.39	0.22	0.37	0.31	0.56	0.33	0.40	0.40	0.33	0.34	0.46	0.40
Al_2O_3	15.57	13.46	13.92	13.69	15.33	22.17	21.58	21.82	24.93	20.97	22.74	22.75
Fe_2O_3*	2.67	2.34	2.77	2.42	3.85	6.43	5.64	5.67	4.96	6.13	6.02	5.42
MnO	0.05	0.07	0.08	0.05	0.03	0.12	0.12	0.11	0.08	0.12	0.12	0.09
MgO	0.59	0.33	0.84	0.25	0.97	5.12	5.54	6.06	3.98	5.41	4.01	5.19
CaO	3.19	1.48	3.43	1.52	0.61	13.24	11.99	12.02	12.77	10.65	13.14	13.32
Na_2O	3.76	4.35	3.88	4.49	3.45	2.21	2.24	2.02	2.35	2.56	2.62	2.27
K_2O	2.39	3.28	1.36	3.07	2.69	0.21	0.19	0.21	0.16	0.53	0.45	0.21
P_2O_5	0.08	0.02	0.11	0.03	0.05	0.05	0.04	0.04	0.03	0.03	0.04	0.05
LOI	1.11	0.85	-0.53	0.40	2.64	0.52	2.02	2.18	1.55	1.93	0.58	1.24
Total	98.58	100.18	100.26	99.69	100.4	98.65	100.29	100.04	100.19	100.26	100.49	100.23
Cr	9	11	7	3	66	148	111	121	80	91	56	128
Ni	3	4	4	3	18	21	18	21	14	16	12	18
V	55	22	32	18	78	122	151	143	126	105	144	125
Pb	15	25	27	35	25	13	14	25	6	15	4	8
Zn	47	37	227	24	73	112	57	56	49	120	44	40
Rb	98	122	89	97	217	39	13	27	9	87	85	15
Ba	727	752	280	730	709	101	449	1163	180	443	136	182
Sr	203	124	211	124	249	376	352	353	407	332	393	382
Ga	17	16	19	18	18	18	18	14	24	20	20	18
Nb	5	8	6.0	6	10.0	2	2	2	2	2	2	2
Zr	139	213	158	115	201	31	28	48	37	41	38	32
Y	22	27	14	29	22	6	10	12	19	8	7	8
Th	9	12	10	10	12	1	1	3	2	1	1	1
La	24	40	17	31	63	5	5	5	5	5	5	5
Ce	49	78	43	59	62	8	5	5	5	7	5	5

Appendix E.3. Kaingaroa lithics XRF

Sample Name	*KA428d*	*KA428a*	*KA428e*	*KA3*	*KA13c*	*KA15*	*KA18*	*KA19*	*KA24*	*KA26*	*KA28*	*KA74*
Rock Type	GB	GB	GB	andesite	andesite	andesite	andesite	andesite	andesite	andesite	andesite	andesite
SiO_2	49.68	49.48	49.08	54.36	54.96	54.76	55.40	55.10	56.64	59.64	53.78	57.29
TiO_2	0.41	0.42	0.47	0.93	1.01	1.01	0.90	0.95	0.81	0.88	0.88	0.80
Al_2O_3	23.17	20.25	19.94	19.74	19.40	20.13	17.36	18.56	18.19	20.53	17.61	18.48
Fe_2O_3*	6.36	7.02	7.20	8.49	8.46	8.05	8.99	8.56	7.61	4.86	9.18	7.03
MnO	0.12	0.11	0.13	0.13	0.13	0.15	0.16	0.13	0.13	0.09	0.16	0.12
MgO	4.49	5.89	7.07	2.87	2.72	2.69	4.57	3.25	4.07	1.54	4.84	4.25
CaO	13.14	11.26	13.60	8.71	8.04	9.06	7.36	7.96	6.70	6.90	8.15	6.24
Na_2O	2.29	2.24	1.79	3.18	3.13	2.77	2.79	2.99	2.74	3.48	3.01	2.36
K_2O	0.32	0.30	0.20	1.38	1.45	1.42	1.43	1.50	1.13	1.58	1.27	1.09
P_2O_5	0.04	0.05	0.04	0.19	0.20	0.19	0.15	0.17	0.11	0.19	0.18	0.07
LOI	0.42	1.72	0.84	0.30	0.31	0.34	0.82	0.01	1.13	0.72	0.19	1.65
Total	100.45	98.74	100.35	100.28	99.81	99.6	99.91	99.18	99.16	100.42	99.24	99.37
Cr	90	224	227	17	17	13	51	18	31	16	52	39
Ni	18	24	25	8	10	8	25	10	11	7	21	14
V	157	134	184	203	193	209	198	171	178	178	214	202
Pb	19	16	16	13	9	13	12	9	10	11	11	14
Zn	111	96	57	72	79	74	78	74	77	75	84	72
Rb	90	11	12	44	47	49	52	52	55	63	46	48
Ba	119	528	85	348	394	326	406	398	428	499	367	421
Sr	414	363	322	409	386	416	359	355	290	300	378	277
Ga	20	18	17	17	19	18	23	21	20	20	21	19
Nb	2	0	2	2	4	2	2	4	4	4	3	2
Zr	31	6	36	135	118	132	138	120	105	117	119	120
Y	6	13	9	26	26	23	20	37	23	53	19	25
Th	1	1	1	7	4	5	5	7	4	5	5	6
La	5	8	5	18	13	17	15	67	16	64	11	14
Ce	11	7	7	29	29	31	33	40	27	30	21	33

Appendix E.3. Kaingaroa lithics XRF

Sample Name	*KA77*	*KA80*	*KA81*	*KA83*	*KA84*	*KA85*	*KA90*	*KA92*	*KA93*	*KA94*	*KA96*	*KA98*
Rock Type	andesite	andesite	andesite	andesite	andesite	andesite	andesite	andesite	andesite	andesite	andesite	andesite
SiO_2	55.01	55.81	55.35	58.04	54.08	60.39	56.21	53.08	52.88	56.57	53.60	55.68
TiO_2	0.84	0.86	0.97	0.73	0.93	0.78	0.74	0.99	0.97	0.90	0.95	0.85
Al_2O_3	17.75	17.78	19.11	18.27	17.40	17.47	17.51	20.51	18.62	17.29	19.76	17.43
Fe_2O_3*	8.71	7.91	8.55	8.22	10.03	7.19	7.83	8.66	9.25	8.91	8.04	8.38
MnO	0.17	0.14	0.13	0.18	0.17	0.12	0.14	0.14	0.16	0.15	0.14	0.15
MgO	3.98	4.43	3.03	3.02	4.69	2.88	4.79	2.74	4.84	4.20	3.21	4.22
CaO	7.09	7.25	7.46	5.97	7.56	5.50	8.00	8.81	8.47	6.91	9.07	7.05
Na_2O	3.14	2.40	2.92	2.56	2.29	3.14	2.57	2.75	2.49	2.53	2.61	2.80
K_2O	1.28	1.26	1.38	1.11	1.28	1.53	1.11	1.02	0.93	1.96	1.05	1.32
P_2O_5	0.13	0.13	0.18	0.11	0.16	0.11	0.11	0.18	0.13	0.20	0.02	0.14
LOI	1.03	1.81	1.40	0.00	1.20	0.94	0.22	0.97	1.24	0.20	0.99	0.58
Total	99.13	99.8	100.48	100.2	99.79	100.07	99.24	99.84	99.98	99.82	99.58	98.61
Cr	27	26	21	79	23	22	56	15	47	32	30	25
Ni	9	10	17	17	9	8	13	9	18	12	9	11
V	182	199	198	200	236	201	202	224	238	216	212	202
Pb	11	9	13	13	7	10	10	12	10	13	11	16
Zn	74	65	76	91	83	78	65	79	90	90	90	76
Rb	49	50	47	54	50	57	36	36	33	62	40	48
Ba	377	374	448	463	386	431	298	319	347	445	262	447
Sr	306	299	367	209	352	238	281	412	357	397	398	297
Ga	18	20	20	22	23	16	19	19	16	18	12	18
Nb	3	2	3	2	2	4	2	4	3	5	4	3
Zr	115	111	138	119	121	141	95	134	127	130	121	115
Y	20	26	32	33	25	22	18	21	20	22	33	23
Th	8	4	5	2	4	4	4	6	5	3	8	7
La	13	17	25	41	25	19	12	16	13	22	25	19
Ce	23	23	24	30	32	35	17	32	31	49	28	27

Appendix E.3. Kaingaroa lithics XRF

Sample Name	*KA156*	*KA194*	*KA428c*
Rock Type	dacite	LPA	UB
SiO_2	65.51	56.56	56.29
TiO_2	0.39	0.69	0.69
Al_2O_3	15.07	17.15	17.29
Fe_2O_3*	3.68	8.01	7.71
MnO	0.07	0.15	0.24
MgO	2.49	4.60	4.33
CaO	3.72	7.62	9.70
Na_2O	2.81	2.69	2.09
K_2O	2.78	1.22	0.52
P_2O_5	0.06	0.12	0.11
LOI	2.04	0.07	0.84
Total	98.63	98.88	99.81
Cr	60	42	82
Ni	13	12	33
V	81	185	182
Pb	14	8	14
Zn	51	72	247
Rb	104	44	60
Ba	657	353	351
Sr	155	245	266
Ga	16	18	17
Nb	5	5	5
Zr	98	97	100
Y	23	19	20
Th	10	4	2
La	16	5	7
Ce	38	18	20

Appendix E.4. Wheao and Kawerau ignimbrites XRF

Sample Name	*KA65A*	*KA65B*	*KA67A*	*KA67B*	*KA110*	*KA114*	*KA119*	*KA139*	*KA152*
Unit	Wheao	Wheao	Wheao	Wheao	Kawerau	Kawerau	Kawerau	Kawerau	Kawerau
Pumice Type					A	B	B	A	A
SiO_2	71.72	71.81	72.09	72.39	71.60	66.60	63.73	72.29	73.19
TiO_2	0.17	0.28	0.22	0.18	0.28	0.59	0.61	0.29	0.21
Al_2O_3	14.46	13.93	12.97	13.49	13.93	15.09	17.19	13.60	12.98
Fe_2O_3*	2.08	1.69	1.98	2.20	1.69	3.20	3.61	1.65	1.51
MnO	0.07	0.09	0.06	0.07	0.09	0.12	0.12	0.09	0.09
MgO	0.15	0.30	0.15	0.34	0.30	0.86	0.48	0.50	0.21
CaO	1.03	1.43	0.95	1.34	1.43	2.69	2.16	1.43	1.29
Na_2O	3.74	4.41	3.96	4.05	4.41	4.48	4.04	4.34	4.29
K_2O	3.43	2.62	3.43	3.45	2.62	2.18	1.98	2.65	2.79
P_2O_5	0.04	0.05	0.03	0.04	0.05	0.14	0.12	0.05	0.03
LOI	3.10	2.87	2.71	2.44	2.87	3.26	5.36	2.16	2.64
Total	99.97	99.78	98.56	99.99	99.27	99.21	99.39	99.05	99.23
Cr	3	3	3	3	3	3	3	3	7
Ni	3	3	3	3	3	3	3	3	4
V	9	7	8	8	7	12	11	7	11
Pb	32	42	85	91	15	19	21	14	13
Zn	63	64	80	84	58	148	386	54	48
Rb	118	118	125	126	81	67	61	84	88
Ba	839	858	786	783	778	648	620	833	877
Sr	86	86	82	85	137	219	198	135	121
Ga	18	18	17	17	16	16	20	14	14
Nb	10.0	10.0	10.0	10.0	9	8	9	9	9
Zr	221	220	208	210	244	622	675	241	221
Y	35	37	35	36	34	42	40	37	33
Th	15	14	13	13	9	6	7	8	8
La	29	29	27	30	23	24	19	26	21
Ce	64	75	70	66	69	60	61	59	67

Appendix E.5. ICP-MS analyses

Sample No	*KA3*	*KA84*	*KA92*	*KA156*	*KA428C*	*KA173*	*KA194A II*	*KA428A*
	andesite	andesite	andesite	dacite	UB	GB	GB	GB
La	16.3	24.5	13.8	20.5	10.5	5.1	4.6	11.0
Ce	32.7	31.9	32.0	42.6	24.2	11.8	10.4	10.7
Nd	19.9	27.7	17.0	16.6	12.0	6.7	5.9	14.2
Sm	4.9	5.9	4.1	3.2	2.9	1.7	1.4	3.1
Eu	1.78	1.59	1.38	0.73	0.96	0.74	0.66	0.96
Gd	5.0	5.6	4.2	3.2	3.1	1.7	1.6	3.1
Dy	4.4	5.2	4.1	3.3	3.3	1.8	1.7	3.1
Er	2.9	2.7	2.4	2.1	2.0	1.0	0.9	1.6
Yb	2.7	2.3	2.4	2.2	1.9	1.0	0.8	1.5
Lu	0.8	0.3	0.4	0.4	0.3	0.2	0.1	0.2
Hf	3.3	3.2	3.3	3.1	1.2	0.3	0.6	0.4
Ta	1.4	1.1	1.2	0.8	1.0	1.3	0.8	0.9
Th	4.74	4.75	4.99	11.3	4.11	1.6	0.9	1.17
U	1.55	1.08	1.12	2.38	0.76	0.27	0.11	0.31

Appendix E.6. INAA analyses

Sample No.	KA45B	KA50	KA45B3	KA269C	KA386f	KA110	KA114
Unit	Kaingaroa	Kaingaroa	Kaingaroa	Kaingaroa	Kaingaroa	Kawerau	Kawerau
Sc	7.22	6.32	6.26	9.20	17.22	5.92	15.29
As	5.30	3.90	4.60	4.40	4.50	3.10	3.20
Br	4.20	4.10	4.50	4.95	3.20	4.70	5.50
Sb	0.37	0.28	0.37	0.18	0.43	0.13	0.17
Cs	5.51	5.04	5.36	5.11	3.23	2.87	2.55
La	26.75	25.63	25.69	26.12	17.60	23.87	23.70
Ce	53.50	55.50	56.10	63.20	39.10	54.00	53.80
Sm	4.77	4.65	4.55	4.46	3.86	5.37	6.79
Eu	0.77	0.69	0.73	0.82	0.97	1.14	1.74
Tb	0.77	0.71	0.70	0.68	0.58	0.87	1.17
Yb	3.01	2.99	2.94	2.92	2.05	3.63	4.64
Lu	0.474	0.423	0.386	0.433	0.313	0.561	0.707
Hf	5.98	4.89	5.03	7.39	5.05	7.15	13.31
Ta	0.73	0.74	0.75	0.94	0.61	0.66	0.63
Th	13	13	13	16	10	8	7
U	3	3	3	3	2	2	2

Appendix E.7. Isotope analyses

Sample No.	*KA25*	*KA42*	*KA45A*	*KA45B*	*KA45B3*	*KA50*
Rock Type	Pumice	Kairuru	Pumice	Pumice	Pumice	Pumice
$^{87}Sr/^{86}Sr$	.705832/23	.705416/37	.705751/51	.705827/28	.705707/29	.705567/17
$^{143}Nd/^{144}Nd$	.512676/12	.512721/14	.512678/11	.512672/11	.512679/11	.512700/10

Sample No.	*KA53*	*KA377*	*KA386f*
Rock Type	Pumice	Pumice	Bleb
$^{87}Sr/^{86}Sr$	.705658/22	.705784/18	.706251/21
$^{143}Nd/^{144}Nd$	.512694/10	.512672/9	.512623/12

Abbreviations

Lithic types

- PPA Plagioclase-phyric andesites
- LPA Large pyroxene-phyric andesites
- UB Uralitised andesites
- WHAK Whakamaru-group ignimbrites
- WAI Waiotapu Ignimbrite
- MAT Matahina Ignimbrite
- SB Sandy black ignimbrites
- MISC Miscellaneous ignimbrites
- ALT Altered ignimbrites
- KG Kaingaroa Ignimbrite
- RHY Rhyolite
- OB Obsidian
- GB Gabbros
- META Metavolcanics
- RGW Rounded greywacke
- GW Greywacke
- SED Sediments
- TERT Tertiary sediments

Stratigraphic units

BT	Basal Tephras
RBU	Reporoa Boundary Unit
TZ	Transition Zone
BTI	Brown Transitional Ignimbrite
TTI	TanTransitional Ignimbrite
OWR	Old Waiotapu Rd unit
TOK	Tokiaminga valley subunit
WIU	Webb Ignimbrite Unit

Beresford (1997)

Distribution maps of the Kaingaroa Ignimbrite

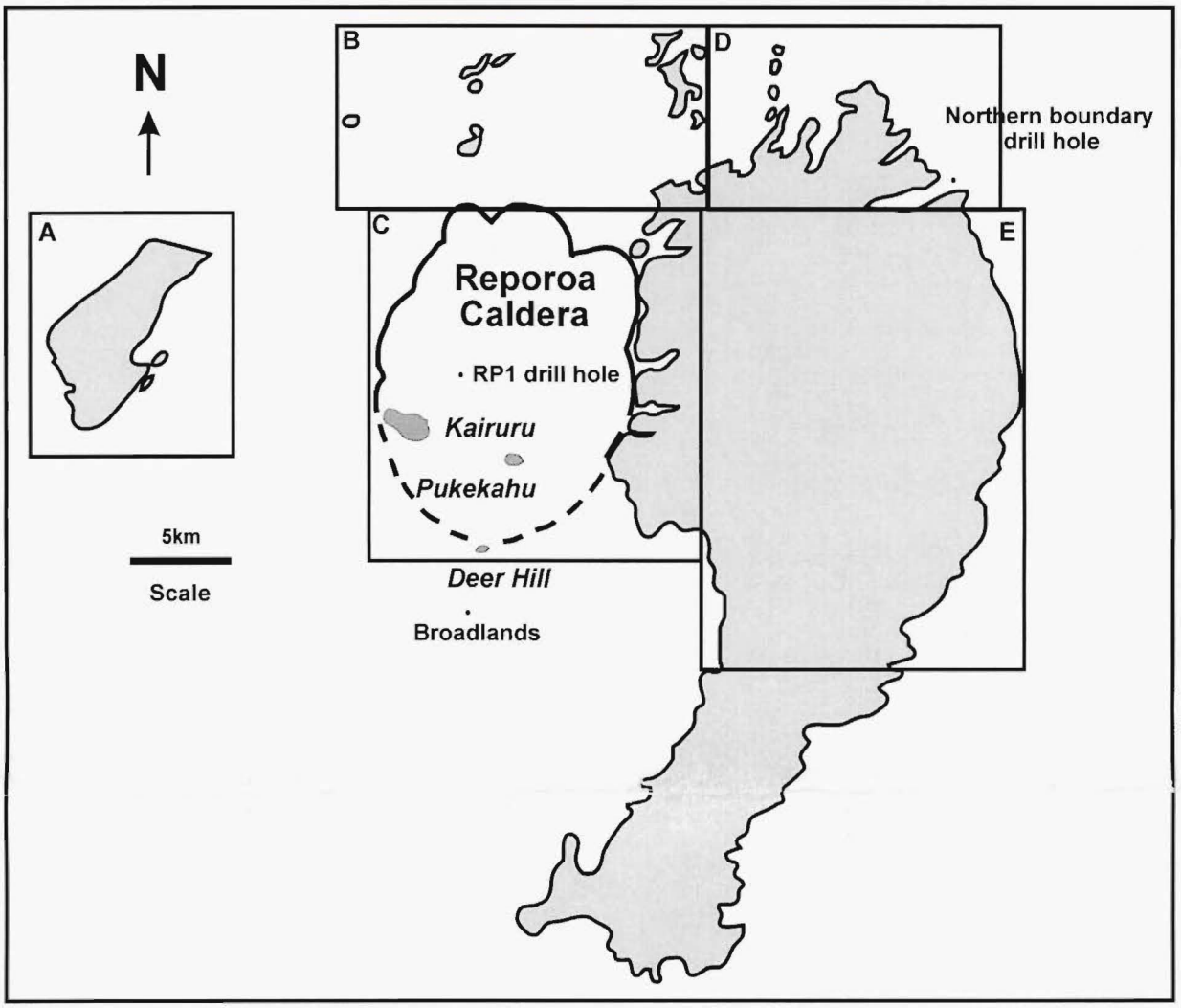

Distribution of the Kaingaroa Ignimbrite and individual outcrop maps.
Grid coordinates refer to NZMS 260 series maps U16, U17, V16 and V17.
Kaingaroa Ignimbrite distribution is denoted in maroon on all maps.
Outcrop and distribution is illustrated relative to major roads, trig stations and rivers (streams) and lakes.

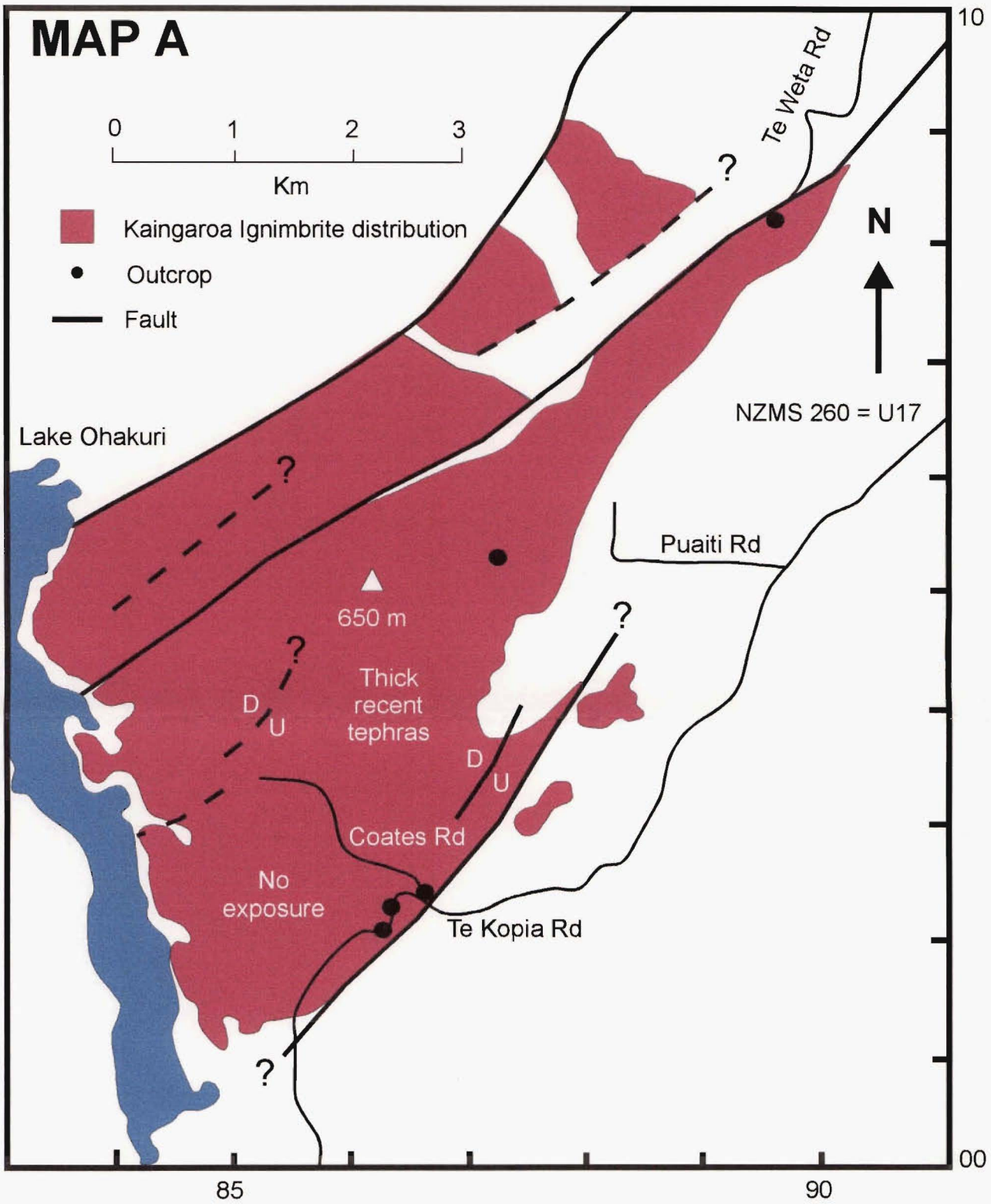

Beresford (1997)

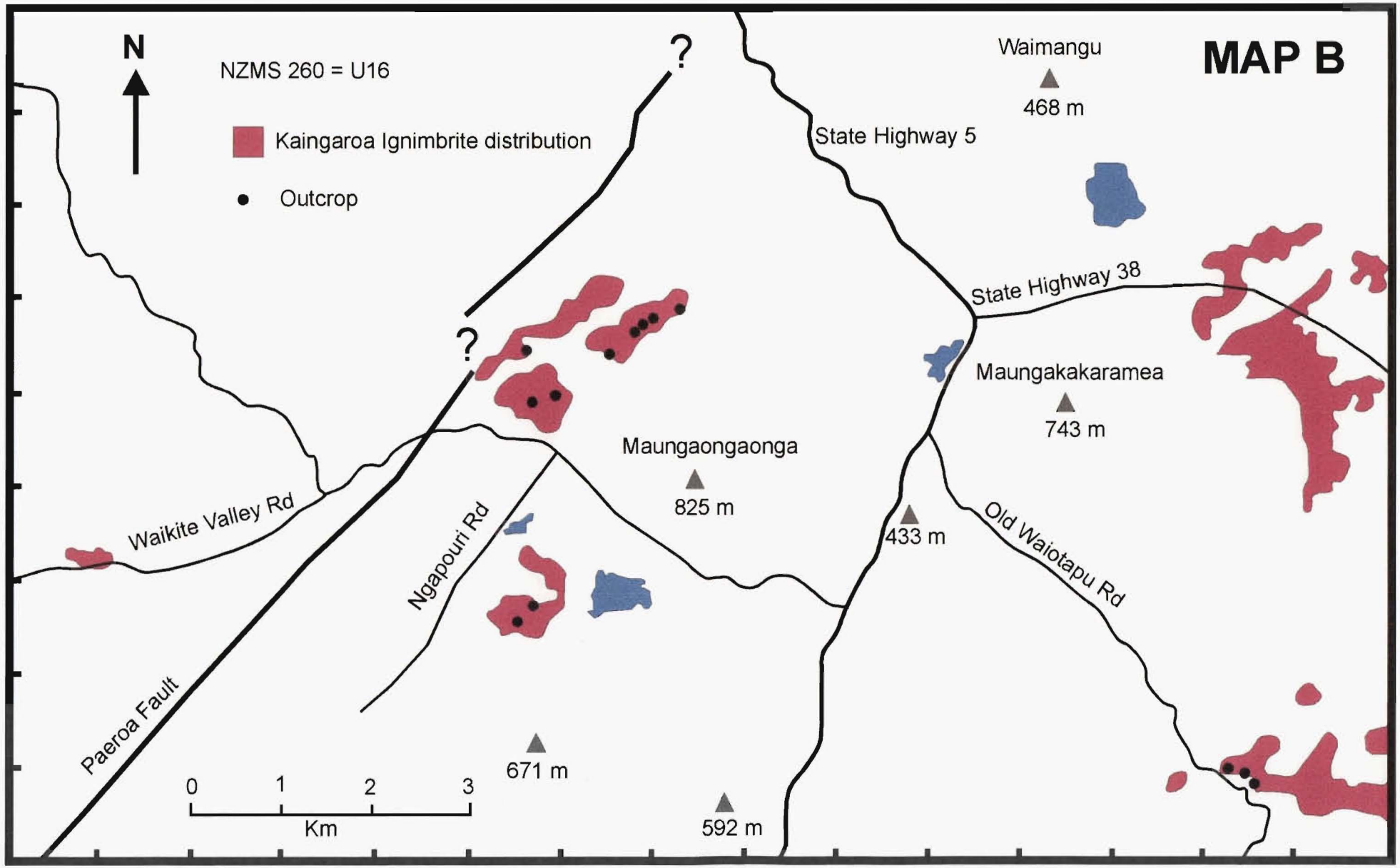

Beresford (1997)

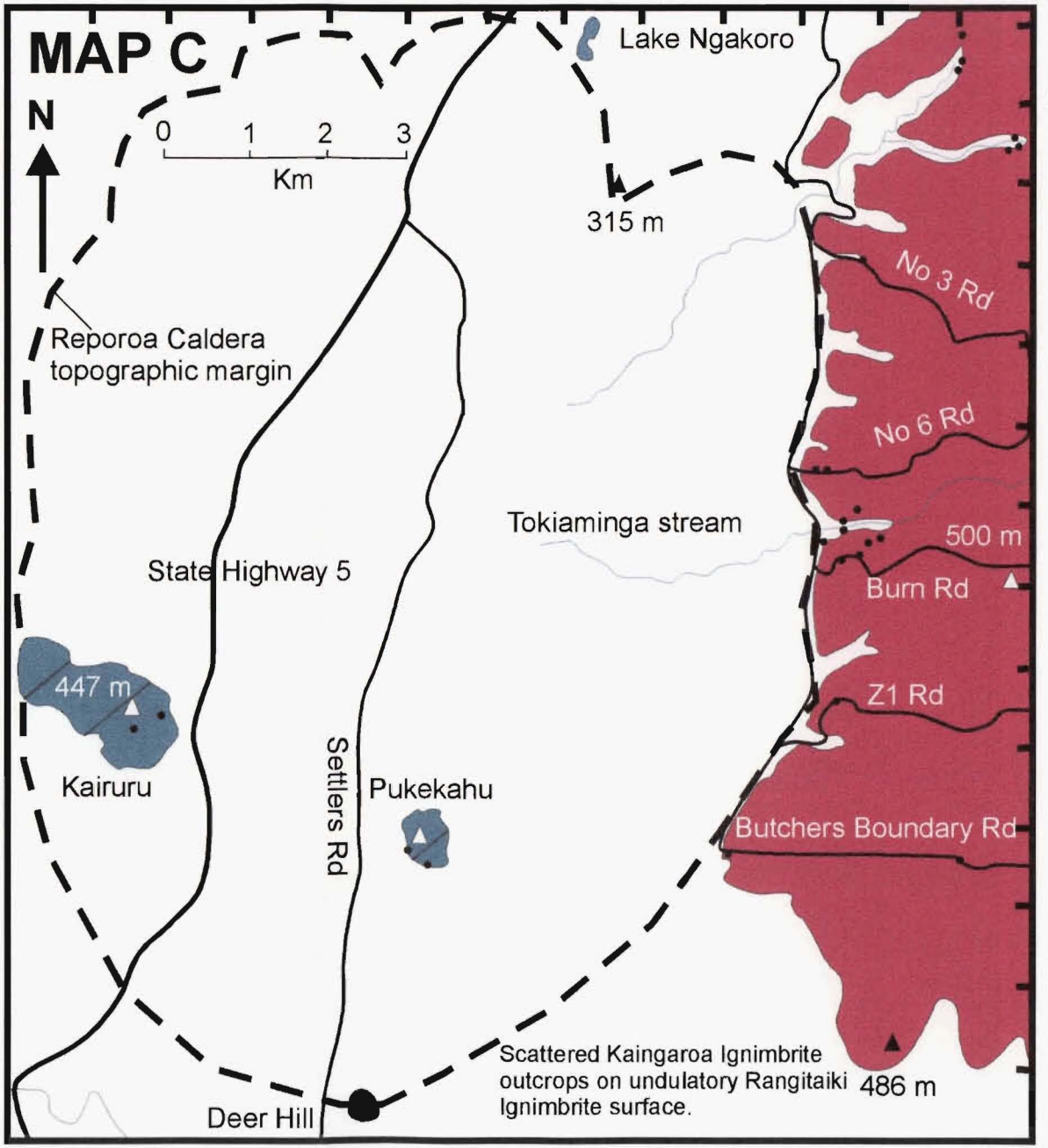

NZMS 260 = U17

Kaingaroa Ignimbrite distribution

Outcrop

Post-caldera rhyolites

Beresford (1997)

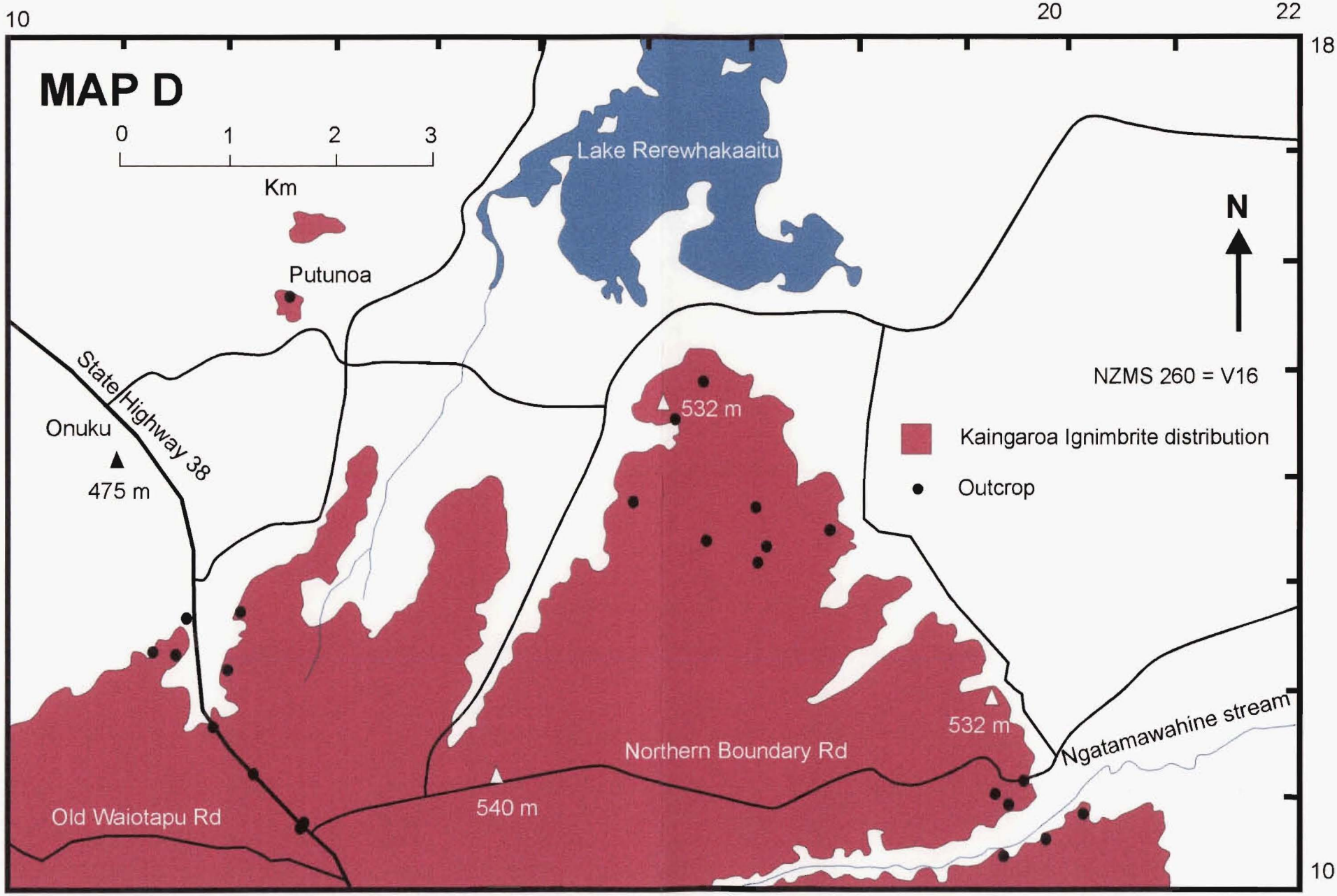

Beresford (1997)

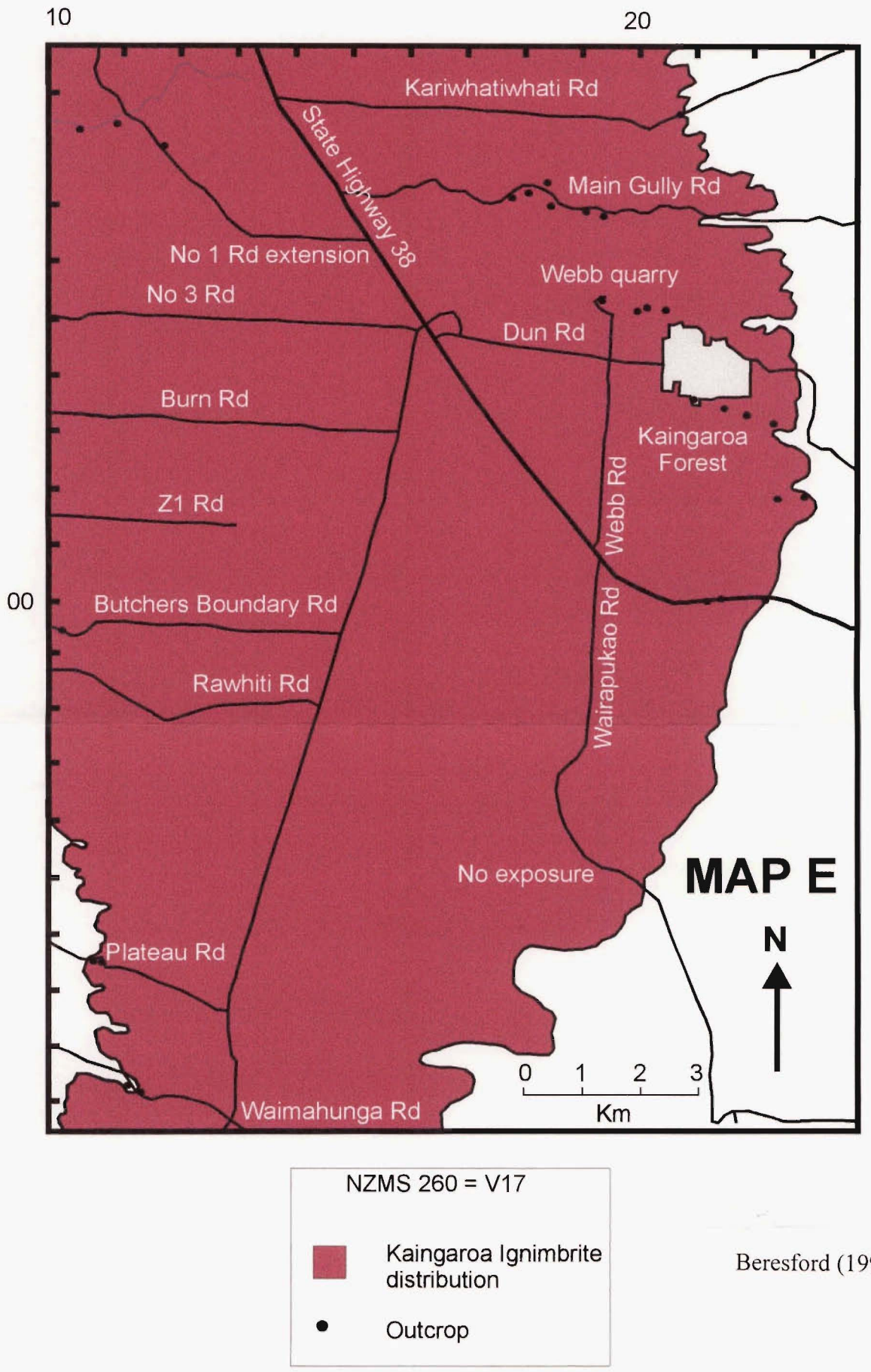

NZMS 260 = V17

Kaingaroa Ignimbrite distribution

Outcrop

Beresford (1997)

Lithic componentry variation in climactic phase deposits

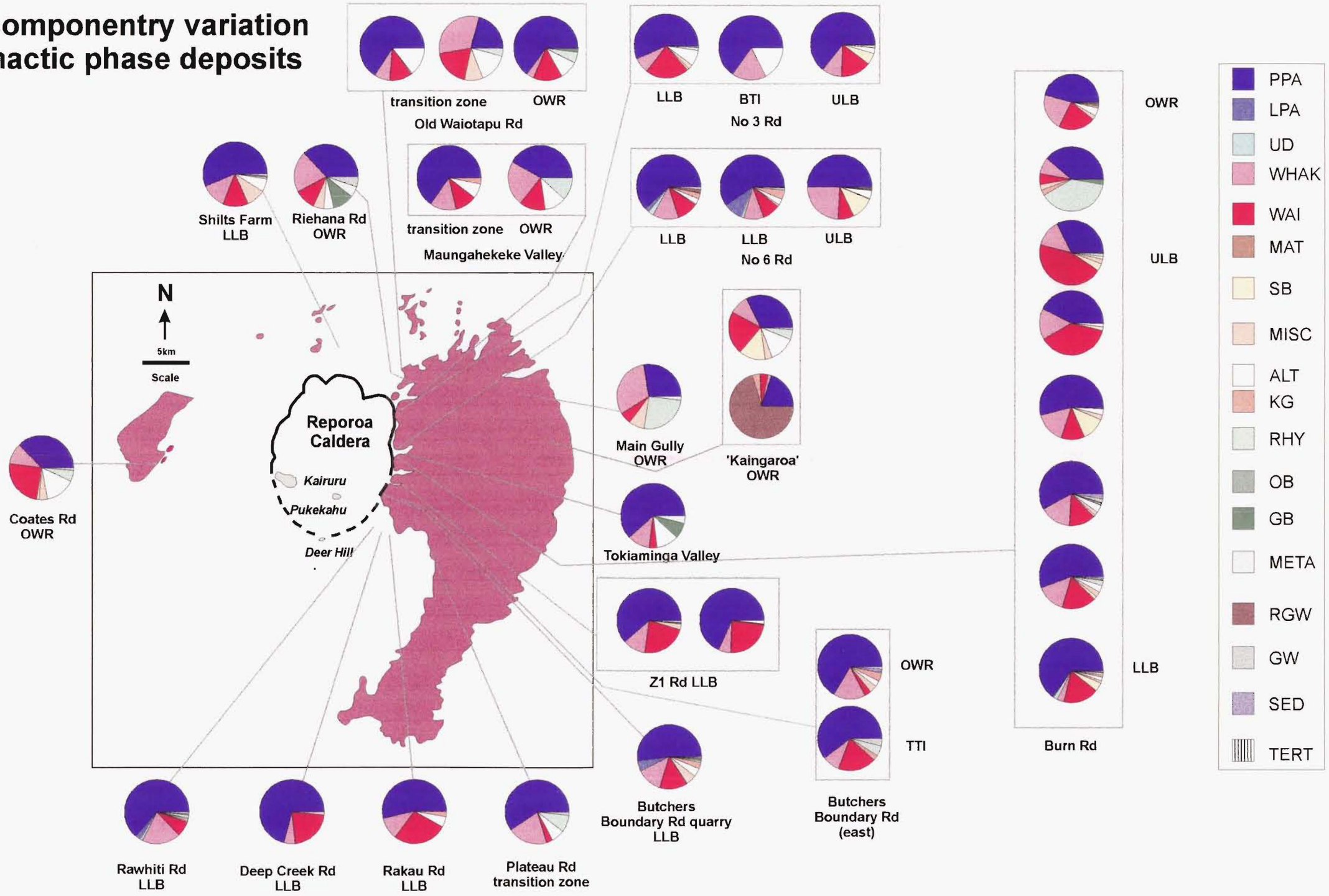

Figure 5.4 enlargement